BJR

THE BRITISH JOURNAL OF RADIOLOGY

Volume 63 Number 754 October 1990

UCM UK-H06215-23-P25855

23

X-ray Diagnosis • Ultrasound • Interventional Radiology
Radiotherapy • Oncology • Hyperthermia
Nuclear Medicine • Nuclear Magnetic Resonance
Radiation Physics • Radiobiology • Radiation Protection

BJR is published by The British Institute of Radiology BIR

You Can Depend On Our Diode Detectors For Patient Dose Verification During Treatment

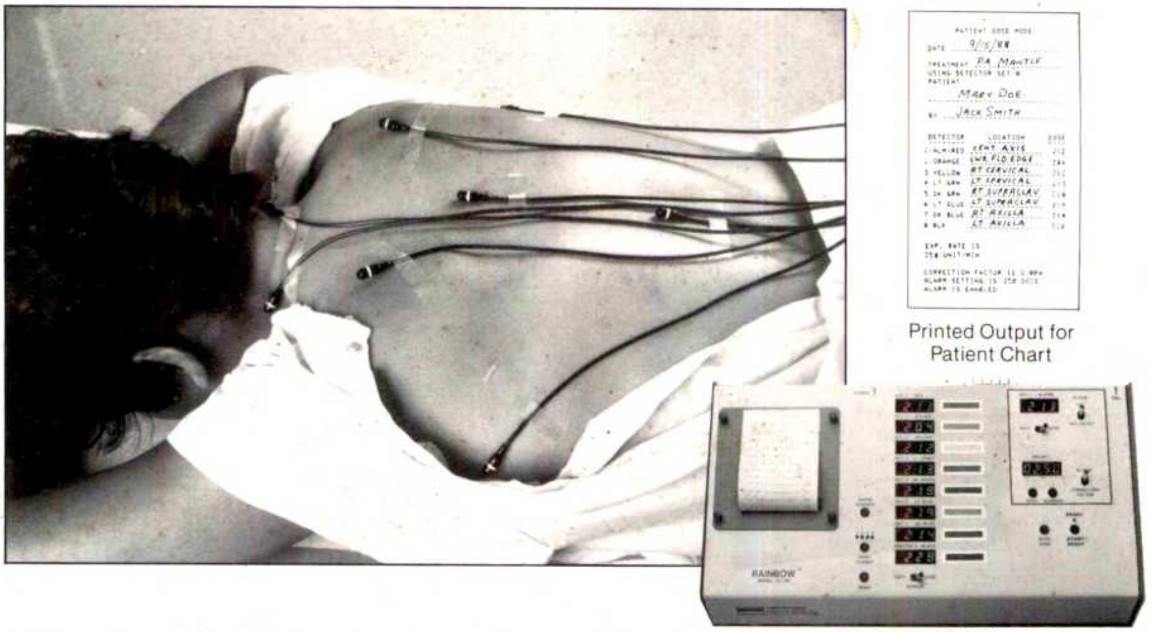

PATIENT DOSE MODE

DATE 9/15/88

TREATMENT PA MANTLE

USING DETECTOR SET A

PATIENT

MARY DOE

BY JACK SMITH

DETECTOR	LOCATION	DOSE
1 [illegible]	CENT AXIS	[illegible]
2 ORANGE	LWR FLD EDGE	[illegible]
3 YELLOW	RT CERVICAL	[illegible]
4 LT GRN	LT CERVICAL	[illegible]
5 DK GRN	RT SUPRACLAV	[illegible]
6 LT BLUE	LT SUPRACLAV	[illegible]
7 DK BLUE	RT AXILLA	[illegible]
8 BLK	LT AXILLA	[illegible]

EXP. RATE IS
250 UNIT/MIN

CORRECTION FACTOR IS [illegible]
ALARM SETTING IS 250 DOSE
ALARM IS ENABLED

Printed Output for Patient Chart

RAINBOW™
Patient Dose Verification and QA Beam Analyzer with 8 Displays for 8 Detectors

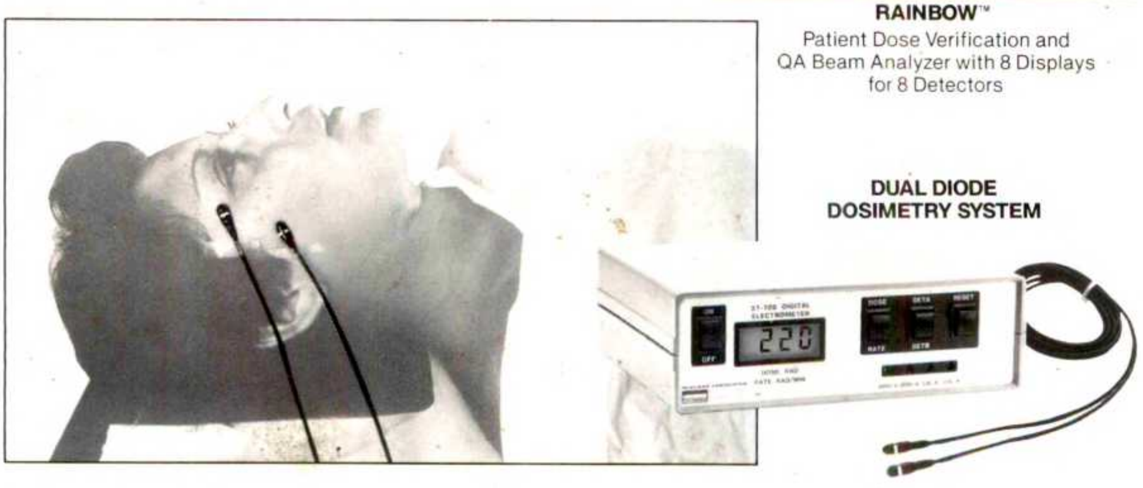

DUAL DIODE DOSIMETRY SYSTEM

- **Instant measurements will help prevent accidental overexposure to patients.**
- **Over 10 years of proven, reliable, dependable performance in the clinical environment.**
- **Detectors for photons and electrons.**
- **Unlimited versatility — use with your electrometer or ours.**

When coupled with a precision electrometer, our Diode Detectors offer the unique combination of high accuracy, ruggedness, small size, immediate readout, and simplicity of operation. The use of noble metal dopings, sophisticated mounting methods and special low noise cable have substantially reduced radiation induced damage, directional sensitivity and induced noise from cable movements, making these detectors perfect for the application of patient dose verification.

For complete details on our Diode Detectors and Diode Dosimetry Systems, request Bulletin 371-14

NUCLEAR ASSOCIATES

VICTOREEN

A Division of VICTOREEN, INC.
100 VOICE ROAD
CARLE PLACE, NY 11514-1593 U.S.A.
(516) 741-6360
FAX (516) 741-5414

™Victoreen, Inc.

P25855

VOL 63 NO 754 OCTOBER 1990

The British Journal of Radiology

Contents

Papers

Page

Stereotactic multiple arc radiotherapy 745
E. S. Thomson, S. S. Gill and D. Doughty

Chronic anaemia, hyperbaric oxygen and tumour radiosensitivity 752
M. McCormack and A. H. W. Nias

The relative biological effectiveness of fractionated doses of fast neutrons (42 $\text{MeV}_{d \rightarrow Be}$) for normal tissues in the pig
II. Late effects on cutaneous and subcutaneous tissues 760
J. W. Hopewell, D. W. H. Barnes, M. E. C. Robbins, M. Corp, J. M. Sansom, C. M. A. Young and G. Wiernik

Lipiodol computerized tomography: how sensitive and specific is the technique in the diagnosis of hepatocellular carcinoma? 771
H. Ngan

Quantitative γ-ray computed tomography of the radius in normal subjects and osteoporotic patients 776
D. A. S. Smith, C. J. Hosie, A. D. Deacon and D. L. Hamblen

Choroid plexus cysts and chromosomal defects 783
J. G. Thorpe-Beeston, C. M. Gosden and K. H. Nicolaides

Ultrasonography in patients with suspected acute appendicitis: a prospective study 787
P. Skaane, P. F. Amland, T. Nordshus and K. Solheim

Sedation in children scanned with high-field magnetic resonance; the experience at The Hospital for Sick Children, Great Ormond Street 794
J. K. Shepherd, M. A. Hall-Craggs, J. P. Finn and R. M. Bingham

Technical notes

A man with three knees? False "hot spot" with dual isotope imaging 798
K. A. Miles and R. W. Barber

Additive filtering 800
S. Marugg, K. Streule, W. Hedtler and C. Berchtold

Computerized calculation of radiation dose to patients from radiography 801
C.-L. Chapple and K. Faulkner

Case reports

Progressive systemic sclerosis (diffuse scleroderma) and radiotherapy 804
S. G. Cooper and J. W. Denham

Spinal cord sarcoidosis with intramedullary cyst formation 805
A. G. Clifton, J. M. Stevens, R. Kapoor and P. Rudge

Ultrasonic appearances of the early changes in fibrodysplasia ossificans progressiva 809
E. J. McAteer, L. A. Hallam and G. M. A. Hendry

Cystic lymphangioma of the pelvis in childhood 813
J. C. Hoeffel, A. L. Marchal, E. Pierre and J. Derelle

Unusual presentation of non-Hodgkin's lymphoma of the small bowel 814
D. A. Nicholson

Ultrasound appearances of extramedullary haematopoiesis in the liver and spleen 816
M. J. Bradley and C. Metreweli

Case of the month

A case of post-operative paresis 819
J. F. C. Olliff, S. J. Gwyther and G. Hart

Short communications

Mathematical models of repopulation and reoxygenation in radiotherapy 821
O. C. A. Scott

Contrast medium imbibition in osteoarthritic cartilage 823
M. W. Spring and J. C. Buckland-Wright

Proceedings

Proceedings of the British Institute of Radiology
Imaging towards 2000: practical integration of new technologies, 21 March 1990 826
The combination of chemotherapy and radiotherapy in clinical practice, 10 May 1990 828

Book reviews

Computed Tomographic Angiography of the Mediastinum. *L. Chiu, W. Stanford and V. Yiu-Chiu* 832
Ultrasound Mammography. Methods, Results, Diagnostic Strategies. *B.-J. Hackeloer, V. Duda and G. Lauth* 832
Hysterosalpingography and Pelvic Ultrasound: Imaging in Infertility and Gynecology. *I. C. Yoder* 832

BIR Bulletin *facing page* 832

© 1990: The British Institute of Radiology. This publication is copyright under the Berne Convention and the Universal Copyright Convention. All rights reserved, apart from any relaxations permitted under national copyright laws, no part of this publication may be reproduced, stored in a retrieval system or transmitted in any form or by any means without the prior permission of the copyright owners. Permission is not, however, required to copy abstracts of papers or of articles on condition that a full reference to the source is shown. Multiple copying of the contents of the publication without permission is always illegal. Published by The British Institute of Radiology, 36 Portland Place, London W1N 4AT. Origination by BPCC Whitefriars Ltd, Tunbridge Wells, and printed and bound in Great Britain by BPCC Wheatons Ltd, Exeter.
ISSN 0007 1285

VOL 63 NO 755 NOVEMBER 1990

The British Journal of Radiology

Contents

Papers

Page

Echo planar imaging of the human fetus *in utero* at 0.5 T 833
P. Mansfield, M. K. Stehling, R. J. Ordidge, R. Coxon, B. Chapman, A. Blamire, P. Gibbs, I. R. Johnson, E. M. Symonds, B. S. Worthington and R. E. Coupland

Magnetic resonance imaging in idiopathic retroperitoneal fibrosis: measurement of T_1 relaxation time 842
A. P. Brooks, R. H. Reznek and J. A. W. Webb

The relationship of "high risk" mammographic patterns to histological risk factors for development of cancer in the human breast 845
J. E. Arthur, I. O. Ellis, C. Flowers, E. Roebuck, C. W. Elston and R. W. Blamey

The role of Indium-labelled leukocyte imaging in pyrexia of unknown origin 850
S. G. Davies and N. W. Garvie

Urinary tract dilatation in constipated children 855
J. Herbetko and I. Hyde

A clinical application of iodine quantitation using digital fluorography 858
W. D. Thompson, C. J. Kotre, J. P. Owen and M. F. Laker

A model for hematopoietic death in man from irradiation of bone marrow during radioimmunotherapy 862
B. R. Scott and L. E. Dillehay

Lack of late skin necrosis in man after high-dose irradiation using small field sizes: experiences of grid therapy 871
H. Shirato, N. K. Gupta, T. J. Jordon and J. H. Hendry

The relative biological effectiveness of fractionated doses of fast neutrons ($42\,\mathrm{MeV}_{d\rightarrow Be}$) for normal tissues.
III. Effects on lung function 875
M. Rezvani, D. W. H. Barnes, J. W. Hopewell, M. E. C. Robbins, J. M. Sansom, P. J. V. Adams and R. Hamlet

Technical notes

A rapid method of production of irregular-shaped fields for use with patients receiving electron radiotherapy 882
J. H. Plane and C. Usher

Calibration of radiotherapy beams using a PC-based dosimetry recording system 883
M. B. Kenny and R. M. Millar

A survey of the radiation exposures received by the staff at two cardiac catheterization laboratories 885
B. J. McParland, J. Nosil and B. Burry

Case reports

Ultrasound cystography: a valuable technique 889
R. A. Coulden, D. C. Hanbury and P. Farman

Skeletal abnormalities in a case of congenital erythropoietic porphyria 891
M. Ito, K. Hayashi, M. Uetani, I. Isomoto and H. Irifune

Computed tomography in volvulus of the midgut 893
A. B. Paul and D. M. Dean

The value of computed tomography in the diagnosis of atlanto-axial rotatory fixation 894
J. B. Murray and M. Ziervogel

Multifocal central nervous system lesions and retropharyngeal lymphadenopathy on magnetic resonance imaging: an association that suggested progressive multifocal leukoencephalopathy in a patient with acute aphasia 897
J. G. Llewelyn, A. R. Valentine, C. Bradley, K. King and M. L. P. Gross

The nidus of an osteoid osteoma mimicking an os supratrochleare dorsale 899
P. Roberts, A. M. Davies, C. M. Starkie and R. J. Grimer

Radiological diagnosis and management of a solitary tuberculous hepatic abscess 902
D. H. Reed, A. F. Nash and P. Valabhji

Case of the month

A case of colonic defection 905
R. Butterworth and H. Adams

Short communication

High resolution, high field magnetic resonance imaging of joints: unexpected features in proton images of cartilage 907
P. R. Cole, M. K. Jasani, B. Wood, A. J. Freemont and G. A. Morris

Correspondence

Major contamination from an iodine-131 therapy patient 910
F. J. F. Madden, R. J. Aukett, M. Y. Early, M. J. Dunn and J. Rampton

Temporary enlargement of penumbra on linear accelerators 911
J. B. Tuohy and A. M. Morgan

Proceedings

Proceedings of the British Institute of Radiology
The repair of radiation damage: molecules to man, 11 May 1990 912

Book reviews

Endovaginal Ultrasound. *S. R. Goldstein* 916
Neonatal and Pediatric Ultrasonography. Clinics in Diagnostic Ultrasound, No. 24. *D. S. Babcock* (Ed.) 916
Digital Subtraction Imaging in Infants and Children. *E. N. Faberer* (Ed.) 916
Cardiac Application of Digital Angiography. *A. G. Wasserman and A. M. Ross* 916
Handbook of Cardiovascular and Interventional Radiologic Procedures. *K. Kandarpa* 917
Diagnostic and Interventional Radiology: A Clinical Manual. *G. M. Gaylord, L. P. Davis and S. R. Baker* 917
Breast Imaging: Diagnosis and Morphology of Breast Diseases. *R. L. Egan* 918
Diagnostic Imaging of the Acute Abdomen: A Clinical and Radiologic Approach. *D. Beyer and U. Modder* 918

BIR Bulletin *facing page* 918

© 1990: The British Institute of Radiology. This publication is copyright under the Berne Convention and the Universal Copyright Convention. All rights reserved, apart from any relaxations permitted under national copyright laws, no part of this publication may be reproduced, stored in a retrieval system or transmitted in any form or by any means without the prior permission of the copyright owners. Permission is not, however, required to copy abstracts of papers or of articles on condition that a full reference to the source is shown. Multiple copying of the contents of the publication without permission is always illegal. Published by The British Institute of Radiology, 36 Portland Place, London W1N 4AT. Origination by BPCC Whitefriars Ltd, Tunbridge Wells, and printed and bound in Great Britain by BPCC Wheatons Ltd, Exeter.
ISSN 0007 1285

1990, *The British Journal of Radiology*, *63*, 745–751

VOLUME 63 NUMBER 754 OCTOBER 1990

The British Journal of Radiology

Stereotactic multiple arc radiotherapy

By E. S. Thomson, PhD, *†S. S. Gill, FRCS and D. Doughty, MSc

Radiation Physics Department, St Bartholomew's Hospital, London and †Neurosurgery Department, The National Hospitals for Nervous Diseases, London

(Received March 1990 and in revised form May 1990)

Abstract. A radiotherapy technique is presented for delivering a concentrated pattern of absorbed dose to intracranial lesions. Treatment takes place on a conventional, isocentrically mounted linear accelerator, rotated in several planes around a single target site. A new, relocatable sterotactic frame is used which enables fractionated radiotherapy to be administered if required. Calculations of the absorbed dose distribution in three orthogonal planes are performed using specially prepared software on a computer used for standard treatment planning. In this way, the need for excessive computing power is avoided.

Leksell (1951) introduced the term "radiosurgery" to describe a technique in which narrow radiation beams from an orthovoltage X-ray unit were used to irradiate an intracranial target from several angles. It was called radiosurgery because it was seen as an alternative to surgical removal of the volume of tissue (Leksell, 1949, 1951). To improve the dosimetric efficacy of the technique, Leksell's group next began to use high energy proton beams (Larsson et al, 1958), an approach later adopted at several other centres (Lawrence et al, 1962; Kjellberg, 1977; Kjellberg et al, 1978, 1983; Fabrikant et al, 1983, 1984).

In 1968, a dedicated radiosurgery unit incorporating 179 converging beams from cobalt-60 sources was introduced (Leksell, 1968, 1971). Adaptations of this unit were produced commercially and these devices are in use at several centres, treating a variety of clinical conditions (Backlund et al, 1972, 1974; Backlund, 1979; Bradshaw, 1986; Walton et al, 1987).

Following the development of isocentrically mounted linear accelerators, it became possible to undertake high precision radiosurgery without such specialized equipment (Betti & Derichinski, 1983; Colombo et al, 1985; Hartmann et al, 1985; Podgorsak et al, 1988; Lutz et al, 1988). Steep absorbed dose gradients were achieved by rotating the beam in a series of non-coplanar arcs around the target volume. In practice, these non-coplanar arcs are usually obtained by positioning the target volume at the isocentre and for a series of static couch positions, rotating the gantry through a predetermined angle whilst irradiating.

The purpose of this paper is to describe the technique developed at St Bartholomew's Hospital. The procedure uses minimal specialized equipment and could be introduced without complications into the majority of radiotherapy centres. Treatment planning is achieved using specially prepared software running on a standard treatment planning computer (Thomson, 1990). The linear accelerator used for treatment is a Varian, Clinac 6/100, 6 MV unit with minor modifications and few additional attachments. The resulting simplicity of the technique is intentional. It is considered that a sufficient degree of positional and dosimetric accuracy can be achieved with standard, low cost radiotherapy equipment.

Radiosurgery techniques are most applicable for the treatment of small target volumes, usually in the range 1.0 to 3.5 cm in diameter, although some dosimetric benefit may exist for volume sizes up to 5.0 cm in diameter (Thomson, 1990). Treatment of such small target volumes requires a high degree of positional accuracy and in order to achieve this, a stereotactic frame is required. Use of conventional stereotactic frames, however, places severe restrictions on the treatment process. Historically, invasive methods have been used to fix stereotactic frames to patients, for example, steel tipped screws indented into the skull and once removed these frames cannot be repositioned with sufficient accuracy. For this reason radiosurgery has been restricted to the administration of a single fraction of radiotherapy and has, as a result, found its widest use in the treatment of benign conditions such as arterio venous malformations (AVMs) where there is probably no radiobiological advantage to be gained from a fractionated regime. The technique described in this paper makes use of a stereotactic relocation device developed at the National Hospitals for Nervous Diseases (Gill, 1987). The frame can be rigidly secured to the head by non-invasive means and can be precisely repositioned as often as is required. This makes it possible to define a target position and volume from a combination of imaging techniques if required. In addition, more time is made available for performing the necessary dosimetric calculations and checks prior to repositioning the frame for stereotactic radiotherapy. A fractionated form of treatment is also made possible, with the ability to monitor the long term effects subsequently by repositioning the frame and re-imaging through the same anatomical plane.

---

*Present address: Department of Neurosurgery, Charing Cross Hospital, London.

It is felt that the term "radiosurgery" is not applicable to the method described and the alternative, "stereotactic multiple arc radiotherapy (SMART)", is used.

Method

The planning procedure for a patient receiving a SMART treatment is spread over several days. On the first visit, the stereotactic frame is fitted to the patient. On the following day, computerized tomography (CT) scans are performed during which the data necessary for treatment planning and target localization are collected. Treatment takes place approximately 1 week after the planning CT scan.

Each step in the planning and treatment procedure will be described in turn.

Patient immobilization

Patient immobilization and stereotactic localization of the target site are achieved using a relocatable stereotactic frame (Gill, 1990). The frame comprises a rectangular base plate to which is secured a dental impression of the patient's upper jaw. Non-invasive and yet rigid fixation of the frame is accomplished by bringing the dental cast into firm contact with the upper jaw. This position is maintained by means of a series of straps which pass over the head. An adjustable and calibrated head rest, containing an individually moulded occipital impression, provides additional stability by preventing forward tilting of the frame. The head rest also makes the frame more comfortable when the patient is supine (Fig. 1). The relocatable frame has fixation points to which the Brown–Roberts–Wells (BRW) stereotactic frame system (Heilbrun et al, 1983) may be attached. It could, however, be used with any other stereotactic system.

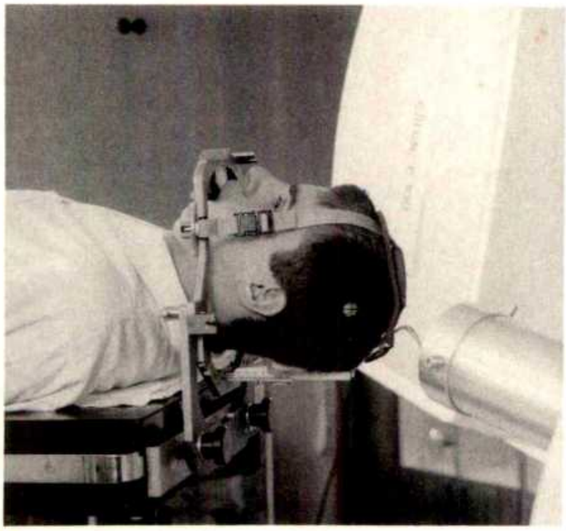

Figure 1. A patient fitted with the relocatable stereotactic frame.

To verify reproducibility of frame position, radiographs are taken on the treatment simulator (Varian Ximatron-CX). For these, the patient lies on the simulator couch, with the frame attached to the end of the couch by means of an intermediary bracket. A three-sided Perspex box is then placed over the patient's head and fixed to the frame. When fixed in position, the box is aligned with the cardinal axes of the BRW coordinate system and these are engraved on the Perspex plates for reference.

With the patient attached to the simulator couch, linear couch movements are made to move the centre of the coordinate system to the isocentre. Anteroposterior (AP) and lateral radiographs are then recorded. The position of the central axis of the beam is indicated on these radiographs by the position of the cross-wires (Fig. 2). As these are aligned with the Perspex box, the position of the cross-wires gives an indirect indication of the position of the frame. Once the images are recorded, the Perspex box and the relocatable frame are removed, refitted and repeat radiographs are taken exactly as described above. Corresponding radiographs can then be overlaid, with the anatomical detail of the patient on each image superimposed. Under these circumstances, the position of the frame relative to the patient in each case can be compared, using the image of the cross-wires for reference.

CT scanning

The planning CT scan of the patient serves three purposes. The first is to find the stereotactic coordinates of the centre of the target volume in order to enable its positioning at the isocentre of the treatment unit. The

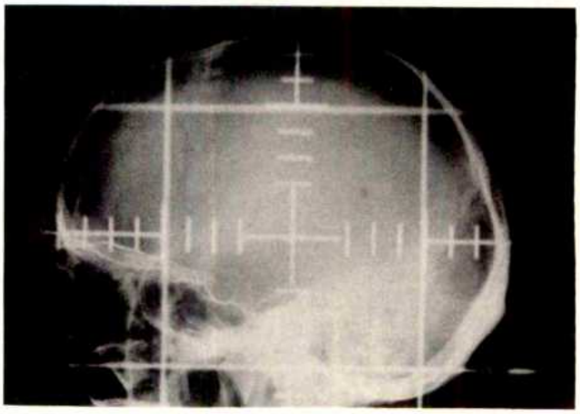

Figure 2. A lateral radiograph of a patient with the relocatable frame fitted. The image of the cross-wires indicates the position of the frame, relative to the patient.

second purpose is to assess the dimensions of the target volume so that the optimum field size may be chosen and the third is to obtain sufficient information to compute an absorbed dose distribution. At present, all treatment plans are prepared solely from CT scan data. It is intended to introduce stereotactic angiography, as an aid to target localization for AVMs, in the near future. For full three-dimensional reconstruction of patient outline data, however, CT scans will still be required.

Immediately prior to CT scanning, the relocatable frame is fitted to the patient. Anteroposterior and lateral radiographs are recorded on the simulator and correct positioning of the frame is verified as described above. The radiographs recorded before CT scanning form an important reference and it is essential that the frame is not removed between the recording of these images and the end of the CT session.

The patient is fixed in position on the couch of the CT scanner (International General Electric, IGE, 9800) in an identical position to that used on the simulator. To obtain the stereotactic coordinates of the centre of the target volume, the BRW CT localizer is fitted to the relocatable frame. With the frame attached to the end of the CT couch, the image plane of the scanner should be parallel to the base plane of the BRW coordinate system. Under these circumstances, there should be a linear relationship between CT image coordinates and BRW frame coordinates. In practice, small deviations in the linearity of couch movements, caused by sagging and twisting of the couch as it is extended, mean that this linear relationship cannot be relied upon. The target coordinates are therefore found using the BRW calculation software which is independent of the scanner alignment. In contrast, for computation of the absorbed dose distribution, a linear relationship is assumed. Contiguous slices are considered to be parallel to the end of the couch when their relative positions are transferred to the treatment planning computer. The significance of these alignment factors is small as the extent of couch deviation is not usually detectable when consecutive images are compared. With such small target volumes, however, it is considered safer to calculate the target coordinates using a system that is independent of scanner alignment in case any deviation should occur.

Treatment planning

Preparation of a treatment plan for non-coplanar arc therapy is a complex process involving consideration of the shape of the patient's head and the relative beam orientation in three dimensions. With other stereotactic frame systems, planning data must be acquired, a treatment plan prepared and treatment administered before the stereotactic frame is removed. This places great emphasis on speed in the treatment planning process and the few commercial systems available have made use of powerful and expensive computer systems to minimize this problem. With a relocatable frame system, the necessity for speed is removed and the need for excessive computing power reduced. At St Bartholomew's Hospital software has been prepared on the computer system used for conventional treatment planning (Data General, Eclipse).

A full description of the treatment planning software is given by Thomson (1990). The beam data required for each field size consists of a set of percentage depth dose (%DD) values and a beam profile through the isocentre. As all beams are circular in cross-section, a single beam profile can be considered to be representative of radial dose fall-off in all directions perpendicular to the beam central axis. The beam profiles were recorded using film placed at 8.0 cm depth in water substitute phantom material. In planes at different distances from the source, adjustment factors are used to correct the beam profile data.

An assessment of the accuracy of the treatment planning programme is also presented by Thomson (1990). The accuracy of the calculation of the absolute values of absorbed dose at the isocentre has been verified using measurements made with an ionization chamber and dosemeter combination (0.2 cm^3 Nuclear Enterprises, 2515/3, ionization chamber and Farmer dosemeter) and thermoluminescent dosimetry (TLD) detectors (Vinten,

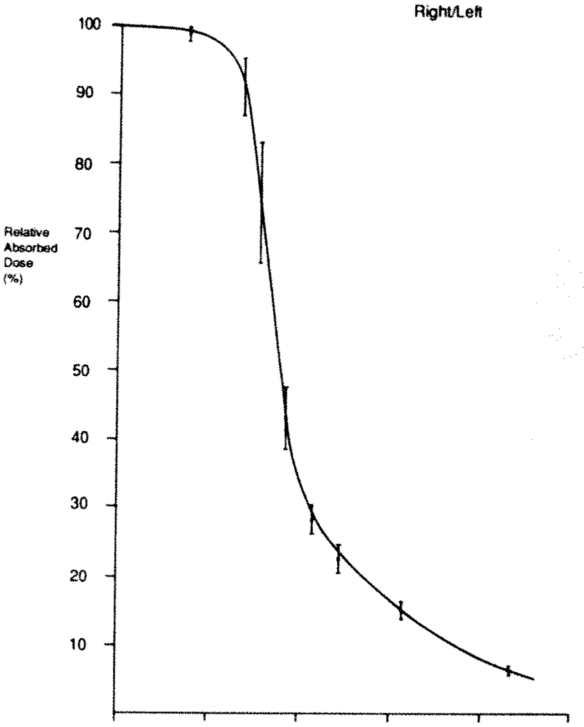

Figure 3. Comparison of calculated (solid line) and measured (points) relative absorbed dose at varying distance from the isocentre. Measured values were recorded using TLD pellets and the uncertainties indicate twice the standard deviation of the mean result at each point. Measurements were made inside a spherical, water substitute phantom irradiated with five arcs of 140° each and the 3.0 cm diameter beam.

LiF-7, 99.5%). The isocentre was placed at various positions within a 16.5 cm diameter, spherical, water substitute phantom. Under these circumstances, the calculated values were found to agree with the measured values, within the limits of uncertainty, at all measurement sites.

The calculated distribution of relative absorbed dose around the isocentre has also been verified using the TLD detectors described above. Measurements were made at various distances from the isocentre and the results are illustrated in Fig. 3. Again, there is agreement, within the limits of uncertainty, at all measurement sites.

Absorbed dose distributions are calculated in sagittal, transverse and coronal planes through the isocentre (Fig. 4). Although the treatment planning software could be modified to perform absorbed dose calculations in any plane, these three planes have, in practice, been found to be sufficient.

The stereotactic coordinates of the centre of the target

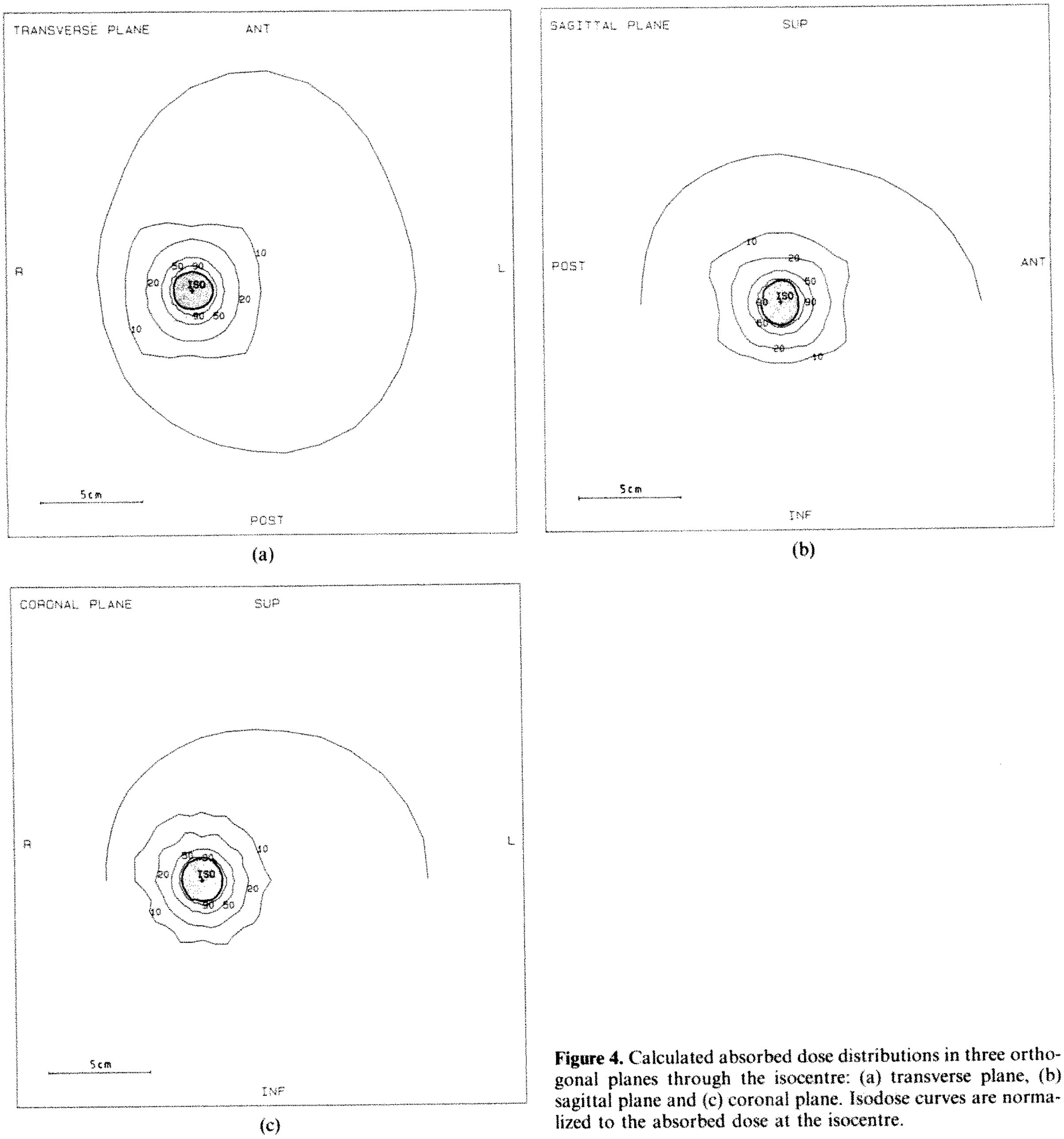

(a)

(b)

(c)

Figure 4. Calculated absorbed dose distributions in three orthogonal planes through the isocentre: (a) transverse plane, (b) sagittal plane and (c) coronal plane. Isodose curves are normalized to the absorbed dose at the isocentre.

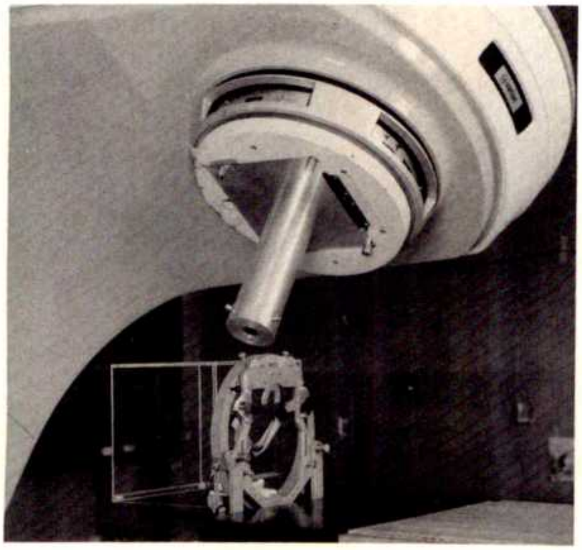

Figure 5. Illustration of the SMART treatment set-up showing the Varian Clinac 6/100 linear accelerator with external collimating applicator. The relocatable frame is fitted to the end of the treatment couch.

volume are calculated using the standard BRW calculation software. These are then marked on the Perspex box described above.

Treatment

On the day of treatment, the relocatable frame is fitted to the patient. To verify that its position is identical to that when the patient had the planning CT scan, the AP and lateral radiographs are repeated on the simulator. The films are overlaid, as described above.

Treatment takes place on a 6 MV linear accelerator. The important factors in choosing a unit on which to perform SMART have been found to be variation in its isocentre with gantry and couch rotation, and its characteristic penumbra (Thomson, 1990). The unit used is known to have an isocentric variation of less than 1 mm from the central point, in any direction, with combined couch and gantry movements. In order to reduce geometric penumbra, a cylindrical collimating applicator has been made which fits to the front face of the treatment unit (Fig. 5). This extends to a distance of 75 cm from the radiation source, leaving 25 cm between the end of the applicator and the isocentre. The length of the applicator is considered to be the maximum possible, without risking collision with the treatment couch. A trial run of each arc is made prior to treatment to ensure that there is no danger of such a collision.

Field size is determined by a series of interchangeable circular collimating inserts, 12 cm thick, machined from low melting point alloy. The inserts locate into the end of the applicator and produce beam diameters in the range 1.5 cm to 5.0 cm, in 0.5 cm steps.

The patient, in the frame, is secured to the couch of the treatment unit in the same way as on the CT and simulator couches. The Perspex box is then attached, marked with the stereotactic coordinates of the centre of the target volume. This point is then brought to the isocentre, as indicated by the alignment lasers, using linear couch movements. Once this is achieved, the Perspex box is removed and no further linear couch movements are made until the treatment is finished.

In terms of the absorbed dose distribution, the optimum treatment strategy has been assessed (Thomson, 1990) to be five arcs of 140° each with equal angular separation between arcs. During treatment, the couch is therefore rotated to five fixed positions. The prescribed couch angles, together with the gantry start and stop angles and all the machine settings necessary for treatment are pre-calculated and documented on the patient's treatment card. The order of the arcs is calculated such that couch rotation between arcs is in one direction only; this simplifies the treatment process.

The treatment usually takes approximately 20 minutes. The standard dose prescription is based on 90% of the absorbed dose at the isocentre.

Positional accuracy

The positional accuracy of the technique can be determined by considering the contributory factors. The uncertainty in target localization, using the BRW CT localization device, will depend on the slice thickness of the CT images. For 3.0 mm slice thickness, the mean uncertainty has been assessed by Saunders et al (1988) to be 1.3 mm. This figure will be less when angiographic localization is implemented. Gill (1990) has measured the mean additional uncertainty introduced by the use of the relocatable stereotactic frame as 0.3 mm ± 0.3 mm (two standard deviations of the mean) for a thalamic target. This value is independent of the use of a checking procedure such as that described. The accuracy of the alignment lasers on the treatment unit used is checked daily. The uncertainty attached to their use in positioning the target centre at the isocentre is difficult to assess but is considered to be less than 0.5 mm. The total uncertainty in isocentre position, found by summing these individual values, is therefore approximately ±2.4 mm (taking the maximum value, 0.6 mm, for the uncertainty in relocatable frame position).

Any variation in isocentre position as the couch and gantry are rotated will reduce the absorbed dose gradient at the edge of the treatment volume (Thomson, 1990). This variation cannot therefore be considered as a positional inaccuracy, as long as the stereotactic coordinates of the target centre are aligned with the mean isocentre position. The variation in the isocentre of the treatment unit used for SMART has been measured as less than 1 mm in any direction. The significance of this can be assessed by comparing the measured and calculated values of absorbed dose around the isocentre (Fig. 3). The computed values represent the ideal case, with no variation in isocentre position as couch and gantry are rotated, whereas the measured values represent the situation in practice. Figure 3, together with similar studies in other planes (Thomson, 1990), illustrates that the effect of isocentre variation on the final absorbed dose pattern cannot be detected. Measured and calculated values agree, within the limits of uncertainty at all measurement sites. In addition, at the majority of positions, measured values and their associated uncertainties lie within 1 mm of the calculated curve. This implies an uncertainty in the calculated position of corresponding isodose curves in the treatment plan of around 1 mm. The exception to this is where the absorbed dose gradients are shallow and relative absorbed dose changes more slowly with distance. Under these circumstances, the statistical variation in TLD measurements will create a greater positional uncertainty.

Conclusions

Radiosurgery has become an established method of treatment for a variety of inoperable brain lesions. The use of linear accelerator techniques should, potentially, make this treatment an option in the majority of radiotherapy centres. The dedicated systems produced commercially, however, are elaborate, costly and out of the reach of a large number of departments. The system presented in this paper requires minimal specialized equipment and few modifications to a standard linear accelerator. Using a relocatable stereotactic frame, the possibility of fractionated radiotherapy is provided and this will increase the clinical applications of the procedure. The positional accuracy of the technique has been estimated to be ±2.4 mm and this should improve once stereotactic angiography is introduced for target localization. Calculation of the absorbed dose distributions is achieved using a computer program developed on a conventional treatment planning computer and the need for excessive computing power is therefore also avoided.

In summary, a technique is described for delivery of a concentrated pattern of absorbed dose to an intracranial target. A new stereotactic device is used, enabling fractionated radiotherapy treatments. The name "radiosurgery" is no longer felt to be applicable and the alternative, "stereotactic multiple arc radiotherapy (SMART)" is suggested.

Acknowledgments

We are grateful for the assistance of Dr P. N. Plowman of the Radiotherapy Department of St Bartholomew's Hospital for his help with the clinical aspects of this work. In addition, we would like to thank Mr D. Thomas of the National Hospitals for Nervous Diseases for his advice during the development of the frame and for his subsequent interest in the treatment procedure.

We are grateful to the workshop staff of the Radiation Physics Department at St Bartholomews's Hospital for their technical assistance and to all the staff of the Radiotherapy Department for their cooperation.

We would like to thank the workshop staff at Hammersmith Hospital for their work on the prototype version of the relocatable stereotactic frame.

Much of this work was funded by the Imperial Cancer Research Fund and we are grateful to them for their continued support.

References

Backlund, E. O., 1979. Solid craniopharyngiomas treated by stereotactic radiosurgery. In *Stereotactic Cerebral Irradiation*, ed. by G. Szilka (Elsevier/North Holland Biomedical Press, Amsterdam), pp. 271–281.

Backlund, E. O., Rahn, T., Sarby, B., DeSchryver, A. & Wennerstrand, J., 1972. Closed stereotaxic hypophysectomy by means of Co-60 gamma radiation. *Acta Radiologica, Therapy, Physics, Biology, 11*, 545–555.

Backlund, E. O., Rahn, T. & Sarby, B., 1974. Treatment of pinealomas by stereotaxic radiation surgery. *Acta Radiologica, Therapy, Physics, Biology, 13*, 368–376.

Betti, O. & Derichinski, V., 1983. Irradiation stéréotaxique multifasceux. *Neurochirurgia, 29*, 295–298.

Bradshaw, J. D., 1986. The stereotactic radiosurgery unit in Sheffield. *Clinical Radiology, 37*, 277–279.

Colombo, F., Benedetti, A., Pozza, F., Aranzo, R. C., Chierego, G., Marchetti, C. & Zanardo, A., 1985. A stereotactic external irradiation by linear accelerator. *Neurosurgery, 16*, 154–160.

Fabrikant, J. I., Lyman, J. T. & Hosobuchi, Y., 1983. Stereotactic heavy-ion Bragg peak radiosurgery for intracranial vascular disorders. In *Heavy Particle Irradiation of Intracranial Lesions*, ed. by J. H. Lawrence, Lawrence Berkeley Laboratory Report No LBL-166011 (University of California, Berkeley), pp. 35, 1–42.

—— 1984. Stereotactic heavy-ion Bragg peak radiosurgery for intracranial vascular disorders: method for treatment of deep arteriovenous malformations. *British Journal of Radiology, 57*, 479–490.

Gill, S. S., 1987. United Kingdom patent application no. 8728150.

—— 1990. *A Relocatable Stereotactic Frame* (MD Thesis, University of London, in preparation).

Hartmann, G. H., Schlegal, W., Sturm, V., Kober, B., Pastyr, O. & Lorenz, W. J., 1985. Cerebral radiation surgery using moving field irradiation at a linear accelerator facility. *International Journal of Radiation Oncology, Biology, Physics, 11*, 1185–1192.

Heilbrun, M. P., Roberts, T. S., Apuzzo, M. L. J., Wells Jr, T. H. & Sabshin, J. K., 1983. Preliminary experience with the Brown–Roberts–Wells (BRW) computerized tomography stereotaxic guidance system. *Journal of Neurosurgery, 59*, 217–222.

Kjellberg, R. M., 1977. Stereotactic Bragg peak proton radiosurgery results. In *Stereotaxic Cerebral Irradiation* ed. by G. Szikla (INSERM Symposium No. 12, Amsterdam), pp. 233–240.

Kjellberg, R. M., Polletti, C. E., Robertson, G. H. & Adams, R. D., 1978. Bragg peak proton beam treatment of arteriovenous malformations of the brain. In *Neurological Surgery with Emphasis on Non-Invasive Methods of Diagnosis and Treatment*, ed. by R. Carrea and D. LeVay (Excerpta Medica, Amsterdam), pp. 184–187.

Kjellberg, R. M., Hanamura, T., Davis, K. R., Lyons, S. L. & Adams, R. D., 1983. Bragg-peak proton-beam therapy for arteriovenous malformations of the brain. *New England Journal of Medicine, 309*, 269–274.

Larson, B., Leksell, L., Rexed, B., Sourander, P., Mair, W. & Anderson, B., 1958. The high energy proton beam as a neurosurgical tool. *Nature, 182*, 1222–1223.

Lawrence, J. H., Tobias, C. A., Born, J. L., Wang, C. & Linfoot, J. A., 1962. Heavy-particle irradiation in neoplastic and neurological disease. *Journal of Neurosurgery, 19*, 717–722.

Leksell, L., 1949. A stereotactic apparatus for intracerebral surgery. *Acta Chirurgica Scandinavica, 99*, 229–233.

—— 1951. The stereotaxis method and radiosurgery of the brain. *Acta Chirurgica Scandinavica, 102*, 316–319.

—— 1968. Cerebral radiosurgery. I. Gamma thalanotomy in two cases of intractable pain. *Acta Chirurgica Scandinavica, 134*, 585–595.

—— 1971. *Stereotaxis and Radiosurgery. An Operative System* (Springfield, Charles Thomas).

LUTZ, W., WINSTON, K. R. & MALEKI, N., 1988. A system for stereotactic radiosurgery with a linear accelerator. *International Journal of Radiation Oncology, Biology, Physics, 14*, 373–381.

PODGORSAK, E., OLIVIER, A., PLA, M., LEFEBVRE, P. Y. & HAZEL, J., 1988. Dynamic stereotactic radiosurgery. *International Journal of Radiation Oncology, Biology, Physics, 14*, 115–125.

SAUNDERS, W. M., WINSTON, K. R., SIDDON, R. L., SVENSSON, G. H., KIJEWSKI, P. K., RICE, R. K., HANSEN, J. L. & BARTH, N. H., 1988. Radiosurgery for arteriovenous malformations of the brain using a standard linear accelerator: rationale and technique. *International Journal of Radiation Oncology, Biology, Physics, 15*, 441–447.

THOMSON, E. S., 1990. *Stereotactic Brain Radiotherapy* (PhD Thesis, University of London).

WALTON, L., BOMFORD, C. K. & RAMSDEN, D., 1987. The Sheffield stereotactic radiosurgery unit: physical characteristics and principles of operation. *British Journal of Radiology, 60*, 897–906.

1990, *The British Journal of Radiology*, *63*, 752–759

Chronic anaemia, hyperbaric oxygen and tumour radiosensitivity

By Mary McCormack, BSc, MSc, PhD, A. H. W. Nias, DM, FRCR, MRCPath and Eileen Smith, BSc, PhD

Richard Dimbleby Department of Cancer Research, UMDS, St Thomas' Hospital, London SE1 7EH

(*Received January 1990 and in revised form April 1990*)

Abstract. Anaemia is an important factor in the response of some human tumours to radiotherapy. The outcome is also influenced by whether the treatment is given in air or high pressure oxygen (HPO). The present study examined the relationship between anaemia and tumour response to radiation given in air or HPO in C_3H mice transplanted with a mammary adenocarcinoma using a growth delay assay to assess the radiation response. Chronic anaemia was induced by the use of a low iron diet and was characterized by a significant reduction in host haematocrit and whole blood viscosity. In addition, anaemia was associated with a right shift in the oxyhaemoglobin dissociation curve and an increase in the volume doubling time of the tumour; but there was no change in the concentration of 2,3-diphosphoglycerate in the red cells. Radiation studies with these anaemic mice demonstrated that the tumour radiosensitivity was decreased when treatment was given in air. HPO was successful in overcoming the increased radioresistance associated with anaemia. This result suggested that tumours grown in anaemic mice have a higher hypoxic fraction than those grown in control mice. Changes in host physiology with chronic anaemia may contribute to the benefit seen with HPO but such alterations *per se* may be inadequate to maintain tumour oxygenation when treatment is given in air.

It has long been recognized that the response of tumours to radiotherapy in anaemic patients is less satisfactory than in those with normal haemoglobin (Hb) levels. Thus, in a study of 895 patients with carcinoma of the cervix, Evans and Bergsjo (1965) found that for Stage II and Stage III disease there was a significantly lower survival in those patients who were anaemic at the time of treatment compared with non-anaemic patients. The authors suggested that the normal compensatory mechanism in the presence of anaemia might fail to overcome tissue hypoxia in the abnormal vascular system of tumours.

A report by Bush et al (1978) supported the thesis that hypoxia influences the local control rate with radiotherapy for patients with advanced carcinoma of the cervix. In this study of 2803 patients there was a significant difference in the local control rates, for all patients, analysed according to Hb levels. Those patients with Hb concentrations <12 g% had a poorer prognosis than those with higher Hb concentrations.

Relatively few studies have evaluated the usefulness of hyperbaric oxygen (HPO) in the treatment of anaemic cancer patients. In 1972, Dische and Hewitt reported on one patient with carcinoma of the cervix with severe anaemia (Hb 4.3 g%) who was treated by radiotherapy in HPO (six fractions in 3 weeks) without a blood transfusion, followed by a radium implant. The immediate response was satisfactory and with cessation of bleeding the Hb concentration rose to a normal value. This patient was still alive and well 16 years after treatment.

A retrospective analysis, according to Hb concentrations, of patients in the Medical Research Council (MRC) trials of HPO in the radiotherapy of carcinoma of the cervix was carried out by Dische et al (1983). All patients with Hb concentrations below 10 g% were given a blood transfusion prior to therapy and again during therapy if required. Local tumour control rates for anaemic transfused patients treated in HPO were significantly better than those for similar patients treated in air. Sealy et al (1989) report a beneficial effect when they treated patients with carcinoma of the cervix by inducing anaemia (by exchange transfusion) followed by its correction prior to therapy in HPO.

The aim of the present study was to elucidate the relationship between anaemia and tumour response to radiation, with particular regard to HPO as an adjunct to such treatment. This investigation centred on three main themes.

(i) To establish a good model of chronic anaemia in the mouse.
(ii) To examine the relationship between anaemia and tumour radiosensitivity in air and HPO.
(iii) To examine the role, if any, of physiological adaptation to anaemia on tumour radiation response.

Materials and methods

A serially transplanted C_3H mouse mammary adenocarcinoma (Nias et al, 1980) was used in SPF-derived inbred C_3H mice. Single doses of 250 kVp X rays (0.83 mm Cu half-value thickness) were delivered at 200 cGy/min to mice in the chamber used for hyperbaric oxygen studies (Tozer et al, 1984), with all but the tumour shielded by 2 mm of lead. Ketamine (45 mg/kg) and diazepam (0.5 mg per mouse) anaesthesia was used. Tumour volume was determined from three perpendicular measurements and growth expressed in terms of the mean (and standard error (SE) of the mean) time taken by a group of tumours to reach 3.5 times the treatment volume, which was approximately 200 mm^3. The exact end-point sizes of individual tumours were related to their individual treatment volumes. At least 10 animals were used for each experimental point.

Diet

A pelleted diet (Tecklad, USA) with an iron content of < 5 mg/kg was fed *ad libitum* for 9 weeks to weaned mice (approximately 21 days old) obtained from Bantin and Kingman Ltd. Mice were usually maintained on the low iron diet for 9–10 weeks prior to treatment and were subsequently fed on a normal laboratory diet. Haematocrit determinations were made at weekly intervals from tail-vein samples during the 9-week period.

Blood viscosity

The viscosity of whole blood taken from control and anaemic mice was determined by Mr Nigel Westwood (Clinical Haematology, St Thomas' Hospital) using an LS-30 Contraves Viscometer (Contraves AG, Zurich).

Oxyhaemoglobin dissociation curve

The oxyhaemoglobin (O_2-Hb) dissociation curve was determined in blood using a hem-o-scan (Aminco). The oxygen haemoglobin dissociation analyser produced an O_2-Hb equilibrium curve by exposing a heparinized blood sample to various partial pressures of oxygen (pO_2) and measuring the fraction of O_2-Hb. The pO_2 was monitored by a Clark oxygen electrode and the fraction of O_2-Hb was monitored by a dual wavelength spectrophotometer at 560 and 576 nm.

2,3-diphosphoglycerate (2,3-DPG) in blood

All reagents were obtained from Sigma Chemical Co., Procedure No. 35-UV.

Mice were bled via cardiac puncture, the blood was collected into heparinized tubes and processed according to the technique of Lenfant et al (1969).

The initial and final absorbances were read at 340 nm on a Pye-Unicam 8820 UV-VIS spectrophotometer, against water as a reference.

Calculation of packed red cell 2,3-DPG

Change in absorbance (ΔA) = initial A − final A.
Corrected ΔA = ΔA − 0.030.
Blood 2,3-DPG (μmol/ml) = corrected ΔA × 7.7.
Packed cell 2,3-DPG = blood 2,3-DPG (μmol/ml)/haematocrit (%) × 100.

Growth curves

Growth curves were constructed for mammary tumours grown in both control and anaemic mice. A single-cell suspension of 10^6 cells was injected, in a volume of 0.05 ml intradermally in the lumbar region of the dorsum of male mice after 9 weeks on the diet (when they were 12 weeks old). Control mice were injected at the same age. Mice were observed daily and measurements of tumour dimensions commenced when the tumours became palpable and were subsequently made on alternate days until the tumours reached a volume of 700–1000 mm^3.

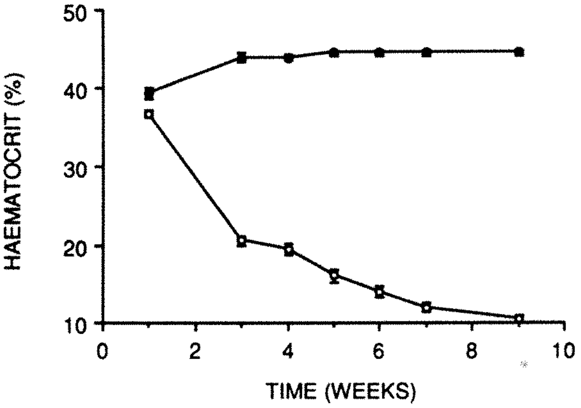

Figure 1. The relationship between haematocrit and time for mice fed a special diet (—○—) and controls (—●—). (All values are means ±1 SEM.)

A log-linear plot of tumour volume against time was constructed for tumours grown in both control and anaemic mice. The regrowth delay assay was used to assess tumour response to different treatment techniques in all experiments with the mammary tumour.

Statistical analysis of data

All data (unless otherwise stated) were subjected to statistical analysis using the Student's unpaired *t*-distribution. Probability (*p*) values greater than 0.05 were not deemed to be statistically significant. In all cases where significance was inferred, the level of significance was quoted.

Results

Haematocrit and body weight

The haematocrit (HCT) achieved in 30 mice fed on the special diet compared with those in 20 mice fed a normal laboratory diet are presented in Fig. 1. In the mice on the special diet the HCT fell to a value of 20% within the first 3 weeks and by 9 weeks the average HCT was 10%, *i.e.* 22% of the control value. The body weights of the control and anaemic mice at the end of the 9-week feeding period were 31.5 ± 0.8% and 19.8 ± 0.4%, respectively. Twenty-eight days after irradiation the HCT was still only 29.8 ± 1.2%.

Viscosity

A small study of whole blood viscosity was made in control and anaemic mice in which the mean HCT was 41.2 ± 0.5% and 12.4 ± 0.2%, respectively. At shear rates of 0.695 s^{-1} and 1.747 s^{-1}, the mean viscosity of blood from control mice was 16.5 and 4.69 mPas, whilst that from anaemic mice was 1.75 and 1.61 mPas. The difference in viscosity at both shear rates between the two groups of mice was statistically significant ($p < 0.001$). Thus the non-Newtonian behaviour of whole blood, which is particularly pronounced at low

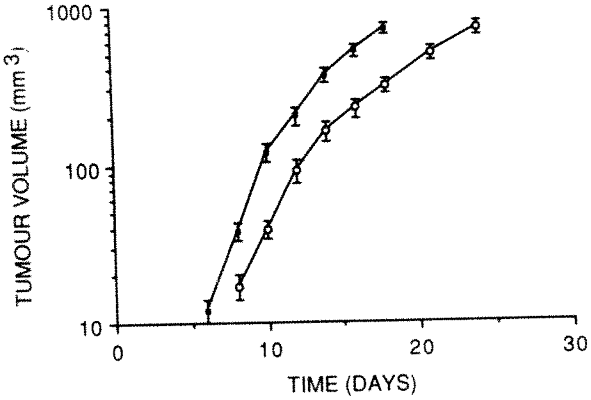

Figure 2. The relationship between tumour volume and time after tumour transplantation in control (—■—) and anaemic (—○—) mice. (All values are means ±1 SEM.)

shear rates, was not apparent in blood obtained from anaemic mice.

Oxyhaemoglobin dissociation curve

The oxyhaemoglobin (O_2-Hb) dissociation curve was shifted to the right in anaemic mice with respect to that obtained in control mice. This shift in the O_2-Hb dissociation curve was accompanied by a significant ($p<0.001$) increase in the partial pressure of oxygen at which the haemoglobin is 50% saturated (P_{50}). The P_{50} values were 43.4±1.1 and 52.3±1.0 mm Hg for control and anaemic mice, respectively.

Diphosphoglycerate in red blood cells

The packed cell 2,3-DPG concentrations in control and anaemic mice were 9.4±0.4 and 9.9±0.5 μm/ml. Thus there was no significant difference in the red cell concentrations of 2,3-DPG between the two groups. The mean HCT was 40±0.4% and 16.6±1.0% in the control and anaemic mice, respectively.

Growth of the C_3H/He mammary tumour

The growth pattern of the mammary tumour grown intradermally in control and chronically anaemic mice is illustrated in Fig. 2. Typical Gompertz curves were observed in both groups of mice, showing a decrease in growth rate as the tumour increased in size. The mean HCT at the time of tumour transplantation was 41.5±0.4% and 12.2±0.5% in the control and anaemic mice, respectively. Tumours grown in control hosts became palpable usually on Day 6 and started to reach treatment size between Days 10 and 12. However, those tumours grown in anaemic hosts generally became palpable on Day 8 and reached treatment size on about Day 14. The difference in the tumour volume doubling time between both groups of tumours appeared to increase with increasing tumour volume above 200 mm^3 (Table I). For this reason the tumour data for anaemic mice have been corrected by dividing the growth delay by a constant factor of 1.26.

Table I. Estimated volume doubling times for the mammary tumour in control and anaemic mice as determined from the growth curves (n = number of mice)

Tumour volume (mm^3)	Volume doubling time (days)		Difference
	Control (n = 20)	Anaemic (n = 23)	
100–200	2.4	3.0	0.6
200–400	2.6	3.4	0.8
300–600	3.4	4.6	1.2

This factor was derived as follows.

(i) The mean time taken for untreated tumours in anaemic animals to reach 3.5 × treatment size was 7.12 days±0.26 ($n=43$).
(ii) The mean time taken for untreated tumours grown in control hosts to reach 3.5 × treatment size was 5.65 days±0.16 ($n=36$).

The ratio of anaemic/control = 7.12/5.65 = 1.26.

Growth delay of irradiated tumours

Figure 3 shows the results of a typical experiment. With all four doses given in air, tumours in control mice responded significantly better ($p<0.05$) than those in anaemic mice. With 15 Gy and 25 Gy given in HPO both groups of tumours responded in a similar manner (*i.e.* the presence of anaemia did not adversely affect the tumour response). Furthermore, at 25 Gy there was no significant difference between the response of tumours in control mice treated in either air or HPO. However, tumours in anaemic mice that were given 25 Gy in HPO responded better ($p<0.001$) than those given the same dose in air.

Another experiment is shown in Fig. 4 where the effect of anaesthesia was also studied. At 15 Gy there was no difference in the response of tumours in anaemic and control mice when both groups were treated in

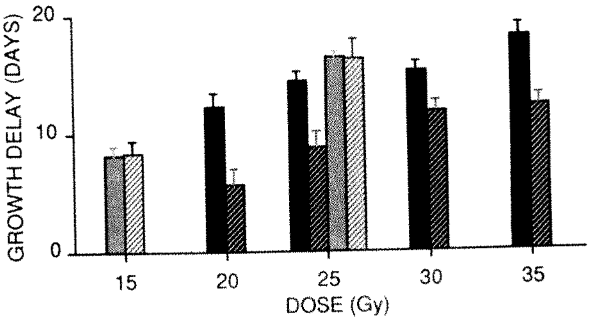

Figure 3. The relationship between growth delay and radiation dose for tumours grown in control mice treated in air (■) or HPO (▦) and anaemic mice treated in air (▨) or HPO (▧). The growth delay in the anaemic groups has been corrected by a factor of 1.26. (All values are means ±1 SEM.)

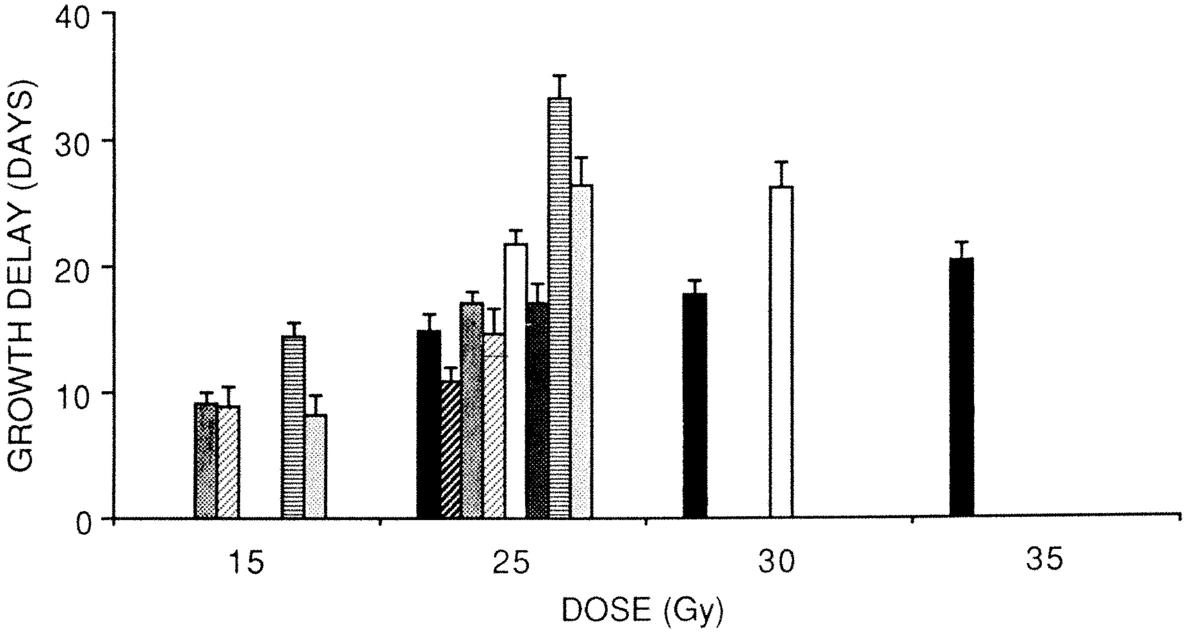

Figure 4. The relationship between growth delay and radiation dose for tumours grown in control mice treated in air with (□) and without (■) anaesthesia or treated in HPO with (▤) and without (▦) anaesthesia, and anaemic mice in air with (▩) and without (▨) anaesthesia or treated in HPO with (□) and without (□) anaesthesia. The growth delay in the anaemic groups has been corrected by a factor of 1.26. (All values are means ± 1 SEM.)

HPO (as was shown in Fig. 3). The anaesthetic did not appear to alter the response of tumours in anaemic mice treated in HPO from that observed for the non-anaesthetized group treated in HPO. However, tumours in control anaesthetized mice treated with 15 Gy in HPO responded significantly better ($p < 0.002$) than the other groups treated at the same radiation dose.

Further similarities with the data in Fig. 3 were that the radiation response of tumours in control mice treated in air at 25 Gy was significantly better ($p < 0.05$) than that in anaemic mice given the same treatment. Host anaemia had no adverse effect on the response of tumours given 25 Gy in HPO as compared with that in control mice given a similar treatment. Furthermore, tumours in anaemic mice treated in HPO responded significantly better ($p < 0.05$) than those treated in air.

Tumours in control anaesthetized mice treated with 25 Gy in air responded significantly better than those in anaemic anaesthetized mice in air ($p < 0.02$) and all other non-anaesthetized groups treated in air or HPO ($p < 0.01$). Tumours in control mice responded significantly better ($p < 0.02$) than those in anaemic mice when both groups were anaesthetized and treated in HPO at 25 Gy. The effect of anaesthesia on the radiation response of the tumour was most pronounced when the control mice were treated in HPO compared with air.

At 30 Gy the response of tumours in control mice treated in air was equivalent to that in anaemic anaesthetized mice given 25 Gy in air, and also equivalent to that in control mice given 25 Gy in HPO. Again the response of tumours in control anaesthetized mice treated in air was significantly better ($p < 0.01$) than that seen in non-anaesthetized mice given the same treatment. The growth delay for tumours in control mice treated with 35 Gy in air was equivalent to that seen in a similar group that were anaesthetized and given 25 Gy in air.

Analysis of tumour growth after a radiation dose of 25 Gy in HPO

A retrospective analysis of each individual tumour growth curve in both control and chronically anaemic mice treated with 25 Gy in HPO was carried out with four of the experiments including those shown in Figs 3 and 4. The most striking observation in each case was the tremendous variation in the response amongst the tumours in anaemic mice in comparison with that in control mice treated in exactly the same way. In anaemic mice, 25 out of 55 tumours regressed at some stage after treatment, whereas this effect was observed in only one control mouse out of 61 (Table II). The number of

Table II. The number of tumours in control and anaemic mice which regressed to a relative volume of at least 0.75 at any stage after a single dose of 25 Gy un HPO

Experiment	1	2	3	4
Control	1/19	0/13	0/15	0/14
Anaemic	9/14*	8/14*	3/12	5/15*

*Significantly different at $p < 0.05$.

tumours which regressed (to an arbitrary relative volume of 0.75) or not, in both anaemic and control mice, was subjected to a 2×2 table statistical analysis using the Fisher test.

Discussion

Models of anaemia

The models of anaemia which have been used include: phlebotomy and exchange transfusion (Hirst & Wood, 1987), the use of the haemolytic agent, phenylhydrazine hydrochloride (Photiou, 1986), bilateral kidney irradiation (Rojas et al, 1987) and tumour-induced anaemia (Hill et al, 1971).

In addition to these methods, a number of studies have been employed using dietary manipulations to produce anaemia (Choi & Simone, 1973; Webster, 1981; Ranasinghe et al, 1983; Walker et al, 1987). Since chronic blood loss with neoplasia ultimately leads to an iron-deficiency anaemia (Lynch & Jackson, 1983), the manipulation of the dietary iron content to produce anaemia was considered to be a relevant model and worthy of investigation.

Chronic anaemia

For our pilot studies we used a low iron diet from Special Diet Services (SDS) but this was very disappointing. Following a period of 9 weeks on this diet the haematocrit was reduced by only 8%. Furthermore, there was a lot of inter-animal variation in the haematocrit levels. In the study by Walker et al (1986) using this diet they noted a considerable variation in the degree of anaemia from experiment to experiment. In fact, in some of their experiments the host haematocrit after 9 weeks on the diet was only very slightly below normal.

For our present studies we utilized a very low iron diet (< 5 mg/kg iron) imported from the United States. This diet successfully reduced the haematocrit to approximately 25% of control within 9 weeks resulting in a severe anaemia (Fig. 1). Post-weaning C_3H/He mice only within the weight range 9–11 g were fed on the low iron diet. This strict control on the age and weight of mice at the start of the 9-week feeding period was necessary, since it had been observed that mice outside of this weight range either died (if under 9 g) or failed to become sufficiently anaemic (if over 12 g) within this time period. Anaemic mice were lethargic and weighed much less than age-matched controls although they appeared to eat normally. This finding was in agreement with that reported by Ranasinghe et al (1983) who fed a similar diet to Syrian hamsters. This failure to gain weight has been attributed to an iron deficiency-induced anorexia (Canale & Lanzkowsky, 1970).

The anaemia produced in this study resulted in a significant fall in whole blood viscosity such that the non-Newtonian behaviour of whole blood was totally lost. This finding is in agreement with Walker et al (1987) who also observed a similar change in blood viscosity with chronic iron deficiency anaemia. A study by Photiou (1986) demonstrated a positive correlation between haematocrit and blood viscosity. The consequences of a reduction in whole blood viscosity at low shear rates are probably most pronounced in the post-capillary vessels, since these vessels exhibit the largest cross-sectional area and therefore the lowest mean flow velocity in the whole circulation. Thus a reduction in blood viscosity in these vessels may lead to an increase in blood flow (Messmer, 1975).

There was a significant right shift in the oxyhaemoglobin dissociation curve in anaemic mice (*i.e.* significant increase in P_{50}). This means that a higher proportion of oxygen will be released from haemoglobin for a given partial pressure of oxygen. An increase in the P_{50} is usually attributable to a decrease in pH and/or an increase in the concentration of 2,3-DPG in the blood. In addition, an increase in the concentration of CO_2 or an increase in temperature can also shift the curve to the right (Lenfant et al, 1969; McConn, 1975). However, in this study there was no significant change in the concentration of 2,3-DPG in anaemic mice when compared with controls. Walker et al (1987) also reported that the concentration of 2,3-DPG remained unchanged with chronic anaemia. Thus in these studies the increase in P_{50} does not appear to be mediated through changes in the concentration of 2,3-DPG. Therefore, in view of the findings in the present study it is questionable whether one can predict changes in the P_{50} on the basis of the concentration of 2,3-DPG in the blood in this mouse model.

Effect of anaemia on tumour growth

When the mammary tumour was implanted intradermally in both control and anaemic mice typical Gompertz-like curves were observed. This relationship was also found for the mammary tumour grown subcutaneously (Tozer, 1982). There was a small but reproducible increase in the observed tumour volume doubling time in the anaemic mice (Fig. 2). There was a difference in the "latency" period (*i.e.* time to palpability) between the two groups. However, it was not possible to determine whether the growth curves would converge if they were extrapolated backwards into the sub-macroscopic phase of growth. Hence it cannot be said whether the difference in time to palpability results from a difference in latent period or a difference in growth rates. There was a noticeable difference in the apparent tumour volume doubling time between the two groups as shown in Table I. This finding is not in agreement with those of Rojas et al (1987) or Walker et al (1987). In these studies there was no reported change in tumour growth rate with anaemia. However, a study by Hann et al (1988) reported a decrease in the growth rate of a colonic adenocarcinoma, a hepatoma and a mammary adenocarcinoma implanted in iron deficient mice of the BALB/c, C3H/He and DBA/2 strains, respectively. The time of initial tumour appearance was similar in all groups of mice. It is possible that the observed change in growth rate in the present study is tumour specific since there was no difference in the growth rate of the KHT tumour implanted in anaemic mice when compared with that in control mice (data not shown).

In most radiobiological studies the experimental conditions *per se* do not affect tumour growth and so conventional calculations of growth delay are used. In the present study, however, it was decided that the corrected version of the data permitted a more meaningful comparison of the growth delay in different groups, where the volume doubling time of the untreated tumours in the anaemic and control groups was not the same.

Effect of radiation

The growth delay in the anaemic groups was corrected by a factor of 1.26 and the findings (Figs 3 and 4 and Table II) can be summarized as follows.

(i) Tumours grown in anaemic mice were significantly less radiosensitive than those grown in control mice when irradiated in air.
(ii) Treatment of tumours grown in anaemic mice in HPO resulted in a significant increase in tumour radiosensitivity compared with similar tumours (in anaemic mice) treated in air.
(iii) Tumours grown in anaemic mice showed significantly more regression than tumours grown in control mice, when treated in HPO.

All the radiation doses were below the "hypoxic breakpoint" for this tumour, which was found to be at approximately 50 Gy by Abdelaal and Nias (1979).

There have been relatively few experimental studies on the influence of chronic anaemia on tumour radiation response. One such study by Rojas et al (1987), using bilateral kidney irradiation to produce anaemia, demonstrated that CA NT tumours grown in anaemic mice were more radiosensitive than those in control mice when treatment was given in air. Data from Walker et al (1987) showed that RIF-1 tumours (grown intradermally) in anaemic mice (with iron deficiency anaemia) were more radiosensitive in both air and HPO than those grown in control mice. Our data do not confirm the findings in either of those papers.

Rojas et al (1987) explained their findings in terms of the following physiological adaptations in anaemic mice.

(i) Reduction in cord diameter due to a reduced oxygen diffusion distance.
(ii) An increase in the concentration of 2,3-DPG and hence an increase in P_{50}.
(iii) A fall in blood viscosity.

If indeed all of the above changes did occur, then one might expect that tumours in anaemic mice would be at least as radiosensitive as those in control mice when treated in air. However, Walker et al (1987) reported that there was no change in the concentration of 2,3-DPG in anaemic mice compared with control mice. They did find, however, that the blood viscosity was greatly reduced with anaemia. Thus it might be anticipated that such a reduction in blood viscosity would lead to an increase in cardiac output and ultimately an increase in tumour blood flow.

In the present study there was a significant reduction in blood viscosity with anaemia. Also the oxyhaemoglobin dissociation curve was shifted to the right with a concomitant increase in P_{50}. Thus, although host adaptation to anaemia had occurred, this did not result in an improved tumour response to radiation given in air. These anomalies pose the question whether host adaptation had any effect on the radiation response of the mammary tumours when treatment was given in air.

It is possible, however, in situations where the anaemia is less severe (*i.e.* where the haematocrit is reduced by 50% or less as opposed to the 65–75% reduction in the present study) that host adaptation via a decrease in blood viscosity, and/or an increase in P_{50} and nutritive blood flow, could compensate for the decrease in the oxygen-carrying capacity of the blood and thereby sensitize the tumour to radiation. Other experimental findings also suggest that the increase in nutritional flow is sufficient to compensate for the reduction in oxygen content only during limited haemodilution. Below haematocrits of 25% the oxygen consumption and muscle performance were progressively restricted (Messmer, 1975). The improvement in the radiation response of the mammary tumour in anaemic mice when treatment was given in HPO could be attributed to an increase in the concentration of dissolved oxygen in the blood. This, together with a fall in blood viscosity, may increase the oxygen availability at the tumour level due to oxygen transport advantages.

The anaesthetic agent hypnomidate was used in one experiment to assess the effect, if any, of physical restraint on the radiation response of the mammary tumour (Fig. 4). Anaesthesia significantly improved the response of tumours in both anaemic and control mice in air and HPO compared with that observed in the absence of anaesthesia. In the absence of anaesthesia the HPO/anaemic and HPO/control groups responded equally well, whilst with anaesthesia the HPO/control group responded better than the HPO/anaemic group. Tozer et al (1984) had shown that anaesthesia enhanced the radiosensitizing effect of HPO on such mammary tumours in control mice treated with single doses of radiation.

It was concluded that the results obtained with the anaesthetic were due to the physiological effects of this agent rather than the lack of restraint in these groups. The precise mechanism of the "anaesthetic effect" remains unknown. However, Nias and Perry (1989) have shown that, in non-anaemic mice, the duration of anaesthesia prior to treatment in either air or HPO will determine whether the agent protects or sensitizes the tumours to radiation.

A retrospective analysis revealed differences in the post-irradiation growth pattern of tumours in anaemic mice treated with 25 Gy in HPO compared with that in control mice treated in a similar manner. The observation of post-treatment regression in the anaemic group

(Table II) may simply reflect an increase in the rate of clearance of dead cells. Alternatively, it may reflect an increase in tumour cell kill with a compensatory increase in the growth rate of the surviving cells. This may explain the similar growth delay observed in both the anaemic and control tumours treated with 25 Gy in HPO without anaesthesia.

The data presented here support the clinical evidence that anaemic patients with cervical cancer, who were not given blood transfusions before treatment, had a higher rate of local recurrence and poorer 5-year survival rates after radiotherapy than those patients who were not anaemic at the time of treatment (Evans & Bergsjo, 1965; Bush et al, 1978). However, there is only one reported case of an anaemic patient treated in HPO without a blood transfusion (Dische & Hewitt, 1972). This patient responded very well despite a pre-treatment haemoglobin level of 4.3 g%. The present study lends support to the thesis that in the absence of a blood transfusion, treatment in HPO is at least marginally better than a similar treatment given in air.

Clearly, the positive effect of HPO was only sufficient to overcome the negative effect of anaemia. There was an analogous finding with the clinical trial of metronidazole in patients with carcinoma of the cervix (Revesz & Balmukhanov, 1987). Local control in anaemic patients was only increased by the drug to the same level as achieved by radiotherapy alone in non-anaemic patients.

In the retrospective analysis of the MRC trial of HPO in the treatment of carcinoma of the cervix, it was noted that at Glasgow the moderately anaemic patients (Hb 10–12 g%), who were not given a blood transfusion, responded significantly worse than non-anaemic patients when treated in air but equally well when treated in HPO (Dische et al, 1983). The present data support this finding, although the haemoglobin levels in the present study were much lower (approximately 4 g%) than those in the clinical trial.

Acknowledgments

The authors are grateful to Mr Phillip Perry for scientific assistance, Drs David Hirst, Oliver Scott and Peter Twentyman for helpful discussion and Mrs Valerie Nunn for typing this manuscript.

This study was supported by an endowment from the Richard Dimbleby Cancer Fund.

References

Abdelaal, A. S. & Nias, A. H. W., 1979. Regression, recurrence and cure in an irradiated mouse tumour. *Journal of the Royal Society of Medicine, 72*, 100–105.

Bush, R. S., Jenkin, D. T., Allt, W. E. C., Beale, F. A., Bean, H., Dembo, A. J. & Pringle, J. F., 1978. Definitive evidence for hypoxic cells influencing cure in cancer therapy. *International Journal of Radiation Oncology, Biology, Physics, 12*, 2047–2050.

Canale, V. & Lanzkowsky, P., 1970. Cellular growth in specific nutritional deficiency states in rats. I. Iron deficiency anaemia in post-weaning period. *British Journal of Haematology, 19*, 579–585.

Choi, S. I. & Simone, J. V., 1973. Platelet production in experimental iron deficiency anaemia. *Blood, 42*, 219–227.

Dische, S. & Hewitt, H. B., 1972. Carcinoma of cervix with severe anaemia. Treatment by radiotherapy without blood transfusion using hyperbaric oxygen. *British Journal of Radiology, 45*, 848–850.

Dische, S., Anderson, P. J., Sealy, R. & Watson, E. R., 1983. Carcinoma of the cervix: anaemia, radiotherapy and hyperbaric oxygen. *British Journal of Radiology, 45*, 848–850.

Evans, J. C. & Bergsjo, P., 1965. The influence of anaemia on the results of radiotherapy in carcinoma of the cervix. *Radiology, 84*, 709–717.

Hann, H.-W. L., Stahlhut, M. W. & Blumberg, B. S., 1988. Iron nutrition and tumour growth: decreased tumour growth in iron deficient mice. *Cancer Research, 48*, 4168–4170.

Hill, R. P., Bush, R. S. & Yeung, P., 1971. The effect of anaemia on the fraction of hypoxic cells in an experimental tumour. *British Journal of Radiology, 44*, 299–304.

Hirst, D. G. & Wood, P. J., 1987. The adaptive response of mouse tumours to anaemia and retransfusion. *International Journal of Radiation Biology, 51*, 597–609.

Lenfant, C., Torrance, J. D. & Finch, C. A., 1969. The regulation of haemoglobin affinity for oxygen in man. *Transcriptions of the Association of American Physicians, 82*, 121–128.

Lynch, E. C. & Jackson, D., 1983. Anaemia and malignancies. *Heart & Lung (Grand Rounds in Critical Care), 12*, 447–453.

McConn, R., 1975. The oxyhaemoglobin dissociation curve in acute disease. Symposium on physiologic approach to critical care. *Surgical Clinics of North America, 55*, 627–658.

Messmer, K., 1975. Haemodilution. *Surgical Clinics of North America, 55*, 659–675.

Nias, A. H. W., Chamberlain, S. M. & Abdelaal, A. S., 1980. The serially transplanted C_3H mouse mammary tumour as a clinically relevant model system. *British Journal of Cancer, 41, Suppl. IV*, 157.

Nias, A. H. W. & Perry, P. M., 1989. Variation of tumour radiosensitivity with time after anaesthetic. *British Journal of Radiology, 62*, 932–935.

Photiou, A., 1986. *Physiological Manipulation of Tumour Oxygen Environment and Radiation Response* (PhD Thesis, University of London).

Revesz, L. & Balmukhanov, S. V., 1987. Anaemia as a prognostic factor for the therapeutic effect of radiosensitizers. *International Journal of Radiation Biology, 51*, 591–595.

Ranasinghe, A. W., Johnson, N. W. & Rowntree, R., 1983. Experimental iron deficiency in Syrian hamsters. *Laboratory Animals, 17*, 210–212.

Rojas, A., Stewart, F. A., Smith, K. A., Soranson, J. A., Randhawa, V. S., Stratford, M. R. L. & Denekamp, J., 1987. Effect of anaemia on tumour radiosensitivity under normo and hyperbaric conditions. *International Journal of Radiation Oncology, Biology, Physics, 13*, 1681–1689.

Sealy, R., Jacobs, P., Wood, L., Levin, W., Barry, L., Boniaszczuk, J. & Blekkenhorst, G., 1989. The treatment of tumors by the induction of anaemia and irradiation in hyperbaric oxygen. *Cancer, 64*, 646–652.

Tozer, G. M., 1982. *Hyperbaric Oxygen and Tumour Response to Radiation in the C_3H Mouse* (PhD Thesis, University of London).

Tozer, G. M., Penhaligon, M. & Nias, A. H. W., 1984. The use of ketamine plus diazepam anaesthesia to increase the radiosensitivity of a C_3H mouse mammary adenocarcinoma in hyperbaric oxygen. *British Journal of Radiology, 57*, 75–80.

WALKER, H. C., MYERS, R. & HORNSEY, S., 1987. Site differences in the radiation response of RIF tumours in anaemic mice. *British Journal of Radiology, 60*, 103.

WALKER, H. C. et al, 1986. *Personal communication.*

WEBSTER, D. J. T., 1981. Tumour induction by carcinogens in iron deficient rats. *Anticancer Research, 1*, 293–294.

P25855

1990, *The British Journal of Radiology*, 63, 760–770

The relative biological effectiveness of fractionated doses of fast neutrons (42 $\text{MeV}_{d\rightarrow Be}$) for normal tissues in the pig

II. Late effects on cutaneous and subcutaneous tissues

By J. W. Hopewell, PhD, *D. W. H. Barnes, MD, M. E. C. Robbins, PhD, *M. Corp,
*J. M. Sansom, C. M. A. Young, DPhil and G. Wiernik, MD

CRC Normal Tissue Radiobiology Research Group, Research Institute (University of Oxford), Churchill Hospital, Oxford OX3 7LJ and *MRC Radiobiology Unit, Chilton, Didcot, Oxfordshire OX11 0RD

(Received February 1990 and in revised form May 1990)

Abstract. The late effects of irradiation with single and fractionated doses of X rays (250 kV) and fast neutrons (42 $\text{MeV}_{d\rightarrow Be}$), on the cutaneous and subcutaneous tissues of the pig, have been evaluated from measurements of changes in relative field length. These were determined at intervals of 26–104 weeks after irradiation. For fractionated irradiation with X rays the average fractions exponent, N, obtained from a log–log plot of iso-effect dose (ED_{50}) against fraction number was 0.41. This was independent of the period of assessment, with no significant indication of a time factor. However, the exponent N did vary with the level of effect and was in the range 0.33–0.51. It was greatest for a $\geqslant 10\%$ reduction in relative field length. Assuming the validity of the linear quadratic model of cell survival, the α/β ratio was 1.95 Gy. However, this model fitted the data less well for the least severe levels of damage, and for these the α/β ratios were not significantly different from zero. Irradiation with fast neutrons showed a small effect of fractionation for doses given in $\geqslant 6$ fractions compared with a single dose. There was no significant increase in iso-effect dose when the dose was given in 30 fractions compared with 6 fractions. The relative biological effectiveness for late cutaneous and subcutaneous damage for the energy of fast neutrons used did not vary with the period of assessment, *i.e.* 26–52 weeks compared with 65–104 weeks, and was not significantly different from that previously obtained for ischaemic dermal necrosis, seen after higher doses, at 12–20 weeks after irradiation.

In fast neutron therapy the possible increased risk of late morbidity in normal tissues is still considered to be one of its major limitations (*e.g.* Ornitz et al, 1980; Duncan et al, 1986). Some of the earlier reports of increased late tissue damage may be explained by the difficulties encountered in obtaining an adequate dose distribution in large treatment volumes (Pointon et al, 1985; Duncan et al, 1986). This was because the first generation of clinically used neutron beams, produced by 16 $\text{MeV}_{d\rightarrow Be}$ or D-T generators, were significantly inferior to megavoltage photon beams currently used (Geraci, 1981). However, this may not be the only explanation since, even with neutron beams from higher energy cyclotrons, late radiation morbidity can still be a problem (Hussey et al, 1974; Maor et al, 1981; Cohen et al, 1981, 1989) although the incidence of such late effects may be less. This has been suggested by the results of an initial retrospective comparison, in the United States, of patients treated with either low or high energy cyclotron-produced neutrons (Griffin, personal communication).

This paper is the second report of a series of studies in which the relative biological effectiveness (RBE) of fractionated doses of fast neutrons have been determined for the normal tissues of the pig. These investigations were carried out using the Variable Energy Cyclotron (VEC) at the Atomic Energy Research Establishment (AERE), Harwell. This produces fast neutrons (42 $\text{MeV}_{d\rightarrow Be}$) with an average energy similar to that of the new hospital-based high energy cyclotron (62 $\text{MeV}_{p\rightarrow Be}$) at the Clatterbridge Hospital, Merseyside, UK (Bonnett et al, 1988). Information is now provided on late radiation damage to cutaneous and subcutaneous tissue for follow-up periods up to 2 years after irradiation. This will be complemented by data for late effects in the lung (Rezvani et al, 1990a), kidney and rectum. Damage to the cutaneous and subcutaneous tissue has been assessed by measuring relative changes in skin field length. This end-point has been used previously to determine late skin changes following fractionated irradiation between 5 and 12 months after X rays (Hopewell et al, 1979) or ^{60}Co γrays (Withers et al, 1978a) and, in a very limited study, the RBE for fast neutrons produced by 50 $\text{MeV}_{d\rightarrow Be}$ (Withers et al, 1978b). The results relating to X rays have now been extended to cover the period up to 2 years after irradiation and have been compared with those for fast neutron irradiation. The skin fields evaluated in the present study had previously been used to examine the initial changes in the epidermis (6 weeks) and in the dermis at 12–20 weeks (Hopewell et al, 1988).

Materials and methods

Female pigs of the Large White strain were used in these investigations. The animals were approximately 12 weeks of age (20–25 kg) when they were brought into the animal house, 2 weeks prior to any experimental procedures being carried out. Details of the method for marking out the skin fields on the flank and the irradiation protocol have been described previously (Hopewell et al, 1988). The skin sites, which have now been assessed for late effects on cutaneous and subcutaneous tissues, were first used to evaluate the initial epithelial and intermediate dermal responses of the skin in the first 20 weeks after irradiation. Late changes were assessed at regular intervals from 26–104 weeks after irradiation.

Briefly, prior to irradiation 16 × 4 cm fields were marked out on the left and right flank of each pig, by tattooing with India ink. In the case of pigs irradiated with 250 kV X rays (half value layer 1.4 mm Cu; focus–skin distance 50 cm; dose rate 69 cGy/min), 2–4 fields, separated by 4 cm, were exposed on the left flank. Fields in the corresponding position on the right flank acted as "unirradiated" controls since the $<8\%$ exit doses, even after the highest doses used, have not been shown to produce any later radiation-induced changes in the skin. For irradiations with fast neutrons ($42\ \mathrm{MeV}_{d \rightarrow Be}$; target–skin distance 150 cm; dose rate 54 cGy/min), only two fields were marked out on the left flank of each pig. These fields were separated from each other by 12 cm. Only a single control field was used, positioned between the irradiated fields on the opposite flank. The exit dose in this instance was $\sim 30\%$ of the applied dose and could not be ignored. Full skin build-up of 10 mm of tissue equivalent material was used for the fast neutron irradiation studies. In addition, in order to protect against the effects of stray radiation, mainly in the form of low energy protons, the adjacent skin field was always shielded by 4 mm of lead while the other was being irradiated.

Irradiation with X rays was with either a single dose or fractionated doses given as 6 or 14 fractions in 18 days and 6, 14 or 30 fractions over 39 days. Fast neutrons were also given as a single dose or as 6 or 12 fractions over 18 days and 6, 12 or 30 fractions over 39 days.

At periods of 26, 39, 52, 65, 78, 91 and 104 weeks after irradiation, the degree of late radiation-induced damage to the cutaneous and subcutaneous tissues was assessed by measuring the length of the long axis of each of the irradiated skin fields and comparing this with the length of a matching field on the opposite flank of the same pig. For each field, measurements were taken of the length of the field edges and that of the central axis and the mean of these measurements was calculated. After X irradiation, the comparison was always with the matching site on the opposite flank. However, after fast neutron irradiation only, a single "control" site was used per pig and hence a differential allowance had to be made for small differences in the growth patterns of the fields on the various sites on the flank. Rostrally positioned fields were $\sim 10\%$ longer than the central site, 26–104 weeks after the initial tattooing procedure. No correction was needed for the caudally positioned field.

The ratio of the lengths of the irradiated to the control sites was referred to as the "relative field length". Measurements carried out between 26 and 52 weeks after irradiation were averaged, as described previously (Hopewell et al, 1979), as were the data for the period 65–104 weeks after treatment. In addition to examining the dose-related changes in the "mean relative field length" at 26–52 weeks and 65–104 weeks after irradiation, the measurements taken over these two time periods were also converted into quantal data. At each dose level, for each fractionation schedule of X rays or fast neutrons, the proportion of skin fields showing a relative field length of <0.9, <0.875, <0.85 or <0.825 was assessed. Using these data the doses associated with a 50% incidence ($ED_{50} \pm SE$) of these four increasing levels of effect were determined by probit analysis. This provided a more objective method by which to compare different fractionated irradiation schedules.

Results

The dose-related changes in the relative length of skin fields at 26–52 weeks after irradiation with single and fractionated doses of fast neutrons are shown in Fig. 1. For the purposes of this evaluation the results for irradiation over 18 and 39 days, given either in 6 or 12 fractions, have been combined since there was no evidence of a singificant effect related to treatment time. The fitting of response curves to such data is somewhat subjective but general patterns of change do emerge. There was apparently an initial shoulder region to the dose–effect curves corresponding to a "mean reduction in relative field length" of $\sim 8\%$. In this respect, the curves are similar to those previously reported for X rays (Hopewell et al, 1979). Then, after exceeding a threshold dose, the degree of reduction in relative field length increases rapidly with increasing radiation dose.

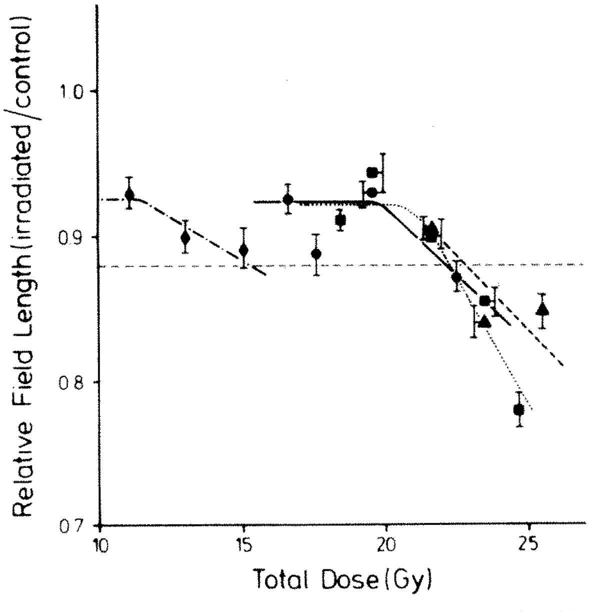

Figure 1. Dose-related changes in relative field length for skin fields on the pig irradiated with both single and fractionated doses of fast neutrons ($42\ \mathrm{MeV}_{d \rightarrow Be}$). (Single dose ◆ ·—·— ◆, 6 fractions ●——●, 12 fractions ■ ····· ■ and 30 fractions ▲ — — — ▲; error bars indicate ±SE.)

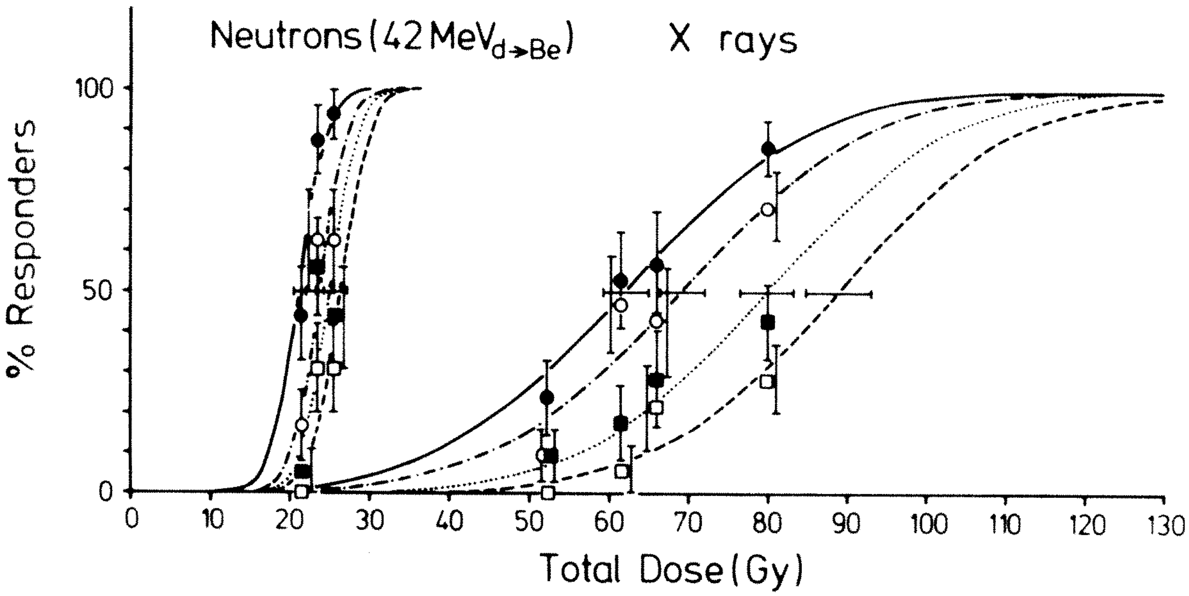

Figure 2. Dose-related changes in the proportion of skin fields showing four incremental degrees of reduction in relative field length after irradiation given as 30 fractions in 39 days of either fast neutrons (42 MeV$_{d \rightarrow Be}$) or X rays (250 kV). The selected level of changes in relative field length were <0.9 (●), <0.875 (○), <0.85 (■) or <0.825 (□). (Error bars indicate ±SE.)

A significant shift in this component of the curve can be seen when single doses of fast neutrons are compared with fractionated doses. For a relative field length of 0.88 (*i.e.* a reduction in relative field length of 12%) this represented a change in total iso-effect dose from ~15 Gy to 22–23 Gy. There was no evidence for a significant effect of fractionation between 6 and 30 fractions of fast neutrons. When compared with similar data for X rays (Hopewell et al, 1979), this would suggest a change in RBE from ~1.35 to ~3.4 for X-ray doses/fraction of 21 Gy and 2.6 Gy, respectively.

Measurements of relative field length, averaged over the period 65–104 weeks after irradiation, produced similarly shaped dose–effect curves. However, the initial plateau region was lower, representing a mean reduction in relative field length of ~10%. Thus a comparison with earlier data (26–52 weeks), at a level of damage represented by a 12% reduction in relative field length, was not possible. Comparisons based on more severe levels of effect were not evaluated because of the subjective aspect of fitting the dose–effect curves by eye.

In an attempt to overcome this problem, the results from the X-ray and fast neutron studies were re-analysed by assessing, for each of the two time periods (26–52 weeks and 65–104 weeks), the dose-related incidence of fields exceeding four specified levels of effect, namely <0.9, <0.875, <0.85 and <0.825 relative field length. Examples of this type of dose–effect curve are illustrated in Fig. 2. These specific curves were based on the results of irradiation with X rays and fast neutrons given as 30 fractions/39 days. For each data set, parallel dose–effect curves were fitted; for the majority of data sets there was good statistical evidence to support the use of such parallel dose–effect curves. The ED$_{50}$ values (±SE) for the selected levels of effect were calculated for both the initial (26–52 weeks) and the later (65–104 weeks) follow-up time periods and these are listed in Tables I and II. For X rays there was a marked increase in the ED$_{50}$ with increasing fraction number, irrespective of the irradiation treatment time (18 or 39 days) or the assessment period. However, as illustrated by the results for the period 26–52 weeks after irradiation (Figs 3 and 4) the slope of the log–log plot of the ED$_{50}$, iso-effect dose, against fraction number depended on the selected threshold level of effect, the slope decreasing with increasing level of effect. The results of these analyses, which exclude the single dose findings, are given in Table III. The ED$_{50}$ values for 12 fractions/39 days and 12 fractions/18 days of X rays were estimated from these iso-effect plots, as illustrated in Figs 3 and 4.

In contrast to X rays, irradiation with fast neutrons showed no marked effect of dose fractionation, apart from the significant increase in the ED$_{50}$ iso-effect dose, between a single dose and 6 fractions (Figs 3 and 4).

Examination of the ED$_{50}$ values for irradiation with X rays, given as 6 or 14 fractions, provided some evidence for the presence of a time factor for this measurement of late radiation-induced damage to the cutaneous and subcutaneous tissues. In general, the ED$_{50}$ values for irradiation given over 39 days were lower than those for treatment given over 18 days, as illustrated in Fig. 5. However, of the 16 intercomparisons that can be made, only in four was there a significant negative time factor ($p < 0.05$). When the means of these ED$_{50}$ values for the four levels of damage were compared, no significant differences were found.

Table I. Iso-effect doses (Gy) and RBE values for late changes in relative length of skin fields in the pig 26–52 weeks after X-ray and fast neutron (42 MeV$_{d\rightarrow Be}$) irradiation

Fractionation (fractions/days)	Relative field length	ED$_{50}$ (±SE) X rays	ED$_{50}$ (±SE) Neutrons	RBE (±SE)
Single dose	<0.9	21.2 ±0.65	13.43±0.85	1.58±0.11
	<0.875	21.93±0.69	17.07±1.78	1.28±0.14
	<0.85	23.22±0.8	18.58±2.32	1.25±0.16
	<0.825	23.38±0.82	—	<1.25
6/18	<0.9	32.47±2.39	19.3 ±0.73	1.68±0.14
	<0.875	37.56±2.23	21.56±0.76	1.74±0.12
	<0.85	50.43±2.56	24.24±1.19	2.08±0.15
	<0.825	55.91±2.99	23.51±1.16	2.38±0.17
12/18	<0.9	48.5 ±2.54*	21.46±0.38	2.26±0.12
	<0.875	53.0 ±2.28	23.0 ±0.43	2.3 ±0.11
	<0.85	58.5 ±2.2	23.93±0.52	2.45±0.11
	<0.825	62.5 ±2.42	25.16±0.7	2.48±0.12
14/18	<0.9	53.48±1.59	—	—
	<0.875	57.47±1.5	—	—
	<0.85	60.24±1.25	—	—
	<0.825	64.1 ±1.51	—	—
6/39	<0.9	22.27±4.73	21.27±1.45	1.05±0.23
	<0.875	31.55±3.88	25.66±2.71	1.23±0.2
	<0.85	40.68±3.56	29.03±3.92	1.40±0.23
	<0.825	48.98±3.81	34.43±6.05	1.42±0.27
12/39	<0.9	36.0 ±6.57*	20.53±0.52	1.75±0.32
	<0.875	43.0 ±5.44	22.23±0.7	1.93±0.25
	<0.85	55.5 ±5.13	23.61±0.9	2.35±0.23
	<0.825	63.0 ±5.51	22.84±0.58	2.76±0.25
14/39	<0.9	41.15±5.55	—	—
	<0.875	45.45±6.02	—	—
	<0.85	59.88±6.01	—	—
	<0.825	66.23±6.11	—	—
30/39	<0.9	62.14±2.8	21.14±0.7	2.94±0.16
	<0.875	69.15±2.78	23.79±0.57	2.91±0.14
	<0.85	79.93±3.31	24.88±0.62	3.21±0.16
	<0.825	88.87±4.17	26.36±0.79	3.37±0.19

*ED$_{50}$ values (±SE) estimated by extrapolation from log–log iso-effect curves, as illustrated in Figs 3 and 4.

However, the mean values for irradiation in 39 days were still consistently lower than those for 18 days (Fig. 5).

In the absence of any clearly defined time factor, the data for irradiation given in 18 and 39 days have been combined in a further evaluation of the effects of dose fractionation with X rays and fast neutrons. For these combined data, there was a high linear correlation ($r>0.88$), on a log–log plot, between fraction number and the ED$_{50}$ iso-effect dose when the single dose results were excluded. Although the slope of the lines still varied with the level of effect, and was greatest for a relative field length of <0.9 (Table IV), the differences were not significant ($p \gg 0.05$). The average slope of these iso-effect lines was 0.41, irrespective of the period of assessment. The combined data still showed no evidence for a significant fractionation effect between 6 and 30 fractions of fast neutrons.

In an alternative analysis, the reciprocals of the ED$_{50}$ values were plotted as a function of the X-ray or fast neutron dose/fraction. For X rays given in 6–30 fractions, there was not always a strong correlation between these two parameters (Fig. 6). This would account for the large uncertainty associated with the α/β ratios estimated from these plots (Table V). The α/β ratios after X irradiation were not significantly different from zero for relative field lengths of <0.9 and <0.875. The average α/β ratio of ~ 1.95 Gy did not vary significantly with the period of assessment.

Larger α/β ratios were obtained for cutaneous and subcutaneous tissues after fast neutron irradiation (Table V). These were also, to some extent, dependent on the level of damage but were independent of the period of assessment. The overall average α/β ratio for fast neutrons was 30.62 ± 3.5 Gy.

The variations in the RBE for cutaneous and subcuta-

Table II. Iso-effect doses (Gy) and RBE values for late changes in relative length of skin fields in the pig 65–104 weeks after X-ray and fast neutron (42 $\mathrm{MeV}_{d\rightarrow Be}$) irradiation

Fractionation (fraction/days)	Relative field length	ED_{50} (±SE) X rays	ED_{50} (±SE) Neutrons	RBE (±SE)
Single dose	<0.9	17.06±1.75	11.05±1.02	1.54±0.21
	<0.875	19.63±1.5	14.85±0.96	1.32±0.13
	<0.85	24.68±2.35	16.29±1.47	1.52±0.20
	<0.825	25.77±2.66	—	—
6/18	<0.9	24.42±3.18	14.96±1.85	1.63±0.29
	<0.875	31.17±2.71	18.37±1.15	1.70±0.18
	<0.85	40.03±2.51	20.33±1.04	1.97±0.16
	<0.825	50.54±2.09	24.3 ±1.64	2.08±0.16
12/18	<0.9	44.5 ±2.5*	20.47±0.93	2.17±0.16
	<0.875	48.5 ±2.0	22.49±0.92	2.16±0.13
	<0.85	53.0 ±2.0	24.94±1.39	2.13±0.14
	<0.825	59.5 ±2.0	28.15±2.31	2.11±0.19
14/18	<0.9	50.35±1.70	—	—
	<0.875	53.74±1.52	—	—
	<0.85	56.58±1.42	—	—
	<0.825	61.61±1.36	—	—
6/39	<0.9	17.44±5.72	16.95±1.40	1.03±0.34
	<0.875	24.92±5.13	19.09±1.25	1.31±0.28
	<0.85	33.55±4.14	21.90±1.51	1.31±0.19
	<0.825	40.2 ±3.79	25.63±2.32	1.57±0.21
12/39	<0.9	31.0 ±5.0*	19.82±0.46	1.56±0.25
	<0.875	38.25±4.5	21.02±0.45	1.82±0.22
	<0.85	49.0 ±4.5	22.01±0.46	2.23±0.21
	<0.825	59.0 ±4.5	22.81±0.47	2.59±0.20
14/39	<0.9	37.35±5.1	—	—
	<0.875	45.22±4.4	—	—
	<0.85	55.37±4.14	—	—
	<0.825	67.09±4.02	—	—
30/39	<0.9	45.95±6.03	—	—
	<0.875	49.16±5.55	20.08±2.16	2.45±0.38
	<0.85	68.9 ±4.25	24.23±1.54	2.84±0.25
	<0.825	84.57±5.34	28.58±2.88	2.96±0.35

*ED_{50} values (±SE) estimated by extrapolation from log–log iso-effect curves.

Table III. Variation in the slope (±SE) of log–log plots of iso-effect dose against fraction number with level of effect and time of assessment

Irradiation treatment time (days)	Relative field length	Period of assessment 26–52 weeks	Period of assessment 65–104 weeks
39	<0.9	0.64±0.04	0.61±0.13
	<0.875	0.49±0.02	0.43±0.12
	<0.85	0.42±0.02	0.45±0.06
	<0.825	0.37±0.01	0.46±0.06
	Average	0.48±0.05	0.49±0.05
18	<0.9	0.59	0.85
	<0.875	0.5	0.64
	<0.85	0.21	0.41
	<0.825	0.14	0.23
	Average	0.37±0.09	0.53±0.12

neous damage for the fast neutron beam used in these investigations, with respect to the dose/fraction of 250 kV X rays, was calculated from the ED_{50} iso-effect

Table IV. Variation in the slope (±SE) of the log–log plot of iso-effect dose with level of cutaneous and subcutaneous damage against fraction number (6–30 fractions) after irradiation with X rays (the correlation coefficient of each plot is given in parentheses)

Relative field length	Period of assessment 26–52 weeks	Period of assessment 65–104 weeks
<0.9	0.51±0.06 (r=0.99)	0.50±0.23 (r=0.90)
<0.875	0.43±0.02 (r=0.99)	0.35±0.20 (r=0.88)
<0.85	0.35±0.01 (r=0.99)	0.39±0.06 (r=0.99)
<0.825	0.33±0.03 (r=0.99)	0.39±0.02 (r=0.99)
Average	0.41±0.04	0.41±0.05

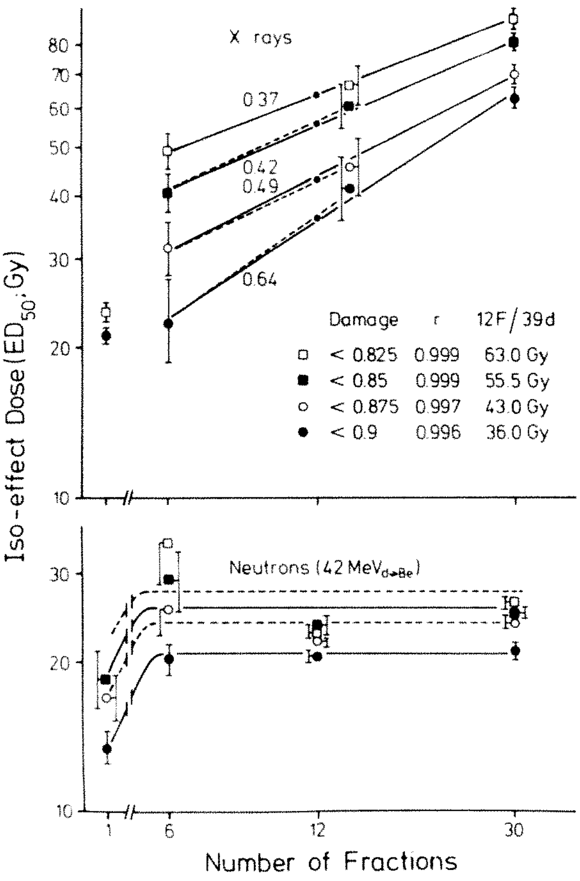

Figure 3. Log–log plot of ED$_{50}$ values (±SE) for changes in relative field length of <0.9 (●), <0.875 (○), <0.85 (■) and <0.825 (□) in pig skin, against number of fractions of either X rays or fast neutrons (42 MeV$_{d\to Be}$), given over 39 days. An estimate of the ED$_{50}$ values for 12 fractions/39 days was obtained by interpolation between the 6 and 14 fraction data as indicated. The data are for the assessment period 26–52 weeks after irradiation.

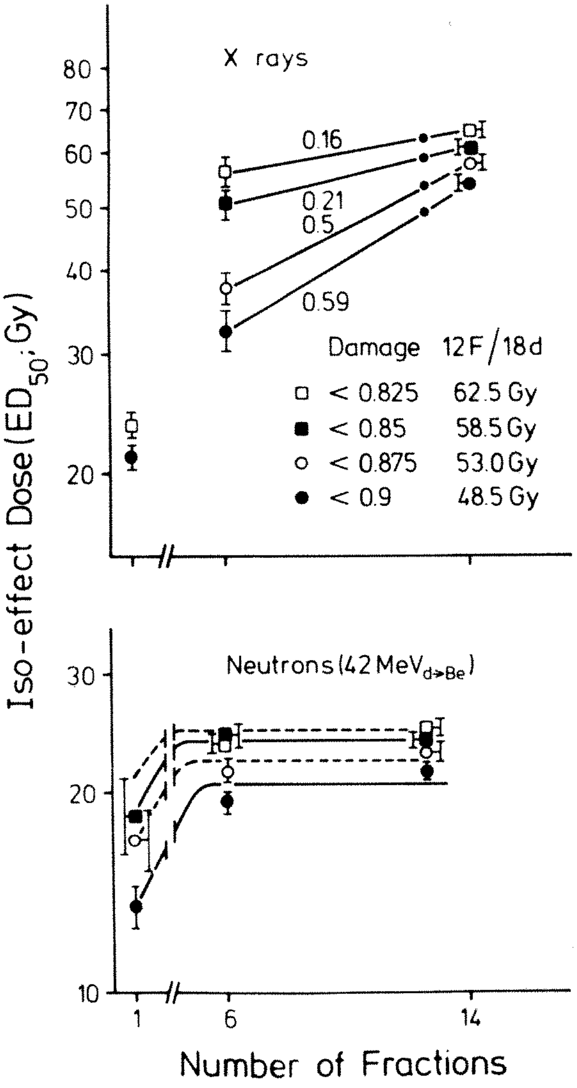

Figure 4. Log–log plot of ED$_{50}$ values (±SE) for changes in relative field length in pig skin against number of fractions of either X rays or fast neutrons (42 MeV$_{d\to Be}$), given over 18 days. An estimated ED$_{50}$ value for 12 fractions/18 days was obtained from this plot. For key to symbols see Fig. 3. The data are for the assessment period 26–52 weeks after irradiation.

doses given in Tables I and II. For both periods of assessment, there was an increase in the RBE with increased fractionation of the radiation dose, except in the case of irradiation with 6 fractions/39 days, where the RBE values tended to be similar to or below those for large single doses. From the individual values of RBE and X-ray dose/fraction, for the different effect levels, mean values were calculated; these results are presented in Fig. 7. A good linear correlation was obtained between the log of the RBE and the log of the X-ray dose/fraction for both periods of assessment ($r > 0.96$), when the data for 6 fractions/39 days were excluded. The slopes of the plots, -0.354 ± 0.022 for 26–52 weeks and -0.266 ± 0.023 for 65–104 weeks, were not significantly different ($p \gg 0.05$) and could be equally well fitted by a single line with a slope of -0.335 ± 0.025. The low RBE values for irradiation, given as 6 fractions/39 days, reflect mainly the higher than anticipated ED$_{50}$ values for the different severities of changes in relative field length for animals irradiated with fast neutrons.

Discussion

Late damage to cutaneous and subcutaneous tissues of the pig has been assessed after local irradiation with single and fractionated doses of 250 kV X rays and fast neutrons (42 MeV$_{d\to Be}$) by measuring the change in length of skin fields relative to that of unirradiated areas

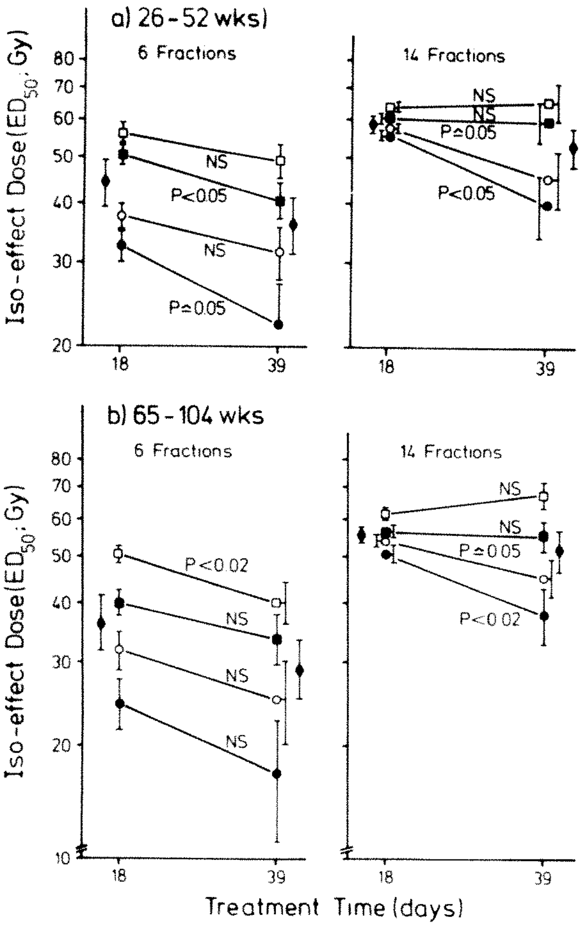

Figure 5. Log–log plot of ED_{50} values (±SE) for changes in relative field length in pig skin against overall treatment time for irradiation given as 6 or 14 fractions of X rays. Data are presented for the assessment period 26–52 weeks (upper panels) and 65–104 weeks (lower panels) after irradiation. For key to symbols see Fig. 3. (◆ indicates average ED_{50} values at 18 and 39 days.)

on the same animals. Measurements were made at regular intervals from 26–104 weeks after iradiation. A previous investigation with X rays, of the time-related changes in relative field length and referred to as "relative field contraction", has suggested that the effect was progressive over this time period after irradiation (Young & Hopewell, 1982). This result has been confirmed by the present findings; the severity of damage, as determined from measurements of relative field length, averaged over 65–104 weeks, was greater than those at 26–52 weeks after both X-ray and fast neutron irradiation. The ED_{50} values for four selected levels of effect also tended to be lower for the later assessment time, although there was some variation in this.

Using a non-invasive ultrasound technique, recent measurements of skin thickness after both X (Baker et al, 1989) and $^{90}Sr/^{90}Y$ β irradiation (Hopewell et al, 1989a), have shown that dermal damage is characterized by two distinct phases of tissue thinning. The first develops over the period 14 and 20 weeks after irradiation, the second between 52 and 65 weeks. As the pigs grew, there was an increase in skin thickness in the first 14 weeks after irradiation. This, and the subsequent growth between 20 and 52 weeks was unaffected by the radiation, the rate of increase in dermal thickness being the same in irradiated and unirradiated skin. The underlying mechanisms leading to dermal thinning are believed to be of vascular origin, albeit with the involvement of at least two different target cell populations (Hopewell et al, 1989b). The reduction in relative field length, after irradiation, is in part related to the atrophy of dermal tissue but may also have been influenced by the atrophy of the underlying subcutaneous fat and the panniculus muscle (Hopewell, 1980).

The complex biological basis of the end-point characterized by the change in relative field length may provide an explanation of the equally complex fractionation responses observed. Based on the results for quantal data, for fractionated irradiation, the slope of the log–log plot of the iso-effect dose against fraction number

Table V. Variation in α/β ratios (±SE) with level of cutaneous and subcutaneous damage after irradiation with 6–30 fractions of X rays and 1–30 fractions of fast neutrons (correlation coefficients given in parentheses)

	Relative field length	Period of assessment	
		26–52 weeks	65–104 weeks
X rays	<0.9	−0.31±0.81 (r=0.95)	0.44±3.37 (r=0.77)
	<0.875	1.06±0.19 (r=0.99)	2.29±2.34 (r=0.78)
	<0.85	4.23±0.61 (r=0.99)	1.77±0.68 (r=0.98)
	<0.825	6.54±1.59 (r=0.97)	2.63±0.06 (r=0.99)
	Average	2.13±1.31	1.78±0.42
Neutrons	<0.9	19.38±1.33 (r=0.99)	11.98±2.21 (r=0.98)
	<0.875	39.53±3.63 (r=0.98)	34.69±4.22 (r=0.96)
	<0.85	47.81±8.8 (r=0.91)	32.3±2.09 (r=0.99)
	<0.825	—	23.68±5.35 (r=0.87)
	Average	35.57±6.89	25.66±2.22

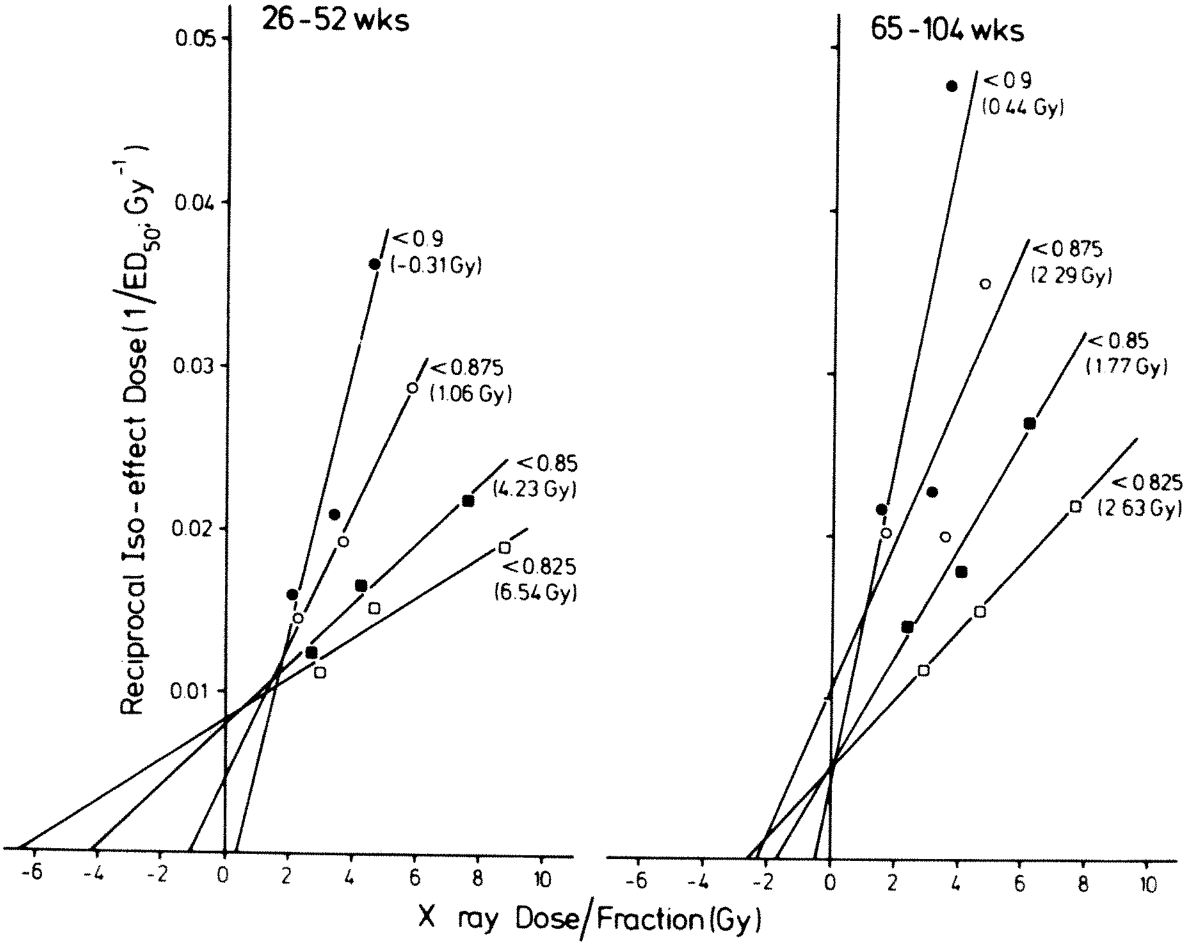

Figure 6. Plots of the reciprocal of the iso-effective doses ($1/ED_{50}$) for changes in relative field length in pig skin as a function of the X-ray dose per fraction. Data for the period of assessment of 26–52 weeks and 65–104 weeks are presented. (For key to symbols see Fig. 3.)

tended to decrease with increasing level of effect. This effect was seen irrespective of whether treatment was given in 18 or 39 days. The slopes were particularly steep for a relative field length of <0.9, representing exponents of N in a modified Ellis (1969) formula of $\geqslant 0.5$. The size of the N exponent was almost always $\leqslant 0.5$, for a relative field length of <0.875, *i.e.* when measurements of field length of between <0.9 and $\geqslant 0.875$ were excluded from the analysis. Despite the wide variations in the individual slopes of the iso-effect plots for different levels of effect, the majority did not differ significantly from the average slope fitted to the combined data. The only exception was that for fractionated irradiation given over 39 days for measurements collected over the earlier of the two assessment periods (26–52 weeks). None of the analyses suggested any change in the fractionation response with the period of assessment.

The results of the present analysis are in agreement with those presented earlier (Hopewell et al, 1979) where slopes of 0.55 and 0.45 were obtained for fractionated irradiation given in 18 and 39 days, respectively. This is encouraging given that these iso-effect doses were based on what was termed "12% linear field contraction" (0.88 relative field length) obtained from dose–effect curves drawn by eye. The subjective difficulties of fitting such curves were emphasized on the present studies with fast neutrons, where only a very limited number of data points were available. The present findings are also in very good agreement with the results of others. For the pig a slope of 0.46 was obtained for field contraction, measured between 5 and 8 months after irradiation, for the very limited comparison of 13 fractions with 32 fractions given in 6 weeks (Withers et al, 1978a). For human skin, the slope was 0.42 for clinically detectable subcutaneous induration measured between 6 and 36 months after the completion of radiotherapy (Gauwerky & Langheim, 1978). This end-point effectively represents a combination of the atrophy of the dermal and subcutaneous fatty tissues (Hamlet et al, 1986), which is seen

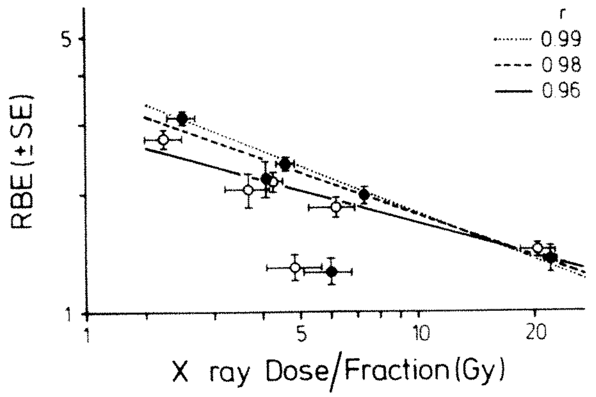

Figure 7. Log–log plot to show the variation in the RBE for fast neutrons (42 $\mathrm{MeV}_{d\to Be}$) with X-ray dose/fraction for changes in relative field length. For each fractionation schedule the average RBE (±SE) based on four levels of damage is plotted against the associated average X-ray dose/fraction (±SE). Data for the periods of assessment of 26–52 weeks (● — — — ●) and 65–104 weeks (○——○) are presented and compared with the data for ischaemic dermal necrosis in pig skin (·····) taken from Hopewell et al (1988).

in >60% of patients who develop the effect within 12 months and in ~80% after 36 months (Rezvani et al, 1990b). Telangiectasia, a lesion appearing later in human skin (after 52 weeks), was also reported as a histological finding associated with the second phase of dermal thinning in the pig (Hopewell et al, 1989a,b). For telangiectasia the slope of the iso-effect slope was approximately 0.4 (Cohen & Ubaldi, 1977); again in good agreement with the present results. For the earlier appearing dermal lesion in pig skin, ischaemic necrosis after 12–16 weeks, the slope of the iso-effect plot was 0.38 ± 0.01 (Hopewell et al, 1988).

The slope of iso-effect plots was also reported to vary with the severity of the effect for leg contraction in mice, 250 days after ^{137}Cs γ irradiation (Masuda et al, 1987). Here again, the multiple components possibly combining to produce the measured parameter of leg contraction were proposed as a major contributory factor. Although the data obtained using this assay in mice were not well fitted by the linear quadratic (LQ) model, α/β ratios were calculated and were found to be within the range 1.48–5.02 Gy for a total contraction of 4–8 mm, respectively. For pig skin, late damage to the cutaneous and subcutaneous tissues was again not well described by the LQ model, and after fractionated irradiation with X rays the α/β ratios were not significantly different from zero for severities of damage represented by a <0.9 and <0.875 change in relative field length. According to the basic concept of the LQ model the α/β ratio should not vary with the degree of injury used to determine iso-effect doses (Masuda et al, 1987). The present observations and those of Masuda et al (1987), in a different mammalian species, have still to be fully explained.

The average α/β ratio obtained from the present studies in the pig, which was of the order of 1.95 for X rays, did not vary significantly with the period of assessment and was in line with values obtained for other late responding normal tissues (*e.g.* Fowler, 1989). These included late cutaneous and subcutaneous changes in human skin (Overgaard, 1985) where values of 1.9–2.3 Gy are quoted. The most recent best estimate of the α/β ratio for late cutaneous and subcutanous injury in human skin is 1.9 Gy (Bentzen et al, 1989). For late telangiectasia in human skin, a value of 2.8 Gy was found when no time correction was applied to the results (Turesson & Thames, 1989). This did not vary with the follow-up time, albeit that the assessments were made at 3 and 5 years after the completion of radiotherapy. This α/β ratio for telangiectasia was increased to ~4.0 when account was taken of a small positive time factor for this end-point (Turesson & Thames, 1989). Evidence for a small positive time factor has also been demonstrated for the end-point of ischaemic dermal necrosis in pig skin when daily fractionation was compared with fractions with a 48–72 h interfraction interval (Hopewell & van den Aardweg, 1991). The interpretation, incomplete repair within 24 h, was in accord with the results of Turesson & Thames (1989).

For late damage to the cutaneous and subcutaneous tissues of the pig, a previous analysis had suggested a *negative* time exponent when doses given as 6 fractions were spread over 39 days as compared with 18 days (Hopewell et al, 1979). While a similar trend was reported here for both 6 and 14 fractions, using a more objective method by which to compare the different fractionation schedules, overall, these differences were not considered to be significant. In general terms, assuming the complete repair of sublethal damage, the overall time factor for late responding tissues is believed to be zero (Fowler, 1989) and indeed should be for a slowly proliferating tissue. For leg contraction in mice, Masuda et al (1987) found no evidence for a significant time factor for radiation given in 2–32 fractions.

A major objective of the present investigation was to determine the variation in RBE with fraction size for a truly late occurring lesion in pig skin. Changes in relative field length were assessed at 26–52 weeks after irradiation and after 65–104 weeks when the severity of damage was greater after both X-ray and fast neutron irradition. These same skin fields had been used previously to assess epithelial changes and more specifically ischaemic dermal injury (Hopewell et al, 1988). Thus information, related at least in part to dermal damage, is available for three widely separate time intervals after irradiation. The trend was for the RBE to decrease slightly with time, most noticably with smaller doses/fraction, but this did not prove to be statistically significant. This is in agreement with the results of studies in mouse lung (Parkins et al, 1985) where again the RBE tended to decrease with the time of assay for X-ray doses/fraction of 2–3 Gy. Our observations would appear to be at variance with previous clinical impressions, which could have been interpreted as suggesting an increase in the RBE with longer follow-up times (Stone, 1948; Duncan, 1983). However, this view was not derived from the concepts of RBE but from the clinical observation that late sequelae, including damage to subcutaneous tissues, were more severe than would have been expected on the basis of the acute reactions observed after neutron therapy (Hussey et al, 1974; Ornitz et al, 1980; Duncan et al, 1986).

The present results for late damage to pig skin are in agreement with those of Withers et al (1987b), who reported a RBE value of >3.11 <3.94 for fast neutrons of a similar energy (50 $\mathrm{MeV}_{b\rightarrow Be}$), for a dose/fraction of ^{60}Co γ rays of 2 Gy with a follow-up time of 5–8 months. For this order of dose/fraction the RBE for dermal damage at 12–16 weeks was greater than that for early epithelial changes after ~6 weeks (Hopewell et al, 1988). The present results, which suggest a slight decrease in RBE with a longer follow-up time for late damage, would tend to reduce the significance of this difference.

Thus in summary, the fractionation response of the cutaneous and subcutaneous tissues of the pig to both X rays and fast neutrons are similar to those of other late responding normal tissues. The RBE for fast neutrons increased with decreasing fraction size but there was no significant evidence for any change in the RBE value with follow-up time from 26–104 weeks after irradiation, the time scale over which most patients who would develop detectable late atrophy of the skin do so.

Acknowledgments

The authors gratefully acknowledge the support and collaboration of the staff of the Churchill Hospital Research Institute, the MRC Radiobiology Unit and the team at the AERE Variable Energy Cyclotron, without whose help this whole series of experiments could not have been carried out. Special thanks are given to D. T. Goodhead and D. A. Bance for the calibration of the beam line, P. J. V. Adams, D. C. Campling and T. K. Yeung for dosimetry with P. Gray and A. Thompson providing back-up electronics support. P. C. Bates, F. W. Dickinson, N. Hubbard and P. C. Monk are thanked for their help with the anaesthesia and the care of the animals, and R. H. Simmonds, M. Rezvani, J. F. Knowles, R. Hamlet and E. M. Whitehouse for help with irradiation and the subsequent measurements of the irradiated fields. The work was supported jointly by the Cancer Research Campaign and the Medical Research Council, including a special MRC Programme Grant awarded to Dr J. W. Hopewell.

References

BAKER, M. R., BADER, D. & HOPEWELL, J. W., 1989. The effects of single doses of X rays on the mechanical properties of pig skin *in vivo*. *British Journal of Radiology, 62*, 830–837.

BENTZEN, S. M., THAMES, H. D. & OVERGAAD, M., 1989. Latent-time estimation for late cutaneous and susbcutaneous radiation reactions in a single follow-up clinical study. *Radiotherapy and Oncology, 15*, 267–274.

BONNETT, D. E., BLAKE, S. W., SHAW, J. F. & BEWLEY, D. K., 1988. The Clatterbridge high energy cyclotron: specification and performance. *British Journal of Radiology, 61*, 38–46.

COHEN, L. & UBALDI, S. E., 1977. Dose–time relationships for post-irradiation cutaneous telangiectasia. *International Journal of Radiation Oncology, Biology, Physics, 2*, 421–426.

COHEN, L., HENDRICKSON, F. R., MANSELL, J. A., AWSCHALOM, M., HREJSA, A., KAUL, R. & ROSENBERG, I., 1981. Late reactions and complications in patients treated with high energy neutrons p (66 MeV) Be (49 MeV). *International Journal of Radiation Oncology, Biology, Physics, 7*, 179–184.

COHEN, L., SCHULTHEISS, T. E., HENDRICKSON, F. R., MANSELL, J. A., SAROJA, K. R. & LENNOX, A., 1989. Normal tissue reactions and complications following high energy neutron beam therapy: Crude response rates. *International Journal of Radiation Oncology, Biology, Physics, 16*, 73–78.

DUNCAN, W., 1983. Clinical experience of fast neutron therapy at Edinburgh. In *Proceedings of the 13th International Cancer Congress, Part D, Research and Treatment*, ed. by E. A. Mirand, W. B. Hutchinson and E. Mihich (Alan R. Liss, New York), pp. 261–265.

DUNCAN, W., WILLIAMS, J. R., KERR, G. R., ARNOTT, S. J., QUILT, P. M., ROGER, A., MACDOUGALL, R. H. & JACK, W. J. L., 1986. An analysis of the radiation related morbidity observed in a randomized trial of neutron therapy for bladder cancer. *International Journal of Radiation Oncology, Biology, Physics, 12*, 2085–2092.

ELLIS, F., 1969. Dose, time and fractionation: a clinical hypothesis. *Clinical Radiology, 20*, 1–7.

FOWLER, J. F., 1989. The linear-quadratic formula and progress in fractionated radiotherapy. *British Journal of Radiology, 62*, 679–694.

GAUWERKY, F. & LANGHEIM, F., 1978. Der zeitfaktor bei der strahleninduzierten subkutanen fibrose. *Strahlentherapie, 154*, 608–616.

GERACI, J. P., 1981. Efficacy of neutrons in radiotherapy. *Health Physics, 40*, 41–53.

HAMLET, R., REZVANI, M. & HOPEWELL, J. W., 1986. Ultrasound measurements of atrophy in pig skin following X- and β-irradiation. *Bioengineering and Skin, 2*, 49–57.

HOPEWELL, J. W., 1980. The importance of vascular damage in the development of late radiation effects in normal tissues. In *Radiation Biology in Cancer Research*, ed. by R. E. Morgan and H. R. Withers (Raven Press, New York), pp. 449–459.

HOPEWELL, J. W., FOSTER, J. L., YOUNG, C. M. A. & WIERNIK, G., 1979. Late radiation damage to pig skin: the effects of overall treatment time and fraction number. *Radiology, 130*, 783–788.

HOPEWELL, J. W., BARNES, D. W. H., ROBBINS, M. E. C., SANSOM, J. M., KNOWLES, J. F. & VAN DEN AARDWEG, G. J. M. J., 1988. The relative biological effectiveness of fractionated doses of fast neutrons (42 $\mathrm{MeV}_{d\rightarrow Be}$) for normal tissues in the pig. I. Effects on the epidermal and dermal vascular/connective tissues. *British Journal of Radiology, 61*, 928–938.

HOPEWELL, J. W., CALVO, W., CAMPLING, D., REINHOLD, H. S., REZVANI, M. & YEUNG, T. K., 1989a. Effects of radiation on the microvasculature: implications for normal tissue damage. *Frontiers of Radiation Therapy and Oncology, 23*, 85–95.

HOPEWELL, J. W., CALVO, W. & REINHOLD, H. S., 1989b. Radiation damage to late-reacting normal tissues. In *Biological Basis of Radiotherapy (2nd Edition)*, ed. by G. G. Steel, G. Adams and A. Horwich (Elsevier Scientific Publishers, Amsterdam) pp. 101–113.

HOPEWELL, J. W. & VAN DEN AARDWEG, J. M. J., 1991. Studies of dose-fractionation on early and late responses in pig skin: a reappraisal of the importance of overall treatment time and its effects on radiosensitization and incomplete repair. *International Journal of Radiation Oncology, Biology, Physics* (in press).

HUSSEY, D. H., FLETCHER, G. H. & CADERAA, J. W., 1974. Experience with fast neutrons using the Texas A & M variable energy cyclotron. *Cancer, 34*, 65–77.

Masuda, K., Hunter, N., Stone, H. B. & Withers, H. R., 1987. Leg contracture in mice after single and multifractionated ^{137}Cs exposure. *International Journal of Radiation Oncology, Biology, Physics, 13,* 1209–1215.

Maor, M. H., Hussey, D. H., Fletcher, G. H. & Jesse, R. H., 1981. Fast neutron therapy for locally advanced head and neck tumors. *International Journal of Radiation Oncology, Biology, Physics, 7,* 155–163.

Ornitz, R. D., Bradley, F. W., Mossman, K. L., Fender, F. M., Schnell, M. C. & Rogers, C. C., 1980. Clinical observations of early and late normal tissue injury in patients receiving fast neutron irradiation. *International Journal of Radiation Oncology, Biology, Physics, 6,* 273–279.

Overgaard, M., 1985. The clinical implications of non standard fractionation. *International Journal of Radiation Oncology, Biology, Physics, 11,* 1225–1229.

Parkins, C. S., Fowler, J. F., Maughan, R. L. & Roper, M. J., 1985. Repair in mouse lung up to 20 fractions of X rays or neutrons. *British Journal of Radiology, 58,* 225–241.

Pointon, R. S., Read, G. & Greene, D., 1985. A randomised comparison of photons and 15MeV neutrons in the treatment of carcinoma of the bladder. *British Journal of Radiology, 58,* 219–224.

Rezvani, M., Barnes, D. W. H., Hopewell, J. W., Robbins, M. E. C., Sansom, J. M., Adams, P. J. V. & Hamlet, R., 1990a. The relative biological effectiveness of fractionated doses of fast neutrons (42 $\mathrm{MeV}_{\mathrm{d}\rightarrow\mathrm{Be}}$) for normal tissues in the pig. III. Effects on lung function. *British Journal of Radiology* (in press).

Rezvani, M., Alcock, C. J., Fowler, J. F., Haybittle, J. L., Hopewell, J. W. & Wiernik, G., 1990b. Results of the BIR study of 3F/week versus 5F/week in the treatment of carcinoma of the laryngo-pharynx by radiotherapy: Normal tissue reactions. *International Journal of Radiation Oncology, Biology, Physics,* (submitted).

Stone, R. S., 1948. Neutron therapy and specific isonisation. *American Journal of Roentgenology, 54,* 771–785.

Turesson, I. & Thames, H. D., 1989. Repair capacity and kinetics of human skin during fractionated radiotherapy: erythema, desquamation and telangiectasia after 3 and 5 years follow up. *Radiotherapy and Oncology, 15,* 169–188.

Withers, H. R., Thames, H. D., Flow, B. L. & Mason, K. A., 1978a. The relationship of acute to late skin injury in 2 and 5 fraction/week γ-ray therapy. *International Journal of Radiation Oncology, Biology, Physics, 4,* 595–601.

Withers, H. R., Thames, H. D., Hussey, D. H., Flow, B. L. & Mason, K. A., 1978b. Relative biological effectiveness (RBE) of 50MV(Be) neutrons for acute and late skin reactions. *International Journal of Radiation Oncology, Biology, Physics, 4,* 603–608.

Young, C. M. A. & Hopewell, J. W., 1982. Functional and morphological changes in pig skin after single or fractionated doses of X rays. *International Journal of Radiation Oncology, Biology, Physics, 8,* 1539–1547.

1990, *The British Journal of Radiology*, *63*, 771–775

Lipiodol computerized tomography: how sensitive and specific is the technique in the diagnosis of hepatocellular carcinoma?

By Henry Ngan, FRCP, FRCPE, FRCR

Department of Diagnostic Radiology, University of Hong Kong, Queen Mary Hospital, Hong Kong

(*Received March 1990*)

Abstract. Computerized tomography (CT) following the intra-arterial injection of Lipiodol (Lipiodol-CT) was performed on 60 patients suspected of having a hepatocellular carcinoma (HCC). Four main patterns of uptake of the Lipiodol within the liver were seen on CT. Of the 14 well circumscribed lesions with dense homogeneous uptake of Lipiodol, 13 were confirmed to be HCCs. Of the 25 lesions with dense patchy uptake of Lipiodol at the periphery and/or in the centre, 19 were confirmed to be HCCs. In 18 patients, in whom only ill defined faint patchy uptake of Lipiodol was present in the liver, or in whom no hepatic uptake was present at all, only one patient was found later to have an HCC. Of the three hypodense lesions in the liver with no Lipiodol uptake, one was found to be necrotic HCC, one a cholangiocarcinoma and one a regenerative nodule. In the diagnosis of HCC, Lipiodol-CT had an overall sensitivity of 97.1%, an accuracy of 88.3% and a specificity of 76.9%. Of the 34 patients with HCC, only 23 were solitary at diagnosis. The size of the HCCs ranged from 0.8 cm to 11 cm in diameter with the median size at 2.2 cm. Eleven of 34 HCCs (32.3%) were resectable. We conclude that, as part of a screening programme for high risk patients, Lipiodol-CT is useful in the early detection of HCCs. The technique also plays an important role in determining whether the tumour should be resected or managed with chemotherapy. By detecting HCCs while still small, the resectability rate can also be improved.

The incidence of hepatocellular carcinoma (HCC) is extremely high in South-East Asia. In Hong Kong, HCC is the third commonest malignant tumour and ranks second amongst the main causes of death from cancer. By the time an HCC becomes symptomatic, it is invariably large and the prognosis extremely poor. The median survival in an untreated HCC is as short as 3.5 weeks (Lai et al, 1981). If the outlook in patients with HCC is to be improved, the tumour must be detected while it is still small and asymptomatic. The procedure of computerized tomography (CT) after the intra-arterial injection of Lipiodol ultrafluid into the hepatic artery (Lipiodol-CT) has been reported by Yumoto et al (1985), Ohishi et al (1985) and Choi et al (1989) as a useful method of detecting small HCCs. However, apart from two papers (Maki et al, 1985; Raby et al, 1989), there has been hardly any detailed description and analysis of the pattern of uptake of Lipiodol in the liver on CT. Moreover, the specificity of the technique of Lipiodol-CT has never been reported. Lipiodol-CT was therefore performed on 60 patients to investigate these two issues and to see if Lipiodol-CT can detect an HCC while it is still small and if resectability rate can be improved.

Materials and methods

Lipiodol-CT was performed on 60 patients during a 4-year period. The series included 53 men and seven women with age ranging 16–78 years. Most of these patients were hepatitis-B surface antigen positive and were closely followed up at 3–6-monthly intervals because of chronic active hepatitis, cirrhosis or a history of hepatic resection for HCC. They were referred for Lipiodol-CT if during follow-up the serum alpha feto-protein was found to be persistently elevated above 20 ng/ml or if the ultrasonogram of the liver was abnormal.

In the technique of Lipiodol-CT, a conventional hepatic angiogram was first performed. Then 2–5 ml of Lipiodol ultrafluid was selectively infused into the common hepatic artery, or into the coeliac axis if selective catheterization of the common hepatic artery was not possible. Computerized tomography of the upper abdomen was performed 6–13 days after the injection of the Lipiodol with contiguous 10 mm slices through the liver at 10 mm intervals.

Results

There were four main patterns of uptake of the Lipiodol within the liver on CT and the results are summarized in Table I. Of the 14 well circumscribed lesions with dense homogenous uptake of Lipiodol, 13 were confirmed to be HCCs (Fig. 1). Of the 25 lesions, some of which were hypodense, with dense patchy uptake of Lipiodol at the periphery and/or in the centre, 19 were confirmed to be HCCs (Fig. 2). In 18 patients, in whom there was only ill defined faint patchy uptake of the Lipiodol in the liver (Fig. 3), especially in the subcapsular region, or in whom no uptake was seen in the liver, only one patient was found later to have an HCC; the rest had either cirrhosis or chronic active hepatitis. Of the three hypodense lesions in the liver with no Lipiodol uptake, one was found to be a necrotic HCC, one a cholangiocarcinoma, and one a regenerative nodule.

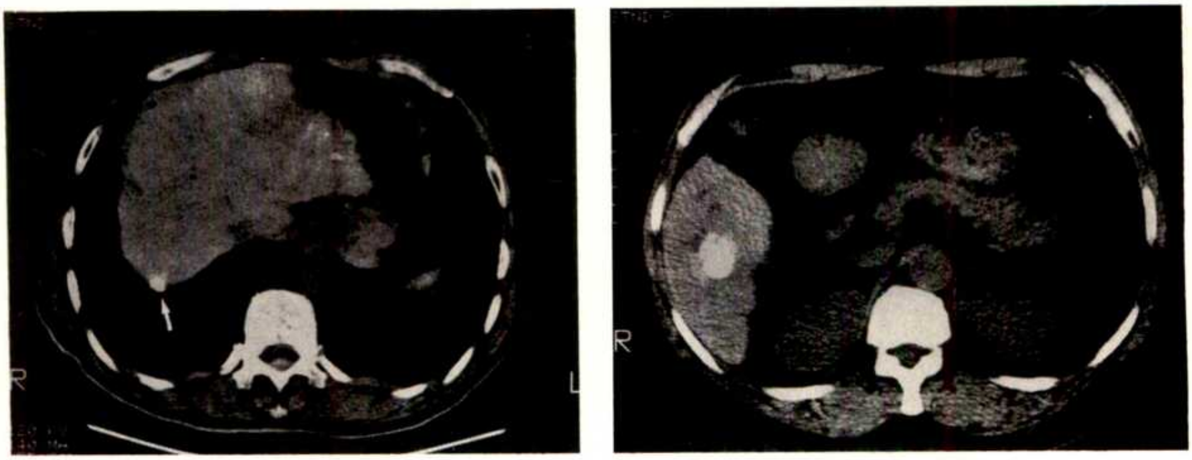

(a) (b)

Figure 1. (a) A 0.8 cm HCC with dense homogeneous uptake of Lipiodol (arrow) in right lobe of the liver. (b) An HCC 2.5 × 1.8 cm with dense homogeneous uptake in the right lobe.

The overall results of Lipiodol-CT in the diagnosis of HCC are summarized in Table II. Thirty-three HCCs were correctly diagnosed. There were, however, six false positives: two lesions turned out to be focal nodular hyperplasia, two haemangiomata (Fig. 4), one a metastasis and one a regenerative nodule. Hepatocellular carcinoma was correctly excluded in 20 patients. One patient, in whom no focal uptake was present in the liver, turned out to have an HCC on follow-up. In the diagnosis of HCC, Lipiodol-CT has therefore a high sensitivity of 97.1%, an accuracy of 88.3%, but a specificity of only 76.9%. Conventional hepatic angiography was performed on all 34 patients with HCCs and nine angiograms were either normal or only suspicious. Hepatic angiography therefore detected the HCCs with certainty in 25 patients (73.6%). Ultrasound was performed on 21 patients with HCCs and detected the tumours in only 10 patients (47.6%).

Table I. Pattern of Lipiodol uptake in liver

Final Diagnosis	Dense homogeneous uptake within lesion	Dense patchy uptake at periphery and/or centre of lesion	Ill defined faint patchy uptake or no uptake in liver	No uptake in hypodense area
Hepatocellular carcinoma	13	19	1	1
Focal nodular hyperplasia	1	1	—	—
Haemangioma	—	3	—	—
Metastasis	—	2	—	—
Cholangiocarcinoma	—	—	—	1
Cirrhosis/ Chronic hepatitis	—	—	17	—
Regenerative nodule	—	—	—	1
Total	14	25	18	3

Hepatocellular carcinoma was present in 34 out of 60 patients. The HCCs were solitary on the Lipiodol CT in the 23 patients. In seven patients, two HCCs were present in the liver and in four patients, three or more HCCs were present in the liver (Fig. 5). The size of the HCCs ranged from 0.8 cm to 11 cm in diameter with the median size being 2.2 cm. The median size of HCCs with dense homogeneous uptake of Lipiodol was 2 cm, while the median size of HCCs with dense patchy uptake of Lipiodol was 4 cm. If a "small HCC" is defined as one of 3 cm or less in diameter (Chen et al, 1982), then 20 of the 34 HCCs (59%) were "small HCCs". Eleven out of 34 HCCs (32.3%) were resectable. However, nine of the 20 "small HCCs" detected (45%) were resectable.

Discussion

When Lipiodol is infused into the hepatic artery, most of the Lipiodol droplets flow into an HCC by virtue of the increased blood supply to the tumour. The Lipiodol is then trapped within the tumour because of the presence of pathological vessels with abnormalities such as lack of contractibility, slow rate of blood flow and enhanced permeability. There is thus a preferential uptake of the Lipiodol in an HCC. Once deposited in the tumour, the Lipiodol droplets disappear at a slower

Table II. The results of Lipiodol-CT in diagnosing HCC

True positive	33
False positive	6
True negative	20
False negative	1

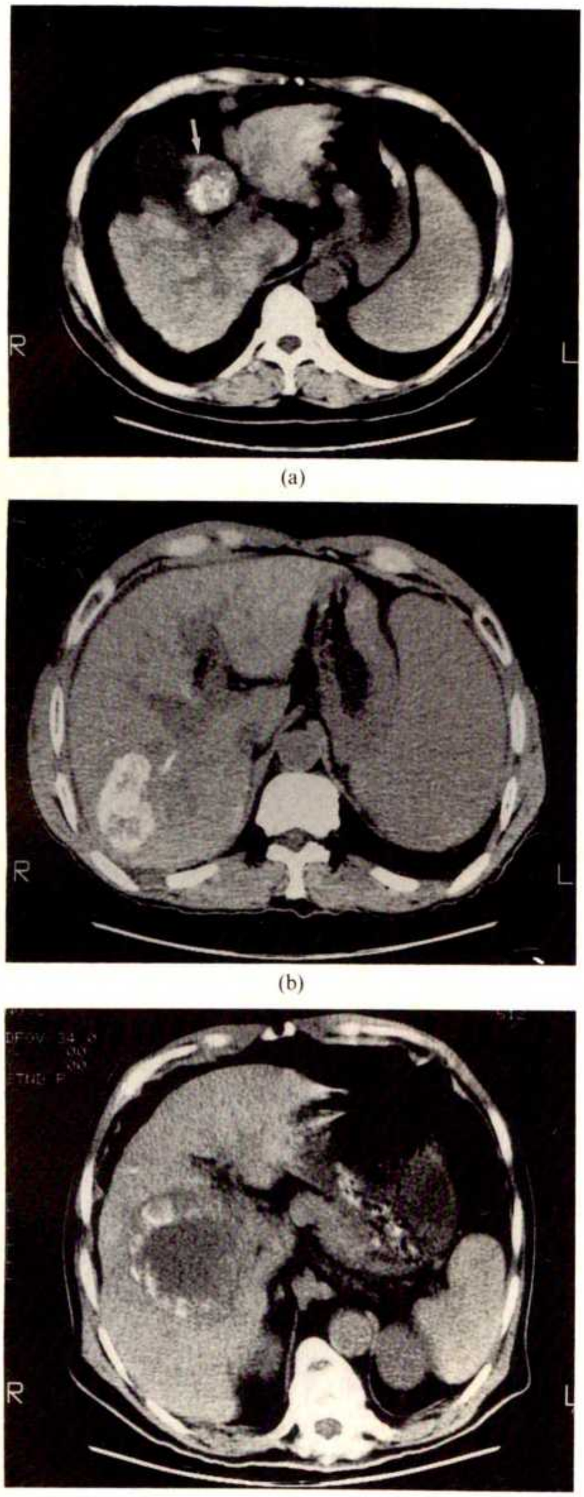

(a)

(b)

(c)

Figure 2. (a) A 2.8 cm HCC with dense patchy uptake of Lipiodol (arrow). (b) An HCC with dense patchy uptake in the periphery and centre of tumour. (c) A hypodense HCC with dense patchy uptake at the periphery of tumour.

rate compared with those deposited in the normal liver tissue. It is uncertain as to the exact mechanism responsible for the faster clearance of Lipiodol from the normal liver tissue. Lipiodol deposited in the normal liver is cleared partly through the hepatic lymphatics. Hepatic Kupffer cells may also play an important role in the elimination of the Lipiodol. The absence of both lymphatics and Kupffer cells within an HCC may account for the difference in the clearance rate. Thus a CT performed a week or so after infusion of the Lipiodol would enhance the differentiation of HCC from normal liver tissue.

Our study revealed that there were four main patterns of uptake of Lipiodol in the liver on CT. When dense homogeneous uptake was present in a well circumscribed lesion, 13 out of 14 (92.8%) turned out to be HCCs, the exception being a case of focal nodular hyperplasia. In the clinical setting of a patient with known chronic hepatitis B virus infection and a persistently elevated alpha fetoprotein, this pattern is highly suggestive of an HCC. When dense patchy uptake was present within a lesion, only 19 out of 25 (76%) turned out to be HCCs. Three haemangiomata, two metastases and one focal nodular hyperplasia demonstrated this pattern. This appearance is therefore not always diagnostic of an HCC and cannot by itself distinguish an HCC from a haemangioma as suggested by Yumoto et al (1985) or from a metastasis as reported by Maki et al (1985). The patchy uptake of the Lipiodol is probably partly related to the type of vascular channels present and the amount of fibrotic and necrotic tissue within the lesion. Since an HCC tends to undergo necrosis as it enlarges, it is expected that patchy uptake is more likely to be seen in larger tumours than in smaller ones. Raby et al (1989) found that homogeneous uptake of the Lipiodol occurred in small HCCs (<5 cm) while uptake with peripheral distribution occurred in larger HCCs (>5 cm) and concluded that the type of distribution of Lipiodol within an HCC is related to tumour size and vascular supply rather than to the histological type. This is in keeping with our observation that the median size of HCCs with homogeneous uptake was 2 cm while that with dense patchy uptake was 4 cm.

In 18 patients, there was either an ill defined and faint patchy uptake of the Lipiodol, especially noticeable at the sub-capsular region, or no uptake at all within the liver. On follow-up, all those patients with the exception of one were found to have only cirrhosis or chronic active hepatitis. Such an appearance is a result of deposition of Lipiodol in the normal liver tissue which has not yet been cleared completely by the time of CT and therefore would exclude the presence of an HCC in the majority of patients. In three patients, a hypodense lesion without any Lipiodol uptake inside was encountered. One was a very necrotic HCC and another a cholangiocarcinoma. The total absence of uptake must be due to the avascular nature of the tumour. In the third case, the hypodense lesion was a regenerative nodule, which is in agreement with the observation by Yumoto et al (1985), who also noted that none of the

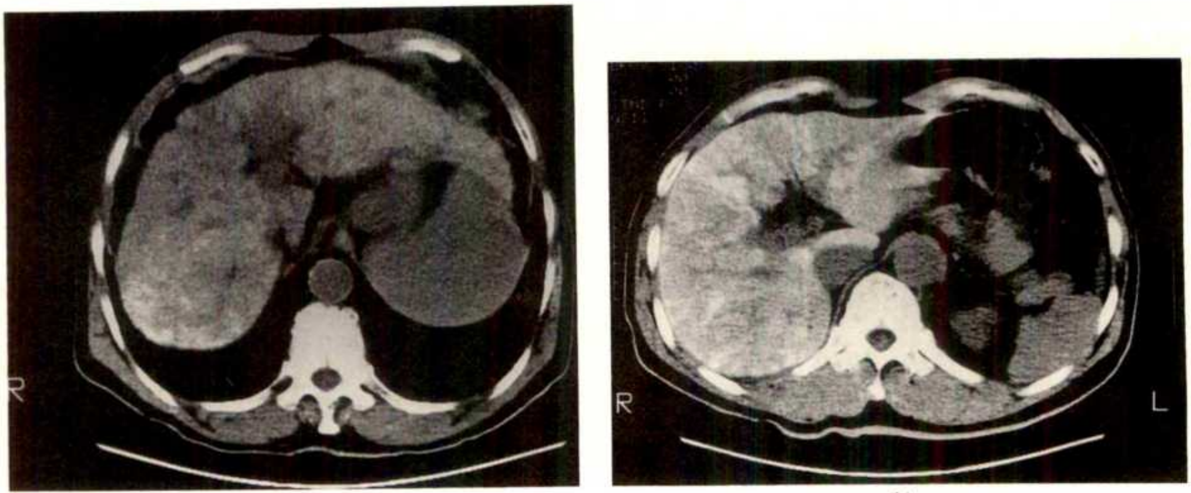

(a) (b)

Figure 3. (a) Ill defined faint uptake of Lipiodol in both lobes of the liver, especially in the sub-capsular region posteriorly of the right lobe. (b) Faint patchy uptake in both lobes of the liver.

regenerative nodules in their study contained Lipiodol.

The overall sensitivity of Lipiodol-CT in the diagnosis of HCC in our series was as high as 97.1%. This is in concordance with the results in the study by Choi et al (1989), in which the overall detectability rate of HCC was reported as 96%. For the detection of small HCCs, Lipiodol-CT is therefore superior to hepatic angiography, which could detect an HCC with certainty in only 73.6% of our patients. Ultrasound detected an HCC in only 47.6% of our cases, whereas Choi et al (1989) could detect 73% in their series. The presence of cirrhosis and the small size of the HCC in our patients probably contributed towards this poor result.

The overall specificity of Lipiodol-CT in the diagnosis of HCC in our series was only 76.9%. This relatively low specificity is mainly a result of the inability of the technique to differentiate an HCC from other abnormalities when there is dense patchy uptake of the lipiodol within a lesion. If such a pattern is encountered, fine needle aspiration biopsy or even "Trucut" biopsy of the lesion under either ultrasound or CT guidance is essential to clarify the diagnosis before surgical resection is undertaken. On the other hand, when dense homogeneous uptake is present in a discrete mass, the chance of it being an HCC is high with the post-test probability being 92.8%. Likewise, when ill defined and faint patchy uptake is present in the liver, or when no uptake occurs at all, an HCC can be excluded with a high degree of certainty, the post-test probability of the liver harbouring an HCC being only 5.5% (Armstrong & Black, 1989).

In our study, the median size of the HCCs was only 2.2 cm, and 59% of the HCCs were 3 cm or less.

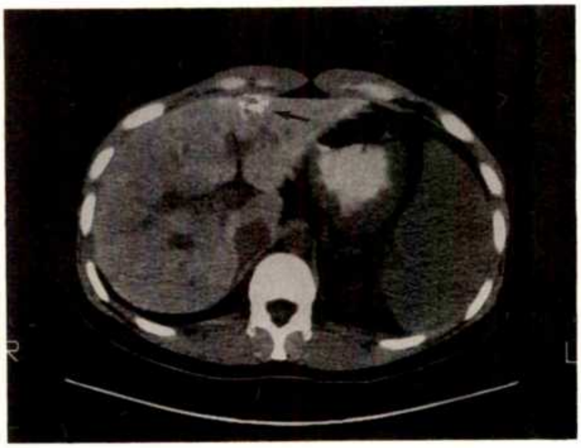

Figure 4. A haemangioma 1.6 cm across with dense patchy uptake of Lipiodol (arrow).

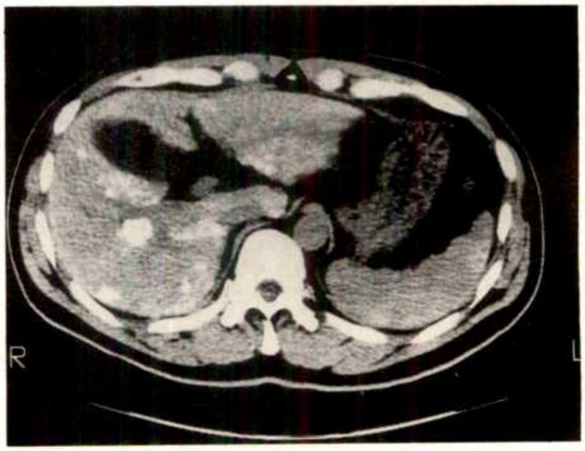

Figure 5. A 1.8 cm HCC with dense homogeneous uptake of Lipiodol in the right lobe. Many other smaller daughter nodules are also present.

Lipiodol-CT can therefore detect an HCC while it is still small.

Although most of the HCCs in our series detected by Lipiodol-CT were small, unfortunately 11 out of 34 (32.3%) were multicentric at the time of diagnosis. Moreover, many of our patients had severely impaired liver function and some of the solitary HCCs were situated deep within the liver making a wedge resection impossible. Notwithstanding these unfavourable features, 11 out of 34 HCCs (32.3%) were resectable. If only "small HCCs" were included, then nine out of 20 tumours (45%) were resectable. The resectability rate compares favourably with the 17.6% reported by Lee et al (1982), the 7.3% reported by Balasegaram (1975) and the 3% reported by Lai et al (1981).

We conclude that, as part of a screening programme for high risk patients, Lipiodol-CT is useful in the detection of HCCs while they are relatively small. In view of its ability to demonstrate daughter nodules at times not seen by conventional CT or hepatic angiography, the technique helps to determine whether the tumour is suitable for surgical resection or whether it would better be treated with chemotherapy, including transarterial chemo-embolization. In spite of the often multicentric nature of HCC, our results demonstrated that by detecting the tumour earlier, improvement in the previously reported resectability rate could be achieved.

References

ARMSTRONG, P. & BLACK, W. C., 1989. Optimum utilisation of radiological tests: the radiologist as advisor. *Clinical Radiology, 40,* 444–447.

BALASEGARAM, M., 1975. Management of primary liver cell carcinoma. *American Journal of Surgery, 130,* 33–37.

CHEN, D. S., SHEU, J. C., SUNG, J. L., LAI, M. Y., LEE, C. S., SU, C. T., TSANG, Y. M., HOW, S. W., WANG, T. H., YU, J. Y., YANG, T. H., WANG, C. Y. & HSU, C. Y., 1982. Small hepatocellular carcinoma—a clinicopathological study in thirteen patients. *Gastroenterology, 83,* 1109–1119.

CHOI, B. I., PARK, J. H., KIM, B. H., KIM, S. H., HAN, M. C. & KIM, C. W., 1989. Small hepatocellular carcinoma: detection with sonography, computed tomography (CT), angiography and Lipiodol-CT. *British Journal of Radiology, 62,* 897–903.

LAI, C. L., LAM, K. C., WONG, K. P., WU, P. C. & TODD, D., 1981. Clinical features of hepatocellular carcinoma: Review of 211 patients in Hong Kong. *Cancer, 47,* 2746–2755.

LEE, N. W., WONG, J. & ONG, G. B., 1982. The surgical management of primary carcinoma of the liver. *World Journal of Surgery, 6,* 66–75.

MAKI, S., KONNO, T. & MAEDA, H., 1985. Image enhancement in computerized tomography for sensitive diagnosis of liver cancer and semiquantitation of tumour selective drug targeting with oily contrast medium. *Cancer, 56,* 751–757.

OHISHI, H., UCHIDA, H., YOSHIMURA, H., OHUE, S., UEDA, J., KATSURAGI, M., MATSUO, N. & HOSOGI, Y., 1985. Hepatocellular carcinoma detected by iodized oil. Use of anticancer agents. *Radiology, 154,* 25–29.

RABY, N., KARANI, J., MICHELL, M., GIMSON, A., NUNNERLEY, H. & WILLIAMS, R., 1989. Lipiodol enhanced CT scanning in assessment of hepatocellular carcinoma. *Clinical Radiology, 40,* 480–485.

YUMOTO, Y., JINNO, K., TOKUYAMA, K., ARAKI, Y., ISHIMITSU, T., MAEDA, H., KONNO, T., IWAMOTO, S., OHNISHI, K. & OKUDA, K., 1985. Hepatocellular carcinoma detected by iodized oil. *Radiology, 154,* 19–24.

1990, *The British Journal of Radiology*, 63, 776–782

Quantitative γ-ray computed tomography of the radius in normal subjects and osteoporotic patients

By D. A. S. Smith, BSc, MD, FRCP, *C. J. Hosie, BSc, PhD, CPhys, A. D. Deacon, MB, ChB, FFARCS and †D. L. Hamblen, MB, BS, FRCS

Bone Metabolism Research Unit, Western Infirmary, *West of Scotland Health Boards, Department of Clinical Physics and Bio-engineering and †Department of Orthopaedic Surgery, Western Infirmary, Glasgow

(Received September 1989 and in final form May 1990)

Abstract. A new design of γ-ray computed tomography (CT) scanner was used to measure bone density in 516 normal adults and in 116 female patients with osteoporotic fractures. Trabecular bone density (TBD) was measured for a core of the ultradistal radius; cortical bone mass per unit length (MLS) and mass per unit volume (MVS) were computed for the radius shaft. TBD, MLS and MVS peaked at the age of about 40 in females and fell by 32%, 15% and 24%, respectively, by the age of 65. In males, TBD decreased from the third decade and MLS and MVS peaked in the fourth decade. The corresponding falls by 65 years were 20%, 6% and 7%. In patients with Colles' fracture TBD and MLS were reduced by 13% and 10%, respectively, relative to age matched normal female subjects. For patients with vertebral crush fracture the reductions relative to age matched normal females were 36%, 17% and 16% for TBD, MLS and MVS. In fracture patients the deficit in TBD was significantly greater than that for cortical bone but TBD was no better at discriminating normal and osteoporotic individuals because of its larger normal range. We conclude that γ-ray CT may best be used for monitoring changes in bone rather than as a diagnostic screening tool.

Osteoporosis is a common problem in the elderly and is associated with an increasing incidence of fractures of the distal forearm, spine and proximal end of the femur (Nilsson & Westlin, 1974; Riggs et al, 1982). The cost to the National Health Service of hospital care is estimated to be £700 million per year (Purdie, 1988). While other factors are involved, the reduced strength of bone is largely determined by reduced bone mass (Weaver & Chalmers, 1966; Smith & Smith, 1976). Bone densitometric studies indicate that bone loss is a long gradual process and that the pattern of bone loss is dependent on a number of factors including sex, age and measurement site (Riggs et al, 1981; Mazess, 1982). Two major objectives of bone densitometry are to select patients who are at high risk of osteoporotic fracture and to monitor patients' response to treatment.

Conventional single photon absorptiometry is limited to the measurement of predominantly cortical bone in the forearm (Wahner et al, 1985), while the fractures associated with osteoporosis occur at skeletal sites which have a high proportion of trabecular bone. Computed tomography (CT) is the only method which can separately measure trabecular and cortical bone. Cann and Genant (1980) pioneered the use of commercial whole-body CT scanners for quantitative measurement of the lumbar spine, while others have designed special purpose scanners for the peripheral skeleton (Ruegsegger et al, 1976; Hangartner & Overton, 1982). We have developed a new low radiation dose γ-ray CT scanner of this type for the precise measurement of trabecular and cortical bone mass in the radius (Hosie et al, 1985; Hosie & Smith, 1986). At present, data on age variation of trabecular bone in the radius is limited (Ruegsegger et al, 1981; Hesp et al, 1985).

In this paper we present new data on the age variation of trabecular and cortical bone density in the radius of normal adults. Measurements were also made on osteoporotic female patients to examine the relative usefulness of radial trabecular and cortical bone measurement in the diagnosis of osteoporosis.

Materials and methods

Computed tomographic measurements were made on the right radius of 338 healthy women aged 20–79 years and 178 healthy men aged 20–76 years. The subjects consisted of hospital staff, their relatives and friends, and visitors to the hospital. For each subject a questionnaire was completed and subjects who had conditions or medication likely to have affected bone mass were excluded from the trial. Bone density measurements were also made on the unfractured arm of 52 female patients aged 20–70 years (mean 56 years) with recent fracture of the wrist subsequent to minor trauma such as a fall from the standing position. Women who had a previous fracture or a condition related to bone mineral loss were not included. A further group of 64 women aged 52–80 years (mean 67 years) with known vertebral crush fracture were also measured. These osteoporotic women represented a random subgroup of patients entering a trial to assess their response to treatment.

The CT scanner used was of the second generation translation-rotation type equipped with an 18.5 GBq iodine-125 source (effective energy 28.5 keV) (Hosie et al, 1985). This design enabled the achievement of excellent long-term stability and low radiation dose of typically 0.4 mSv to the skin (Hosie & Smith, 1986). The

---

Address for correspondence: C. J. Hosie, PhD, West of Scotland Health Boards, Department of Clinical Physics and Bio-engineering, 11 West Graham Street, Glasgow G4 9LF.

ulnar length, between the palpable tip of the styloid process and the olecranon, was measured with the arm in extreme flexion using a specially manufactured gauge. Computed tomographic slice measurements (2 mm sections) were made of the radius at sites corresponding to 4% (ultradistal) and 25% (shaft) of the length of the ulna from the distal end. The ultradistal region is the usual site of Colles' fracture (Eastell et al, 1989). The tomograms represent arrays of linear attenuation coefficients for the mixture of bone and marrow in each picture element. To enable comparisons to be made with other techniques, the attenuation coefficients were converted to physical bone density under the assumption that the composition of bone marrow was the same for all subjects (Hangartner & Overton, 1982). For the ultradistal site the trabecular bone density (TBD) was computed for a 50% core of the radius. This core excluded the outer shell of cortical bone. At the shaft site, which contains very little trabecular bone, the bone cross-sectional area and the total bone mass per unit volume (MVS) were calculated. The mass per unit length at the shaft (MLS), which is equivalent to bone mineral content measured by single photon absorptiometry, was also computed in order to assess the effect of bone size on the diagnostic usefulness of the shaft measurement. The computation of bone density was carried out automatically and was independent of the operator. The long-term *in vivo* precision of the measurements were 0.7%, 1.6% and 1.4% for TBD, MVS and MLS, respectively (Hosie & Smith, 1986). The subjects' height was measured using a wall mounted height gauge and the unsupported stretch technique (subjects were told to stretch up maximally, but without the observer holding their head).

The age-decade bone density data were checked to ensure that each distribution was a normal Gaussian distribution. The significance of difference between age decades was computed using Student's t-test. The difference between fracture patients and age matched controls was assessed by the Wilcoxon paired rank test. Least squares linear regression analysis was used to assess the variation of height and bone area with age to relate bone density to height and weight.

Results

Normal women

The values obtained for the normal women are shown in Table I. There is no evidence of loss of height with age until 70–79 years when a 4% deficit is apparent. There is a 2.5% per decade increase in radial shaft area until the age group 70–79 years which shows an 8% fall compared with the previous decade. The mean ulna length was 4% shorter in this older group. TBD peaked at about the age of 40. A marked and highly significant mean fall of 19% was found in the 50–59 age group compared with the previous decade. A further large fall of 17% occurred in the seventh decade. The mean fall between the ages of 40 and 65 was 32%. Cortical bone MLS also peaked at the age of 40 and began to fall after the age of 50, although a statistically significant decrease relative to the previous decade was not found until the 60–69 age group. The mean fall by the age of 65 was 15%. A significant fall in MVS was found after the age of 40, with a total mean loss of 24% by the age of 65. A reduced normal range was noted for the area corrected radial shaft measurement (MVS), 9% (coefficient of variation (cov)) compared with 12% for MLS. There was no evidence of change in variance with age for any of the measured parameters.

Normal men

The mean height of the male subjects decreased by 1.3 cm (0.7%) per decade while the radial shaft area increased by 1% per decade (Table II). Trabecular bone

Table I. Ten-year means (and standard deviations) for height, weight and radial bone parameters in 338 women

Age group (years)	Number	Height (cm)	Weight (kg)	Radial shaft area (cm²)	Trabecular bone density (TBD) (g/cm³)	Mass per unit length shaft (MLS) (g/cm)	Mass per unit volume shaft (MVS) (g/cm³)
20–29	79	162.7 (5.8)	58.1 (8.5)	1.00 (0.13)	0.290 (0.071)	1.43 (0.14)	1.44 (0.12)
30–39	52	161.4 (6.8)	61.5^a (9.3)	1.01 (0.15)	0.307 (0.092)	1.48 (0.19)	1.47 (0.11)
40–49	55	159.9 (5.8)	62.3 (12.4)	1.03 (0.14)	0.308 (0.069)	1.45 (0.19)	1.42^a (0.15)
50–59	84	161.9 (6.3)	63.3 (9.5)	1.06 (0.15)	0.251^c (0.083)	1.39 (0.18)	1.32^c (0.13)
60–69	45	161.4 (5.6)	62.9 (10.3)	1.10 (0.14)	0.209^b (0.073)	1.23^c (0.21)	1.12^c (0.14)
70–79	23	155.6^c (6.7)	60.0 (9.8)	1.01 (0.16)	0.234 (0.087)	1.12^a (0.18)	1.11 (0.14)
25–44	113				0.304 (0.077)	1.46 (0.18)	1.45 (0.13)

$^a p < 0.05$, $^b p < 0.01$ and $^c p < 0.001$ (Student's t-test comparison with preceding decade).

Table II. Ten-year means (and standard deviations) for height, weight and radial bone parameters in 178 men

Age group (years)	Number	Height (cm)	Weight (kg)	Radial shaft area (cm^2)	Trabecular bone density (TBD) (g/cm^3)	Mass per unit length shaft (MLS) (g/cm)	Mass per unit volume shaft (MVS) (g/cm^3)
20–29	51	179.0 (7.4)	74.4 (11.5)	1.40 (0.21)	0.370 (0.080)	1.96 (0.22)	1.41 (0.12)
30–39	36	177.4 (7.0)	76.2 (10.0)	1.45 (0.21)	0.352 (0.095)	2.08^a (0.26)	1.44 (0.11)
40–49	22	175.3 (7.8)	76.1 (9.7)	1.40 (0.20)	0.351 (0.069)	2.01 (0.21)	1.45 (0.11)
50–59	26	174.2 (8.4)	76.6 (11.4)	1.47 (0.22)	0.325 (0.109)	1.94 (0.24)	1.34^b (0.15)
60–69	28	171.6 (5.7)	72.3 (10.6)	1.45 (0.18)	0.295 (0.096)	1.96 (0.27)	1.35 (0.14)
70–79	15	173.6 (8.8)	72.2 (14.9)	1.49 (0.23)	0.297 (0.079)	1.79^a (0.26)	1.22^a (0.18)
25–44	68				0.366 (0.092)	2.04 (0.25)	1.44 (0.11)

$^a p < 0.05$ and $^b p < 0.01$ (Student's t-test comparison with preceding decade).

Table III. Correlations between bone density parameters and height and weight in 113 women and 68 men aged 25–44 years

Bone parameter	Women		Men	
	Height	Weight	Height	Weight
TBD	−0.22^a	0.09	0.01	0.23
MLS	0.33^c	0.25^b	0.36^b	0.39^b
MVS	−0.27^b	−0.08	−0.04	−0.18
Area	0.46^c	0.26^b	0.31^a	0.39^b

$^a p < 0.05$.
$^b p < 0.01$.
$^c p < 0.001$.

density decreased from the third decade, falling by 20% by the age of 65. In young men the mean TBD was 17% higher than for similarly aged women. The cortical MLS peaked in the fourth decade at a value 41% greater than women and fell by 6% by the age of 65. MVS peaked at the age of about 40 with a 7% fall by the age of 65. Peak MVS was not different from that for women.

Correlation of bone density with height and weight

The correlation coefficients for the regression of bone densitities with age in 181 adults aged 25–44 years are presented in Table III. Trabecular bone density and cortical MVS were significantly negatively correlated with height in female subjects. Bone area and MLS were positively correlated with height and weight in both men and women.

Fracture patients

Osteoporotic fractures in women are relatively uncommon before the age of 45 (Knowelden et al, 1964). We have therefore arbitrarily defined low bone density for each measurement parameter as the fifth percentile of young normal adult women (25–44 years). A similar definition has been used by others (Nordin et al, 1980; Firooznia et al, 1984). The values for TBD, MLS and MVS were 0.177 g/cm^3, 1.17 g/cm and 1.23 g/cm^3, respectively. A previous study has shown, in women, no difference between left and right TBD and only a small difference (2%) between left and right MVS and MLS (Hosie, 1986). The measurements carried out

Table IV. Comparison of radial bone density in 52 patients with Colles' fracture of the wrist and normal subjects

Bone parameter	Age matched normals	Colles' patients	Deficit relative to age matched normals		Deficit relative to young adults	Percentage of patients below the 5th percentile young adults
			%	Z-score		
TBD (g/cm^3)	0.236 (0.098)	0.206 (0.060)	13^a	−0.31	32%^{b}	37
MLS (g/cm)	1.32 (0.20)	1.24 (0.17)	10^a	−0.36	15%^{b}	29
MVS (g/cm^3)	1.23 (0.19)	1.20 (0.18)	2	−0.15	17%^{b}	60

$^a p < 0.05$.
$^b p < 0.001$.

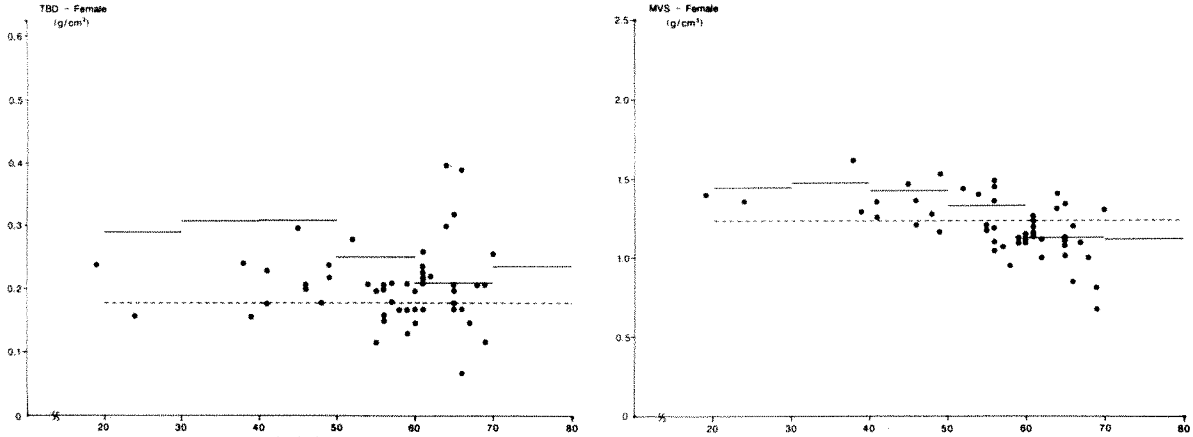

Figure 1. Bone density *versus* age for patients with Colles' fracture for TBD and MVS. The bars indicate 10-year means for normal females and the dotted line indicates the 5th percentile for young normal females.

on the left forearm in some fracture patients have therefore not been corrected.

Colles' fracture

The results of bone density measurements in patients with Colles' fracture of the wrist and control subjects are shown in Table IV and Fig. 1. TBD and MLS were significantly lower in the fracture patients compared with age matched normal subjects. There was no significant deficit in the MVS measurement. Relative to the young normal females the percentage deficit was greatest for trabecular bone ($p<0.001$), although the deficit was highly significant for all density measurements. MVS showed the largest proportion of patients with low bone density.

Vertebral crush fracture

Patients with crush fractures had significant reductions in both trabecular and cortical bone relative to age matched controls and young females (Table V, Fig. 2). Relative to the young adults, the percentage trabecular bone deficit in the fracture patients was greater than that for cortical bone ($p<0.001$).

Discussion

Increasing bone cross-sectional area with age is well known (Garn, 1972). We found that the increase in radial shaft area in males was less than that of females and may be partly explained by the males' reduction in stature with age. This is a cross-sectional study with some of the limitations inherent in such studies (Geusens et al, 1986). The younger subjects may have experienced different growth patterns compared with earlier generations. Thus apparently age-dependent trends, such as the males' decrease in height with age and the rather anomalous values of bone area and trabecular bone density for the oldest female group, might be in part due to this secular effect. The fall in

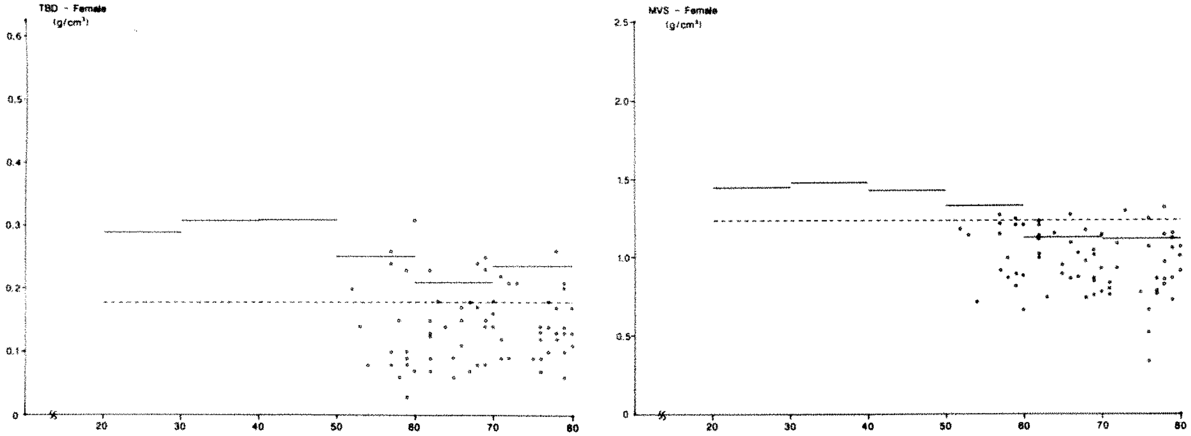

Figure 2. Bone density *versus* age for patients with vertebral fracture for TBD and MVS. The bars indicate 10-year means for normal females and the dotted line indicates the 5th percentile for young normal females.

Table V. Comparison of radial bone density in 64 patients with vertebral crush fracture and normal subjects

Bone parameter	Age matched normals	Crush fracture patients	Deficit relative to age matched normals		Deficit relative to young adults	Percentage of patients below the 5th percentile young adults
			%	Z-score		
TBD (g/cm^3)	0.221 (0.082)	0.141 (0.060)	36[a]	−0.98	54%[a]	78
MLS (g/cm)	1.21 (0.19)	1.01 (0.24)	17[a]	−1.08	31%[a]	73
MVS (g/cm^3)	1.16 (0.19)	0.98 (0.18)	16[a]	−1.18	33%[a]	89

[a] $p < 0.001$.

height with age in males was similar to that reported by Rosenbaum et al (1985). Loss of height with age in individuals is not simply related to osteoporotic vertebral fractures, but may also be attributable to loss of fluid and volume from intervertebral discs (Posner, 1988).

Many studies have been carried out to assess the age variation of cortical bone. Mazess (1982) has reviewed 10 reports and concluded that cortical bone mass in women peaks in the mid-thirties followed by a slow decline until age 45–50, when there is an accelerated loss of about 9% per decade. In men a steady loss of 3–4% per decade occurred after the age of 45. Similar results were found in our present study. For cortical MLS the average fall was 8% per decade in women and 3% in men. The continuing increase in the outer circumference of bone with age resulted in a greater percentage bone loss for MVS compared with MLS.

There is no consensus on the variation of trabecular bone density with age. The review paper by Mazess (1982) concluded that the decrease in trabecular density begins in young adulthood and continues at 6–8% per decade in both men and women. More recently, CT spinal measurements in women (Reinbold et al, 1986) have found trabecular bone density in the spine to peak at about 30 years and fall by up to 17% per decade in later life. In men bone loss at a rate of 0.9% per year was found (Genant et al, 1984). Compston et al (1988), using CT, have found a linear annual loss from the age of 20 of 0.8% in men and 1.1% in women. Similar annual rates of bone loss from the spine in women have been reported for dual photon absorptiometry measurement (Hansson & Roos, 1986; Riggs et al, 1986). Using a γ-ray CT scanner Ruegsegger et al (1984) found that trabecular bone in the distal tibia decreased in women at a rate of 0.8% per year after the age of 50. A cross-sectional study carried out in England using a similar scanner failed to show any significant loss in radial TBD until age 70 in women and 60 in men (Hesp et al, 1985). Longitudinal studies using various techniques have shown accelerated bone loss of between 3 and 9% per year immediately following the menopause (Genant et al, 1982; Nilas & Christiansen, 1988; Muller et al, 1989).

The present study finds that TBD in women peaks at about 40 years and falls steadily at up to 19% per decade. In men a steady loss of about 5% per decade was found beginning in young adulthood. In young adults TBD was 17% lower in women relative to men. By 65 years the difference was nearly 30%. Values for TBD measured in women aged 21–50 years were not significantly different from the values reported for a smaller group of subjects in England (Hesp et al, 1985). However, our study found TBD to start to fall 20 to 30 years earlier, resulting in a difference between the two populations of approximately 30% by the age of 65. While both scanners are of similar design, the added feature of a scout scan enabled our measurements to be carried out at a site approximately 10 mm more distal. The measurement of TBD in men aged 21 to 50 years was almost 10% higher in the English study. This may reflect the inclusion of some cortical bone at the more proximal measurement site rather than any significant geographical variation (Hosie, unpublished data). As with previous cross-sectional studies we were unable to detect an increase in bone loss immediately following the menopause. This is a reflection of the large normal variation in bone density in the population and the probable short duration of any accelerated bone loss.

In agreement with other studies of the peripheral skeleton, we found that bone mineral content of the radius shaft and bone area were positively correlated with subject height and weight (Garn, 1972; Hesp et al, 1985; Compston et al, 1988). When bone mineral content was corrected for bone width no significant correlation with height or weight was found (Hesp et al, 1985; Compston et al, 1988). The negative relation between height and TBD and MVS bone mineral density in the present study is probably a result of TBD and MVS being equivalent to bone mineral content divided by bone area, a second order correction.

Bone densitometry of the forearm has recently been shown to be a useful predictor of future osteoporotic fractures (Gardsell et al, 1989). There have been a number of other retrospective studies comparing patients with Colles' fracture and age matched controls. Significant deficits of between 3% and 12% have been reported for single photon absorptiometry of the forearm (Nilsson & Westlin, 1974; Nilas et al, 1987; Horowitz et al, 1988; Eastell et al, 1989). Using γ-ray CT, Hesp et al (1984) found a deficit in radial cortical MLS and trabecular TBD of 9% and 23%, respectively, in fracture patients. We have found a similar deficit in

MLS but, because of our lower values in older normal women, the reduction in trabecular bone was only 13% in patients. In agreement with this previous study, we found no difference between fracture patients and controls for the MVS measurement.

The deficits in both trabecular and cortical bone were greater in the vertebral crush fracture patients than in those with Colles' fracture. This is partly because the spine fracture patients were older and the density measurements were not carried out until some years after the first fracture occurred. Our finding of a 36% deficit in TBD in vertebral fracture patients relative to age matched normals is similar to that found for the tibia and radius using CT (Ruegsegger et al, 1984; Hesp et al, 1985) and greater than that reported for dual photon absorptiometry measurement of the spine (Riggs et al, 1981; Grubb et al, 1984). The 54% deficit relative to young adults is similar to that reported for CT of the spine (Reinbold et al, 1986). There is considerable overlap between osteoporotic fracture patients and age matched controls. While the control group were believed to be normal, and they were certainly asymptomatic, this group would almost certainly contain osteopaenic subjects who were at risk of fracture requiring only sufficient trauma.

In common with other studies we have found that the percentage deficit of trabecular bone was significantly greater than that of cortical bone for both Colles' and vertebral fracture patients (Riggs et al, 1981; Grubb et al, 1984; Hesp et al, 1985). However, we are unable to say that TBD is the best parameter to use in the diagnosis of osteoporosis. This is largely because of the relatively large normal range for trabecular bone. The statistical significance of the difference between fracture patients and age matched control subjects was similar for both MLS and TBD. MVS was the best discriminator of fracture patients and young normal adults. While we have found that there is no great advantage in a single measurement of trabecular bone in the diagnosis of osteoporosis, other researchers have used the high precision of peripheral TBD measurement to diagnose "fast" and "slow" bone losers following menopause and to monitor patients treated for osteoporosis (Muller et al, 1989; Ruegsegger et al, 1982). As a measure of cortical bone γ-ray CT is certainly more complex than single photon absorptiometry. However, it offers a number of advantages, such as the accurate measurement of bone cross-sectional area, and CT is unaffected by the unknown variable amount of fat in the surrounding soft tissue.

We have established the normal range and variation of trabecular and cortical bone in the distal radius. These data will be used to estimate if referred patients have abnormally low bone mass and if they are losing bone at a different rate from the normal population. We conclude however that γ-ray CT may best be used to monitor changes in trabecular bone during the course of disease and its response to treatment rather than as a diagnostic screening tool using a single measurement of bone density.

Acknowledgments

This work was supported by grants from the Scottish Home and Health Department, Tenovus-Scotland and the National Fund for Research into Crippling Diseases. We thank Eileen Miller for carrying out the bone density measurements.

References

CANN, C. E. & GENANT, H. K., 1980. Precise measurement of vertebral mineral content using computed tomography. *Journal of Computer Assisted Tomography*, *4*, 493–500.

COMPSTON, J. E., EVANS, W. D., CRAWLEY, E. O. & EVANS, C., 1988. Bone mineral content in normal UK subjects. *British Journal of Radiology*, *61*, 631–636.

EASTELL, R., WAHNER, H. W., O'FALLON, W. M., AMADIO, P. C., MELTON III, L. J. & RIGGS, B. L., 1989. Unequal decrease in bone density of the lumbar spine and ultradistal radius in Colles' and vertebral fracture syndromes. *Journal of Clinical Investigation*, *83*, 168–174.

FIROOZNIA, H., GOLIMBU, C., RAFII, M., SCHWARTZ, M. S. & ALTERMAN, E. R., 1984. Quantitative computed tomography assessment of spinal trabecular bone. II. In osteoporotic women with and without vertebral fractures. *CT: The Journal of Computed Tomography*, *8*, 99–103.

GARDSELL, P., JOHNELL, O. & NILSSON, B. E., 1989. Predicting fractures in women by using forearm bone densitometry. *Calcified Tissue International*, *44*, 235–242.

GARN, S. M., 1972. The course of bone gain and the phases of bone loss. *Orthopedic Clinics of North America*, *3*, 503–520.

GENANT, H. K., CANN, C. E., ETTINGER, B. & GORDAN, G. S., 1982. Quantitative computed tomography of the vertebral spongiosa: A sensitive method for detecting early bone loss after oöphorectomy. *Annals of Internal Medicine*, *97*, 699–705.

GENANT, H. K., CANN, C. E., ETTINGER, B., GORDAN, G. S., KOLB, F. O., REISER, I. & ARNAUD, C. D., 1984. Quantitative computed tomography for spinal mineral assessment. In *Osteoporosis*, ed. by C. Christiansen, C. D. Arnaud, B. E. C. Nordin, A. M. Parfitt, W. A. Peck and B. L. Riggs (Aalborg Stiftsbogtrykkeri), pp. 65–71.

GEUSENS, P., DEQUEKER, J., VERSTRAETEN, A. & NIJS, J., 1986. Age-, sex-, and menopause-related changes of vertebral and peripheral bone: Population study using dual and single photon absorptiometry and radiogrammetry. *Journal of Nuclear Medicine*, *27*, 1540–1549.

GRUBB, S. A., JACOBSEN, P. C., AWBREY, B. J., MCCARTNEY, W. H., VINCENT, L. M. & TALMAGE, R. V., 1984. Bone density in osteopenic women: A modified distal radius density measurement procedure to develop an "at risk" value for use in screening women. *Journal of Orthopaedic Research*, *2*, 322–327.

HANGARTNER, T. N. & OVERTON, T. R., 1982. Quantitative measurement of bone density using gamma-ray computed tomography. *Journal of Computer Assisted Tomography*, *6*, 1156–1162.

HANSSON, T. & ROOS, B., 1986. Age changes in the bone mineral of the lumbar spine in normal women. *Calcified Tissue International*, *38*, 249–251.

HESP, R., KLENERMAN, L. & PAGE, L., 1984. Decreased radial bone mass in Colles' fracture. *Acta Orthopaedica Scandinavica*, *55*, 573–575.

HESP, R., DORE, C., PAGE, L. & SUMMERS, R., 1985. Normal values for trabecular and cortical bone in the radius measured by computed tomography. *Clinical Physics and Physiological Measurement*, *4*, 303–310.

HOROWITZ, M., WISHART, J. M., BOCHNER, M., NEED, A. G., CHATTERTON, B. E. & NORDIN, B. E. C., 1988. Mineral density of bone in the forearm in premenopausal women with fractured wrists. *British Medical Journal, 297,* 1314–1315.

Hosie, C. J., 1986. Measurement of bone density using I-125 computed tomography. PhD Thesis (Council for National Academic Awards, London), pp. 240–242.

Hosie, C. J. & Smith, D. A. S., 1986. Precision of measurement of bone density with a special purpose computed tomography scanner. *British Journal of Radiology, 59,* 345–350.

Hosie, C. J., Richardson, W. & Gregory, N. L., 1985. A gamma-ray computed tomography scanner for the quantitative measurement of bone density. *Journal of Biomedical Engineering, 7,* 30–34.

Knowelden, J., Buhr, A. J. & Dunbar, O., 1964. Incidence of fractures in persons over 35 years of age. *British Journal of Preventative and Social Medicine, 18,* 130–141.

Mazess, R. B., 1982. On aging bone loss. *Clinical Orthopaedics and Related Research, 165,* 239–252.

Muller, A., Ruegsegger, E. & Ruegsegger, P., 1989. Peripheral QCT: a low risk procedure to identify women predisposed to osteoporosis. *Physics in Medicine and Biology, 34,* 741–749.

Nilas, L. & Christiansen, C., 1988. Rates of bone loss in normal women: evidence of accelerated trabecular bone loss after the menopause. *European Journal of Clinical Investigation, 18,* 529–534.

Nilas, L., Podenphant, J., Riis, B. J., Gotfredsen, A. & Christiansen, C., 1987. Usefulness of regional bone measurements in patients with osteoporotic fractures of the spine and distal forearm. *Journal of Nuclear Medicine, 28,* 960–965.

Nilsson, B. E. & Westlin, N. E., 1974. The bone mineral content in the forearm of women with Colles' fracture. *Acta Orthopaedica Scandinavica, 45,* 836–844.

Nordin, B. E. C., Heyburn, P. J., Peacock, M., Horsman, A., Aaron, J., Marshall, D. & Crilly, R. G., 1980. Osteoporosis and osteomalacia. *Clinics in Endocrinology and Metabolism, 9,* 177–205.

Posner, J. B., 1988. Intervertebral disc disease. In *Textbook of Medicine,* ed. by J. B. Wyngaarden and L. H. Smith (W. B. Saunders, Philadelphia), pp. 2252–2254.

Purdie, D. W., 1988. Broken bones—a gynaecological problem. *British Journal of Obstetrics and Gynaecology, 95,* 737–739.

Reinbold, W.-D., Genant, H. K., Reiser, U. J., Harris, S. T. & Ettinger, B., 1986. Bone mineral content in early-postmenopausal osteoporotic women: Comparison of measurement methods. *Radiology, 160,* 469–478.

Riggs, B. L., Wahner, H. W., Dunn, W. L., Mazess, R. B., Offord, K. P. & Melton III, L. J., 1981. Differential changes in bone mineral density of the appendicular and axial skeleton with aging. *Journal of Clinical Investigation, 67,* 328–335.

Riggs, B. L., Wahner, H. W., Seeman, E., Offord, K. P., Dunn, W. L., Mazess, R. B., Johnson, K. W. & Melton III, L. J., 1982. Changes in bone mineral density of the proximal femur and spine with aging. *Journal of Clinical Investigation, 70,* 716–723.

Riggs, B. L., Wahner, H. W., Melton III, L. J., Richelson, L. S., Judd, H. L. & Offord, K. P., 1986. Rates of bone loss in the appendicular and axial skeletons of women. *Journal of Clinical Investigation, 77,* 1487–1491.

Rosenbaum, S., Skinner, R. K., Knight, I. B. & Garrow, J. S., 1985. A survey of heights and weights of adults in Great Britain, 1980. *Annals of Human Biology, 12,* 115–127.

Ruegsegger, P., Elsasser, U., Anliker, M., Gnehm, H., Kind, H. & Prader, A., 1976. Quantification of bone mineralisation using computed tomography. *Radiology, 121,* 93–97.

Ruegsegger, P., Anliker, M. & Dambacher, M., 1981. Quantification of trabecular bone with low dose computed tomography. *Journal of Computer Assisted Tomography, 5,* 384–390.

Ruegsegger, P., Stebler, B. & Dambacher, M., 1982. Quantitative computed tomography of bone. *Mayo Clinic Proceedings, 57,* 96–103.

Ruegsegger, P. Dambacher, M. A., Ruegsegger, E., Fischer, J. A. & Anliker, M., 1984. Bone loss in premenopausal and postmenopausal women. *Journal of Bone and Joint Surgery, 66-A,* 1015–1023.

Smith, C. B. & Smith, D. A., 1976. Relations between age, mineral density and mechanical properties of human femoral compacta. *Acta Orthopaedica Scandinavica, 47,* 496–502.

Wahner, H. W., Eastell, R. & Riggs, B. L., 1985. Bone mineral density of the radius: Where do we stand? *Journal of Nuclear Medicine, 26,* 1339–1341.

Weaver, J. K. & Chalmers, J., 1966. Cancellous bone: Its strength and changes with aging and an evaluation of some methods for measuring its mineral content. *Journal of Bone and Joint Surgery, 48-A,* 289–308.

1990, *The British Journal of Radiology*, *63*, 783–786

Choroid plexus cysts and chromosomal defects

By J. G. Thorpe-Beeston, MRCOG, †C. M. Gosden, PhD and *K. H. Nicolaides, MRCOG

Harris Birthright Research Centre for Fetal Medicine, Department of Obstetrics and Gynaecology, King's College Hospital of Medicine and Dentistry, Denmark Hill, London SE5 8RX and †MRC Human Genetics Unit, Western General Hospital, Edinburgh EH4 2XU

(*Received January 1990 and in revised form April 1990*)

Abstract. During a 4-year period, 83 pregnant women with fetal choroid plexus cysts were investigated in our unit. Abnormal karyotypes were found in 20 fetuses, including trisomy 18 ($n=16$), trisomy 13 ($n=1$), triploidy ($n=1$) and translocation Down's syndrome ($n=2$). All fetuses with chromosomal defects had structural malformations in addition to the choroid plexus cysts.

The ultrasound diagnosis of fetal choroid plexus cysts was first reported in 1984; in all five fetuses the cysts had resolved spontaneously by 23 weeks and it was suggested that the cysts were of no pathological significance (Chudleigh et al, 1986). However, it was subsequently noted that if the cysts are associated with other malformations, such as cerebral ventriculomegaly, congenital diaphragmatic hernia, exomphalos or obstructive uropathy, they may indicate the presence of an underlying trisomy 18 (Nicolaides, 1986). A series of reports have since reinforced this possible association between choroid plexus cysts and chromosomal abnormalities (Ricketts et al, 1987; Furness, 1987; Chitkara et al, 1988; Ostlere et al, 1989; Khouzam & Hooker, 1989; Gabrielli et al, 1989). This study reports the findings in 83 fetuses with choroid plexus cysts that were examined in our centre.

Patients and methods

In a 4-year period (September 1985–November 1989) we investigated 83 cases of fetal choroid plexus cysts. The indication for referral to our centre included the detection of choroid plexus cysts ($n=39$) or other fetal malformations ($n=27$) at the routine ultrasound examination in the referring hospitals, pre-natal diagnosis of haemophilia A or epidermolysis bullosa ($n=2$), raised maternal serum alpha feto-protein ($n=4$), oligohydramnios ($n=3$) and fetal karyotyping for maternal age or low maternal alpha feto-protein ($n=8$).

In our centre, a detailed ultrasound examination was performed for fetal biometry and the exclusion or diagnosis of fetal malformations. The choroid plexuses were examined in the standard biparietal diameter view, but care was taken to examine both hemispheres and avoid the mistaken diagnosis of unilateral lesions. The best view to determine bilaterality is one midway between the transaxial and coronal sections (Fig. 1).

Subsequently, parents were counselled as to the possible association with chromosomal defects and it was explained that in the presence of additional malformations the risk was thought to be high whereas if the cysts were isolated the risk was likely to be extremely small. The parents were also told that the procedure related risks of fetal loss from the various invasive techniques for karyotying was approximately 1%.

In 46 of the cases, the parents requested fetal karyotyping and cordocentesis ($n=43$) or amniocentesis ($n=3$) was performed as an outpatient procedure. In all cases where karyotyping was not undertaken, and in those where the karyotype was normal, patients were rescanned at 4-weekly intervals until resolution of the cysts was observed. Subsequent management of the pregnancies was undertaken by the referring obstetricians, who also provided details on outcome.

Results

In 82 of the 83 cases the choroid plexus cysts were bilateral. The size of the cysts varied considerably, ranging from 3–21 mm in maximum diameter. No relationship was found between the size or shape of the cysts and other findings.

Additional malformations were found in 34 fetuses (Table I) and in all cases karyotyping was undertaken. In 20 (59%) of these fetuses there were chromosomal defects including trisomy 18 ($n=16$), trisomy 13 ($n=1$), triploidy ($n=1$) and translocation Down's syndrome ($n=2$). The predominant malformations in the chromosomally abnormal group were exomphalos ($n=7$), congenital diaphragmatic hernia ($n=4$), congenital heart disease ($n=5$), oesophageal atresia ($n=2$) and polyhydramnios ($n=3$). Furthermore, 16 of the 20 fetuses were severely growth retarded. The characteristic facial and digital defects of trisomy 18 and 13 were found in 14 cases. Both infants with translocation Down's syndrome had nuchal skin oedema. In contrast, in the chromosomally normal group the predominant associated malformations were renal.

In the chromosomally abnormal group, 18 of the 20 pregnancies were electively terminated and two resulted in an intrauterine or neonatal death. In the chromosomally normal group, six infants were liveborn and of

---

*Author for correspondence.

Table 1. Ultrasonic findings, karyotype and outcome of 34 fetuses with choroid plexus cysts and additional malformations

Case number	Gestational age (weeks)	Karyotype	Biometry	Other malformations	Outcome (weeks)
1	15	47,XY,+18	SGA	Exomphalos, strawberry head, atrioventriculoseptal defect	TOP (19)
2	17	47,XX,+18	SGA	Exomphalos, strawberry head, digital defects, facial cleft, mild hydronephrosis, ventriculoseptal defect	TOP (21)
3	18	47,XX,+18	SGA	Exomphalos, strawberry head	TOP (20)
4	18	47,XY,+18	SGA	Exomphalos, digital defects	TOP (19)
5	18	47,XY,+18	SGA	Exomphalos, digital defects, talipes, micrognathia, mild hydronephrosis	TOP (20)
6	20	46,XY,−14 +t(14q21q)	SGA	Nuchal oedema	TOP (22)
7	20	47,XX,+18	AGA	Diaphragmatic hernia, micrognathia, strawberry head, digital defects	TOP (22)
8	21	47,XY,+18	SGA	Diaphragmatic hernia, facial cleft	TOP (23)
9	21	47,XY,+18	SGA	"Absent stomach", digital defects, talipes	TOP (26)
10	21	47,XY,+18	SGA	Exomphalos, digital defects, ventriculoseptal defect, rocker-bottom feet	TOP (22)
11	22	47,XX,+18	SGA	Diaphragmatic hernia, facial cleft	TOP (22)
12	22	47,XX,+18	AGA	Digital defects, facial cleft, talipes	IUD (40)
13	23	47,XY,+18	AGA	Exomphalos, strawberry head, ventriculoseptal defect, digital defects	TOP (25)
14	24	46,XY,−14 +t(14q21q)	AGA	Ascites, skin oedema, mild hydronephrosis	TOP (25)
15	24	47,XY,+18	SGA	Diaphragmatic hernia, rocker-bottom feet	TOP (25)
16	24	47,XY,+18	SGA	Ventriculoseptal defect, talipes, strawberry head	TOP (25)
17	25	47,XX,+18	SGA	"Absent stomach", digital defects, strawberry head, micrognathia	TOP (26)
18	24	47,XY,+18	SGA	Strawberry head, micrognathia, digital defects	TOP (26)
19	27	69,XXX	SGA	Digital defects, microcephaly	TOP (27)
20	37	47,XY,+18	SGA	Posterior fossa cyst	NND
21	17	46,XY	AGA	Bilateral mild hydronephrosis	LB (41)
22	18	46,XY	AGA	Bilateral mild hydronephrosis	Continuing
23	18	46,XX	AGA	Exomphalos, kyphoscoliosis	TOP (22)
24	19	46,XY	AGA	Bilateral mild hydronephrosis	Continuing
25	19	46,XY	AGA	Bilateral severe hydronephrosis	TOP (22)
26	21	46,XY	AGA	Bilateral renal dysplasia, ascites	TOP (23)
27	21	46,XY	AGA	Ventriculoseptal defect, right multicystic renal dysplasia	LB (40)
28	21	46,XY	AGA	Bilateral mild hydronephrosis	LB (39)
29	21	46,XY	AGA	Bilateral mild hydronephrosis	LB (40)
30	21	46,XY	AGA	Bilateral severe hydronephrosis, kyphoscoliosis	TOP (23)
31	22	46,XX	AGA	Ventriculoseptal defect, bilateral mild hydronephrosis	LB (42)
32	24	46,XY	AGA	Bilateral severe hydronephrosis	TOP (27)
33	32	46,XX	AGA	Holoprosencephaly, facial cleft	NND
34	33	46,XY	SGA	Left moderate hydronephrosis, microcephaly	LB (39)

TOP: Termination of pregnancy.
IUD: Intrauterine death.
NND: Neonatal death.
SGA: Small for gestational age.
AGA: Appropriate for gestational age.
LB: Livebirth.

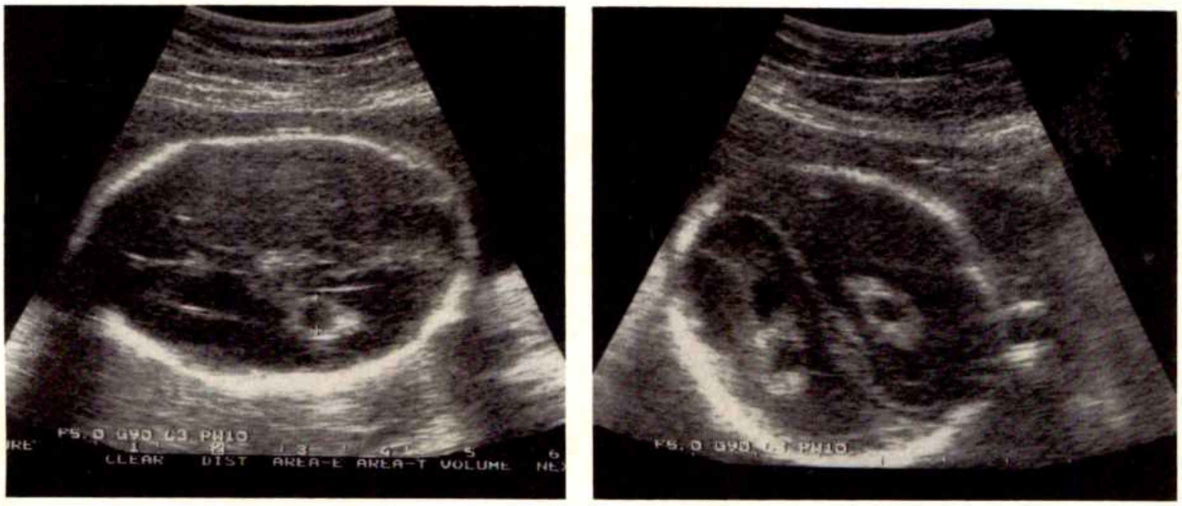

Figure 1. Coronal section demonstrating bilateral choroid plexus cysts.

these, one infant with Fallot's tetralogy underwent successful surgical repair and another with microcephaly, diagnosed in the post-natal period, died at 8 months of age. Five of the pregnancies were electively terminated because of the associated malformations. One infant with holoprosencephaly died in the neonatal period and two pregnancies are continuing.

In 49 of the 83 fetuses there were no additional malformations and in all but one case the cysts resolved by 28 weeks' gestation. In 12 pregnancies the mothers elected to have karyotyping performed and this was found to be normal. Forty-two pregnancies resulted in healthy normal livebirths, one pregnancy in an unexplained stillbirth at term with no detectable abnormality at post-mortem and one in an intrauterine death at 25 weeks, 9 weeks after a skin biopsy. Five pregnancies are continuing. In one case the cysts persisted throughout the antenatal period and were also present at the post-natal scan, but the infant, who is now 2 years old, has normal neurological development.

Discussion

The findings of this study confirm the association between choroid plexus cysts and chromosomal abnormalities. Although trisomy 18 is by far the commonest chromosomal defect, this is not exclusive as choroid plexus cysts were also present in one fetus with trisomy 13 and in two cases of translocation Downs' syndrome. All the chromosomally abnormal fetuses had additional malformations and in addition the majority of the fetuses were growth retarded. Therefore, the finding of choroid plexus cysts should prompt a diligent search for both major defects such as exomphalos and congenital diaphragmatic hernia but also for more subtle markers of trisomy 18 and 13 such as facial cleft, digital abnormalities, talipes, rocker-bottom feet and a strawberry shaped skull or prominent occiput. In the case of trisomy 21 the diagnosis may be suspected from a combination of features such as brachycephaly, relative shortening of the femur in relation to the biparietal diameter, nuchal skin oedema, atrio-ventricular septal defect, mild hydronephrosis and clinodactyly or hypoplasia of the midphalanx of the fifth finger.

In this series, chromosomal abnormalities were found in 59% of the fetuses noted to have choroid plexus cysts and additional malformations. These results are in agreement with the findings of Chitkara et al (1988) and Gabrielli et al (1989) who reported trisomy 18 in a total of five of seven cases of choroid plexus cysts in association with other structural anomalies seen at three referral centres. In these circumstances fetal karyotyping should be performed. Karyotyping is of value even in the third trimester of pregnancy, because knowledge that the fetus is chromosomally normal would allow the parents, obstetrician and paediatrician to discuss the appropriate mode, place and timing of delivery. Alternatively, if the fetus is chromosomally abnormal, the parents and attending obstetrician may decide that obstetric interventions, such as delivery by caesarean section, should be avoided. Fetal blood karyotyping can be achieved within 2–4 days, thereby alleviating parental anxiety associated with the 3–4 week delay in the UK if karyotyping from amniotic fluid. Karyotyping by placental biopsy using direct preparations of cytotrophoblastic cells can provide results in a few hours, but there is a significant risk of false positive results, especially for trisomy 18 and 13.

During the last 5 years in our centre, cordocentesis and fetal blood karyotyping was undertaken in 1265 cases. An abnormal karyotype was found in 204 cases. The most common were trisomy 18 ($n=56$), trisomy 13 ($n=19$), trisomy 21 ($n=36$) and triploidy ($n=30$). Choroid plexus cysts were present in 29%, 5%, 6% and 3% of the cases, respectively. Although the sensitivity is relatively low even for trisomy 18, it compares favourably with the sensitivity of screening for chromosomal defects on the basis of maternal age alone, which is approximately 25%. Furthermore, choroid plexus cysts are useful markers because they are easily seen in the standard biparietal view which is obtained for all routine ultrasound scans. Alternative lesions detected by ultrasound screening that may potentially have much higher sensitivities for chromosomal abnormalities are presently not easy to detect at a routine examination. For example, congenital heart disease, such as ventricular septal defects, may be found in 90–99% of fetuses with trisomy 13 and 18 and in 50–80% of those with trisomy 21; however, these defects may be impossible to detect even in the second trimester by specialist echocardiographers (Allan et al, 1984; Copel et al, 1986).

Choroid plexuses are derived from neuroepithelial folds. The aetiology is poorly understood but has been thought to be a variant of normal development. However, in some fetuses, as in our case with microcephaly, choroid plexus cysts may be a manifestation of abnormal brain development. The choroid plexus is easily visualized from 9 weeks' gestation when it occupies almost the entire hemisphere. Thereafter, and until 24 weeks' gestation, there is a rapid decrease in both the size of the choroid plexus and of the lateral cerebral ventricle in relation to the hemisphere. Therefore, in normal fetuses cysts are most commonly seen during this phase of a relatively large choroid plexus, and the vast majority will resolve by 24 weeks. Although the natural history of the cysts in chromosomally abnormal fetuses is less well documented, because many of the pregnancies are electively terminated, it is possible that the high incidence of these cysts may be another manifestation of the delayed neurological development in such fetuses.

At present there is considerable controversy as to whether fetal karyotyping should be undertaken for choroid plexus cysts found in the absence of other malformations. There are three reported cases of trisomy 18 or 21 where choroid plexus cysts were the only antenatal finding, but a chromosomal anomaly was detected post-natally (Ricketts et al, 1987; Furness, 1987; Ostlere, 1989). Furthermore, the possibility of isolated choroid plexus cysts being the sole abnormality in fetuses with trisomy 18 is strongly suggested by the extremely worrying findings of a very careful pathological study by Fitzsimons et al (1989). Although 12 of 14 fetuses with trisomy 18 studied at post-mortem had other structural anomalies, bilateral choroid plexus cysts were the only abnormality in two of their fetuses. It was intimated that the risk of finding isolated choroid plexus cysts in a fetus with trisomy 18 was higher than the risk of a 35-year-old woman having a child with trisomy 21 and therefore karyotyping in these circumstances is justified. Although this is an attractive argument, the risk of fetal loss as a consequence of invasive techniques should not be underestimated, particularly as improving ultrasound technology and training will undoubtedly lead to increased detection of this condition. This is already well demonstrated in the study of Ostlere et al (1989) who reported a trebling in the incidence of choroid plexus cysts at 16–18 weeks' gestation with improving resolution of the ultrasound equipment used.

Fetal choroid plexus cysts are found in 0.18–2.3% of pregnancies (Clark et al, 1989; Gabrielli et al, 1989). Their detection should be an indication for detailed ultrasonography and the search for other markers of chromosomal defects. In the absence of additional malformations the parents should be made aware of the existing controversies concerning the association with chromosomal defects and allowed to have fetal karyotyping if they wish. Furthermore, serial scans should be undertaken to document resolution of the cysts and normal brain devlopment.

References

ALLAN, L. D., CRAWFORD, D. C., ANDERSON, R. H. & TYNAN, M. J., 1984. Echocardiographic and anatomical correlations in fetal congenital heart disease. *British Heart Journal, 52,* 542–548.

CHITKARA, U., COGSWELL, C., NORTON, K., WILKINS, I. A., MEHALEK, K. & BERKOWITZ, R. L., 1989. Choroid plexus cysts in the fetus: A benign anatomic variant or pathologic entity? Report of 41 cases and review of the literature. *Obstetrics and Gynaecology, 72,* 185–189.

CHUDLEIGH, P., PEARCE, J. M. & CAMPBELL, S., 1986. The prenatal diagnosis of transient cysts of the fetal choroid plexus. *Prenatal Diagnosis, 4,* 135–137.

CLARK, S. L., DEVORE, G. R. & SABEY, P. L., 1989. Prenatal diagnosis of the fetal choroid plexus. *Obstetrics and Gynaecology, 72,* 585–586.

COPEL, J. A., PILU, G. & KLEINMAN, C. S., 1986. Congenital heart disease and extracardiac anomalies: associations and indications for fetal echocardiography. *American Journal of Obstetrics and Gynaecology, 154,* 1121–1132.

FITZSIMONS, J., WILSON, D., PASCOE-MASON, J., MEI SHAW, C., CYR, D. R. & MACK, L. A., 1989. Choroid plexus cysts in fetuses with trisomy 18. *Obstetrics and Gynaecology, 73,* 257–260.

FURNESS, M. E., 1987. Choroid plexus cysts and trisomy 18. *Lancet, 2,* 693.

GABRIELLI, S., REECE, A. R., PILU, G., PEROLO, A., RIZZO, N., BOVICELLI, L. & HOBBINS, J. C., 1989. The clinical significance of prenatally diagnosed choroid plexus cysts. *American Journal of Obstetrics and Gynaecology, 160,* 1207–1210.

KHOUZAM, M. N. & HOOKER, J. G., 1989. The significance of prenatal diagnosis of choroid plexus cysts. *Prenatal Diagnosis, 9,* 213–216.

NICOLAIDES, K. H., RODECK, C. H. & GOSDEN, C. M., 1986. Rapid karyotyping in non-lethal fetal malformations. *Lancet, 1,* 283–287.

OSTLERE, S. J., IRVING, H. C. & LILFORD, R. J., 1989. A prospective study of the incidence and significance of fetal choroid plexus cysts. *Prenatal Diagnosis, 9,* 205–211.

RICKETTS, N. E. M., LOWE, E. M. & PATEL, N. B., 1987. Prenatal diagnosis of choroid plexus cysts. *Lancet, 1,* 213–214.

1990, *The British Journal of Radiology*, *63*, 787–793

Ultrasonography in patients with suspected acute appendicitis: a prospective study

By P. Skaane, MD, *P. F. Amland, MD, T. Nordshus, MD and *K. Solheim, MD

Departments of Radiology and *Surgery, Ullevaal University Hospital, Oslo, Norway

(*Received March 1990 and in revised form May 1990*)

Abstract. The diagnostic accuracy of high-resolution real-time ultrasonography was prospectively studied in 240 patients admitted to the hospital with suspected acute appendicitis. The criteria for ultrasound diagnosis of appendicitis included a sausage-shaped, aperistaltic, hypoechoic structure when imaged along its longitudinal axis, with a target-like appearance on transverse section. The ultrasonographic findings were correlated with surgical-pathological outcome in 82 cases with proven appendicitis, with laparotomy findings in another 21 patients and with clinical follow-up in the remainder. The overall sensitivity, specificity and accuracy of ultrasonography in the diagnosis of acute appendicitis were 78%, 92% and 87%, respectively. The positive predictive value was 84% and the negative predictive value was 88%. Ultrasonography may significantly improve the diagnostic accuracy in patients with suspected acute appendicitis and should be performed in all patients in whom the clinical diagnosis is equivocal. The ultrasonographic findings must be interpreted in light of the clinical findings.

The diagnosis of acute appendicitis remains one of the most challenging in surgery. The rate of unnecessary laparotomy for suspected acute appendicitis is as high as 20–25%, and the perforation rate varies between 15% and 30% in most reported series (Lewis et al, 1975). It is difficult to reduce the negative appendicectomy rate without increasing the risk of perforation caused by delayed diagnosis. Most cases of acute appendicitis can be accurately diagnosed by a combination of careful history, physical examination and laboratory parameters of inflammation. The need for objective diagnostic methods has, however, been advocated to improve diagnostic accuracy. A variety of diagnostic approaches has been described, including intensive inpatient observation, predictive scoring systems, computer-aided diagnosis, conventional radiographic examinations, isotope scanning, computed tomography and laparoscopy (Hoffmann & Rasmussen, 1989). None of these procedures has, however, gained general acceptance in the pre-operative evaluation of patients with suspected acute appendicitis.

High-resolution real-time ultrasonography has recently been reported to be useful in the diagnosis of acute appendicitis. In a previous report we have compared the accuracy of ultrasonography and parameters of inflammation with that of clinical findings. Clinical judgment and ultrasonography were statistically highly significant as predictors of acute appendicitis, whereas none of the other predictors attained statistical significance (Amland et al, 1989). This report summarizes our experience with ultrasonography in the diagnosis of 240 patients with suspected acute appendicitis.

Materials and methods

During an 18-month period from September 1987 to May 1989, 240 patients (115 male and 125 female; age range 4–85 years; mean age 27.0 years) admitted to the department of surgery with a diagnosis of suspected acute appendicitis underwent ultrasonography. All patients were initially evaluated by a surgical resident or a staff surgeon and divided into one of the following three categories based on this initial clinical examination: (I) acute appendicitis, emergency operation indicated; (II) acute appendicitis equivocal, inpatient observation indicated; (III) acute appendicitis unlikely. The patients were then examined sonographically by a radiologist without knowledge of further clinical history or laboratory findings.

All ultrasonographic examinations were performed by radiologists (P.S. or T.N.) well trained in ultrasonography. The random choice of patients for the study was based on days when the patients could be examined by one of these two radiologists. All ultrasound studies were obtained with a 5 MHz linear-array transducer (General Electric RT 3000). The method of examination of the right lower quadrant was similar to the graded compression technique previously described (Puylaert, 1986). Unless an inflamed appendix was shown, compression was increased until bowel gas could be expressed from the area of interest. Gently reducing and then increasing the pressure of the transducer allowed assessment of compressibility of the normal bowel. If an inflamed appendix was not seen, an ultrasound survey of the adjacent regions, including liver and biliary system, right kidney, retroperitoneum and pelvis, using a 3.5 MHz sector scanner, was then usually performed.

The inflamed non-perforated appendix is seen as a sausage-shaped, non-compressible, blind-ending, hypoechoic structure usually with a thin echogenic rim surrounding the hypoechoic centre (Fig. 1a). On transverse section a target-like appearance is seen (Fig. 1b).

Address correspondence to Dr Per Skaane, Ullevaal University Hospital, Department of Radiology, Kirkeveien 166, N-0407 Oslo 4, Norway.

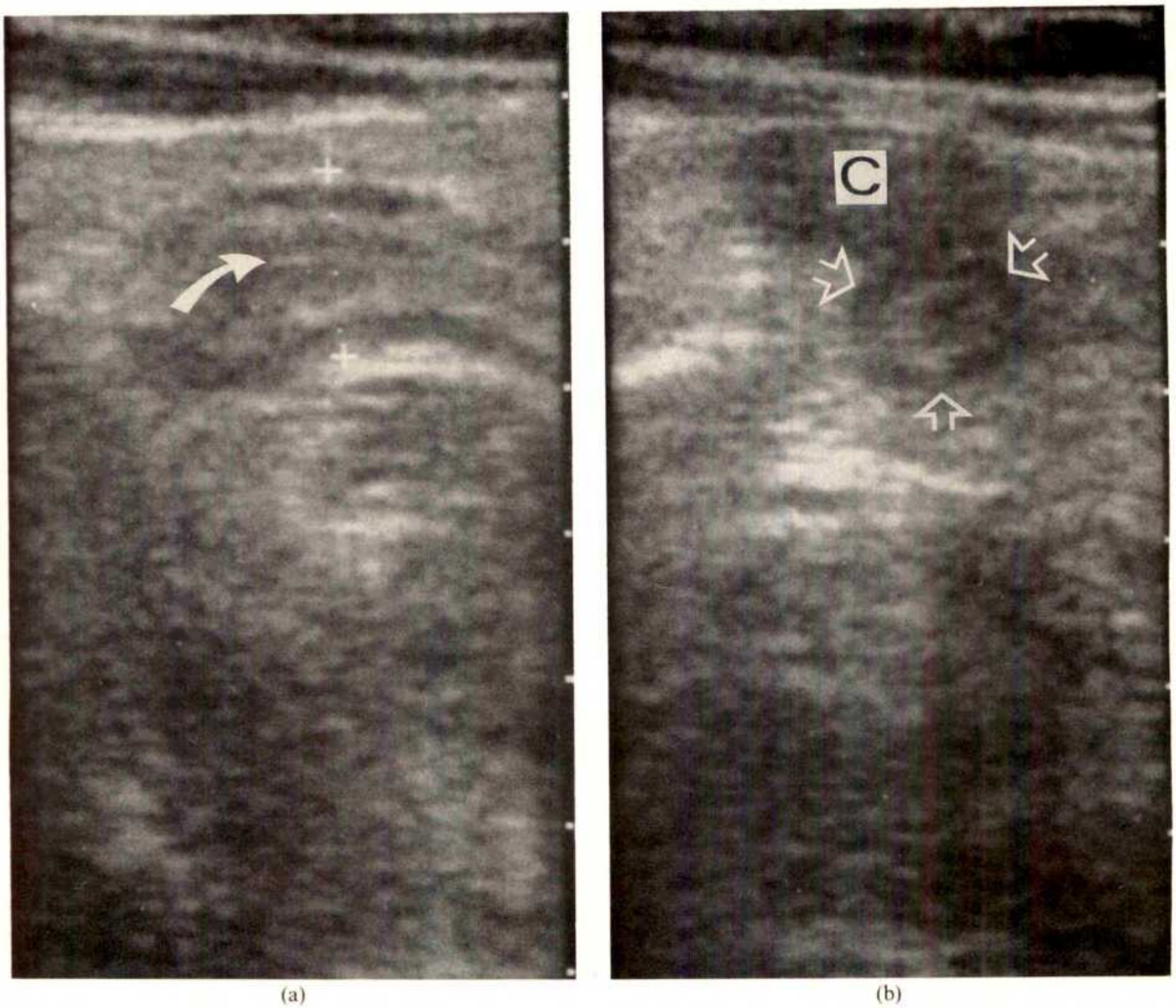

(a) (b)

Figure 1. (a) Longitudinal scan of an inflamed appendix showing a sausage-shaped structure with an outer diameter of 12 mm. The obliterated appendiceal lumen is indicated by a thin echogenic line (curved arrow). (b) On transverse scan the inflamed appendix appears as a "target-like" lesion (arrows) with a hypoechoic centre. The tip of the caecum (C) is seen anteriorly.

The echogenic layer may be absent and the inflamed appendix appears then as an anechoic tubular structure (Fig. 2a), with a "cyst-like" appearance on transverse section (Fig. 2b). The outer diameter of the non-perforated inflamed appendix is usually in the range of 7–15 mm. The size, shape, lack of peristalsis or of change in configuration and location help to differentiate the inflamed appendix from a fluid-filled loop of bowel. Appendicoliths are demonstrated as intraluminal hyperechoic foci with distal acoustic shadowing (Fig. 3). A hypoechoic mass adjacent to an inflamed appendix is consistent with periappendiceal abscess (Fig. 4). It was occasionally difficult to identify an inflamed appendix within a mixed hypoechoic-echogenic inflammatory mass (Fig. 5). Thickening of the adjacent caecal wall was occasionally found. Transverse and longitudinal views of the inflamed appendix were obtained with magnification. A negative sonographic diagnosis of appendicitis was based on non-visualization of the appendix. The ultrasonographic findings were reported to the surgeon, but the decision whether to operate was not based on the ultrasonographic diagnosis.

Final discharge records were reviewed for all patients included in the study. A true positive diagnosis of acute appendicitis was based on intra-operative findings and histological examination. In the group that did not undergo surgery, final diagnoses were substantiated by a combination of clinical findings, laboratory results, radiographic examinations, laparoscopy and clinical follow-up.

Results

Laparotomy for suspected acute appendicitis was carried out in 103 of the 240 patients, of which 82 had

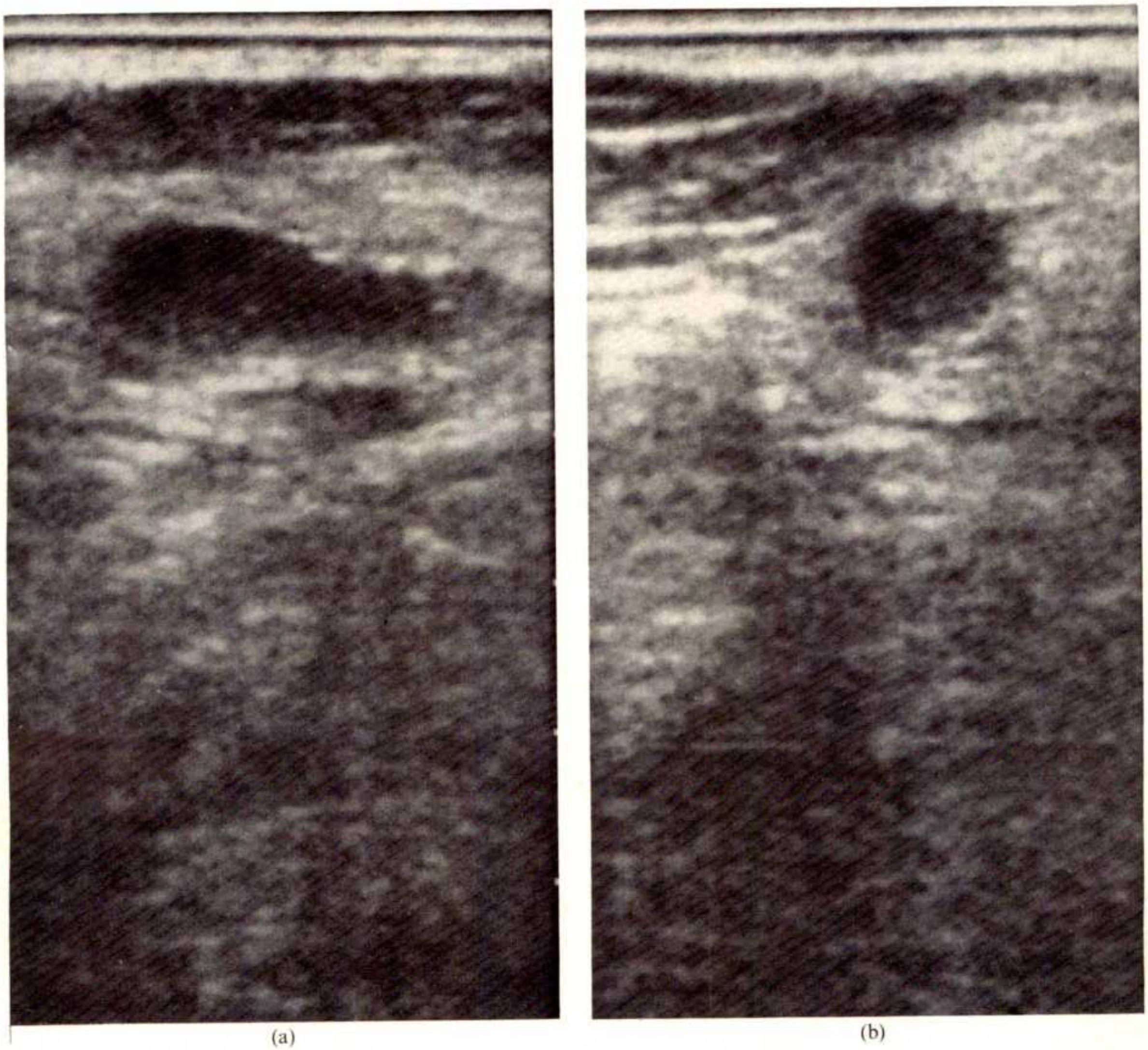

Figure 2. Acute appendicitis. (a) Longitudinal scan showing the inflamed appendix as a hypoechoic tubular structure. (b) The inflamed appendix appears as a small "cystic" mass on cross section.

proved acute appendicitis (Table I). Four patients with perforated appendicitis and periappendiceal abscess were treated conservatively with antibiotics. Thus, a total of 86 (35.8%) of the 240 patients included in the study had acute appendicitis (Table II). Six patients suffered from disorders justifying laparotomy, whereas 15 patients underwent unnecessary laparotomy (negative appendectomy rate 20.0% and negative laparotomy rate 14.6%).

True positive ultrasonographic diagnoses of acute appendicitis were made in 63 of the 82 cases proven at laparotomy and in all four cases manifest as a periappendiceal abscess. Thirty-nine (42.7%) of the 82 cases of acute appendicitis confirmed at laparotomy were classified as category I on initial clinical examination, whereas 63 (76.7%) of these 82 patients were correctly diagnosed on ultrasonography (Table I). Of the four patients with proved acute appendicitis classified as category III on initial clinical examination, two were correctly diagnosed on ultrasonography whereas the other two inflamed appendices were not seen (false negative ultrasonic diagnoses).

True negative ultrasonographic diagnoses were made in 141 patients (Table II). Of 15 patients with a normal finding on laparotomy and thus undergoing unnecessary laparotomy, three were classified as category I on initial clinical examination, 11 as category II and one as category III. Twelve of these 15 patients were diagnosed as normal on ultrasonography (true negative diagnoses) whereas appendicitis was suspected in three cases (false

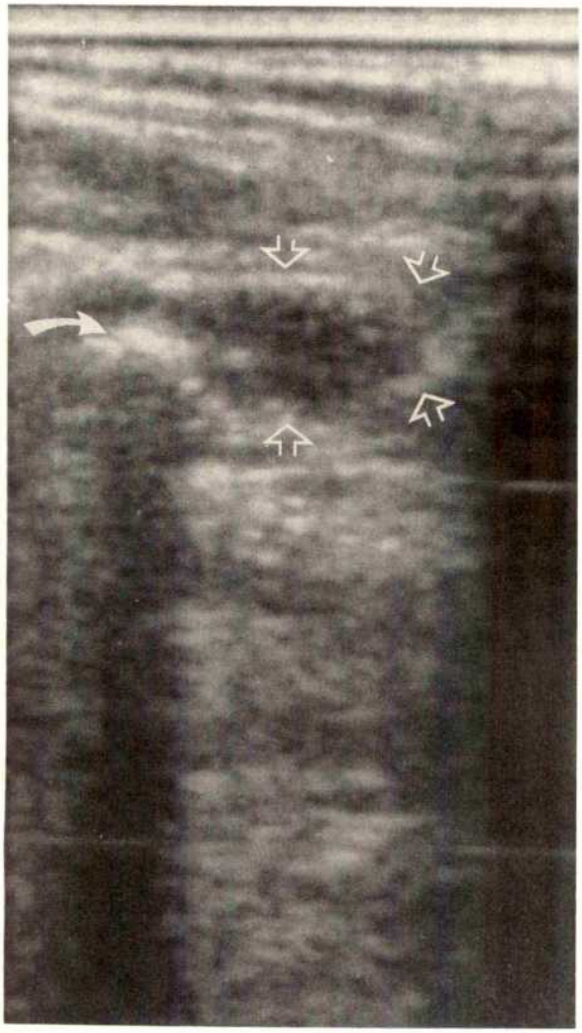

Figure 3. Longitudinal ultrasound scan of an inflamed appendix (arrowheads) demonstrating an appendicolith (curved arrow) within the appendiceal lumen with distal acoustic shadowing.

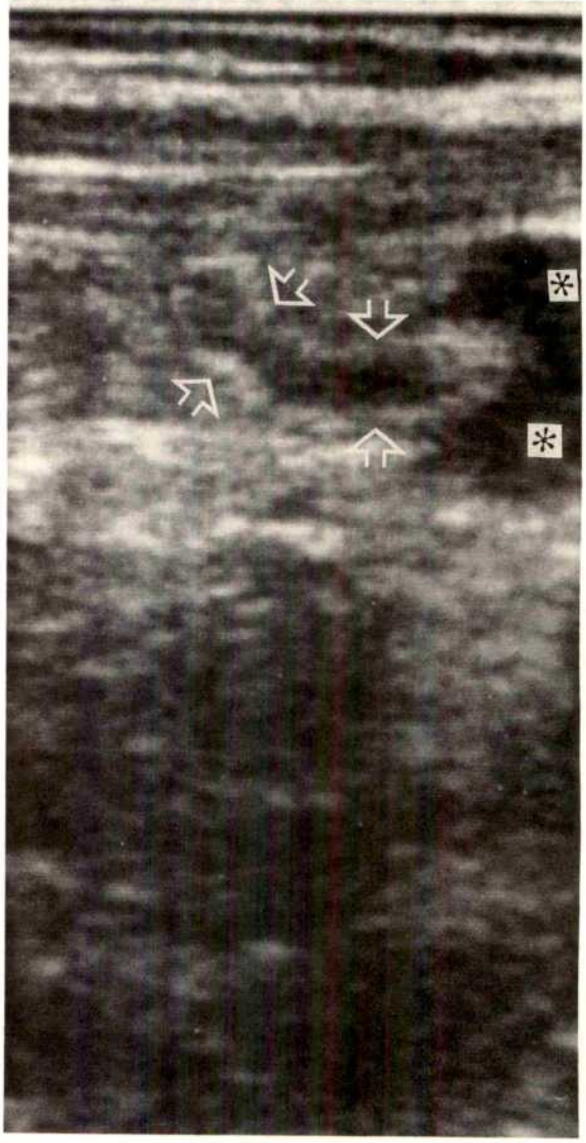

Figure 4. Perforated appendicitis. Longitudinal scan showing a sausage-shaped inflamed appendix (arrowheads). The anechoic mass (asterisks) around the tip of the appendix is consistent with abscess formation.

positive diagnoses), of whom one patient was classified as category I and two patients were classified as category II on initial clinical examination.

Of the 19 patients with false negative diagnoses (inflamed appendices not demonstrated on ultrasound), seven patients were classified as category I, 10 patients as category II and two patients as category III on initial clinical examination. Three of the 19 patients with false negative ultrasonic diagnoses had perforated appendicitis, six patients had retrocaecal appendices and two patients had inflamed appendices adherent to the surrounding mesentery manifest as an "omental mass" at operation. One of the eight other inflamed appendices showed inflammation only at the tip.

False positive sonographic diagnoses were made in 13 patients, of which one patient was classified as category I, 11 patients as category II, and one patient as category III on initial clinical examination (Table II). Three of the 13 patients were classified as false positive sonographic diagnoses although appendiceal abnormality was found on histological examination: lymphoid hyperplasia in a patient with terminal ileitis, granulocytes in the mucosa of a patient with ulcerative colitis and inflammation in the mesoappendix of unknown origin in a patient without any inflammatory changes in the appendix itself. These three cases were classified as

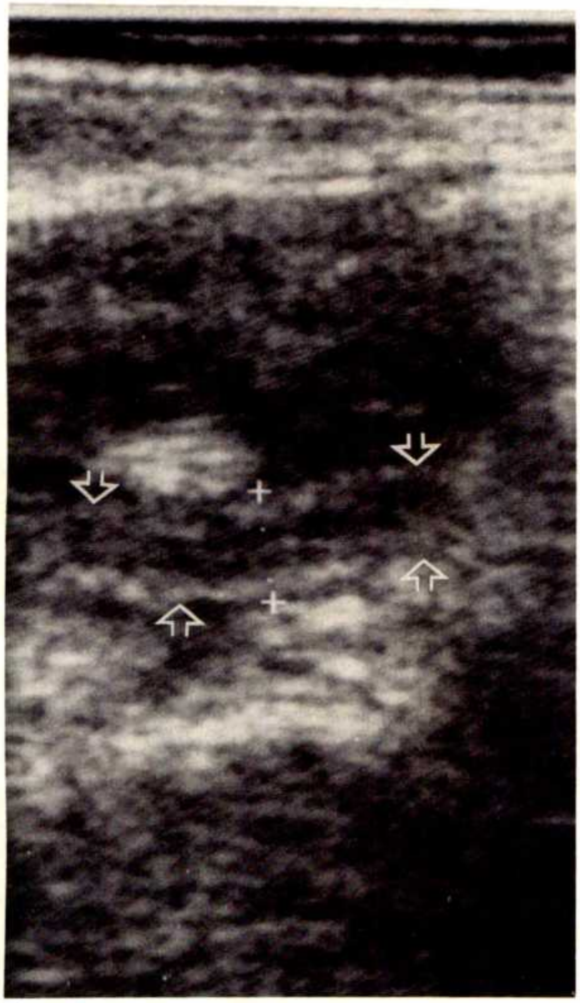

Figure 5. Perforated appendicitis. The inflamed appendix (arrowheads) with a diameter of 8 mm is localized eccentrically within the hypoechoic inflammatory mass.

false positive diagnoses because the ultrasonographic record films did not show findings consistent with appendicitis. Three patients had a final diagnosis of mesenteric lymphadenitis (Table III). Two patients had sonographic findings "characteristic" of acute appendicitis, and also laboratory findings were consistent with appendicitis in one of these two patients. However, the symptoms resolved spontaneously and laparotomy was not performed. Two patients with a false positive sonographic diagnosis proved to have gynecological disorders: one patient had a right-sided tubal pregnancy and the other patient had a ruptured corpus luteum cyst of the right ovary.

The overall sensitivity of sonography in the diagnosis of acute appendicitis in this study was 78% (ultrasonographer variability 59–88%), the overall specificity was 92% (ultrasonographer variability 87–95%) and the overall accuracy 87% (ultrasonographer variability 78–92%). The predictive value of a positive diagnosis was 84% (ultrasonographer variability 68–91%) and the negative predictive value was 88% (ultrasonographer variability 82–93%).

Discussion

The ultrasonographic appearance of an inflamed appendix is in by far the most cases quite different from the characteristic "target lesion" seen in benign and malignant conditions elsewhere in the gastrointestinal tract. This latter "target lesion" consists of a small hyperechoic centre surrounded by a thicker hypoechoic rim. On the other hand, the "target-like" appearance of the inflamed appendix on cross section consists of a hypoechoic centre surrounded by a thin hyperechoic rim (Fig. 1b). This appearance has been explained by purulent exudate filling the lumen and oedema of the mucosa (Karstrup et al, 1986). A thin echogenic line corresponding to the obliterated appendiceal lumen may occasionally be seen on longitudinal scans (Fig. 1a) (Puylaert, 1986). A "target lesion" as seen in conditions elsewhere in the gastrointestinal tract was found in only one patient in our study, and histological examination of this case revealed extensive mesoappendiceal inflammation due to perforating diverticulitis of the appendix. The detection rate of inflamed appendices by ultrasonography has been reported to depend on the severity of the inflammation (Takada et al, 1986). On the other hand, a lower sensitivity has been reported in patients with perforated appendicitis than in those with acute non-perforated appendicitis, probably owing to reflex rigidity preventing adequate compression, atonous dilatation of bowel loops caused by the peritonitis, and ill defined pus collections around the inflamed appendix (Puylaert et al, 1987). Ultrasonographic findings "typical" of acute appendicitis were seen in two patients

Table I. Comparison of initial clinical diagnosis and ultrasonography in 103 patients operated for suspected acute appendicitis

	Number	Clinical diagnosis			Ultrasonography			
		I	II	III	TP	TN	FP	FN
Surgically proved acute appendicitis	82	39	39	4	63	—	—	19
Normal appendix at laparotomy	21	5	15	1	—	15	6	—

TP = true positive.
TN = true negative.
FP = false positive.
FN = false negative.

Table II. Initial clinical diagnosis and ultrasonography in 240 patients with suspected acute appendicitis

Clinical category	Initial clinical diagnosis	Proved acute appendicitis	Ultrasonography			
			TP	TN	FP	FN
I	52	40	33	11	1	7
II	150	42	32	97	11	10
III	38	4	2	33	1	2
Total	240	86	67	141	13	19

TP = true positive.
TN = true negative.
FP = false positive.
FN = false negative.

in whom the symptoms resolved spontaneously and a laparotomy was not carried out. Both patients, categorized as group II on initial clinical examination, were classified as false positive ultrasonic diagnoses. However, we suggest that these two patients might have had spontaneously resolving appendicitis. Resolving appendicitis is a controversial subject, but the existence of this has been favoured by recent ultrasonographic studies (Takada et al, 1986; Jeffrey et al, 1987; Puylaert et al, 1987; Adams et al, 1988).

Ultrasonography may suggest alternative diagnoses in patients with clinically suspected acute appendicitis. A correct ultrasonic diagnosis has been reported in 70% of the patients without acute appendicitis, in whom a specific diagnosis was established (Gaensler et al, 1989). In our study, ultrasonography suggested the correct diagnosis in 23 (82%) of 28 patients with acute gynaecological diseases, an overall sensitivity which is similar to previous reports (Table III) (Gaensler et al, 1989). Furthermore, ultrasonography may be especially useful in differentiating appendicitis from mesenteric lymphadenitis and bacterial ileocaecitis (Puylaert et al, 1989). Enlarged mesenteric lymph nodes may occasionally be found in patients with acute appendicitis, but they are in general smaller and not as numerous as in patients with mesenteric lymphadenitis and bacterial ileocaecitis. The mural thickening of the terminal ileum in patients with bacterial ileocaecitis has usually an appearance different from an inflamed appendix, but the mural thickening of the terminal ileum and caecum as seen in bacterial ileocaecitis may easily be confused with Crohn's disease of the ileocaecal region (Puylaert et al, 1989). In our study, ultrasonography suggested the correct diagnosis in five (42%) of 12 patients with a final diagnosis of mesenteric lymphadenitis (Table III).

The overall sensitivity of 78%, specificity of 92% and accuracy of 87% are comparable to that of previous studies (Abu-Yousef et al, 1987; Adams et al, 1988). Specificity rate of 100% has been reported in two series (Puylaert et al, 1987; Kang et al, 1989). A high sensitivity rate of 89% has been reported, but in these studies "uncertain" and "non-diagnostic" groups on ultrasonography were excluded from the final evaluation (Adams et al, 1988; Jeffrey et al, 1987). Obesity, extensive gas-filled bowel loops or exquisite tenderness with severe abdominal guarding were noticed in our reports, but all these "non-diagnostic" examinations were classified as negative for appendicitis. We feel that surgeons are not at all pleased with equivocal ultrasonic diagnoses and have consequently abandoned this category. A high sensitivity rate and a high specificity rate of ultrasonography in the evaluation of 523 patients with suspected

Table III. Final diagnoses, initial clinical diagnoses, and ultrasonic diagnoses in 240 patients with suspected acute appendicitis

Final diagnosis	Number	Clinical diagnosis			Ultrasonography			
		I	II	III	+	−	Pos.	Neg.
Acute appendicitis	86	40	42	4	67	19	67	19
Mesenteric lymphadenitis	12	1	10	1	3	9	5	7
Gastroenteritis	17	0	13	4	1	16	1	16
Other gastrointestinal disorders	15	1	13	1	3	12	8	7
Non-specific abdominal pains	71	7	49	15	4	67	0	71
Gynaecological disorders	28	3	17	8	2	26	23	5
Urinary tract disorders	7	0	4	3	0	7	3	4
Other conditions	4	0	2	2	0	4	2	2
Total	240	52	150	38	80	160	109	131

Ultrasonography: + = acute appendicitis; − = appendix not seen; Pos. = final diagnosis suggested on ultrasound; Neg. = final diagnosis not suggested on ultrasound.

acute appendicitis has recently been reported (Schwerk et al, 1989).

Ultrasonography is recommended in patients with suspected acute appendicitis and equivocal clinical findings. Our study confirms the findings of previous studies that high-resolution real-time sonography is fairly accurate and specific, although slightly less sensitive in the diagnosis of acute appendicitis. Ultrasonography is of greatest value either when it definitively confirms appendicitis in patients with equivocal or atypical clinical findings or when it excludes appendicitis by diagnosing an alternative condition mimicking appendicitis. Patients with positive ultrasound findings and clinical or laboratory findings suggestive of appendicitis should undergo laparotomy. However, a small percentage of patients will have false positive ultrasonic examinations and the surgical decisions must rely on the clincal examination in conjunction with ultrasonography. In patients with a low clinical suspicion and negative ultrasonography, we recommend inpatient observation until symptoms resolve.

References

Abu-Yousef, M. M., Bleicher, J. J., Maher, J. W., Urdaneta, L. F., Franken, E. A. & Metcalf, A. M., 1987. High-resolution sonography of acute appendicitis. *American Journal of Roentgenology*, *149*, 53–58.

Adams, D. H., Fine, C. & Brooks, D. C. 1988. High-resolution real-time ultrasonography. A new tool in the diagnosis of acute appendicitis. *American Journal of Surgery*, *155*, 93–97.

Amland, P. F., Skaane, P., Rønningen, H., Nordshus, T. & Solheim, K., 1989. Ultrasonography and parameters of inflammation in acute appendicitis. A comparison with clinical findings. *Acta Chirurgica Scandinavica*, *155*, 185–189.

Gaensler, E. H. L., Jeffrey, R. B., Laing, F. C. & Townsend, R. R., 1989. Sonography in patients with suspected acute appendicitis: Value in establishing alternative diagnoses. *American Journal of Roentgenology*, *152*, 49–51.

Hoffmann, J. & Rasmussen, O. Ø., 1989. Aids in the diagnosis of acute appendicitis. *British Journal of Surgery*, *76*, 774–779.

Jeffrey, R. B., Laing, F. C. & Lewis, F. R., 1987. Acute appendicitis: High-resolution real-time US findings. *Radiology*, *163*, 11–14.

Kang, W. M., Lee, C. H., Chou, Y. H., Lin, H. J., Lo, H. C., Hu, S. C. & Peng, F. K., 1989. A clinical evaluation of ultrasonography in the diagnosis of acute appendicitis. *Surgery*, *105*, 154–159.

Karstrup, S., Torp-Pedersen, S. & Roikjaer, O., 1986. Ultrasonic visualisation of the inflamed appendix. *British Journal of Radiology*, *59*, 985–986.

Lewis, F. R., Holcroft, J. W., Boey, J. & Dunphy, J. E., 1975. Appendicitis. A critical review of diagnosis and treatment in 1000 cases. *Archives of Surgery*, *110*, 677–684.

Puylaert, J. B. C. M., 1986. Acute appendicitis: US evaluation using graded compression. *Radiology*, *158*, 355–360.

Puylaert, J. B. C. M., Rutgers, P. H., Lalisang, R. I., De Vries, B. C., van der Werf, S. D. J., Doerr, J. P. J. & Blok, R. A. P. R., 1987. A prospective study of ultrasonography in the diagnosis of appendicitis. *New England Journal of Medicine*, *317*, 666–669.

Puylaert, J. B. C. M., Vermeijden, R. J., van der Werf, S. D. J., Doornbos, L. & Koumans, R. K. J., 1989. Incidence and sonographic diagnosis of bacterial ileocaecitis masquerading as appendicitis. *Lancet*, *ii*, 84–86.

Schwerk, W. B., Wichtrup, B., Rothmund, M. & Rueschoff, J., 1989. Ultrasonography in the diagnosis of acute appendicitis: A prospective study. *Gastroenterology*, *97*, 630–639.

Takada, T., Yasuda, H., Uchiyama, K., Hasegawa, H. & Shikata, J. I., 1986. Ultrasonographic diagnosis of acute appendicitis in surgical indication. *International Surgery*, *71*, 9–13.

1990, *The British Journal of Radiology*, *63*, 794–797

Sedation in children scanned with high-field magnetic resonance; the experience at The Hospital for Sick Children, Great Ormond Street

By J. K. Shepherd, DCR, *M. A. Hall-Craggs, BA, MRCP(UK), FRCR, **J. P. Finn, MSc, MRCP(UK), FRCR and †R. M. Bingham, MB, BS, FFARCS

NMR Unit, Department of Radiology and †Anaesthetics Department, Hospital for Sick Children, Great Ormond Street, London WC1N 3JH

(*Received March 1990*)

Abstract. Patient movement is the most common cause of image degradation when performing magnetic resonance scans in children. This is a particular problem scanning at high field, as noise levels of up to 90 dB may be reached. Movement can be reduced by adequate sedation. We present the results of two sedation protocols when scanning with a 1.5T Magnetom scanner. Optimal scan quality can be achieved in up to 85% of scans using Pethco combined with triclofos in children aged 1 month–2 years, and trimeprazine combined with papaveretum in children over 2 years. When heavy sedation is used, patient selection must be cautious, and there is a minimum acceptable level of monitoring including close physical observation, electrocardiographic and apnoea monitoring.

Patient movement is the main cause of image degradation when performing magnetic resonance (MR) scans in children. At our hospital, a Siemens Magnetom MR scanner operating at 1.5T is used for imaging. Gradient switching during sequences generates noise levels of up to 90 dB (±5 dB), which is frightening for children and prevents speech being heard. For a successful abdominal scan, a child must be able to tolerate lying still for 1–2 hours, and must lie completely still for periods of up to 15 min during the data acquisition of each sequence. Most young children find it impossible to keep still for any length of time, yet in a scanner the child lies in a confined, enclosed space with restricted parental contact.

This problem can be partly solved by sedating children who are unable to tolerate these conditions. A number of different sedation regimens have been described for use in MR, most based on modifications of those used in computed tomography (CT) units. Most authors report having to sedate children up to the ages of 3–7-years (Smith, 1983; Cohen et al, 1986; Dietrich & Kangerloo, 1988). Chloral hydrate has been widely advocated in doses of 50–100 mg/kg (Cohen et al, 1986; Dietrich & Kangerloo, 1988), although Ringertz et al (1985) found pentobarbitone more successful than chloral. These studies have all been performed at low field, when the noise generated is a background hum. Because of the additional problems anticipated with the higher noise levels of a high-field system, a more aggressive approach to sedating children was adopted than that described by other investigators. The sedation protocols devised and the results of sedation are reported.

Patients and methods

Two sedation protocols were assessed. Initially, the protocol used for CT scanning in our hospital was adopted (Protocol 1, Fig. 1). All patients undergoing scans were sedated according to this regimen. Patient age, the region scanned, drugs administered, the requirement for a "top-up" with intravenous diazepam (Diazemuls®), and the total examination time were recorded. The quality of the examination was assessed and classified as optimal, suboptimal or as an abandoned procedure. An examination was considered optimal if a complete diagnostic scan, with insignificant movement artefact was obtained. If movement artefact significantly degraded images, or if the examination was curtailed because the patient awoke, the examination was classed as suboptimal. Scanning was abandoned when movement produced non-diagnostic images.

Early experience of this regimen suggested that the success rate in obtaining satisfactory scans was not adequate. A new protocol was devised (Protocol 2, Fig. 1), and the results of this compared with those of Protocol 1. The χ^2 test was used to analyse the statistical significance of the results.

Children were not sedated when parents refused permission for sedation, when the child was considered old enough (*i.e.* over 10 years) and co-operative enough to tolerate the procedure and when clinicians particularly wished that a younger, compliant child should be scanned without drugs. In these cases, whenever possible, the child was shown the scanner prior to the scan, was warned of the noise, and had a parent present

---

*Author for correspondence. M. A. H.-C. is a Research Fellow supported by Action Research for the Crippled Child.
**Present address: Department of Radiology, New England Deaconess Hospital, Boston, USA.

Protocol 1

Age	Weight	Sedation
<3months		Feed
3months -8years	<15kg	Pethco* 0.1ml/kg IM
	>15kg	Trimeprazine 3mg/kg PO +droperidol 0.7mg/4kg PO
>8years		Nothing or Trimeprazine 3mg/kg PO +droperidol 0.7mg/4kg PO

Drugs administered 40-60 minutes before the scan
Plus diazepam (Diazemuls™), 0.5mg/kg IV if necessary

Protocol 2

Age	Sedation
1 month - 2 years	Triclofos 50 mg/kg PO +Pethco* 0.06 ml/kg IM
2-5 years	Trimeprazine 3mg/kg PO +papaveretum 250 µg/kg IM
>5 years	Trimeprazine 3mg/kg PO +papaveretum 400 µg/kg IM

Drugs administered 40-60 minutes before the scan
Plus diazepam (Diazemuls™), 0.2-0.4mg/kg IV if necessary

* Pethidine 25mg, Promethazine 6.25mg, Chlorpromazine 6.25mg in 1ml

Figure 1. Sedation protocols.

during the scanning procedure. Parents were encouraged to hold the child's feet (hands are inaccessible), and to talk to the child between sequences.

Results

A total of 375 examinations was assessed and comparison of the results using Protocols 1 and 2 is shown in Table I.

Protocol 1

Pethco. Thirty-six patients with a mean age of 21 months (range 5 weeks–5 years) were sedated with Pethco alone (a combination of 25 mg pethidine, 6.25 mg promethazine and 6.25 mg chlorpromazine in 1 ml). Optimal scans were obtained in 66.7% of children scanned and 55% of patients required an intravenous "top-up" with Diazemuls.

Droperidol and trimeprazine. Seventy-nine patients with a mean age of 6.2 years (range 10 weeks–17 years) were sedated with droperidol and trimeprazine. Optimal scans were obtained in 74.7% of patients and 44% of children required a "top-up" with intravenous Diazemuls in addition to their initial sedation.

Protocol 2

Pethco and triclofos. Seventy-nine patients with a mean age of 9.5 months (range 1 week–28 months) were sedated with Pethco combined with triclofos. Optimal scans were obtained in 83.5% of patients scanned and 38% required a "top-up".

Trimeprazine and papaveretum. One hundred and twenty-seven patients with a mean age of 6.0 years (range 6 months–15 years) were sedated with trimeprazine and papaveretum. Optimal scans were obtained in 85% of children scanned and additional intravenous Diazemuls was required in 46% of children.

Patients receiving no sedation

Fifty-five children were scanned with no sedation given prior to the procedure. The mean age for this group was 11.7 years, with an range of 4–20 years, and the results are presented in Table II. Intravenous diazepam was given in three children (5.5%), and the scans were optimal in each case. The abandoned scans occurred in children aged 4, 8, 9, 9, 10 and 15 years.

Since the age profiles are similar, the results of Pethco alone can be compared with Pethco and triclofos, and droperidol and trimeprazine can be compared with papaveretum and trimeprazine. Compared with Pethco alone, combining Pethco with triclofos increased the proportion of optimal examinations from 67% to 84%, and reduced the number scans of less than optimal quality from 33% to 16% ($0.05>p>0.02$), despite an overall increase in examination time. Compared with trimeprazine and droperidol, papaveretum and trimeprazine increased the proportion of optimal scans from 75% to 85% and reduced the number of scans of less

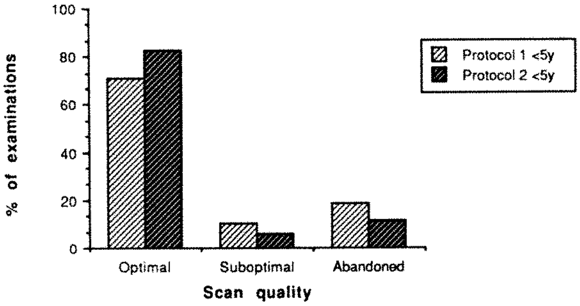

Figure 2. Scan quality using Protocol 1 compared with Protocol 2 in children under 5 years.

Table 1. Comparison of Protocols 1 and 2

	Protocol 1		Protocol 2	
	Pethco (%)	Trimeprazine and Droperidol (%)	Pethco and Triclofos (%)	Trimeprazine and Papaveratum (%)
Number	36	79	79	127
Age range	5 w–5 y	10 w–17 y	1 w–28 m	6 m–15 y
Mean age	21 m	6.2 y	9.5 m	6.0 y
Region scanned				
Head	27 (75)	47 (59.5)	50 (63.3)	82 (64.6)
Spine	4 (11.1)	18 (22.8)	6 (7.6)	18 (14.2)
Other	5 (13.9)	14 (17.7)	23 (29.1)	27 (21.3)
Scan quality				
Optimal	24 (66.7)	59 (74.7)	66 (83.5)	108 (85)
Suboptimal	3 (8.3)	11 (13.9)	6 (7.6)	7 (5.5)
Abandonded	9 (25)	9 (11.4)	7 (8.9)	12 (9.4)
Scan time (mins)				
< 30	2 (5.5)	4 (5.1)	1 (1.3)	4 (3.1)
30–60	18 (50)	48 (60.8)	25 (31.6)	47 (37.0)
61–90	11 (30.5)	16 (20.3)	35 (44.3)	52 (40.9)
> 90	5 (13.8)	11 (13.9)	18 (22.8)	24 (18.9)

than optimal quality from 25% to 15% ($0.05 > p > 0.02$), despite increased examination times.

Alternatively, the two protocols can be compared by age group, and the results for each protocol in children (a) under and (b) over 5 years are shown in Table III and Figs 2 and 3. Modifying the sedation protocol improved the proportion of optimal examinations from 71% to 83% for children under 5 years ($0.10 > p > 0.05$), and from 75.5% to 88% ($0.10 > p > 0.05$) in children over 5 years.

Unwanted effects

Two patients sedated with Pethco developed upper airway obstruction when placed in the supine position within the scanner. Both children recovered when placed in the "coma" position and a scan was not attempted in either child. One child with Stage 4S neuroblastoma, with extensive hepatic infiltration slept for a prolonged period (24 h), after being sedated with Pethco and triclofos.

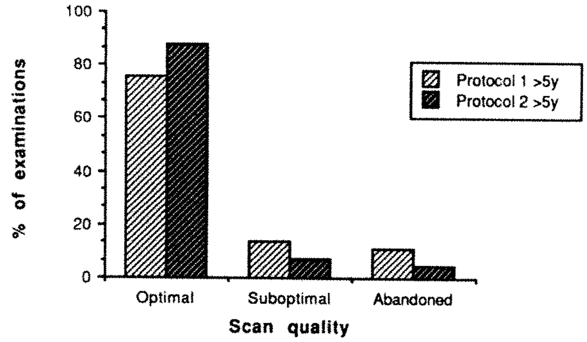

Figure 3. Scan quality using Protocol 1 compared with Protocol 2 in children over 5 years.

Discussion

The difference between sedation and general anaesthesia lies in the potential for patients to be roused by harmful, noxious stimuli. A sedated patient should be

Table II. Patients scanned without sedation

	Total (%)
Number	55
Age range	4 y–20 y
Mean age	11.65 y
Region scanned	
Head	27 (49.1)
Spine	20 (36.4)
Other	8 (14.5)
Scan quality	
Optimal	38 (69.1)
Suboptimal	11 (20)
Abandoned	6 (10.9)
Scale time (mins)	
< 30	2 (3.6)
30–60	36 (65.5)
61–90	12 (21.8)
> 90	5 (9.1)

Table III. Comparison of Protocols 1 and 2 by age

	Protocol 1		Protocol 2	
	Under 5 y (%)	Over 5 y (%)	Under 5 y (%)	Over 5 y (%)
Number	70	45	122	83
Age range	10 w–4 y 11 m	5–17 y	1 w–4 y 11 m	5–15 y
Mean age	2.5 y	8.9 y	1.5 y	7.6 y
Region scanned				
Head	49	25	79	53
Spine	8	13	10	14
Other	13	7	34	16
Scan quality				
Optimal	50 (71.4)	34 (75.6)	101 (82.8)	73 (88)
Suboptimal	7 (10)	6 (13.3)	7 (5.7)	6 (7.2)
Abandoned	13 (18.6)	5 (11.1)	14 (11.5)	4 (4.8)

able to protect himself from the damaging effects of such stimuli, and should not require the full-time attention of an anaesthetist. In practice, it is difficult to draw such a clear distinction since sedation is designed to prevent arousal to mildly noxious stimuli. In the case of MR scanning, this includes the discomfort of lying still for prolonged periods and the high noise levels. Since there is considerable individual variation in response to sedative drugs, it is difficult to avoid unwanted side effects in some patients, if success is to be achieved in the majority.

The most serious unwanted effect is respiratory depression and, because of this, we tried to avoid the exclusive use of opioids. Nevertheless, intramuscular opioids give very reliable sedation, hence when the protocol was modified, an injected opioid (papaveretum) was combined with an oral hypnotic in older children. In younger children, triclofos, which has little effect on respiration, was chosen in combination with Pethco, a recognized respiratory depressant. Naloxone reverses the respiratory depressive action of narcotic analgesics, and as a precaution, is kept available at all times.

As with any sedative technique, care must be exercised in the choice of patient. There are four groups of patients in whom sedation should be used with extreme caution.

(1) Those with upper airway abnormalities causing obstruction, including obstructive sleep apnoea syndrome.
(2) Those with abnormalities of the respiratory centre, *e.g.* mitochondrial cytopathies and brain stem tumours, or conditions causing desensitization of the respiratory centre to carbon dioxide, *e.g.* chronic lung disease with a raised carbon dioxide level.
(3) Those with abnormalities of metabolism or excretion, *e.g.* renal and hepatic dysfunction. This group also includes normal neonates (*i.e.* children less than 45 weeks gestational age), in whom the pharmacokinetics of sedative drugs are extremely variable.
(4) Those with conditions in which a rise in carbon dioxide levels would be detrimental, in particular patients with raised intracranial pressure.

Modifying the sedation protocol has increased the proportion of children successfully scanned. If sedation is inadequate, either the scan has to be abandoned or performed under general anaesthesia. This has cost and time implications, and general anaesthesia may be undesirable in a child undergoing further anaesthetics for other investigative procedures or surgery.

Because of the individual variation in response to sedative drugs, and because the doses used in these protocols are at the upper end of those which may be safely used, adequate monitoring of vital functions is essential. This is very difficult in the setting of a high-field strength MR scanner. We feel that close physical observation, supplemented by electrocardiogram and apnoea monitoring (Graseby Medical MR 10) is the minimum acceptable. Pulse oximetry would be ideal but despite trying several we have not, as yet, found an oximeter which performs reliably within the bore of the magnet, operating at high field.

References

Cohen, M. D., Weetman, R. W., Provisor, A. J., Grosfeld, J. L., West, K. W., Cory, D. A., Smith, J. A. & McGuire, W., 1986. Efficacy of magnetic resonance imaging in 139 children with tumors. *Archives of Surgery, 121,* 522–529.

Dietrich, R. B. & Kangerloo, H., 1988. Pediatric body imaging. In *Magnetic Resonance Imaging*, ed. by D. D. Stark and W. G. Bradley (Mosby, St. Louis), pp. 1434–1452.

Ringertz, H. G., Brasch, R. C. & Gooding, C. A., 1985. Artifacts, variants, and factors degrading image quality in pediatric magnetic resonance imaging. *Pediatric Radiology, 15,* 173–178.

Smith, F. W., 1983. The value of NMR imaging in pediatric practice: A preliminary report. *Pediatric Radiology, 13,* 141–147.

1990, *The British Journal of Radiology*, 63, 798–800

Technical notes

A man with three knees? False "hot spot" with dual isotope imaging

By *K. A. Miles, MB, BS, FRCR and †R. W. Barber, MSc, MInstP

Department of Nuclear Medicine and †Department of Medical Physics, Addenbrooke's Hospital, Hills Road, Cambridge

(*Received February 1990*)

Radionuclide imaging is subject to a wide range of potential artefacts. We have recently come across an unusual example which we have not seen previously described (Wells & Bernier, 1988; Ryo et al, 1985) . A 66-year-old man presented with a pyrexia, 3 months after undergoing bilateral upper tibial osteotomies. The patient was referred for a ^{99}Tc^{m} methylene diphosphonate (MDP) bone scan followed by ^{111}In labelled white blood cell (WBC) scanning to determine whether one of the osteotomy sites was infected. Three hours before imaging, 400 MBq of ^{99}Tc^{m} MDP was administered. Blood was taken for white cell labelling 90 min prior to MDP imaging. The MDP images showed intense uptake at the osteotomy sites, but were otherwise normal (Fig. 1a).

Immediately after the MDP bone scan images had been obtained, 15.4 MBq of ^{111}In WBC were injected. Three hours later, the knees were imaged with the same gamma camera (IGE 400A) fitted with a high energy collimator. Energy windows were reset to include the two ^{111}In peaks at 170 and 245 keV. An area of activity was seen at the site of each osteotomy with an additional area located between the knees (Fig. 1b). This additional area of activity proved not to be contamination as it could be eliminated by moving one or other knee out of the field of view. The artefact was not seen when images were obtained at 21 h, the only abnormality being low grade activity in the right knee with a synovial distribution.

It was suggested that the artefact resulted from technetium photons arising from each osteotomy site entering the camera simultaneously, with summation of their energies to create an event falling within the indium window but positioned between the two osteotomy sites. To confirm this, and to evaluate the phenomenon further, two technetium sources were imaged on the gamma camera with 5 cm of scatter material placed between the sources and the collimator. The experiment was repeated using pairs of technetium sources of 50,

---

*Author for correspondence.

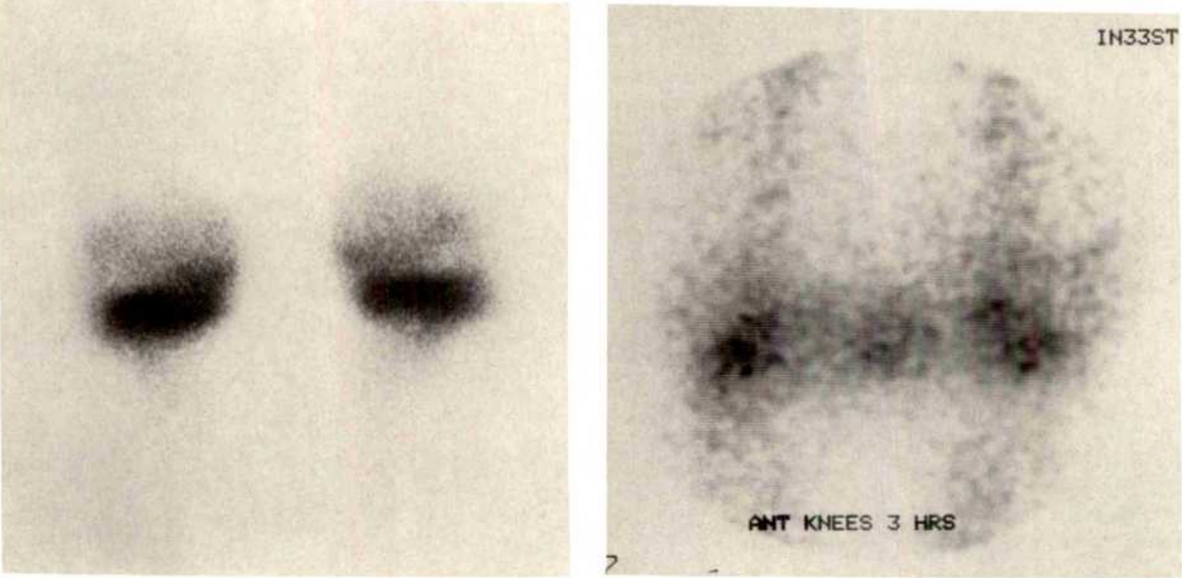

(a) (b)

Figure 1. (a) Technetium-99m MDP image demonstrating increased activity at the osteotomy sites. (b) Image collected using indium window demonstrating false hot spot between the knees (third knee!)

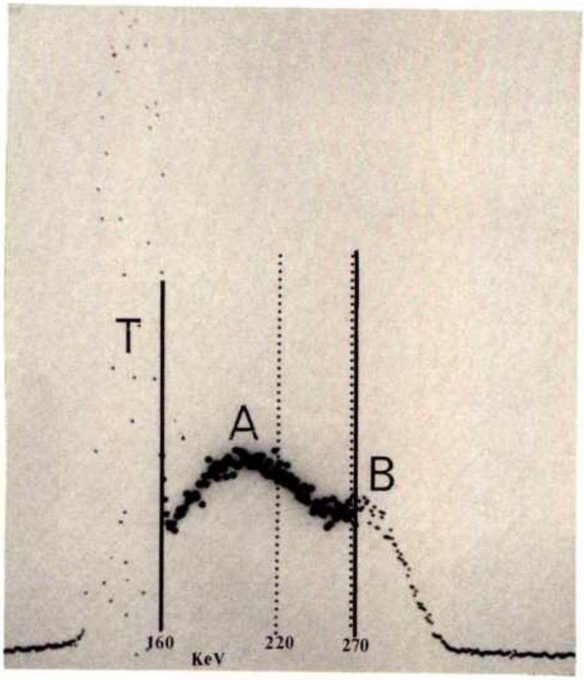

Figure 2. Pulse-height spectrum obtained from two $^{99}Tc^m$ sources. The technetium 140 keV photopeak (T) has been allowed to overflow. Secondary scatter (A) and 280 keV sum peak (B) fall within the wide (solid line) and narrow (dotted line) ^{111}In windows.

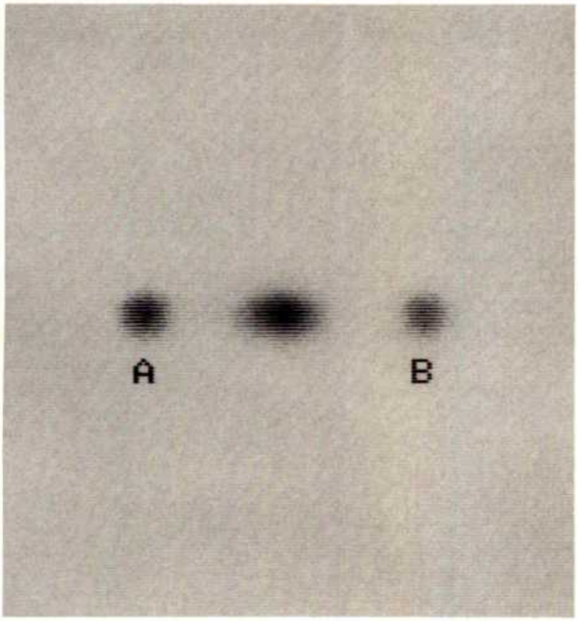

Figure 3. Simulation of artefact showing apparent activity in the region of the two technetium sources (A and B), and between them.

100 and 200 MBq and the count rates for each pair were measured in the technetium window and in two indium windows: a narrow window (220–270 keV) and a wide window (160–270 keV). The count-rates were also compared with the count-rates in the indium windows from a small (7 MBq) ^{111}In source (Table I). Examples of pulse-height spectra were also recorded (Fig. 2).

The artefact was reproduced (Fig. 3) when imaging with either of the indium windows, but not seen when using the technetium window.

Discussion

It is well known when imaging in dual energy mode that scattered events from the higher energy nuclide will appear in the lower energy window. It is perhaps not so well known that events can occur in the higher energy window from the lower energy nuclide.

The images and pulse-height spectra obtained from the pairs of technetium sources confirmed the presence of recorded events in the indium windows. These events arise from the inability of the gamma camera to process the pulses correctly from two events closely spaced in time. The pulses "pile-up" and are treated by the gamma camera as a single event whose energy is the sum of the energies of the individual events. The pulse-height spectrum of energies above the photopeak of technetium (Fig. 2) shows a peak at 280 keV due to the summation of two unscattered 140 keV photons. Other events above the technetium photopeak arise from the summation of two scattered photons, or one scattered and one unscattered photon. Activity localized over the two sources themselves (Fig. 3) results from the summation of two photons from the same source, whereas the activity between the sources results from summation of one photon from each source. In both cases the summed event is positioned between the two original interactions. Horton et al (1978) show two examples of such an effect when imaging technetium with an energy window centred on 280 keV. Sorenson (1987) shows a similar effect when imaging with a technetium window, but this did not create an observable artefact in the $^{99}Tc^m$ MDP images of the patient.

The data in Table I show that, as the activity of

Table I. Count rates from paired $^{99}Tc^m$ and single ^{111}In sources. High energy collimator: 5 cm scatter. Count s^{-1} MBq^{-1} (background corrected)

Window Source	125–155 keV	160–270 keV	220–270 keV
2 × 200 MBq $^{99}Tc^m$	65.5	2.65	1.16
2 × 100 MBq $^{99}Tc^m$	70.4	1.58	0.67
2 × 50 MBq $^{99}Tc^m$	74.0	0.77	0.35
1 × 7 MBq ^{111}In	48.4	168	62

1990, *The British Journal of Radiology*, *63*, 800–801

technetium increases, there is a loss of counts from the technetium window, but an increase in the appearance of "false" counts in the indium windows. The effect is clearly related to the dead-time of the gamma camera. Although the count-rate per MBq of technetium appearing in the indium windows is much less than the count-rate per MBq of indium, when there is significantly more technetium than indium activity in the patient it is possible that "false" indium counts could exceed "true" indium counts. It is also clear that there is little to gain by attempting to reduce the effect by adjusting the indium window. Narrowing the window reduces the number of false events, but at the expense of true indium events.

In this particular patient we estimated that there was approximately 70 MBq of technetium in the field of view compared with only 0.15 MBq of indium. The false indium count-rate was about 35 counts/s compared with a true indium count-rate of 25 counts/s. The effect was further exacerbated by the fact that the ^{99}Tc^{m} MDP was much more localized than the ^{111}In WBC uptake.

There are other situations in radionuclide imaging where awareness of this phenomenon is important. When performing dual isotope techniques, such as liver subtraction with ^{99}Tc^{m} colloid during ^{111}In labelled WBC scanning, a proportion of the counts in the indium window will in fact arise from the technetium activity and thus represent the colloid distribution. For instance, if 14 MBq of ^{111}In labelled WBC are distributed to liver and spleen and subtraction is performed with 100 MBq of ^{99}Tc^{m} colloid, then up to 5% of the indium counts may be spurious, arising from this artefact. A localized area of false activity would be unlikely in this circumstance owing to the relatively diffuse distribution of the technetium activity. However, the case presented demonstrates that there are occasions in clinical practice when a ghost image may be created. The effect should be minimized by keeping the technetium activity as low as possible during dual energy imaging with ^{111}In.

References

HORTON, P. W. (Ed.), 1978. *The Theory, Specification and Testing of Anger Type Gamma Cameras* (The Hospital Physicists' Association, London), p. 36.

RYO, U. V., BEKERMAN, C. & PINSKY, S. M., 1985. *Atlas of Nuclear Medicine Artifacts and Variants* (Year Book Medical Publishers, Chicago).

SORENSON, J. A. & PHELPS, M. E., 1987. *Physics in Nuclear Medicine* (W. B. Saunders, Philadelphia), p. 327.

WELLS, D. L. & BERNIER, D. R., 1980. *Radionuclide Imaging Artifacts* (Year Book Medical Publishers, Chicago).

Additive filtering

By Silvio Marugg, MD, Karl Streule, MD, Wolfgang Hedtler, MD and Cyril Berchtold, MD

Department of Radiology, University Hospital Basel, Switzerland

(Received March 1990)

One of the major goals of diagnostic radiology is to produce a radiograph of high quality while maintaining radiation exposure to the patient at a low level. In addition, the public is more aware of and concerned about radiation exposure (Kohn et al, 1988). Therefore the use of aluminium or plexiglass filters for compensating and eliminating over-penetration in special regions such as shoulders, arch aortograms, chest radiographs and lateral decubitus films has been described (Crow et al, 1983; Feczko et al, 1983; Vyborny & MacMahon, 1984; Vezina, 1985). For an overall reduction of radiation exposure, yttrium, niobium and copper filters are in use. The shape and thickness of the different filters are highly variable. To achieve a correct positioning a sliding teflon mount was used by Crow et al (1983).

A filtering system with ferromagnetic plates at the tube-housing and magnets glued onto the filters has been developed and used by us. The system allows free positioning of filters of different sizes, the use of more than one filter at the same time and, with a second coupling plate, even the addition of two filters. This

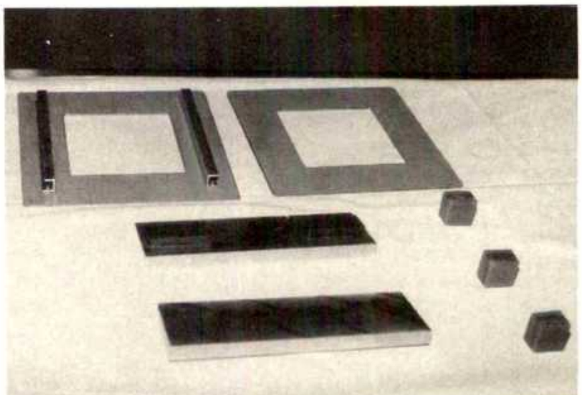

Figure 1. Material needed for additive filtering: coupling plates (top), filter with magnetic holders (front) and "distance-holders" (right).

Address correspondence to Dr S. Marugg, Kantonsspital Basel, Department of Radiology, 4031 Basel, Switzerland.

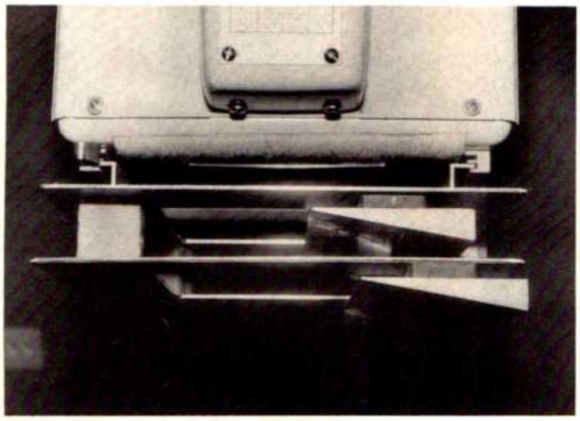

Figure 2. Filters "added" with coupling plates.

approach combines the advantages of the filtering systems mentioned above.

The coupling plate of ferromagnetic material is attached to the tubehousing (Fig. 1) and aluminium filters with magnetic holders are added to the system. Because the magnetic grip is tight but not fixed, filters can be moved without problems up and down. Even the use of two filters at the same time from two different sides is possible.

By placing one filter on the first plate, the addition of a second plate and a second filter is possible. This allows the addition of two filters for examination of the thoraco-lumbar region, for example (Fig. 2).

Flat, long magnets (0.5 × 3 × 6 cm) are glued onto the filters and square magnets 3 cm across act as distance holders between two coupling plates.

With this device it is possible to move filters around freely or add filters without disturbing the patient, and a quicker examination is achieved as well as a better quality of radiograph.

Acknowledgments

We thank J. Binda for construction of the plates and filters and J. Lehmann for secretarial assistance.

References

CROW, W., GUINTO, F. C. JR & SEGURA, T., 1983. Aluminium-wedge filter for improved arch aortograms. *Radiology*, *146*, 542.

FECZKO, P. J., HAGGAR, A. M., RAUCH, P. L., HALPERT, R. D. & SIMMS, S. M., 1983. Compensation filtration for decubitus radiography during double-contrast barium enema examinations. *Radiology*, *149*, 848–850.

KOHN, S. S., GOOCH, M. S. & KELLER, W. S., 1988. Filters for radiation reduction: a comparison. *Radiology*, *167*, 255–257.

VEZINA, J. A., 1985. Compensation filter for shoulder radiography. *Radiology*, *158*, 823.

VYBORNY, C. & MACMAHON, H., 1984. Foil filters for equalized chest radiography. *Radiology*, *151*, 524.

Computerized calculation of radiation dose to patients from radiography

By C.-L. Chapple, BA, MSc and *K. Faulkner, BSc, MSc, PhD

Regional Medical Physics Department, Newcastle General Hospital, Westgate Road, Newcastle-upon-Tyne NE4 6BE

(*Received January 1990 and in revised form February 1990*)

There are a number of occasions on which it may be necessary to make a retrospective calculation of the radiation dose to a patient. For instance, a fetal dose may need to be determined. Irradiation during pregnancy is avoided whenever possible, but sometimes the patient's condition may be considered to necessitate a radiological examination, or a pregnancy may be unsuspected at the time of the examination. When this occurs the radiation dose, and the associated risk of harm, to the fetus from the X-ray examination should be estimated. Dose estimates may also be requested for a patient who has received an unusually large number of radiographs over a period of time, to assess the cumulative dose to that patient.

Current procedures for making retrospective dose calculations, which are usually performed manually, can be quite lengthy, and require thorough error checking. A computerized method for estimating fetal doses using tissue-air-ratio data has been described (Clarkson & Brennen, 1987), but this requires considerable data preparation and knowledge of the exact area of irradiation.

This article describes a method of automatically estimating patient doses with a microcomputer, using exposure information typed in by the operator and normalized organ dose data (Jones & Wall, 1985) already stored in the computer memory. The software has been derived from that written for an on-line automated quality assurance and dosimetry system which has been described previously (Faulkner et al, 1990).

The program requests the operator to enter the required patient and exposure details, and then calculates either the dose and risk to the fetus alone, or a full set of organ doses, effective dose equivalent and associated risks to the patient. The information is displayed on the screen, and a permanent hard copy record can be printed.

---

*Author for correspondence.

Further details concerning the computer programs are available from the authors.

The computer used is a CAS 286 PC/AT, with a 40 MegaByte hard disk, and the program is written using a commercial software package (SMART II, Informix Inc.).

Data input

When the program is run, the operator is first prompted to enter the patient's name, the number of radiographs taken and the gestation period, if this is applicable. An option is given between calculating just the fetal dose, or the effective dose equivalent to the patient in addition.

The exposure factors must then be entered for each exposure taken. The parameters required are the phase of the supply, tube filtration, tube voltage, mAs (product of tube current and exposure time), focus–skin distance, examination type and projection, and the tube output if it is known. If no entry is made for the tube output, then the program will calculate it by assuming an output of 80 Gy/mAs at 80 kVp (Birch et al, 1979) and a distance of 1 m, and correcting for the actual tube voltage used (output $\propto kV^2$).

Data entry is facilitated by providing menus of choices for selecting the phase of supply, tube filtration, and type of examination.

Calculations

Organ doses are derived by multiplying the entrance skin dose by the appropriate organ dose factors. Normalized organ dose data is taken from Jones and Wall (1985), and consists of tables of factors for different examinations at a number of discrete values of tube voltage. Curves have been fitted to this data (Chapple & Faulkner, 1990), and the coefficients of a series of equations have been stored within the computer. The entrance skin dose is determined from the tube output, the mAs, the focus–skin distance and a backscatter factor. The backscatter factors are also taken from Jones and Wall (1985), and stored within the computer.

The effective dose equivalent is given by a weighted sum of organ doses, with the weighting factors taken from the International Commission on Radiological Protection (1977). When a full set of organ doses has been calculated, the somatic risk is estimated by multiplying each organ dose by the corresponding somatic risk factor and summing the results. Genetic risk is estimated by multiplying the gonad dose by the genetic risk factor. Risk factors are based on those suggested by the National Radiological Protection Board (Stather et al, 1988).

Fetal dose is taken as being equivalent to the dose to the uterus, which is considered to be a valid assumption for the earlier stages of pregnancy when the majority of fetal estimations are requested. Two separate fetal risks are considered. The risk of mental retardation is 4.5×10^{-4} mGy^{-1} at 8–15 weeks gestation and nil at all other times, and the risk factor for cancer induction is 6.0×10^{-5} mGy^{-1} for all stages of gestation. For fetal doses of more than 10 mSv, the risk factor is multiplied by three, in accordance with the advice given by the National Radiological Protection Board (Stather et al, 1988).

Output and storage of data

When the calculations are completed, the dose and risk information is displayed on the screen as shown in Tables I and II. The operator is given the option of printing out the data, after viewing it.

The information is stored within a database. One file contains the information from the fetal dose calculations, with a separate record for each patient. This file contains data for individual exposures as well as the cumulative dose and risk to the fetus. A second file

Table I. Display of calculated dose and risk information: dose summary

Patient name/ID A. N. Other
Number of X-rays: 5
(All doses in mSv)

Brain	0.298	Liver	3.459	Urinary bladder	0.451
Breasts	4.187	Lungs	3.012	Uterus	1.111
Stomach	5.311	Ovaries	0.979	Head region	0.331
Small intestine	1.559	Pancreas	2.701	Trunk region	2.394
U. large intestine	2.183	Skin	1.227	Total bone	1.725
L. large intestine	0.692	Testicles	0.018	Red marrow	0.878
Kidneys	0.746	Thyroid	2.609		

Effective dose equivalent 2.486
Somatic risk $34.8 \times E\text{-}06$
Genetic risk (M) $0.18 \times E\text{-}06$
Genetic risk (F) $9.79 \times E\text{-}06$
Fetal dose 1.111 mSv
Risk to fetus $500 \times E^{-6}$ (mental retardation)
$66.67 \times E^{-6}$ (cancer induction)

Table II. Display of calculated dose and risk information: fetal dose

Patient name/ID A. N. Other
Number of X-rays: 3

X-ray no.	Dose (mSv)	Risk of retardation	Risk of cancer	X-ray no.	Dose (mSv)	Risk of retardation	Risk of cancer
1	3.321	0.0015	0.0002	2	11.44	0.0051	0.0007
3	11.44	0.0051	0.0007				

Total fetal dose 26.20 mSv
Total risk to fetus $0.0117 \times E^{-6}$ (mental retardation)
$0.0016 \times E^{-6}$ (induction of cancer)

contains the cumulative organ doses, effective dose equivalents, somatic and genetic risks for each patient for whom the information was required. Complete dose details for the individual exposures are stored in a separate file, as are the exposure details entered by the operator for both types of calculation.

Discussion

The program displays dose and risk estimates very quickly after the appropriate exposure details have been entered—the exact time depends on the number of radiographs taken. A calculation of effective dose equivalent for 10 radiographs takes approximately 1 min, whereas a fetal dose calculation for the same number of radiographs takes just over 40 s.

The calculations performed by this program are similar to those carried out manually in this department, and may be more accurate, as the curve fitting procedure may produce better estimates of organ dose factors for intermediate tube voltages than does the simple extrapolation method used in the manual technique.

The program has been tested by using it to perform specific fetal dose calculations that had previously been carried out manually, using the same data. The results were in good agreement with those originally determined.

The program can also be used for making prospective dose calculations. These are useful when a radiograph of a pregnant woman is planned, or to compare the doses arising from different radiological techniques.

Acknowledgments

This work was partially funded by the Commission of the European Communities, under contract number B16.0315.UK(H). We wish to thank Professor K. Boddy for his encouragement and support.

References

Birch, R., Marshall, M. & Ardran, G. M., 1979. *Catalogue of Spectral Data for Diagnostic X-rays. Scientific Report Series 30* (Hospital Physicists' Association, London).

Chapple, C.-L. & Faulkner, K., 1990. Computer curve fitting to normalised organ dose data. In *Computers in Radiology* (Institute of Physical Sciences in Medicine, York), in press.

Clarkson, D. McG. & Brennen, S. E., 1987. Use of a microcomputer for the estimation of X-Ray dose received by the fetus. *British Journal of Radiology, 60,* 1119–1123.

Faulkner, K., Chapple, C.-L., Hedley, P., Kotre, C. J. & Harrison, R. M., 1990. Automated quality assurance and patient dosimetry in diagnostic radiology. *Journal of Biomedical Engineering, 12,* 228–232.

International Commission on Radiological Protection, 1977. *Recommendations of the International Commission on Radiological Protection, ICRP Report 26* (Pergamon Press, Oxford).

Jones, D. G. & Wall, B. F., 1985. *Organ Doses from Medical X-ray Examinations Calculated Using Monte Carlo Techniques. National Radiological Protection Board Report NRPB-R186* (HMSO, London).

Stather, J. W., Muirhead, C. R., Edwards, A. A., Harrison, J. D., Lloyd, D. C. & Wood, N. R., 1988. *Health Effects Developed from the 1988 UNSCEAR Report. National Radiological Protection Board Report NRPB-R226* (HMSO, London).

1990, *The British Journal of Radiology*, *63*, 804–805

Case reports

Progressive systemic sclerosis (diffuse scleroderma) and radiotherapy

By Stephen G. Cooper, MB, BS and James W. Denham, MD, FRCR, FRACR

Radiotherapy Department, Newcastle Mater Misericordiae Hospital, Waratah, NSW 2298, Australia

(*Received November 1989 and in revised form February 1990*)

The rheumatological manifestations of cancer are many and varied. Progressive systemic sclerosis has been reported both as an initial manifestation of malignancy (Caldwell & McCallum, 1986) and, of course, as coexisting with malignant disease. Surprisingly, only one case report is to be found in the literature reporting on the interaction between radiotherapy and scleroderma (Ransom & Cameron, 1987), the consequences of which may carry significant morbidity.

Case report

Our patient was 49 years old in May 1987 when referred for the management of a mass in the right neck. This right cervical node measured 6 × 5 cm, was fungating through the skin, with biopsy confirming metastatic squamous cell carcinoma. No primary site was identified either on direct ear, nose and throat examination or with computed tomography.

His past medical history included heavy smoking (50 per day for 25 years) and intermittent heavy alcohol consumption. Otherwise, he had been well, working as a surgical dresser for 19 years. There was no noteworthy family history.

Radical irradiation was planned and delivered in a beam direction immobilization shell. This entailed coverage of the nasopharynx and upper neck to a dose of 40 Gy in 20 fractions, given over 26 days with an opposed lateral pair, using 6 MV X rays, measured at the midplane. The nasopharynx was boosted by a further 10 Gy in five fractions. The lower neck was treated with an anterior split neck field to 50 Gy in 25 fractions over 33 days, measured to a depth of 3 cm. The right and left lower posterior neck was boosted by a further 10 Gy in five fractions using 12 MeV electrons, assessed at 3 cm depth. A final boost of 20 Gy to the neck node in 10 fractions, measured at D max was administered, using 12 MeV electrons. Spinal cord dose was less than 47 Gy. Maximum calculated point dose was 74.5 Gy in 35 fractions.

The treatment was well tolerated. In particular, no severe or untoward normal tissue reactions were observed. Initial tumour response was slow, with incomplete regression 2 months after completion. The patient was subsequently lost to follow-up.

Two years after initial therapy, the patient was referred back to the clinic. During this time he had lost 8 kg in weight owing to increasing difficulty in swallowing. The patient was unable to extend his neck and there was marked limitation of movement of both shoulders. Questioning elicited symptoms consistent with Raynaud's Syndrome. Additionally, over the last 6–7 months he had noted increasing dyspnoea on exertion.

Clinical examination revealed findings typical of scleroderma (Fig. 1). He had widespread skin thickening, beyond the field of radiation, apparent in both sets of limbs, trunk and face. The thickening was maximal within the neck, completely limiting

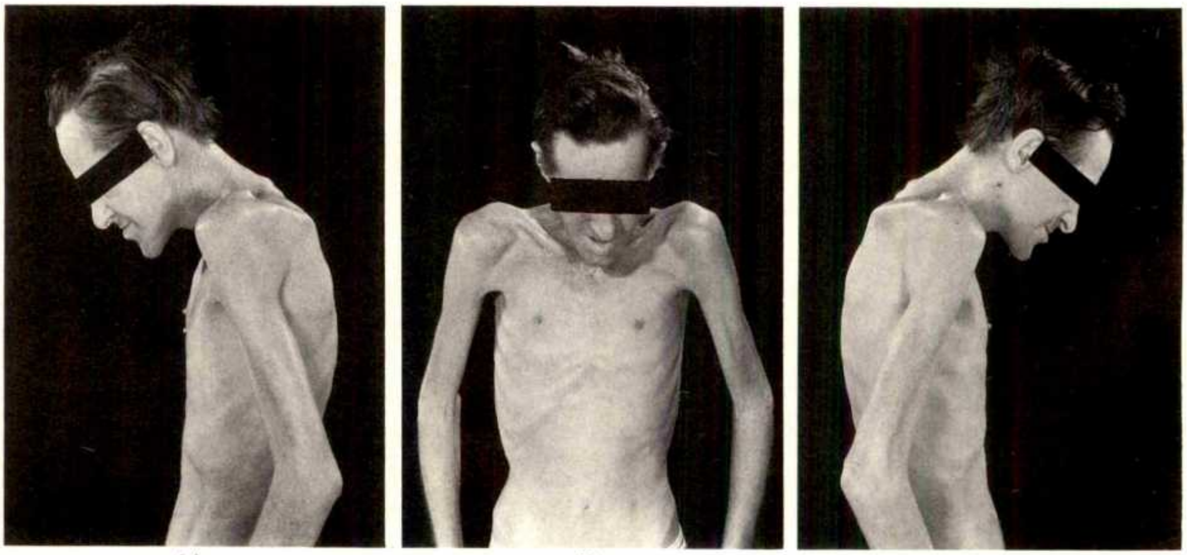
(a) (b) (c)

Figure 1. Clinical photographs showing a severe flexion deformity.

any flexion, extension or rotation involving the cervical spine. A severe flexion deformity was present. Similarly, there was limitation of abduction of both shoulders to about 70 or 80 degrees, and he has a flexion deformity in both elbows. Surprisingly, there was very minimal sclerodactylia in comparison to his skin changes elsewhere. There was no evidence of persistent or recurrent tumour.

Investigations included a barium swallow examination, which could not be completed satisfactorily owing to regurgitation into the bronchial tree. His immunological profile was consistent with scleroderma, with ANA being highly positive, titre greater than 1 in 2560, with the immunofluorescent pattern being homogenous, nucleolar and speckled. The usual extractable nuclear antigens were not detected. Anti-DNA antibodies were not elevated. Skin biopsy from an unirradiated area was typical of scleroderma, but pulmonary function studies were more compatible with his pre-existing emphysema than with scleroderma. Marked air trapping improved by bronchodilators and a reduced carbon monoxide diffusion were noted.

He was referred to a rheumatologist who recommended D-Penicillamine, 125 mg bd, increasing at monthly intervals by 125 mg to a maximum of 500–625 mg daily. Dietary advice was obtained, with some early weight gain. Subsequent follow-up at this stage has been too short to assess the utility of systemic therapy.

Discussion

The vascular and fibrotic changes of scleroderma are well documented, though their precise aetiology is poorly understood (Gilliland, 1988). Similarly, the late normal tissue effects of radiotherapy and their variations with such factors as total dose, fraction size, volume are well known and documented (Hall, 1988). When occurring together, significant morbidity may develop secondary to dense subcutaneous and soft-tissue fibrosis. In this case, diffuse scleroderma manifested some 2 years after the completion of radical irradiation to the head and neck region. Whilst small areas received greater than 70 Gy, the bulk of the neck received only 50 Gy in 25 fractions. Nevertheless, major morbidity developed because of severe bilateral fibrosis involving all structures in the neck. Importantly, however, no evidence of tumour recurrence is to be found. Response to D-Penicillamine therapy will be monitored.

This is only the second case report we have been able to identify regarding the adverse interaction between radiation therapy and scleroderma.

Acknowledgment

Mrs Kim Lusis is thanked for preparing the manuscript.

References

CALDWELL, D. S. & MCCALLUM, R. M., 1986. Rheumatological manifestations of cancer. *Medical Clinics of North America*, *70*, 385–417.

GILLILAND, B. C., 1988. Progressive systemic sclerosis (Diffuse scleroderma). In *Harrisons Principles of Internal Medicine, 11th edn* (McGraw Hill, Maidenhead), pp. 1428–1432.

HALL, E. J., 1988. *Radiobiology for the Radiobiologist, 3rd edn* (J. B. Lippincott, Philadelphia), pp. 57–58; 239–261.

RANSOM, D. T. & CAMERON, F. G., 1987. Scleroderma—a possible contraindication to lumpectomy and radiotherapy in breast carcinoma. *Australasian Radiology*, *31*, 317–318.

Spinal cord sarcoidosis with intramedullary cyst formation

By A. G. Clifton, MA, MRCP, FRCR, J. M. Stevens, DRACR, FRCR, *R. Kapoor, MA, MRCP and *P. Rudge, FRCP

Departments of Radiology and *Neurology, The National Hospitals for Nervous Diseases, Maida Vale, London W9

(*Received November 1989 and in revised form February 1990*)

We report a case of spinal cord sarcoidosis with surgically confirmed localized cyst formation and probably syringomyelia involving almost the entire spinal cord, an association which has not been documented previously. The magnetic resonance (MR) findings before and after gadolinium diethylenetriamine-pentaacetic acid (Gd-DTPA) are described. There has been only one previous report of the MR findings in histologically confirmed spinal cord sarcoidosis, and in this case Gd-DTPA was not given.

Case report

A 49-year-old man presented with a 3-week history of progressive urinary hesitancy and weakness of both legs. Three years previously he was diagnosed as having sarcoidosis on the basis of bilateral hilar adenopathy on plain chest radiography, and a positive Kveim test. Ten months before this admission he had developed granulomatous uveitis.

Clinical findings

On initial examination there was moderate reduction of muscle power in all four limbs, whilst tone and co-ordination were normal. Reflexes were generally brisk, abdominal reflexes were absent, and there were bilateral extensor plantar responses. Vibration and joint position sensation were absent bilaterally in his feet, and there was a spinothalamic sensory level at C8 on the right and D6 on the left.

Routine blood tests were normal. The erythrocyte sedimentation rate was 70 mm/h. Serum angiotensin converting enzyme activity was 15 iu/l. At lumbar puncture, the cerebrospinal fluid (CSF) pressure was 140 mm and the fluid was xanthochromic; the CSF protein concentration was 14 g/l and glucose 2.1 mmols (blood glucose 8 mmols/l). There were 21 mature lymphocytes and one red blood cell per cubic mm. Oligoclonal studies were negative.

Radiology

Imaging revealed abnormalities on the following tests.

Myelogram (Fig. 1): marked expansion of the spinal cord was shown from the foramen magnum to the third thoracic vertebra.

Post-myelography computed tomography (CT) (Fig. 2): immediate images showed symmetrical expansion of the spinal cord from the foramen magnum to the upper thoracic region, maximal in the cervical region. Delayed CT 20 h after the myelogram showed pathological accumulation of contrast medium in the spinal cord from the level of the third to the 10th thoracic vertebrae, but not in the cervical region. The spinal cord was slightly expanded throughout the thoracic region.

Magnetic resonance imaging (Fig. 3): T_1 and T_2 weighted images showed expansion of the spinal cord from the medulla oblongata down to the tenth thoracic vertebra, with maximum expansion from about C6 to the lower border of T1. On T_1 weighted images the region of maximum expansion showed

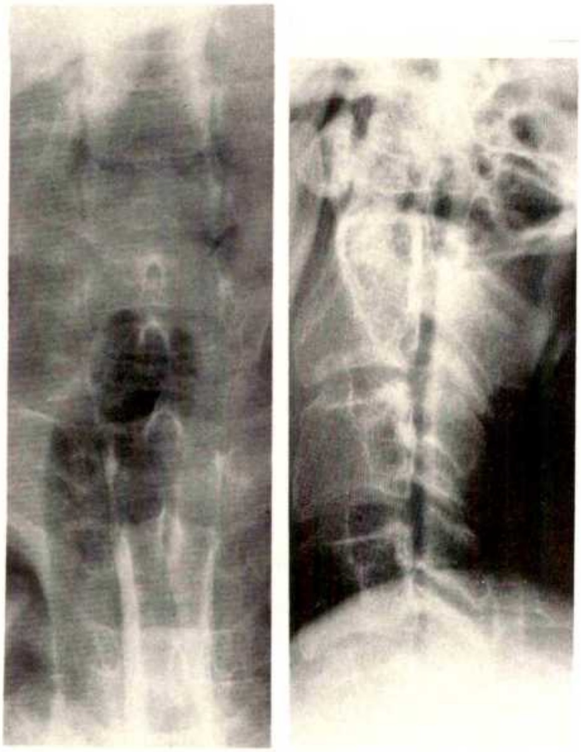

(a) (b)

Figure 1. Conventional myelography using water soluble contrast medium. Contrast medium was introduced by lumbar puncture. The expanded cervical cord is shown in the antero-posterior and lateral projections. Note the mild undulation of the lateral margins of the spinal cord in the upper thoracic and lower cervical regions.

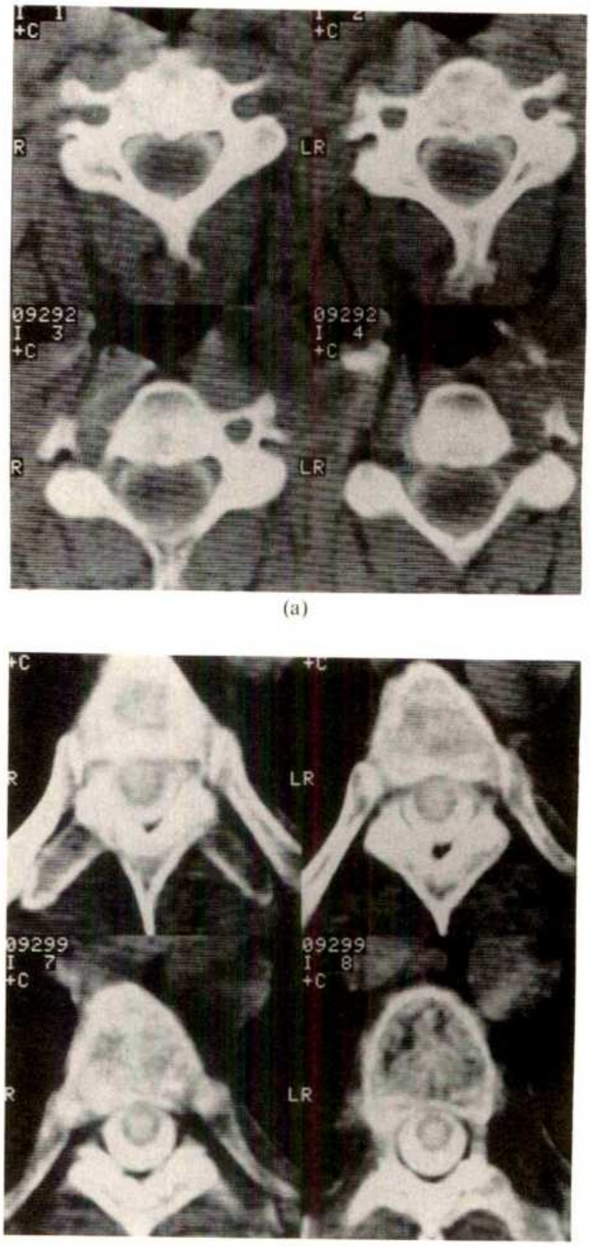

(a)

(b)

Figure 2. (a) Computed myelography showing a series of 5 mm thick axial sections through the mid-cervical region immediately after the myelogram. The spinal cord is symmetrically expanded. (b) A series of axial 5 mm thick CT sections through the thoracic region made 20 h after the myelogram, showing a conspicuous accumulation of contrast medium in the central part of a mildly expanded spinal cord.

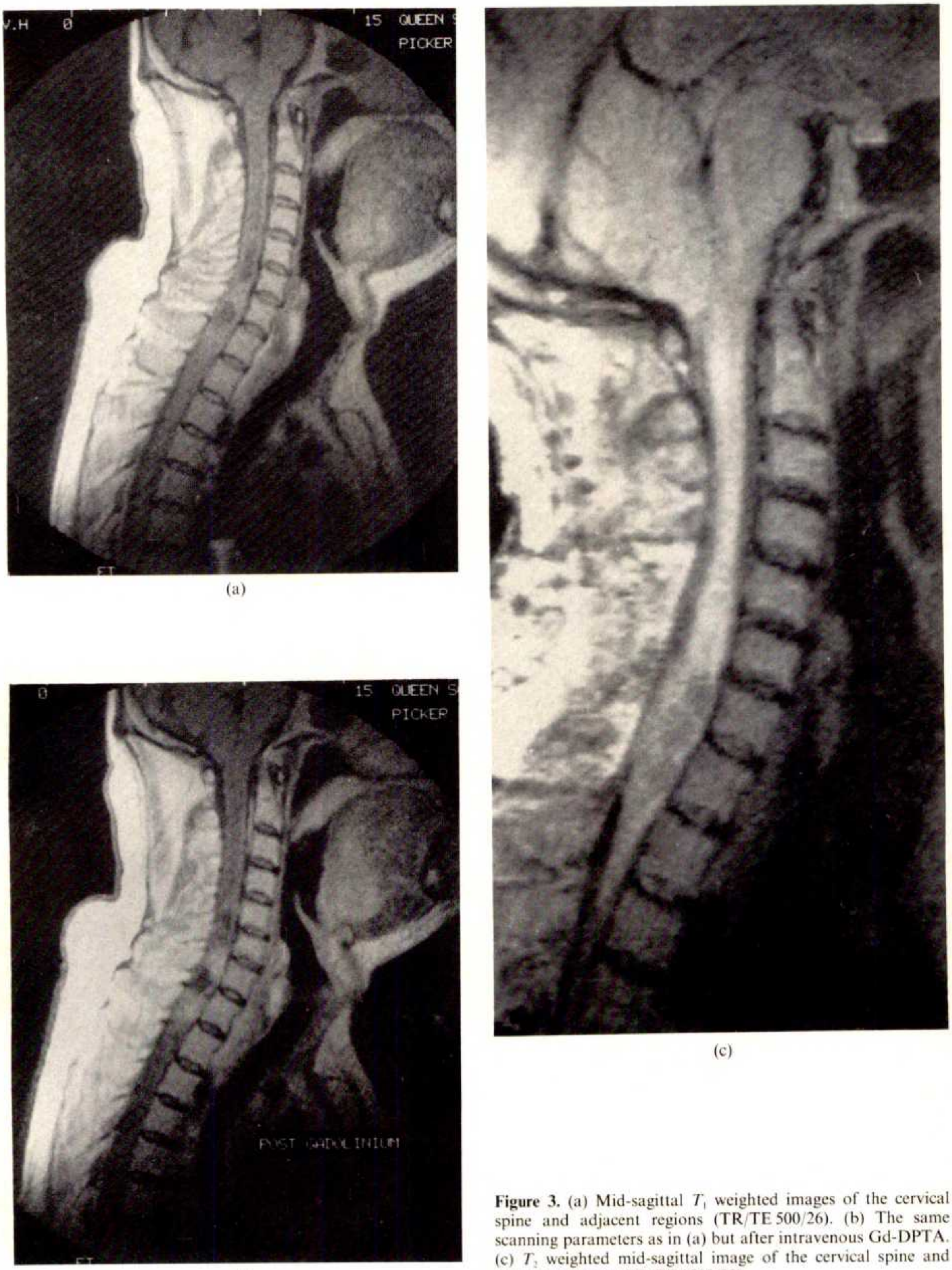

(a)

(b)

(c)

Figure 3. (a) Mid-sagittal T_1 weighted images of the cervical spine and adjacent regions (TR/TE 500/26). (b) The same scanning parameters as in (a) but after intravenous Gd-DPTA. (c) T_2 weighted mid-sagittal image of the cervical spine and adjacent regions (TR/TE 1500/80).

diffusely increased signal in which were located two circumscribed areas of low signal. Extended both cranially and caudally from this region were central areas of slightly reduced signal, suggestive of syringomyelia, reaching at least as high as C2 and to T10 below. After intravenous Gd-DTPA, the relatively hyperdense areas in the region of maximum expansion showed well circumscribed enhancement. On T_2 weighted images there was diffusely increased signal from the level of the foramen magnum down to the upper thoracic region. In the region of maximum expansion, signal was inhomogenous, and with some irregular, poorly circumscribed areas of reduced signal, not definitely indicating cystic change.

The MR study shows mild cerebellar ectopia, but on the computed myelogram using overlapping 5 mm thick sections there was no evidence of cerebellar ectopia. We conclude that probably there was minimal and almost certainly insignificant cerebellar ectopia.

Clinical management

The patient was treated with Dexamethasone 4 mg q.d.s. prior to operation which consisted of laminectomy between C5 and T1. Intramedullary cysts containing clear xanthochromic fluid were incised at C5 and at C7 to T1. Biopsy of abnormal solid material revealed, on histological examination, intense astrocytic gliosis surrounding non-caseating granulomas composed of centrally placed epithelioid cells and a peripheral rim of lymphocytes, consistent with sarcoidosis. There were a few multinucleated giant cells, but neither caseation nor acid fast bacilli were seen. Subsequent cultures of this material and of the CSF were also negative for acid fast bacilli.

There was considerable clinical improvement, with return of normal bladder function. A mild sensory type ataxia, right leg weakness and impaired position sensation in the feet persisted. Treatment with oral steroids was continued.

Discussion

Sarcoidosis is a common idiopathic granulomatous disease which may involve any organ system, resulting in varied manifestations. The overall frequency of clinical neurological involvement is 5% (Delaney, 1977). Although patients usually have other stigmata of the disease, neurological dysfunction can be the presenting feature. Involvement of the spinal cord is much less frequent than the brain and peripheral nerves. Hitchon et al (1984) described only 24 cases of histologically confirmed sarcoidosis documented in the literature up to 1984. Our search of the literature has revealed no case with a syrinx. An intramedullary mass lesion is the most common manifestation; however arachnoiditis and intradural–extramedullary mass lesions have also been described (Kelly et al, 1988). Biopsy is usually needed for diagnosis because the myelographic appearance of an expanded spinal cord is non-specific; and may be seen with, for example, intramedullary neoplasms, syringomyelia, multiple sclerosis and other inflammatory lesions. Operative diagnosis is necessary and may permit a useful decompression as in this case. Subsequent treatment with systemic steroid has been shown to be beneficial in spinal cord sarcoidosis (Hitchon et al, 1984).

The MR findings of spinal cord sarcoidosis are poorly documented. There have been several reports in intracerebral sarcoidosis (Poole, 1984; Ketonen et al, 1987; Miller et al, 1988), but our literature review has revealed only one biopsy proven case with spinal cord involvement (Kelly et al, 1988), which did not include imaging after intravenous injection of Gd-DPTA. This case demonstrated expansion of the cervical cord, and diffuse signal increase on T_2 weighted images extending from the medulla oblongata into the upper thoracic cord.

Pathologically, central nervous system involvement is in the form of either sarcoid tissue in meninges or nervous tissue, or infarction secondary to occlusion of small vessels by granulomata (Herring et al, 1969). On MRI both appear as increase in T_1 and T_2 relaxation times (Miller et al, 1988). The enhancement characteristics of intramedullary disease after Gd-DTPA are similar to those in disease of the brain, enhancement depending on the presence of an intact blood supply and the state of the physiological barriers that regulate the passage of contrast medium into the extracellular space (Sze et al, 1989). In this case enhancement assisted in establishing the presence of pathological solid elements in the spinal cord. Cystic change was confirmed surgically in the lower cervical region. The more extensive involvement of the spinal cord in the form of circumscribed central persistent contrast accumulation on delayed post-myelography CT and signal changes on MRI were most likely to represent syringomyelia but could conceivably have represented only central necrosis (myelomalacia). The presence of mild expansion of the affected region of the spinal cord on CT, however, makes the presence of syringomyelia almost certain (Williams et al, 1987).

References

DELANEY, P., 1977. Neurologic manifestations in sarcoidosis. *Annals of Internal Medicine, 87*, 336–346.

HERRING, A. B. & URICH, H., 1969. Sarcoidosis of the central nervous system. *Journal of Neurological Sciences, 9*, 405–422.

HITCHON, P. W., UL HAQUE, A., OLSON, J. J., JACOBS, S. K. & OLSON, S. P., 1984. Saracoidosis presenting as an intramedullary spinal cord mass. *Neurosurgery, 15*, 86–90.

KELLY, R. B., MAHONEY, P. D. & CAWLEY, K. M., 1988. MR demonstration of spinal cord sarcoidosis: report of a case. *American Journal of Neuroradiology, 9*, 197–199.

KETONEN, L., OKSANEN, V. & KUVLIALA, I., 1987. Preliminary experience of magnetic resonance imaging in neurosarcoidosis. *Neuroradiology, 29*, 127–129.

MILLER, D. H., KENDALL, B. E., BARTER, S., JOHNSON, G., MACMANUS, D. G., LOGSDUIL, S. J., ORMEROD, I. E. C. & MCDONALD, W. I., 1988. Magnetic resonance imaging in central nervous system sarcoidosis. *Neurology, 38*, 378–383.

POOLE, C. J. M., 1984. Argyll Robertson pupils due to neurosarcoidosis, evidence for site of lesions. *British Medical Journal, 289*, 356.

SZE, G., BRAVO, S. & KROL, G., 1989. Spinal lesions: Quantitative and qualitative temporal evolution of gadopentate dimeglumine enhancement in MR imaging. *Radiology, 170*, 849–856.

WILLIAMS, A. L., HAUGHTON, V. M. & POJUNAS, K. W., 1987. Differentiation of intramedullary neoplasms and cysts by MR. *American Journal of Neuroradiology, 8*, 527–523.

1990, *The British Journal of Radiology*, *63*, 809–812

Ultrasonic appearances of the early changes in fibrodysplasia ossificans progressiva

By E. J. McAteer, MRCP, DMRD, FRCR, *L. A. Hallam, MB, BSc, MRCPath and G. M. A. Hendry, MB, BS, DMRD, FRCR

Departments of Radiology and *Pathology, the Royal Hospital for Sick Children, Edinburgh

(*Received February 1990 and in revised form April 1990*)

Progressive heterotopic ossification and congenital skeletal anomalies characterize the very rare and relentless condition of fibrodysplasia ossificans progressiva (FOP) or myositis ossificans progressiva (MOP) (McKusick, 1972). These patients frequently present with subcutaneous masses which are often painful (Lindhout & Golding, 1985) and therefore ultrasound may be used in the initial investigation. We report a case of FOP presenting with recurrent soft-tissue swellings and demonstrate the ultrasonic appearances not previously documented in this condition.

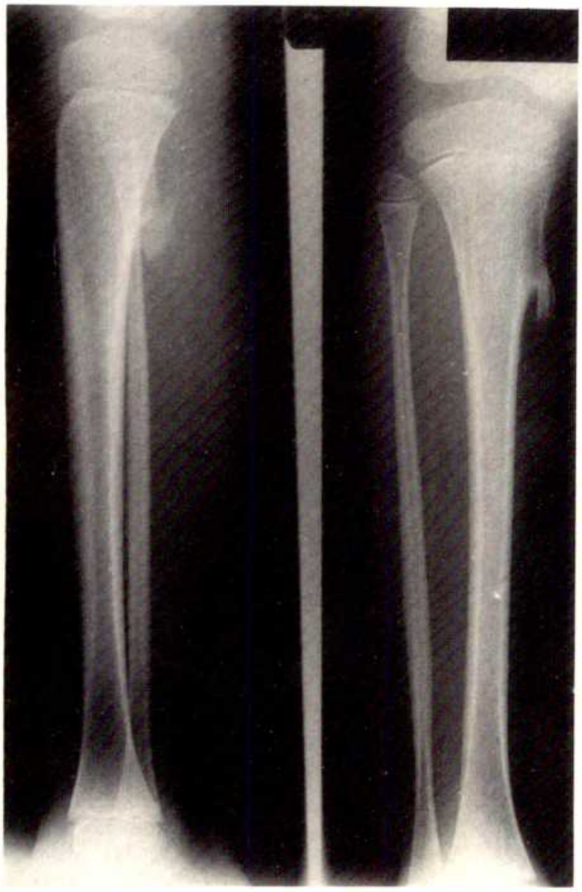

Figure 1. Lower limb radiograph demonstrates pseudoexostosis arising from the upper medial tibial shaft.

Case report

A 5-year-old boy first presented with a history of pain in his right knee following a minor injury. Radiographs showed an apparent simple exostosis arising from the medial side of the proximal tibial metaphysis (Fig. 1); no further investigations were performed at this time. He presented again several months later with a swelling in the subcutaneous tissues of the left anterior thigh and with pain on walking. No soft-tissue abnormality was identified on the radiographs. Ultrasonic examination using a Diasonics 5 MHz rotating transducer demonstrated an increase in the thickness of the soft tissues and a well defined hypoechoic lesion with an echogenic central region in the deep compartment of the anterior thigh (Fig. 2). When radiographs were repeated 3 months later ossification had taken place in this area (Fig. 3.).

Further similar swellings developed in the para-vertebral tissues of the lumbar region and around the right scapula. Ultrasound now demonstrated separation of the normal muscular fasicular planes by echogenic material together with increase in the muscle size (Fig. 4). Computed tomography of the thorax showed that the right posterior thoracic and scapular muscles were expanded and separated by tissue which enhanced less than the adjacent muscles. No calcification or ossification was present in the soft tissues of the thorax at this time (Fig. 5). A biopsy of this mass revealed a florid proliferation of plump fibroblasts with a focal proliferation of blood

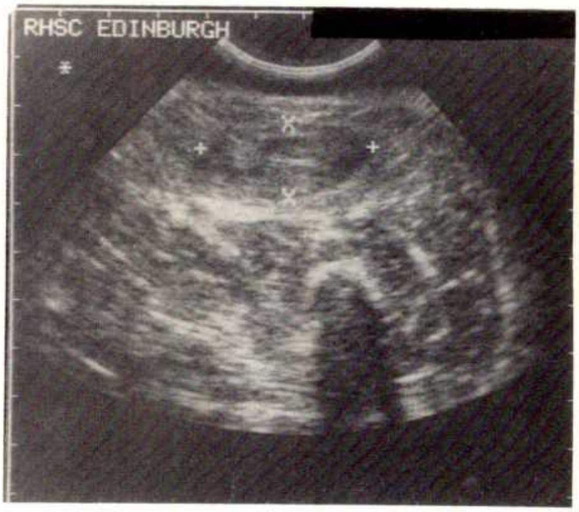

Figure 2. Transverse ultrasound scan of the thigh. The femoral shaft is causing acoustic shadowing. Lying within the quadraceps femoris is an oval hypoechoic lesion (crosses) with a moderately echoic central region.

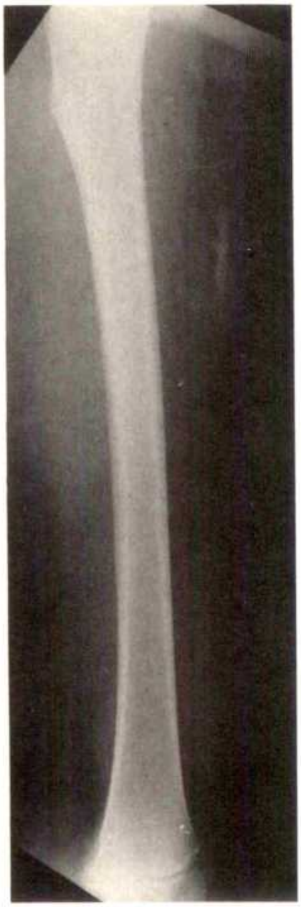

Figure 3. Lateral radiograph of the left femur showing ossification at the site of the previous soft-tissue swelling.

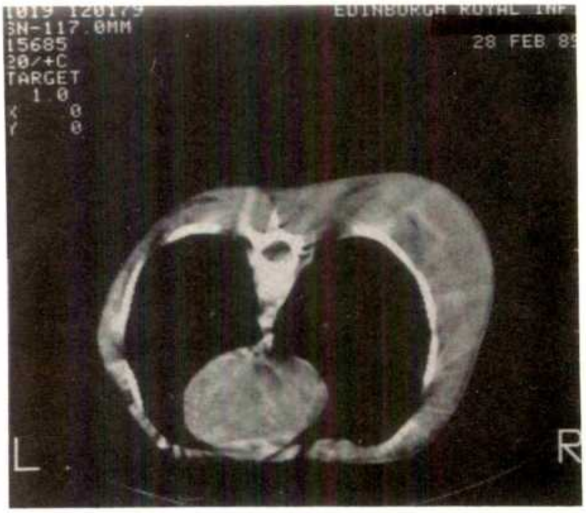

Figure 5. Contrast-enhanced CT through the lower thorax showing the right infra scapular muscles expanded and separated by tissue which enhances less than the adjacent muscles.

vessels (Fig. 6). In many areas there was much myxomatous ground substance, whilst elsewhere collagenization was prominent. There was infiltration of fat and muscle, both around and within fascicles resulting in some myofibre atrophy. Although calcification and ossification were not a feature, the findings were in keeping with FOP (Enzinger & Weiss, 1988).

At this time, a limited skeletal survey showed hypoplasia of the first metacarpals and metatarsals with hallux valgus deformity and a hypoplastic deformed first phalanx of the great toe (Fig. 7). The cervical spine had relatively enlarged posterior elements and shortening of the antero-posterior diameter of the cervical bodies (Fig. 8). The diagnosis of FOP was established by these characteristic appearances.

Discussion

Fibrodysplasia ossificans progressiva is a congenital disease of connective tissue of unknown origin. It can be inherited as an autosomal dominant trait with a variable

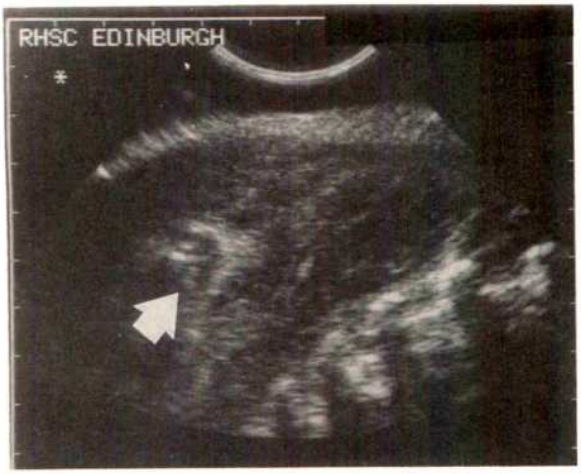

Figure 4. Longitudinal paramedian scan of the right infrascapular region. The arrow indicates the lower border of the scapula, the ribs are casting acoustic shadowing. There is a diffuse increase in thickness of the infrascapular soft tissues and separation of the muscle fasicular planes by echogenic material not causing acoustic shadowing.

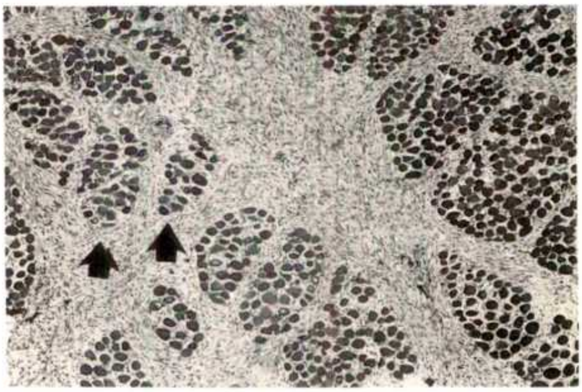

Figure 6. Low power view of infrascapular biopsy showing fibroblastic proliferation around and within muscle fasicles (arrows) with some atrophy of the myofibres (HeE × 50).

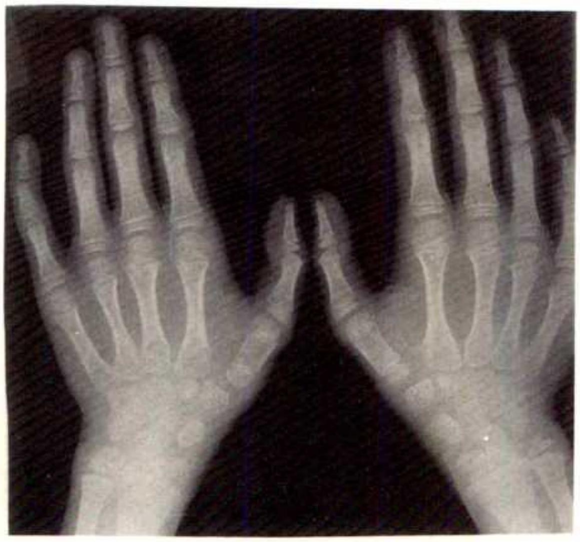

(a)

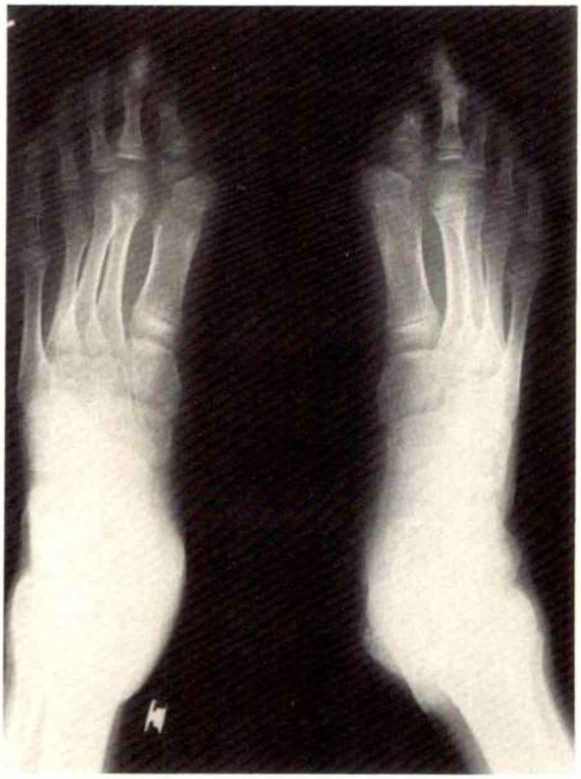

(b)

Figure 7. (a) Radiograph of the hands showing bilateral short first metacarpals. (b) Radiograph of the feet showing bilateral hallux valgus and malformed hypoplastic proximal phalanges and pseudoepiphysis at the heads of the first metatarsals.

penetrance, but most often as in this case arises sporadically (Wynne-Davies et al, 1985). The radiographic features are well documented with characteristic changes in the hands and feet (Fig. 7) in almost all cases (Rogers & Geho, 1979; Schroeder & Zasloff, 1980; Connor & Evans, 1982; Thickman et al, 1982). The cervical spine is also a common site of congenital abnormality; the vertebrae may have small bodies with enlarged pedicles (Fig. 8) and fusion abnormalities (Hall & Sutcliffe, 1979; Cremin et al, 1982; Connor & Smith, 1982).

The radiologist has a central role to play in establishing a diagnosis of FOP so avoiding biopsy, as it is well recognized that any type of trauma will accelerate the ossification process (Rosenstirn, 1918; Rogers & Geho, 1979; Connor & Evans, 1982). Histological appearances may be misleading (Rogers & Geho, 1979; Carter et al, 1989). Delay in diagnosis may occur however, owing to the varied presentations (Smith, 1975; Rogers & Geho, 1979; Connor & Evans, 1982). The earliest clinical findings are typically a diffuse soft-tissue swelling or a more discrete soft-tissue mass, usually in the neck or back. The plain radiographs in the acute phase are unlikely to show any calcification or ossification and, as the differential diagnosis of the soft-tissue mass includes sarcoma and fibromatosis, further imaging is appropriate.

Isotope bone scanning will demonstrate soft-tissue uptake prior to radiographic changes in FOP (Susuki et al, 1974; Fang et al, 1986) but will not be abnormal in the most acute phase (Carter et al, 1989). Computed tomography can show early changes in the soft tissues very well (Rogers & Geho, 1979; Reinig et al, 1986; Carter et al, 1989), with variable amounts of oedema in the soft-tissue planes (Fig. 5) and the early development of ossification.

Ultrasound is widely available and has become established in the imaging of soft tissues. There have been few reports of the ultrasonic appearances in established myositis ossificans (Kramer et al, 1979; Giron & Senac, 1985; Roy & Challan-Belval, 1985) and several of the early ultrasonic features (Kirkpatrick et al, 1987; Peck & Metreweli, 1988; Fornage & Eftekhari, 1989) but none of FOP. The early ultrasonic changes appear similar. Kirkpatrick et al (1987) and Fornage and Eftekhari (1989) described well defined elongated hypoechoic mass lesions within muscle similar to the present case (Fig. 2); however, in both cases calcification developed peripherally around the lesions rather than centrally as occurred in this patient (Figs 2 and 3). Peck and Metreweli (1988) showed sheets of echogenic material with acoustic shadowing in the muscle fasicular planes because of early calcification. Echogenic material was found in the scapular region in the present case, causing

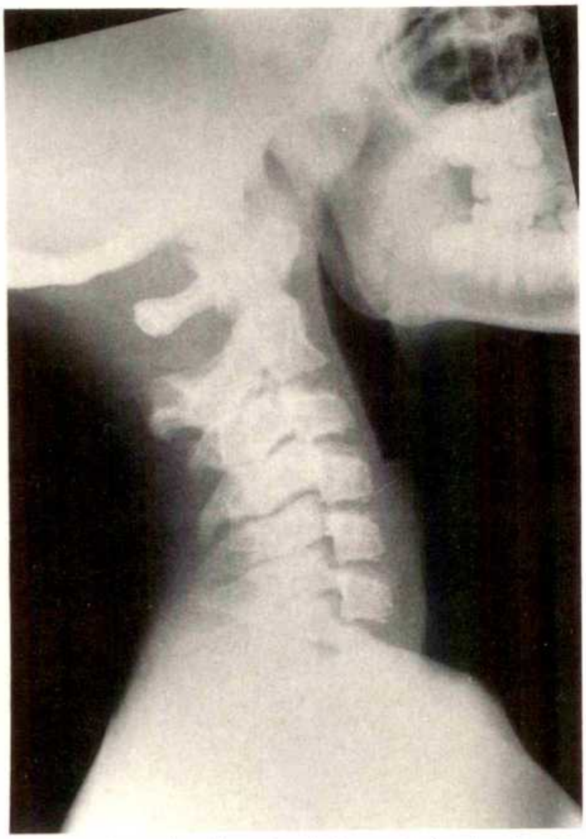

Figure 8. Lateral radiograph of the cervical spine showing relative enlargement of laminae and shortening of the anteroposterior diameter of the cervical bodies.

expansion of the muscle layers but no acoustic shadowing to suggest calcification, and this was most likely the result of infiltration of the muscle layers by myxoid tissue and collagenization as seen on histological examination (Fig. 6).

Conclusion

Ultrasound can demonstrate the early changes of fibrodysplasia ossificans progressiva as a soft-tissue mass lesion or echogenic material causing expansion in a more widespread area of muscle and connective tissue. While these changes may not be specific for FOP, in the correct clinical context they should lead to a search for the characteristic features in the hands, feet and cervical spine, to circumvent biopsy of the lesions.

References

Carter, S. R., Davies, A. M., Evans, N. & Grimer, R. J., 1989. Value of bone scanning and computed tomography in fibrodysplasia ossificans progressiva. *British Journal of Radiology, 62*, 269–272.

Connor, J. M. & Evans, D. A. P., 1982. Fibrodysplasia ossificans progressiva: the clinical features and natural history of 34 patients. *Journal of Bone & Joint Surgery, 64B*, 76–83.

Connor, J. M. & Smith, R., 1982. The cervical spine in fibrodysplasia ossificans progressiva. *British Journal of Radiology, 55*, 492–496.

Cremin, B., Connor, J. M. & Beighton, P., 1982. The radiological spectrum of fibrodysplasia ossificans progressiva. *Clinical Radiology, 33*, 499–508.

Enzinger, F. M. & Weizz, S. W., 1988. *Soft Tissue Tumours, 2nd edn* (C. V. Mosby, St. Louis, USA), pp. 890–894.

Fang, M. A., Reinig, J. W., Hill, S. C., Marini, J. & Zasloff, M. A., 1986. Tc^{99m} MDP demonstration of heterotopic ossification in fibrodysplasia ossificans progressiva. *Clinical Nuclear Medicine, 11*, 8–9.

Fornage, B. D. & Eftekhari, F., 1989. Sonographic diagnosis of myositis ossificans. *Journal of Ultrasound in Medicine, 8*, 463–466.

Giron, J. & Senac, J. P., 1985. Myosite circonscrite hyperaigue, pseudomaligne. Apports et limites de l'échographique. Revue de la littérature. A propos d'un cas. *Journal de Radiologie, 66*, 151–156.

Hall, C. M. & Sutcliffe, J., 1979. Fibrodysplasia ossificans progressiva. *Annales de Radiologie, 22*, 119–123.

Kirkpatrick, J. S., Korman, L. A. & Rovere, G. D., 1987. The role of ultrasound in the early diagnosis of myositis ossificans. *The American Journal of Sports Medicine, 15*, 179–181.

Kramer, F. L., Kurtz, A. B., Rubin, C. & Goldberg, B. B., 1979. Ultrasound appearance of myositis ossificans. *Skeletal Radiology, 4*, 19–20.

Lindhout, D. & Golding, R. P., 1985. Fibrodysplasia ossificans progressiva. *Pediatric Radiology, 15*, 211–213.

McKusick, V. A., 1972. *Heritable Disorders of Connective Tissue, 4th edn* (C. V. Mosby, St. Louis, USA), pp. 687–702.

Peck, R. J. & Metreweli, C., 1988. Early myositis ossificans: a new echogenic sign. *Clinical Radiology, 39*, 586–588.

Reinig, J. W., Suvimol, C. H., Fang, M., Marini, J. & Zasloff, M. A., 1986. Fibrodysplasia ossificans progressiva: CT appearance. *Radiology, 159*, 153–157.

Rogers, J. R. & Geho, W. B., 1979. Fibrodysplasia ossificans progressiva: a survey of 42 cases. *Journal of Bone & Joint Surgery, 61A*, 909–914.

Rosenstirn, J. A., 1918. A contribution to the study of myositis ossificans progressiva. *Annals of Surgery, 68*, 591–637.

Roy, C. & Challan-Belval, P., 1985. Myosite ossificante non traumatique. Aspects échographique et scanographique. A propos d'un cas. *Journal de Radiologie, 66*, 473–475.

Schroeder, H. W. & Zasloff, M. A., 1980. The hand and foot malformations in fibrodysplasia ossificans progressiva. *Johns Hopkins Medical Journal, 147*, 73–78.

Smith, R., 1975. Myositis ossificans progressiva: a review of current problems. *Seminars in Arthritis and Rheumatism, 4*, 369–380.

Susuki, Y., Hisada, K. & Takeda, M., 1974. Demonstration of myositis ossificans by Tc^{99m} pyrophosphate bone scanning. *Radiology, 111*, 663–664.

Thickman, D., Bonakdapour, A., Clancy, M., Orden, J. V. & Steel, H., 1982. Fibrodysplasia ossificans progressiva. *American Journal of Roentgenology, 139*, 935–941.

Wynne-Davies, R., Hall, C. M. & Apley, A. G., 1985. *Atlas of Skeletal Dysplasias* (Churchill Livingstone, Edinburgh), p. 547.

1990, *The British Journal of Radiology*, *63*, 813–814

Cystic lymphangioma of the pelvis in childhood

By *J. C. Hoeffel, MD, A. L. Marchal, MD, †E. Pierre, MD and ‡J. Derelle, MD

Departments of Radiology, †Surgery and ‡Medicine, Hôpital d'Enfants, 5, allée du Morvan, 54511 Vandoeuvre, France.

(*Received January 1990 and in revised form March 1990*)

We report a case of a multicystic retroperitoneal lymphangioma appearing in an infant as an inguinal mass.

Case report

A 1-year-old boy presented with a right inguinal mass which had the appearance of a lymph node. After biopsy, the pathologist reported "non-specific adenitis". Six weeks later the boy was admitted because of a recurrent swelling. The inguinal mass was large and irreducible. On urography, the bladder was displaced to the left and there was a right hydronephrosis.

A barium enema demonstrated upward displacement of the ascending colon.

Ultrasound examination showed a large inguinal mass of 8 cm, with solid and liquid areas (Fig. 1). The right ureter was dilated and displaced by the tumour.

On computed tomography (CT), a large tumour was demonstrated (Fig. 2) extending from the aortic bifurcation down to the right inguinal area. It contained fluid levels and areas of mixed density from 25 to 100 Hounsfield Units. Posteriorly, the tumour extended to the right ileo-psoas and anteriorly to the abdominal wall. There was no enhancement after an intravenous injection of contrast medium but the vessels were clearly visible (Fig. 3) within the mass. A diagnosis of cystic lymphangioma was made because of the association of fluid levels with solid areas.

At surgery, the mass could not be removed completely as there was adherence posteriorly where the obturator nerve was partially involved by the tumour. Further elements of the tumour could not be removed at the levels of the greater sciatic notch and obturator foramen. Parts of the anterior abdominal wall and ileo-psoas had to be excised because of infiltration by the tumour. Histological examination proved it to be a cystic lymphangioma of 298 g containing numerous cavities. Five years later, there has been no recurrence of the tumour.

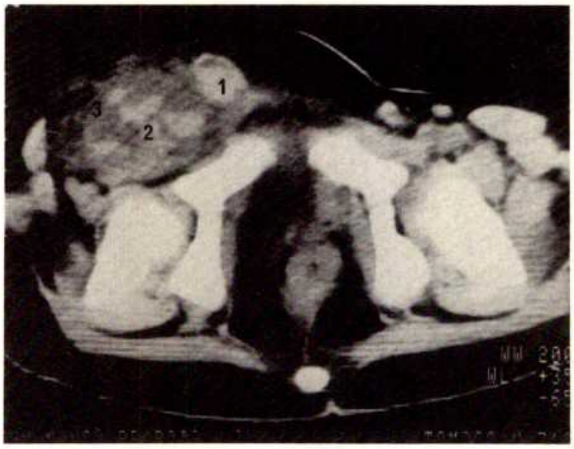

Figure 2. Computed tomographic scan showing extension of the tumour to the anterior part of the right thigh. Levels of liquid are also visible (1 = fluid level; 2 = liquid areas; 3 = solid areas).

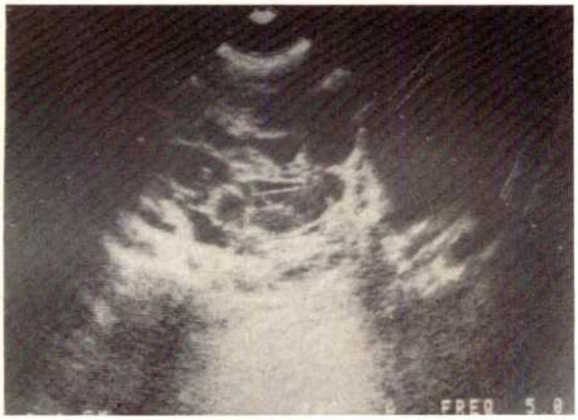

Figure 1. Heterogeneous echogenic mass with some cystic areas inside. The bladder is displaced to the right.

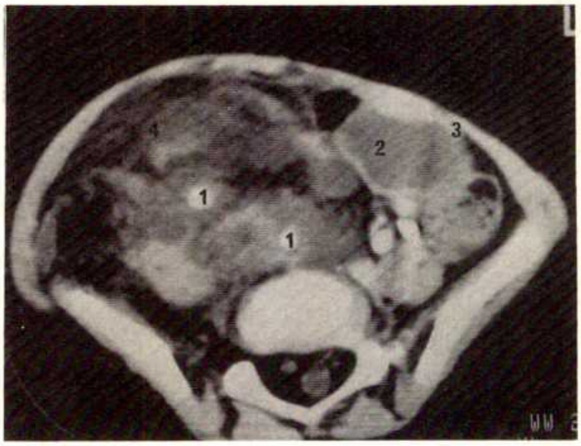

Figure 3. Computed tomographic scan taken after the injection of contrast medium; vessels are visible inside the tumour (1 = vessels; 2 = liquid; 3 = Wall of the cystic area; 4 = solid area of the lymphangioma).

---

*Author for reprint requests.

Discussion

Lymphangiomas are classified histologically into simple, cavernous and cystic, according to the size of the dilated lymphatics. Cystic lymphangiomas are unilocular or multilocular masses containing serous or chylous fluid. The cyst wall and septum consist of fibrous tissues, lymphatic tissues, vessels and smooth muscles with an inner surface of endothelial cells.

Cystic lymphangiomas arise as the result of congenital malformation of the lymphatic system (Godart, 1966) and are considered to be lymphatic hamartomas. There is a lack of adequate drainage from the sequestrated lymphatic vessels to the venous system because of insufficiency or atresia of the afferent channels. About 50% of these lesions are present at birth and up to 90% are evident by 2 years of age. Lymphangiomas enlarge during the early growth of the infant.

Ninety five per cent of lesions arise in the neck and the axilla. The rest arise in various sites.

In the literature, we have found 15 cases of scrotal lymphangioma (MacMillan et al, 1984). We have also found six lymphangiomas of the inguinal area.

In three cases, children of 70 days, 5 months and 3 years developed lymphangiomas mimicking an inguinal hernia (Hoffman, 1965; Kafka & Novak, 1970; Aboulola et al, 1975).

In two further cases, children of 2½ years and 2 years and 4 months, the lymphangioma appeared as an inguinal/abdominal tumour (Aboulola et al, 1975). The case described by Singh et al (1975) contains no clinical information. On CT or ultrasound, it is usual to find cystic areas with multiple septa. In our case, hemorrhage inside the cystic area explained the fluid levels.

Cystic lymphangiomas seldom cause acute clinical symptoms, but these may manifest themselves when the retroperitoneal cystic lymphangiomas are large enough to cause pressure on adjacent structures, such as the bowel and the ureters, or when they are complicated by infection, hemorrhage, or rupture.

Conclusion

We report a case of a rare inguinal lymphangioma where the diagnosis was facilitated pre-operatively by ultrasound and CT.

Acknowledgments

The authors would like to thank Dr P. B. Guyer, Royal South Hants Hospital, Southampton, for his help.

References

ABOULOLA, M., BOUKHELOUA, A., DANIEL, F. & BOUHADAFF, A., 1975. Lymphangiomes kystiques abdominaux chez l'enfant. *Chirurgie*, *101*, 852–857.

GODART, S., 1966. Embryological significance of lymphangioma. *Archives of Disease in Childhood*, *41*, 204–205.

HOFFMAN, E., 1965. Multicystic retroperitoneal lymphangioma presenting as an indirect inguinal hernia in a newborn. *American Surgeon*, *31*, 525–531.

KAFKA, V. & NOVAK, K., 1970. Multicystic retroperitoneal lymphangioma in an infant appearing as an inguinal hernia. *Journal of Pediatric Surgery*, *5*, 573.

MACMILLAN, R. W., MACDONALD, B. R. & ALPHERN, H. D., 1984. Scrotal lymphangioma. *Urology*, *23*, 79–80.

SINGH, S., BABOO, M. L. & PATHAK, I. C., 1971. Cystic lymphangioma in children; report of 32 cases including lesions at rare site. *Surgery*, *69*, 947–951.

Unusual presentation of non-Hodgkin's lymphoma of the small bowel

By D. A. Nicholson, BMedSci, BM, BS, FRCR

Department of Radiology, University Hospital of South Manchester, Nell Lane, West Didsbury, Manchester M20 8LR

(*Received February 1990 and in revised form March 1990*)

Small bowel non-Hodgkins lymphoma (NHL) usually present with abdominal pain (72%), vomiting and diarrhoea (28%); however, gastrointestinal (GI) bleeding is an uncommon mode of presentation (4%) (Makepeace et al, 1987). A case is presented where a patient with coexisting small bowel NHL and an abdominal aortic aneurysm presented with clinical symptoms suggestive of an aortoenteric fistula.

The mode of presentation for NHL is unusual, with computed tomography (CT) playing a significant role in the diagnosis and management.

Case report

A 75-year-old man presented with a 1-month history of intermittent episodes of non-colicky upper abdominal pain, mild weight loss, malaise, and black stools. Past medical history was unremarkable.

On examination he was anaemic with a pulsatile abdominal mass. Investigation revealed a haemoglobin of 4.9 g/dl, with normal urea, electrolytes, liver function tests and white count. Severe melaena with positive occult bloods was confirmed.

An abdominal ultrasound scan showed the presence of an 8 cm abdominal aortic aneurysm, with no evidence of leakage. Initially the patient was transfused with 6 units of blood. An urgent fibre-optic gastroscopy revealed no gastric or proximal duodenal abnormality. A presumptive diagnosis of aortoenteric fistula was made, on the clinical triad of upper GI bleeding, abdominal pain and abdominal aortic aneurysm (Ferguson & Arden, 1966).

An abdominal CT scan confirmed a large infrarenal aortic aneurysm which, although thin walled and close to the duodenum, showed no leak or erosion into bowel. In the upper

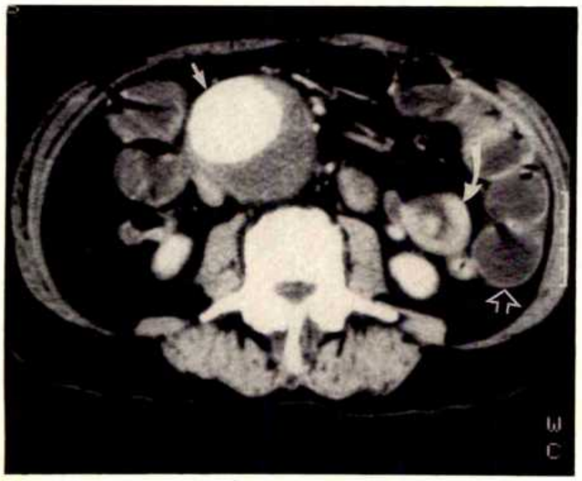

Figure 1. Computed tomographic scan during dynamic intravenous contrast infusion (level of lower poles of kidneys). Thin-walled aneurysm with mural thrombus (small arrow). Circumferential thickening of a small bowel loop is seen (curved arrow), with further dilated loops of small bowel (open arrow).

abdomen there were multiple loops of fluid-filled dilated small bowel. In addition, two separate abnormal areas of bowel were demonstrated; one with circumferential thickening of the bowel wall (Fig. 1), the second showing a lobular mass (4 × 3 cm) with proximal small bowel dilatation (Fig. 2). The liver and spleen were normal with no evidence of adenopathy.

At laparotomy, the proximal 1.5 m of small bowel were dilated leading to a 4 cm segment of intussuscepted nodular, haemorrhagic bowel. A further 3 cm long annular tumour was found 40 cm distal to the first lesion. No further intraperitoneal disease was seen. The diseased small bowel was resected and an end to end anastomosis performed. On inspection of the aortic aneurysm no aortoenteric fistula was identified. A routine aneurysm repair was performed with a Dacron tube graft. Histology confirmed the neoplasms as high grade diffuse non-Hodgkin's lymphoma extending through the bowel wall and involving peri-intestinal fat. No involved lymph nodes were identified.

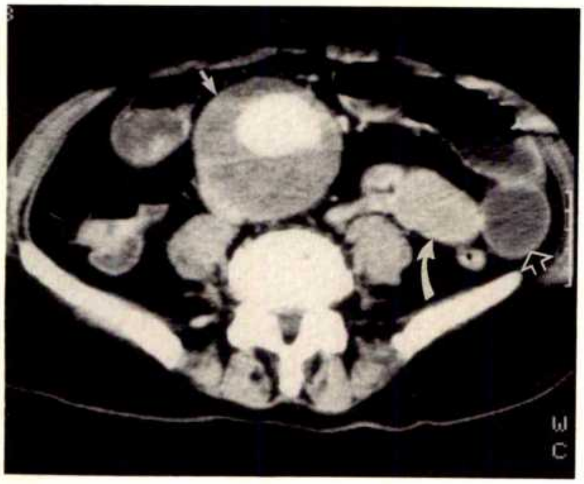

Figure 2. Computed tomographic scan during dynamic intravenous contrast infusion (level of iliac blades). A separate lobular mass is seen in the small bowel (curved arrow).

Discussion

Primary lymphoma is one of the commonest tumours of the small bowel accounting for about 40% of primary malignant neoplasms (Good, 1963). The most common site of involvement is the distal ileum, because of its abundance of lymphatic tissue; the duodenum is rarely involved (Brady & Ashell, 1980). Non-Hodgkin's lymphoma has a tendency to involve extranodal areas as its primary site, with the GI tract being the commonest involved organ (Freeman et al, 1972). However, 50–70% of patients with disseminated lymphoma will have incidental GI involvement (Rosenburgh et al, 1961). Mesenteric involvement and adenopathy is found in 50% of NHL, but only 4% of those with Hodgkin's disease (Spjut & Navarrtte, 1978). Multifocal tumours occur in 30% (Zornoza & Dodd, 1980), tending to be in the same organ (Green et al, 1979), as in this case.

According to most reports, surgery alone can be curative if the tumour is resectable (Lim et al, 1977). However, GI lymphoma is usually of an aggressive histology which adversely affects the prognosis: 5-year survival is 40% (Lim et al, 1977; Paulson et al, 1983). In addition, surgery carries a significant risk in the elderly, with a reported operative mortality of 9–19% (Maor et al, 1984).

Gastrointestinal bleeding, along with prodromal symptoms, is relatively uncommon in small bowel NHL, although abdominal pain is invariable. A small proportion present with malabsorption (Isaacson & Wright, 1978). A striking feature is the high incidence of perforation in contrast to other more common small bowel pathology such as Crohn's disease, with which confusion is common (Green et al, 1979). Further diagnostic difficulty occurs in distinguishing GI-NHL from carcinoma and carcinoid, although lymphomas often involve longer segments and are frequently multiple.

The most common radiological appearance of small bowel lymphoma is luminal narrowing, including stricture formation (Gourtsoyiannis & Nolan, 1988), intussuseption is uncommon. Other appearances include polypoid, infiltrating, ulceration, cavitation, thickened valvulae, multiple nodules, mesenteric masses and aneurysmal dilatation. The CT manifestations again exhibit a broad spectrum of radiological changes which depend on the underlying pattern of pathological involvement. Marked thickening of the bowel may be the only abnormality. Mesenteric involvement produces typical irregular lobulated masses that tend to displace bowel and may cause obstruction. Areas of reduced attenuation within the mesenteric masses occasionally occur owing to tumour necrosis.

Because of non-specfic presentation of small bowel lymphoma, the tumour is rarely diagnosed prior to surgery (Green et al, 1979). Although an aortoenteric fistula was clinically suspected in this patient, the CT revealed two abnormal areas of bowel at different sites, with associated obstruction. This raised the suspicion of a co-existing NHL with the aortic aneurysm, giving the opportunity to perform a formal staging laparotomy, adding valuable additional information in planning further treatment.

References

Brady, L. W. & Ashell, S. O., 1980. Malignant lymphoma of the gastointestinal tract. *Radiology*, *137*, 291.

Ferguson, J. P. & Arden, M. J., 1966. Gastrointestinal haemorrhage secondary to rupture of the aorta. *Archives of Internal Medicine*, *117*, 133–140.

Freeman, C., Berg, J. W. & Cutler, S. J., 1972. Occurence and prognosis of extranodal lymphomas. *Cancer*, *29*, 252–260.

Good, C. A., 1963. Tumours of the small intestine. *American Journal of Roentgenology*, *89*, 685–705.

Gourtsoyiannis, N. C. & Nolan, D. J., 1988. Lymphoma of the small bowel: radiological appearances. *Clinical Radiology*, *39*, 639–645.

Green, J. A., Dawson, A. A., Jones, P. F. & Brunt, P. W., 1979. The presentation of gastrointestinal lymphoma: study of a population. *British Journal of Surgery*, *66*, 798–801.

Issacson, P. & Wright, D. H., 1978. Intestinal lymphomas associated with malabsorption. *Lancet*, *i*, 67–70.

Lim, F. E., Haetman, A. S., Tan, E. G., Cady, B. & Meissner, W. A., 1977. Factors in the prognosis of gastric lymphoma. *Cancer*, *39*, 1715–1720.

Makepeace, A. R., Fermont, D. C. & Bennett, M. H., 1987. Gastrointestinal non-Hodgkin's lymphoma. *Clinical Radiology*, *38*, 609–614.

Maor, M. H., Maddux, B., Osbourne, B. M., Fuller, L. M., Sullivan, J. A. & Nelson, R. S., 1984. Stages IE and IIE non-Hodgkin's lymphoma of the stomach. *Cancer*, *54*, 2330–2337.

Paulson, S., Sheehan, R. G. & Stone, M. J., 1983. Large cell lymphomas of the stomach: improved prognosis with the resection of all intrinsic gastrointestinal disease. *Journal of Clinical Oncology*, *1*, 263–269.

Rosenberg, S. A., Diamond, H. D., Jaslowitz, B. & Craver, L. F., 1961. Lymphosarcoma: a review of 1209 cases. *Medicine*, *40*, 31–84.

Spjut, A. J. & Navarette, A., 1978. *Alimentary Tract Roentgenology* (C. V. Mosby, St Louis), p. 787.

Zornoza, J. & Dodd, G. D., 1980. Lymphoma of the gastrointestinal tract. *Seminars in Roentgenology*, *15*, 272–287.

Ultrasound appearances of extramedullary haematopoiesis in the liver and spleen

By M. J. Bradley, MB, ChB, FRCR and C. Metreweli, FRCR, FRCP

Department of Radiodiagnosis and Organ Imaging, Prince of Wales Hospital, Shatin, Hong Kong

(Received December 1989)

Extramedullary haematopoiesis is an uncommon finding in the adult patient. Many sites have been described, the liver and spleen being more common. The ultrasound appearances have not been well documented. Two cases of extramedullary haematopoiesis in the liver and spleen are presented.

Case reports

Case 1

A 58-year-old man presented with a history of a cough, haemoptysis, dyspnoea and weight loss. On examination he had finger clubbing, no significant chest signs and hepatomegaly. A bronchial neoplasm was suspected clinically and the initial chest radiograph demonstrated a right lung mass adjacent to the hilum. Full blood count was normal and the erythrocyte sedimentation rate was raised at 52 mm/h. Bronchoscopy revealed extrinsic compression of the right upper lobe bronchus but biopsy was unsuccessful. Ultrasound examination of the abdomen demonstrated multiple echogenic lesions in an enlarged liver (Fig. 1). Some of these lesions contained central echo-poor areas. The spleen was of normal size, and contained one echogenic mass similar to those in the liver. No other abnormality was shown in the remainder of the abdomen and pelvis.

The most likely diagnosis for these lesions was metastatic

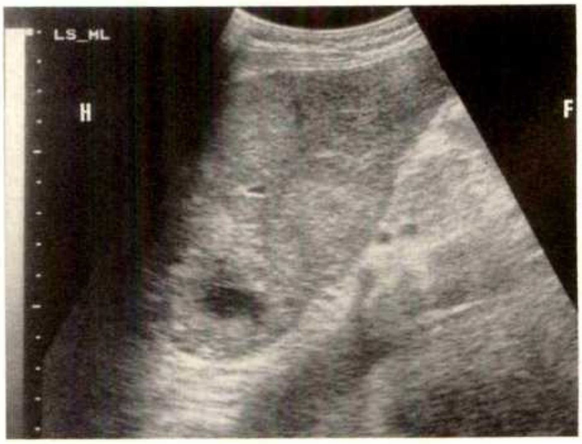

Figure 1. Longitudinal section of the right lobe of liver showing several echogenic foci, one with central necrosis.

Address for correspondence: University Department of Radiodiagnosis, Royal Liverpool Hospital, Prescot Street, Liverpool L7 8XP.

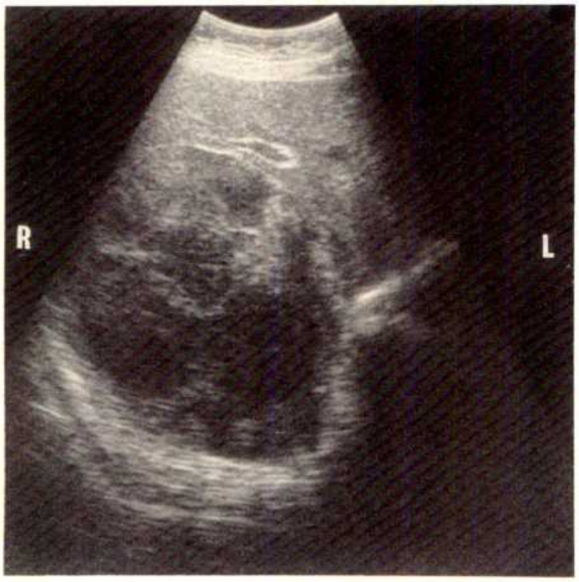

Figure 2. Transverse section through the right lobe of liver showing the large heterogeneous mass displacing the right portal vein.

carcinoma. Ultrasound-guided Trucut biopsy was performed. The lesion chosen was peripheral and without any central echo-poor area.

Histology revealed immature and mature cells of the myeloid and erythroid series with occasional megakaryocytes. Dilated sinusoids and portal tracts contained pleomorphic infiltrate. These are the features of hepatic extramedullary haematopoiesis. An isotope bone scintigram using ^{99}Tc^{m} MDP revealed multiple hot spots in the femora, ribs, skull and spine, interpreted as being metastases. A repeat bronchial biopsy was successful and this confirmed the presence of a small cell carcinoma.

Case 2

A 31-year-old woman with β thalassaemia intermedia presented with right upper quadrant pain and mass. On examination she had Mongoloid facies. She looked pale and had hepatomegaly but no jaundice. There was a large mass in the right upper quadrant. The presence of hepatoma was suspected. The haemoglobin was 8.8 g/dm^3 with 3% reticulocytes. The blood film showed schistocytes, target cells and poikilocytosis. Electrophoresis confirmed Hb-A and increased levels of HbF and HbA2. Alpha-Feto protein and liver function tests were normal. A skull radiograph revealed the typical spiculated vault of haemoglobinopathy. The chest radiograph was normal.

Ultrasound showed hepatosplenomegaly with a large, fairly well defined, inhomogenous solid mass in the right lobe of liver, 15 cm in diameter (Fig. 2). There was no vessel invasion or signs of cirrhosis. Computed tomography (CT) showed a mixed attenuation pattern, with patchy contrast enhancement. It did not have any demonstrable fat content (Fig. 3). An ultrasound-guided Trucut biopsy was performed. Histology revealed extramedullary haematopoiesis.

Discussion

Hepatic extramedullary haematopoiesis is a normal feature in the fetus and in the neonatal liver up to 5 weeks of age. It may persist in the presence of anaemia. In adults, extramedullary haematopoiesis is uncommon (MacSween et al, 1987). It is associated with loss of bone marrow due to myeloproliferative disease. Other causes include aplastic anaemia, marrow replacement syndromes, disseminated carcinomatosis, multiple myeloma and Albers Schonberg (Marble bone) disease.

Extramedullary haematopoiesis is well recognized in the thoracic paravertebral region, sometimes with intraspinal extension even causing paraplegia (Mann et al, 1987). It has been reported to arise in a wide variety of tissues including spleen, liver, adrenal, retroperitoneal fat, gastrointestinal lymphatic, breast, skin and dura mater (Ross & Logan, 1969; Bronn et al, 1980).

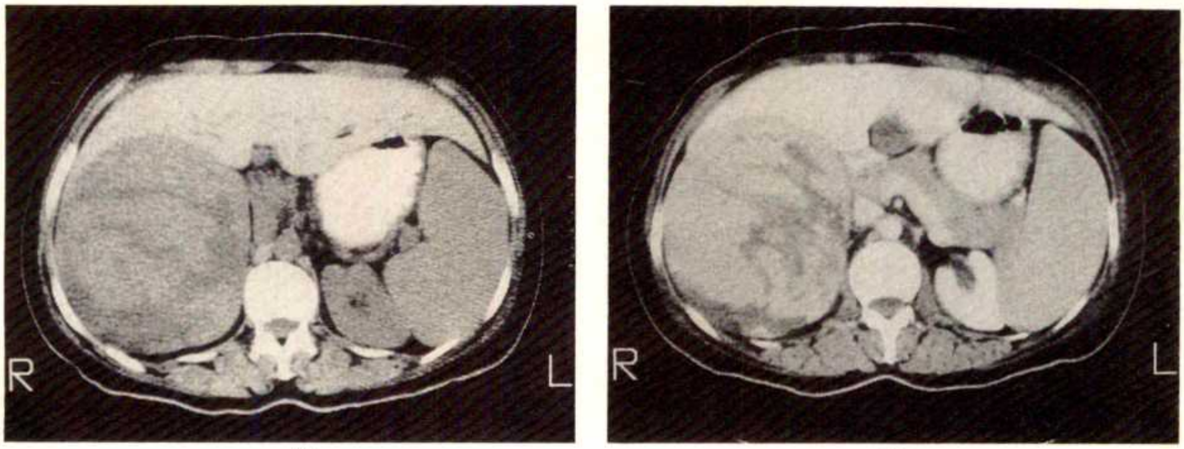

(a) (b)

Figure 3. (a) Plain CT slice showing the heterogeneous mass right lobe of liver. (b) The mass enhanced heterogeneously with contrast medium.

There have only been two previously reported cases of the echography of extramedullary haematopoiesis in a patient with agnogenic myeloid metaplasia in the liver (Weiner et al, 1987) and in a woman with polycythaemia rubra vera (Abbitt & Teates, 1989). In both cases, ultrasound demonstrated hepatosplenomegaly with a large heterogenous solid mass in the right lobe of liver, similar to Case 2 reported here. Case 1 had different ultrasound appearances, in that the lesions were multiple in both liver and spleen; they were echogenic, some with central echo-poor areas, interpreted as necrosis.

The differential diagnosis of ultrasonically echogenic liver lesions is wide, and includes haemangiomas, abscesses, focal nodular hyperplasia, adenoma, haemorrhage, focal fatty infiltration, hepatoma and metastases (Cosgrove & McCready, 1982). It is now necessary to include extramedullary haematopoiesis to this list especially in the presence of marrow disease. Histology obtained by guided biopsy is needed for the definitive diagnosis.

The typical histology of extramedullary haematopoiesis shows plesmorphic clumps of erythroid and myeloid precursors along with megakaryocytes in the sinusoids, the space of Disse and portal tracts. The pleomorphism differentiates this from the infiltrations of leukaemia, infections mononucleosis and tropical splenomegaly syndrome (MacSween et al, 1987). Extramedullary haematopoietic tissue may constitute parts of some other tumours such as angiomyoliopoma of the liver, adenoma, angiosarcoma and hepatoblastoma but these are differentiated by the histology (Miyahara et al, 1988).

The echographic appearances described would normally be attributed to metastases, especially when there is a known primary malignancy. This raises the question that extramedullary haematopoiesis in the liver may be more common in cases with marrow replacement than has been previously suspected. An increased awareness of this possibility may discover more such cases.

Conclusion

Solitary or multifocal heterogenous solid masses in the liver and spleen have a wide differential diagnosis. Extramedullary haematopoiesis should be included in the differential diagnosis of these echographic appearances, especially when there is marrow replacement or anaemia. Ultrasound-guided biopsy is diagnostic.

References

ABBITT, P. L. & TEATES, C., 1989. The sonographic appearance of extramedullary haematopoiesis in the liver. *Journal of Clinical Ultrasound, 17,* 280–282.

BRONN, L. J., PAQUELET, J. R. & TETALMAN, M. R., 1980. Intrahepatic extramedullary haematopoiesis: appearance on 99M TcSulfur colloid marrow scan. *American Journal of Roentgenology, 134,* 1245–1255.

COSGROVE, D. & MCCREADY, R., 1982. *Ultrasound Imaging of the Liver* (Wiley Medical, Chichester), pp. 149–194.

MACSWEEN, R. N. M., ANTHONY, P. P. & SCHEUER, P. J., 1987. *Pathology of the Liver, 2nd edn* (Churchill Livingstone, Edinburgh), p. 665.

MANN, K. S., YUE, C. P., CHAN, K. H., MA, C. T. & NGAN, H., 1987. Paraplegia due to extramedullary haematopoiesis in thalassaemia. *Journal of Neurosurgery (United States), 66,* 938–940.

MIYAHARA, M. et al, 1988. Giant hepatic angiomyolipoma simulating focal nodular hyperplasia. *Japanese Journal of Surgery, 18,* 346–350.

ROSS, P. & LOGAN W., 1969. Roentgen findings in extramedullary haematopoiesis. *American Journal of Roentgenology, 106,* 604–613.

WEINER, M. D., HALVORSEN, R., VOLLMER, R., FOSTER, W. & ROBERTS, L., 1987. Focal intrahepatic extramedullary haematopoiesis mimicking neoplasm. *American Journal of Roentgenology, 149,* 1171–1172.

1990, *The British Journal of Radiology*, 63, 819–820

Case of the month

A case of post-operative paresis

By J. F. C. Olliff, MRCP, FRCR, S. J. Gwyther, MB, FRCS and G. Hart, FRCR

The Royal Marsden Hospital, Downs Road, Sutton, Surrey SM2 5PT and *Atkinson Morley Hospital, Copse Hill, Wimbledon SW20 0NE

(*Received September 1989 and in revised form November 1989*)

An 82-year-old man was admitted for biopsy of an anal mass lesion. Histology revealed a moderately well differentiated squamous cell carcinoma originating at the anal margin. Post-operative pyrexia resolved with intravenous antibiotics. Five days after this he developed neck stiffness, urinary retention and left-sided weakness with a sensory level at C4. Radiographs of the cervical spine were obtained and a cervical myelogram performed (Figs 1 and 2).

What features are seen on the two examinations and what are the likely causes?

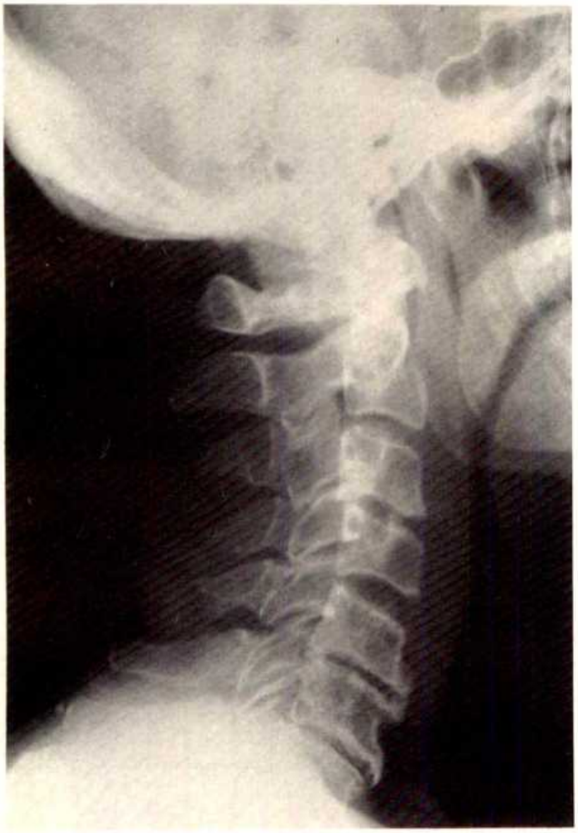

Figure 1. Lateral plain radiograph of the cervical spine.

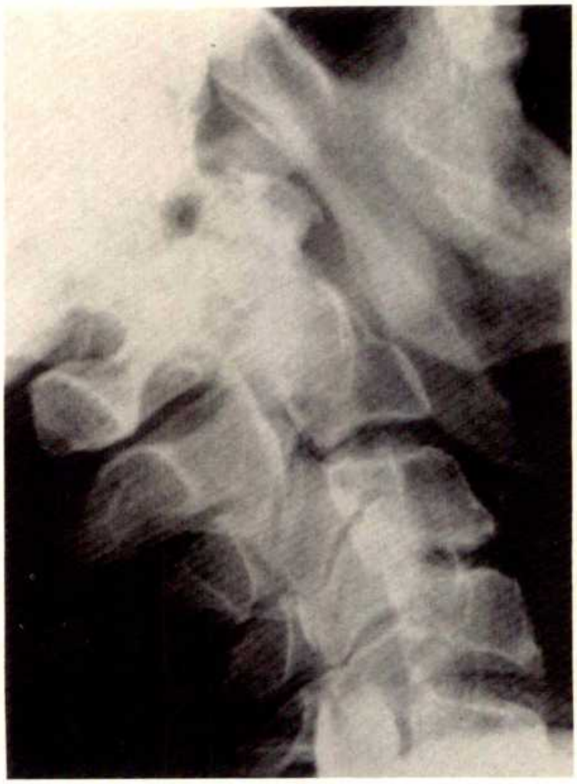

Figure 2. Prone lateral view of the cervical spine from a myelographic series.

The cervical spine radiograph (Fig. 1) shows degenerative changes with reduced height of the disc joint and osteophyte formation at C5/6 and C6/7. The height of the disc joint is also reduced at C3/4 with grade 1 backward slip of C3 on C4. The marginal hypertrophic changes are relatively slight. Subtle prevertebral soft-tissue swelling can be recognized anteriorly at this level. The myelogram shows almost complete obstruction to flow of contrast medium at the level of the C4/5 disc joint. The theca is displaced posteriorly at this level and the appearances would be in keeping with an extradural obstruction: only a small amount of contrast medium being visible superiorly at C2.

Magnetic resonance imaging (MRI) of the neck was undertaken. The sagittal T_1 weighted (time to repeat (TR) 500 ms, time to echo (TE) 17 ms) image demonstrates abnormal low signal in the vertebral bodies of C3 and C4 with thickening of the pre-vertebral, retropharyngeal soft tissues anteriorly (Fig. 3a). Abnormal soft tissue is also shown extending in a linear fashion posterior to these vertebral bodies within the spinal canal, anterior to the spinal cord. On the T_2 weighted (TR 2.1 s, TE 90 ms) image, abnormal high signal can be seen in the vertebral bodies of C3 and C4 adjacent to the intervening intervertebral disc which also shows high signal only at this level (Fig. 3b). The soft-tissue swelling anteriorly and posterior to these vertebral bodies is also confirmed by abnormal high signal. This T_2 weighting gives a "myelographic effect" and the extradural soft-tissue mass anterior to the cord at C3/4 is better appreciated on this image than on the T_1 weighted image.

These are the features of a discitis and associated vertebral osteomyelitis. On the plain film the slight loss of disc joint height at C3/4 could be interpreted as being a result of degenerative disease, although there is little marginal hypertrophy and subtle soft-tissue swelling is seen anteriorly. At this level the prevertebral soft tissues should not measure greater than one third of the sagittal diameter of the vertebral body or more than 4 mm, provided conventional examination can be made without magnification (Weir, 1975). The myelogram showed the pattern of extradural obstruction to flow of contrast from the level of C4/5. The differential diagnosis of an extradural block includes extradural malignancy, degenerative hypertrophy, infection and haematoma.

Squamous cell carcinomas of the anal margin very rarely metastasize to bone and with the recent history of pyrexia, infection seemed the most likely cause.

The three major pathogenetic mechanisms of acute osteomyelitis are haematogenous spread, direct inoculation secondary to trauma or surgery and contiguous spread from adjacent or soft tissue infection (Wald, 1985). In this patient with no history of the last two causes it would seem that haematogenous spread was the underlying mechanism. Acute haematogenous osteomyelitis predominantly affects the long tubular bones. In adults the vertebral bodies are also often affected. In a post-surgical patient, one risk factor is the use of indwelling catheters for vascular access, another factor is a distant focus of infection such as an abscess or cellulitis.

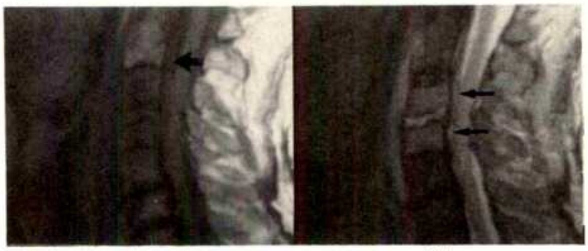
(a) (b)

Figure 3. (a) Sagittal T_1 weighted (TR 50 msec TE 17 msecs) view of the neck demonstrates abnormal low signal in the vertebral bodies of C3 and C4. Subtle soft-tissue swelling is noted anterior to these vertebral bodies. Abnormal signal is also seen extending in a linear fashion posterior to the vertebral bodies of C3 and C4 (arrow). (b) Sagittal T_2 weighted (TR 2.1 s TE 90 ms) view of the neck which demonstrates abnormal high signal within the vertebral bodies of C3 and C4 with high signal in the intervening disc joint. Abnormal high signal is also seen in the soft tissues anteriorly and extending posterior to these vertebral bodies within the spinal canal (arrows).

Magnetic resonance imaging elegantly demonstrates the features of an infective process centred on the C3/4 disc joint with adjacent vertebral osteomyelitis. Inflammation causes prolongation of the T_1 and T_2 relaxation times of the vertebral marrow and adjacent soft tissue. On the T_1 weighted images there is reduction of signal from the marrow of the infected vertebral bodies. On T_2 weighted images the infected vertebral bodies, disc and inflamed tissue have a higher signal intensity than adjacent normal structures. The multiplanar imaging ability of MR allows accurate assessment of the superior and inferior limits of the extradural mass. This is not always possible on myelography which is less precise.

Magnetic resonance imaging has been shown to be more sensitive and specific for vertebral osteomyelitis than either plain radiography or radio-isotope bone scans, providing diagnostic accuracy similar to combined Gallium and ^{99}Tc^{m} HDP bone scans, and also providing more information regarding the thecal sac and neural structures. Changes of vertebral osteomyelitis on MRI are apparent sooner than on plain radiographs, but appear at about the same stage in evolution as can be detected by increased isotope concentration on radionuclide scan. In follow-up of treated patients, the resolution of disc joint infection with appropriate therapy is accompanied by a return to normal of the signal intensity changes on both T_1 and T_2 weighted images (Modic et al, 1985).

References

MODIC, M. T., FEIGLIN, D. H., PIRAINO, D. W., BOUMPHREY, F., WEINSTEIN, M. A., DUCHESNEAU, P. M. & REHM, S., 1985. Vertebral osteomyelitis assessment using MR. *Radiology*, *157*, 157–166.

WEIR, D. C., 1975. Roentgenographic signs of cervical injury. *Clinics in Orthopaedics*, *109*, 9–17.

WALD, R. W., 1985. Risk factors for osteomyelitis. *The American Journal of Medicine*, *78*, 206–212.

1990, *The British Journal of Radiology*, 63, 821–823

Short communications

Mathematical models of repopulation and reoxygenation in radiotherapy

By O. C. A. Scott, MD

The Richard Dimbleby Department of Cancer Research, UMDS, St Thomas' Hospital, London SE1 7EH

(*Received January 1990 and in final form May 1990*)

Mathematical models of the effect of ionizing radiation on tumours have not, so far, received general acceptance, and Wheldon (1989) warns of the dangers of over-generalization. Nevertheless, the construction of models may have a certain value, in that we are forced to define our assumptions with clarity.

It is interesting to compare two models which have been described in the columns of the *BJR*: "Misonidazole in fractionated radiotherapy: are many small fractions best?" (Denekamp et al, 1980) and "The linear-quadratic formula and progress in fractionated radiotherapy" (Fowler, 1989). The former gives a detailed description of the possible effect of reoxygenation on tumour response, but excludes repopulation. The latter is much concerned with repopulation, but excludes reoxygenation. Evidence that hypoxic cells may be important in the clinical response of tumours has been published recently (Gatenby et al, 1988; Whittle et al, 1990), and it would appear to be logical to combine the two models.

Denekamp et al give a full description of their model, and any computer-literate reader could reconstruct the programs from which they worked. The addition of repopulation is a simple matter, but the marriage of the two programs forces us to face an interesting question: which class of cells repopulates, the oxic or the hypoxic? The work of Tannock (1968), also quoted by Suit et al (1977), suggests that cells deprived of both oxygen and nutrients in a tumour cord are less likely to divide. It may be useful to investigate the consequences of the rather extreme hypothesis that all tumour cell repopulation occurs initially in the oxic compartment.

The addition of another parameter to the model of Denekamp et al implies that there is a very large number of possible combinations of dose and fractionation which could be investigated. A single example is provided in Fig. 1. Here, accelerated repopulation is considered to begin immediately after the first fraction. This is case "a" in Figs 3–6 of Fowler's article, where the effect of repopulation is at a maximum. The linear-quadratic equation is assumed with $\alpha = 0.35\ \mathrm{Gy}^{-1}$ and $\alpha/\beta = 10$ Gy. For the case where no hypoxic cells are present in a tumour, the calculated plot of $-\log_{10}$ cell kill against doubling time of clonogenic cells agrees with the line shown in Fig. 3a of Fowler's article, for a conventional 30 F × 2 Gy/6 week treatment. As can be seen, increasing the doubling times from 2 to 20 days predicts a massive change in cell kill of 5 logs or a factor of 100 000.

However, if we postulate a 10% hypoxic fraction and an oxygen enhancement ratio (OER) of 2.7 (as did Denekamp et al), and there is no reoxygenation, then repopulation restricted to oxic cells would have a negligible effect on total cell kill. Levels of reoxygenation of 10% or 20% per day of treatment give intermediate results. My model assumes that as soon as a hypoxic cell is reoxygenated, it has a chance of dividing within 24 hours. It was found that the order of the two processes, reoxygenation and repopulation, in a given interval, had little effect on the computation, and I have arbitrarily assumed that repopulation of existing oxic cells precedes reoxygenation in each daily interval. The regrowth of hypoxic cells returned to an oxic environment has been investigated by Wilson et al (1990).

Do we have a testable hypothesis here? Experiments of the type described by Suit et al (1977) could be helpful. They compared the results of 10 fractions, in an overall time of 9 or 18 days, on a mouse mammary tumour. The TCD_{50} (120 days) was found to be 105 Gy at 9 days and 100.1 Gy at 18 days, implying no repopulation in the critically important class of cells, if the irradiation was carried out in air. The response of these tumours is dominated by the response of the hypoxic cells, as can be seen from the reduction of TCD_{50} due to HPO. If the tumours were clamped at the time of irradiation (in which case the survival of the normally oxic cells becomes significant) then the TCD_{50} increased from 129.6 Gy at 9 days to 149.1 Gy at 18 days, a highly significant change, suggesting that repopulation was confined to the oxic compartment.

In a rapidly growing rodent tumour, the picture could be blurred at long time intervals by islands of repopulating oxic cells forming a new hypoxic centre, (called "re-hypoxygenation" by H. R. Withers, personal communication). This possibility was also considered by Suit et al (page 444).

If further work should confirm the idea that repopulation may be relatively unimportant in those tumours where the

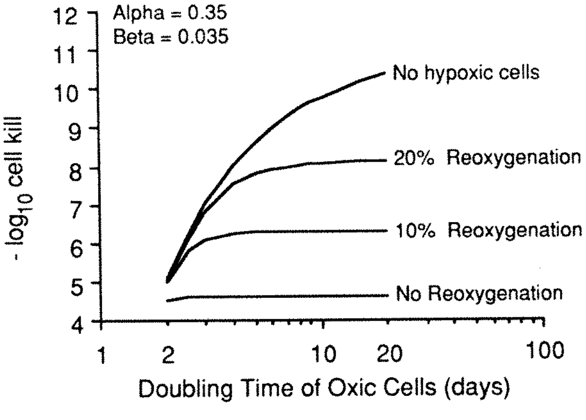

Figure 1. Calculated $-\log_{10}$ cell kill as a function of assumed doubling times of tumorigenic cells from 2 to 20 days, for a standard schedule of 30 fractions of 2 Gy in 6 weeks. The case of no hypoxic cells was considered by Fowler (1989) in his Fig. 3a. (Repopulation commences immediately after the first fraction.) The other three cases were based on the assumption of an initial hypoxic fraction of 10%.

response is dominated by hypoxic cells, the consequences for the planning of future clinical trials could be significant.

Fowler (1989) made an interesting comparison between the continuous hyperfractionated accelerated radiation therapy (CHART) treatment (36 fractions in 12 days, Saunders & Dische, 1986) and conventional treatment (daily treatment in 6 or 7 weeks). His model, based on repopulation, predicts that CHART would not be more effective than conventional treatment in terms of tumour cell kill, unless the doubling time of clonogenic cells is short. Just how short depends on the time of onset of accelerated repopulation and the absolute value of α, the α/β ratio being held constant (Fowler, 1989, Fig. 4).

The same point can be demonstrated in terms of the crossing point of the curves of log cell kill against clonogen doubling time. CHART will only kill more tumour cells than conventional treatment if the clonogen doubling time is shorter than that at the crossing point. In Table I, the points where the curves computed for CHART (36 F/1.5 Gy) and for 35 F/2 Gy in 7 weeks, cross are given, in days, as shown by Fowler in his Fig. 4. For the case of all cells oxic, the computed crossing points agree with Fowler's curves. (The 7-week treatment involves 46 repopulation cycles, and repopulation was assumed to start immediately after the first treatment). For example, if $\alpha = 0.25\,\text{Gy}^{-1}$ and all the cells are oxic, there will be no increased tumour cell kill, using CHART, unless the clonogen doubling time is less than 4.45 days.

The addition of a hypoxic fraction, with or without reoxygenation, reduces the doubling time at the crossing point for all values of α, and therefore reduces the number of cases where the use of CHART might be expected to have more effect on the tumour. However, it should be pointed out that the model under consideration is a gross over-simplification and the fact that good tumour responses have been observed in the clinic is of far greater significance than the predictions of any model.

It may also be of interest to look at the possible influence of a hypoxic sensitizer. Table II shows the computed enhancement ratios (ERs) in terms of dose ratio (*i.e.* changing the dose per fraction) for iso-effect on the tumour, if the sensitizer enhancement ratio (SER) for hypoxic cells is equal to 2, assuming a hypoxic fraction of 10% and no reoxygenation. The hypoxic sensitizer is predicted to be much more effective when combined with CHART than with conventional treatment, if the doubling time of the oxic clonogens is short, and the values of α are low. The reason for this result is that if relatively few oxic cells are killed and if the survivors repopulate rapidly, then repopulation can counterbalance cell kill. For instance, if $\alpha = 0.1444\,\text{Gy}^{-1}$ and $\alpha/\beta = 10\,\text{Gy}$ then 2 Gy per day would balance a doubling time of 2 days, *i.e.* the oxic population would remain constant with repeated daily doses of 2 Gy, whereas the hypoxic cells, which do not repopulate according to this model, would be gradually eliminated. In other words, an oxic, but dividing, cell could be a greater danger than a hypoxic non-dividing one. According to the present model, a reoxygenated cell also starts to divide, so we have the paradox that reoxygenation could sometimes be a disadvantage. The recent work of Wilson et al (1990) suggests that reoxygenated cells may divide, but at a slower rate.

Table I. Crossing points, in terms of clonogen doubling time (CDT) in days for the plots of log cell kill against CDT for CHART (36 F/1.5 Gy) and standard treatment (35 F/2 Gy)

α	10% Hypoxic fraction reoxygenation per day			All cells oxic
	None	10%	20%	
0.25	2.39	2.59	2.84	4.45
0.3	1.93	2.07	2.24	3.69
0.35	1.62	1.72	1.84	3.17
0.4	1.39	1.47	1.56	2.76
0.45	1.22	1.28	1.35	2.46

Table II. Enhancement ratios for iso-effect on a tumour, assuming a sensitizer enhancement ratio of 2 on hypoxic cells and an OER of 2.7. Hypoxic fraction = 0.1. No reoxygenation. Standard treatment (35 F/2 Gy)

α	Standard treatment		CHART	
	2 day CDT	5 day CDT	2 day CDT	5 day CDT
0.25	1.001	1.69	1.7	1.93
0.3	1.01	1.85	1.85	1.97
0.35	1.14	1.94	1.93	1.99
0.4	1.35	1.98	1.97	2
0.45	1.51	1.99	1.99	2

In summary, if α is small and clonogenic cell doubling time is short, oxic cells dominate the picture. If α is large and the doubling time is long, then hypoxic cells determine the tumour response, as seen in Fig. 1. Since there is less repopulation with CHART, hypoxic cells become relatively more important, and therefore the gain from using a hypoxic sensitizer is increased.

However, other factors could operate in the opposite sense. If sensitization by hypoxic sensitizers is reduced at low doses per fraction, as has been claimed for oxygen (Révész & Palcic, 1985; Watts et al, 1986), then the gain from combining a hypoxic sensitizer with CHART would be reduced.

The assumption of no reoxygenation in Table II may seem rather extreme, but the encouraging results obtained with hyperbaric oxygen (Whittle et al, 1990) suggest that hypoxic cells may persist after some fractionation regimes.

It is to be hoped that the hypothesis that repopulation is restricted to oxic cells will stimulate further work.

References

DENEKAMP, J., MCNALLY, N. J., FOWLER, J. F. & JOINER, M. C., 1980. Misonidazole in fractionated radiotherapy: are many small fractions best? *British Journal of Radiology, 53,* 981–990.

FOWLER, J. F., 1989. The linear-quadratic formula and progress in fractionated radiotherapy. *British Journal of Radiology, 62,* 679–694.

GATENBY, R. A., KESSLER, H. B., ROSENBLUM, J. S., COIA, L. R., MOLDOFSKY, P. J., HARTZ, W. H. & BRODER, G. J., 1988. Oxygen distribution in squamous cell carcinoma metastases and its relationship to outcome of radiation therapy. *International Journal of Radiation Oncology, Biology, Physics, 14,* 831–838.

RÉVÉSZ, L. & PALCIC, B., 1985. Radiation dose dependence of the sensitization by oxygen and oxygen mimic sensitizers. *Acta Radiologica Oncology, 24,* 209–217.

SAUNDERS, M. I. & DISCHE, S., 1986. Radiotherapy employing three fractions in each day over a continuous period of 12 days. *British Journal of Radiology, 59,* 523–525.

SUIT, H. D., HOWES, A. E. & HUNTER, N., 1977. Dependence of response of a C3H mammary carcinoma to fractionated irradiation on fractionation number and intertreatment interval. *Radiation Research, 72,* 440–454.

1990, *The British Journal of Radiology*, *63*, 823–825

Tannock, I. F., 1968. The relationship between cell proliferation and the vascular system in a transplanted mouse mammary tumour. *British Journal of Cancer*, *22*, 258–273.

Watts, M. E., Hodgkiss, R. J., Jones, N. R. & Fowler, J. F., 1986. Radiosensitization of Chinese hamster cells by oxygen and misonidazole at low X-ray doses. *International Journal of Radiation Biology*, *50*, 1009–1021.

Wheldon, T. E., 1989. Radiobiological rationales in radiotherapy: the role of models. *British Journal of Radiology*, *62*, 1113–1114.

Whittle, R. J. M., Fuller, A. P. & Foley, R. R., 1990. Glottic cancer: results of treatment with radiotherapy in air and hyperbaric oxygen. *Clinical Oncology*, *2*, 214–219.

Wilson, R. E., Keng, P. C. & Sutherland, R. M., 1990. Changes in growth characteristics and macromolecular synthesis on recovery from severe hypoxia. *British Journal of Cancer*, *61*, 14–21.

Contrast medium imbibition in osteoarthritic cartilage

By M. W. Spring, BSc and J. C. Buckland-Wright, PhD

Macroradiographic Research Unit, Department of Anatomy, United Medical and Dental Schools of Guys' and St Thomas's Hospitals, Guys' Campus, London Bridge, London

(*Received November 1989 and in revised form February 1990*)

Double contrast arthrography is routinely used in the examination of synovial joints as the articular cartilage and capsular surfaces are more clearly delineated than with a single contrast technique. Tears, pitting and thinning of articular and meniscal cartilages are readily identified (Stoker, 1980; Fujikawa, 1981). Stoker (1980) has described the way that osteoarthritic changes in articular cartilage are heralded by the absorption of the contrast agent. This observation forms the basis of a current investigation into the articular changes in patients with osteoarthritis of the knee using high definition microfocal radiography (Buckland-Wright, 1989; Buckland-Wright & Bradshaw, 1989). To understand the process of contrast medium imbibition into articular cartilage, the present *in vitro* study was undertaken to determine whether the rate and the volume of contrast medium diffusing into articular cartilage was related to the histological condition of the tissue.

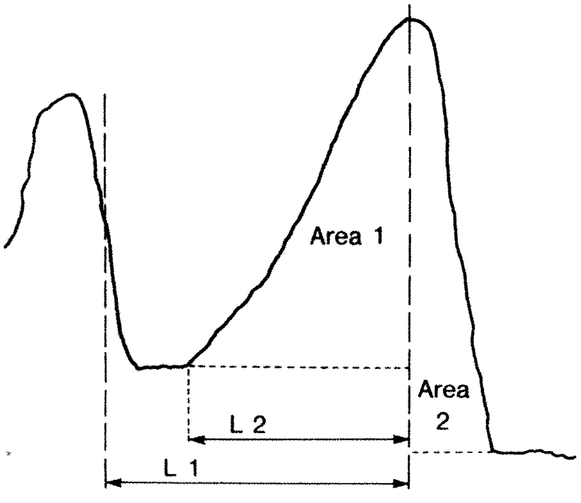

Figure 1. Diagram of a densitometric trace of a macroradiograph of contrast medium imbibition in articular cartilage illustrating the measurements taken from the trace. L1 is the thickness of the cartilage and L2 the depth to which the contrast had penetrated the tissue. Area 1, above the broken line, represents the increased density corresponding to the volume of absorbed contrast medium in the cartilage and Area 2 is the increased density corresponding to the volume of the medium on the samples' surface.

Materials and methods

Thirty-seven samples of visually intact articular cartilage were obtained from the tibial plateau of fresh post-mortem subjects, three women and two men with early osteoarthritis and a mean age of 67.2 ± 15.0 years. Only five subjects were obtained for this study as we were not examining inter-subject variation but variation between samples, which were taken

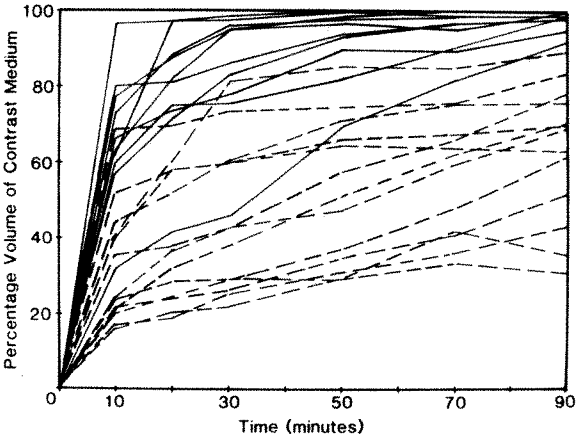

Figure 2. Graph showing the percentage volume of contrast medium absorbed by articular cartilage against time. Refer to text for explanation.

Address for correspondence: Dr J. C. Buckland-Wright, Anatomy Department, Guys' Hospital Medical School, London Bridge, London SE1 9RT.

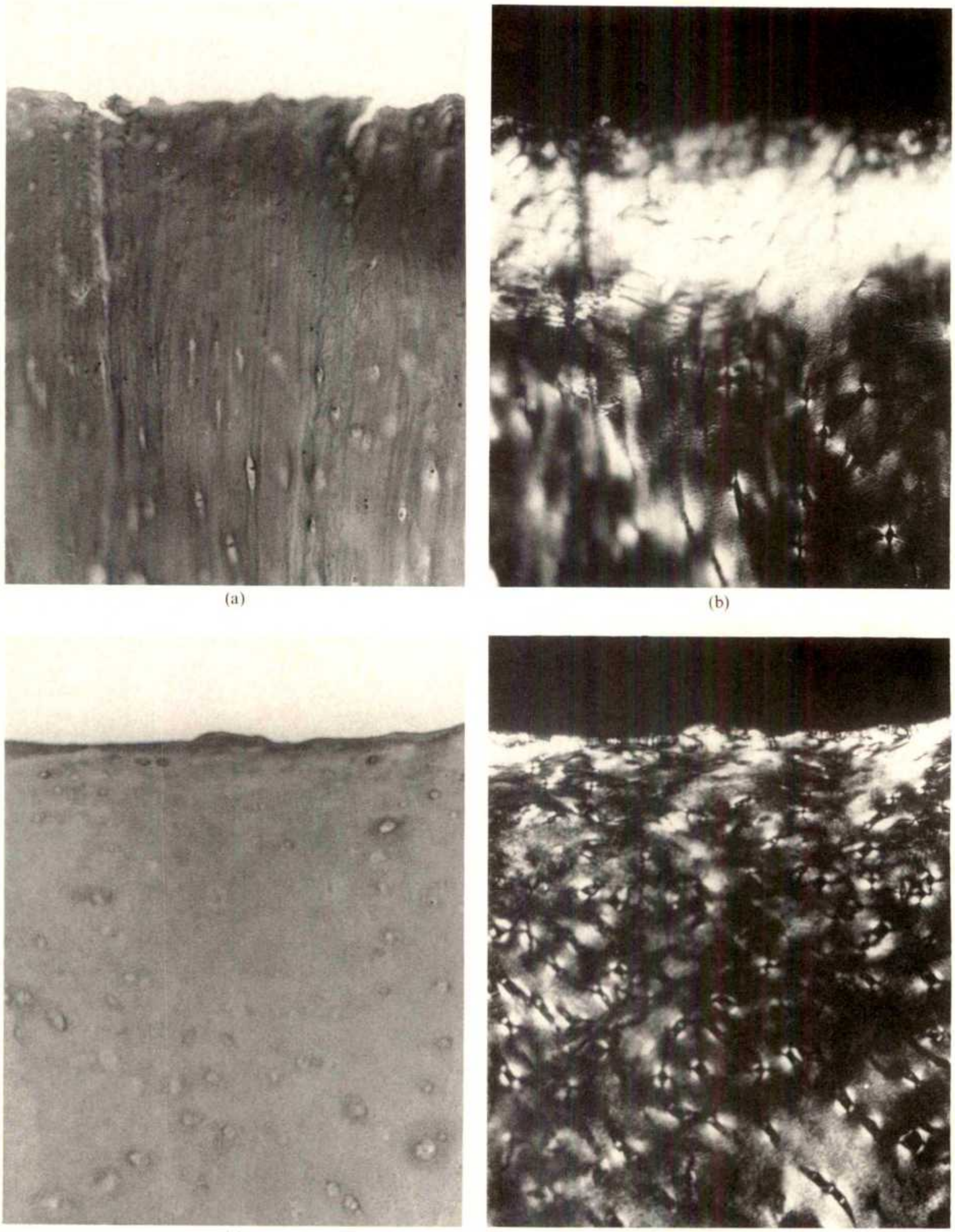

(a) (b) (c) (d)

Figure 3. Photomicrographs taken with transmitted and polarized light of histological sections of articular cartilage obtained from (a) and (b) Group A and (c) and (d) Group B samples. The Group A samples show fibrillation and splits within the articular cartilage and an altered collagen pattern at the tissue surface compared with the normal histological tissue seen in (c) and (d). (Magnification × 75.)

from different areas of the central articular regions of the medial and lateral tibial surfaces. The cartilage samples were cut to 3 × 10 mm in area, supported on approximately 10 mm of subchondral bone. As the X-ray beam of the microfocal unit (Buckland-Wright, 1989) is aligned horizontally, the samples were mounted onto a platform with their broad side facing the tube. A scale and step wedge were added for calibration. Macroradiographs at ×5 magnification were taken using Trimax 8 screens and XD film. After the initial radiograph, 0.02 ml of Niopam 200 (E. Merck Ltd, Hampshire) was placed on the surface of each cartilage sample. A contrast medium with 200 mg of iodine/ml had been found previously to provide better definition of the articular cartilage in macroradiographs of the knee than contrast media with higher iodine concentrations. The cartilage samples were re-X-rayed at 10, 20, 30, 50, 70 and 90 minute intervals. The radiographs of each sample were scanned with a microdensitometer (Joyce Loebl) and the data transferred to a microcomputer. After calibration, the thickness of the cartilage was measured for each sample, together with the depth to which the contrast medium had penetrated and the volume that had been absorbed at the different times. The depth to which contrast medium had penetrated was expressed as a percentage of the cartilage thickness. The volume of contrast medium below the cartilage surface was obtained from the measurement of the area below the density trace for that region (Fig. 1). This volume was expressed as a percentage of the total volume of contrast medium, *i.e.* that still lying on the surface as well as that below.

The cartilage samples were prepared for routine histology. The sections were stained with Weigert and Sirius Red and examined under transmitted and polarized light with a Zeiss Axiophot Microscope.

Results

Within a mean cartilage thickness of 1.62 ± 0.46 mm the contrast medium had penetrated to 53.0 ± 10.7% of that depth 10 min after its addition to the surface of the cartilage and 84.2 ± 6.3% after 90 min. Evaluation of the rate of contrast medium diffusion into the articular cartilage samples showed a Gaussian distribution.

The percentage volume of contrast medium imbibed into the cartilage against time, for a representative selection of samples, is illustrated in Fig. 2. The solid lines were those samples in which the percentage volume of the medium had reached 90% in the cartilage within 90 min (Group A), whilst the broken lines were those samples with a percentage volume less than 90% in the cartilage with the same period (Group B). Within the first 10 min, Group A samples had absorbed a significantly larger volume of contrast medium (mean 70.5 ± 11.7%) compared with Group B (mean 31.0 ± 13.6%).

Histological sections of the samples showed that those from Group A had fibrillation and fissures extending into the cartilage (Figs 3a, b). The latter were frequently accompanied by the presence nests of chondrocytes or "brood capsules" (Fassbender, 1982). Under polarized light, disruption of the collagen structure at the surface of the tissue was indicated by the thick bright band lying above the deeper undisturbed layer of cartilage. In contrast, sections from Group B samples showed normal appearance of articular cartilage with only a narrow bright line at the tissue surface (Figs 3c, d).

Discussion

The condition of the articular cartilage in the knees of the elderly subjects showed evidence of early osteoarthritis. The samples chosen were from areas of least damage in which disruption of the surface was not obvious on naked eye inspection. The tissue, thus obtained, ranged from areas with intact surface to those with early fibrillation and fissuring. High definition macroradiography of the articular cartilage samples produced radiographs large enough to permit accurate measurements from the densitometer trace of the depth and quantity of contrast medium imbibed by the tissue.

The results of this study revealed that the rate of diffusion showed a Gaussian distribution. In all samples the contrast medium diffused rapidly, to approximately half the depth of the cartilage, within 10 min. From then on, the rate of diffusion decreased with the increasing depth of the cartilage. By comparison, the volume of contrast medium imbibed by the cartilage showed a wide variation. Two groups were identified on the basis of the volume of medium imbibed and the histological appearance of the tissue. In cartilage samples with intact surface, a small volume of contrast medium diffused into the tissue over a long period of time (< 90 min) compared with samples with fibrillation and fissuring in which a large volume of the medium diffused within a short period (> 10 min). Contrast medium imbibition would be further assisted in these samples by the increased hydration of the tissue associated with such structural changes (Maroudas & Venn, 1977).

Thus, in the radiographic assessment of osteoarthritic changes in joints, exposures taken with a delay of 10 min or more following the introduction of the double contrast agents should allow sufficient time for contrast medium imbibition to reveal the extent of articular cartilage damage. Furthermore, joint movement prior to radiography would accelerate the process of imbibition. In diagnostic radiology, the advantages in determining the extent of contrast medium absorption can lead to increased precision in detecting the early pathological changes in cartilage of either osteo- or rheumatoid arthritis, prior to joint space narrowing, or in chondromalacia. In these conditions, contrast medium imbibition will differ from the focal absorption association with trauma. In our continuing study of disease progression in osteoarthritis of the knee, macroradiographs of the knee arthrograms have been taken. Densitometry will be used to quantify the volume of contrast medium absorbed *in vivo* by the femoral and tibial articular cartilages in this study. The findings will be compared with the measurements for joint space narrowing to determine the extent of the correlation.

Acknowledgments

We would like to express our thanks to Ciba Geigy Pharmaceuticals for their financial support and to E. Merck Ltd for the contrast medium used in this study.

References

BUCKLAND-WRIGHT, J. C., 1989. A new high definition microfocal X-ray unit. *British Journal of Radiology, 62*, 201–208.

BUCKLAND-WRIGHT, J. C. & BRADSHAW, C. R., 1989. Clinical applications of high definition microfocal radiology. *British Journal of Radiology, 62*, 209–217.

FASSBENDER, H. G., 1982. *Osteoarthrosis—Not Simply a Degenerative Process.* (Documenta Geigy, Basle), pp. 7–29.

FUJIKAWA, K., 1981. Arthrographic study of the rheumatoid knee. Part 2. Articular cartilage and menisci. *Annals of the Rheumatic Diseases, 40*, 344–349.

MAROUDAS, A. & VENN, M., 1977. Chemical composition and swelling of normal and osteoarthritic femoral head cartilage. *Annals of the Rheumatic Diseases, 36*, 399–406.

STOKER, D. J., 1980. *Knee Arthrography* (Chapman & Hall, London).

1990, *The British Journal of Radiology*, *63*, 826–828

Proceedings of the British Institute of Radiology

Imaging towards 2000: practical integration of new technologies

Abstracts of papers presented at a BIR meeting held at the Scientific Societies Lecture Theatre, New Burlington Place, London NW1, on Wednesday, 21 March 1990

Chairman: Professor P. Wells

A low cost CT in every hospital, by Mr J. Williams. Abstract not received
The expanding role of interventional radiology, by A. Hemingway
Clinical ultrasound and ultrasound contrast media, by W. R. Lees. Abstract not received
The impact of recent technical advances on clinical magnetic resonance, by M. Smith. Abstract not received

Chairman: Professor Ian Isherwood

How is the clinical usefulness of PET to be assessed? by R. Frakowiak
A digital department? by H. Nunnerley
Lithotripsy—role of radiology, by J. Haworth
Total health data file system based on optical-magnetic disc, by I. Mano
Computed radiography—a step towards the filmless department, by M. Vizor
MRI and PET—convergence of anatomical and functional imaging, by A. Hinds. Abstract not received
PACS—the way forward, by P. Layzell

The expanding role of interventional radiology

A. P. Hemingway

Academic Department of Radiology, University of Sheffield, Floor P, Royal Hallamshire Hospital, Glossop Road, Sheffield S10 2JF

Interventional radiology represents one of the major growth areas within the field of medical imaging. The range of procedures undertaken includes angioplasty, biopsy, drainage, extraction and embolization. A survey performed by the Royal College of Radiologists' Working Party revealed an overall increase of 116% in the number of procedures performed in 1986 compared with 1982, and this trend continues. The areas which have shown the greatest expansion, both in terms of numbers of procedures and number of centres performing them, are biopsy drainage and dilatation. Biopsy procedures, carried out under fluoroscopic, ultrasound or CT guidance represent the most commonly performed interventional procedure. The development of a wide range of biopsy instruments combined with the various imaging modalities for localization means that there are few if any sites or organs remaining that cannot be biopsied under imaging control. Puncture and drainage techniques, performed most widely in the renal and biliary systems for the relief of obstruction, remain commonplace. Abscess drainage under imaging control particularly in the management of post-operative infection has revolutionized the management of these patients who would otherwise have undergone further surgery. Percutaneous transluminal angiography is now an established treatment option for stenotic and occlusive vascular disease in the peripheral vascular system, renal arteries and coronary vessels. Developments in balloon, catheter and guidewire technology continue to be made. The introduction of other devices including the atherectomy catheter, laser systems and stents has increased the interventionalist's armamentarium but their value and place in the effective management of vascular disease is still undergoing proper evaluation. The area where vascular stents have made an immediate impact is in the management of malignant and benign superior vena caval obstruction. Extraction of calculi from the renal and biliary systems is an area that is undergoing rapid evolution. The primary management of renal calculi via lithotripsy and/or percutaneous drainage and extraction (nephrolithotomy) is now well established. Similar techniques in the biliary system are being evaluated. Therapeutic vascular embolization has not increased significantly in numerical terms over the past 5 years. However, the indication for the procedure and types of lesion treated have changed dramatically. Whereas 5 years ago most embolizations were performed for malignant disease (*e.g.* preoperative embolization of a renal cell carcinoma), now a significant proportion are undertaken in the management of systemic and pulmonary arteriovenous malformations. Interventional radiological techniques have developed and will continue to expand because of the close co-operation between radiologists and clinicians. Further developments in instrumentation and imaging technology are likely to improve further the scope of procedures that can be performed. One area of major controversy remains the adequate staffing and funding of departments undertaking this work. Many interventional radiological techniques have replaced more invasive and expensive surgical treatment options and others represent the only viable treatment available for that disease. The vast majority of radiology departments have had to absorb the increased workload and cost within their existing staffing complement and budget at the expense of other diagnostic imaging services. However, they are now faced with increasing demand and diminishing or static resources and this problem must be urgently addressed.

How is the clinical usefulness of PET to be assessed?

R. S. J. Frackowiak

MRC Cyclotron Unit, Hammersmith Hospital, DuCane Road, London W12 0HS

Position Emission Tomography (PET) is characterized by giving functional rather than anatomical information. It uses methods which are in principle common to all three dimensional reconstruction technologies involving external detection of radiation. It is characterized by its high sensitivity to the detection of gamma radiation emitted from the annihilation of positrons. The high sensitivity allows the injection of small masses of tracer permitting the application of tracer methods to human tissue *in vivo*. Positron tomography is characterized by uniform sensitivity through a precisely defined, electronically collimated field of view. Correction for attenuation effects is possible by direct measurement and this results in the recording of an accurate distribution of radioactivity in absolute units in the tissue. Data can be collected as a function of time to give time–activity relationships in the tissue of interest. The activity data can be combined with mathematical expressions of the biodistribution of the tracer to derive, in conjunction with data obtained from the arterial blood, scans of relevant functional variables. The most commonly used are measures of blood flow, energy metabolism and also various aspects of neurotransmitter storage and binding to specific receptors. The technique has implications for diagnosis in diseases which have no structural correlate. It has implications for the objective monitoring of pharmacotherapy and for performing pharmacodynamic studies *in vivo* in the tissue of interest. It provides an objective means of monitoring the results of therapy. Finally, it is a technique which can be applied to increasing understanding of the pathogenesis and pathophysiology of disease and thus providing new perspectives for treatment. It is suggested that the clinical usefulness of PET cannot be measured in the simple, utilitarian, single-patient directed ways that are common for structural diagnostic imaging. Examples are shown to justify this position.

A digital department?

Heather B. Nunnerley

King's College Hospital, Denmark Hill, London SE5 9RS

One of the most exciting and challenging projects for a radiologist is to design a new department. Currently, the very fast moving technical advances make decisions even more difficult. Eventually, I am sure that all the majority of departments will become digital departments. The problems of how and when will be discussed. The current state of the art in image management and communication has to be reviewed and the possibility of introducing digitization in stages considered. This is all going to be very costly and the benefits must be identified for this additional cost. An attempt will be made to discuss the influence a digital department will have on the work of the radiologist, the role of the radiographer and the relationship with one's clinical colleagues, as well as the impact on education.

Lithotripsy—role of radiology

J. M. Haworth

Department of Radiology, Southmead Hospital, Bristol

Lithotripsy is well established in the treatment of renal stones. Since 1985 there has been increasing interest in using lithotripsy in the treatment of gall stones. Following the development by Dornier, there are now about 10 manufacturers developing lithotripter machines. The machines initially used either ultrasound or X-ray localization techniques, although the majority of the newer machines now incorporate both. The shock waves themselves are generated by one of three methods, these being either spark gap generation, electro-magnetic shock wave generation or piezo electric shock wave generation. In the treatment of renal stones, the role of the radiologist revolves round the imaging and localization techniques, whether these be in the pre-treatment assessment, the actual treatment or in follow-up. In the newer and slightly more controversial subject of biliary lithotripsy, the radiologist should remain involved at a similar level as for renal stones, with, however, considerably more involvement in the treatment phase, particularly in the accurate localization and targetting of the gall stones for lithotripsy. The special requirements of biliary lithotripsy will also involve the radiologist in the selection and suitability of cases. In summary, lithotripsy involves both in renal and biliary adaptation the use of a multidisciplinary approach, and the radiologist has an important contribution to make in both spheres.

Total health data file system based on optical-magnetic disc for company employees

Isamu Mano

Toshiba General Hospital, Tokyo, Japan

For every company employee, an enormous amount of health data are generated throughout the period of employment. Such data are obtained during periodic health checks and temporary hospitalization(s). These personal data are, in most cases, managed by individual hospitals or clinical facilities independently. Moreover, in the same hospital, X-ray images and endoscopic images are stored in different forms. Consequently, it is difficult to retrieve complete personal data. For these reasons, we plan to develop the Toshiba Personal Health Data File System (T-PHD) to manage the total health data for Toshiba employees based on 3.5- or 5-inch read/write optical discs. This system is expected to make rapid progress. "Total health data" refers to all image data including descriptions, numerics, sketches, endoscopic images, X-ray images, and CT images. Our current research and development activities with regard to the above goals are presented.

Computed radiography—a step towards the filmless department

M. Vizor

Philips Medical Systems, London

Computed radiography has yet to establish itself in the United Kingdom, but it is only a matter of time as many prospective users now see computed radiography as a step down the filmless path. This paper describes the assumptions made in talking about a filmless department. Should it be described as having less film rather than as filmless? What are the implications of running such a department and how may this be achieved with today's technology? Computed radiography principles and the manner in which computed radiography replaces conventional techniques either as part of a phased or "big bang" implementation are discussed. The approach that should be adopted by both supplier and customer to ensure that pitfalls are avoided and a successful implementation is achieved are also addressed.

PACS—the way forward

P. A. Layzell

General Electric-CGR, 283 rue de la Minière, 78530 BUC, France

Picture, archiving and communication systems (PACS) will be required if all digital radiology departments are to become a reality. Small PACS started to operate in a clinical environment in the late 1980s. The results of these evaluations indicate that 1024 × 1024 resolution displays are not adequate for primary diagnosis, that network speeds of 10 mbits/s would be insufficient for all-digital departments and that integration of images with other patient data such as reports would be required for efficient, cost effective system performance. Technology in the 1990s will provide the capability for operational PACS and all-digital radiology departments. The major issues affecting purchase of these systems will be cost and acceptance by the medical community. New hospitals planned for the 1990s will have to decide whether to open their doors as an all-digital hospital or to follow the pattern of existing hospitals who must choose the best path to the filmless environment. The steps taken should be practical, enhance patient care or solve an existing problem. Each step must be planned with the final implementation in mind using equipment which is capable of being integrated into the final total digital system.

The combination of chemotherapy and radiotherapy in clinical practice

Abstracts of papers presented at a BIR meeting held at 36 Portland Place, London W1N 4AT, on Thursday, 10 May 1990

Chairman: Professor A. Horwich

Biological principles of combined modality therapy, by G. G. Steel
Hodgkin's disease, by A. Timothy. Abstract not received
Non-Hodgkin's lymphoma, by M. Brada. Abstract not received
Head and neck cancer, by J. Tobias. Abstract not received
Small cell lung cancer, by P. Hoskins. Abstract not received
Combined chemotherapy and radiotherapy in carcinoma of the bladder, by A. Horwich
The combination of chemotherapy and radiotherapy in the treatment of childhood rhabdomyosarcoma, by N. Plowman

Chairman: Dr J. Tobias

Anal canal, by S. J. Arnott
Cancer of the cervix, by P. R. Blake
The combination of chemotherapy and radiotherapy in breast cancer, by J. R. Arnold
Prostate cancer. Combined modality treatment with hormones and radiotherapy, by D. P. Dearnaley

Chairman: Dr S. Arnott

The combination of chemotherapy and radiotherapy in Ewing's sarcoma, by D. Spooner
Medulloblastoma, by D. Tait
Directions of future research, by M. Slevin. Abstract not received

Biological principles of combined modality therapy

G. Gordon Steel

Department of Radiotherapy Research, Institute of Cancer Research, Sutton, Surrey SM2 5NG

The problem of understanding the response of tumours and normal tissues to combinations of chemotherapy and radiotherapy are complex. The ways in which chemotherapy added to radiotherapy may lead to an improved therapeutic index can be considered under three headings. *Spatial co-operation:* the use of drugs and radiation to hit disease in different anatomical sites (primary, metastatic). *Independent cell kill:* if the chemotherapy does not compromise the delivery of a full course of radiotherapy then any cell kill from the drugs should carry a benefit. *Enhancement of tumour response:* greater than expected tumour cell kill from the combination. The first two mechanisms do not imply interaction between the effects of drugs and radiation. Gains observed in the clinic are probably attributable to one or other of these processes. Synergism between drugs and radiation in the clinical setting is elusive. The optimum therapy probably consists of the best available radiotherapy combined with the best chemotherapy, reducing as far as possible interactions between them in critical normal tissues. Such detrimental interactions can be minimized by choice of chemotherapeutic agents and by maintaining as large a time interval as possible between chemotherapy and radiotherapy.

Combined chemotherapy and radiotherapy in carcinoma of the bladder

A. Horwich

Radiotherapy Research Unit, Institute of Cancer Research, 15 Cotswold Road, Sutton, Surrey SM2 5NG

The results of radical radiotherapy for localized muscle invasive bladder cancer (Stage T2 and T3) are unsatisfactory with long-term local control in only 40–60% of patients and survival in only 20–40%. The disease is drug-sensitive with single agent responses between 15% and 30%; the most active agents being cis-platin and methotrexate. Combination chemotherapy achieves complete remissions in 15–35% with a further similar number of partial remissions, the most widely investigated regimens being CMV (cis-platin, methotrexate and vinblastine) and M-VAC (methotrexate, vinblastine, adriamycin and cis-platin). The rationale for considering combined modality are, first, that each modality can achieve significant numbers of complete remissions and, secondly, that a recent trial of adjuvant cis-platin, adriamycin and cyclophosphamide combination chemotherapy following radical cystectomy reported from California indicates significantly improved disease-free survival and survival in those having chemotherapy. Neo-adjuvant single-agent chemotherapy has been investigated in bladder cancer in prospective randomized trials, first with methotrexate by the Cooperative Urological

Cancer Group and secondly with cis-platin, by a number of groups including a combined report from the Australian and West Midland Cooperative Groups. These studies were negative. Simultaneous cis-platin radiotherapy has been investigated with high response rates but no evidence has yet suggested that survival is improved. Current studies in bladder cancer are investigating neo-adjuvant combination chemotherapy and these include a Medical Research Council trial of neo-adjuvant CMV chemotherapy which allows considerable flexibility of the method of local control and which is actively seeking patient entry. The observation that patients who achieve a significant response to chemotherapy have a good prognosis has led to the development of the policy in America of using chemotherapy to select for conservative treatment. The scheme developed in Boston begins treatment with combination chemotherapy using CMV and this goes on to whole pelvic irradiation to a dose of 40 Gy over 4 weeks. If re-evaluation reveals persisting tumour, patients have a cystectomy, but if there has been complete response, they go on to boost radiotherapy and adjuvant chemotherapy. During radiotherapy, single-agent cis-platin is administered. Recently, this approach has included a randomized comparison between CMV and single-agent cis-platin. The current situation is that the case for combining chemotherapy with radiotherapy remains unproven.

The combination of chemotherapy and radiotherapy in the treatment of childhood rhabdomyosarcoma

P. N. Plowman

Department of Oncology, The Hospital for Sick Children, Great Ormond Street and Department of Radiotherapy, St Bartholomew's Hospital, London

The definitive treatment of childhood rhabdomyosarcoma (RMS) is now based around primary chemotherapy with local treatment being employed after 3–4 months of therapy. Local treatment is usually radiotherapy but can be surgery alone. After local therapy, chemotherapy is continued for a total of 1 year. Studies of the results of such treatment have allowed us to define good prognosis patients (*e.g.* localized orbital RMS, paratesticular and vaginal RMS) and bad prognosis patients (parameningeal RMS and prostatic RMS). Modern therapy is aimed at reducing intensity of therapy for good prognostic patients, *e.g.* for orbital RMS: omitting alkylating agent therapy and reducing the radiation dose, or for vaginal RMS: omitting alkylating agents and using vaginal brachytherapy (after ovarian transposition). Meanwhile, the poor prognosis patients receive more aggressive therapy, with six drugs being alternated in different triplets. Chemotherapy drugs with radiosensitizing properties are omitted during radiotherapy and cyclophosphamide/iphosphamide during bladder radiotherapy. Arguing differently, the SIOP group have attempted to omit local therapy but in attempting this, large doses of alkylating agents are administered.

Anal canal

S. J. Arnott

Department of Radiotherapy, St Bartholomew's Hospital, West Smithfield, London EC1A 7BE

Anal carcinoma is a rare tumour. However, modern developments in clinical management are having a great impact on the quality of life experienced by patients who develop this disease. Traditionally, management has been by surgical excision. Whilst local excision is possible for tumours arising around the anal margin, in the majority of tumours developing in the anal canal, radical surgical excision with the loss of the anal sphincter is necessary. As cancers arising in the anal canal are nearly three times more common than those arising at the margin, the treatment for such patients assumes relatively greater importance. The average survival of patients being managed surgically for anal cancers by radical excision is only of the order of 55%, largely on account of the fact that, in spite of dealing with a disease which tends to remain loco-regionally for a considerable part of its natural history, surgery is not effective in dealing with patients with involved lymph nodes. In such patients, the average 5-year survival is only of the order of 29%. The early radiotherapy experience was based largely on interstitial implantation. Although survival rates were similar to those achieved by surgery, complication rates were high. However, recent reports have described complication rates of only 5–8% and 5-year survival rates of 51–68%. It would seem therefore that radiotherapy is as effective as radical surgery in dealing with such patients, in spite of the fact that interstitial treatment does not attempt to treat nodal metastases. Efforts were made in the early 1970s to improve the results of surgery by using a pre-operative radiotherapy treatment in which a dose of 3000 cGy in 15 treatments was given. During the first week of this treatment, Mitomycin C as a bolus dose on Day 1 and 5-fluorouracil by continuous infusion was combined with the radiotherapy. At surgery, many of these patients were found to have either no evidence of tumour or only microscopic residual disease. As a result, many centres in the United States began to use this as primary treatment for such patients and did not carry out surgery unless there was evidence of gross residual disease or progressive tumour. There has not been a randomized clinical trial which has compared this chemo/radiotherapy programme with radiotherapy alone. However, a review at the Princess Margaret Hospital in Toronto suggested that whilst overall 5-year survival rates may be the same, the combined chemo/radiotherapy treatment improved local tumour control, reducing the need for radical salvage surgery. The UKCCCR has now embarked on a large multi-centre national trial to compare the effectiveness of radiotherapy alone with radiotherapy combined with Mitomycin C and 5-fluorouracil in patients with this disease.

The combination of chemotherapy and radiotherapy in the treatment of carcinoma of the cervix

P. R. Blake

The Royal Marsden Hospital, London SW3 6JJ

The treatment of advanced carcinoma of the cervix has remained disappointing with 5-year survival rates of approximately 50% for Stage IIb, 30% for IIIb and 10% for IV. It was thought that the hypoxic cell population in these tumours accounted for some lack of response to radiation and trials of hyperbaric oxygen, hypoxic cell sensitizers and, more recently, neo-adjuvant chemotherapy have attempted to improve the results of radiotherapy. It now seems more likely that any interaction between chemotherapy and radiotherapy in the treatment of cervical cancers is one of "additive cell kill" rather than a true "co-operation" between modalities. If this is so, then the chemotherapy used must be effective in its own right. Cis-platinum is the most effective single agent and when used in combination regimens can produce an overall response rate of 60–70%. At the present time regimens based on cis-platinum and bleomycin, with the addition of methotrexate, vincristine or ifosphamide, are under study in a neo-adjuvant role in UK trials. Early results show satisfactory response rates but long-term complication rates, disease-free and overall survival rates have not yet been published. These results are awaited as are those of other studies in which chemotherapy has been given concomitantly with radiotherapy to "enhance" the radiotherapy effect.

The combination of chemotherapy and radiotherapy in breast cancer

J. R. Yarnold

Academic Unit of Radiotherapy and Oncology, The Royal Marsden Hospital, Downs Road, Sutton, Surrey SM2 5PT

Adjuvant chemotherapy and breast radiotherapy are routinely combined after tumour excision in the conservative management of pre-menopausal women with node positive breast cancer. Retrospective analyses, and the preliminary results of one large randomized trial, suggest that breast recurrence rates are reduced by the concurrent use of adjuvant chemotherapy and radiotherapy, compared with breast radiotherapy alone, after wide local excision. However, the impact of combined modality therapy on breast cosmesis has not been recorded, and previous experience suggests that improved local control may be gained only at the expense of overall cosmetic result. In locally advanced, non-metastatic breast cancer, three randomized trials have reported the results of local-regional radiotherapy with and without cytotoxic chemotherapy. In none of these trials was there an improvement in overall survival associated with systemic therapy, although there was a modest improvement in the local-disease-free survival. It is not clear whether a therapeutic gain is achieved in terms of local control using combined modality therapy because no data on normal tissue damage are presented. It is quite possible that the same levels of local control might have been achieved for equivalent levels of normal tissue damage by higher doses of radiation alone.

Prostate cancer. Combined modality treatment with hormones and radiotherapy

D. P. Dearnaley

Institute of Cancer Research and Royal Marsden Hospital, Downs Road, Sutton, Surrey SM2 5PT

Radical radiotherapy is the most commonly used potentially curative treatment for localized prostate cancer in the UK. Although life expectancy may approach that of the normal population for small well differentiated tumours, local failure occurs in 30% or more of T3 cancers. Post-treatment biopsies remain positive in up to 60% of such cases and are associated with the development of distant metastases. The combination of hormone pre-treatment with radiotherapy may produce benefit in three ways: (1) reduction in tumour and radiation target volume leading to an improved therapeutic ratio, (2) additive or enhanced effect of combined modality treatment on the primary tumour and (3) spatial co-operation with reduction in development of metastases. We have treated 25 patients with advanced localized prostate cancer using Zoladex before and during radical irradiation. Prostate volume was monitored using trans-rectal ultrasound and radiation treatment given after maximum response was achieved. Reductions in radiation target volume were measured using 3-D CT planning before and after hormone treatment. Mean prostate volume reduced from 68 cm^3 (range 40–130 cm^3) to 32 cm^3 (range 12–45 cm^3) with a mean percentage reduction in volume of 61%. Median time to stabilization of prostate volume was 13 weeks (range 9–31 weeks). Although previous studies using oestrogen and radiotherapy have reported improved local control and a reduced incidence of distant metastases, survival has been unaltered, perhaps owing to an increase in cardiovascular complications. Treatment with LH-RH analogues and radiotherapy gives the opportunity for combined modality therapy without increased toxicity.

The combination of chemotherapy and radiotherapy in Ewing's sarcoma

D. Spooner

Children's Hospital, Ladywood Middleway, Birmingham B16 8ET and The Woodlands Hospital, Northfield, Birmingham

The development of early and intensive cytotoxic chemotherapy has been responsible for the improvement in survival in patients with Ewing's sarcoma. Although a radio-responsive tumour, local measures alone produce less than 10% survival. The addition of systemic treatment has increased 5-year disease-free survival to 45% or more. Radiation therapy was used as the local treatment of choice to avoid amputation but produced considerable long-term toxicity when treating developing childhood limbs, especially with the introduction of chemotherapy. Fifty Gray in 25 daily fractions will produce significant soft-tissue atrophy and radiation induced fractures (humerus 33%, femur 43%, tibia 33%). The recent development of specialist limb preserving surgery and expandable "growing" prothesis is likely to reduce the role of radiotherapy in the local management of Ewing's sarcoma. In Birmingham, only 30% of patients with Ewing's sarcoma treated in the current MRC/UKCCSG study have been given radiation therapy. Any attempts at comparison of the effectiveness of local control must take into consideration the systemic cytotoxic chemotherapy regime, original tumour volume, tumour site as well as the local treatment modality, which are all determinants of primary tumour sterilization. The optimal time for local therapy is still controversial: 18 weeks is thought to be too long by the German group; possibly 9–12 weeks is optimal. The interruption or delay of early chemotherapy by radiotherapy or surgery is undesirable and a pilot study of pulse, hyperfractionated megavoltage radiation with chemotherapy is being studied in large inoperable pelvic tumours.

Medulloblastoma

Diana M. Tait

Department of Radiotherapy, Royal Marsden Hospital, Downs Road, Sutton, Surrey SM2 5PT

Overall survival figures for medulloblastoma remain in the region of 55%, which means that almost half the children with this diagnosis are still dying of their disease. There is good reason for looking to chemotherapy to improve these results as medulloblastoma, a small round cell tumour of childhood, is histologically very similar to other paediatric malignancies where chemotherapy has had a dramatic impact. In addition, there are well documented examples of responses to chemotherapy in children with recurrent disease. In the mid-1970s two multi-centre randomized trials were organized in Europe (SIOP I) and in North America (CSG-942) to see whether the addition of chemotherapy, using vincristine and CCNU, could have any impact on survival. Although the early results from SIOP I were extremely promising, neither study has had any sustained effect on disease-free survival on the group as a whole. However, in both studies, retrospective subgroup analysis has shown an advantage for those patients with advanced disease treated with chemotherapy. The subsequent criticism of these earlier trials has been that sub-optimum chemotherapy was used in terms of the drugs investigated, the dose intensity and the scheduling. A second SIOP study was therefore designed to overcome some of these problems and the main design feature was to bring the chemotherapy upfront so that it was given as a sandwich between the surgery and the radiotherapy. This trial closed in December 1988, but early analysis has failed to show any advantage for the sandwich chemotherapy. This result has been met with further criticism in terms of the drugs employed and the dose intensity. As a result, the proposal for the third SIOP trial is to randomize to a much more intensive sandwich chemotherapy, before radiotherapy. The details of this have not yet been resolved but will involve children in 3–4 months of chemotherapy before cranio-spinal irradiation. One's concern is that the delay, and possible compromise in delivery, of radiotherapy, the proven adjuvant treatment, may have an adverse effect. Inadequate drug access may be the critical limiting factor. Although drug access may be assumed in relapsed patients where the blood–brain barrier is disrupted, it may be that in the adjuvant setting, where disease burden is minimal, chemotherapy is not reaching malignant cells in sufficient concentration.

1990, *The British Journal of Radiology*, *63*, 832

Book reviews

Computed Tomographic Angiography of the Mediastinum. By Lee Chiu, William Stanford and Vicky Yiu-Chiu, pp. x + 214, 1986 (Warren H. Green, Missouri, USA), £41.25.
ISBN 0-87527-363-7

This book is an atlas of dynamic, contrast-enhanced CT scans of the mediastinum. It covers three areas, namely, technique, normal anatomy and abnormal anatomy. The quality of the CT images is acceptable rather than outstanding, although the anatomy and pathological features are clear on all scans. The book is well written and clearly laid out. There have been many publications covering this topic, but this book is succinct with a good mix of mediastinal pathology related to both pulmonary and cardiovascular problems. The chapter of superior vena cava obstruction is particularly well presented.

The book will be of value to all radiologists involved in thoracic CT scanning but, because of the price and the competition, I feel that it will be predominantly bought by libraries rather than individuals.

Denis H. Carr

Ultrasound Mammography. Methods, Results, Diagnostic Strategies. By B.-J. Hackeloer, V. Duda and G. Lauth, pp. xii + 144, 1989 (Springer Verlag, New York), DM164.00.
ISBN 0-387-96494-0 (New York)
3-540-96494-0 (Berlin)

This book is primarily concerned with breast sonography and covers basic technical aspects, benign and malignant disease in some detail, effects of iatrogenic procedures and blood flow assessment. It describes the evolution and illustrates the present state of breast sonography well. The chapter on benign breast disease is particularly informative and well illustrated, covering a wide range of topics from ductectasia, benign and other unusual benign tumours and indicates the difficulty in distinguishing a carcinoma from fibrocystic disease. Useful line drawings help to illustrate the text.

The editorial standard of the book is good, and the book is easy to read. It is reasonably indexed and very well referenced. There are an appropriate number of illustrations which are mainly of automated immersion scans with some real time scans. Both are of a high standard making interpretation of the former easy for ultrasonographers not used to this type of breast sonogram. The quality of reproduction is very high and labelling usually accurate. Many of the lesions are arrowed but there are still several rather subtle lesions which are not. Colour illustrations for thermography are included.

In the preface the authors suggest that ultrasound can detect microcalcifications suggesting its potential use as a screening tool. I accept that ultrasound can detect the former but remain unconvinced about it being reliable enough to be used for screening, and this is supported by an extremely useful policy statement from the American College of Radiologists, which the authors include, outlining the present indications for breast sonography.

There are some minor irritations in the book. I have reservations about ultrasound being used to assess what the skin looks like and think the list for the differential diagnosis of liver metastases far too wide (including simple cysts and normal variants) to be of any practicable help. Interventional techniques under ultrasound control is well done and illustrated but I do not find it helpful to see a poorly positioned needle in one of the few mammograms included in the book.

Throughout the book and in a dedicated chapter the authors attempt to define the role of sonography in breast disease. There are too few mammograms to assess this comparison fully and the book is inherently biased towards sonography. Indeed, the authors state that in their institution sonography has become a routine part of every breast examination anyway. However, sonography is well covered indicating the great expertise the authors obviously have with this technique.

In summary, I enjoyed reading the book and would strongly recommend registrars in training and radiologists who have recently developed an interest in breast sonography to read it. They may find it a little expensive to buy, but the quality of the book is such that I would recommend its purchase by individual radiology departments.

P. J. Shaw

Hysterosalpingography and Pelvic Ultrasound: Imaging in Infertility and Gynecology. By I. C. Yoder, pp. xviii + 204, 1988 (Little, Brown and Company, Boston, USA), £52.00.
ISBN 0-316-96881-1

This book is divided into three parts. The first concentrates on the technique of hysterosalpingography and normal radiological appearances while the other sections are concerned with hysterosalpingographic findings in tubal and uterine abnormalities. The author's preference lies with the increasingly popular balloon catheter method for hysterosalpingography. Complications of the technique, as well as anatomical variants, are also described in the first section. A particular strength of the subsequent sections is a relating of clinical and pathological aspects to radiological findings. Further virtues are the large and clear illustrations, with the use of accompanying line drawings where appropriate, and a concise text with up-to-date references. The chapter on fallopian tube surgery is particularly good.

There are relatively few ultrasound illustrations. The failure to describe vaginal ultrasound, save for a brief mention in regard to ectopic pregnancy, is a disappointment. The role of ultrasound in the diagnosis of cervical incompetence receives no mention. However, the failure to include the use of ultrasound for follicular screening, IVF and GIFT is an important deficiency.

In summary, this book gives a useful coverage of hysterosalpingography but is far from comprehensive in regard to ultrasound in gynaecology and infertility.

D. W. Pilling
G. H. Whitehouse

1990, *The British Journal of Radiology*, *63*, 833–841

VOLUME 63 NUMBER 755 NOVEMBER 1990

The British Journal of Radiology

Echo planar imaging of the human fetus *in utero* at 0.5 T

By P. Mansfield, BSc, PhD, FRS, M. K. Stehling, Dr med, R. J. Ordidge, BSc, PhD, R. Coxon, BSc, PhD, B. Chapman, BSc, PhD, A. Blamire, BSc, P. Gibbs, BSc, *I. R. Johnson, BSc, MB, BS, DM, MRCOG, *E. M. Symonds, MD, FRCOG, †B. S. Worthington BSc, LIMA, MB, BS, DMRD, FRCR and †R. E. Coupland, MD, PhD, DSc, FRSE

Departments of Physics, *Obstetrics and Gynaecology and †Human Morphology, University of Nottingham, Nottingham NG7 2RD

(Received November 1989 and in revised form April 1990)

Abstract. The snap-shot capability of the echo-planar imaging technique is used to freeze motion effectively in human fetal studies *in utero*. These first results obtained at 0.5 T demonstrate diagnostic quality images without the need for averaging. Although averaging improves the image signal to noise ratio, it is shown that significant image blurring is produced even when only eight separate images are averaged over a period of a few seconds. Results are presented showing anatomical detail of the internal organs of the fetus. Some pathology is also demonstrated. These results were obtained using the modulus blipped echo-planar single-pulse technique (MBEST). Running at 10 frames/second, the modulus version of the fast low-angle excitation echo-planar technique (FLEET) is used to produce ungated fetal cardiac movies.

Echo-planar imaging (EPI) (Mansfield, 1977; Mansfield & Morris, 1982) is a real time snap-shot imaging method which has evolved from the principles of nuclear magnetic resonance imaging introduced by Mansfield and Grannell (1973). Echo planar imaging produces complete images in times ranging from 64 to 128 ms.

Improvements in our home-built equipment, especially the increase in magnetic field strength to 0.5 T, have enabled us to produce snap-shot images of diagnostic quality comprising up to 128 × 128 pixels.

In this paper we present a range of human fetal images *in utero* which are the first to be obtained by EPI. Preliminary accounts of this work have been presented elsewhere (Johnson et al, 1989; Mansfield et al, 1989; Stehling et al, 1988, 1989b, 1990). Previous fetal imaging studies using commercial magnetic resonance imaging (MRI) equipment looked at pregnancies immediately before termination (Johnson et al, 1984). Later, when the safety of the technique was established, fetal imaging was carried out in the third trimester (Powell et al, 1988). Since that time fetuses from several hundred pregnancies have been imaged using conventional slow MRI techniques. Although the speed of imaging has increased with the introduction of faster imaging regimes, it is still not possible to obtain accurate definition of fetal structures with commercial equipment. This is because repetitive data acquisition, as employed in two-dimensional Fourier transform techniques, is susceptible to fetal movement resulting in movement degradation, ghosting in the phase encoding direction and image blurring.

The snap-shot ability of EPI overcomes most of these problems, and consequently fetal motion is effectively frozen in time. Avoidance of movement degradation in images and excellent soft-tissue contrast offer the potential for improved evaluation of normal and abnormal fetal structure, improved measurement of tissue parameters and the study of physiological function of the viscera.

Method

All low repetition rate images were obtained at 22 MHz using the modulus blipped echo-planar single pulse technique (MBEST) (Howseman et al, 1988; Ordidge et al, 1989b; Turner et al, 1988; Stehling et al, 1989a) variant of the original echo-planar technique (Mansfield, 1977; Mansfield & Morris, 1982). High frame rate sequences were obtained with the modulus version of the fast low-angle excitation echo-planar technique (FLEET) (Chapman et al, 1987; Doyle et al, 1987). Results were obtained on our home-built imaging machine. With current gradient strengths, the MBEST technique yields a complete two-dimensional magnetic resonance image in either 64 or 128 ms after a single excitation of the spin system.

The pulse and gradient timing sequence for MBEST and FLEET is shown in Fig. 1a. Prior to the slice selection process, a chemically shifted radiofrequency pulse and spin phase scrambling gradient (shaded) are

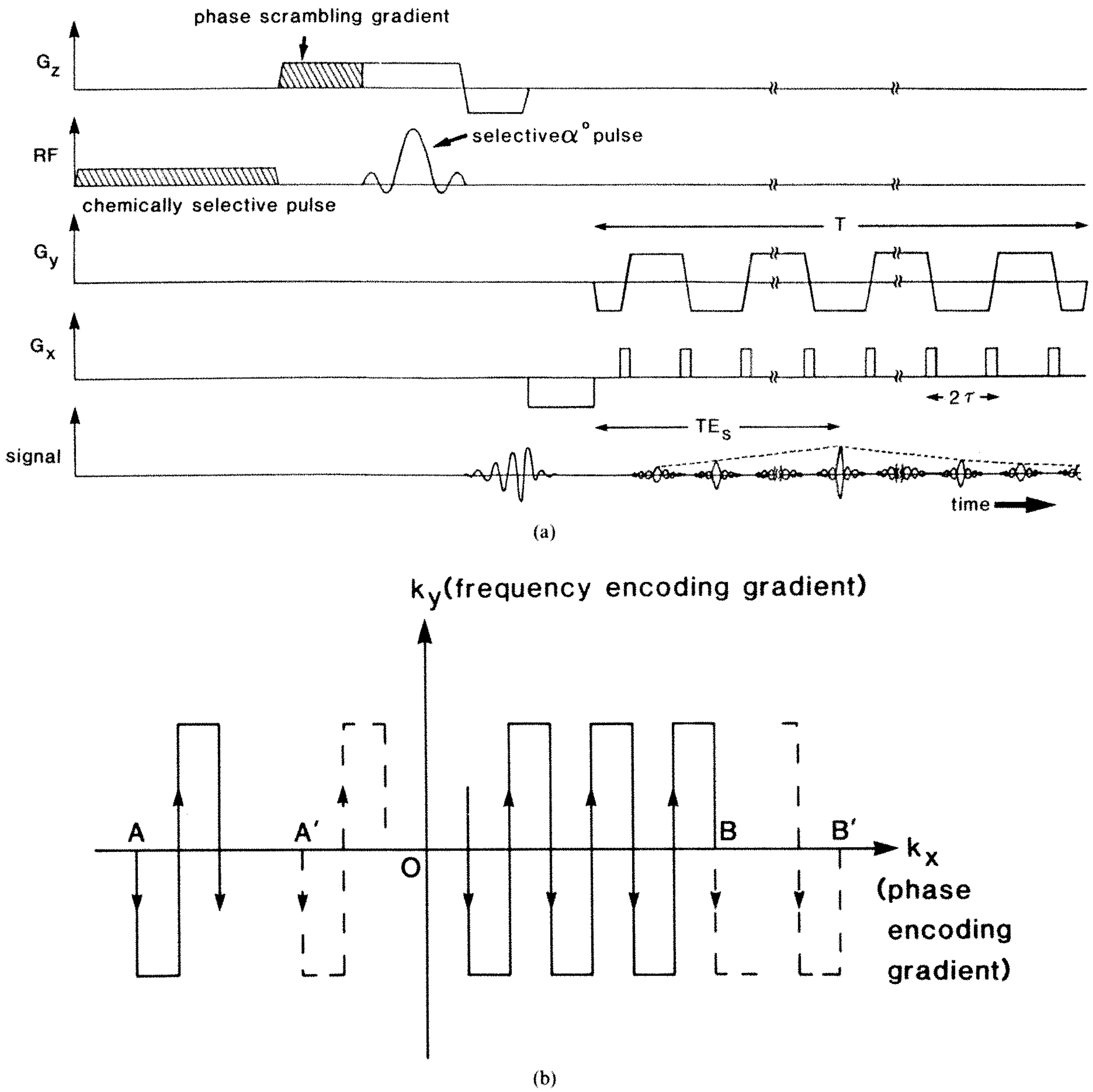
phase scrambling gradient
G_z
RF
selective α° pulse
chemically selective pulse
T
G_y
G_x
2τ
TE_s
signal
time
(a)
k_y(frequency encoding gradient)
A
A'
O
B
B'
k_x
(phase encoding gradient)
(b)

Figure 1. (a) Pulse timing diagram for MBEST. The prepulse on G_x can be adjusted to cause the slow echo peak at TE_s to occur at times in the range 1/4 T to 1/3 T. The fast $TE = \tau$. (b) Normal k-space scan (solid line) and shifted k-space scan (dotted line) for the MBEST sequence of Fig. 1a.

applied to saturate the chemically shifted fatty tissues (Ordidge et al, 1989b). Immediately following this, a 10 mm slice of the so-far undisturbed water signal is then selectively excited (Garroway et al, 1974). During the ensuing free induction decay of the excited transverse magnetization signal, the y-gradient is rapidly switched in a trapezoidally modulated waveform, modulo 2τ, to create a train of gradient echoes in a total data capture time T. The effective echo time $(TE) = \tau$. Phase encoding along the x-axis is achieved by applying a burst of gradient blips as indicated. Prior to this burst, a negative x-gradient pre-pulse is applied which sets the initial spin phase to a predetermined value prior to signal sampling. This has the effect of causing successive gradient echoes to grow to a maximum in a time TE_s producing a slow gradient echo superimposed on the faster echoes. Although TE_s should be set to $\frac{1}{2}T$ according to conventional theory, we find empirically that the best image quality is obtained when $TE_s \simeq T/4$ (Bowtell et al, 1990). The image formation process may be understood in terms of the scanning trajectory in k-space (Mansfield & Grannell, 1973; Ljunggren, 1983). This is sketched in Fig. 1b. The continuous data sampling trajectory covers the whole of the k_x,k_y plane in a single pass. The initial negative G_x pulse serves to start the scan at point A. Making TE_r less than $\frac{1}{2}T$ has the effect of moving the scan start from A to A′ and the scan finish from B to B′ (Fig. 1b) thereby producing a shifted k-space scan. The 64 ms version of MBEST yields an image comprising 64 × 128 pixels. With the 128 ms version of MBEST images with 128 × 128 pixels can be obtained. In-plane resolution varies between 3 and 1.5 mm, depending on the strength of both frequency and phase encoding gradients, which can be adjusted in real-time to optimize resolution and signal to noise ratio (S/N).

For fetal imaging we use sequential continuous image acquisition. Complete echo-planar images have been obtained with our current equipment in real time at rates up to 20 frames/second (Doyle et al, 1987). However, we operate typically at slower rates of around 1–0.5 frames/second. In this case images are displayed immediately on the video screen. The appropriate imaging plane can thus be determined in real-time and is easily readjusted in an interactive manner when the fetus moves.

For very slow frame rates a repetition period (TR) of 3–5 seconds allows almost complete T_1 relaxation between acquisition of consecutive images. This ensures maximum S/N. The excellent soft-tissue contrast in MBEST images arises from the intrinsic T_2 contrast characteristic of this technique arising from the use of long values of TE_r.

For fetal heart studies, higher repetition rates are required. Low angle selective excitation pulses (Garroway et al, 1974; Mansfield, 1984), typically less than 45°, ensure S/N optimization at up to 10 frames/second. Thus, MBEST allows acquisition of up to five complete two-dimensional images in a single fetal heart cycle.

Subject and protocol

Eight fetuses were imaged in this study at gestations ranging from 21 weeks to term. From ultrasound and clinical evidence, three of the fetuses were suspected of having mild intrauterine growth retardation. In one fetus with pathology, a gastroschisis was demonstrated (Stehling et al, 1989b). In another case, a fetal diaphragmatic hernia was evident. In one case there was doubt about the degree of significance of placenta praevia. One patient presented with oligohydramniosis. One patient had an abnormally raised serum concentration of alpha feto-protein. Fully informed written consent was obtained from all eight patients. Magnetic resonance imaging of pregnant women has been performed for 5 years following the guidelines suggested by the National Radiological Protection Board. Approval for imaging of pregnant women in Nottingham, excluding those in the first trimester, was obtained from the local ethical committee.

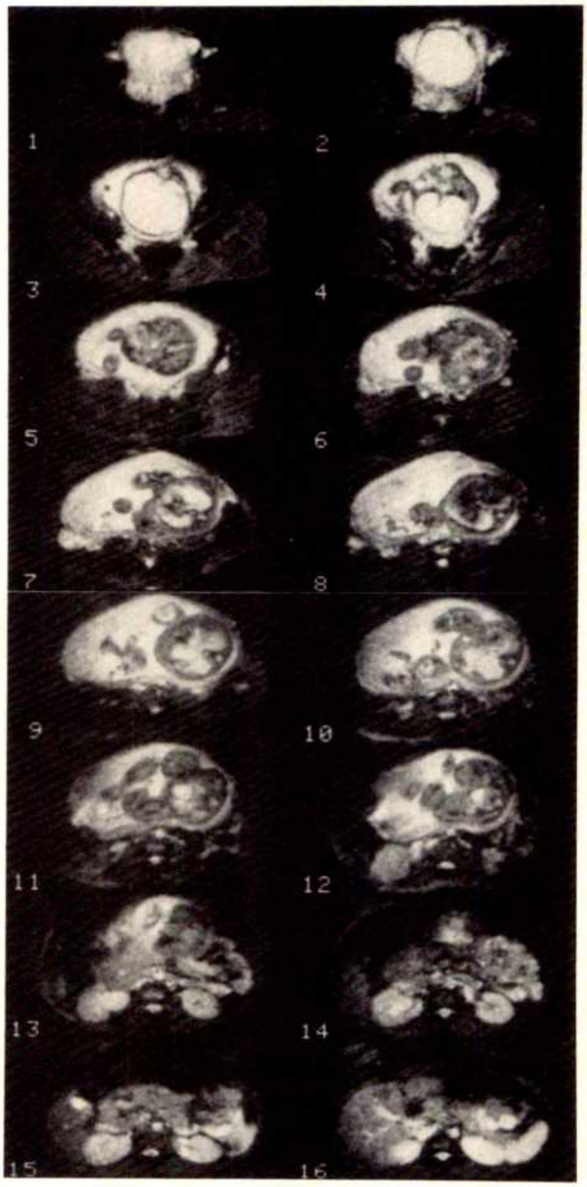

Figure 2. Sixteen transaxial snap-shot images from a full contiguous set of 32 images of a fetus with a gestation period of 36 weeks. Each image comprises 64 × 128 pixels and was acquired in 64 ms. (13301.)

Results

Figure 2 shows 16 alternate planes from a full scan of 32 planes through a fetus in the 36th week of pregnancy. The original three-dimensional data set comprises 32 contiguous 10 mm thick slices, each of which was obtained in 64 ms. The patient was advanced through the EPI scanner and images from contiguous planes were recorded sequentially. This allowed depiction of the uterus and its contents in approximately 1 minute.

Images 1–4 show cross-sections through the fetal

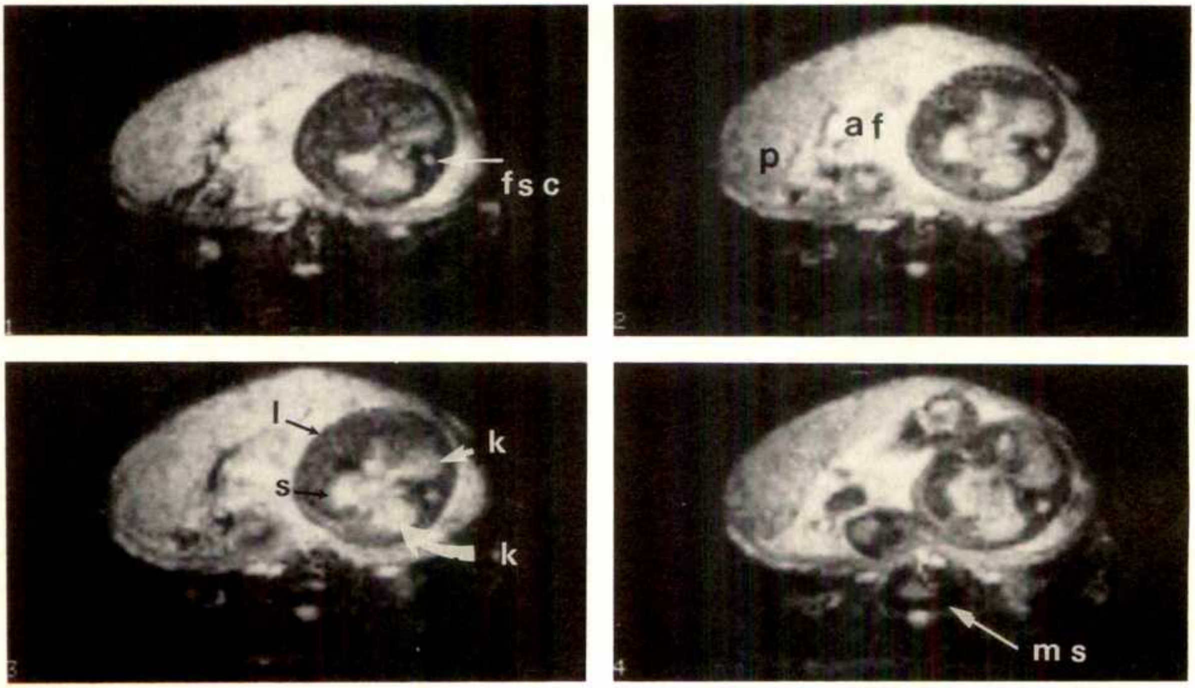

Figure 3. Four different and enlarged snap-shots from the same patient as Fig. 2. These images highlight the fetal cross-sections, placenta and amniotic fluid within the amniotic sac.

head. The fetal brain is differentiated from the surrounding amniotic fluid by the skull which appears black. The high water content of the unmyelinated fetal brain accounts for the high signal intensity of the parenchyma.

Image 5 demonstrates features of the fetal neck with the cerebrospinal fluid-filled spinal canal shown in an oblique section. By Plane 6 the lung apices have appeared. Fetal lungs are filled with alveolar and amniotic fluids which yield high signal intensity owing to the long T_2 time of these fluids. In Image 7, detail of the chambers of the fetal heart can be seen.

In Images 9 and 10 detail of fetal liver, spleen, kidneys, stomach and intestines is apparent. Also clearly apparent in Images 7–12 is the fetal spinal canal. The slices continue through the pelvis and also show the lower limbs in longitudinal section in Image 11, and the fetal bladder in 12. The maternal hydronephrosis shown in Images 13 and 14 was an incidental finding, which is of little significance in pregnancy.

Figure 3 shows four different but interesting planes of the same data set as Fig. 2. The maternal spine (ms) can be seen at the bottom of the images, the uterus occupying the majority of the image anteriorly. The amniotic fluid (af) showing starkly white outlines the placenta (p), the fetal trunk and fetal limbs.

Image 1 shows particular heterogeneity in the placenta, anterolaterally on the left, representing areas of different perfusion. The insertion of the umbilical cord can be seen on the fetal surface. The fetus is facing towards the placenta. The fetal spinal canal (fsc) can be seen posteriorly, white, with the black area of the vertebral body immediately in front of it. To either side of the vertebral body a small portion of the kidneys can be seen, with the stomach and liver lying anterior to them. The low signal line between the stomach and the liver represents the left umbilical vein. In Image 2, the transverse section through the fetus shows the fetal spinal canal and vertebral body. The kidneys (k) to either side of the vertebral body show some internal structure, probably the renal pelvis. The renal veins appear as white structures, arching around the vertebral body joining the inferior vena cava, showing white, to the left side of which can be seen the black circle representing the fast moving blood in the aorta. Anterior to the left kidney the high signal of the stomach (s) can be seen and following this across, fluid can be seen in the first part of the duodenum. Anterior to the stomach, in the midline, the dark areas pointing towards the anterior abdominal wall of the fetus is the left hepatic vein linking with the umbilical vein. The liver (l) is seen as a heterogeneous area filling the anterior portion of the fetal trunk. Image 3, obtained further down the fetal trunk, again shows fetal spine, kidneys, great vessels, stomach and first part of the duodenum. The left hepatic vein and the liver can be seen. The spleen can be seen as a slightly darker area than that of the left kidney which lies antero-laterally to it. Image 4 completes the sequence with a slice showing the umbilical cord from the fetus lying in the amniotic fluid.

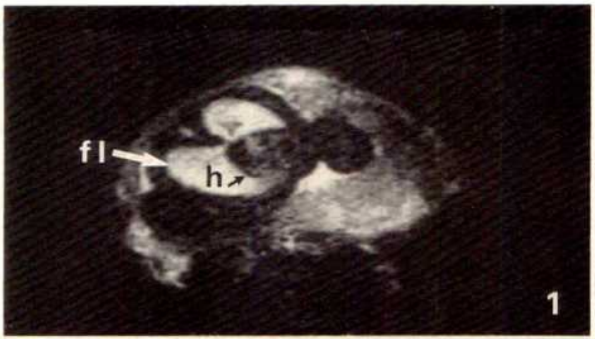

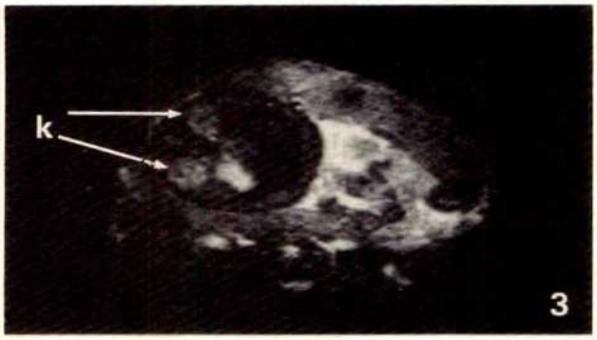

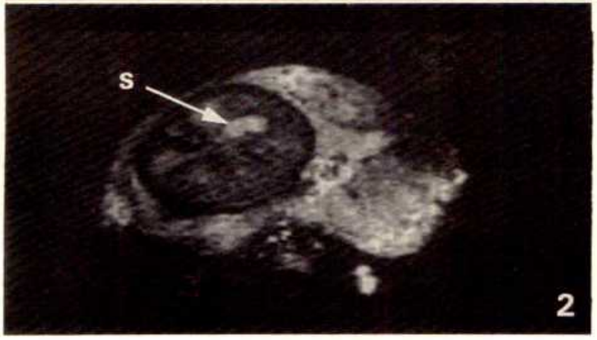

Figure 4. Three EPI snap-shots of a 37-week fetus. Each image comprises 128 × 128 pixels and was acquired in 128 ms. These shifted *k*-space images have $TE_r = 32$ ms. Image 1 shows lung fields, Image 2 shows detail of the liver and stomach while Image 3 shows the kidneys. All three images clearly show the spinal canal. (13201.)

Figure 4 shows three 128 ms MBEST images of a 37-week fetus. The original images comprise an array of 128 × 128 pixels. The phase encoding x-gradient was chosen to yield twice the resolution in the x-direction than in the y-direction. The x and y resolutions were 1.5 mm and 3.0 mm, respectively. For display the image array was linearly interpolated to 512 × 256 pixels in order to preserve the correct dimensional ratio of the object.

The TE_r of 32 ms accounts for the stronger T_2 weighting in 128 ms MBEST images.

Image 1 shows the fan-like structure of the fetal lungs (fl) on either side of the mediastinum. In these more strongly T_2-weighted images they are sharply delineated from the thoracic wall, spine and heart (h), which are of low signal intensity. This allows the outline of the fetal lungs to be traced with a cursor. Summation of the measured area over all thoracic planes and multiplication by the slice thickness yields an approximate fetal lung volume. This measurement may be refined by accounting for lung tissue density.

The main bronchi can be seen emerging from the pulmonary hilus. Their cartilaginous wall accounts for the low signal intensity. The heart lies antero-medially in the thorax. The placenta is on the right lateral aspect of the amniotic cavity and a fetal limb can be seen in front of the chest wall. Image 2 shows a cross-section through the fetal stomach and liver immediately below the diaphragm. The stomach (s) is filled with amniotic fluid and secretions and displays high signal intensity. Part of the left hepatic vein is apparent towards the origin of the umbilicus in the fetal abdominal wall. The liver appears with medium signal intensity and shows a typical granular appearance.

In Image 3 the fetal kidneys (k) are depicted, with differentiation between renal pelvis and parenchyma. Anterior to the right kidney lie the lower part of the fluid-filled fetal stomach and the duodenum.

Figure 5 shows transaxial cross-sections through a fetus at term. Images numbered A are single snap-shots, obtained in 128 ms. Images numbered B are corresponding averages of eight snap-shots taken at the same plane. The TR between acquisition of consecutive images was 5 seconds. Higher S/N in the averaged images is vitiated by the introduction of a significant amount of motional blurring, even though this fetus at term displayed little movement compared with others, particularly earlier in pregnancy. In none of the images does averaging facilitate image interpretation.

In Figure 6 four cross-sectional images are shown through a fetus at 21 weeks of gestation. This case was a breech presentation. In Image 1, the placenta (p) can be seen lying dorsally. The fetal head (fh) is lying anteriorly to the placenta and yields a homogeneous signal because of the lack of myelination, although the interhemispheric fissure (arrow) can be seen.

In Image 2, a cross-section through the fetal thorax shows both lungs (l) and the fetal heart (h). The vertebral column (v) can be seen dorsally and continues in Images 3 and 4. In Image 3, the fetal liver (l) lies anteriorly in the abdomen. The central circular black structure (arrow) is the ductus venosus. The dark zone within it indicates rapid blood flow. The fetal stomach can be seen lying to the left of it, fluid-filled and of high signal intensity. The kidneys are obscured by a partial volume effect, merging with the posterior costo-diaphragmatic recesses. In Image 4, little differentiation of the lower abdominal structures was obtained, apart from the left portal vein seen in the small rim of liver

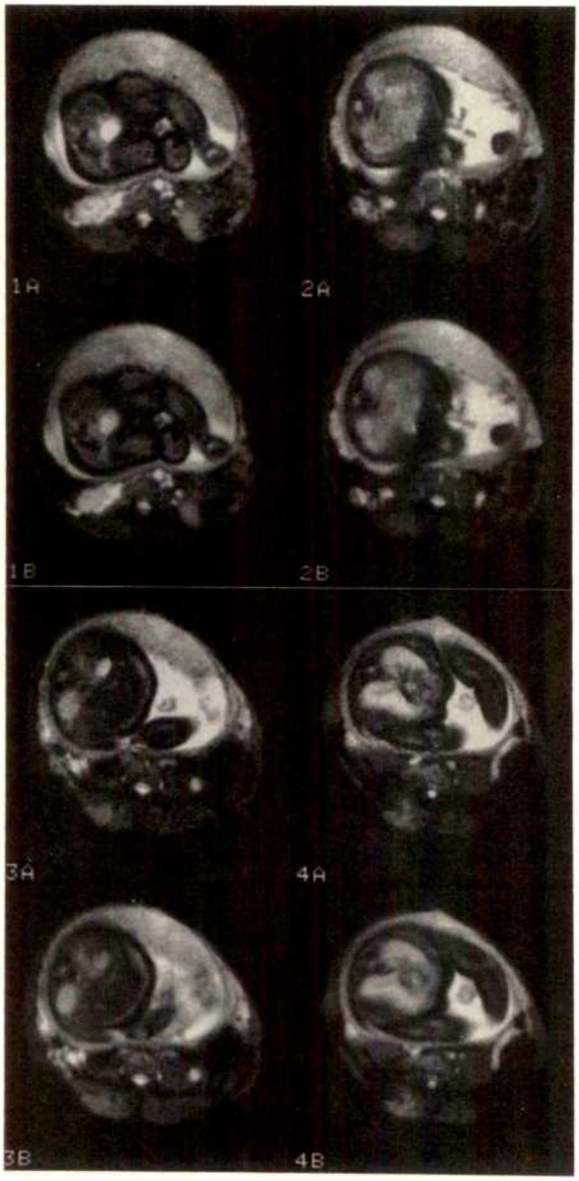

Figure 5. Transaxial images of a fetus at term. Images marked A are four snap-shots showing detailed morphology. These were obtained in 128 ms and comprise 128 × 128 pixels. Note the fetal bladder and limbs in 1A, liver in 2A, right kidney in 3A and lungs in 4A. Images marked B are the averages of eight snap-shots corresponding to the same transaxial views as in set A. There is clearly some improvement in signal to noise ratio but also evidence of some blurring due to motion over the extended acquisition time of 35 seconds. Note the dark outline in all images arising from the lost subcutaneous fat signal. (13401.)

immediately posterior to the abdominal wall.

Figure 7 shows two 64 ms MBEST transectional images through the thorax of a 26-week fetus. These images were taken at random points in the fetal cardiac cycle. A TR of approximately 5 seconds allowed full longitudinal spin relaxation between consecutive image acquisitions and also allowed a normal 90° flip angle to be used. Image 1 shows a four-chamber view of the fetal heart (h) in systole. Blood flow in both atria and ventricles is fast and results in signal loss, outlining the intracardiac spaces. The intraventricular septum is depicted particularly well. Image 2 shows the heart in late systole. Blood flow in the ventricles is still fast, resulting in signal loss. Slowly moving blood in the atria yields high signal intensity in this phase of the cardiac cycle. In diastole, not shown here, depiction of cardiac structure is more difficult, owing to the similar signal intensity from sluggish blood and other thoracic tissues.

Figure 8 shows the first nuclear magnetic resonance movie sequence of a fetal heart entirely ungated and obtained from within a single cardiac cycle. We have used the 64 ms MBEST version with a low angle selective pulse (FLEET) of 45° in this case, to optimize image intensity at a repetition rate of 10 frames/second.

The images presented here give an in-plane resolution of better than 2 mm with a slice thickness of ~ 10 mm. Improvement of S/N has been achieved with the Fourier filtering method (Doyle & Mansfield, 1986) which allows reduction of image noise while retaining essential motion information. With a fetal heart rate of about 120 beats/minute, approximately three complete cardiac cycles were covered in a 16-frame fast sequence. Images 1–5 are transaxial sections acquired at five different phases from a single fetal heart beat. Both lung fields yield high signal intensity (l) owing to the presence of amniotic and alveolar fluids. The chest wall and paraspinal muscles are of intermediate signal intensity, due to the shorter T_2 of these tissues.

Images 1, 2 and 5 show the fetal heart in diastole. Delineation of the intracardiac spaces is poor, because slowly moving blood in diastole yields a signal smilar to that of the surrounding lungs. In systole, both left (lv) and right ventricles (rv) can be seen. The descending aorta (a) is also indicated.

Figure 9 shows two abdominal cross-sections through a fetus at 36 weeks' gestation. A gastroschisis is evident in Image A, the gap in the abdominal wall (g) and the intra-abdominal amniotic fluid (af) being clearly demonstrated. In Image B, the prolapsed intestines (i) can be seen floating in the amniotic cavity. Fetal limbs (l) and placenta (p) are also depicted.

A thoracic cross-section at 36 weeks' gestation is shown in Image C. A diaphragmatic hernia accounts for the prolapse of the fetal stomach (s) into the left hemithorax causing displacement of the lungs (l) and heart (h) to the right. In normal pregnancies, the fluid-filled fetal lungs appear bright on MBEST images, as shown in Image D. The low signal intensity in the case of the diaphragmatic hernia indicates the compression and hypoplasticity of the lungs with diminished intra-alveolar fluid. This child died of respiratory failure soon after birth. With the acquisition of contiguous image planes in rapid succession (5 planes/second), quantitative assessment of fetal lung volumes is feasible.

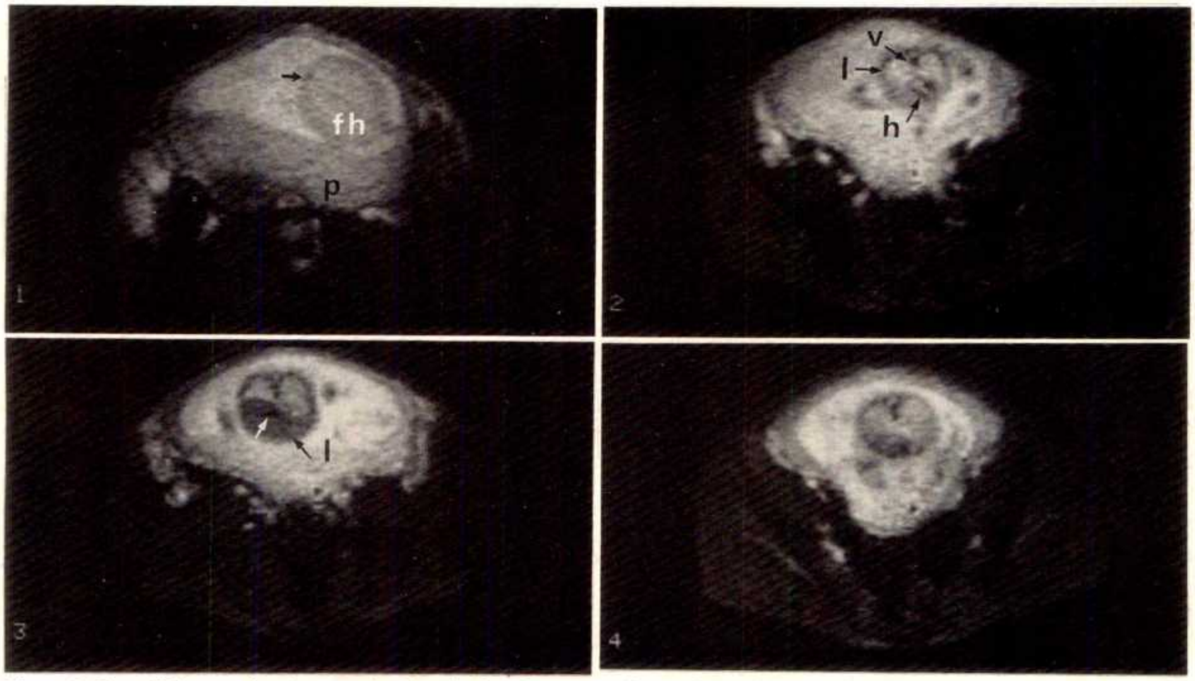

Figure 6. Four EPI snap-shot images of a fetus in breech presentation at 21 weeks' gestation. Each image comprises 128 × 128 pixels and was acquired in 128 ms. See text for detail. (14101.)

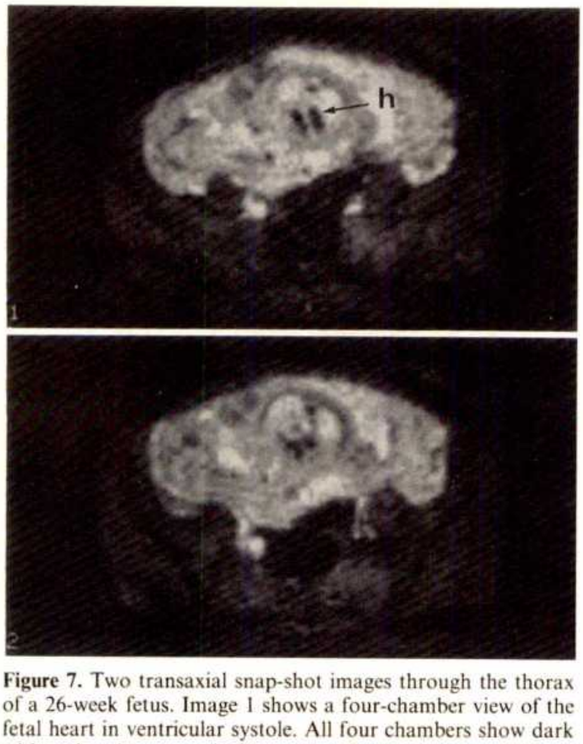

Figure 7. Two transaxial snap-shot images through the thorax of a 26-week fetus. Image 1 shows a four-chamber view of the fetal heart in ventricular systole. All four chambers show dark with a clear inter-ventricular septum. Image 2 shows the same section of the heart in late systole. Here the ventricles are still dark but the atria are brighter indicating blood close to stand-still. (13001.)

Discussion and conclusions

Using the snap-shot EPI technique, which effectively freezes in time the motion of an object, we have obtained the first motion-artefact-free magnetic resonance images of the human fetus *in utero*. This is of particular importance for imaging the fetus early in pregnancy or when it is in breech presentation. In both cases a considerable amount of random fetal motion excludes conventional MRI. Abrupt positional changes of the mobile fetus are at least an order of magnitude more rapid than image acquisition with fast MRI techniques like FLASH (Frahm et al, 1986). Indeed, fetal motion could also present problems for the more recent snap-shot FLASH technique (Haase et al, 1989), where the current data acquisition times are around $\frac{1}{2}$ second. Although some useful results might be obtainable with those techniques in relatively static phases of the fetus, data acquisition would be a trial and error process. This is not the case with EPI.

The strongest competitor to obstetric MRI is ultrasound. Ultrasound has real-time capability and yields excellent resolution of fetal structures as early as a few days after implantation of the morula. However, ultrasound images are based on acoustic impedance changes at tissue interfaces. This means that they contain essentially tissue density information. This mono-parametric signal intensity dependence accounts for the poor soft-tissue contrast and specificity in ultrasound. Magnetic resonance images are inherently multiparametric, being based on tissue T_1, T_2, proton density, flow, diffusion etc. Using specific pulse sequences, a high level of tissue

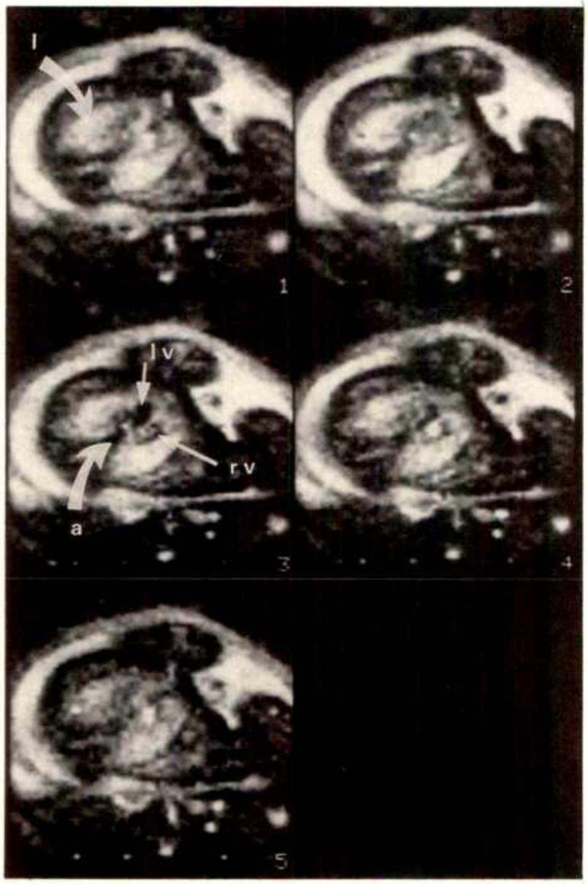

Figure 8. Five snap-shot image frames from a movie sequence showing cardiac motion in the fetal heart. Each frame was acquired in 64 ms following a low angle excitation pulse of 45°. The frame repetition rate was 10 frames/second. These images cover five different phases of the same cardiac cycle. (17401.)

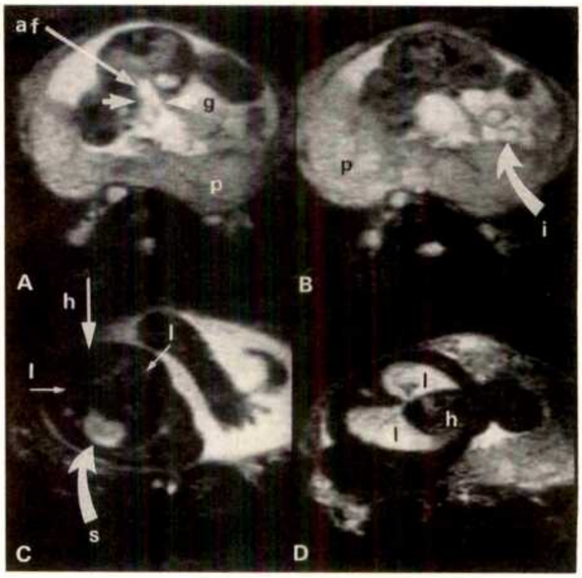

Figure 9. Echo planar imaging transaxial snap-shots through two 36-week fetuses. Images A and B show a gastroschisis with prolapsed intestines. The gap (g) in the abdominal wall is shown clearly in A. Image C is of a fetus with diaphragmatic hernia. It shows the prolapsed fetal stomach (s) protruding into the left hemi-thorax with corresponding displacement of lungs (l) and heart (h) to the right. Image D shows normal fluid filled lungs (bright signal) for comparison.

characterization is obtainable. A particular advantage of EPI in this context is its ability to be used easily in conjunction with spin preparation phases like spin echo, saturation recovery, inversion recovery or bipolar gradient encoding for flow information (Ordidge et al, 1989a). This would be harder, if not impossible, to achieve with two-dimensional Fourier transform fast imaging regimes.

In this work we have simply moved the patient through the EPI scanner at a constant speed to obtain different image planes. The image acquisition repetition rate is not limited by the proton T_1 relaxation, because new planes are imaged consecutively. The data sets thus obtained allow volumetric evaluation of organ size, for instance, lung volumes. Echo planar imaging has already been used for lung volume measurement in paediatrics (O'Callaghan et al, 1987). A report of fetal lung volume measurements is in preparation. Organ size assessment in conjunction with tissue characterization might prove to be a sensitive tool for pre-natal prediction of post-partum functional abnormalities of the organ concerned.

Chemically selective presaturation of either fat or water protons preceded every EPI experiment. In water proton images, the fat signal is absent so that the subcutaneous fat layer appears black. The complementary fat image allows assessment of the thickness of the subcutaneous fat layer and might serve as a sensitive indicator of intra-uterine growth retardation of the fetus.

Image acquisition rates of 10 frames/second with the ultrafast modulus version of the low flip angle technique FLEET have for the first time allowed the acquisition of a single fetal heart cycle movie loop. Single cardiac cycle data acquisition is the only way to obtain a fetal heart movie, since gating to the fetal R-wave is notoriously difficult owing to the prevailing electrical activity from the maternal heart which obscures the fetal signal. Also, in most cases, the fetus would not remain in the same position for the length of time required for a gated heart study. The low signal, created by the rapidly flowing blood in the cardiac lumina, serves as a natural contrast agent and facilitates the interpretation of cardiac anatomy. This clearly has potential for intra-uterine assessment of congenital cardiac malformations.

We believe that EPI has great potential for intra-uterine assessment of the human fetus. Its multiparametric soft-tissue contrast and good resolution (currently ~1.5 mm) makes it a sensitive imaging technique for the depiction of normal and pathological fetal anatomy. Real-time image display in EPI makes the imaging procedure interactive, allowing rapid choice of the region of interest and control over all imaging parameters, with immediate feed-back. Echo planar imaging offers the potential for clarification of specific questions in situations where the information obtained by ultrasound is incomplete or ambiguous. In such cases, a degree of tissue characterization or quantitative volumetric assessment could be valuable in providing new insights into fetal pathology. This could be of importance in planning pre- and post-natal treatment.

Acknowledgments

We thank the Medical Research Council, the Department of Health and Social Security and the British Heart Foundation for financial support of the echo-planar imaging programme. A.B., P.G. and A.M.H. wish to thank the Science and Engineering Research Council for Research Studentships. M.K.S. thanks the Deutsche Forschungsgemeinschaft for a stipend.

References

BOWTELL, R., STEHLING, M. K., BLAMIRE, A. M., GUILFOYLE, D. N. & MANSFIELD, P., 1990. Effects of shifted k-space scanning. *Magnetic Resonance in Medicine* (in press).

CHAPMAN, B., TURNER, R., ORDIDGE, R. J., DOYLE, M., CAWLEY, M. G., COXON, R., GLOVER, P. & MANSFIELD, P., 1987. Real-time movie imaging from a single cardiac cycle by NMR. *Magnetic Resonance in Medicine, 5*, 246–254.

DOYLE, M. & MANSFIELD, P., 1986. Real-time movie image enhancement in NMR. *Journal of Physics E: Scientific Instruments, 19*, 439–444.

DOYLE, M., CHAPMAN, B., TURNER, R., ORDIDGE, R. J., CAWLEY, M. G., COXON, R., GLOVER, P., COUPLAND, R. E., MORRIS, G. K., WORTHINGTON, B. S. & MANSFIELD, P., 1987. Real-time cardiac imaging of adults at video frame rates by MRI. *Lancet, ii*, 964–965.

FRAHM, J., HAASE, A. & MATTHAEI, D., 1986. Rapid NMR imaging of dynamic processes using the FLASH technique. *Magnetic Resonance in Medicine, 3*, 321–327.

GARROWAY, A. N., GRANNELL, P. K. & MANSFIELD, P., 1974. Image formation in NMR by a selective irradiative process. *Journal of Physical Chemistry, 7*, L457–L460.

HAASE, A., MATTHAEI, D. & NORRIS, D., 1989. Snap-shot FLASH imaging. *Proceedings of the Society of Magnetic Resonance in Medicine, 8th Annual Meeting, Amsterdam, 1*, 364.

HOWSEMANN, A. M., STEHLING, M. K., CHAPMAN, B., COXON, R., TURNER, R., ORDIDGE, R. J., CAWLEY, M. G., GLOVER, P., MANSFIELD, P. & COUPLAND, R. E., 1988. Improvements in snap-shot NMR imaging. *British Journal of Radiology, 61*, 822–828.

JOHNSON, I. R., SYMONDS, E. M., KEAN, D. M., WORTHINGTON, B. S., BROUGHTON-PIPKIN, F., HAWKES, R. C. & GYNGELL, M., 1984. Imaging the pregnant human uterus with nuclear magnetic resonance. *American Journal of Obstetrics and Gynecology, 148*, 1136–1139.

JOHNSON, I. R., MCPHERSON, M. B. A., STEHLING, M. K., ORDIDGE, R. J., COXON, R., BLAMIRE, A. M., GIBBS, P. & MANSFIELD, P., 1989. Fetal anatomy assessed by echo-planar imaging. *Proceedings of the Society of Magnetic Resonance in Medicine 8th Annual Meeting, Amsterdam, 1*, 200.

LJUNGGREN, S., 1983. A simple graphical representation of Fourier based imaging methods. *Journal of Magnetic Resonance, 54*, 338–343.

MANSFIELD, P., 1977. Multi-planar image formation using NMR spin echoes. *Journal of Physical Chemistry, 10*, L55–L58.

MANSFIELD, P., 1984. Spatial mapping of the chemical shift in NMR. *Magnetic Resonance in Medicine, 1*, 370–386.

MANSFIELD, P. & GRANNELL, P. K., 1973. NMR "diffraction" in solids? *Journal of Physical Chemistry, 6*, L422–L426.

MANSFIELD, P. & MORRIS, P. G., 1982. *NMR Imaging in Biomedicine* (Academic Press, New York).

MANSFIELD, P., ORDIDGE, R. J., COXON, R., STEHLING, M. K., CHAPMAN, B., BLAMIRE, A. M., GIBBS, P., JOHNSON, I. R., SYMONDS, E. M., WORTHINGTON, B. S. & COUPLAND, R. E., 1989. Echo-planar imaging in obstetrics at 0.5 T. *Proceedings of the 6th Radiological Symposium, Graz*, 180.

O'CALLAGHAN, C., SMALL, P., CHAPMAN, B., COXON, R., GLOVER, P., TURNER, R., JAROSZKIEWICZ, G., HOWSEMAN, A. M., MANSFIELD, P., COUPLAND, R. E., MILNER, A. D. & MILNER, M., 1987. Determination of individual and total lung volumes using NMR echo-planar imaging. *Annals of Radiology, 30*, 470–472.

ORDIDGE, R. J., GUILFOYLE, D. N., GIBBS, P. & MANSFIELD, P., 1989a. Real-time flow measurements using echo-planar imaging. *Proceedings of the Society of Magnetic Resonance in Medicine, 8th Annual Meeting, Amsterdam, 2*, 889.

ORDIDGE, R. J., HOWSEMAN, A. M., COXON, R., TURNER, R., CHAPMAN, B., GLOVER, P., STEHLING, M. K. & MANSFIELD, P., 1989b. Snap-shot imaging at 0.5 T using echo-planar techniques. *Magnetic Resonance in Medicine, 10*, 227–240.

POWELL, M. C., WORTHINGTON, B. S., BUCKLEY, J. M. & SYMONDS, E. M., 1988. Magnetic resonance imaging in obstetrics; fetal anatomy. *British Journal of Obstetrics & Gynaecology, 95*, 38–46.

STEHLING, M. K., JOHNSON, I. R., CHAPMAN, B., HOWSEMAN, A. M., ORDIDGE, R. J., COXON, R. & MANSFIELD, P., 1988. Imaging of the mobile fetus *in utero* with echo-planar imaging. *Proceedings of the 7th Annual Meeting of the Society of Magnetic Resonance in Medicine, San Francisco, WIP*, p. 152.

STEHLING, M. K., HOWSEMAN, A. M., ORDIDGE, R. J., CHAPMAN, B., TURNER, R., COXON, R., GLOVER, P., MANSFIELD, P. & COUPLAND, R. E., 1989a. Whole body echo-planar MR imaging at 0.5 T. *Radiology, 170*, 257–263.

STEHLING, M. K., MANSFIELD, P., ORDIDGE, R. J., COXON, R., CHAPMAN, B., BLAMIRE, A. M., GIBBS, P., JOHNSON, I. R., SYMONDS, E. M., WORTHINGTON, B. S. & COUPLAND, R. E., 1989b. Echo-planar MRI in abnormal pregnancies. *Lancet, ii*, 157.

STEHLING, M. K., MANSFIELD, P., ORDIDGE, R. J., COXON, R., CHAPMAN, B., BLAMIRE, A. M., GIBBS, P., JOHNSON, I. R., SYMONDS, E. M., WORTHINGTON, B. S. & COUPLAND, R. E., 1990. Echo-planar imaging of the human fetus *in utero*. *Magnetic Resonance in Medicine, 13*, 314–318.

TURNER, R., CHAPMAN, B., HOUSEMAN, A. M., ORDIDGE, R. J., COXON, R., GLOVER, P. & MANSFIELD, P., 1988. Snap-shot Magnetic Resonance Imaging at 0.1 T using double-screened gradients. *Journal of Magnetic Resonance, 80*, 248–258.

1990, *The British Journal of Radiology*, *63*, 842–844

Magnetic resonance imaging in idiopathic retroperitoneal fibrosis: measurement of T_1 relaxation time

By *Alan P. Brooks, Rodney H. Reznek and Judith A. W. Webb

Department of Diagnostic Radiology, St Bartholomew's Hospital, West Smithfield, London EC1A 7BE

(*Received February 1990 and in revised form May 1990*)

Abstract. Magnetic resonance imaging at 0.08 Tesla was performed in nine patients with proven idiopathic retroperitoneal fibrosis. A total of 11 scans was performed. Three patients were scanned before diagnosis; one of these also had two follow-up scans. A further six patients were scanned a variable time after diagnosis and treatment. On each scan, a periaortic soft-tissue mass was readily identified, the distribution corresponding to that seen on computed tomography. There was no difference in the mean T_1 relaxation time of the mass between patients scanned before diagnosis and those scanned after treatment. However, the patient followed with serial scans showed a progressive reduction in the T_1 value of the mass with time. Comparison with results obtained in patients with lymphoma suggests that the T_1 values in retroperitoneal fibrosis are lower than in lymphoma, particularly non-Hodgkin's lymphoma.

The differential diagnosis of a periaortic retroperitoneal soft-tissue mass demonstrated on computed tomography (CT) includes retroperitoneal fibrosis (RPF), lymphoma and metastatic carcinoma. Chisholm et al (1986) studied such a group of patients: of 24 patients not known to have malignant disease, the cause of the mass proved to be lymphoma in 46%, "periaortitis" (RPF) in 17%, and a variety of malignancies in 38%. Identification of discrete para-aortic or mesenteric lymph node enlargement appears to be the most reliable sign of malignancy on CT. Differentiation of RPF from malignancy by the CT features is particularly difficult when a confluent mass is present (Chisholm et al, 1986; Degesys et al, 1986).

It is not yet clear whether magnetic resonance imaging (MRI) can distinguish prospectively between idiopathic RPF and malignancy. The purpose of this study was to measure the T_1 relaxation time of the periaortic mass in patients with RPF, and to compare the results with those obtained in patients with lymphoma.

Patients and methods

Nine patients (eight male, one female; age range 44–59 years) with biopsy-proven idiopathic RPF were examined (Table I). One patient was scanned three times, thus a total of 11 scans were performed. Three patients were scanned before diagnosis, and the remainder were scanned at varying intervals after diagnosis and treatment. Patients were examined using an MD 800 resistive MRI scanner operating at 0.08 Tesla. The technique for obtaining T_1 measurements using this scanner has been described (Richards et al, 1988). Briefly, a T_1 map is generated using an interleaved saturation recovery/inversion recovery sequence. Axial scans through the retroperitoneum were obtained using a slice thickness of 1.6 cm and a slice interval of 2 cm. T_1 measurements of the periaortic soft-tissue mass were made using a region of interest cursor, and a mean T_1 of the mass was calculated for each patient. The number of readings obtained varied between two and eight, depending on the size and extent of the retroperitoneal mass. The results were compared with T_1 values in patients with lymphoma reported from this unit previously (Richards, 1987). In 10 of the 11 scans, a T_1 measurement of skeletal muscle (psoas) and of subcutaneous fat was also taken. All patients had had a previous CT scan.

Results

The periaortic mass was readily identified on MRI, the distribution corresponding to that present on CT (Fig. 1). Even relatively small masses present on some follow-up scans were clearly identified. This included the smallest residual mass, which measured about 0.5 cm in thickness. The T_1 values of the periaortic masses are shown in Table I (unfortunately, the actual T_1 measurements obtained in three patients scanned early in the study are no longer available). The mean T_1 values for all the examinations ranged between 254 and 364 ms. The overall mean T_1 values were the same for the three patients scanned before diagnosis (315 ms; range 254–364 ms), the eight follow-up scans (311 ms; range 258–340 ms), and for the 11 scans combined (313 ms; standard deviation 33). The patient scanned before diagnosis and twice afterwards showed a progressive reduction in the mean T_1 of the mass (302 ms before diagnosis, decreasing to 258 ms at 12 months). The mean T_1 value for psoas muscle was 247 ms (standard deviation 8; range 233–257) and for subcutaneous fat was 146 ms (standard deviation 5; range 140–157): these results are similar to those previously obtained in a group of normal volunteers (Richards et al, 1988).

The results of the current study are compared in

---

*Author for correspondence.

Table I. Patient details and MR scan results

Scan number	Patient number	Steroid treatment	Diagnosis–scan interval	T_1 measurement of periaortic mass (ms)	
				Mean	Range
1	1	No	Pre-diagnosis	302	N/A
2	1	No	6 months	294	266–332
3	1	No	12 months	258	237–278
4	2	No	Pre-diagnosis	254	218–277
5	3	No	Pre-diagnosis	364	N/A
6	4	Yes	9 months	321	258–407
7	5	Yes	6 years	340	336–343
8	6	Yes	9 years	320	N/A
9	7	Yes	26 months	339	320–349
10	8	Yes	17 months	337	322–353
11	9	Yes	13 months	317	268–365

(N/A: Actual T_1 readings no longer available).

Table II with those obtained in a previous study from this unit of T_1 measurements of lymph node masses in patients with a variety of types of lymphoma (Richards, 1987). The mean T_1 measurement in RPF is significantly lower than that seen in Hodgkin's lymphoma ($p < 0.001$) and much lower than that seen in non-Hodgkin's lymphoma ($p \ll 0.001$).

Discussion

A growing number of cases of RPF have been examined using MRI (Hricak et al, 1983; Lee et al, 1984; Cullenward et al, 1986; Arrive et al, 1989; Mulligan et al, 1989; Yuh et al, 1989). The periaortic mass demonstrated by MRI is comparable in size and extent to that shown by CT, and can be imaged directly in the sagittal and coronal as well as axial planes. A major advantage of MRI over CT is the ability to demonstrate patent vascular structures without the administration of intravenous contrast medium. This facilitates the identification of even quite small masses (Yuh et al, 1989). These can be difficult to identify on unenhanced CT, particularly on post-treatment scans (Brooks et al, 1987).

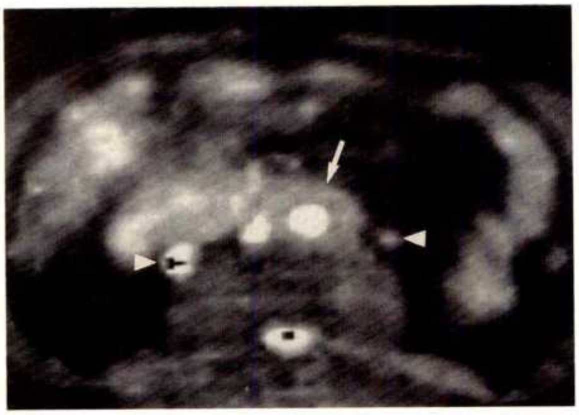

Figure 1. Calculated T_1 image in a patient with RPF. The lumen of both the aorta and inferior vena cava appear as regions of very high "signal". These are enveloped by a retroperitoneal mass of intermediate T_1 (arrow). Dilated ureters are also visible (arrowheads).

Previous studies of MRI in RPF have been performed using higher field strength scanners than ours (0.35 and 0.5 Tesla), usually making use of a qualitative rather than a quantitative analysis. This is usually described in terms of signal intensity of the periaortic mass relative to that of psoas muscle and fat on spin echo images. However, the relative signal intensities on T_1-weighted spin echo images will depend on the relative values of both T_1 and T_2, and on the precise timing of the sequence, especially the repetition time. As a result, published descriptions of the signal intensity of RPF compared with that of muscle on T_1-weighted images differ (Hricak et al, 1983; Arrive et al, 1989; Mulligan et al, 1989). Two articles from the same group have reported T_1 and T_2 relaxation time measurements obtained at 0.35 Tesla in RPF. The first found that both the mean T_1 and T_2 values of RPF were longer than those of muscle (Hricak et al, 1983). The second studied eight patients with non-malignant RPF and found the mean T_1 value to be 917 ms with a standard deviation of

Table II. T_1 measurements in RPF and lymphoma

Condition	T_1 measurements (ms)		
	Mean	Standard deviation	Range
RPF (11 scans)	313	33	254–364
Hodgkin's lymphoma (6 patients)	387	34	330–422
Non-Hodgkin's lymphoma (12 patients)	447	42	382–509

(Modified from Richards, 1987).

370 ms (Arrive et al, 1989). We have confirmed that RPF has a longer T_1 relaxation time than muscle. The different T_1 values obtained by ourselves and by Arrive et al (1989) reflect the shorter T_1 values obtained at lower magnetic field strengths, with a possible contribution from the different methods of calculating T_1 values used by the two scanning systems. The precision and reproducibility of T_1 measurement at 0.08 Tesla using the MD 800 scanner is established (Richards et al, 1987). The relatively wide spread of T_1 values obtained for the periaortic mass in patients with RPF indicates considerable heterogeneity of this tissue. This probably reflects the inhomogeneity found on histology in RPF (Catino et al, 1967).

In order to investigate the possibility of distinguishing RPF from retroperitoneal malignancy, Arrive et al (1989) compared quantitatively T_1 and T_2 measurements in malignant and non-malignant RPF. The mean T_1 value of RPF at 0.35 Tesla was found not to be significantly different from that obtained in a group of patients with a variety of metastatic carcinomas. The T_2 value of malignant masses was however significantly longer than that of benign RPF. Our study has shown that the T_1 measurement in RPF at 0.08 Tesla is significantly lower than that in lymphoma. Whether this degree of T_1 contrast is confined to very low field strength MRI, whether it also applies to other malignant disease of the retroperitoneum, and what role T_2 relaxation time measurements have, will be resolved with further studies.

Patients with RPF who receive steroid treatment almost invariably show shrinkage of the periaortic mass at follow-up CT, and some patients are left with a stable residual mass (Brooks et al, 1987). A possible explanation for this is that steroids cause the inflammatory cellular portion of the mass to regress, leaving a residual fibrous tissue "scar". One might anticipate that the T_1 value of the periaortic tissue would differ between "new" patients and those with treated disease. The one patent in this study followed with serial scans over a 12-month period (even though not treated with steroids) showed a progressive reduction in the mean T_1 value of the mass from 302 ms to 258 ms. However, as a whole, this study failed to show any overall difference between treated and untreated patients. Yuh et al (1989) performed follow-up scans on four patients with RPF, three of whom had been treated with steroids. In only one case was there a subjective decrease in signal intensity at follow-up compared with the pre-treatment scan; this was in a patient given steroids.

Our results suggest that MRI, at least at low field strength, may be of some value in the prospective differentiation between RPF and malignant disease of the retroperitoneum.

References

Arrive, L., Hricak, H., Tavares, N. J. & Miller, T. R., 1989. Malignant versus nonmalignant retroperitoneal fibrosis: differentiation with MR imaging. *Radiology, 172,* 139–143.

Brooks, A. P., Reznek, R. H., Webb, J. A. W. & Baker, L. R. I., 1987. Computed tomography in the follow-up of retroperitoneal fibrosis. *Clinical Radiology, 38,* 597–601.

Catino, D., Torack, R. M. & Hagstrom, J. W. C., 1967. Idiopathic retroperitoneal fibrosis: histochemical evidence for lateral spread of the process from the midline. *Journal of Urology, 98,* 191–194.

Chisholm, R. A., Coltart, R. S., Cooper, P. & Dixon, A. K., 1986. Circumferential para-aortic masses: computed tomographic observations. *Clinical Radiology, 37,* 531–535.

Cullenward, M. J., Scanlan, K. A., Pozniak, M. A. & Acher, C. A., 1986. Inflammatory aortic aneurysm (periaortic fibrosis): radiologic imaging. *Radiology, 159,* 75–82.

Degesys, G. E., Dunnick, N. R., Silverman, P. M., Cohan, R. H., Illescas, F. F. & Castagno, A., 1986. Retroperitoneal fibrosis: use of CT in distinguishing among possible causes. *American Journal of Roentgenology, 146,* 57–60.

Hricak, H., Higgins, C. B. & Williams, R. D., 1983. Nuclear magnetic resonance imaging in retroperitoneal fibrosis. *American Journal of Roentgenology, 141,* 35–38.

Lee, J. K. T., Ling, D., Heiken, J. P., Glazer, H. S., Sicard, G. A., Totty, W. G., Levitt, R. G. & Murphy, W. A., 1984. Magnetic resonance imaging of abdominal aortic aneurysms. *American Journal of Roentgenology, 143,* 1197–1202.

Mulligan, S. A., Holley, H. C., Koehler, R. E., Koslin, D. B., Rubin, E., Berland, L. L. & Kenney, P. J., 1989. CT and MR imaging in the evaluation of retroperitoneal fibrosis. *Journal of Computer Assisted Tomography, 13,* 277–281.

Richards, M. A., 1987. Magnetic resonance imaging in lymphoma—the role of spin lattice relaxation time measurement. *Cancer Surveys, 6,* 315–341.

Richards, M. A., Gregory, W. M., Webb, J. A. W., Jewell, S. E. & Reznek, R. H., 1987. Reproducibility of spin lattice relaxation time (T_1) measurement using an 0.08 Tesla MD 800 magnetic resonance imager. *British Journal of Radiology, 60,* 241–244.

Richards, M. A., Gregory, W. M. & Webb, J. A. W., 1988. Detection of a systemic effect of malignancy in vivo by magnetic resonance imaging. *Magnetic Resonance Imaging, 6,* 557–565.

Yuh, W. T. C., Barloon, T. J., Sickels, W. J., Kramolowsky, E. V. & Williams, R. D., 1989. Magnetic resonance imaging in the diagnosis and followup of idiopathic retroperitoneal fibrosis. *Journal of Urology, 141,* 602–605.

1990, *The British Journal of Radiology*, *63*, 845–849

The relationship of "high risk" mammographic patterns to histological risk factors for development of cancer in the human breast

By Justine E. Arthur, MB, BS, I. O. Ellis, MB, BS, MRCPath, *C. Flowers, MRCS, LRCP, FRCR, *E. Roebuck, DMRD, FRCR, C. W. Elston, MD, MRCPath and †R. W. Blamey, MD, FRCS

Departments of Histopathology and †Surgery, City Hospital and *Department of Radiology, University Hospital, Nottingham

(*Received February 1990 and in revised form May 1990*)

Abstract. In the UK Trial for the Early Detection of Breast Cancer in Nottingham, 119 women were identified as having fibrocystic change with epithelial hyperplasia or *in situ* carcinoma. Their mammograms were classified according to Wolfe's criteria and the corresponding histology for each patient was classified for degrees of epithelial hyperplasia, atypia and *in situ* neoplasia using Page's criteria. A control population of patients presenting for breast screening was used to represent the general population. No correlation was found between the four mammographic Wolfe patterns, N1, P1, P2 and DY and histological evidence of epithelial hyperplasia, atypia or *in situ* carcinoma. A further study was carried out to determine histological features of Wolfe pattern, using radiological examination of resected breast tissue. The variation in Wolfe pattern was related to the distribution of fibrous and adipose tissue in the breast interlobular stroma and appeared to have no relationship to epithelial parenchymal content. This information does not support the hypothesis that radiographic densities of P2 and DY patterns correspond to high risk epithelial proliferation.

Each year 15 000 women in England and Wales die from breast cancer and 1 in 15 women will develop the disease in their lifetime (OPCS, 1983, HMSO, 1983). The current lack of any prospect for primary prevention increases the need to develop more effective and less expensive techniques for early detection of breast cancer. Selection of women at high risk might reduce the number who need to attend for regular mammographic screening. The work of Wolfe shows that women exhibiting certain mammographic breast parenchymal patterns are at greater risk of developing breast cancer (Wolfe, 1976, 1987; Wolfe et al, 1983). He has described the following breast parenchymal patterns:

- N1 the breast is composed primarily of fat, often with a fine trabeculated appearance;
- P1 "prominent" ducts occupy 25% or less of the volume of the breast;
- P2 "prominent" ducts occupy more than 25% of the volume of the breast;
- DY mammary dysplasia (fibrocystic change) with sheet-like areas of increased density.

Wolfe states that the mammographic patterns most often related to breast cancer and premalignant epithelial alterations, especially after the age of 50, are the P2 and DY breast patterns, N1 and P1 being rarely associated with these conditions. He reports that the incidence of subsequent carcinoma development, per 1000 women, over a period of 3 years increases 30 fold, from 1.45 cases per 1000 women with N1 patterns to 44.60 cases per 1000 women with DY patterns. (P1 = 3.85 and P2 = 17.45)

Several categories of epithelial proliferation have been described in the female breast (Page & Anderson, 1988): regular epithelial hyperplasia of mild, moderate and florid degree, atypical ductal hyperplasia and atypical lobular hyperplasia; and ductal and lobular carcinoma *in situ*. Increasing risks of subsequent development of breast carcinoma have been demonstrated with these conditions (Page et al, 1978, 1982, 1985). Mild hyperplasia carries the same risk as the general population of the subsequent development of invasive breast carcinoma. Moderate and florid hyperplasia carry a risk double that of the general population for cancer development. Atypical hyperplasia of ductal and lobular types are associated with four times the risk for subsequent development of invasive carcinoma. Ductal and lobular carcinomas *in situ* are associated with a risk for invasive carcinoma development 10 times that of the general population (Hutter et al, 1986; Page et al, 1978, 1982; Page & Anderson, 1988).

Despite these detailed studies of histopathological and radiological risks for carcinoma development in the breast, little work has been undertaken to relate these phenomena to each other. One study, performed by Wellings and Wolfe (1978) correlated the radiographic densities of P1, P2 and DY mammographic patterns with fibrosis and a variety of lesions of the terminal duct lobular units particularly "atypical lobules Type A". Two of these lesions were described previously by Wellings and Jensen (1975) but both were thought to arise from a similar histogenetic pathway. Type A

Address for correspondence: Dr I. O. Ellis, Department of Histolopathology, City Hospital, Hucknall Road, Nottingham NG5 1PB.

Table I. The study population identified from the Nottingham Breast Self Examination (BSE) arm of the UK Trial for the Early Detection of Breast Cancer 1979–1986

Women attending for BSE	28 759	(49.86% of those invited)
Number of biopsies in the study group for malignant conditions	546	119 borderline biopsies*
Number of biopsies in the study group for benign conditions	449	

* Borderline biopsies indicates the number of biopsies for carcinoma *in situ* (included in the malignant category) and epithelial hyperplasia (included in the benign category).

lesions represent the spectrum of ductal hyperplasia, atypical ductal hyperplasia and ductal carcinoma *in situ*. Type B lesions represent the lobular equivalents, that is, atypical lobular hyperplasia and lobular carcinoma *in situ*. Wellings and Wolfe (1978) found that the degree of fibrosis and the grade of Type A atypical lobules increased from P1 to DY. A recent study by Urbanski et al (1988) demonstrated a weak relationship between the extent of mammographic "dysplasia" and histological evidence of epithelial atypia and carcinoma *in situ* in women younger than 50 years old. Such findings could explain the increased risk for cancer development associated with P2 and DY breasts.

We have investigated this putative relationship between Wolfe pattern and epithelial proliferation with two studies. First, a retrospective study was carried out of the mammographic appearances and histology of women from the Nottingham arm of the UK Trial for the Early Detection of Breast Cancer. Secondly a prospective study was performed combining radiological and histological examination of mastectomy specimens from women undergoing treatment for breast carcinoma.

Method

Between 1979 and 1986, 56 000 women aged 45–64 years in Nottingham were invited for education in Breast Self Examination as part of the United Kingdom Trial of Early Detection of Breast Cancer. Women participating in this programme were offered an open access mammography and clinical examintion service should they detect a breast abnormality through self examination. If a significant lesion was identified at clinic attendance, open biopsy was performed. During this study period biopsies were carried out on 995 of the study group. One hundred and nineteen cases were identified as "borderline lesions" of epithelial hyperplasia and *in situ* carcinoma (Table I).

In our study, these 119 patients with borderline lesions were taken to represent women with histological evidence of increased risk. Forty-three women who underwent biopsies which showed benign non-proliferative fibrocystic change are taken to represent women with no histological evidence of increased risk (Table II). To represent the general population, 91 women, aged between 50 and 64, consecutively attending for mammographic breast screening at the Nottingham City Hospital during 1998, were used to determine the frequency of each mammographic pattern. All mammograms on the patients were available. The Wolfe classification of all these mammograms was reviewed by a single radiologist to elimiate interobserver variation in the objective grading of mammograms. The radiological classification based on the mammographic pattern was then compared with the histological findings. Improvement of mammographic technique has occurred between 1979 and 1988. However, the differences was not considered sufficient to alter interpretation of the Wolfe pattern.

The histological slides were stained in Ehrlich's haematoxylin and eosin (H&E), and were assessed by two pathologists using Page's method of classification (Page & Anderson, 1988). Mild regular hyperplasia is defined by the recognition of between two and four

Table II. Distribution of the cases according to Wolfe mammographic pattern categories (percentages in parentheses)

	Screened population	FCC	All pathological "borderline" groups	Pathological "borderline" groups					
				Mild EH	Mod EH	ADH	DCIS	ALH	LCIS
N1	15 (16)	1 (2)	13 (11)	0 (0)	3 (10)	0 (0)	8 (14)	0 (0)	2 (18)
P1	12 (13)	9 (21)	24 (20)	2 (12)	8 (28)	0 (0)	12 (21)	0 (0)	2 (18)
P2	16 (18)	15 (35)	32 (27)	3 (19)	9 (31)	2 (40)	15 (26)	0 (0)	3 (27)
DY	48 (53)	18 (42)	50 (42)	11 (69)	9 (31)	3 (60)	23 (39)	0 (0)	4 (36)
Total	91 (100)	43 (100)	119 (100)	16 (100)	29 (100)	5 (100)	58 (100)	0 (0)	11 (100)

FCC = fibrocystic change.
Mild EH = mild epithelial hyperplasia.
Mod EH = moderate and florid epithelial hyperplasia.
ADH = atypical ductal hyperplasia.
DCIS = ductal carcinoma *in situ*.
ALH = atypical lobular hyperplasia.
LCIS = lobular carcinoma *in situ*.

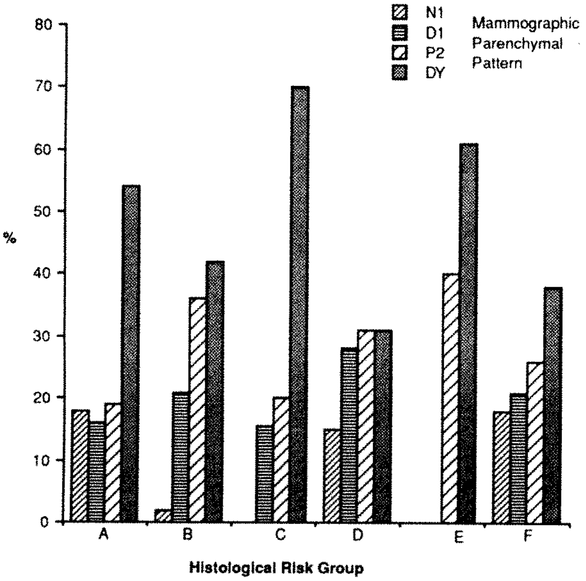

Figure 1. The distribution of Wolfe mammographic breast parenchymal patterns in various histological subgroups. A: Screened/general population; B: non-proliferative fibrocystic change; C: mild regular epithelial hyperplasia; D: moderate florid regular epithelial hyperplasia, mild atypical hyperplasia; E: atypical epithelial hyperplasia; F: carcinoma *in situ* (ductal and lobular).

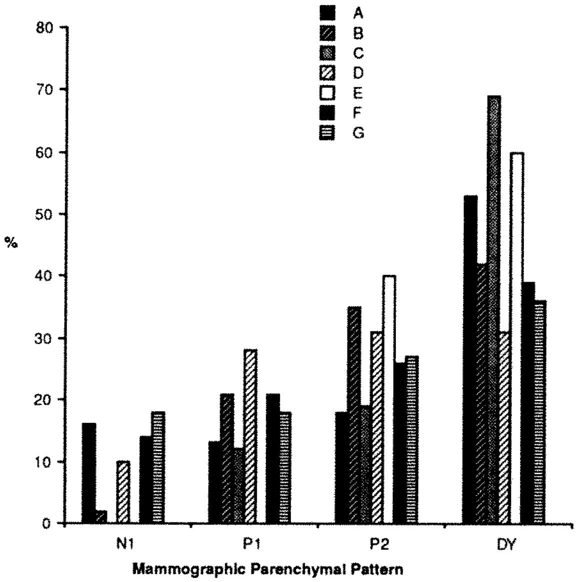

Figure 2. The distribution of the normal population and histological risk groups found in each of the Wolfe mammographic parenchymal patterns. A–E: as in Fig. 1; F: ductal carcinoma *in situ*; G: lobular carcinoma *in situ*.

epithelial cells above the basement membrane. Moderate and florid regular hyperplasia are recognized as five or more cells above the basement membrane, with a tendency to distension and crossing of the space by hyperplastic cells which do not show the cytological and architectural patterns of atypical hyperplasia and ductal carcinoma *in situ*. Atypical ductal hyperplasia is recognized by its histological pattern which is intermediate between that of regular hyperplasia and ductal carcinoma *in situ*, that is, with some but not all the histological features of ductal carcinoma *in situ*. Ductal carcinoma *in situ* in its various subtypes is recognized by its characteristic architectural and cytological features, well described by Page and Anderson (1988). Atypical lobular hyperplasia and lobular carcinoma *in situ* are recognized by an expansion of small uniform cells with lobular units which may extend to involve ducts in a Pagetoid manner. Filling of all acini within the lobule with distortion of at least 50% of the lobule is used as the arbitrary divide between the two conditions.

An additional prospective study was also performed involving a radiographic and histological study of breast slices from 17 consecutive women who had undergone mastectomy. All of these patients had had pre-operative mammography. It is not possible to examine the entire breast in a histological section. Specimen radiography was used to confirm that the areas of breast sampled had a radiographic appearance representative of the mammographic pattern. Slices measuring 1–2 cm in thickness were taken from each mastectomy specimen. The slice included the nipple and was taken from as near as possible to the 3–9 o'clock position in the horizontal plane. A specimen radiograph was taken and correlated with the pre-operative cranio-caudal mammographic view. Using the specimen radiograph and mammogram it was possible to sample areas of tissue containing the radiographic densities characteristic of the mammographic pattern. On average, 10 blocks were taken from each slice, and between four and six sections were cut and stained in Ehrlich's H & E. The direction and position of each block was recorded on diagrams corresponding with the mammograms and specimen radiographs.

Results

The distribution of breast patterns seen in the control group and in each histological group is shown in Table II and illustrated in Fig. 1. There was no correlation between the radiological and the histological risk factors for development of breast cancer. Figure 2 shows the overall distribution of the histological conditions seen in each mammographic subgroup. These results demonstrate that any increased risk associated to P2 and DY patterns cannot be attributed to a greater proportion of high risk epithelial abnormalities in the breasts.

From the study of specimen radiology of women who had undergone mastectomy, it appears that the variation in Wolfe pattern was a result of the ratio of fibrous to adipose tissue in the breast with no apparent relationship to epithelial parenchymal content. A varying distribution of collagenous fibrous tissue and adipose tissue was observed in the breasts examined. A classification of this distribution based on the arrangement of these tissues was devised. Three basic patterns were observed: (1) septae, where fibrous tissue was confined to thin fibrous septae usually containing vessels and subsegmental ducts; (2) islands, where the fibrous tissue was arranged in nodular collections, usually containing parenchymal structures, and surrounded by adipose tissue; (3) confluent, where the fibrous tissue was arranged as a diffuse sheet with little adipose tissue present. Within some breasts, more than one type of distribution was observed across the breast disc. The dominant pattern was recorded in these instances. The results of this aspect of the study are shown in Table III. In addition, the proportion of epithelial parenchymal structures present was recorded. This was highly variable between cases with no apparent relationship to mammographic background pattern or histological fibrous tissue and adipose tissue distribution.

Discussion

We have examined the putative link between mammographic breast parenchymal pattern and histological evidence of epithelial proliferation, a documented risk factor for the development of breast cancer. If the high risk associated with P2 and DY Wolfe patterns is to be attributed to high grades of epithelial premalignant abnormality, one would expect the proportion of these high risk mammographic patterns to be increased in the high risk histological groups. No such distribution is seen in this study and our findings do not support the results reported by Wellings and Wolfe (1978). In fact, the ratio of high risk (P2 and DY) to low risk (N1 and P1) mammographic patterns is increased in the low risk histology control group and screening control group compared with in the high risk histological groups of *in situ* carcinoma. In all the histological groups, and in the two control populations, the commonest mammographic categories were P2 and DY (Figs 1 and 2). This observation, although well recognized by radiologists, is not well documented. It could provide an alternative explanation why an increased incidence of carcinoma was demonstrated with these two mammographic patterns.

The failure of this study to confirm a correlation between Wolfe mammographic parenchymal pattern and histological epithelial alteration suggests that any high risk for carcinoma development associated with P2 and DY patterns is not due to an epithelial abnormality. Instead, the variation in mammographic patterns appears to be related to the variable ratio and distribution of fibrous tissue and adipose tissue in the breast interlobular stroma. N1 patterns reflect a stroma predominantly composed of adipose tissue with only thin fibrous tissue septae being present. The P1 and P2 patterns result from stroma composed of islands and septae of fibrous tissue within adipose tissue. In DY patterns there is coalescence of extensive fibrous islands and septae to produce large areas of virtual confluence of fibrous connective tissue (Table III).

Table III. Histological distribution of fibrous tissue within Wolfe radiological groups

Breast Pattern	Septae	Islands*	Confluent*
N1 (*n* = 1)	1	0	0
P1 (*n* = 1)	0	1	0
P2 (*n* = 8)	4	8	2
DY (*n* = 7)	3	4	7

* Variable epithelial parenchymal content.

These descriptions of the association of high risk mammographic patterns with the distribution of fibrous tissue are consistent with the findings of Fisher et al (1978) and Mansel (personal communication), but are contrary to prevailing views that associate the radiographic densities of P2 and DY patterns and their corresponding risk for breast cancer development with proliferative fibrocystic change (Wellings & Wolfe, 1978). Although Urbanski et al (1988) have demonstrated a significant association between epithelial atypia and carcinoma *in situ* and mammographic "dysplasia", this associaton was very weak and could not be reproduced on independent review by a second radiologist. They recognized that the epithelial changes observed were not directly responsible for the mammographic findings.

We are unable in this study to address directly the association between subsequent risk of breast cancer and mammographic background pattern. Our observation that these radiographic densities, which are characteristic of the four mammographic patterns, are simply a result of variation in fibrous tissue in the interlobular stroma does not necessarily dispel claims of risk associated with P2 and DY patterns. To our knowledge there are no studies which have investigated the distribution of stromal components to risk or development of breast cancer. Further evaluation of the radiographic determinants of risk and these stromal alterations in the development of breast carcinoma is required.

Acknowledgments

We wish to thank the administrative staff of the Nottingham Breast Screening Service for their help in identification of the cases studied, the audiovisual department for assistance in preparing the figures and Julie Rainbow and Jinny Spence for preparing the manuscript.

References

Fisher, E. R, Palekar, A., Kim, W. S. & Redmond, C., 1978. The histopathology of mammographic patterns. *American Journal of Clinical Pathology, 69*, 241–426.

HMSO, 1983. *Cancer Statistic Registrations* (HMSO, London).

Hutter, R. P. V., 1986. Consensus meeting: Is 'fibrocystic disease' of the breast precancerous? *Archives of Pathology and Laboratory Medicine, 110*, 171–173.

OPCS, 1983. Cancer Statistics Registrations (OPCS, England and Wales).

Page, D. L. & Anderson, T. J., 1988. *Diagnostic Histopathology of the Breast* (Churchill Livingstone, Edinburgh).

Page, D. L., Zwagg, R. V., Rogers, L. W., Williams, L. T., Walker, W. E. & Hartmann, W. H., 1978. Relation between the component parts of fibrocystic disease complex and breast cancer. *Journal of the National Cancer Institute*, *61*, 1055–1063.

Page, D. L., Dupont, W. D., Rogers, L. W. & Landenberger, M., 1982. Intraductal carcinoma of the breast: follow-up after biopsy. *Cancer*, *49*, 751–758.

Page, D. L., Dupont, W. D., Rogers, L. W., Williams, L. T., Walker, W. E. & Hartmann, W. H., 1985. Atypical hyperplastic lesions of the female breast—long term follow study. *Cancer*, *55*, 2698–2708.

Urbanski, S., Jensen, H. M., Cooke, G., McFarlane, D., Shannon, P., Kruikov, V. & Boyd, N. F., 1988. The association of histological and radiological indicators of breast cancer risk. *British Journal of Cancer*, *58*, 474–479.

Wellings, S. R. & Jensen, H. M., 1979. An atlas of subgross pathology of the human breast with special reference to precancerous lesions. *Journal of the National Cancer Institute*, *55*, 231–273.

Wellings, S. R. & Wolfe, J. N., 1978. Correlative studies of the histological and radiographic appearances of the breast with special reference to possible precancerous lesions. *Diagnostic Radiology*, *129*, 299–306.

Wolfe, J. N. 1976. Breast patterns as an index of risk for developing breast cancer. *American Journal of Roentgenology*, *126*, 1130–1139.

Wolfe, J. N., Albert, S., Belle, S. & Balane, M., 1983. Breast patterns and their relationship to risk for having or developing carcinoma. *Radiological Clinics of North America*, *21*, 127–136.

Wolfe, J. N., Saftlas, A. F. & Salane, M., 1987. Mammographic parenchymal patterns and quantitative evaluation of mammographic densities: a case-control study. *American Journal of Roentgenology*, *148*, 1087–1092.

1990, *The British Journal of Radiology*, *63*, 850–854

The role of Indium-labelled leukocyte imaging in pyrexia of unknown origin

By S. G. Davies, MRCP, FRCR and N. W. Garvie, MRCP, FRCR

Radioisotope Department, The London Hospital, Whitechapel, London E1 1BB

(*Received April 1990 and in final form June 1990*)

Abstract. Indium-111-labelled white blood cell scanning is often used in the investigation of pyrexia of unknown origin (PUO) to locate an otherwise occult source of sepsis. From a series of 166 white blood cell studies performed for sepsis, 28 cases of true PUO were identified and reviewed. The sensitivity was 60% and specificity 70%, with a positive predictive value of 38% and negative predictive value of 90%. Only 11% of studies revealed a pyogenic cause for PUO. These results are discussed and the potential role of gallium scanning in PUO is raised.

Indium-111-labelled white blood cell scintigraphy is an established imaging technique in the investigation of abdominal sepsis (Knochel et al, 1980; Carrol et al, 1981; Goodwin, 1983; Goldman et al, 1987; Syrjala et al, 1987) with values for sensitivity of 84–93% and specificity of 91–100%. Other well recognized indications include the investigation of inflammatory bowel disease (Saverymuttu et al, 1985) and osteomyelitis. Previous studies have emphasized the role of white cell scanning in pyrexia of unknown origin (PUO) (Schell-Frederick et al, 1984; Froelich & Swanson, 1984; Syrjala et al, 1987). It was observed by Syrjala et al (1987) that whilst the sensitivity and specificity were 91% and 85%, respectively, there was a relatively low predictive value of a positive result (73%) in the PUO group. It has recently been suggested that the yield from white cell scanning in PUO may not be as high as expected (Peters, 1989a) and that only 10% of cases of PUO are identified as having a pyogenic cause (Peters, 1989b). This study was undertaken in order to assess the role of labelled white cell scanning in PUO.

Materials and methods

A total of 166 white cell scans performed in this department were reviewed retrospectively. Using the criteria established by Syrjala et al (1987), of the 166 patients examined, 28 cases fulfilled the criteria for PUO. This was defined as a fever of at least 2 weeks' duration, including a week of inpatient investigation with full biochemical and haematological analysis of blood and negative blood, sputum and urine cultures. Appropriate radiographic investigation, including a chest radiograph with no positive findings to indicate the cause of fever, was also required. All patients who had undergone surgery within the previous 6 months were excluded. A minimum period of follow-up of 3 months was required.

Labelled white cells were obtained using a standard method modified from the technique described by Thakur et al (1977). Briefly, this involved withdrawal of 50 ml of the patient's blood into a syringe containing 9 ml of acid-citrate dextrose. After sedimentation, the leukocyte-rich supernatant was withdrawn and a leukocyte pellet obtained by centrifugation at 150 g for 5 minutes. The leukocytes were then resuspended in plasma and labelled with Indium-111-tropolonate followed by incubation at room temperature for 5 minutes. This resulted in a preparation of Indium-labelled white cells with between 9 and 14 MBq of activity.

Imaging was performed at 4, 24 and 48 hours after re-injection using a large field-of-view γ camera equipped with a medium-energy parallel hole collimater with 20% windows set on the 173 keV and 247 keV photopeaks of Indium-111. In all cases the chest, abdomen and pelvis were imaged at 24 and 48 hours. In only three cases was imaging of the head and neck performed. White cell scanning followed ultrasound or computed tomography (CT), except in the three cases where neither ultrasound nor CT was undertaken.

Analysis of scintigrams

A scan was regarded as a "true positive" when the abnormal uptake was confirmed by further investigation, biopsy, surgery or follow-up as representing an infective cause for the pyrexia. Non-infective causes were, therefore, not included in this group. A false negative scan was a normal white cell study where an infective cause for PUO was subsequently established. A separate analysis was undertaken where all causes (*i.e.* infective and non-infective) were considered. In this analysis, a true positive scan was one in which an abnormal area of uptake was demonstrated to be a result of an infective or non-infective cause of PUO.

Results

A total of 28 cases of true PUO were identified. In 25 (89%) cases the fever was of greater than 3 weeks'

Address for correspondence: Dr S. G. Davies, Alex-Wing X-Ray Department, The London Hospital, Whitechapel, London E1 1BB.

Table I. Analysis of data showing levels of white cells (total number of cases: 28)

	True positive	True negative	False positive	False negative
Infective causes of PUO	3 (11%)	18 (64%)	5 (18%)	2 (7%)
% with raised white blood cells	67%	61%	60%	100%
% receiving antibiotics	100%	56%	60%	100%
All causes of PUO	5 (18%)	18 (64%)	3 (11%)	2 (7%)
% with raised white blood cells	80%	61%	30%	100%
% receiving antibiotics	80%	56%	67%	100%

Table II. Analysis of scan results giving sensitivity, specificity and positive and negative predictive values

	Sensitivity	Specificity	Predictive value	
			Positive	Negative
Infective causes of PUO	60%	78%	38%	90%
All causes of PUO	71%	86%	63%	90%

duration at the time of performing the white cell scan; in the remaining three cases the fever was of 2–3 weeks' duration at the time of scanning. It is interesting to note that in these three cases, fever persisted at 3 weeks and that no diagnosis was reached in these patients. The scan results are presented in Tables I and II. These give values of 60% sensitivity, 78% specificity; a positive predictive value of 38% and negative predictive value of 90% for infective causes of PUO. Considering all causes of PUO the sensitivity was 71%, specificity 86%, positive predictive value 63% and negative predictive value 90%.

When considering infective causes of PUO, the three true positive cases (11% of total) were caused by liver abscess, diverticulitis and pneumonia (Cases 1–3, *vide infra*). The five false positive cases included collagen-vascular diseases responsive to steroids in two, non-specific bowel activity in two (presumed to be because of swallowed leukocytes from a respiratory inflammatory process), and renal transplant activity. The two false negative cases were a fungal liver infection in an immunosuppressed patient and a tuberculous pleural effusion (Case 4, *vide infra*).

In two cases, collagen-vascular diseases were responsible for positive scans. In one, marked uptake of the sternoclavicular and shoulder joints was present, and although serology was negative, the rapid resolution of joint and systemic symptoms in response to steroid therapy suggested an autoimmune aetiology. These two cases were regarded as true positives when the broader definition of all causes of fever was used, as the uptake accurately reflected the site of inflammation causing fever.

Considering all modes of investigation, a diagnosis was only ever made in 15 (53%) of all cases, of which only five resulted from infection. The remaining 10 cases were of non-infective aetiology including neoplasia and collagen-vascular disease. In none of the cases did the 48-hour image contribute any further information. There were 13 cases (46%) in whom no diagnosis was made despite the minimum follow-up period of 3 months.

There was no clear trend in the level of white cells (Table I). The upper limit of normal was defined as 11 000 cells per mm^3. Sixty-four per cent of patients were receiving antibiotics at the time of scanning. Again, no clear trend emerges (Table I).

The following case reports are illustrative. The first three cases form the true positive group (infective causes) and illustrate the value of white cell scanning in those cases where initial investigation has not yielded the diagnosis, and where the result of the scan has made further definitive investigation or treatment possible. The fourth case serves to illustrate that a negative white cell scan does not exclude important infection or inflammation.

Case 1

An 80-year-old woman being investigated for a transient ischaemic attack was found to have a persistent temperature of between 37.5 and 38°C. General examination was unremarkable. The erythrocyte sedimentation rate (ESR) was 110 and the white cell count was 16 000 per mm^3. Abdominal ultrasound and CT did not reveal sepsis. A white cell scan demonstrated uptake in the left iliac fossa (Fig. 1). A barium enema demonstrated diverticulitis in the sigmoid colon (Fig. 2).

Case 2

A 52-year-old Indian man presented with a 10-day history of fever and right upper quadrant pain. Ultrasound revealed a rather non-specific pattern suggestive of fatty infiltration of the liver. The gallbladder was normal. No other abnormality was seen in the abdomen or pelvis. Despite antibiotic therapy, the fever continued. The white cell scan demonstrated marked uptake in the right lobe of the liver (Fig. 3), although a repeat ultrasound and biopsy failed to demonstrate evidence of sepsis. A large abscess containing Gram-negative organisms was drained at surgery.

Case 3

A 29-year-old man with non-Hodgkin's lymphoma presented with a 2-week history of fever and general malaise. Laboratory investigations of urine, blood and sputum were normal, as was a chest radiograph. A white cell scan demonstrated high grade lung uptake on the

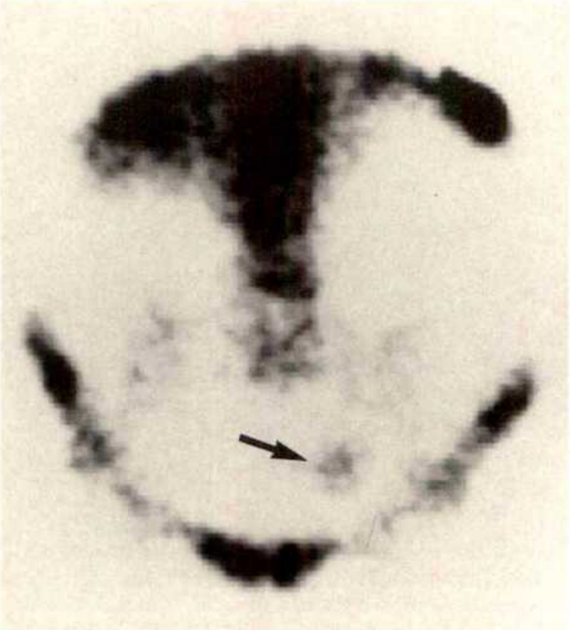

Figure 1. *Case 1.* Indium-labelled white cell scan demonstrating an abnormal focus of activity in the left iliac fossa (arrow).

24-hour image (Fig. 4), which was confirmed as an infiltrate on CT (Fig. 5). Subsequently the patient developed chest signs. These and the infiltrate on CT disappeared with broad-spectrum antibiotics. The chest radiograph remained normal throughout.

Case 4

A 31-year-old Indian woman presented with an 8-week history of fever, weight loss and general malaise associated with pain in the right hypochondrium. Chest radiography and two ultrasound examinations of the abdomen and pelvis were normal. A white cell scan was normal. Three weeks later the patient developed a large left pleural effusion. The effusion, fever and systemic symptoms resolved with anti-tuberculous therapy.

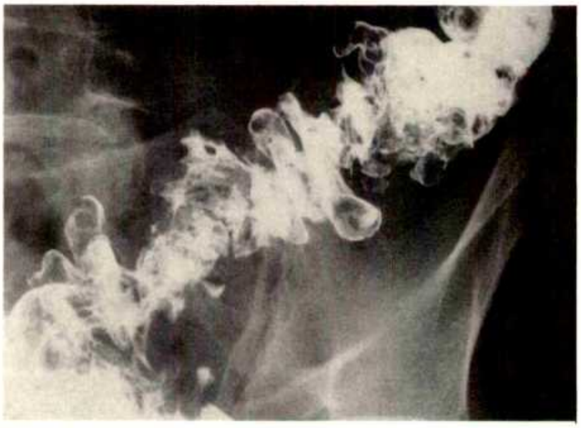

Figure 2. *Case 1.* Barium enema showing changes of diverticulitis in the sigmoid colon.

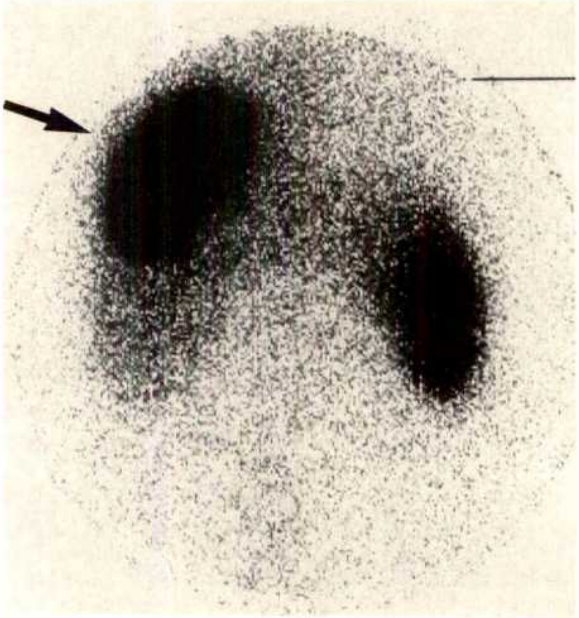

Figure 3. *Case 2.* Indium-labelled white cell scan demonstrating markedly increased uptake in the right lobe of the liver.

Discussion

Previous studies have reported favourably on the role of white cell scanning in PUO (Froelich et al, 1984;

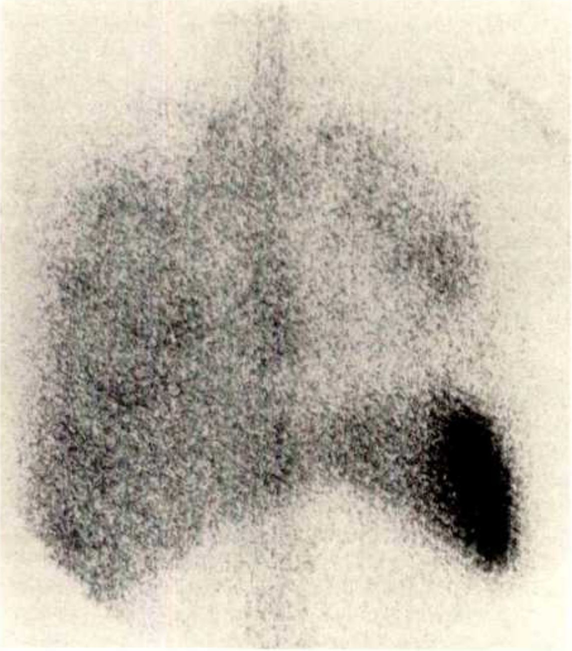

Figure 4. *Case 3.* Indium-labelled white cell scan demonstrating high grade uptake in the thorax.

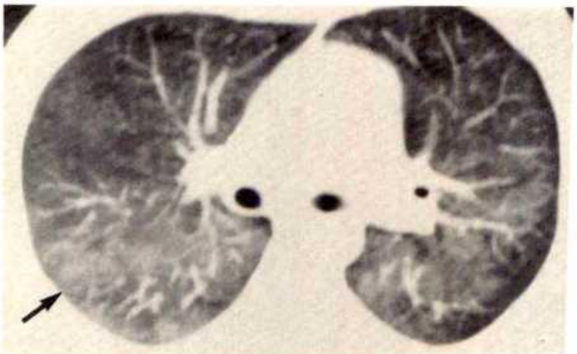

Figure 5. *Case 3.* Computed tomographic scan of the thorax demonstrating areas of increased attenuation in both lungs.

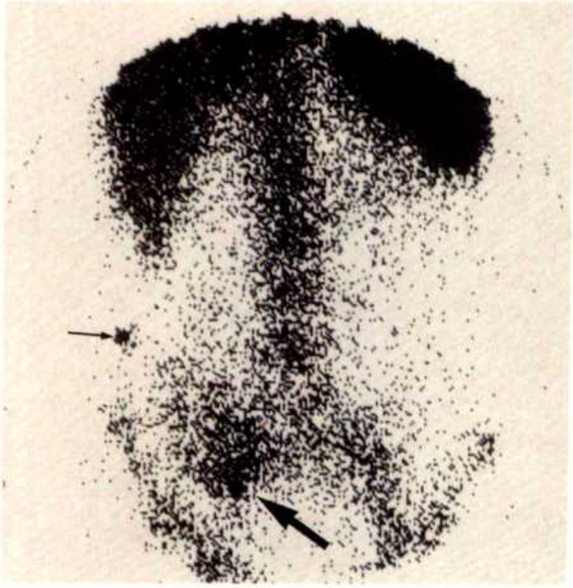

Figure 6. Indium-labelled white cell scan demonstrating an abnormal focus (large arrow) corresponding to the site of the renal transplant. The smaller arrow indicates a cobalt source used as a marker.

Schell-Frederick et al, 1984) although the relatively poor positive predictive value of 73% of this investigation has been noted (Syrjala et al, 1987). This study confirms the poor positive predictive value (38%) of white cell scanning in infective causes of PUO but also demonstrates a relatively low sensitivity (60%) and specificity (78%).

The true positive group (infective causes) included the cases described above of diverticulitis, a hepatic abscess and pulmonary infection. In the case of the hepatic abscess a positive diagnosis was possible without the colloid subtraction technique, although this was performed in cases where upper abdominal pathology was suspected, as recommended by Fawcett et al (1980) and Rovekamp et al (1983). Diverticulitis is a recognized cause of gastrointestinal uptake (McAfee & Samin, 1985).

Of interest was the case of pulmonary infiltrate in a young man with non-Hodgkin's lymphoma (Case 3). Although bilateral pulmonary uptake of Indium-labelled white blood cells was present, it was uneven in distribution. This pattern has been described as diffuse (Cook et al, 1984; Segall & McDougall, 1986) and although less likely to indicate an infective aetiology than a focal pattern, infection was the cause in our patient as the fever and lung changes disappeared promptly with antibiotics. Seabold et al (1984) have stressed the importance of extra-abdominal sites of infection in the investigation of PUO, where pneumonitis was found unexpectedly on several occasions.

There were five false positive cases in the infective group. In one, renal transplant uptake was present (Fig. 6). Although this has been thought to be a reliable indicator of transplant rejection or infection (Forstrum et al, 1981), this case had a negative biopsy and no serological or pulmonary evidence of cytomegalovirus. This finding was, therefore, more in keeping with the view of Collier et al (1984), who demonstrated that Indium-labelled white blood cells may be taken up normally by renal transplants.

Bowel activity was present in two false positives (infective causes), a finding which is well recognized (Datz & Thorne, 1986a) and may indicate sepsis of the sinuses or lung. The importance of including the head and neck in a survey for PUO has been stressed (Hawker et al, 1985) and it is noted that the head and neck were only included in three cases in this series. None of these three cases was, however, found to have pulmonary or sinus sepsis on follow-up. The other two false positive cases are described above.

The two false negative cases (infective group), *i.e.* that of tuberculosis (Case 4) and that of a fungal infection of the liver in an immunosupressed patient, emphasize that a negative white cell scan in PUO does not exclude serious life threatening infection or inflammation.

In the overall analysis a diagnosis was achieved in only 15 of the 28 patients undergoing white cell scanning. Of the total of 15 cases, five were of infective aetiology and 10 were of non-infective aetiology. These figures are broadly in line with the classic study of Petersdorf & Beeson (1961), where 36% of their series resulted from infective causes.

In the series of patients presented here, 64% were already receiving antibiotics at the time of the white cell scan. It has, however, previously been noted that the presence of antibiotic therapy is unlikely to influence the result (Datz & Thorne, 1986b). In this study there was no clear trend in the level of the white cell count at the time of scanning. All groups contained a relatively high percentage of patients with elevated white cell counts (Table I).

The question of duration of infection has been raised with reference to the success of white cell scanning in prolonged pyrexia. Sfakianakis et al (1982) recommended from a study of 32 cases that gallium should be considered for subacute and chronic infections where white cell scintigraphy may be falsely negative. Indium-labelled white cells were proposed as the preferable agent for acute infections of less than 2 weeks' duration. This view has been challenged by Datz and Thorne (1986c) who found no statistical difference in the sensitivity of white cell scanning between acute and subacute groups of patients. Nevertheless, the potential value of gallium scintigraphy in PUO should perhaps be reconsidered, particularly in patients in whom white cell scanning is negative but in whom the clinical suspicion of an infective, or perhaps more importantly a non-infective, aetiology for PUO is strongly suspected. Previous studies have demonstrated the value of gallium scintigraphy in febrile patients (McNeil et al, 1981), despite the recognized drawbacks of using this agent.

Conclusion

This study has demonstrated that the yield from white cell scanning in PUO is poor, with only 18% of studies providing a positive result and only 11% of cases representing a pyogenic cause. The importance of non-pyogenic causes for PUO is raised, as is the potential role of gallium scanning.

References

Carroll, B. C., Silvermann, P. M., Goodwin, D. A. & McDougall, I. R., 1981. Ultrasonography and Indium 111 white blood cell scanning for the detection of intraabdominal abscesses. *Radiology*, *140*, 155–160.

Collier, B. D., Isitman, A. T., Kaufman, H. M., Rao, S. A., Knobel, J., Hellman, R. S., Zielonka, J. S. & Pelc, L., 1984. Concentration of In-111-Oxine labeled autologous leukocytes in noninfected and nonrejecting renal allografts: concise communication. *Journal of Nuclear Medicine*, *25*, 156–159.

Cook, P. S., Datz, F. L., Disbro, M. A., Alazraki, N. P. & Taylor, A. T., 1984. Pulmonary uptake in Indium-111 leukocyte imaging: clinical significance in patients with suspected occult infections. *Radiology*, *150*, 557–561.

Datz, F. L. & Thorne, D. A., 1986a. Gastroinestinal tract radionuclide activity on In-111 labeled leukocyte imaging: clinical significance in patients with fever of unknown origin. *Radiology*, *160*, 635–639.

——1986b. Effect of antibiotic therapy on the sensitivity of Indium-111-labelled leukocyte scans. *Journal of Nuclear Medicine*, *27*, 1849–1853.

——1986c. Effect of chronicity of infection on the sensitivity of the In-111-labeled leukocyte scan. *American Journal of Roentgenology*, *147*, 809–812.

Fawcett, H. D., Lantieri, R. L., Frankel, A. & McDougall, I. R., 1980. Differentiating hepatic abscess from tumour: combined 111-In white blood cell and 99mTc liver scans. *American Journal of Reontgenology*, *135*, 53–56.

Forstrum, L. A., Loken, M. K., Cook, A., Chandler, R. & McCullough, J., 1981. In-111-labelled leukocytes in the diagnosis of rejection and cytomegalovirus infection in renal transplant patients. *Clinical Nuclear Medicine*, *6*, 146–148.

Froelich, J. W. & Swanson, D., 1984. Imaging of inflammatory processes with labeled cells. *Seminars in Nuclear Medicine*, *14*, 128–140.

Goldman, M., Ambrose, N. S., Droic, Z., Hawker, R. J. & McCollum, C., 1987. Indium-111-labelled leukocytes in the diagnosis of abdominal abscess. *British Journal of Surgery*, *74*, 184–186.

Goodwin, D. A., 1983. Clinical use of In-111 leukocyte imaging. *Clinical Nuclear Medicine*, *8*, 36–38.

Hawker, R. J., Hall, C. E., Droic, Z. & Rhys-Evans, P. H., 1985. Indium leukocyte imaging in true pyrexia of unknown origin. *European Journal of Nuclear Medicine*, *10*, 172–174.

Knochel, J. Q., Koehler, P. R., Lee, T. G. & Welch, D. M., 1980. Diagnosis of abdominal abscesses with computed tomography, ultrasound, and 111-In leukocyte scans. *Radiology*, *137*, 425–432.

McAfee, J. G. & Samin, A., 1985. In-111 labeled leukocytes: a review of problems in image interpretation. *Radiology*, *155*, 221–229.

McNeil, B. J., Sanders, R., Alderson, P. O., Hessel, S. J., Finberg, H., Siegelman, S. S., Adams, D. F. & Abrams, H. L., 1981. A prospective study of computed tomography, ultrasound and gallium imaging in patients with fever. *Radiology*, *139*, 647–653.

Peters, A. M., 1989a. Imaging with white cells. *Clinical Radiology*, *40*, 453–454.

——1989b. Communication at BIR meeting: *Imaging in Abdominal Sepsis*.

Petersdorf, R. G. & Beeson, P. B., 1961. Fever of unexplained origin: report on 100 cases. *Medicine*, *40*, 1–30.

Rovekamp, M. H., van Royen, E. A., Folmer, S. C. C. & van der Schoot, J. B., 1983. Diagnosis of upper abdominal infections by In-111 labeled leukocytes with Tc-99m colloid subtraction technique. *Journal of Nuclear Medicine*, *24*, 212–216.

Saverymuttu, S. H., Peters, A. M., Crofton, M. E., Rees, H., Lavender, J. P., Hodgson, H. J. F. & Chadwick, V. S., 1985. 111-Indium autologous granulocytes in the detection of inflammatory bowel disease. *Gut*, *26*, 955–960.

Schell-Frederick, E., Fruhling, J., van der Auwera, P., Laethem, Y. & Klastersky, J., 1984. 111-Indium-Oxine-labeled leukocytes in the detection of localized infection in patients with neoplastic disease. *Cancer*, *54*, 817–824.

Seabold, J. E., Wison, D. G., Liebermann, L. M. & Boyd, C. M., 1984. Unsuspected extra-abdominal sites of infection: scintigraphic detection with Indium-111-labeled leukocytes. *Radiology*, *151*, 213–217.

Segall, G. M. & McDougall, I. R., 1986. Diagnostic value of lung uptake of Indium-111 Oxine-labeled white blood cells. *American Journal of Roentgenology*, *147*, 601–606.

Sfakianakis, G. N., Al-Sheikh, W., Heal, A., Rodman, G., Zeppa, R. & Serafini, A., 1982. Comparisons of scintigraphy with In-111 leukocytes and Ga-67 in the diagnosis of occult sepsis. *Journal of Nuclear Medicine*, *23*, 618–626.

Syrjala, M. T., Valtonen, V., Liewendahl, K. & Myllyla, G., 1987. Diagnostic significance of Indium-111 granulocyte scintigraphy in febrile patients. *Journal of Nuclear Medicine*, *28*, 155–160.

Thakur, M. L., Coleman, R. E. & Welch, M. J., 1977. Indium-111 labeled leukocytes for the localization of abscesses: preparation, analysis, tissue distribution and comparison with 67Ga citrate in dogs. *Journal of Laboratory and Clinical Medicine*, *82*, 217–228.

1990, *The British Journal of Radiology*, *63*, 855–857

Urinary tract dilatation in constipated children

By J. Herbetko, MRCP, FRCR and I. Hyde, FRCP(Ed), FRCR

Department of Paediatric Radiology, Southampton General Hospital, Tremona Road, Southampton
SO9 4XY

(*Received April 1990 and in revised form June 1990*)

Abstract. Abnormalities of the upper urinary tract were sought retrospectively in 180 children with constipation who had been investigated surgically over a 5-year period. Of those in whom an intravenous urogram had been performed, the incidence of dilatation of the upper renal tract was high, but only 12% of the patients with non-organic constipation had been so investigated.

Constipation in children is conventionally divided into those cases for which there is an organic cause, such as Hirschsprung's disease, and those where no organic cause is found ("functional constipation").

The literature on the association of urinary tract abnormalities and constipation in children is patchy, often inconclusive and sometimes questionable, for example when the diagnosis is based on rectal manometry. One problem is that definitions of what constitutes constipation and its severity lack consistency, making comparisons difficult. It is generally agreed that there is a higher incidence of urinary tract infection (UTI) in both groups of children (Neuman et al, 1973; Yazbeck & O'Regan, 1986), particularly in girls (O'Regan et al, 1985). Functional constipation usually improves with time but decisions on treatment will be influenced by the potential for urinary tract infection. One might therefore expect investigation of the urinary tract to play a crucial part in management.

Bladder and ureteric abnormalities have been described in both groups. Swenson & Fisher (1955) reported an incidence of 2.5% of megaureters, bladders with high residual volumes and high intravesical pressures in children with Hirschsprung's disease. Leibowitz & Bodian (1963) found normal ganglion cell distributions in the bladders of children with megaureter/megacystis, megaureter, Hirschsprung's disease, bladder neck obstruction and myelomeningocoeles when compared with normal controls, implying that abnormality of ganglion cells was not the cause of the abnormal urinary tract.

Of 278 cases of treated Hirschsprung's disease in that series, no case of megaureter was found either at surgery or in the 25 cases who had intravenous urograms (IVUs).

Kottmeier & Clattworthy (1965) noted four incidental cases of megaureter in 13 children with functional megacolon but only three cases of megaureter in 27 children with aganglionic megacolon. They presumed the cause to be a mechanical pressure phenomenon.

Shopfner (1968) found 12 cases of mild hydronephrosis (three with reflux) and slight tortuosity of the ureters in 39 children with severe functional constipation but these were from a group of children with known abnormalities of their urinary tract. He found no evidence of mechanical obstruction but did find a high incidence of bladder abnormalities including a cone-shaped bladder base plate (26), elongated urethra (18) and mural irregularity localized to the pressure area from the faecal mass (12). In cases with hydronephrosis there was normal ureteric peristalsis and emptying. Hence he found no supporting evidence of an obstructive cause but could not exclude mild dilatation secondary to chronically raised intravesical pressure.

Neuman et al (1973) found mural bladder irregularities in every case of 30 children with UTI and constipation who underwent cystometry and IVUs, but abnormality of the upper tracts was not mentioned.

O'Regan et al (1985) reported a series of 47 girls with recurrent UTI and large faecal reservoirs; all had abnormal uninhibited bladder contractions and normal upper tracts on IVU.

Method

We investigated the incidence of urological abnormalities on the IVUs and micturating cystograms (MC) of constipated children.

All those children who had had any of the following procedures performed between 1982 and 1987 were reviewed: manual evacuation of faeces, anal stretch, rectal biopsy, rectal manometry, surgery for Hirschsprung's disease, colostomy or examination under anaesthesia of the anal region. From these, we selected those where constipation was the primary indication for the procedure. We reasoned that this would identify a group of children with unequivocal constipation severe enough to warrant an invasive procedure. This avoided problems of defining severity.

Of 308 cases reviewed 180 were selected by this definition, 144 were functional and 36 organic.

Table I lists the numbers of IVUs and the abnormalities found.

Functional group ($n = 144$)

Eighteen had IVUs and seven showed upper tract dilatation. Six of the seven had MCs with only one showing vesico-ureteric reflux. Dilatation therefore has little correlation with reflux.

Thirty-five had mid-stream specimens of urine (MSU) taken and 11 were infected. Of the latter, six had dilated

Table I. Constipation and urinary tract investigation

	Functional	Organic[a]	Total
Number of patients	144	21	165
IVU	18	11	29
Urinary tract dilatation	7[b]	6[c]	13
Others	1	1	2
MSU	35	20	55
Proven UTI	11	5	16

[a] Excluding ano-rectal anomalies.
[b] Micturating cystograms, six: five normal, one reflux. Five had UTI.
[c] Micturating cystograms, four: two normal, two reflux. Six had UTI.

upper tracts. Thus of the seven children with dilated upper tracts, six contracted urinary infections.

Organic group (n = 36)

In this group there were 15 children with ano-rectal anomalies (imperforate anus, 12; ectopic anterior anus, three). Thirteen had IVUs and the other two children had normal renal tracts on ultrasound. One case had a duplex system with dilatation of the upper part of the upper moiety but no evidence of reflux or of a ureterocele. A second child had a unilateral dilated upper tract associated with reflux and a small scarred kidney and a third case had a unilateral dilated upper tract but no evidence of reflux. The first two cases had proven UTIs as did a third case with a normal IVU. No other renal tract abnormalities were found in this subgroup.

The other cases were Hirschsprung's disease (19) and spina bifida (2), both with some dilatation of their upper tracts. Nine with Hirschsprung's disease had IVUs, with upper tract dilatation seen in four. None showed reflux but each of these developed at least one UTI, as did one case with spina bifida.

Table II indicates the sides affected and the incidence of reflux. If the loaded sigmoid had any influence on dilatation one would have expected this to be commoner on the left, but distributions were equal in both groups, excluding the ano-rectal anomalies.

Table II. Intravenous urograms and micturating cystograms (excluding ano-rectal anomalies)

Renal tract	Functional	Organic
Dilatation	7	5
Left	2	1
Right	2	1
Bilateral	3	3
Reflux	1	0
Others	1[a]	1[b]

[a] Pelvi-ureteric junction stenosis.
[b] Absent kidney.

Table III. *Functional Group.* Eleven patients with urinary tract infections

IVU	Normal		Abnormal		None	
	4		6[a]		1[b]	
MC	N	R	N	R	N	R
	0	3	5	1	1	0

[a] Five dilated tracts; one pelvi-ureteric obstruction.
[b] Normal MC and ultrasound.
N = normal; R = reflux.

Discussion

In this highly selective group of severely constipated children we have found a relatively high incidence of dilatation of the upper urinary tract where this has been sought but the rate of investigation was low overall (8% in the functional group and 67% in the organic group). Where dilatation was present infection was common,

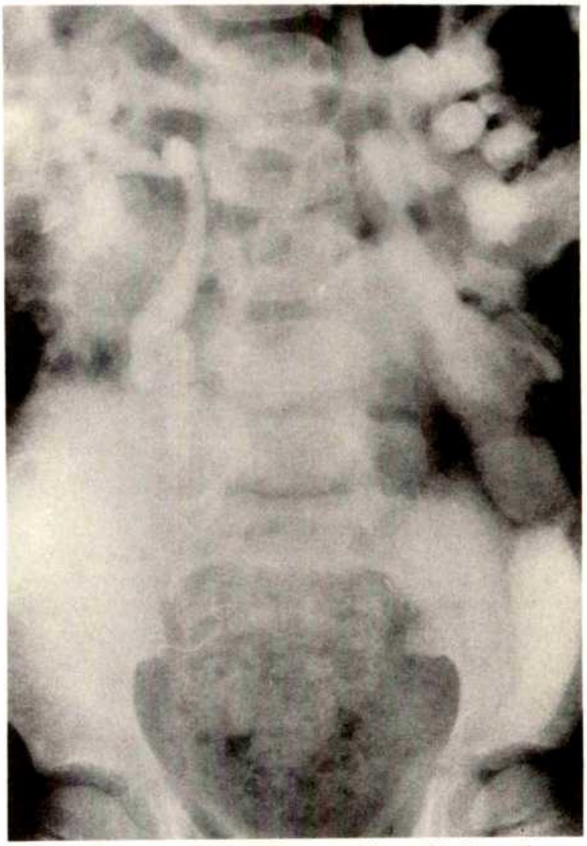

Figure 1. A 9-year-old boy with severe bilateral hydronephroses and hydroureters and marked bladder displacement from the rectal faecal mass.

suggesting an association between them (Table III). As expected, renal tracts were carefully investigated in those cases with ano-rectal anomalies, but less well investigated with other organic causes and poorly investigated in functional constipation, even when severe, unless infection or poor renal function was present.

The infrequent use of ultrasound in this retrospective series was disappointing, especially in view of its simplicity and relative accuracy in detecting dilatation of the renal collecting systems. Many of these investigations were performed when the constipation was improving or being treated so that urinary tract dilatation may have been under-estimated.

Three cases with functional constipation and without reflux were associated with marked hydroureters. One of these is illustrated (Fig. 1). One case resulted in severe renal failure.

The aetiology of upper tract dilatation is unclear and from previous studies is unlikely to be a simple obstructive mechanical effect. It may be related to increased bladder volume or pressure. We feel it is important to be aware that there might be an association with functional constipation and a case can be made out for investigating by MSU and ultrasound the urinary systems of all those children with severe chronic constipation of this degree. More detailed investigations can then be reserved for those showing abnormalities on these screening tests.

If every child presenting to our clinics with chronic constipation had had their renal tracts investigated, perhaps the incidence of dilatation would have been low, as has been found in other published series; but our criteria select a group of greater severity who require more active management.

References

KOTTMEIER, P. K. & CLATTWORTHY, H. W., 1965. Aganglionic and functional megacolon in children—a diagnostic dilemma. *Pediatrics*, *36*, 572–582.

LEIBOWITZ, S. & BODIAN, M., 1963. A study of the vesical ganglia in children and the relationship to the megaureter megacystis syndrome and Hirschsprung's disease. *Journal of Clinical Pathology*, *16*, 342–350.

NEUMANN, P. Z., DEDOMENICO, I. J. & NOGRADY, M. B., 1973. Constipation and urinary tract infection. *Pediatrics*, *52*, 241–245.

O'REGAN, S., YAZBECK, S. & SCHICK, E., 1985. Constipation, bladder instability, urinary tract infection syndrome. *Clinical Nephrology*, *23*, 152–154.

SHOPFNER, C. E., 1968. Urinary tract pathology associated with constipation. *Radiology*, *90*, 865–877.

SWENSON, O. & FISHER, J. H., 1955. The relation of megacolon and megaureter. *The New England Journal of Medicine*, *253*, 1147–1150.

YAZBECK, S. & O'REGAN, S., 1986. Hirschsprung's disease and urinary tract infection: Unrecognised association. *Nephron*, *43*, 211–213.

1990, *The British Journal of Radiology*, *63*, 858–861

A clinical application of iodine quantitation using digital fluorography

By W. D. Thompson, MRCP, FRCR *C. J. Kotre, BSc, MSc, †J. P. Owen, MBBS, DMRD, FRCR and §M. F. Laker, MD, FRCPath

Department of Radiology, North Tees General Hospital, Stockton on Tees TS19 8PE, *Regional Medical Physics Department, Newcastle General Hospital, Newcastle upon Tyne NE4 6BE, †University Department of Radiology and §Department of Clinical Biochemistry and Metabolic Medicine, Royal Victoria Infirmary, Newcastle upon Tyne NE1 4LP

(*Received January 1990 and in final form June 1990*)

Abstract. A preliminary clinical study of 20 patients is described in which a method of iodine quantitation *in vitro* using digital fluoroscopy was applied to the intravenous urogram. It was possible to quantitate iodine levels, in terms of mass thickness, in both the renal parenchyma and collecting system in 38 of 40 kidneys studied (20 patients). In the two kidneys on which measurements could not be made, the cause of failure was subtraction artefact due to movement of bowel gas, compounded in one case by poor renal opacification. The variations of iodine mass thickness against time were plotted and their forms were similar to dynamic computed tomography and magnetic resonance imaging studies of transplanted kidneys. Potential clinical applications of this method, in particular the functional assessment of the dilated upper urinary tract, are suggested based on its ability to offer quantitative information in addition to anatomical images.

The intravenous urogram (IVU) is a standard radiographic examination which provides anatomical information with high spatial resolution but little functional information (Saxton, 1988). To gain quantitative information it is usual to perform a radio isotope examination such as a Tc-DPTA renogram, though anatomical detail is poor. Dynamic computed tomography (CT) has also been used to provide physiological information in the assessment of renal transplants (Fuld et al, 1984).

Digital subtraction radiography is an established technique which, in addition to good spatial resolution and high contrast resolution, allows quantitation of the displayed image, as the mean pixel values of chosen areas can be measured (Hunter et al, 1986). Previous studies have used digital subtraction time–density analysis to assess blood flow (Kruger et al, 1983), left ventricular ejection fraction (Detrano et al, 1985) and transplanted kidneys (Fiechner et al, 1983).

Recent work has shown that it is possible to express absolute (as opposed to relative) iodine concentration *in vitro* in a subtracted image (in terms of mass thickness at a point expressed) as mg/cm^2 (Kotre et al, 1989). The aim of this pilot study was to see if this method could be successfully applied to the IVU.

Method

Digital fluorography system

A Picker International DAS 211 digital imaging system was used, the analogue video data being acquired under the control of a DEC PDP 11/23 processor via a 10 bit analogue-to-digital converter and stored as image arrays of 512 × 512 pixels. Images were acquired under manual control and standard mask mode subtraction performed using a logarithmic mapping function. The radiation dose to the patient was reduced by using the widest iris on the TV camera without appreciable degradation of image quality.

Summary of physical principle

Reference images were acquired which contained a tin step wedge of known composition suspended from the light beam diaphragm above the patient. Tin is used in preference to iodine because of the practical difficulties in handling iodine in suitably low concentrations either in solution or in epoxy resins. The atomic numbers of tin and iodine are 50 and 53, respectively, and it has been shown that for X-ray tube voltages in the range 75–120 kV, the relationship of the attenuation coefficients is such that it is possible to calculate the mass thickness of iodine equivalent to a given mass thickness of tin (Kotre et al, 1989).

There are, however, certain physical effects which mean that this equivalence is difficult to apply in practice (Kotre et al, 1989). The most important is the effect of veiling glare which occurs in the image intensifier. This effect was measured in the image intensifier used in the study and a corrective deconvolution filter derived and incorporated into the software. Correction is also required for the effect of iodine in the background tissues. A standard method of subtracting the iodine concentration in a chosen area of interest of the background soft tissues from that in the area under study was not used, as the choice of this area is subjective and therefore potentially unreliable. Instead, the modal value of the whole image was used as the background correction. This also has the effect of correcting for frame to frame variation of X-ray tube output.

Address for correspondence: Dr J. P. Owen, Imaging Laboratory, Royal Victoria Infirmary, Queen Victoria Road, Newcastle upon Tyne NE1 4LP.

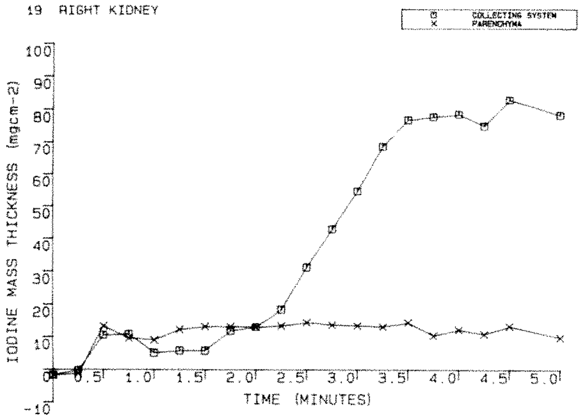

Figure 1. A plot of iodine mass thickness against time for the renal pelvis (boxes) and parenchyma (crosses) of a normal kidney during the course of an IVU examination.

Patients

Patients were chosen from routine clinical requests for IVU but, because of the sessions available, urgent examinations could not be included in the study. In addition, all patients under the age of 18, all women of reproductive age and those with a history of iodine sensitivity or thyrotoxicosis were specifically excluded. The project received the agreement of the local Joint Ethics Committee and informed consent was obtained from each participating patient. Twenty patients were entered into the study, their ages ranging from 19 to 78 years (mean age 45.5 years). Ten were women (aged 39–78 years) and 10 were men (aged 19–56 years).

Height and weight were recorded so that expected creatinine clearance could be estimated and at the time of the IVU a blood sample and 24-hour urine collection were taken for estimation of urea, creatinine and creatinine clearance.

In order to minimize the amount of bowel gas, patients received no bowel preparation prior to the examination, as the initial use of Picolax (sodium picosulphate) had been associated with excess bowel gas.

Examination procedure

Following a preliminary plain abdominal film, two digitally acquired mask films were obtained. Mask 1 was an image of the renal areas incorporating the reference tin step wedge placed clear of bowel gas shadows or bone. Mask 2 was of the same area but without the step wedge. The contrast medium was Iopamidol (Niopam 370, Merck) given as a rapid intravenous injection in a dose of 250 mg/kg body weight. Digital images were acquired of the same field as the mask films every 15 seconds for 4.5 minutes and also at 5 and 10 minutes; a total of 21 images. Following acquisition of the digital images the examination was completed with a full length abdominal film and any other projections necessary to solve the clinical problem. Hard copy of the 5 and 10 minute digital images was used in reporting and included in the patients' records.

Image processing and analysis

The aim of image processing is to produce a digital subtraction image corrected for veiling glare and frame to frame variation from which the iodine mass thickness of a chosen area can be calculated.

A subtracted image of the reference step was obtained by subtracting mask 2 from mask 1, and subtracted images of the IVU sequence were obtained by subtracting mask 2 from each of the 21 post-contrast images. The pixel values of each step on the wedge, corrected for veiling glare and frame to frame variation, were plotted against the known equivalent iodine mass thickness and from this plot the iodine mass thickness of a chosen area in the kidney could be calculated from the corrected pixel value. Two points were sampled in each kidney in each image, ideally in the same place on each image and away from overlying gas or bone:

1. in the parenchyma, typically in the upper or lower pole;
2. in the collecting system, either the renal pelvis or a major calyx.

The time taken for the first appearance of contrast medium in the collecting system was recorded in each case (analogous with the parenchymal transit time in isotope studies). Opacification of the abdominal aorta could be detected in most cases and this was taken as a more reliable time from which to count than the time of the intravenous injection.

For each kidney a graph was plotted of iodine mass thickness against time for both parenchyma and collecting system.

Results

Figure 1 shows typical curves for the parenchyma and collecting system of a normal kidney. The plot of the parenchyma shows an initial rapid rise over the first 30–60 seconds as the contrast bolus enters the kidney. Following this, the level remains essentially constant for the length of the examination. This was a consistent feature and is thought to represent the balance between excretion of contrast medium into the collecting system and recirculation of unfiltered contrast.

The collecting system curve shows an initial rise above background which may be spurious, owing to inclusion of renal tissue in the sampling area, but at between 2 and 2.5 minutes there is a rapid rise as the contrast medium accumulates in the collecting system. The peak level depends on the physical size of the renal pelvis, in addition to the concentration of iodine within the pelvis. Fluctuations in the peak level occur and comparison with the corresponding images shows that these coincide with peristaltic activity in the renal pelvis.

The time taken for the contrast medium to appear in the collecting system was recorded by studying the subtracted images. In all cases with normal urographic findings or minor abnormalities, such as uncomplicated calculi, this time was 120–135 seconds. This is analagous with the parenchymal transit time measured in isotope

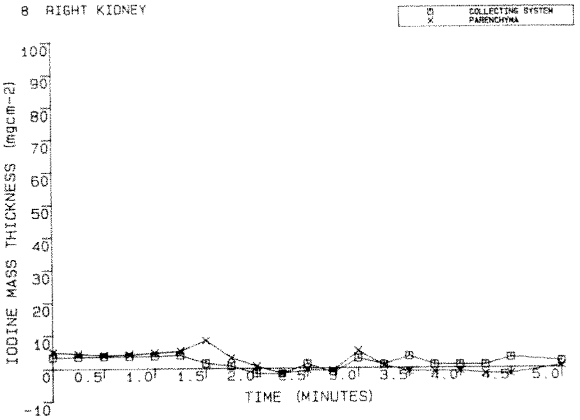

Figure 2. A plot of iodine mass thickness against time for the renal pelvis (boxes) and parenchyma (crosses) of a poorly functioning kidney. The glomerular filtration rate was 35 ml/min. The IVU showed bilaterally small kidneys with caliectasis and cortical scarring consistent with chronic pyelonephritis.

studies (Britton et al, 1987) where it is used as an indicator of urinary obstruction. Times of 165 seconds (left) and 150 seconds (right) were recorded in one case with hydronephrosis associated with a bladder tumour, while in one case with unilateral idiopathic pelvi-ureteric junction obstruction but good drainage, the time was normal at 135 seconds.

Figure 2 shows an example of an abnormal plot in a patient with reduced renal function and a creatinine clearance of 35 ml/min. The IVU showed small scarred kidneys with delayed and greatly reduced concentration of contrast medium which is reflected in the digital fluorographic study by flat curves for the parenchyma and collecting system. Both curves show low iodine levels and neither shows the typical rise in levels seen in normal patients.

In all patients the calculated creatinine clearance was compared with a predicted range based on age and sex and corrected for body surface area. Of the 20 patients studied, 14 had plasma creatinine levels within the normal range, and of these, 11 had calculated creatinine clearances within the predicted range. In the other three, one had a calculated creatinine clearance of 2 ml/min below the predicted range, whilst the other two were 9 and 15 ml/min below the predicted range. Six patients with elevated plasma creatinine levels all had calculated creatinine clearances lower than predicted. In one the plasma creatinine was marginally elevated at 94 μmol/l (normal 50–92 μmol/l), although the creatinine clearance was unexpectedly low at 76 ml/min (predicted range 95–135 ml/min). In only two patients were the creatinine clearances markedly reduced at 22 and 35 ml/min, respectively.

The plasma creatinine and creatinine clearance values were compared with the peak iodine mass thickness reached in the renal parenchyma but no relationship could be observed.

Table I. Percentage of renal area covered by bowel gas artefact on subtracted image

	Right kidney	Left kidney
No artefact	3	2
Up to 25%	6	4
Up to 50%	4	4
Up to 75%	6	6
Greater than 75%	1	4

Total number of kidneys = 40 (20 patients).

Discussion

In digital subtraction radiography movement of a structure in the time between the mask and post-contrast images leads to misregistration shown on the subtracted image as areas with falsely high or low pixel values. Facilities for re-registration can correct for this to a limited degree depending upon the source of the movement. Patient movement and respiratory movement can be minimized in the co-operative patient by acquiring images during normal quiet respiration. Movement of bowel gas, however, is a significant problem both because of the anatomical relationship of the kidneys to large and small bowel and because intestinal peristalsis cannot be successfully corrected for by re-registration. The use of antispasmodic drugs was not sanctioned for this study and misregistration artefact occurred in the renal area in 35 out of 40 kidneys studied in 20 patients (Table I). It was impossible to produce useful measurements in two of the kidneys (in two patients). In one, this was entirely because of bowel gas and in the other it was because of a combination of bowel gas and poor opacification.

The normal iodine uptake curves (Fig. 1) are comparable with results obtained on transplanted kidneys by magnetic resonance imaging (MRI) using a paramagnetic contrast agent (Heintz et al, 1988), and with combined cortical and medullary curves obtained from dynamic CT images (Fuld et al, 1984).

From the intact nephron hypothesis of Bricker (Bricker et al, 1960), it would be expected that the iodine mass thickness in the renal parenchyma would be related to the number of functioning nephrons per unit volume and hence the glomerular filtration rate. It was therefore hoped that an index of renal function could be measured from the parenchymal iodine mass thickness. The measured creatinine clearance was compared with the peak iodine mass thickness in the renal parenchyma and, in a similar way to nuclear medicine studies, with the iodine level at 2 minutes. No relationship was observed, either in this way or after correcting the iodine levels for the total amount of iodine in the contrast medium injection. The small range of observed creatinine clearance values is one possible factor in the lack of a relationship while inaccuracy of the calculated creatinine clearance values is a further possible source of error. In an out-patient population the reliability of the 24-hour urine collection will influence the creatinine clearance estimation and in order to check for any obvious discrepancies the calculated creatinine clearance was compared with the predicted values. In two patients with normal plasma creatinine levels, the calculated clearances were 10–15% below predicted while in one patient with a marginally elevated plasma creatinine, the calculated creatinine clearance was unexpectedly low. These three cases may represent incomplete 24-hour urine collections, but in the other 17 patients the calculated and predicted values were in agreement. In a future study the use of in-patients would reduce this potential source of error. The curves produced by this method represent variations of iodine mass thickness at a point with time and are not directly comparable with nuclear medicine studies. Nevertheless, it is possible to sample the parenchyma and collecting system separately, and it is hoped that the ability to derive quantitative information from the IVU can be used in clinical practice.

This method may be of value in the assessment of the transplanted kidney where information concerning function and possible obstruction are of prime importance. A further potential application is the differentiation of the obstructed from the non-obstructed but dilated upper urinary tract. The effects of pyeloplasty upon pelvi-ureteric junction obstruction could be assessed.

Three measurements which can be obtained and which may be relevant are as follows.

1. Parenchymal transit time.
2. Parenchymal iodine level. A typical urographic feature of acute urinary obstruction is increased density of the nephrogram. The greater contrast sensitivity of this method may allow more subtle degrees of this phenomenon to be detected.
3. The size and configuration of the collecting system curve.

Future studies will assess the role of iodine quantitation of the excretion urogram in clinical practice.

Acknowledgments

We would like to thank the patients for agreeing to take part in the study; Professor R. Wilkinson and Dr M. Ward for advice and support; the radiographers at the Royal Victoria Infirmary, Newcastle for their professional skills; and Mrs P. Gibbon and Mrs J. Stoddart for typing the manuscript.

References

Bricker, N. S., Morrin, P. A. F. & Wesley-Kime, S., 1960. The pathologic physiology of chronic Bright's disease. *American Journal of Medicine*, *28*, 77–98.

Britton, K. E., Nawaz, M. K., Whitfield, H. N., Nimmon, C. C., Carroll, M. J., Granowska, M. & Mlodkowska, E., 1987. Obstructive nephropathy: comparison between parenchymal transit time index and frusemide diuresis. *British Journal of Urology*, *59*, 127–132.

Detrano, R., MacIntyre, W. J., Salcedo, E. E., O'Donnell, J., Underwood, D. A., Simpfendorfer, C., Go, R. T., Houston, J., Butters, K. & Leatherman, J., 1985. Video-densitometric ejection fractions from intravenous digital substraction left ventriculograms: correlation with conventional direct contrast and radionuclide ventriculography. *Radiology*, *155*, 19–23.

Fiechner, S. M., Novick, A. C., Meaney, T. F., Gallagher, J. H., Braun, W. E. & Steinmuller, D., 1983. Simultaneous structural and functional imaging of the transplant kidney using digital subtraction angiography. *The Journal of Urology*, *129*, 248–252.

Fuld, I. L., Matalon, T. A., Vogelzang, R. L., Neiman, H. L., Kowal, L. E., Hutchins, W. W. & Soper, W., 1984. Dynamic CT in the evaluation of physiologic status of renal transplants. *American Journal of Roentgenology*, *142*, 1157–1160.

Heintz, P., Enrenheim, C. & Hundeshagen, H., 1988. Gd-DTPA in MRI and 99m Tc-DTPA in the examination of the perfusion of transplanted kidneys. *Diagnostic Imaging International*, *4*, 20–21.

Hunter, G. J. S., Hunter, J. V. & Brown, N. J. G., 1986. Parametric imaging using digital subtraction angiography. *British Journal of Radiology*, *59*, 7–11.

Kotre, C. J., Harrison, R. M., Faulkner, K. & Owen, J. P., 1989. An approach to iodine quantitation using digital fluorography. *Physics in Medicine and Biology*, *34*, 1795–1808.

Kruger, R. A., Bateman, W., Lui, P. Y. & Nelson, J. A., 1983. Blood flow determination using recursive processing: a digital radiographic method. *Radiology*, *149*, 293–298.

Saxton, H., 1988. Myths and misconceptions in uroradiography. *Clinical Radiology*, *39*, 361–362.

1990, *The British Journal of Radiology*, *63*, 862–870

A model for hematopoietic death in man from irradiation of bone marrow during radioimmunotherapy

By Bobby R. Scott, PhD and *Larry E. Dillehay, PhD

Inhalation Toxicology Research Institute, Lovelace Biomedical and Environmental Research Institute, P.O. Box 5890, Albuquerque, NM 87185 and *Johns Hopkins Oncology Center, 600 N. Wolfe Street, Baltimore, MD 21205, USA

(*Received October 1989 and in final form June 1990*)

Abstract There are numerous institutions worldwide performing clinical trials of radioimmunotherapy (RIT) for cancer. For RIT, an exponentially decaying radionuclide is attached by using a chelating agent to a specific monoclonal or polyclonal tumour antibody (*e.g.* antiferritin IgG). The major limitation to RIT is toxicity to normal tissue in organs other than the one containing the tumour (*e.g.* bone marrow). The focus of this manuscript is on modelling the risk (or probability) of hematopoietic death in man for exponentially decaying patterns of high-energy β irradiation (*e.g.* ^{90}Y) of bone marrow by radioimmunoglobulin injected into the blood. The analytical solutions presented are only applicable to protocols for which significant uptake of radioactivity by the bone marrow does not occur, and only for high energy β emitters. However, the generic equation used to obtain the analytical solutions is applicable to any continuous pattern of high energy β irradiation. A model called the "normalized dose model" was used to generate calculated values for the LD_{50} as a function of the effective half-time for the radioimmunoglobulin in the blood. A less complicated empirical model was used to describe the calculated values. This model is presumed to be valid for effective half-times in blood of up to about 20 days. For longer effective half-times, the LD_{50} can be estimated using the normalized-dose model presented. In this manuscript, we also provide a modified Weibull model that allows estimation of the risk of hematopoietic death for single or multiple injections (in one cycle) of radioimmunoglobulin, for patients with normal susceptibility to irradiation and for patients with heightened susceptibility. With the modified Weibull model, the risk of hematopoietic death depends on the level of medical treatment provided to mitigate radiation injuries.

Immunotherapy with radiolabelled antibodies is a recent development (Beierwaltes, 1976). The use of an immunospecific antibody as a carrier for therapeutic radionuclides requires the establishment of discrete immunologic specificity of the antibody and radiolabelling with an appropriate radionuclide without damaging antibody specificity (Order et al, 1985). The use of radioimmunotherapy (RIT) with radiolabelled monoclonal and polyclonal antibodies in patients with solid tumours and hematologic malignancies has been reported (Leichner et al, 1981; Ettinger et al, 1982; Carrasquillo et al, 1984; Epenetos, 1985; Lenhard et al, 1985; Order et al, 1985; Zimmer et al, 1988). Treatment of lymphoma by using antibodies labelled with the β-emitting isotopes ^{90}Y (physical half-life = 2.7 days) and ^{131}I (physical half-life = 8 days) has given encouraging results. Rosen et al (1987) have conducted initial immunodiagnostic and immunotherapy trials using radioiodinated monoclonal antibody (^{131}I-T101) in six patients with cutaneous T-cell lymphoma. Each of the six patients demonstrated a clinical response that lasted from a few weeks to 3 months after a single immunotherapy dose. However, irradiation of the liver and irradiation of the bone marrow are major limitations to application of RIT.

To develop an optimum therapy scheme, four predictive models may be needed: one for estimating radiation doses to the tumour and to normal tissue; a second for estimating the probability of sterilizing the tumour cells; a third for estimating the risk of producing lethal damage to the bone marrow; and a fourth for predicting the risk of serious damage to other normal tissue.

Mathematical models were recently developed for evaluating absorbed radiation doses to the total body and to a specific tumour (Vaughan et al, 1987), for predicting survival of tumour cells (Dillehay, 1990), and for determining allowable doses to normal organs (O'Donoghue & Wheldon, 1988) for biologically targeted radiotherapy. However, a model is also needed for estimating the risk of hematopoietic death due to irradiation of bone marrow during biologically targeted radiotherapy that takes into consideration protection provided to the patient by good medical care, and variable susceptibility to irradiation for different types of patients. For example, very ill patients that are already hematologically compromised or have other associated medical conditions may be more susceptible to irradiation than more healthy patients.

This paper provides an empirical mathematical model for estimating the risk of hematopoietic death, whereby the risk depends on the patient's susceptibility to irradiation, and on the level of protection provided by medical treatment given to mitigate radiation injuries. The focus of application is on exponentially decaying patterns of irradiation that can arise in RIT.

Because radionuclides decay with specific physical half-lives, and are biologically cleared from the blood, radiation dose rate to the bone marrow from a specific radionuclide in the blood is assumed to decrease as a single, negative-exponential function of time. This assumption is supported by the dosimetry model of Vaughan et al (1987). The pattern of irradiation of the bone marrow depends on the whole-body effective half-life of the radionuclide, which depends on the rate of elimination of activity from the body and on the rate of physical decay of the radionuclide (Vaughan et al, 1987). Radiolabelled antibodies directed against the same antigenic specificity but derived from different species have different whole-body effective half-lives (Klein et al, 1985).

Order et al (1985) obtained results indicating saturation of ^{131}I uptake in the tumour after treating patients with ^{131}I antiferritin for hepatoma. Dosimetric results with ^{131}I antiferritin indicated that 1110 MBq (30 mCi) was sufficient to saturate the tumour. Based on an effective half-life of the radioactive antibody in the tumour of 3–5 days, a protocol was selected whereby 1110 MBq (30 mCi) was administered on Day 0 and 740 MBq (20 mCi) on Day 5. For such protocols, complex patterns of irradiation of the bone marrow can arise.

The focus of this manuscript is on predicting the risk of hematopoietic death after irradiation of the bone marrow by single or repeated injections, in one cycle, of high-energy, β-emitting radioimmunoglobulin. The analytical solutions presented are specific for protocols in which the β-emitting radionuclide (attached to antibody or dislocated) does not accumulate in significant amounts in the bone marrow, so that irradiation of the bone marrow arises mainly from radioimmunoglobulin in the circulating blood. Also, the results provided for repeated injections are only applicable to protocols in which irradiation of the bone marrow occurs with no radiation-free time between the injections.

Estimates of the LD_{50}

An important statistic for evaluating hematopoietic toxicity from brief or protracted irradiation of man is the median lethal dose (LD_{50}) for hematopoietic death (Warren & Bowers, 1950; Bond et al, 1965). Based on extrapolations from animal data and on theoretical calculations, the LD_{50} for hematopoietic death in man depends on several variables including radiation quality (Kaul & Scott, 1984), the spatial distribution of dose over the body (Mole, 1985), and the dose rate of low linear-energy-transfer (LET) radiation (Bateman, 1968). It also depends on the level of medical support received by the irradiated group to mitigate the radiation injuries (Vriesendorp & van Bekkum, 1984; Scott & Hahn, 1989; MacVittie, 1990) and on pre-irradiation health status (Langham, 1967; Lushbaugh et al, 1967).

There are no human data suitable for estimating the LD_{50} for hematopoietic death for protracted internal β irradiation of the bone marrow. However, it is reasonable to assume that the LD_{50} for high-energy β irradiation (*e.g.* with ^{90}Y-labelled antibody) would be similar to that obtained for external γ irradiation, for similar spatial and temporal patterns of irradiation of the bone marrow. Literature on the LD_{50} for hematopoietic death in man after brief or protracted exposure to external γ radiation has been recently reviewed (UNSCEAR, 1988; Scott & Hahn, 1989). Estimates judged to be plausible for individuals with normal susceptibility to irradiation vary from 2.4 to 3.4 Gy for brief exposure; however, these values are only appropriate for circumstances for which medical treatment to mitigate the radiation injuries is not provided.

The impact that medical treatment (to mitigate radiation injuries) has on the LD_{50} must also be considered. Three categories of medical treatment are considered and are the same as those described in a recent report by the US Nuclear Regulatory Commission (NUREG/CR-4214, 1989): minimal, supportive, and intensive treatment.

Basic first aid in a clean environment is considered minimal treatment. Supportive treatment includes hospitalization with routine isolation procedures (*i.e.* not including laminar airflow), electrolyte replacement, administration of blood products (especially fresh platelets), treatment with broad-spectrum antibiotics, antifungals and antivirals, and parenteral feeding.

Intensive treatment includes, in addition to supportive treatment, extraordinary procedures such as bone marrow transplantation. The use of colony stimulating factor (CSF) treatment for hematopoietic injury was also discussed.

The discussion of the three categories of treatment is not intended to be a guide for physicians treating radiation injury in RIT patients. The categories are provided for use in developing dose–response models for hematopoietic death that take into consideration potential protection provided to the irradiated individual by medical treatment to mitigate radiation injury. Protection can be accounted for using a protection factor (PF), which is defined as the ratio of the LD_{50} obtained with treatment for mitigating the radiation injuries to the LD_{50} obtained without such treatment.

For brief exposure of the total body to external γ radiation, a central estimate of 3 Gy to bone marrow has been recommended for the LD_{50}, for individuals with normal susceptibility to irradiation, for the minimal treatment category (Stather et al, 1988; UNSCEAR, 1988 Scott & Hahn, 1989). An LD_{50} of about 3 Gy may also apply for cancer patients that are not extremely ill that receive supportive medical treatment (UNSCEAR, 1988).

The LD_{50} for hematopoietic death is expected to be larger than 3 Gy for individuals of normal susceptibility to irradiation that receive supportive or intensive medical treatment to mitigate radiation injuries. For such individuals receiving supportive treatment, the LD_{50} for brief exposure has been extrapolated from animal data to be about 4.5 Gy, indicating a protection factor (PF) of 1.5 (*i.e.* 4.5 Gy/3.0 Gy = 1.5) (Vriesendorp & van Bekkum, 1984; Scott & Hahn, 1989).

The Chernobyl accident data shown in Fig. 1 would place the LD_{50} at about 6 Gy to the bone marrow for individuals of normal susceptibility to irradiation that received good medical care. In some cases, only supportive treatment was provided; however, 13 victims with

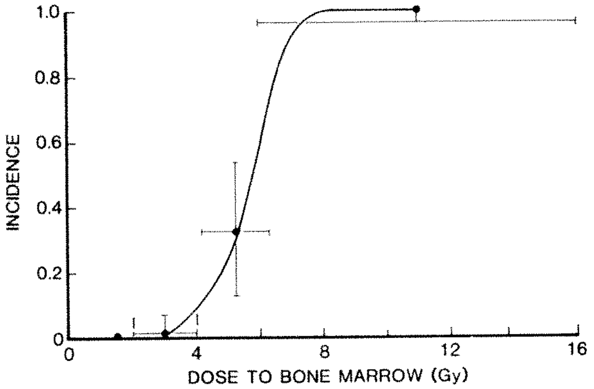

Figure 1. Dose–response curve for acute lethality based on Chernobyl accident data taken from Gos'kova (1987).

very serious radiation injuries received bone marrow transplantation (Gus'kova, 1987). Also, exposures may have been highly non-uniform; radiation doses were quite uncertain, and the data were complicated by the presence of severe skin burns. Bone marrow transplantations were carried out in 13 victims, but were only successful in two cases (Gus'kova, 1987). The Chernobyl data indicate that a PF as large as 2 might be provided by supportive treatment for individuals of normal susceptibility to irradiation when the radiation dose is not uniformly distributed over the body.

For the intensive treatment category, available information on radiation therapy patients would place the LD_{50} for hematopoietic death above 10 Gy, for brief exposure to external γ radiation (Scott & Hahn, 1989). This suggests that a PF greater than 3.3 (*i.e.* 10 Gy/3 Gy = 3.3) is provided by bone marrow transplantation for individuals with supralethal radiation doses.

The use of CSF treatment for radiation injury is also expected to provide some protection from hematopoietic death (MacVittie, 1990). However, the applicability of the CSF treatment for radiation injury is limited to the range of radiation doses over which a critical number of hematopoietic stem cells survive.

Granulocyte-macrophage colony stimulating factor (GM-CSF) was used, along with supportive treatment, in victims of the radiation accident in Brazil involving a 50.9 TBq (1375 Ci) ^{137}Cs source taken from a cancer therapy machine (IAEA, 1988; Butturini, 1990). However, because the GM-CSF was administered after the victims had become profoundly pancytopenic and had demonstrated spontaneous hematopoietic repair, the effectiveness of their GM-CSF therapy is controversial. Granulocyte-macrophage colony stimulating factor was also used in treating radiation injury in the three male victims of the recent radiation accident in San Salvador that involved non-uniform γ irradiation from a 666 TBq (18,000 Ci) ^{60}Co source (Ricks, 1990). Exposures were estimated to range from 3 to 5 minutes, with total-body doses estimated to be about 3, 4, and 8 Gy for the three victims, based on chromosomal aberrations among peripheral blood lymphocytes (Ricks, 1990). There were no hematopoietic deaths among the three victims. The radiation doses were highly non-uniform. The absorbed dose to the feet of the victim receiving the highest exposure was estimated to be about 240 Gy, while the dose to his head was estimated to be only about 3 Gy (Ricks, 1990).

Interesting results have also been observed following application of CSF therapy to mitigate radiation injury in dogs. Dogs receiving a 100% lethal dose of 4 Gy of ^{60}Co γ radiation to the bone marrow were spared from hematopoietic death when GM-CSF was administered (MacVittie, 1990). Based on estimates available in the literature, the LD_{50} for hematopoietic death in Beagle dogs is about 2.6 Gy, after brief, uniform, total-body exposure to external high-energy photons, when no medical treatment for radiation injury is provided (MacVittie et al, 1984). Based on these observations, the PF provided by GM-CSF therapy for radiation injury is greater than 1.5 (4 Gy/2.6 Gy = 1.5), so that supportive treatment, when combined with administration of CSF, should provide greater protection than supportive treatment alone.

As previously stated, CSF therapy alone would be expected to provide protection from radioimmunotherapy over a more limited range of doses than would be provided by intensive treatment involving bone marrow transplantation, since stem cell survival is required for CSF therapy to be successful. It is thought that the survival curve for hematopoietic stem cells is well characterized by a single exponential function that depends on a single parameter, the D_0. Using this cell survival model, the D_0 for the hematopoietic stem cell survival curve was estimated to be 0.73 Gy for ^{60}Co γ radiation (MacVittie, 1990). With a D_0 of 0.73 Gy, a dose of 4 Gy would be expected to reduce the survival of hematopoietic stem cells to about 0.4%. The results indicate that even with survival of less than 1% of the stem cells, the use of CSF therapy can prevent hematopoietic death in dogs.

Because the hematopoietic stem cell survival curve is characterized by a single exponential without a shoulder, one would predict no dose-rate effects in the absence of cell repopulation. The pronounced effects of dose rate on the LD_{50} are therefore thought to be mainly related to cell repopulation.

Dose–response function for hematopoietic death

For brief exposure to external gamma radiation, both the US NRC (NUREG/CR-4214, 1989) and the National Radiological Protection Board (Stather et al, 1988) have adopted a dose–response function based on the two-parameter Weibull model developed for the minimal treatment category (Scott & Hahn, 1989). For the minimal treatment category, the central estimate of risk of hematopoietic death among humans of normal susceptibility to irradiation, at absorbed dose D in Gy to the bone marrow, and after brief, total-body, external-γ irradiation, is given by

$$\text{Risk} = 1 - \exp[-(\ln 2)(D/3)^6] \qquad (1).$$

The exponent 6 represents the central estimate of the shape parameter v, which has upper and lower bounds of 8 and 4 (Scott & Hahn, 1989). The value 3 (in Gy) represents the central estimate of the LD_{50} for dose rates above about 0.6 Gy/h, with upper and lower bounds of 3.5 and 2.5 Gy, respectively (Scott & Hahn, 1989). However, a value of 3 Gy for the LD_{50} may be inappropriate for groups with heightened susceptibility to irradiation such as very ill cancer patients (Langham, 1967; Lushbaugh et al, 1967).

Dose–response model for RIT

The results that follow are specific for RIT protocols whereby the radio-immunoglobulin is not taken up by the bone marrow, and an exponentially decaying pattern of irradiation of the bone marrow arises indirectly from the blood. For exponentially decaying patterns of high-energy, internal β irradiation of the bone marrow, one can adapt the normalized dose model originally developed by Scott et al (1988) for γ irradiation. Model parameters have been revised recently (Scott & Hahn, 1989), based on improved estimates of the LD_{50} for man for different γ radiation dose rates.

With the normalized dose model, the quotient D/LD_{50} in Equation 1 is replaced with the normalized dose X, in units of LD_{50}. For continuous exposure at variable dose rates, X is given by the solution to the integral (Scott & Hahn, 1989; Scott et al, 1988)

$$X(t) = \int \dot{D}\theta(\dot{D})^{-1}\, dt' \qquad (2)$$

where t' represents the variable exposure time and where $\theta(\dot{D})$ estimates the LD_{50} at dose rate $\dot{D}$, based on the dose-rate model shown in Fig. 2. The integral in Equation 2 is evaluated over the exposure period from zero to time t. Equation 2 represents the normalized dose model; a value $X = 1$ corresponds to an LD_{50}-absorbed dose regardless of the continuous pattern of irradiation. A value $X = 0.5$ corresponds to half the LD_{50}-absorbed dose (Scott & Hahn, 1989).

The empirical dose-rate model used in Fig. 2 for $\theta(\dot{D})$ was adopted by the US NRC (NUREG/CR-4214, 1989). While some of the points in Fig. 2 represent data on hematopoietic death in man after exposure to external γ radiation, other points represent judgements (Scott & Hahn, 1989). Langham's two estimates of the LD_{50} based on the linear probit model are shown in Fig. 2, and were derived from data for exposure times of 0–1 day and 1–7 days (Langham, 1967). Total-body doses (not LD_{50}s) are also shown for the five-member Mexican family exposed intermittently in their home to ^{60}Co γ radiation. Only one of the five survived. Total-body doses are also shown for the seven (two points indistinguishable) of the 23 Japanese fishermen exposed to fallout γ radiation that had total-body doses of greater than 4 Gy. The other 16 fishermen had total body doses of less than 4 Gy. None of the 23 Japanese fishermen died from acute effects of irradiation. The solid point at the high dose-rate end represents the current 3 Gy estimate of the LD_{50} for prompt exposure (Stather et al, 1988; Scott & Hahn, 1989). The point labelled Hiroshima (open triangle) represents Rotblat's (1986) estimate based on data from Hiroshima with the LD_{50} dose evaluated at 892 metres from the hypocentre and with doses re-evaluated based on DS86 dosimetry (Fujita et al, 1990). Judgments of the LD_{50} provided by the OTA (Office of Technology Assessment, 1980) for a 1-week exposure period, and by the British Institute of Radiology (BIR Working Party, 1982) for a 1-month exposure period, are also shown in Fig. 2.

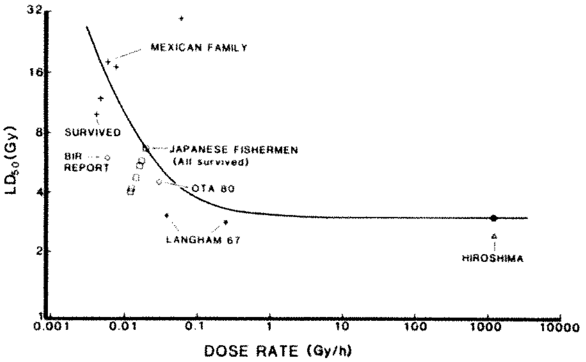

Figure 2. Dose-rate model for LD_{50} for man taken from previous report (Scott & Hahn, 1989). The smooth curve is presumed to apply to groups with normal susceptibility to irradiation. See text for explanation of the data.

The mathematical structure of the dose-rate model was developed from the animal data shown in Fig. 3 which is redrawn from a previous publication (Scott et al, 1988). With the dose-rate model, the LD_{50} as a function of a fixed absorbed dose rate $\dot{D}$ to the bone marrow of a given species is estimated with

$$\theta(\dot{D}) = \theta_1/\dot{D} + \theta_\infty \qquad (3)$$

where $\theta_1/\dot{D}$ estimates the increase in the LD_{50} due to protracted exposure at dose rate $\dot{D}$, and θ_∞ represents the asymptotic value for the LD_{50} expected to be observed after exposure at very high dose rates that overwhelm recovery and repair during irradiation (Scott et al, 1988). Estimates of model parameters θ_1 and θ_∞ for different mammalian species including man are given in Table I.

There are major uncertainties related to the smooth curve in Fig. 2. These uncertainties arise from different sources that include (1) potential systematic error associated with the dose-rate model used; (2) error in cumulative radiation dose; (3) error in average dose rate; (4) error associated with the use of intermittent exposure data for continuous exposure; and (5) error associated with use of non-uniform exposure data for uniform exposure.

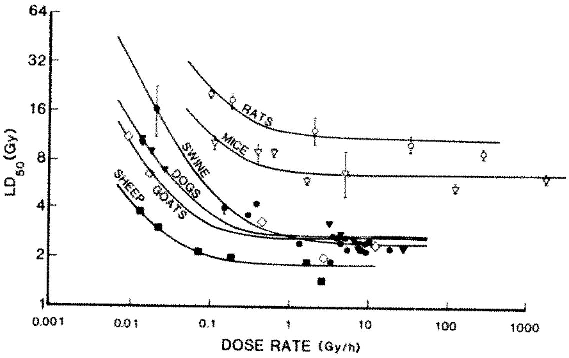

Figure 3. Dose-rate models for LD_{50} for different mammalian species redrawn from previous publication (Scott et al, 1988). The data were obtained from other publications: rats (Logie et al, 1960), mice (Koznova, 1978), swine (Page, 1968), dogs (Page, 1968; McClellan et al, 1982), goats (Page, 1968) and sheep (Page, 1968).

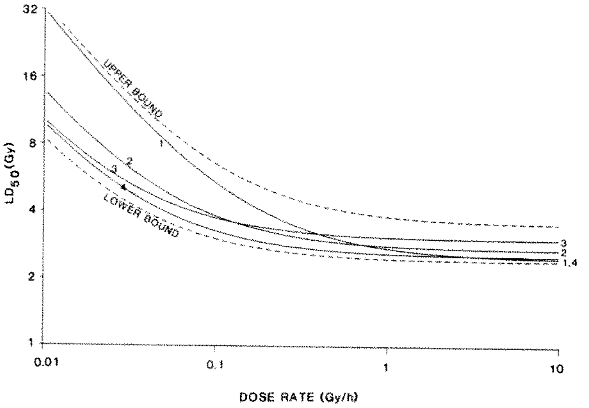

Figure 4. Dose-rate models for the LD_{50} for (1) swine, (2) dogs, (3) man and (4) goats, based on data in Figs 2 and 3. Judgmental upper and lower bounds are also provided for the family of curves.

Available information on the five listed sources contributing to the uncertainties were not sufficient for conducting a formal evaluation of overall uncertainty in the smooth curve presented in Fig. 2. As shown in Fig. 4, the LD_{50} against dose-rate curve derived for man is quite similar to the curve derived for dog and goat. It is also similar to the curve derived for swine, except at low dose rates where swine may be more tolerant to protracted exposure than man, dog, or goat. However, in view of likely large errors associated with each of the curves in Fig. 4, we do not view the curves as being significantly different and use the family of curves to obtain judgmental upper and lower bounds on the curve for man.

Figure 4 shows empirical curves that bound the family of similar curves derived for man, dog, swine, and goat, for dose rates above about 0.01 Gy/h. The bounds were derived using the following empirical equations:

$$\text{Upper bound in Gy} = 0.3/\dot{D} + 3.5 \qquad (4)$$

and

$$\text{Lower bound in Gy} = 0.06/\dot{D} + 2.4 \qquad (5)$$

where $\dot{D}$ is in Gy/h to bone marrow. These empirical equations can be used as judgmental upper and lower bounds on the LD_{50} for uniform γ or high-energy β irradiation of man, for dose rate above about 0.01 Gy/h.

Table I. Estimates of dose-rate model parameters θ_1 and θ_∞ and their asymptotic standard deviations, by species

Species	θ_1 (Gy^2/h)	θ_∞ (Gy)
Rat[a, b]	1.07 ±0.30	10.9 ±1.42
Mouse[a, c]	0.49 ±0.13	6.5 ±0.47
Dog[a]	0.11 ±0.004	2.69±0.13
Swine[a]	0.29 ±0.008	2.45±0.10
Goat[a]	0.073±0.006	2.52±0.35
Sheep[a]	0.027±0.003	1.68±0.10
Man[d]	0.072	3.0

[a] Scott et al, 1988.

[b] Female albino Sprague-Dawley rats.

[c] White non-inbred mice.

[d] Scott & Hahn, 1989; only data for individuals or groups presumed to be of normal susceptibility to irradiation were used to obtain θ_1 and θ_∞.

Exponentially decaying patterns

Normalized dose

The focus of this section is on calculating the normalized dose X for hematopoietic death for exponentially decaying, dose-rate patterns of the form

$$\dot{D}(t) = A\exp[-Bt] \qquad (6)$$

for high-energy β irradiation. A and B are positive parameters, with A representing the initial dose rate to the bone marrow during RIT and B equals ln(2) divided by the effective half-time T for the antibody-associated radioactivity in the blood.

For any continuous pattern of irradiation, the normalized dose for hematopoietic death is given by the solution to the following generic equation (Scott et al, 1988):

$$X(t) = \int \dot{D}[\theta_1/\dot{D} + \theta_\infty]^{-1}\,dt' \qquad (7).$$

While Equation 7 is valid even for cases where significant amounts of the radionuclide are decoupled from the immunoglobulin and are taken up by the bone marrow, the analytical solutions that follow are specific for cases where no significant uptake occurs. For cases where significant uptake occurs, whether an analytical solution can be obtained or not will depend on the overall pattern of irradiation of the bone marrow.

Numerical evaluation of Equation 7 may therefore be required when significant uptake by bone marrow of decoupled radionuclide occurs.

For cases where the dose rate to the bone marrow decreases as a single, negative-exponential function of time, $\dot{D}$ in Equation 7 is given by Equation 6. The integral is evaluated from zero to exposure time t. Model parameters θ_1 and θ_∞ for man are provided in Table I. Equation 7 can also be used for the other species presented in Table I, when the appropriate parameter values for the species of interest are used. However, for rodents, θ_∞ and θ_1 may vary with strain.

Integrating Equation 7 from 0 to the time t of exposure, in hours, with dose rate expressed in Gy/h, one obtains the solution

$$X(t) = D(t)/\theta_\infty - \theta_1 Z(t)/B\theta_\infty^{\,2} \tag{8}$$

where

$$Z(t) = \ln\{(A\theta_\infty + \theta_1)/(A\theta_\infty \exp[-Bt] + \theta_1)\} \tag{9}.$$

The negative sign in Equation 8 arises because recovery from injury during protracted irradiation leads to a reduction in the normalized dose, when compared with that obtained for brief exposure. When the follow-up time t is large in comparison to the effective retention half-time T for the radionuclide in the blood, the expression for $Z(t)$ reduces to $\ln(1+kA)$, where $k = \theta_\infty/\theta_1$. One can obtain the LD_{50}-absorbed dose for short-lived, high-energy, β-emitting radionuclides by replacing $Z(t)$ in Equation 8 with $\ln(1+kA)$ and varying the initial dose rate A to find that initial dose rate (*i.e.* median lethal initial dose rate A_{50}) which makes $X = 1$. The LD_{50}-absorbed dose is then given by the quotient A_{50}/B.

Equation 8 is identical to the solution previously derived for lethality from radiation pneumonitis that is caused by chronic β irradiation of the lung (Scott et al, 1989). However, model parameters for death from pulmonary injury differ from those for hematopoietic death. For death from radiation pneumonitis, θ_1 and θ_∞ have been estimated to be about 30 Gy^2/h and 10 Gy, respectively (Scott & Hahn, 1989; Scott et al, 1989).

An effective reduction in the dose X for hematopoietic death can be brought about through the protection provided by supportive or intensive treatment, or by CSF treatment, to mitigate radiation injury.

Using parameters in Table I for man and for dogs and the normalized dose model, calculated data were generated for the LD_{50} (in Gy) for hematopoietic death in man and in the dog against the effective retention half-time T (in days) and are shown as points in Figs 5 and 6. Also shown are smooth curves based on less complicated empirical models that were fit to the data. In both cases, empirical models of the form

$$LD_{50} = \theta_\infty + aT^b \tag{10}$$

were found to represent the data adequately. For man, a and b were found to be 1.534 and 0.6, respectively, with the LD_{50} in Gy and T in days. For dogs, the corresponding values were 2.03 and 0.6 (0.58 rounded), respectively. Values used for θ_∞ were the same as given in Table I: 3 Gy for man and 2.7 Gy for dogs. The value of 0.6 for the parameter b implies that the increase in the LD_{50} (*i.e.* $LD_{50} - \theta_\infty$) should be linearly related to $T^{3/5}$, for both dogs and man.

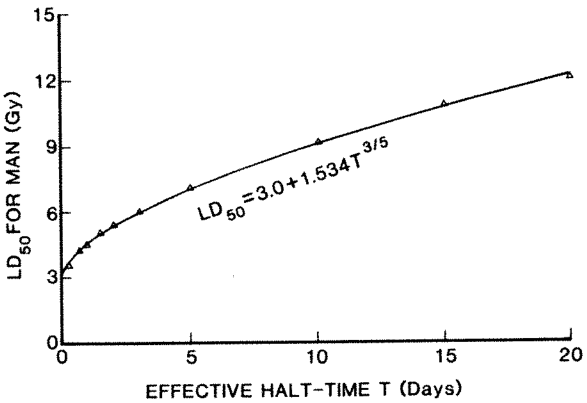

Figure 5. Predicted LD_{50} (in Gy) for hematopoietic death in man as a function of the effective retention half-time T (in days), for uniform high-energy β irradiation of the bone marrow from radiolabelled antibodies in the blood. Data points are calculated values generated with the normalized dose model. The smooth curve is based on the empirical model presented in the text.

Lethality risk, single injection of radioimmunoglobulin

The risk of hematopoietic death in man can be estimated by using the following equation (modified Weibull model), which is a modification of Equation 1, to account for the impact of supportive or intensive treatment of radiation injuries:

$$\text{Risk} = 1 - \exp[-\ln(2)(X/\text{CF})^V] \tag{11}$$

where the dose X is calculated for normal susceptibility to irradiation and for individuals not receiving medical treatment to mitigate radiation injuries. The correction factor (CF) serves two purposes: (1) to account for protection provided by minimal, supportive or intensive medical treatment to mitigate radiation injuries; and (2) to allow for a distinction between normal and heightened susceptibility. The CF actually represents the quotient of two factors, PF/SF, where the susceptibility factor (SF) takes on a value of 1 for individuals with normal susceptibility to irradiation and a value greater than one for individuals with heightened susceptibility.

Langham (1967) provided two estimates of the LD_{50} for brief exposure of very ill patients to external photons: 2.5 Gy, based on the log-normal model, and 2.9 Gy based on the Gaussian model. These values for the LD_{50} would place the SF in the range 1.6 (4.5 Gy/2.9 Gy $\simeq$ 1.6) to 1.8 (4.5 Gy/2.5 Gy = 1.8) for very ill cancer patients. A value of 1.6 was also obtained for the SF, based on an LD_{50} of 2.8 Gy reported by Lushbaugh et al (1967), for brief exposure of very ill patients to external photons.

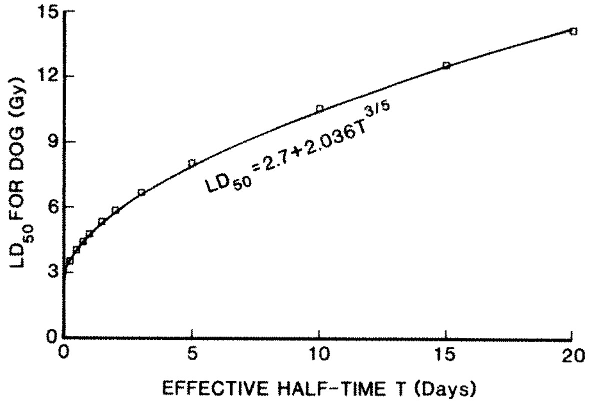

Figure 6. Predicted LD_{50} (in Gy) for hematopoietic death in dogs as a function of the effective retention half-time T (in days), for uniform high-energy β irradiation of the bone marrow from radiolabelled antibodies in the blood. Data points are calculated values generated with the normalized dose model. The smooth curve is based on the empirical model presented in the text.

The protection factor PF is assigned a value of 1 for the minimal treatment category; it was estimated to be 1.5 for the supportive treatment category (when CSFs are not used); greater than 1.5 for supportive treatment supplemented with CSFs; and greater than 3.3 for the intensive treatment category. The shape parameter ν has been estimated to be about 6 with lower and upper bounds of 4 and 8, respectively.

Lethality risk, multiple RIT treatments, single cycle

As previously pointed out, Order et al (1985) obtained results that indicated saturation of ^{131}I uptake in the tumour after treating patients with ^{131}I-labelled antiferritin for hepatoma. Based on this and other considerations, Order et al selected a protocol whereby 1110 MBq (30 mCi) of radioimmunoglobulin was administered on Day 0 and 740 MBq (20 mCi) was administered on Day 5. There was no radiation-free time between the two injections of ^{131}I-labelled antiferritin. For this type of single-cycle, two-injection protocol, Equation 7 can be evaluated by piecewise integration.

The piecewise integration can be carried out over two time intervals: (1) an integral from 0 to T_2 hours (the time of the second injection) with the initial dose rate based on the activity from the first injection; and (2) an integral from T_2 to the end of the radiation exposure with the dose rate at T_2 increased to account for the added activity from the second injection.

Piecewise integration of Equation 7 can be carried out for any combination of activities of radioimmunoglobulin in the single-cycle, two-injection protocol. However, application of the model is limited to time intervals between injections of radioimmunoglobulin that are short enough such that irradiation occurs continuously throughout the interval between the two injections.

For the single-cycle, two-injection protocol, it is useful to change the independent variable in Equations 8 and 9 from t to the variable $n = t/T$ (*i.e.* number of effective half-times), and also to substitute 1.443 T for $1/B$. We replace $D(t)$ and $Z(t)$ in Equations 8 and 9 with interval-specific functions $D(n_1, n_2, A_1)$ and $Z(n_1, n_2, A_1)$, for the interval (n_1, n_2), to facilitate modelling multiple injections; n_1 equals zero and represents the time (in effective half-times) of the first injection. We use n_2 to indicate the number of effective half-times at which the second injection occurs. The parameter A_1 is the initial dose rate to the bone marrow for the interval (n_1, n_2). The interval (n_2, ∞) is associated with the second injection, and activity from the first injection remaining in the blood at n_2 effective half-times after the first injection. The symbol ∞ is used to indicate a large number of effective half-times. The initial dose rate to the bone marrow for the interval (n_2, ∞) is indicated by A_2.

The interval-specific functions of $D(n_1, n_2, A_1)$ and $Z(n_1, n_2, A_1)$ can be evaluated using the following generalized equations for the generalized interval (n_i, n_j) and dose rate A_i at the beginning of the interval:

$$\mathrm{D}(n_i, n_j, A_i) = 1.443TA_i\,(1-\exp[-\ln(2)(n_j-n_i)]) \quad (12)$$

and

$$Z(n_i, n_j, A_i) = \ln\{(A_i\theta_\infty+\theta_1)/(A_i\theta_\infty\exp[-\ln(2)(n_j-n_i)]+\theta_1)\} \quad (13).$$

Interval-specific normalized doses for the intervals (n_1, n_2) and (n_2, ∞) are given by $X(n_1, n_2, A_1)$ and $X(n_2, \infty, A_2)$, respectively, and can be evaluated using the generalized equation

$$X(n_i, n_j, A_i) = \mathrm{D}(n_i, n_j, A_i)/\theta_\infty - 1.443T\theta_1 Z(n_i, n_j, A_i)/\theta_\infty^2 \quad (14).$$

The total dose, X, for the single-cycle, two-injection protocol is obtained by adding $X(n_1, n_2, A_1)$ and $X(n_2, \infty, A_2)$. The radiation doses $\mathrm{D}(n_1, n_2, A_1)$ and $\mathrm{D}(n_2, \infty, A_2)$ can be evaluated using Equation 12.

The model can easily be extended to three or more injections in the same cycle. In this case, Equation 14 would apply to the time interval between the ith and $(i+1)$th injections, for $i = 1, 2, \ldots, m-1$, for m injections. For the interval (n_m, ∞) the normalized dose would be given by $X(n_m, \infty, A_m)$.

We have presented empirical models which should be validated by animal experiments and clinical data. For ^{90}Y-labelled antiferritin injected into dogs, with an effective retention half-time in the blood ranging from 1.7 to 2 days (Vriesendorp et al, 1989), the empirical model for dogs predicts an LD_{50} of between 5.5 Gy and 5.7 Gy when only minimal treatment for radiation injuries is provided, and 8.3 Gy to 8.6 Gy when supportive treatment is provided. The 8.3 Gy to 8.6 Gy range is slightly below the 10 Gy value reported by Vriensendorp et al (1989), suggesting that perhaps some of the marrow was not irradiated (non-uniform irradiation) or that radiation doses may have been overestimated by about 1 Gy. Because the difference between the predicted and reported values may be due to some of the bone marrow being unirradiated, future research should be devoted towards developing lethality models for non-uniform irradiation of the marrow for RIT. This may be especially important when low-energy β emitters, such as ^{131}I, or α emitters are used in RIT. For applications where non-uniform irradiation is judged to be important, models developed for uniform irradiation can be used to provide upper limits on the risk of hematopoietic death.

The analytical solution provided for Equation 7 applies only to cases where no significant uptake of the radionuclide by the bone marrow occurs and for which the dose rate to the bone marrow decreases as a single negative exponential function of time. Future reseach efforts should also be devoted towards applying Equation 7 to more complicated patterns of irradiation including those that involve uptake of the radionuclide by the bone marrow. This may be important for energetic β emitters such as ^{90}Y which could be decoupled in significant amounts from circulating radioimmunoglobulins.

We have described empirical models that focus on toxicity to bone marrow from RIT. However, the modified Weibull model presented could also be adapted to include combinations of external-beam (total-body irradiation) and antibody-targeted radiotherapy. The potential advantage of the external-beam component results from assuming that some of the tumour cells may not be targeted by antibodies (Wheldon & O'Donoghue, 1986). We also obtained crude estimates of the PF for protection from hematopoietic death provided by minimal (PF = 1), supportive (PF = 1.5), and intensive (PF > 3.3) medical treatment to mitigate radiation injuries, along with estimates of the SF (1.6 to 1.8) for very ill cancer patients. However, more accurate values for these factors are needed, as well as validation of the normalized dose model, for exponentially decaying patterns of irradiation, before the modified Weibull model should be used in developing RIT schemes for man.

Acknowledgments

This research was supported by the US Department of Energy under Contract DE-AC04-76EV01013, with partial support by the Defense Nuclear Agency under TASK Code RMRH and Work Unit Code 00091 of IACRO DNA 89-877 and by the US Nuclear Regulatory Commission via Interagency Agreements. The participation by Dr L. E. Dillehay was supported by National Institute of Health Grant PO1 43791. We are grateful to Dr J. R. Williams and H. M. Vriensendorp of the Johns Hopkins Oncology Center for valuable information and discussions related to their RIT research, to Dr T. A. Coons for editorial assistance, and to Drs B. A. Muggenburg, D. L. Lundgren, L. J. Shyr, J. H. Diel, A. F. Hubbs, Mr W. C. Griffith, and Dr B. B. Boecker for review of the manuscript. We are also grateful to the journal referees for their helpful suggestions.

References

Bateman, J. L., 1968. A relation of radiation dose rate effects in mammals and in mammalian cells. In *Dose Rate in Mammalian Radiation Biology, Proceedings of a Symposium held April 29–May 1, 1968, Oak Ridge, TN*, ed. by D. G. Brown, R. G. Cragle and T. R. Noonan (CONF-680410), pp. 23.1–23.19.

Beierwaltes, W. H., 1976. Radioiodine-labeled compounds previously or currently used for tumor localization. In *Tumor Localization with Radioactive Agents* (IAEA, Vienna), IAEA-MG-50/2, pp. 47–56.

Bond, V. P., Fliedner, T. M. & Archambeau, J. O., 1965. *Mammalian Radiation Lethality: A Distribution in Cellular Kinetics* (Academic Press, New York).

BIR Working Party, 1982. *Report of the BIR Working Party on the Radiological Effects of Nuclear War* (British Institute of Radiology, London).

Butturini, A., 1990. Use of GM-CSF in Brazil radiation accident. In *Proceedings of the First Consensus Development Conference on the Treatment of Radiation Injuries*, sponsored by the Medical Radiobiology Advisory Team (MRAT) of the Armed Forces Radiobiology Research Institute, May 10–13, 1989, Washington, DC (in press).

Carrasquillo, J. A., Krohn, K. A., Beaumier, P., McGuffin, R. W., Brown, J. P., Hellström, K. E., Hellström, I. & Larson, S. M., 1984. Diagnosis of and therapy for solid tumors with radiolabeled antibodies and immune fragments. *Cancer Treatment Reports*, *68*, 317–358.

Dillehay, L. E., 1990. A model of cell killing by low-dose-rate radiation including repair of sublethal damage, G2 block, and cell division. *Radiation Research* (in press).

Epenetos, A. A., 1985. Clinical results with regional antibody guided irradiation. *British Journal of Cancer*, *52*, 641–669.

Ettinger, D. S., Order, S. E., Wharam, M. D., Parker, M. K., Klein, J. L. & Leichner, K., 1982. Phase-I-II study of isotopic immunoglobulin therapy for primary liver cancer. *Cancer Treatment Reports*, *66*, 289–297.

Fujita, S., Kato, H. & Schull, W. J., 1990. *The LD_{50} Associated With Exposure to the Atomic Bombings in Hiroshima and Nagasaki: a Review and Reassessment, Technical Report RERF TR 17-87* (Radiation Research Foundation, Hiroshima City 730, Japan).

Gus'kova, A. S. (Ed.), 1987. *Early Acute Effects of the Chernobyl Accident*. ICRP-87-C:G-01, translation provided by R. W. Young (Defense Nuclear Agency, Washington, DC).

IAEA, 1988. *The Radiological Accident in Goiânia* (IAEA, Vienna).

Kaul, D. C. & Scott, W. H., 1984. Dose and cell-survival calculations in anthropomorphic phantoms. In *Response of Differenct Species to Total Body Irradiation*, ed. by J. J. Broerse and T. J. MacVittie, (Martinus Nijhoff, Boston), pp. 29–42.

Klein, J. L., Ling, M. N., Leichner, P. K., Kopher, K. S., Rostock, R. A. & Order, S. E., 1985. A model system that predicts effective half-life for radiolabeled antibody therapy. *International Journal of Radiation Oncology, Biology, Physics*, *11*, 1489–1494.

Koznova, L. B., 1978. Effects of radiation dose rate on median lethal dose for mice with development of hemopoietic and enteric syndromes. *Radiobiologiia*, *18*, 63–69, DOE-TR4/9.

Langham, W. H. (Ed.), 1967. *Radiobiology Factors in Manned Space Flight*. NAS-NRC 1487 (Washington, DC).

Leichner, P. K., Klein, J. L., Garrison, J. B., Jenkins, R. E., Nickoloff, E. L., Ettinger, D. S. & Order, S. E., 1981. Dosimetry of ^{131}I-labeled anti-ferritin in hepatoma: A model for radioimmunoglobulin dosimetry. *International Journal of Radiation Oncology, Biology, Physics*, *7*, 323–333.

Lenhard, R. E. Jr., Order, S. E., Spunberg, J. J., Asbell, S. D. & Leibel, S. A., 1985. Isotopic immunoglobulin: a new systemic therapy for advanced Hodgkin's disease. *Journal of Clinical Oncology, 3,* 1296–1300.

LOGIE, L. C., HARRIS, M. D., TATSCH, R. E. & VAN HOOSER, E. N., 1960. An analysis of the $LD_{50(30)}$ as related to radiation intensity. *Radiation Research, 12,* 349–356.

LUSHBAUGH, C. C., COMAS, F. & HOFSTRA, R., 1967. Clinical studies of radiation effects in man, a preliminary report of a retrospective search for dose-relationships in the prodromal syndrome. *Radiation Research Supplement, 7,* 398–412.

MACVITTIE, T. J., 1990. Rescue of lethally irradiated canines using therapeutic administration rhG-CSF or rhGM-CSF. In *Proceedings of the First Consensus Development Conference on the Treatment of Radiation Injuries,* sponsored by the Medical Radiobiology Advisory Team (MRAT) of the Armed Forces Radiobiology Research Institute, May 10–13, 1989, Washington, DC (in press).

MACVITTIE, T. J., MONROY, R. L., PATCHEN, M. L. & DARDEN, J. H., 1984. Acute lethality and radiosensitivity of the canine hemopoietic system to cobalt-60 gamma and mixed neutron-gamma irradiations. In *Response of Different Species to Total Body Irradiation,* ed. by J. J. Broerse and T. J. MacVittie (Martinus Nijhoff Publishers, Boston), pp. 113–129.

MCCLELLAN, R. O., BOECKER, B. B., CUDDIHY, R. G., GRIFFITH, W. C., HAHN, F. F., MUGGENBURG, B. A., SCOTT, B. R. & SEILER, F. A., 1982. Health effects from internally deposited radionuclides released in nuclear disaster. In *The Control of Exposure of the Public to Ionizing Radiation in the Event of Accident or Attack, NCRP Symposium held April 17–29, 1981, Reston, VA.* (NCRP, Bethesda, MD), pp. 28–39.

MOLE, R. H., 1985. The LD_{50} for uniform low-LET irradiation of man. *British Journal of Radiology, 58,* 98–99.

NUREG/CR-4214, 1989. *Health Effects Model for Nuclear Power Plant Accident Consequence Analysis* (US Nuclear Regulatory Commission).

O'DONOGHUE, J. A. & WHELDON, T. E., 1988. Predicted allowable doses to normal organs for biologically targeted radiotherapy. *British Journal of Radiology, 61,* 264–266.

OFFICE OF TECHNOLOGY ASSESSMENT, CONGRESS OF THE UNITED STATES OF AMERICA, 1980. *The Effects of Nuclear War* (Croom Helm, London).

ORDER, S. E., STILLWAGON, G. B., KLEIN, J. L., LEICHNER, P. K., SIEGELMAN, S. S., FISHMAN, E. K., ETTINGER, D. S., HAULK, T., KOPHER, K., FINNEY, K., SURDYKE, M., SELF, S. & LEIBEL, S., 1985. Iodine 131 antiferritin, a new treatment modality in hepatoma: a radiation therapy oncology group study. *Journal of Clinical Oncology, 3,* 1573–1582.

PAGE, N. P., 1968. The effect of dose-protraction on radiation lethality of large animals. In *Proceedings of a Symposium on Dose Rate in Mammalian Radiation Biology* (CONF-680410, Oak Ridge, TN), pp. 12.1–12.23.

RICKS, R. C., 1990. Radiation accident in San Salvador. In *Proceedings of the First Consensus Development Conference on the Treatment of Radiation Injuries,* sponsored by the Medical Radiobiology Advisory Team (MRAT) of the Armed Forces Radiobiology Research Institute, May 10–13, 1989, Washington, DC (in press).

ROSEN, S. T., ZIMMER, A. M., GOLDMAN-LEIKIN, R., GORDON, L. I., KAZIEKIEWICZ, J. M., KAPLAN, E. H., VARIAKOJIS, D., MARDER, R. J., DYKEWICZ, M. S., PIERGIES, A., SILVERSTEIN, E. A., ROENIGK, H. H. & SPIES, S. M., 1987. Radioimmunodetection and radioimmunotherapy of cutaneous T-cell lymphomas using an ^{131}I-labeled monoclonal antibody: An Illinois cancer council study. *Journal of Clinical Oncology, 5,* 562–573.

ROTBLAT, J., 1986. Acute radiation mortality in a nuclear war. In *Medical Implications of Nuclear War,* Institute of Medicine, National Academy of Sciences (National Academy Press, Washington, DC), pp. 233–250.

SCOTT, B. R. & HAHN, F. F., 1989. Early occurring and continuing effects. Chapter 2, Revision 1, Part II. In *Health Effects Model for Nuclear Power Plant Accident Consequence Analysis* (US Nuclear Regulatory Commission Report, NUREG/CR-5214, Washington, DC).

SCOTT, B. R., HAHN, F. F., MCCLELLAN, R. O. & SEILER, F. A., 1988. Risk estimators for radiation induced bone marrow syndrome lethality in humans. *Risk Analysis, 8,* 393–402.

SCOTT, B. R., FILIPY, R. E. & HAHN, F. F., 1989. *Models for Pulmonary Lethality and Morbidity after Irradiation from Internal and External Sources, Final Report* (US Nuclear Regulatory Commission Report NUREG/CR-5351).

STATHER, J. W., MUIRHEAD, C. R., EDWARDS, A. A., HARRISON, J. D., LLOYD, D. C. & WOOD, N. R., 1988. Health effects models developed from the 1988 UNSCEAR report. In *National Radiological Protection Board Report NRPB-R226* (NRPB, Chilton).

UNSCEAR, 1988. Sources, effects, and risks of ionizing radiation. *United Nations Scientific Committee on the Effects of Atomic Radiations Report to the General Assembly, with Annexes* (United Nations, New York).

VAUGHAN, A. T. M., ANDERSON, P., DYKES, P. W., CHAPMAN, C. E. & BRADWELL, A. R., 1987. Limitations to the killing of tumours using radiolabelled antibodies. *British Journal of Radiology, 60,* 567–578.

VRIESENDORP, H. M. & VAN BEKKUM, D. W., 1984. Susceptibility to total body irradiation. In *Response of Different Species to Total-Body Irradiation,* ed. by J. J. Broerse and T. J. MacVittie, (Martinus Nijhoff, Boston), pp. 43–57.

VRIESENDORP, H. M., STINSON, R., ONYEKWERE, O., KLEIN, J., LEICHNER, P., JACOBSON-KRAM, D., WESSELS, B. & WILLIAMS, J., 1989. Dosimetry studies of polyclonal ^{90}yittrium-labeled antiferritin in rats and dogs. Paper EK-2 presented at the *Thirty-Seventh Annual Meeting of the Radiation Research Society, Seattle, WA, March 18–23, 1989.*

WARREN, S. & BOWERS, J. Z., 1950. The acute radiation syndrome in man. *Annals of Internal Medicine, 32,* 207–216.

WHELDON, T. E. & O'DONOGHUE, J. A., 1986. Prospects for antibody-targeted radiotherapy of cancer. *Lancet, ii,* 580.

ZIMMER, A. M., ROSEN, S. T., SPIES, S. M., GOLDMAN-LEIKIN, R., KAZIKIEWICZ, J. M., SILVERSTEIN, E. A. & KAPLAN, E. H., 1988. Radioimmunotherapy of patients with cutaneous T-cell lymphoma using an iodine-131-labeled monoclonal antibody: analysis of retreatment following plasmapheresis. *Journal of Nuclear Medicine, 29,* 174–180.

1990, *The British Journal of Radiology*, *63*, 871–874

Lack of late skin necrosis in man after high-dose irradiation using small field sizes: experiences of grid therapy

By *H. Shirato, MD, *N. K. Gupta, FRCR, †T. J. Jordan, PhD and ‡J. H. Hendry, PhD

*Department of Radiotherapy, †Department of Medical Physics and ‡Cancer Research Campaign Department of Radiobiology, Paterson Institute for Cancer Research, The Christie Hospital and Holt Radium Institute, Manchester M20 9BX, UK

(*Received April 1990 and in revised form June 1990*)

Abstract. Out of a total of 437 patients with superior vena caval syndrome or advanced malignancy, given single-dose grid radiotherapy, four survived to 7 years. The dose to the skin under each of the 77 holes in the grid was approximately 58 Gy. The lack of skin necrosis in the total of 308 skin circles of 1 cm diameter among these survivors, compared with known necrosis rates in larger irradiated areas, implies that there is a marked field-size effect for late necrosis in small areas of irradiated skin.

Knowledge of the influence of field size on late skin reactions is important not only in radiation therapy but also in accidents. Previous studies regarding *early* skin reactions in man, mouse and pig showed a strong dependence on the area irradiated over a range 1–20 mm in diameter (MacKee et al, 1943; Joyet & Hohl, 1953; von Essen, 1968; Hendry, 1978; Hopewell et al, 1986; Charles et al, 1989; Charles, 1990). However, there are fewer data for late skin reactions. A field-size effect was reported for dermal atrophy in pig skin at 2 years after β-irradiation using ^{90}Sr/Y or ^{170}Tm when the field diameter was less than 2 mm (Hamlet et al, 1986). A field-size effect for late skin necrosis in man was reported for treatments of superficial skin cancer when the field diameter was varied between 10 and 40 mm (Chan et al, 1988; Chan, 1989).

Before the era of megavoltage machines, grid or sieve therapy, using orthovoltage photon beams and a lead sheet with many small holes was one of the most popular techniques employed in order to deliver high doses at depth with avoidance of untoward reactions on the skin surface (*e.g.* Jolles, 1952; Rode, 1962). We have now reviewed the late skin necrosis rate in patients treated using grid therapy and single exposures.

Materials and methods

Irradiation and dosimetry

Grid therapy was performed at Victoria Hospital, Blackpool and at the Christie Hospital, Manchester, UK.

The treatment machine at Blackpool is a Marconi 230 kVp X-ray unit with a half-value thickness (HVT) of 1.55 mm Cu. The grid treatment involved placing on the anterior chest wall of the patient a sheet of lead in which there were holes of 10 mm diameter, centred at 14 mm intervals (Fig. 1). The phantom studies and patient treatments were performed at a focus–surface distance of 50 cm.

The treatment dosage was fixed at a nominal 45 Gy single exposure (surface dose without backscatter), which required about 50 min continuous irradiation. Details of the measurement of nominal dose in grid therapy are described elsewhere (Massey, 1970).

Absolute dosimetry was performed at Blackpool with a 0·6 ml Farmer-type ion chamber, with a calibration traceable back to the National Physical Laboratory (Teddington, Middlesex, UK) primary standard. In addition, for measurements made under the grid, a Farmer thimble chamber with an especially reduced long axis (6 mm × 6 mm diameter) and a volume of 0.15 ml was used. The sensitivity of this chamber was established by direct comparison with the calibrated chamber at 230 kVp on the surface of a Mix D slab phantom (ICRU, 1989) with no grid. Two of the 1 cm Mix D slabs were clamped and drilled with a hole matching the Farmer chamber dimensions. This permitted measurements to be made at depth with minimum air gaps or, by separating the slabs, surface measurements with the ion chamber in "half-sunk" geometry. Using this latter arrangement, the dose rate of the Blackpool unit was measured and the magnitude of the shutter error established.

Film dosimetry was also used extensively to investigate the shape of the dose distribution under the grid and as a second method of determining absolute dosimetry with depth. As a preliminary, the film was given a known range of exposures on the surface of the Mix D phantom, and the relationship between absorbed dose and optical density was established.

The dose rate at the phantom surface irradiated using a 10 cm circle field without the grid was 109.0 ± 0.4 cGy/min. The dose rate at the phantom surface under the central hole of the grid was 108.2 ± 1.6 cGy/min as measured by the 0.15 ml ionization chamber. The total skin dose under the central hole of the grid in the patient treatment was estimated to be 58.0 ± 0.9 Gy. The significant difference between the

---

*Present address of Hiroki Shirato, MD: Department of Therapeutic and Diagnostic Radiology, Obihiro Kosei Hospital, West-6 South-8, Obihiro, Hokkaido, Japan 080. Address correspondence to N. K. Gupta.

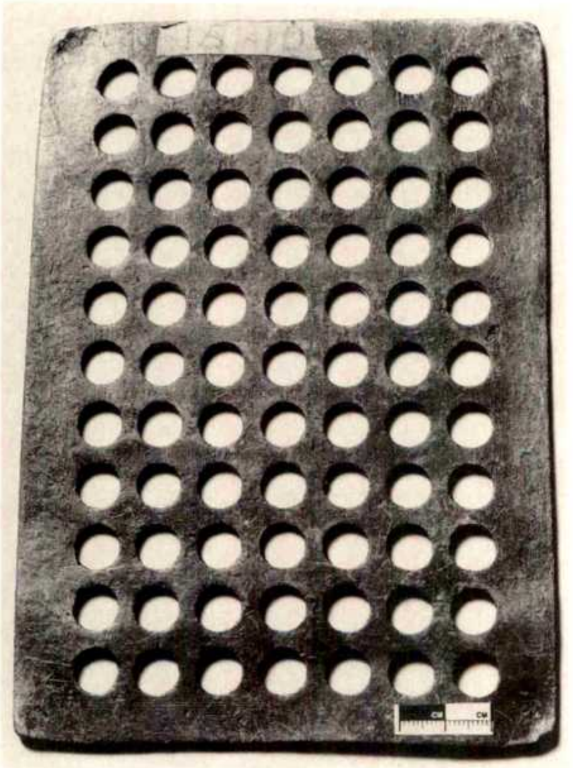

Figure 1. Lead sheet (4 mm thick) for use in grid therapy, with holes 10 mm in diameter with centres at 14 mm intervals.

Table I. Number of patients at risk, number of 1 cm skin circles at risk (none showing necrosis), and the expected number of 2–3 cm skin circles showing necrosis as a function of time following 22.5 Gy (see text)

Months	Number of patients at risk	Number of 1 cm skin circles at risk	Expected number of 2–3 cm skin circles having necrosis at 22.5 Gy
0	437 (127)	33 649	0
12	19	1 463	3
24	7	539	10
36	5	385	25
48	5	385	63
60	4 (3)	308	59
84	4 (3)	308	27[a]

Values in brackets refer to the Blackpool patients only.
[a] Crude rate; other values are actuarial rates (see text).

nominal and the actual dose is attributed mainly to the contribution from backscatter in the Mix D phantom. At orthovoltage energies, the unflattened beam centre is the most intense point. The dose estimated by film densitometry under each hole of the grid gave the following distribution: four holes (5%) received doses between 47.0 and 49.9 Gy, 18 (23%) between 50.0 and 52.9 Gy, 18 (23%) between 53.0 and 55.9 Gy, and 37 (48%) between 56.0 and 58.9 Gy. The skin dose under the lead sheet was estimated to be 12.3 ± 1.5 Gy.

The grid technique used in Manchester was similar to that used in Blackpool except that it used 300 kVp X rays with HVL = 1.7 mm (Holmes, 1963). As the prescribed doses and the type and size of the grid used in the two hospitals were identical, it can be assumed that the surface doses received by the two sets of patients were similar.

Patient treatment and follow-up

Four hundred and thirty-seven patients received orthovoltage therapy using the grid technique, to the anterior mediastinum. Two hundred and sixty-eight patients had treatment for superior vena caval syndrome and 169 patients received treatment for gross dyspnoea/stridor, persistent haemoptysis and/or chest wall pain due to advanced malignancy. Three hundred and nine (70%) were male and the mean age of the group was 58 years (range 26–80). Three hundred and ten patients in this study had treatment in Manchester (1956–1959) and 127 patients were treated in Blackpool (1970–1985). All were in poor general condition with distressing symptoms and were considered unsuitable for protracted fractionation. In view of this and the urgency of institution of palliative therapy, histological diagnoses were not sought and were available only in 66 patients (15%). Of those where histology was available, 57 had squamous cell carcinoma of the bronchus, three with metastatic breast cancer, two with oesophageal cancer and four patients with miscellaneous tumours. There are no survivors. One of the authors (N.K.G.) was involved in the treatment and subsequent follow-up of all his patients at Blackpool. The information about the Manchester patients was collected from the hospital case notes and via postal enquiries from their general practitioners.

Late skin necrosis was defined as necrosis existing at or after 3 months following radiotherapy, which either healed or was excised surgically and histologically proven (Dutreix, 1986). Follow-up of patients was at intervals of at least 2–3 months during the first year, 3–4 months during the second year, and then every 6 months from 3 years.

Results

The poor long-term survival of these patients was expected. All were in poor general condition with advanced cancer and had a simple palliative radiotherapy merely to alleviate the distressing symptoms. All patients had relief of vena caval obstruction within the first week after irradiation, and 75% of these had benefit lasting 2–9 months. Only 19 patients were alive at the end of the first year, seven patients survived for 2 years, five patients lived 3 years and a mere four patients lived for more than 4 years (Table I). Of the seven who were alive more than 2 years, five had treatment in Blackpool (total 127 treated), and three of these survived to 7 years. In one patient, a post-mortem examination 10 years after grid therapy showed radiation fibrosis around the retrosternal thyroid, but there was no evidence of cutaneous or bone necrosis (nor of tumour). However, in all long-surviving patients, deep permanent skin pigmentation matching the grid pattern was evident. No skin necrosis has been detected. Regarding the previous Manchester patients, the annotation on the case notes was not always precise about the status of the skin but a statement of moist desquamation in the treated site was frequently noted at 3 months after therapy (as also observed in the Blackpool patients). Further comments specific to the skin condition were rarely made thereafter, and usually referred to skin atrophy. As auscultation of the chest was done during follow-up visits, it is not unreasonable to assume that a degree of inspection of the chest wall was inevitable. It is unlikely that a clinician could overlook skin necrosis which is painful and takes several weeks to heal.

With an observation of (0/19) patients as a skin necrosis rate at 12 months, the 95% confidence interval of probability of skin necrosis at 1 year is 0–18% assuming a binominal distribution. The number of patients after 24 months was too small to analyse on an individual basis. However, if the probability of late skin necrosis is assumed to be independent of patient characteristics and if there is no interaction between circles, it is possible to use each 1 cm circle as an independent observation (Table I, third column). In this case, the 95% confidence interval would be 0–1.2%, *i.e.* an upper limit of only four events (necroses) in 308 sites even at 7 years.

Discussion

Late radiation morbidity from grid therapy has not been well documented. The technique has only been used for patients with poor prognosis and hence there have been only a few long-term survivors. The first report on the use of grid technique was by Kohler (1909). This form of therapy was developed further (for example: Liberson, 1933; Haring, 1934; Grynkraut, 1945; Jolles 1949, 1952), and individual experiences were reported (for example: Marks, 1952; Tenzel, 1952; Jolles, 1962; Rodé, 1962; Aliev 1976). Anecdotal incidences of skin necrosis after fractionated grid technique were reported by Jolles (1952) and Tenzel (1952), but this seems to have been due to technical errors in grid placement or as a consequence of previous irradiation. Although fractionated therapy has its potential problems with reproducibility of grid placement, the low incidence of skin damage is striking. Our results are very similar to those in an extensive series reported by Rodé (1962) who found no evidence of tissue necrosis occurring in 1200 fields of 800 patients who received 30 Gy in a single (nominal) dose for a mixed group of tumours treated over a period of 7 years. This dose and other doses referred to in the literature do not include the contribution from backscatter, and are in fact 10–30% higher than their prescribed nominal doses. Jolles (1962) reported five small necrotic skin patches in 83 patients with advanced bladder cancer treated with 110 and 120 Gy in 20–25 fractions using an anterior field and a further 90 Gy delivered to the skin by a posterior field in the same overall time. Aliev (1976) noted 19 cases of late skin necrosis in 251 patients who had received doses between 150 and 200 Gy using fractionated grid therapy with a daily dose of between 6 and 10 Gy/fraction.

The results can be compared with those for larger field sizes. A previous study from this Institute has shown that the actuarial skin necrosis rate after a 22.5 Gy single dose for the treatment of skin cancer using a 2.0–3.0 cm diameter field was 0.2%, 1.9%, 6.6%, 16.4% and 19.2% at 1, 2, 3, 4 and 5 years respectively (Chan et al, 1988). The value at 7 years was quoted as a crude rate (8.9%). Using these percentages, Table I (last column) shows the expected number of necroses as a function of time after 22.5 Gy using a 2.0–3.0 cm diameter field. In spite of the large difference in dose between 22.5 Gy and 47–59 Gy, the necrosis rate in the present study (0/308) was significantly lower than for a 2–3 cm diameter field.

Chan et al (1988) have also shown that the crude skin necrosis rate at 7 years was 2.3%, 3.0% and 8.9% after 18 Gy, 20 Gy and 22.5 Gy single dose for the treatment of skin cancer using a 2.0–3.0 cm diameter field. Using those data, a dose–response curve calculated by probit analysis predicts 50% risk of skin necrosis at 29 ± 1 Gy and 99% incidence at about 40 Gy (Chan, 1989). The corresponding dose for 50% incidence in 3–4 cm diameter fields was 28 ± 4 Gy. This is consistent with other data where 50% incidence of necrosis was produced by 24.5 Gy using a field more than 3 cm in diameter and where virtually 100% necrosis was predicted at >30 Gy (Trott et al, 1984). The difference between this and the lack of skin necrosis (0/308) using 58 Gy and 1 cm diameter fields in grid therapy is thus highly significant. This difference occurred in spite of the probability of interaction effects between the neighbouring 1 cm fields which may have increased, not decreased, their response. It was shown by Jolles (1950) that there was no interaction regarding acute skin reactions on the leg when 2 areas each of 1.56 cm^2 were separated by not less than 2 cm of unirradiated skin. In the present studies the holes were separated by a minimum of only 0.4 cm of (shielded) skin.

Another possibility, which would apparently decrease the differential in responses between the different field sizes, is that the 1% of patients who survived to 5 years in the present study were inherently radioresistant. However, there was no evidence for a lack of acute skin reactions in these four individuals compared with the majority. Also, at 2 years five out of the seven survivors were part of the original number of 127 treated in Blackpool, and 4% of individuals more resistant than the other 96% by a factor of as much as 2–3 in terms of tolerance dose is contrary to common radiotherapeutic experience.

It is also noted that the dose as high as 12 Gy to the skin between the high-dose circles did not increase the risk of necrosis. These results are consistent with clinical observations using interstitial treatments, which give ultrahigh doses around the radioactive needles but which result in no tissue necrosis.

The sharp increase in iso-effect dose for areas decreasing to 1.0 cm diameter is similar to data for early skin reactions using single fields previously reviewed (Hopewell & Young, 1982). Although skin reactions are no longer dose limiting in conventional radiotherapy, these dosage increases for both early and late skin reactions are probably applicable to treatment of other tissues as well, such as the use of charged particles in the treatment of occular melanomas and of chordomas and chondrosarcomas abutting the central nervous system, where high doses can be delivered safely to small volumes. Also, it has been suggested that grid therapy may still have a role in treatments involving "series-type" tissues such as the spinal cord where each of a series of critically sized elements is essential for the function of the whole organ (Maruyama et al, 1989). The sparing of single elements due to the field-size effect (*e.g.* Hopewell & van der Kogel, 1988) would enable much higher regional doses to be tolerated.

Acknowledgment

We thank Mr R. Swindell for his help with the statistical aspects of this study.

References

Aliev, E. M., 1976. Möglichkeiten dun Perspektiven einer ungleichmässigen Bestrahlung von malignen Geschwulsten. *Radiobiology-Radiotherapy, 2,* 223–234.

Chan, S., 1989. The effect of field size on late skin necrosis in man following single-exposure radiotherapy. *British Journal of Radiology, 62,* 770.

Chan, S., Lim, J. & Hunter, R. D., 1988. Single fraction radiotherapy for carcinoma of the skin. *British Journal of Cancer, 55,* 520–521.

Charles, M. W., 1990. General considerations of the choice of dose limits, averaging areas and weighting factors for the skin in the light of revised skin cancer risk figures and experimental data on non-stochastic effects. *International Journal of Radiation Biology, 57,* 841–858.

Charles, M. W., Hopewell, J. W., Wells, J. & Coggle, J. E., 1989. Recent trends in radiobiology of the skin and repercussions for dose limitation and personal dosimetry. Radiation protection theory and practice. In *Proceedings of the Fourth International Symposium of the Society for Radiological Protection, Malvern, 1989* (Institute of Physics, Bristol), pp. 419–424.

Dutreix, J., 1986. Human skin: early and late reactions in relation to dose and its time distribution. In *Radiation Damage to Skin* (British Journal of Radiology Supplement 19, British Institute of Radiology, London), pp. 22–28.

von Essen, C. F., 1968. Radiation tolerance of the skin. *Acta Radiologica, Therapy, Physics, Biology, 8,* 311–330.

Grynkraut, B., 1945. Direct and indirect radiotherapy. *American Journal of Roentgenology, 53,* 491–499.

Hamlet, R., Heryet, J. D., Hopewell, J. W., Wells, J. & Charles, M. W., 1986. Late changes in pig skin after irradiation from beta-emitting sources of different energy. In *Radiation Damage to Skin* (British Journal of Radiology Supplement 19, British Institute of Radiology, London), pp. 51–53.

Haring, W., 1934. Siebstrahlung. *Strahlentherapie, 51,* 154–163.

Hendry, J. H., 1978. Radionecrosis of normal tissue: studies on mouse tails. *International Journal of Radiation Biology, 33,* 47–55.

Holmes, K. S., 1963. The treatment of superior vena caval syndrome by high-dose grid technic. *Radiology, 81,* 402–405.

Hopewell, J. W. & Young, C. M. A., 1982. Letter to the Editor. *British Journal of Radiology, 55,* 936–937.

Hopewell, J. W. & van der Kogel, A. J., 1988. Volume effects in the spinal cord. *British Journal of Radiology, 61,* 973–975.

Hopewell, J. W., Coggle, J. E., Wells, J., Hamlet, R., Williams, J. P. & Charles, M. W., 1986. The acute effects of different energy beta-emitters on pig and mouse skin. In *Radiation Damage to Skin* (British Journal of Radiology Supplement 19, British Insititute of Radiology, London), pp. 47–51.

ICRU, 1989. *Report 44: Tissue Substitutes in Radiation Dosimetry and Measurement* (ICRU, Bethesda), p. 189.

Jolles, B., 1949. Radiotherapy of accessible malignant tumors by alternating chess-board method. *Lancet, 2,* 603–606.

Jolles, B., 1950. The reciprocal vicinity of irradiated tissues on a 'diffusible substance' in irradiated tissues. *British Journal of Radiology, 23,* 18–24.

Jolles, B., 1952. The sieve in radiotherapy. *British Journal of Radiology, 25,* 395–405.

Jolles, B., 1962. X-ray sieve therapy of pelvic tumors. *Proceedings of the Royal Society of Medicine, 55,* 493–498.

Joyet, G. & Hohl, K., 1953. Die Biologische Hautreaktion in der Tiefentherapie als Function der Feldgrosse. Ein Gesetz der Strahlentherapie. *Fortschritte auf dem gebiete der Röntgenstrahlung, 82,* 387–400.

Kohler, A., 1909. Zur Röntgentieftherapie mit massendosen. *München med. Wochenschrift, 56,* 2314–2316.

Liberson, F., 1933. The value of a multi-perforated screen in deep X-ray therapy. *Radiology, 20,* 186–195.

MacKee, G. M., Mutscheller, A. & Cipollaro, A. C., 1943. The area factor in roentgen irradiation. *Archives of Dermatology and Syphilology (Chicago), 47,* 657–664.

Marks, H., 1952. Clinical experience with irradiation through a grid. *Radiology, 58,* 338–341.

Maruyama, Y., Yaes, R. J., Urano M., Patel, P. & Hernandez, J. D., 1989. Stem-cell depletion and grid therapy. *British Journal of Radiology, 62,* 386–387.

Massey, J. B., 1970. In *Manual of Dosimetry in Radiotherapy* (International Atomic Energy Agency, Vienna), pp. 59–60.

Rodé, I., 1962. Clinical and economic significance of massive grid irradiation in the therapy of breast cancer. *Acta Chirurgica Acad. Sci. Hungarica, 3,* viii–xx.

Tenzel, W. V., 1952. Experience with grid therapy. *Radiology, 59,* 399–408.

Trott, K.-R., Maciejewski, B., Preuss-Bayer, G. & Skolyszewski, J., 1984. Dose-response curve and split-dose recovery in human skin cancer. *Radiotherapy and Oncology, 2,* 123–129.

1990, *The British Journal of Radiology*, *63*, 875–881

The relative biological effectiveness of fractionated doses of fast neutrons (42 $\mathrm{MeV}_{d\rightarrow Be}$) for normal tissues

III. Effects on lung function

By M. Rezvani, *D. W. H. Barnes, J. W. Hopewell, M. E. C. Robbins, *J. M. Sansom, *P. J. V. Adams and R. Hamlet

CRC Normal Tissue Radiobiology Research Group, Research Institute (University of Oxford), Churchill Hospital, Oxford OX3 7LJ and *MRC Radiobiology Unit, Chilton, Didcot, Oxfordshire OX11 0RD

(*Received April 1990 and in revised form July 1990*)

Abstract. The effect of single and fractionated doses of fast neutrons (42 $\mathrm{MeV}_{d\rightarrow Be}$) on the early and late radiation responses of the pig lung have been assessed by the measurement of changes in lung function using a ^{133}Xe washout technique. The results obtained for irradiation schedules with fast neutrons have been compared with those after photon irradiation. There was no statistically significant difference between the values for the relative biological effectiveness (RBE) for the early and late radiation response of the lung. The RBE of the neutron beam increased with decreasing size of dose/fraction with an upper limit value of 4.39 ± 0.94 for infinitely small X-ray doses per fraction.

The historical development of neutron-therapy and the underlying radiobiological rationale have been discussed extensively (*e.g.* Field, 1976; Brennan, 1977; Fowler, 1981). However, there remain few detailed data on the relative biological effectiveness (RBE) of fast neutrons for different normal tissues and, in particular, for the higher energy neutrons that are now being produced by the new generation of hospital-based cyclotrons.

Relative biological effectiveness values have been found to vary considerably; they are tissue-dependent and are said to be greater for late effects than for early effects (Withers et al, 1978, 1982). The RBE, as was suggested earlier, also varies with fraction size (Hopewell et al, 1988) and with neutron energy (Hall et al, 1975; Kellerer et al, 1976). Considering these different parameters, there is still a great deal to be explored about appropriate RBE values for fast neutrons and their applicability in radiotherapy.

Previous reports on the RBE of fast neutrons for lung tissue have been based on studies with lower energy neutrons (Geraci et al, 1976; Hornsey, 1982; Parkins & Fowler, 1985; Parkins et al, 1985; Herrmann et al, 1986). This paper is one of a series which describe the results of an extensive experimental programme designed to determine the RBE for higher energy neutrons (42 $\mathrm{MeV}_{d\rightarrow Be}$) specifically for late effects in the normal tissues of the pig. The energy of these neutrons is comparable with those produced by the new generation of hospital based cyclotrons now being used for fast neutron therapy (*e.g.* Bonnett et al, 1988). The first two reports in this series (Hopewell et al, 1988, 1990) described the initial epidermal, the later dermal, and late cutaneous and subcutaneous responses of pig skin to fast neutrons. This paper describes the relatively early (pneumonitic) and late (fibrotic) responses of pig lung to single and fractionated doses of fast neutrons and provides information on the variation in RBE for these lung responses after irradiation with this 42 $\mathrm{MeV}_{d\rightarrow Be}$ produced neutron beam.

Materials and methods

Seventy-seven female pigs of the Large White strain were used in these investigations. Animals were brought into the animal house when they were approximately 12 weeks of age (weight 20–25 kg) and were allowed an acclimatization period of at least 2 weeks before any experimental procedures were undertaken. Prior to irradiation the position of the fully ventilated basal lobe of the left lung was determined fluoroscopically and included in a 10 cm × 20 cm triangular shaped field tattooed on the overlying skin. In each animal this field was irradiated with either a single or fractionated dose of fast neutrons using the Variable Energy Cyclotron (VEC) at the Atomic Energy Research Establishment (AERE), Harwell. The physical characterization of this beam has been described in detail previously (Goodhead et al, 1977). Neutrons were produced by the bombardment of a 2 mm thick, gold-backed beryllium target with 42 MeV deuterons. The target to skin surface distance was 150 cm, giving a dose-rate of 0.36–0.55 Gy/min. The quoted doses refer to those at the centre of the fully ventilated lobe of the irradiated lung without a correction for changes in tissue density. The irregular shape of the irradiated lung tissue resulted in a maximum dose variation, across the fully ventilated lung, of ±14%. However, the average dimensions of the lung suggested that a ±9.5% variation in total dose across the lung was more representative. Irradiations were with single doses, 6 or 12 fractions in 18 days and 6, 12 or 30 fractions in 39 days; four to six dose levels were used for each of the dose fractionation regimes.

All procedures were carried out with the animals under anaesthesia, which was maintained with 2% halothane, ~30% nitrous oxide and ~70% oxygen.

Animals were intubated and a closed, non-rebreathable system was used for the irradiations and the subsequent lung function studies. Lung function tests were performed prior to irradiation and then at 13-weekly intervals until 104 weeks after irradiation. The timing of the lung function tests, for irradiation schedules given over 18 days and 39 days, was related to the midpoint of the schedule. Each animal was tested twice on each occasion using a standard ^{133}Xe washout technique, details of which have been described previously (Rezvani & Hopewell, 1986). Briefly, 37–185 MBq (depending on the size of the animal) of ^{133}Xe in saline (370 MBq/ml) was injected as a bolus via an ear vein. The accumulation and clearance of the ^{133}Xe from comparable areas of the irradiated and unirradiated lung, in the same animal, was recorded using two matched, collimated, NaI scintillation detectors. Activity counts against time were integrated over intervals of 0.4 s using a multichannel analyser. Counts were collected for a total period of 160 s. Prior to each functional assessment the position of comparable areas of the left and right lung was established using X-ray fluoroscopy.

The time–activity curves obtained were normalized by taking the peak radioactivity over each lung as 100%. The clearance part of the time–activity curve for each lung was then analysed using a two compartment model (Rezvani & Hopewell, 1986). From each time–activity curve a rate constant for the clearance of ^{133}Xe, which represented the gas exchange capacity of that lung, was obtained. Changes in the function of the irradiated lung were assessed as a "functional index" obtained by the comparison of the rate-constant obtained for the irradiated lung with respect to that of the contralateral unirradiated lung in the same animal. In order to convert these quantitative measurements into quantal data, a threshold level of impairment in lung function of $\geqslant 15\%$ was set for the variation in the function of the irradiated left lung with respect to the unirradiated right lung in the same animal. Thus, any irradiated lung which had a functional index of $\leqslant 85\%$ was considered to be affected. The number of lung function tests showing this response *versus* the number of tests performed in each dose group was scored and classified into different groups according to the time after irradiation, *i.e.* 13–26 weeks for the early (pneumonitic) phase and 39–104 weeks for the late (fibrotic) phase. These quantal data were analysed by probit analysis (Finney, 1964) and ED$_{50}$ values ($\pm$SE) determined. To establish RBE values these results were compared with those obtained previously after irradiation with single and fractionated doses of photons. The results of these studies have been described in detail elsewhere (Rezvani & Hopewell, 1990).

At 104 weeks after irradiation, animals were sacrificed by nitrous oxide asphyxiation. The lungs were infused, *in situ*, with 10% formal-saline at an inflation pressure of 25 cm of fixation fluid. After the lungs had been removed from the thorax they were fixed for a further 2–3 weeks in a 10% formal-saline bath before samples were taken for histology.

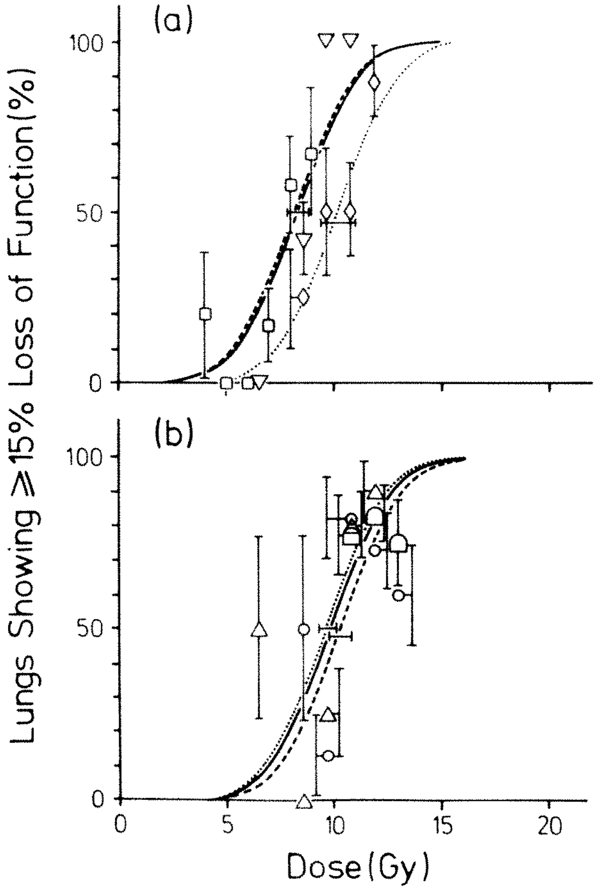

Figure 1. Dose–effect curves indicating the variation in the incidence of $\geqslant 15\%$ loss of lung function in animals irradiated with doses of fast neutrons (42 MeV$_{d\to Be}$) given as (a) a single dose (□—□), 6 F/18 days (▽--▽) or 12 F/18 days (◇···◇), and (b) 6 F/39 days (△—△), 12 F/39 days (▢--▢) or 30 F/39 days (○···○). The period of assessment was from 13–26 weeks after irradiation. Error bars indicate ±SE.

Results

Lung function tests

The dose-related changes in the percentage of lung function tests showing a $\geqslant 15\%$ reduction in function (relative to the unirradiated lung in the same animal) for the time period 13–26 weeks after irradiation are shown in Fig. 1. These dose–effect curves have been drawn parallel to each other since there was no significant difference ($p > 0.5$) between the slopes of the curves for the different fraction schedules. The ED$_{50}$ values obtained from this analysis are listed in Table I along with the comparable values previously reported after ^{60}Co or X irradiation (Rezvani & Hopwell, 1990). The ED$_{50}$ values for the different irradiation schedules with fast neutrons were not significantly different from each other ($p > 0.2$).

Dose–effect curves for the time period 39–104 weeks after irradiation are shown in Fig. 2 and the ED$_{50}$ values

Table I. Variation in ED_{50} values ($\pm$SE) for a $\geqslant 15\%$ reduction in lung function after irradiation with single and fractionated doses of either photons or fast neutrons (42 $MeV_{d \to Be}$), assessed at 13–26 weeks after irradiation (early damage)

Fractionation (fraction/days)	ED_{50} iso-effect doses (Gy)		
	Photons	Neutrons	RBE ($\pm$SE)
Single dose	10.12 ± 0.33^a	8.52 ± 0.50	1.19 ± 0.08
6/18	17.19 ± 2.46	8.51 ± 0.53	2.02 ± 0.31
12/18	26.30 ± 2.40^b	10.19 ± 0.52	2.58 ± 0.27
6/39	22.53 ± 4.13	9.59 ± 0.52	2.35 ± 0.45
12/39	30.44 ± 3.50^b	10.06 ± 0.60	3.03 ± 0.39
30/39	45.29 ± 3.95	9.50 ± 0.51	4.77 ± 0.49

The ED_{50} for photon exposure were those reported by Rezvani and Hopewell (1990) after irradiation with fractionated doses of 250 kV X rays or after single doses of ^{60}Co γ rays^a. The ED_{50} values for 12 F in 18 or 39 days were obtained by extrapolation from the X ray iso-effect plots^b.

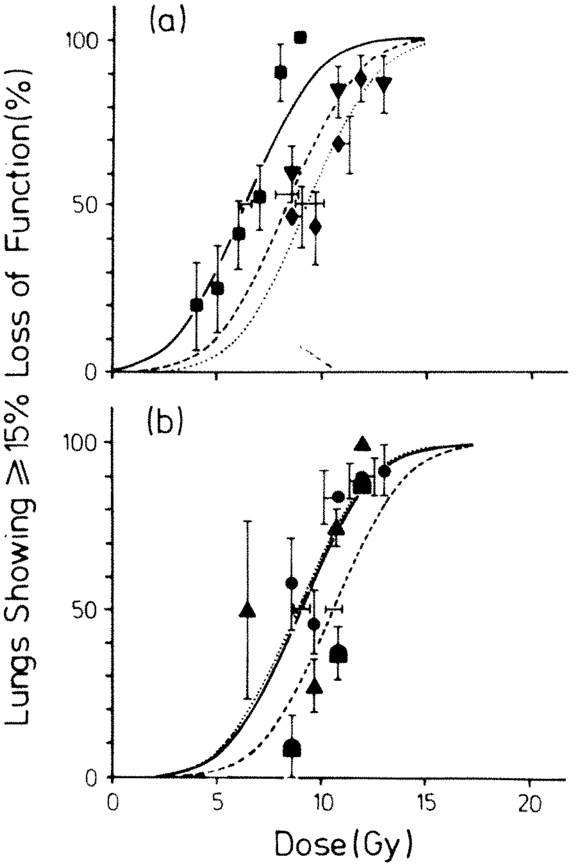

Figure 2. Dose–effect curves indicating the variation in the incidence of a $\geqslant 15\%$ loss of lung function in animals irradiated with doses of fast neutrons (42 $MeV_{d \to Be}$) given as (a) a single dose (■—■), 6 F/18 days (▼---▼) or 12 F/18 days (◆···◆), and (b) 6 F/39 days (▲—▲), 12 F/39 days (☗ ☗) or 30 F/39 days (●···●). The period of assessment was from 39–104 weeks after irradiation. Error bars indicate $\pm$SE.

obtained from these curves are listed in Table II. For this later effect the ED_{50} value for the single dose study was significantly lower than that for the different fractionated irradiation schedules ($p < 0.02$). No significant effect of dose fractionation was found for doses given in 18 days. For an overall treatment time of 39 days the ED_{50} values for 6 F and 30 F were not significantly different from each other; however, the ED_{50} value for 12 F was apparently significantly higher ($p = 0.03$) than the ED_{50} values for the 6 F and 30 F schedules. There was no significant difference between the ED_{50} values obtained for fractionated schedules involving an equal number of fractions delivered over 18 days or 39 days.

When the variation in ED_{50} values for fractionated doses of fast neutrons, for the early effect, was compared with fraction number, on a log–log plot, independent of the overall treatment time, a regression line with a slope of 0.04 ± 0.06 was obtained. The value of the slope was not significantly different from zero ($p = 0.52$). Moreover, although inclusion of the single-dose data from the analysis changed the slope of the regression line slightly, *i.e.* 0.05 ± 0.03, it was still not significantly different from zero ($p = 0.15$). In addition, there was no significant effect of overall treatment time; a time exponent of 0.05 ± 0.09 was obtained, which was not significantly different from zero ($p = 0.59$).

For the late reaction seen after irradiation with fractionated doses of fast neutrons the ED_{50} values were similar to those obtained for the early effect ($p > 0.4$). Therefore, the exponents of fraction number (N) and time (T) of 0.03 ± 0.07 and 0.08 ± 0.11, respectively, were again not significantly different from zero ($p > 0.5$). Inclusion of the single-dose data in the analysis increased the slope of the regression line to the log–log plot of ED_{50} values against number of fractions, with a resulting slope of 0.12 ± 0.05 which just reached the accepted level of statistical significance ($p = 0.05$). This was because the ED_{50} value for the late effect, after a single dose, was significantly lower than that for the early effect ($p = 0.01$).

Because of the similarities in the results for the early and late changes following fast neutron irradiation the data have been combined (Fig. 3). The regression line fitted to the combined data, irrespective of the overall treatment time, indicated a fraction exponent of 0.04 ± 0.04 which was again not significantly different from zero ($p = 0.04$). However, inclusion of the single-dose data resulted in a slope of 0.08 ± 0.03 which was significantly different from zero ($p = 0.01$). When the effects of overall treatment time were examined for these combined data, independent of the number of fractions, a time exponent of 0.07 ± 0.06 was obtained which was not significantly different from zero ($p = 0.3$). Use of a multivariate analysis, which allowed for a simultaneous optimization of the N- and T-exponents, to the data resulted in values of 0.02 ± 0.05 and 0.07 ± 0.07 for the

Table II. Variation in ED_{50} values (±SE) for a $\geqslant 15\%$ reduction in lung function after irradiation with single and fractionated doses of either photons or fast neutrons (42 MeV$_{d\to Be}$), assessed at 39–104 weeks after irradiation (late damage)

Fractionation (fraction/days)	ED_{50} iso-effect doses (Gy)		
	Photons	Neutrons	RBE (±SE)
Single dose	9.73±0.34[a]	6.41±0.38	1.52±0.10
6/18	15.71±1.43	8.40±0.50	1.87±0.20
12/18	24.59±1.88[b]	9.38±0.37	2.62±0.23
6/39	17.13±2.64	8.98±0.39	1.91±0.30
12/39	24.17±2.13[b]	10.58±0.38	2.28±0.22
30/39	38.11±2.50	8.94±0.43	4.26±0.35

The ED_{50} for photon exposure were those reported by Rezvani and Hopewell (1990) after irradiation with fractionated doses of 250 kV X rays or after single doses of ^{60}Co γ rays[a]. The ED_{50} values for 12 F in 18 or 39 days were obtained by extrapolation from the X-ray iso-effect plots[b].

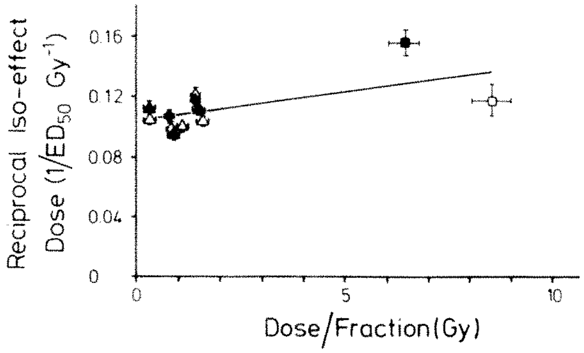

Figure 4. Plot of the reciprocal of ED_{50} iso-effect dose ($1/ED_{50}$) for a $\geqslant 15\%$ reduction in lung function against neutron dose/fraction. Data points are plotted for the early effect from 13–26 weeks (□, ◇, △) and the late effect from 39–104 weeks (■, ◆, ▲) after irradiation. Fractionated irradiation was given over 18 days (◇, ◆) or 39 days (△, ▲). The linear regression line was fitted through all data points ($r = 0.64$). Error bars indicate ±SE.

N- and *T*-exponents, respectively. None of these values was significantly different from zero ($p > 0.45$).

In an alternative analysis, assuming the applicability of the linear quadratic model of cell survival, a plot was made of the reciprocal of the ED_{50} values ($1/ED_{50}$) against the neutron dose/fraction (Fig. 4). The α/β ratios obtained from such plots were 58.63±35.43 Gy and 11.69±2.44 Gy for the early and late effects, respectively. These α/β ratios were not significantly different from each other, and in the case of that for the early effect it was not significantly different from zero ($p = 0.2$). For the combined data for early and late effects the α/β ratio was 26.26±3.83 Gy. This was significantly different from zero ($p = 0.03$). When the single-dose data was excluded from this analysis the α/β ratio of 17.46±17.44 Gy was not significantly different from zero ($p > 0.34$).

The variations in the RBE of fast neutrons with dose fractionation, for both early and late effects on the lung are listed in Tables I and II; the RBE increases with increasing fraction number. The variation in RBE with X-ray dose/fraction is illustrated in Fig. 5. There was no significant difference in the relationship between the RBE and X-ray dose/fraction for the early and the late effect to the lung: for the combined data the relationship, on a log–log plot, was adequately described by a straight line with a slope of −0.52±0.1.

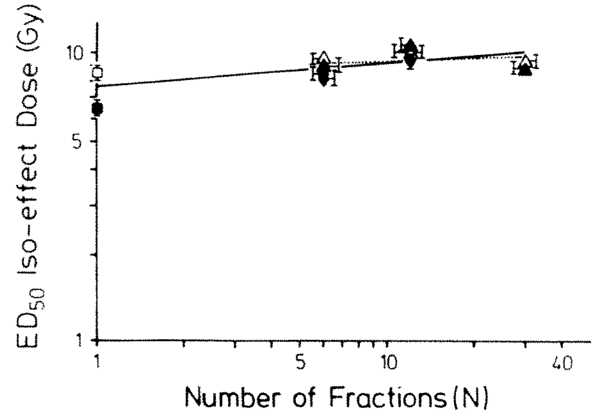

Figure 3. Log–log plot of iso-effect ED_{50} doses of fast neutrons for a $\geqslant 15\%$ reduction in lung function against the number of fractions, assessed from 13–26 weeks (□, ◇, △) or from 39–104 weeks (■, ◆, ▲) after irradiation. Fractionated irradiation was given over 18 days (◇, ◆) or 39 days (△, ▲). Linear regression analysis was carried out either including (—) or excluding (·····) the single dose results. The associated linear correlation coefficients were 0.69 and 0.3, respectively. Error bars indicate ±SE.

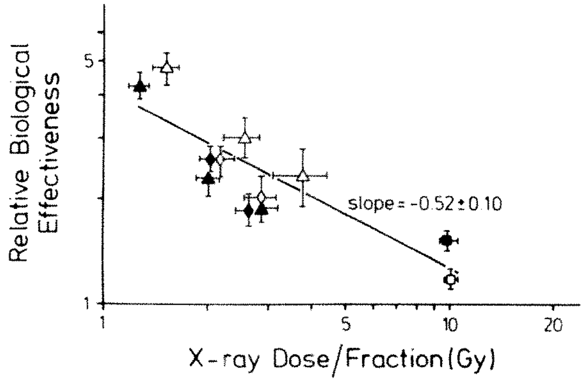

Figure 5. Log–log plot of RBE values against X ray dose/fraction for both the early effect in pig lung from 13–26 weeks (□, ◇, △) and the late effect from 39–104 weeks (■, ◆, ▲) after irradiation. Fractionated irradiation was given over 18 days (◇, ◆) or 39 days (△, ▲). The linear regression line was fitted through all data points ($r = 0.86$). Error bars indicate ±SE.

Histological changes

On post mortem examination, at 104 weeks after irradiation, four of the animals showed adhesions between the irradiated lung and the chest wall. However, this occurred at a similar frequency (6%) between the unirradiated right lobe of the lung and the chest wall.

The most prominent gross feature of the lungs of all the animals irradiated with single doses of >7 Gy of fast neutrons was an atrophy of the irradiated lobe of the left lung. Similar changes were seen after slightly higher fractionated doses of fast neutrons.

In animals showing atrophy of the irradiated lobe of the left lung the histological changes were characterized by the presence of thick bundles of collagen fibres and evidence of tissue degeneration. Collagen accumulation was found in the interlobular septa and alveolar walls; in places there was evidence of local gross scar tissue formation. After lower doses where there was no gross evidence of lung damage, however, some focal fibrotic lesions were found, *e.g.* even in some animals receiving the lowest single dose of 4 Gy.

Discussion

The post mortem appearance and histological changes found in pig lung after fast neutron irradiation were similar to those seen after photon irradiation (Rezvani et al, 1989). This had been anticipated since no qualitative differences had previously been reported in the morphological effects of photon and fast neutron on the lung of mice (Field & Hornsey, 1974) and rabbits (Bradley et al, 1979). The relationship between functional and morphological changes has already been evaluated in pig lung (Rezvani et al, 1989).

It has also been proposed previously, on the basis of assessments of lung function in the pig using the ^{133}Xe washout technique, that late effects in the lung of pig might be a continuation of the earlier damage (Rezvani et al, 1989; Rezvani & Hopewell, 1990). The present results of functional studies obtained after the irradiation of pig lung with fast neutrons support this hypothesis; there was no significant difference between the ED_{50} values obtained for the impairment of lung function for the early and late periods of assessment after fractionated irradiation.

The ED_{50} values obtained from dose–effect curves clearly indicate that the lung is more sensitive to higher LET radiation than to photons. From a comparison of these ED_{50} values it would appear that the response of pig lung was not modified significantly by fractionation of the neutron dose. The N-exponent of 0.04 ± 0.04 and T-exponent of 0.07 ± 0.06, in a modified nominal standard-dose formula, were not significantly different from zero and the N-exponent only became significant after the inclusion of the single-dose data in the analysis. This suggests a small effect of dose fractionation between a single dose and fractionated doses for pig lung for fast neutrons. This is in agreement with the findings of Hornsey et al (1975) and Parkins et al (1985) who only observed a fractionation effect between single dose and a small number of dose fractions but not between 2 and 20 fractions for fast neutrons of a lower energy. In studies on pig skin, using comparable fractionation schedules, with the same neutron beam as used in the present studies a small, but significant, effect of fractionation was found for the endpoint of dermal necrosis of 0.038 (Hopewell et al, 1988), whereas for late cutaneous and subcutaneous lesions there was no significant effect of dose fractionation between 6 and 30 fractions (Hopewell et al, 1990). For both endpoints in the skin the changes from a single dose to 6 fractions produced the largest increase in ED_{50} values. A T-exponent of 0.07 ± 0.06 suggests that there was no significant effect of overall treatment time for neutron irradiation of pig lung. This is in agreement with the findings of Hornsey (1982) who reported no sparing of damage to lung by extending the overall treatment time with fast neutrons; nor indeed was there any strong evidence for such a time factor for late changes in pig skin after neutron irradiation (Hopewell et al, 1990).

The α/β ratios obtained for early and late effects were 58.63 ± 35.43 Gy and 11.69 ± 2.44 Gy, respectively. These values were not significantly different from each other and the α/β ratio for the combined data was 26.26 ± 3.83 Gy. Parkins et al (1985) reported α/β ratios of 18–48 Gy for mouse lung irradiated with lower energy neutrons. These authors suggested a decreasing α/β ratio with increasing time of assessment from 26–68 weeks after irradiation. Comparable α/β ratios would not be expected from these two studies because of the different neutron beam energies.

Although there was no statistically significant difference between the RBE values for fast neutrons for early and late effects on the lung, there was a slight tendency towards lower values for the later effect. This trend supports the findings of Parkins et al (1985) who also reported a slight but not significant difference between the RBE for neutrons for acute (28 weeks) as compared with later lung damage in mice, at least for some fractionation schedules. A similar trend was found with increasing latency in pig skin (Hopewell et al, 1990). In studies on the lung of dogs Bradley et al (1981) assessed effects using a number of functional parameters for up to 104 weeks after irradiation. Fractionation irradiation with total doses of photons within the clinical range of 40–60 Gy were used. For the majority of the parameters they reported RBE values for fast neutrons of >4, in keeping with the present findings. However, considerably higher values were sometimes obtained. These authors did not observe any significant difference in the RBE values obtained by measuring perfusion and ventilation from 13–104 weeks of irradiation. When assessing lung density the results suggested a tendency for an increase in RBE with increasing time of follow up after irradiation. This disparity could be a result of variation in the endpoints or the method of assessment. The limitations of the results obtained by densitometric methods have been discussed by Lehnert and Al-Khatib (1989).

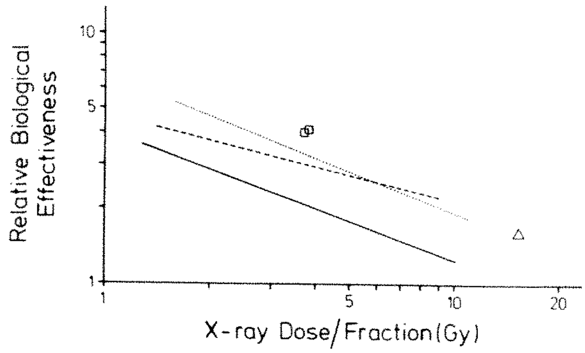

Figure 6. Comparison of the variation in RBE values with X-ray dose/fraction for lung tissue after irradiation with different quality neutron beams. [42 $\text{MeV}_{d\rightarrow Be}$, present study (—), 16 $\text{MeV}_{d\rightarrow Be}$, Hornsey, 1982 (---); 4 $\text{MeV}_{d\rightarrow Be}$, Parkins et al, 1985 (·········); 6.2 MeV neutrons, Herrmann et al, 1986 (□) and 22 $\text{MeV}_{d\rightarrow Be}$, Geraci et al, 1976 (△).]

From a comparison of the *y*-intercepts and the α/β ratios obtained from the Fe-plots for both X rays and fast neutrons, a limiting upper value of the RBE can be calculated for vanishing small X-ray doses/fraction. Applying this procedure a limiting RBE value of 4.39 ± 0.94 was obtained for lung tissue irradiated with fast neutrons (42 $\text{MeV}_{d\rightarrow Be}$); a value not significantly different ($p < 0.01$) from that obtained for the dermal tissue of the pig for the same energy of neutrons of 4.32 ± 0.39 (Hopewell et al, 1988). A limiting value of 5–9 was reported for lower energy neutrons (4 $\text{MeV}_{d\rightarrow Be}$) for mouse lung (Parkins et al, 1985).

There was a strong influence of fraction size on the RBE values. The RBE value decreased markedly with increasing fraction size for X-ray doses/fraction of 1.27–10.12 Gy. The relationship between the RBE value and X-ray dose/fraction could be adequately described by a straight line with a slope of -0.52 ± 0.10 (Fig. 6). A similar trend was reported for neutrons produced by 4 $\text{MeV}_{d\rightarrow Be}$ (Parkins et al, 1985) and 16 $\text{MeV}_{d\rightarrow Be}$ (Hornsey, 1982). The value of -0.55 ± 0.03 for the slope of the line fitted to data of Parkins et al (1985) was similar to that obtained for the present study; however, the line fitted to data of Hornsey (1982) was shallower; a slope of -0.33 ± 0.01 was obtained, more in agreement with that previously reported for late damage to pig skin of -0.34 ± 0.03 (Hopewell et al, 1990). In both these reports the RBE values were higher than those for 42 $\text{MeV}_{d\rightarrow Be}$ produced neutrons. The difference between the RBE for 16 $\text{MeV}_{d\rightarrow Be}$ and 42 $\text{MeV}_{d\rightarrow Be}$ produced neutrons varied, ranging from 25–55%, the difference increasing with increasing fraction size. This is considerably higher than the difference of 20% reported by Bewley et al (1976) for acute skin and intestinal reactions. The energy-dependent distribution of RBE values is also illustrated in Fig. 6 which clearly supports the previously reported neutron-energy dependency of RBE values (Hall et al, 1975; Kellerer et al, 1976). The same effect has been observed for the RBE of different energy neutrons for skin reactions in the mouse (Joiner & Field, 1988).

Thus in conclusion there was no significant difference between the RBE for early and late damage to the lung of pigs. Moreover, for infinitely small X-ray doses/fraction, the upper limiting RBE for lung was similar to that for late damage to skin at ~4.35. However, for X-ray doses/fraction of between 1.5 and 9 Gy, the RBE for the lung decreased more rapidly than that for the skin (Hopewell et al, 1990) suggesting that the risks of severe late complications to the lung after neutron therapy are less than those for the skin at clinically used doses/fraction.

Acknowledgments

The authors gratefully acknowledge the support and collaboration of the staff of the Churchill Hospital Research Institute, the MRC Radiobiology Unit and the team at the AERE Variable Energy Cyclotron, without whose help this whole series of experiments could not have been carried out. Specific thanks are given to D. T. Goodhead and D. A. Bance for the calibration of the beam line, D. C. Campling, M. J. Corp and T. K. Yeung for dosimetry, with P. Gray and A. Thompson providing back-up electronics support. P. C. Bates, F. W. Dickinson, N. Hubbard and P. C. Monk are thanked for the help with the anaesthesia and care of animals, R. H. Simmonds, J. F. Knowles, C. M. A. Young and G. Wiernik for help with the irradiations, and Z. Rezvani for assistance in data analysis. The work was jointly supported by the Cancer Research Campaign and the Medical Research Council, including a special MRC Programme Grant awarded to Dr J. W. Hopewell.

References

Bewley, D. K., Cullen, B., Field, S. B., Hornsey, S., Page, B. C. & Berry, R. J., 1976. A comparison for use in radiotherapy of neutron beams generated with 16 and 42 MeV deutrons on beryllium. *British Journal of Radiology*, *49*, 360–366.

Bonnet, D. E., Blake, S. W., Shaw, J. E. & Bewley, D. K., 1988. The Clatterbridge high energy neutron facility: specification and performance. *British Journal of Radiology*, *61*, 38–46.

Bradley, E. W., Zook, B. C., Casarett, G. W., Mossman, K. L. & Rogers, C. C., 1979. Effects of fast neutrons on rabbits. II. Comparison of pathologic effects of fractionated neutron and photon exposures of the lung and spinal cord. *International Journal of Radiation Oncology, Biology, Physics*, *5*, 795–802.

Bradley, E. W., Alderson, P. O., McWhorter, R. E., Vieras, F., Olmsted, W. W., Fisher, M. P. & Rogers, C. C., 1981. A comparison of neutron RBE values for normal canine lung by densitometry, pulmonary function and radionuclide studies. *International Journal of Radiation Oncology, Biology, Physics*, *7*, 1055–1064.

Brennan, J. T., 1977. History of the use of neutrons in radiation therapy. *International Journal of Radiation Oncology, Biology, Physics*, *3*, 143–148.

Catterall, M., Sutherland, I. & Bewley, D., 1975. First results of a randomized clinical trial of fast neutrons compared with X- or gamma rays in treatment of advanced tumours of the head and neck. *British Medical Journal*, *2*, 653–656.

Field, S. B., 1976. A historical survey of radiobiology and radiotherapy with fast neutrons. *Current Topics in Radiation Research Quarterly, 11*, 1–86.

Field, S. B. & Hornsey, S., 1974. Damage to mouse lung with neutrons and X-rays. *European Journal of Cancer, 10*, 621–627.

Finney, D. J., 1964. *Probit Analysis, 2nd edn* (Cambridge University Press, London).

Fowler, J. F., 1981. *Medical Physics Hand Books, 8, Nuclear Particles in Cancer Treatment* (Adam Hilger, Bristol).

Geraci, J. P., Jackson, K. L., Christensen, G. M., Parker, R. G., Thrower, P. D. & Fox, M., 1976. Single dose fast neutron RBE for pulmonary and esophageal damage in mice. *Radiology, 120*, 701–704.

Goodhead, D. T., Berry, R. J., Bance, D. A., Gray, P. & Stedeford, J. B. H., 1977. High energy fast neutrons from the Harwell variable energy cyclotron. I. Physical characteristics. *American Journal of Roentgenology, 129*, 709–716.

Hall, E. J., Novak, J. K., Kellerer, A. M., Rossi, H. H., Marino, S. & Goodman, L. J., 1975. RBE as a function of neutron energy. I. Experimental observations. *Radiation Research, 64*, 245–255.

Herrmann, T., Voigtmann, L., Knorr, A., Lorenz, J., Johannsen, U. & Welker, K., 1986. Fractionated lung irradiation in young pigs with 6.2 MeV neutrons and cobalt-60. *Radiotherapy and Oncology, 7*, 69–75.

Hopewell, J. W., Barnes, D. W. H., Robbins, M. E. C., Sansom, J. M., Knowles, J. F. & van den Aardweg, G. J. M. J., 1988. The relative biological effectiveness of fractionated doses of fast neutrons (42 $\mathrm{MeV}_{d \rightarrow Be}$) for normal tissues in the pig. I. Effects on the epidermis and dermal vascular/connective tissues. *British Journal of Radiology, 61*, 928–938.

Hopewell, J. W., Barnes, D. W. H., Robbins, M. E. C., Corp, M., Sansom, J. M., Young, C. M. A. & Wiernik, G., 1990. The relative biological effectiveness of fractionated doses of fast neutrons (42 $\mathrm{MeV}_{d \rightarrow Be}$) for normal tissues in the pig. II. Late effects on cutaneous and subcutaneous tissues. *British Journal of Radiology, 63*, 760–770.

Hornsey, S., 1982. RBE for lung and cord. *International Journal of Radiation Oncology, Biology, Physics, 8*, 2099–2102.

Hornsey, S., Kutsutani, Y. & Field, S. B., 1975. Damage to mouse lung with fractionated neutrons and X rays. *Radiology, 116*, 171–174.

Joiner, M. C. & Field, S. B., 1988. The response of mouse skin to irradiation with neutrons from the 62 MV cyclotron at Clatterbridge, U.K. *Radiotherapy and Oncology, 12*, 153–166.

Kellerer, A. M., Hall, E. J., Rossi, H. H. & Teedla, P., 1976. RBE as a function of neutron energy. II. Statistical analysis. *Radiation Research, 65*, 172–186.

Lehnert, S. & El-Khatib, E., 1989. The use of CT densitometry in the assessment of radiation-induced damage to the rat lung: A comparison with other endpoints. *International Journal of Radiation Oncology, Biology, Physics, 16*, 117–124.

Parkins, C. S. & Fowler, J. F., 1985. Repair in mouse lung of multifraction X rays and neutrons: extension to 40 fractions. *British Journal of Radiology, 58*, 1097–1103.

Parkins, C. S., Fowler, J. F., Maughan, R. L. & Roper, M. J., 1985. Repair in mouse lung for up to 20 fractions of X rays or neutrons. *British Journal of Radiology, 58*, 225–241.

Rezvani, M. & Hopewell, J. W., 1986. The validity of different methods of analysis of ^{133}Xe washout curves for the determination of lung function. *Nuclear Medicine and Biology, 13*, 245–251.

Rezvani, M. & Hopewell, J. W., 1990. The response of the pig lung to fractionated doses of X rays. *British Journal of Radiology, 63*, 41–50.

Rezvani, M., Heryet, J. C. & Hopewell, J. W., 1989. Effects of single doses of radiation on pig lung. *Radiotherapy and Oncology, 14*, 133–142.

Withers, H. R., Thames, H. D., Hussey, D. H., Flow, B. L. & Mason, K. A., 1978. Relative Biological Effectiveness (RBE) of 50MV (Be) neutrons for acute and late skin injury. *International Journal of Radiation Oncology, Biology, Physics, 4*, 603–608.

Withers, H. R., Thames, H. D. & Peters, L. J., 1982. Biological basis for high RBE values for late effects of neutron irradiation. *International Journal of Radiation Oncology, Biology, Physics, 8*, 2071–2076.

1990, *The British Journal of Radiology*, *63*, 882–883

Technical notes

A rapid method of production of irregular-shaped fields for use with patients receiving electron radiotherapy

By J. H. Plane, BA, MSc and C. Usher, BSc, MSc

Regional Medical Physics Department, South Cleveland Hospital, Marton Road, Middlesbrough, Cleveland TS4 3BW

(*Received March 1990 and in revised form April 1990*)

This technical note describes a method to produce irregularly-shaped electron fields using a polystyrene shape to form the irregular outline, low melting point alloy and modified electron applicators. The method supports a procedure for irregular-field electron therapy which is rapid, cheap, accurate and provides a permanent record of the field treated.

Physical requirements

A recently commissioned linear accelerator (Siemens M7145) was supplied with five applicators (50 mm circle and squares of side 100, 150, 200 and 250 mm) for radiotherapy with electrons in the energy range 5–14 MeV.

Whilst the applicators provide an adequate range of field size the shape of each field was restrictive. A variable electron applicator (available from the manufacturer) suffered from two disadvantages. First, the weight (approx. 15 kg) was excessive and, secondly, the shape of any chosen field size included straight edges. A method has been developed which removes these restrictions and satisfies several criteria, namely rapid, accurate and applicable up to the largest field size and electron applicator.

Existing methods using stainless steel suffer from the disadvantages of consuming both time and non-recycleable material. An improved alternative was sought.

Several methods were devised but each proved unsuccessful. The preferred method was to modify each applicator. It can be seen in Fig. 1 that a step was milled in the inside edge of each applicator 5 mm wide and 10 mm deep. Two retaining pins were manufactured and added to each applicator. The open applicator was assessed to ensure that the dose distribution had not changed by means of a three-dimensional beam data acquisition system (Wellhofer 600, NE Ltd). Separate half-moulds using steel and an aluminium base were also manufactured. This produced a cast which was smaller than the end of the modified applicator to allow for the growth of the alloy (density 9570 kg/m^3, Ostalloy 158, Fry's Metals Ltd). This also formed the recesses required for the retaining clips in the modified applicators. The mould required pre-heating to about 70°C to avoid immediate solidification of the alloy in contact with a cooler surface. This was done by circulating hot water through a copper heat exchanger. After the alloy had been poured to the required depth, the hot water supply was replaced by a cold water supply to cause solidification of the alloy within 2 minutes. The mould was then split allowing the cast to be freely removed. An example of an irregular-shaped field ready for assembly into the end of the 250 mm square applicator is shown in Fig. 1.

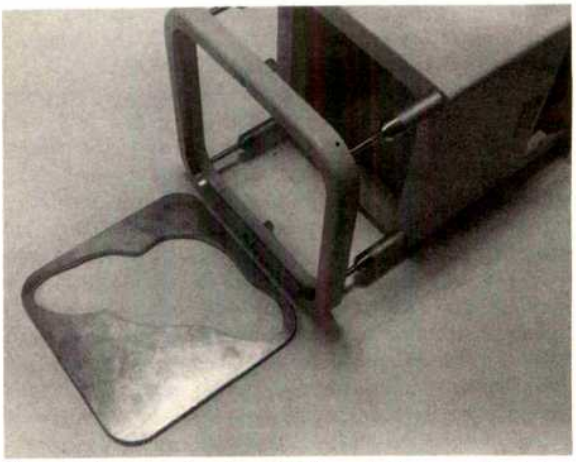

Figure 1. An irregular-shaped field ready for assembly into a 250 mm square applicator.

Radiation measurements suggested the maximum transmission through 8 mm of alloy for 14 MeV electrons and 250 mm square applicator was 5.0%. This thickness of alloy avoided any increase in skin dose under the shielded region (Klevenhagen, 1979).

Clinical requirements

Each patient requiring electron radiotherapy is seen by a Consultant Radiotherapist. The area to be irradiated is drawn on the patient's skin using an alcohol based ink. A photograph of the area on the patient's skin is produced using an instant print system (Polaroid Image System, Polaroid UK Ltd). The size and shape of this area is copied onto a sheet of transparent film in contact with the patient's skin. A lateral margin of 15 mm is added to the indicated area. On the machine concerned, this ensures that the dose at the required depth is at least 90% of the dose at peak depth. The enlarged area is cut from the transparent film and transferred onto a polystyrene block. A copy is cut from the polystyrene to form a blank. The blank is positioned as desired inside the appropriate steel mould and the remaining volume is filled with low melting point alloy as described above. The radiotherapy prescription specifies total dose, number of fractions, fraction duration and therapeutic range. The last parameter is used to select the electron energy and depth of bolus material.

Discussion

The output factor for each cut-out was measured immediately after routine dosimetry using an open 100 × 100 mm applicator had been performed. This avoided any variation in applicator output (Aird & Lambert, 1985). The protocol for electron dosimetry of the Hospital Physicists' Association was used (HPA, 1985). A limited number of cut-outs were verified using radiographic film (XOMATV, Kodak Ltd). The images showed no variations from the expected edges of the field and no gross deficiencies in the shielding properties of the alloy outside the field.

The method described has fulfilled the objectives required. The system is rapid, requiring approximately 30 minutes of workshop time. A patient can be treated as soon as 1 working day after being seen by the consultant. The method has been in routine use for approximately 6 months. Following the initial cost of raw materials, operating costs are minimized because of the availability of reusable materials to be found in most Medical Physics workshops.

Acknowledgments

The authors thank Dr J. K. Haywood for continuous encouragement, Dr S. L. Chawla and Dr P. R. C. Dunlop for clinical involvement and Mr D. K. Owst for assistance in the Medical Physics workshop.

References

Aird, E. G. A. & Lambert, G. D., 1985. Unforeseen variation in electron output with field size following modification of linear accelerator treatment head. *British Journal of Radiology*, *58*, 1229–1230.

HPA, 1985. Code of practice for electron beam dosimetry in radiotherapy. *Physics in Medicine and Biology*, *30*, 1169–1194.

Klevenhagen, S. C., 1979. *High Energy Electrons in Radiotherapy*. (Philips, Eindhoven).

Calibration of radiotherapy beams using a PC-based dosimetry recording system

By M. B. Kenny, MSc, MAIP, MACPSEM and R. M. Millar, MSc, MACPSEM

Unit of Physical Sciences, Peter MacCallum Cancer Institute, Melbourne, Victoria, Australia

(Received April 1990)

Routine calibration of radiotherapy treatment units involves the following steps:

1. radiation measurement under standardized conditions;
2. recording of the resultant data;
3. applying correction factors to the data which take into account the response of the calibrating instrument, the effects of the measurement geometry and the beam type, etc.;
4. scrutinizing the results for significant changes in output from previous calibrations and, if necessary, making appropriate adjustments to the machine's dosimetry system;
5. recording all calculations and sundry other relevant information including date, time, operator, temperature, and barometric pressure etc.;
6. issuing a calibration certificate which either states the machine output or attests that the dosimetry system is set within acceptable tolerances.

In large institutions these data may be measured by members of a team of physicists on a roster basis, and all members of the team need to be familiar with all aspects of each calibration. At the Peter McCallum Cancer Institute (PMCI), the Physical Sciences Unit calibrate 26 separate beams routinely. These beams are derived from two superficial X-ray machines, one orthovoltage machine and six linacs* and range from X-ray beams of 4 mm tissue HVT to 4 mm Cu HVT, higher energy X-ray beams of 4 MV, 6 MV, 18 MV and 25 MV and electron beams from 4 MeV to 22 MeV. There are two calibration instruments routinely used with a variety of chambers: standard Farmer type 0.6 cm^3 chambers, Marcus chambers, a Holt chamber and two 0.03 cm^3 parallel plate chambers. To keep conversant with the various procedures and correction factors, and to perform calculations and data recording with accuracy and confidence, requires continual practice and an appreciable amount of time.

To lighten the load we have developed a system using an IBM compatible PC to facilitate the entire calibration process. The design requirements are that the system should:

---

* Linacs at PMCI are: from Philips, an SL75/6, two SL75/5s and an SL25; and from Varian, a Clinac 4/100 and a 2100C.

1. guide the operator through the calibration;
2. have access to files containing all the relevant data to carry out the calibration, *i.e.* instrument correction factors for dose calculation, and machine calibration history to check for unexpected changes in output or suspected operator error;
3. record all measurements and results in a uniform easily read format;
4. backup all records automatically;
5. be user friendly, with efficient use of keystrokes and comprehensive error recovery routines so that the calibration time taken in running the system can be minimized.

In implementing these concepts, the system has been developed as a complete calibration package guiding the operator through all the steps necessary to perform the calibration. It issues instructions, records readings and performs the calculations using correction factors that it has on file. For linacs, it calculates the magnitude and direction of any adjustments required to correct the linac's dosimetry system if it has drifted significantly, and this leads to a considerable saving in calibration time by removing all the guesswork, especially where adjustments are infrequent and often poorly annotated. It has on file factors for each beam, instrument and relevant chamber. The set-up instructions it issues for each beam comprise: correct chamber, filter (for superficial or orthovoltage qualities), calibration distance, exposure time or monitor units to set, type of phantom (*i.e.* whether in air or at depth in a tissue equivalent material etc.) and field size where applicable. Calibration records are kept on disk, until the software detects that the record is long enough to fill a printed page, at which time hard copies are made. At the completion of each calibration a backup copy of the record is made automatically, and where applicable a calibration certificate is printed.

In changing from a handwritten logbook style of calibration record to a recording system which involves the temporary storage of results on a magnetic medium, it is essential that the records are always correctly backed up. To ensure that this is done the system requests that a properly labelled backup disk be inserted in the appropriate drive, which it then checks. The system will not continue until the presence of the backup disk has been verified. As a further precaution the backup disks are kept in a separate location from the main system.

The system consists of a lead-off programme and four main programmes, written in GWBASIC, to perform the individual functions of:

1. calibration (UNICAL);
2. printing the records (CALPRINT);
3. maintenance of the correction factor file (CF);
4. checking the correction factor file (CFREAD).

UNICAL is the main calibration programme described above. CALPRINT prints the pages of records. It determines the number of integral records that will fit to a page and prints them. When a file is longer than a page, the remaining records are stored back on disk where subsequent records will be appended to them. The programme which stores the instrument correction factors is CF, and is password protected for security reasons. CFREAD is a short programme which prints a list of all the instrument correction factors on file. The system is configured to run on a PC with at least two disk drives and a printer. While UNICAL is written for conditions at PMCI, the concept of the PC-based calibration system is readily adaptable to other institutes. Adapting the system to suit other radiotherapy centres would involve only changes to those parts of UNICAL which were machine specific, and most of the routines would require no changes at all. Certainly, the other three programmes would require only cosmetic changes, and then only if a different printer were used.

Since the system has been introduced, we have used it in the training of new members of staff and find that they have rapidly gained competence and are able to perform calibrations as well as the most experienced staff. All staff find the system easier to use because it does all the tedious calculations without error. Also, because the results are checked automatically, any human errors in data entry etc. are likely to be detected. If required, manual checking for errors is made easier because all entries are recorded legibly and in a standard form. The system would be particularly useful if the intention were to have a trained technician, rather than physicist, perform some or all of the routine calibration.

1990, *The British Journal of Radiology*, *63*, 885–888

Technical notes

A survey of the radiation exposures received by the staff at two cardiac catheterization laboratories

By *Brian J. McParland, PhD, FCCPM, †Josip Nosil, PhD and †Brian Burry

*Division of Radiation Physics, Cancer Control Agency of British Columbia, Victoria Cancer Clinic, Victoria V8R 1J8 and †Department of Medical Imaging, Victoria General Hospital, Victoria, BC Canada

(*Received January 1990 and in revised form April 1990*)

Staff working in cardiac catheterization laboratories receive radiation exposures from primary radiation (if any part of their body is placed within the X-ray beam) or from secondary radiation due to scatter from the patient and image intensifier and to leakage from the X-ray tube. As a result, the radiation exposure distribution over a staff member's body is expected to be non-uniform. In order to evaluate the radiation somatic risk to be assigned to an individual, and to assess the efficacy of the personal shielding used, radiation exposures must be measured at specific anatomical locations.

In the study described here, radiation exposures received by catheterization laboratory personnel were measured at various body locations in two separate laboratories over 3–5 day periods. This study was initiated as a consequence of conventional radiation monitoring by the federal regulatory agency (Bureau of Radiation and Monitoring Devices, Health and Welfare Canada), which had indicated that occasional high exposures were received by some individuals. This conventional monitoring used only a single dosimeter mounted at head level and, consequently, did not provide a measure of the exposure distribution received over the body. The exposures described here were determined using lithium fluoride thermoluminescent dosimeters (TLDs), which have been used successfully in the past for measuring radiation doses during cardiac radiological procedures (Faulkner et al, 1986). The study in one laboratory was at the Royal Jubilee Hospital (RJH) in Victoria, British Columbia, in which interventional procedures were performed almost exclusively. The study included seven cardiologists and one nurse for 25 procedures. The study in the second laboratory was at the Victoria General Hospital (VGH) which was used mainly for diagnostic procedures. This study included three cardiologists and one nurse for 18 cases.

Methods and materials

Lithium fluoride ribbons of dimensions $3.2 \times 3.2 \times 0.9$ mm were sealed in small glass vials during both the study and the calibration exposures. The TLD response to primary X-irradiation was evaluated in air against a calibrated ionization chamber, and that to scattered radiation was determined by comparing TLD measurements at various locations on the surface of an anthropomorphic phantom, exposed to a fluoroscopy beam, against ionization measurements made at the same locations. The maximum uncertainty in the exposure derived from the TLD responses was estimated to be $\pm 15\%$.

Both catheterization units examined in this study used an undercouch tube and overcouch image intensifier arrangement and operated under automatic exposure control with tube potentials and currents during fluoroscopy ranging from 63 to 105 kVp and from 2.8 to 4.5 mA. Exposure rates in air measured during fluoroscopy at the image intensifier without a patient present were 1.32 R/min and 0.5 R/min for the RJH and VGH units, respectively ($1\ \mathrm{R} = 2.58 \times 10^{-4}$ C/kg). The corresponding rates with a patient present and when operated under automatic exposure and brightness control were 54 μR/s and 20 μR/s. Cinefluoroscopy was performed with a pulsed X-ray output under automatic exposure and brightness control at 30 frames/s with tube potentials and currents ranging from 96 to 102 kVp and from 100 to 140 mA, with exposure rates of 94 μR/frame and 28 μR/frame, measured at the image intensifier for the interventional (RJH) and diagnostic (VGH) units, respectively. The total fluoroscopy and cinefluoroscopy exposure times, tube currents and voltages were recorded during each procedure.

All staff wore torso and thyroid shielding, with a minimum manufacturer-specified thickness of 0.25 mm Pb-equivalent. Only the cardiologists wore face protection (specified by the manufacturer as 0.75 mm Pb-equivalent) during the course of this study. No shielding was placed between the image intensifier and the cardiologist. The dosimeters were taped to the following locations:

thyroid shield (outside and inside);
torso shield (outside and inside at level of umbilicus);
left wrist;
cardiologist face mask (outside and inside at eye level);
nurse's forehead.

The cardiologist and nurse worked to the patient's right, with the nurse always to the right of the cardiologist. The image intensifier and tube housing were always to the cardiologist's left; the distances from the image intensifier centre to the cardiologist's torso and eyes and hands were measured as being typically 70 and 100 cm, respectively.

---

*Current address: Physics Division, Ontario Cancer Institute, 500 Sherbourne Street, Toronto, Ontario M4X 1K9, Canada.

Table I. Summary of procedures followed

Site	Number of cardiologists	Number of nurses	Number of procedures	Total workload (mA–min)	Cinefluoroscopy workload (% of total)	Average $\frac{\text{mA–min}}{\text{procedure}}$
RJH	7	1	25	3500	68%	140
VGH	3	1	18	5613	98%	312

It was impractical in this study for each cardiologist to be fitted with individual dosimeters. In order to estimate the radiation exposure per cardiologist, it was assumed that this quantity was proportional to the workload per cardiologist, which was given by the mA–min product recorded for each of the procedures. This assumption was verified by having two cardiologists wearing separate TLDs externally on their torso aprons during the course of the study and then comparing the ratio of the two exposures derived with the ratio of the two recorded mA–min values for each cardiologist. This test indicated an agreement between the two ratios to within ±3%.

Results and discussion

Table I summarizes the procedures covered in this study. The factor of 2.2 increase in the average workload per procedure at VGH over that at the RJH is a reflection of the greater amount of cinefluoroscopy used in the diagnostic procedures at VGH (98% of the total mA–min). A direct comparison of the exposures received at both laboratories is possible from the measured exposures normalized to the workload (given by the mA–min product), as presented in Table II. The data in Table II can be used to assess the effectiveness of the personnel shielding during the catheterization procedures and to provide an upper-estimate of the annual effective dose equivalents received by the staff, as discussed below. Because of the uncertainty in the measured exposures, the data in Table II are rounded off to the nearest 5 μR/mA–min.

The cardiologists' exposure reduction by the torso shielding and face mask differs markedly between the two hospitals. At RJH, the exposure is reduced by the trunk apron by a factor of 20, but is reduced by only a factor of about 2 at VGH. In contrast, at RJH, the exposure is attenuated by the face mask by a factor of less than 2, whereas that at VGH is reduced by a factor of over 3. It was not possible to identify the cause for the first difference, but the second was found to be a result of a tendency of the RJH cardiologists to allow the face mask to slip, exposing the forehead and eyes to radiation scattered from the patient. At both laboratories, the cardiologists' thyroid shields attenuated the thyroid exposure by factors of about 2 to 3. The RJH

Table II. Exposures received by cardiology catheterization laboratory staff (μR/mA–min) (normalized to workload)

Cardiologist

Site	Location						
	Face mask		Thyroid shield		Torso shield		Left wrist
	Outside	Inside	Outside	Inside	Outside	Inside	
RJH	60	35	45	15	300	15	365
VGH	70	20	65	30	60	25	75

Nurse

Site	Location					
	Forehead	Thyroid shield		Torso shield		Left wrist
		Outside	Inside	Outside	Inside	
RJH	20	15	10	15	10	45
VGH	30	15	10	30	10	30

1 R = 2.58×10^{-4} C/kg of air.

Table III. Upper-estimate of annual dose equivalents received by catheterization laboratory staff (mSv/year)

Staff	Site	Organ at risk								
		Lens	Thyroid	Breast	Lung	RBM	Gonads	Left arm	Right arm	WBE
Cardiologist	RJH	10	8	8	8	8	8	100	100	18 (2.4–18)
Cardiologist	VGH	10	13	13	13	13	13	34	34	13 (7.2–14.4)
Nurse	RJH	38	17	17	17	17	17	68	68	19
Nurse	VGH	54	13	13	13	13	13	42	42	14

RBM = red bone marrow.
WBE = whole body equivalent: quantities in brackets are ranges of whole-body exposures determined by conventional radiation monitoring of the cardiologists using a single dosimeter per cardiologist.

cardiologists' trunk shield external exposure and the left wrist exposure are both five times greater than those measured at VGH. On investigation of the respective techniques followed, this was found to be because the cardiologists worked considerably closer to the patient during the interventional procedures. It is interesting to note that the normalized exposures shown in Table II are only 10–20% of those reported for cardiologists working with much older imaging equipment (Stacey, et al, 1974).

With the exception of the exposures measured at the forehead, the nurses' exposures are lower than those of the cardiologists. The thyroid and torso shielding appeared only to reduce exposure a little, which may be because of the exposed head and more internal scatter reaching the thyroid and torso. The RJH nurses' left wrist exposure is elevated by almost a factor of 1.5 over that measured at VGH. This was also believed to be because of the nurse being considerably closer to the patient during the interventional procedures at RJH than during the diagnostic procedures at VGH for extended periods of time.

The data given in Tables I and II give an upper-estimate of the annual whole-body dose equivalent received by the staff. The average weekly number of procedures per cardiologist was 4.2 and 3, and for the nurses was 25 and 9, at RJH and VGH, respectively. A 47-week work-year was assumed for the purposes of the estimate.

The effective whole-body dose equivalent owing to partial exposure is

$$H_E = \sum_T W_T H_T$$

(ICRP, 1977) where H_T is the dose equivalent to tissue T, W_T is the relative risk weighting factor and the summation is over all irradiated tissues. The exposures measured here are strictly those to the skin and, hence, would represent upper limits of the exposure at the organ at risk at depth. The organs considered here to be at risk are the thyroid, lungs, red bone marrow (RBM), breast, gonads and arms with corresponding W_T values provided by the International Commission on Radiological Protection (ICRP, 1977).

The exposures to the eye were estimated by those measured at the inside of the cardiologists' face mask and at the nurses' forehead; both arm exposures were approximated by the left wrist data. Because of variations in exposures measured and expected beneath the thyroid and torso shields, a maximum normalized exposure was used to provide an upper-estimate of the H_T received by the thyroid, lungs, breast, RBM and gonads. The maximum normalized exposures received at these organs by the cardiologists and nurses were set at $30\,\mu$R/mA–min and $10\,\mu$R/mA–min, respectively. For the purpose of estimation, an exposure of 2.58×10^{-4} C/kg of air (1 R) was equated to the dose equivalent of 10^{-2} Sv. Upper estimates of the annual dose equivalents received to the organs at risk for a cardiologist and a nurse at each laboratory are given in Table III; ranges of the cardiologists' whole-body annual dose equivalents derived from the federal regulatory agency radiation monitoring (using a single dosimeter at chest level behind the torso shield) are shown for comparison. The values estimated from the partial exposure measurements described in this paper are in good agreement with the ranges determined from conventional monitoring.

From Table III, it can be seen that no individual receives an annual effective whole-body dose equivalent exceeding 19 mSv/year. In addition, no individual organ receives an annual dose equivalent beyond limits proposed by the ICRP (1977) or the National Council on Radiation Protection and Measurements (NCRP, 1987). The annual dose equivalent to the VGH nurses' eyes do, however, approach the maximum limit set by the NCRP to minimize non-stochastic effects.

The results in Tables II and III have led to modifications in the procedures used at both laboratories, as suggested by Dunlap (1975). Nurses at both laboratories are now required to wear face protection in order to reduce the eye exposure, and the cardiologists' face mask at the RJH laboratory has been corrected to reduce exposure to the eye. The RJH cardiologists have been instructed to modify their tendency to work close to the patient and to allow their extremities to be exposed to the primary beam. On both fluoroscopy units, a protective shield is now placed between the cardiologist and the image intensifier to intercept scattered radiation.

Conclusions

As the radiation exposure received by the staff of a cardiac catheterization laboratory is non-uniform, conventional radiation exposure monitoring with a single dosimeter cannot determine the degree of non-uniformity nor can it accuratley assess the effectiveness of personal shielding. In addition, it is limited in its ability to identify any practices by the staff which can elevate exposures to specific organs.

This paper has described a study determining the radiation exposures received by the cardiologists and nurses, working in two catheterization laboratories, at various anatomical locations. One laboratory performed primarily diagnostic procedures, the other, interventional procedures. The results have been used to assess the efficacy of the personal shielding and to identify procedures followed by the staff which have elevated some levels of exposure. The data have also been used to calculate estimates of the upper limits of the annual effective whole-body dose equivalent, H_E, which ranged from 13 to 19 mSv/year for the staff at the two laboratories. Although these values are lower than the maximum annual effective dose equivalent of 50 mSv/year, they are still significant and have resulted in modifications of procedures in order to reduce the H_E. Of the considered organs, only the nurses' eyes were estimated to receive annual dose equivalents approaching maximum limits. Consequently, the nurses now wear eye protection during the procedures.

Acknowledgments

We are grateful for the co-operation of the medical, nursing and technical staff of both laboratories during the course of the study.

References

DUNLAP, J. H., 1975. Radiation protection considerations in the cardiac catheterization laboratory. *Health Physics, 29*, 415–417.

FAULKNER, K., LOVE, H. G., SWEENEY, J. K. & BARDSLEY, R. A., 1986. Radiation doses and somatic risk to patients during cardiac radological procedures. *British Journal of Radiology, 59*, 359–363.

ICRP, 1977. *Recommendations of the International Commission on Radiological Protection, ICRP Publication 26* (Oxford, Pergamon Press).

NCRP, 1987. *Recommendations on Limits for Exposure to Ionizing Radiation NCRP Report No. 39* (NCRP, Washington).

STACEY, A. J., DAVIS, R. & KERR, I. H., 1974. Personnel protection during cardiac catheterisation with a comparison of the hazards of undercouch and overcouch X-ray tube mountings. *British Journal of Radiology, 47*, 16–23.

1990, *The British Journal of Radiology*, *63*, 889–891

Case reports

Ultrasound cystography: a valuable technique

By R. A. Coulden, MB, MRCP, FRCR, *D. C. Hanbury, MB, FRCS and P. Farman, DCR, DMU

Departments of Radiology and *Urology, Addenbrooke's Hospital, Cambridge

(*Received March 1990*)

Ultrasound is a reliable method for demonstrating dilated upper renal tracts and obstruction (Scheible & Talner, 1979). However, not all dilated pelvicalyceal systems and ureters are obstructed (Flower, 1977). Similar appearances can be seen in vesico-ureteric reflux (VUR), megaureter and pregnancy (Cietak & Newton, 1985). Where there is doubt concerning the cause of dilatation, other techniques are required.

Ultrasound cystography, performed as a part of micturating cystography, has been shown to be useful in demonstrating VUR in children (Kessler & Altman, 1982). In this case report, we demonstrate its wider application in the distinction between obstruction and VUR in a complex urological problem.

Case report

A 22-year-old girl had a sacral meningocoele closed at birth. She developed recurrent urinary tract infections with severe bilateral VUR. A urinary diversion with re-implantation of the ureters into a colonic conduit was performed. She remained well, and at the age of 20, underwent a cystoplasty with anastomosis of the colonic conduit to the dome of the bladder. This was complicated 6 months later by a tight stricture of the colo-vesical anastomosis. After successful dilatation, a cystogram showed free reflux of contrast medium into the colonic conduit and dilated upper renal tracts (Fig. 1). She remained well until, when she was 28 weeks pregnant, she presented with a urinary tract infection and bilateral loin pain. An ultrasound showed bilateral pelvicalyceal dilatation and a fluid filled colonic conduit. The conduit failed to empty on voiding and it was impossible to distinguish between recurrent obstruction at the colo-vesical anastomosis and VUR. Ultrasound cystography was carried out using a 3.5 MHz mechanical sector scanner.

The technique entails catheterization of the bladder which is then emptied. Ultrasound examination of the kidneys and pelvis is performed, with particular attention to the renal pelves and ureters. Imaging continues while the bladder is filled to capacity with a drip infusion of 0.9% saline. Before infusion, the saline is shaken vigorously to provide a suspension of air microbubbles. Vesico-ureteric reflux is suggested by dilatation or the appearance of bubbles in the upper renal tracts. The bladder is emptied and the kidneys and pelvis are re-scanned.

Saline containing microbubbles refluxed freely into the anechoic fluid filled conduit (Fig. 2). The already dilated renal pelves enlarged further during bladder filling (Fig. 3a,b), with microbubbles entering the collecting system. After voiding, the renal pelves and conduit returned to their original size (Fig. 3c).

Discussion

Ultrasound cystography has clearly shown VUR to be the cause of pelvicalyceal dilatation in this case. The subsequent decompression of the upper tracts and conduit on voiding excludes obstruction. This simple test has avoided the need for more invasive investigation, and in particular, tests requiring ionizing radiation.

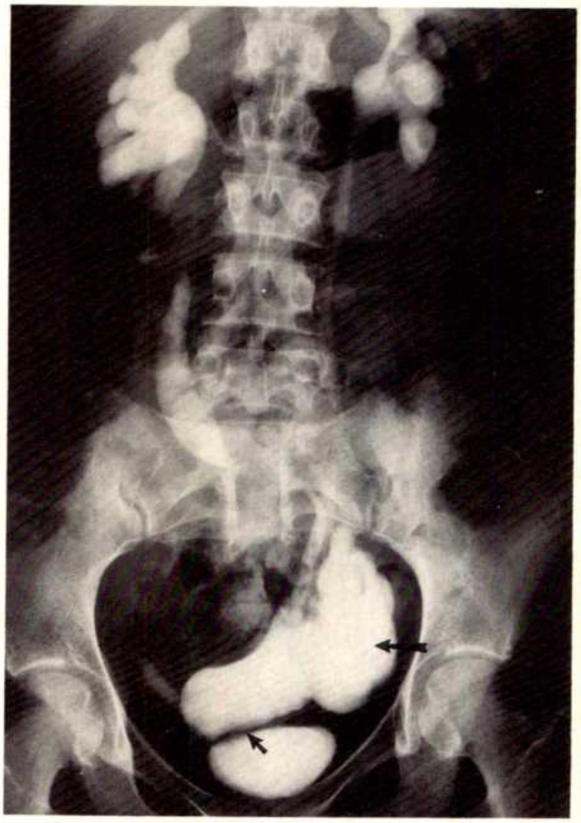

Figure 1. Abdominal radiograph following cystography. This was performed shortly after successful dilatation of the colo-vesical anastomosis (short arrow). There is bilateral grade III reflux and distension of the colonic conduit (long arrow).

Address correspondence to R. A. Coulden, Department of Cardiology, Manchester Royal Infirmary, Oxford Road, Manchester.

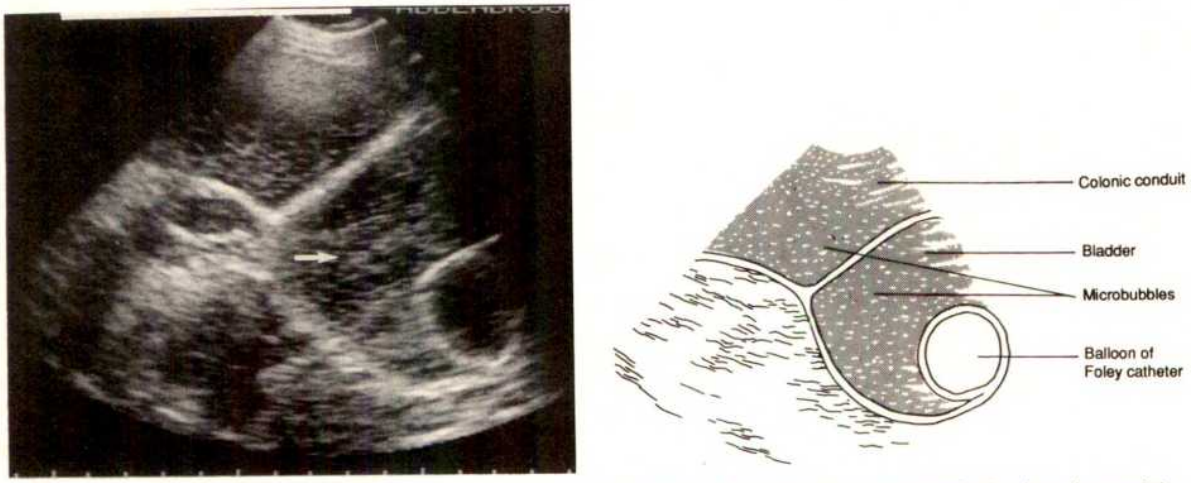

Figure 2. Oblique sagittal section of the bladder and colonic conduit showing microbubbles (arrow) refluxing into the conduit.

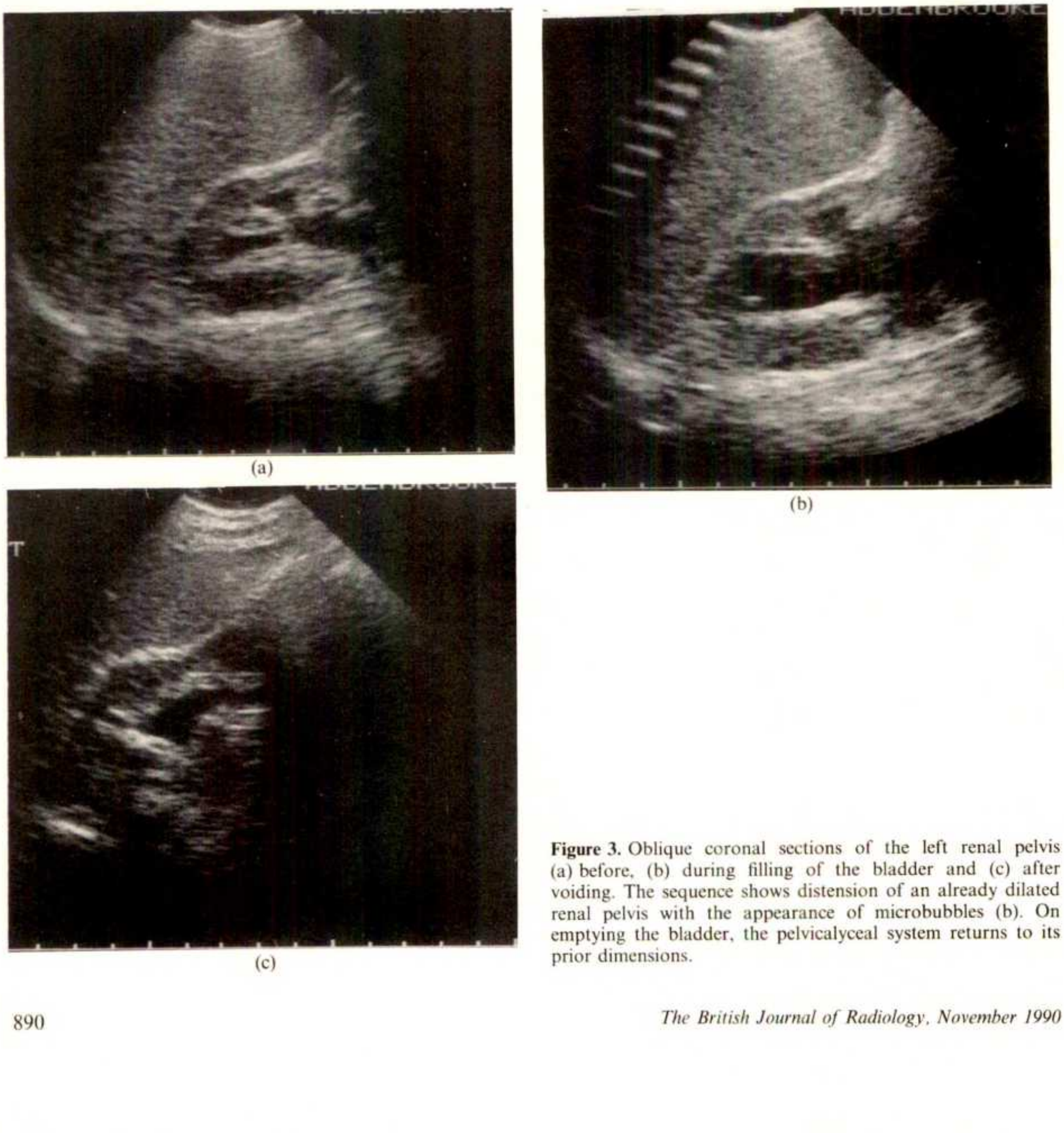
(a)

(b)

(c)

Figure 3. Oblique coronal sections of the left renal pelvis (a) before, (b) during filling of the bladder and (c) after voiding. The sequence shows distension of an already dilated renal pelvis with the appearance of microbubbles (b). On emptying the bladder, the pelvicalyceal system returns to its prior dimensions.

1990, The British Journal of Radiology, 63, 891–893

Agitated saline has been advocated as an ultrasound contrast agent in echocardiography (Gramiac et al, 1969) but is rarely used elsewhere. The authors have successfully adopted it in cystography for childhood reflux (Hanbury et al, 1990), where the technique proved to be a reliable alternative to standard micturating cystography. The addition of microbubbles, although unnecessary in this case, enables the diagnosis of VUR to be made in the absence of pelvicalyceal distension. Platt et al (1989) have recently shown pulsed Doppler ultrasound to be helpful in the distinction between obstructive and non-obstructive pyelocaliectasis. However, the changes in resistive index described in obstruction were non-specific and were also seen in intrinsic renal disease. As such, Doppler could prove misleading in situations where there may be underlying chronic renal disease.

We believe this is a valuable technique which could be more widely adopted. Its main advantage over standard cystography lies in cases where ionizing radiation is relatively contra-indicated.

Acknowledgment

We are grateful to Mr P. D. Doyle, Consultant Urologist, for allowing us to present this case.

References

Cietak, K. A. & Newton, J. R., 1985. Serial quantitative nephrosonography in pregnancy. *British Journal of Radiology*, *58*, 405–413.

Flower, C. D. R., 1977. Wide ureters. *British Journal of Radiology*, *50*, 539–540.

Gramiac, R., Shah, P. M. & Kramer, D. H., 1969. Ultrasound cardiography contrast studies in anatomy and function. *Radiology*, *92*, 939–948.

Hanbury, D. C., Coulden, R. A., Farman, P. & Sherwood, T., 1990. Ultrasound cystography in the assessment of vesico-ureteric reflux. *British Journal of Urology*, *65*, 250–253.

Kessler, R. M. & Altman, D. H., 1982. Real-time sonographic demonstration of vesico-ureteral reflux in children. *American Journal of Roentgenology*, *138*, 1033–1036.

Platt, J. F., Rubin, J. M. & Ellis, J. H., 1989. Distinction between obstructive and non-obstructive pyelocaliectasis with duplex Doppler sonography. *American Journal of Roentgenology*, *153*, 997–1000.

Scheible, W. & Talner, L. B., 1979. Grey scale ultrasound and the genito-urinary tract. *Radiologic Clinics of North America*, *17*, 281–297.

Skeletal abnormalities in a case of congenital erythropoietic porphyria

By Masako Ito, MD, Kuniaki Hayashi, MD, Masataka Uetani, MD, Ichiro Isomoto, MD and *Hiroko Irifune, MD

Departments of Radiology and *Dermatology, Nagasaki University School of Medicine, 7-1 Sakamoto-machi, Nagasaki 852, Japan

(Received February 1990 and in revised form April 1990)

Congenital erythropoietic porphyria (CEP) is an extremely rare disorder of porphyrin metabolism and is characterized by the deposition of porphyrins in soft tissue, bone and teeth. Reported radiographic findings of CEP include acro-osteolysis, scleroderma-like calcifications and demineralization of bone. We report a case of CEP which showed, in addition to these findings, multiple osteolytic and sclerotic lesions.

Case report

A 21-year-old female presented with cutaneous pigmentation, deformity of the hands and nose, and hepatosplenomegaly. Congenital erythropoietic porphyria was discovered shortly after her birth when she passed red urine. The erythema and blistering started to appear in her first year of life. She began to have pigmentation on her face when she was 15 years old. She had a past history of having cholecystolithiasis and acute hepatitis.

Laboratory data showed following values: red blood cell count, 3.16×10^6 µl; haemoglobin 9.3 g/100 ml; total haematocrit, 28.7%; white blood cell count, 3.9×10^3 µl; platelet count, 111×10^3 µl; serum glutamic oxalo-acetic-acid-transaminase, 70 IU (normal <39); serum glutamic pyruvic transaminase, 28 IU (normal <33); total serum bilirubin, 1.3 mg/ml (normal <1.0); direct bilirubin, 0.8 mg/ml (normal <0.5); lactic dehydrogenase, 2007 U (normal <435); serum phosphate, 5.3 mg/dl (normal 2.3–4.5); serum calcium, 8.5 mg/dl (normal 8.2–9.8). The red blood cell protoporphyrin and coproporphyrin level was markedly high, and the urine contained increased coproporphyrin and uroporphyrin.

The skull radiograph (Fig. 1) taken prior to plastic surgery of the face demonstrated round sclerotic and osteolytic lesions in the calvarium, maxilla and mandible, and moderate widening of the diploic space with thin outer table. The bone survey was requested and this showed additional round sclerotic lesions in the pelvic bones, together with generalized osteopenia, acro-osteolysis and soft tissue calcification in the hands (Fig. 2). Computed tomography of the skull showed well circumscribed dense sclerotic and osteolytic lesions in the diploic space of the calvarium (Fig. 3).

Computed tomography of the abdomen demonstrated cholelithiasis, hepatosplenomegaly and fatty infiltration of the pancreas. At laparoscopy, the liver demonstrated fluorescence under ultraviolet light, and chronic active hepatitis was diagnosed by liver biopsy.

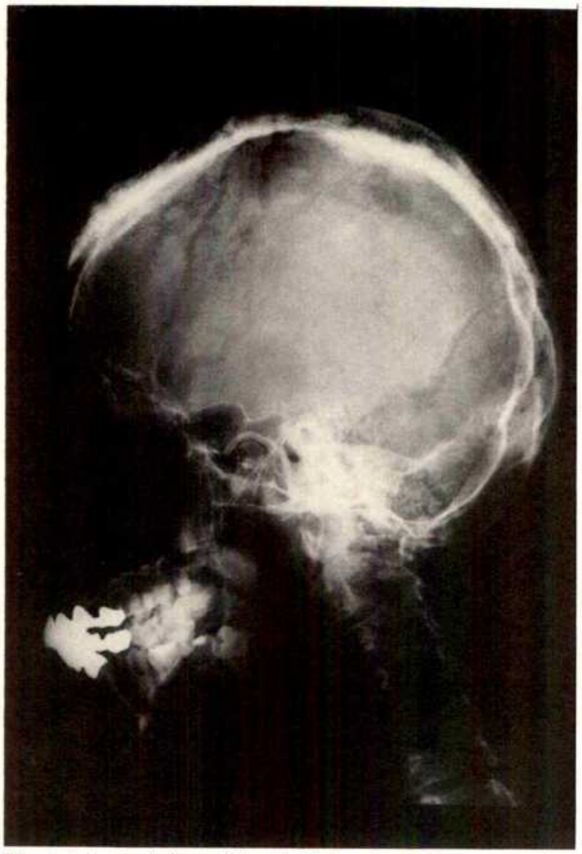

Figure 1. Lateral view of the skull demonstrating spotty sclerotic and osteolytic lesions in the calvarium, and moderate widening of the diploic space with thin outer table.

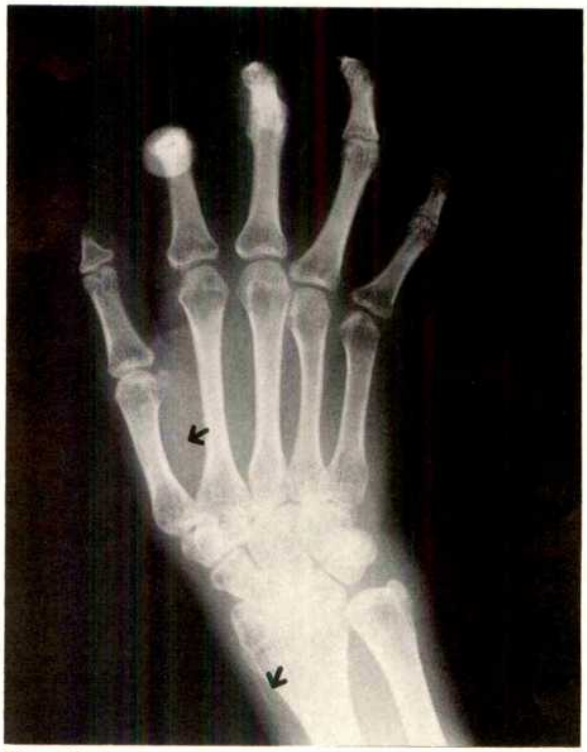

Figure 2. Anteroposterior view of the right hand showing demineralization, acro-osteolysis and soft tissue calcifications (arrows).

Discussion

Congenital erythropoietic porphyria is a generalized metabolic disorder associated with the deposition of porphyrins in all tissues: greater amounts in the liver, gallbladder, intestines and kidneys, possibly because of excretion of large amounts of porphyrin in bile and urine. The porphyrin fluorescence has been observed in the bone, meninges, heart, lungs, liver, kidneys, brain and intestine (Bhutani et al, 1974). The early clinical manifestations are blisters on skin exposed to light, especially on the face and hands. The patients may have extensive mutilation such as loss of the fingers, nose or ears after years of continued photosensitivity. Haemolytic anaemia and splenomegaly are invariably associated with CEP.

The bone changes of CEP are not well known, but acro-osteolysis, scleroderma-like calcifications and demineralization of bone have been reported as typical radiographic findings (Small & Dickson, 1970). Our case showed, in addition, multiple round sclerotic and osteolytic lesions in the calvarium, maxilla, mandible and pelvic bones. No similar case has ever been reported, but we did find one case of CEP in the

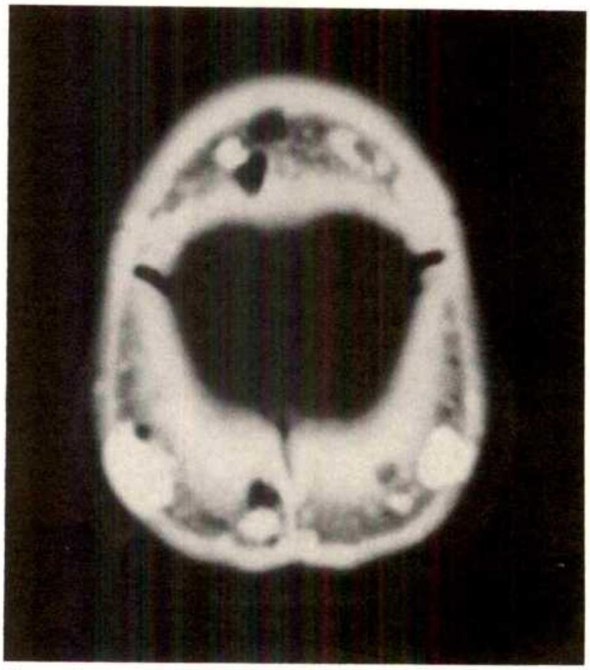

Figure 3. Computed tomographic scan of the skull showing well circumscribed dense sclerotic and osteolytic lesions in the widened diploic space of the calvarium.

1990, *The British Journal of Radiology*, *63*, 893–894

literature which showed calcification of the falx and a sclerotic spot of the calvarium (Levesque et al, 1988). The pathogenesis of sclerotic lesions is not clear. Focal osteolytic lesions may be explained as localized areas of tumorous collections of hyperplastic marrow due to anaemia (Moseley, 1974).

While the combination of lytic and sclerotic lesions may suggest metastatic disease, there has been no evidence of malignancy in this case and she remains well on follow-up a year later. We consider these sclerotic lesions may be a part of the spectrum of skeletal abnormalities in CEP, although no histological evaluation has been made.

References

BHUTANI, L. K., SOOD, S. K., DAS, P. K., DESHPANDE, S. G., MULAY, D. N. & KANDHARI, K. C., 1974. Congenital erythropoietic porphyria: an autopsy report. *Archives of Dermatology*, *110*, 427–431.

LEVESQUE, M., LEGMANN, P., LECLOIREC, A., DEYBACH, J. C. & NORDMANN, Y., 1988. Radiological features in congenital erythropoietic porphria (Gunther's disease): Report of 3 cases. *Pediatric Radiology*, *18*, 62–66.

MOSELEY, J. E., 1974. Skeletal changes in the anemias. *Seminar Roentgenology*, *9*, 169–184.

SMALL, P. & DICKSON, R., 1970. The radiological features of congenital porphyria. *British Journal of Radiology*, *43*, 732–734.

Computed tomography in volvulus of the midgut

By A. B. Paul, MB, ChB and *D. M. Dean, MB, ChB, DMRD, FRCR

Department of Surgery, Eastern General Hospital, Seafield Street and *University Department of Medical Radiology, Edinburgh Royal Infirmary, Lauriston Place, Edinburgh

(*Received December 1989*)

Herniation of the midgut into the umbilical cord and its rotation and return are normally complete by the tenth week of intra-uterine life. Abnormalities of this process lead to the various types of malrotation of the gut. These may lead to a variety of problems in extra-uterine life (Dott, 1923). We recently encountered a patient with such a condition which was diagnosed only at laparotomy. In retrospect the computed tomographic (CT) findings could have allowed a pre-operative diagnosis.

Case report

A 20-year-old male was admitted to hospital with a 1-week history of vomiting 1 hour after each meal. In association was increasingly severe, constant upper abdominal pain radiating to the back. There had been 2 days of abdominal distension. In the previous 2 years he had suffered four similar episodes, all less severe and spontaneously resolving.

On examination he was clinically jaundiced and dehydrated. The epigastrium was tender without signs of peritonism.

Blood chemistry confirmed dehydration (Na 145 mmol/l, Urea 41.7 mmol/l). Amylase was elevated at 231 IU/l. Liver function tests showed bilirubin of 89 μmol/l with a hepatocellular picture. Haematology showed a leucocytosis and dehydration (white blood corpuscles 16.1×10^9; haemoglobin 19.5 g/dl; haematocrit 59.4%).

A pancreatic or other retroperitoneal tumour, or pancreatitis, were thought to be likely diagnoses.

A plain abdominal radiograph was unremarkable. Upper abdominal ultrasonography showed dilatation and peristalsis of the second part of the duodenum but no other abnormality and specifically no hepatic or biliary lesion. Barium meal examination (Fig. 1) showed obstruction at the junction of the second and third parts of duodenum with dilatation of the second part. There was an impression of extrinsic compression of the duodenum on this examination. Upper gastrointestinal endoscopy was normal to the second part of duodenum.

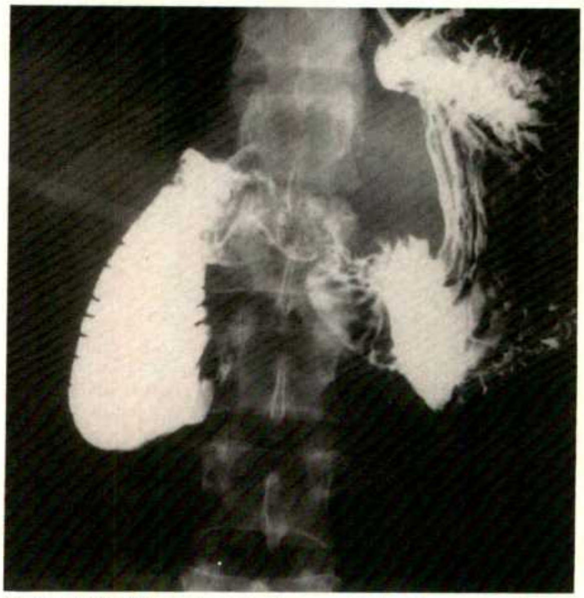

Figure 1. Double contrast barium meal showing obstruction at the distal second part of the duodenum.

Computed tomography showed a mass lying immediately anterior to, and to the left of, the aorta (Fig. 2). This consisted of a number of concentrically arranged, gas-containing whorls. Its exact nature was unclear but was thought to represent a paraduodenal hernia.

At laparotomy the findings were of volvulus of the midgut.

Address correspondence to Dr A. B. Paul, Ward 11/12, Royal Infirmary of Edinburgh, Lauriston Place, Edinburgh.

1990, *The British Journal of Radiology*, *63*, 894–897

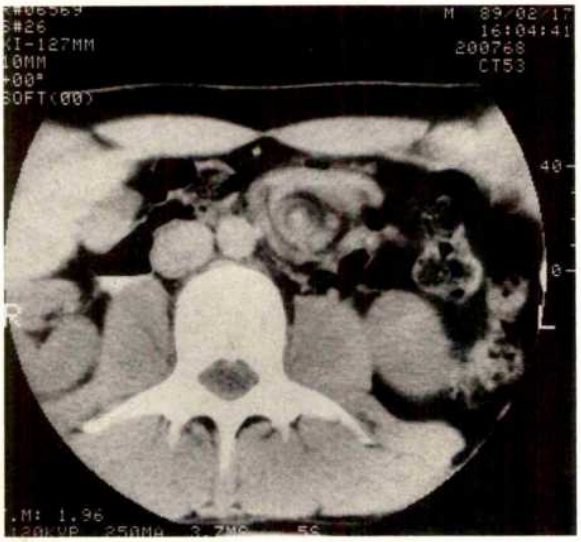

Figure 2. Computed tomographic scan showing characteristic whorls of bowel around the superior mesenteric artery.

The distal duodenum lay anterior to and was compressed by the transverse colon lying on the left. The small bowel and proximal colon, on a narrow mesentery on the right, were twisted about the superior mesenteric artery forming the mass seen on computed tomography. This was presumed to have compressed the biliary and pancreatic ducts causing derangement of liver function tests and amylase.

Discussion

Disorders of rotation of the gut are all uncommon, those of the fore and hind guts extremely so. Those of the midgut are most often encountered in the paediatric age group, but their presentation in adult life is well recognized. Their characteristics are well described by Dott (1923). The most common is volvulus in which the midgut leaves and returns to the abdomen in the first trimester without rotation. The disposition of small and large bowels is explained by the attachments of the fore and hind guts (Moore, 1988).

Malrotation of the gut provides considerable diagnostic difficulty. Computed tomographic scanning may be a useful means of establishing a pre-operative diagnosis in such patients. Although rare, the bizarre CT appearance of volvulus in malrotation showing whorls of bowel around the superior mesenteric artery has been previously described (Fisher, 1981; Mori et al, 1987).

Characteristic changes in the relative positions of superior mesenteric artery and vein may also be seen in malrotation (Nichols & Li, 1983).

It is important that the characteristic appearances of this rare condition are recognized so that a correct pre-operative diagnosis can be made.

References

DOTT, N. M., 1923. Anomalies of intestinal rotation. *British Journal of Surgery*, *11*, 251–286.

FISHER, J. K., 1981. Computed tomographic diagnosis of volvulus in intestinal malrotation. *Radiology*, *140*, 145–146.

MOORE, K. L., 1988. *The Developing Human—Clinically Orientated Embryology* (W. B. Saunders, Philadelphia), pp. 228–236.

MORI, H., HAYASHI, K. & FUTAGAWA, S., 1987. Vascular compromise in chronic volvulus with midgut rotation. *Paediatric Radiology*, *17*, 227–281.

NICHOLS, D. M. & LI, D. K., 1983. Superior mesenteric vein rotation: A CT sign of midgut malrotation. *American Journal of Roentgenology*, *141*, 707–708.

The value of computed tomography in the diagnosis of atlanto-axial rotatory fixation

By J. B. Murray, MB, ChB, DA, FRCR and M. Ziervogel, MB, ChB, FRCR

Department of Radiology, Royal Hospital for Sick Children, Yorkhill, Glasgow G2

(*Received July 1989 and in revised form June 1990*)

Case report

A 10-year-old girl was examined in Casualty complaining of a torticollis with her head looking downwards and to the right, which had developed suddenly that morning as she was drying herself after a bath. She had no neurological signs or symptoms. Interpretation of her cervical spine radiographs was difficult owing to her inability to move her neck for proper radiographic positioning (Fig. 1). She was given a soft collar and sent home.

She returned 10 days later with increased paravertebral muscle spasm in her neck. Further radiographs, including oblique views, were taken of her cervical spine. Interpretation was again difficult owing to her inability to move her neck. She was admitted and further investigations including isotope bone scan and routine bloods were normal. She was unable to tolerate a collar support. Analgesia and muscle relaxants were not successful.

There were two episodes, one at home and one in the ward, where she was noted to have untwisted her neck during the night; but gradually the torticollis returned. Because of her rather odd posturing and anxiety in the ward it was thought this might be a conversion hysteria. An opinion was therefore sought from a child psychiatrist, who concluded that the child was normal and well adjusted. A consultant neurologist examined her and could find no peripheral or central neurological deficit. Wilson's disease was considered because of possible Kayser-Fleischer rings and a slightly raised bilirubin but an ophthalmological opinion discounted this.

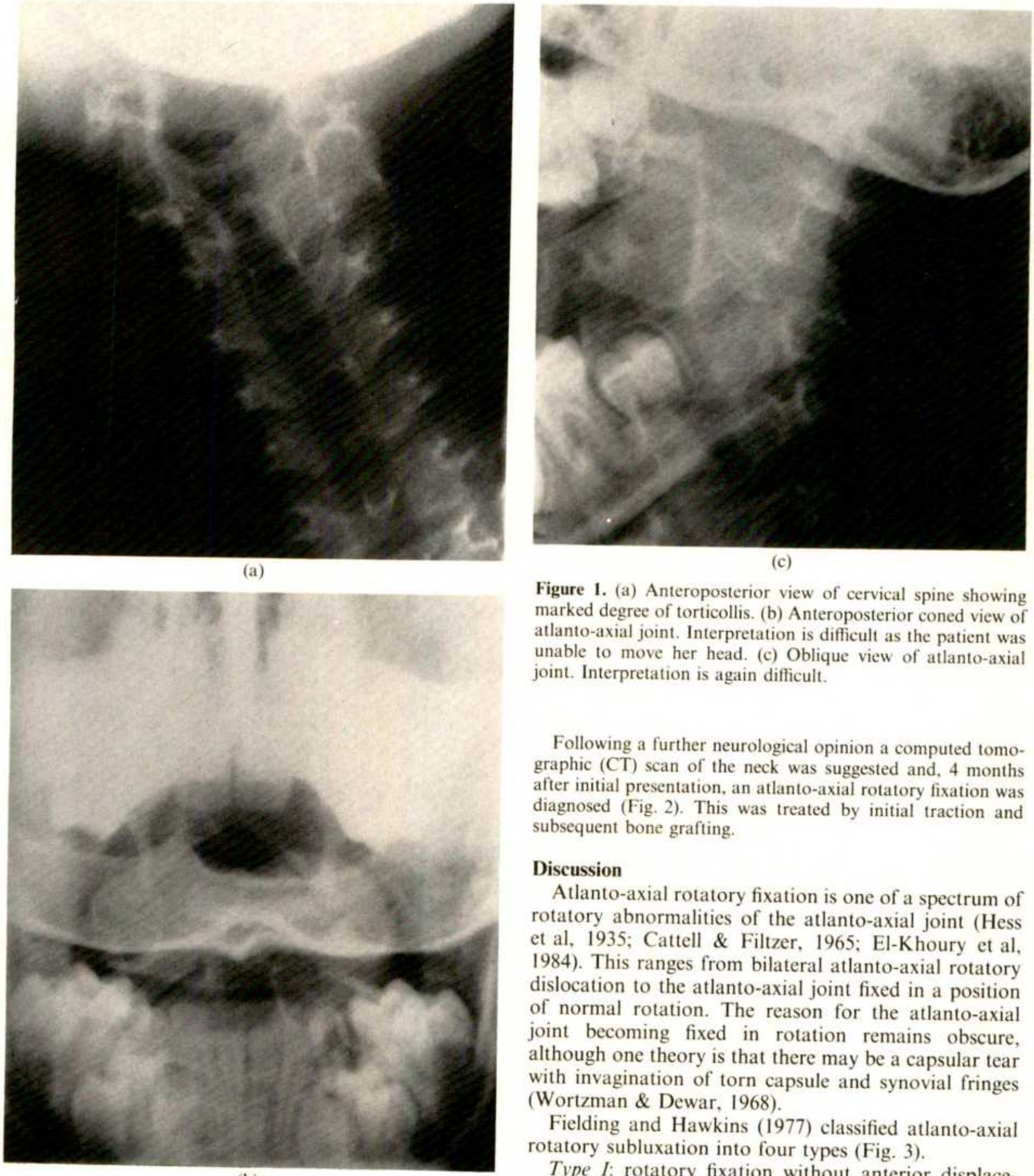
(a)
(b)
(c)

Figure 1. (a) Anteroposterior view of cervical spine showing marked degree of torticollis. (b) Anteroposterior coned view of atlanto-axial joint. Interpretation is difficult as the patient was unable to move her head. (c) Oblique view of atlanto-axial joint. Interpretation is again difficult.

Six weeks after initial presentation she was examined by an orthopaedic surgeon with a paediatric interest. It was concluded that she had a spastic torticollis of unexplained aetiology, probably also to some degree hysterical in origin. In order to exclude an intraspinal lesion, a magnetic resonance scan was performed. No intracranial abnormality and no cervical cord abnormality was identified.

Following a further neurological opinion a computed tomographic (CT) scan of the neck was suggested and, 4 months after initial presentation, an atlanto-axial rotatory fixation was diagnosed (Fig. 2). This was treated by initial traction and subsequent bone grafting.

Discussion

Atlanto-axial rotatory fixation is one of a spectrum of rotatory abnormalities of the atlanto-axial joint (Hess et al, 1935; Cattell & Filtzer, 1965; El-Khoury et al, 1984). This ranges from bilateral atlanto-axial rotatory dislocation to the atlanto-axial joint fixed in a position of normal rotation. The reason for the atlanto-axial joint becoming fixed in rotation remains obscure, although one theory is that there may be a capsular tear with invagination of torn capsule and synovial fringes (Wortzman & Dewar, 1968).

Fielding and Hawkins (1977) classified atlanto-axial rotatory subluxation into four types (Fig. 3).

Type I: rotatory fixation without anterior displacement of the axis. The fixed rotation is within the normal range of atlanto-axial rotation. The transverse ligament is intact so that the dens acts as a pivot. This is the most common.

Type II: rotatory fixation with 3–5 mm anterior displacement of the atlas and is the second most common lesion. This is associated with slackness of the transverse ligament and anterior displacement of the lateral mass while the opposite atlanto-axial joint acts as a pivot.

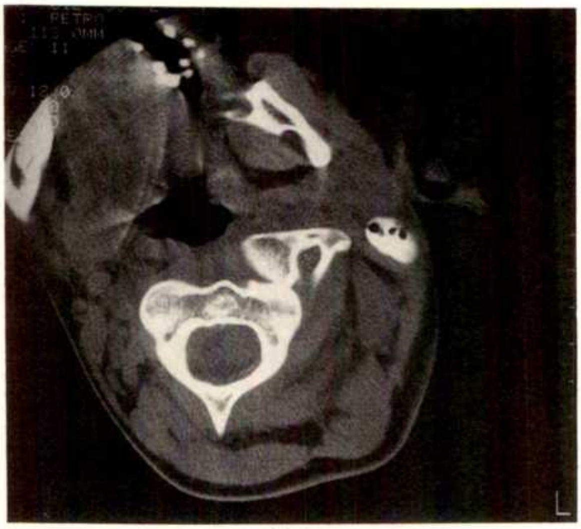

(a)

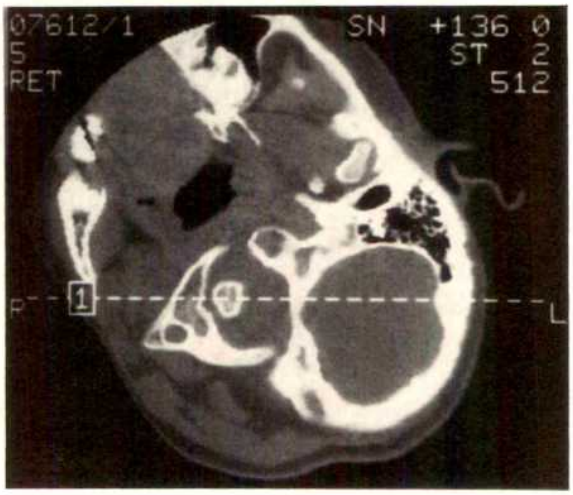

(b)

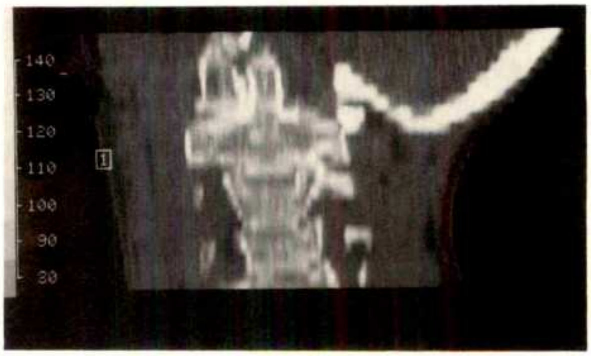

(c)

Figure 2. Axial CT scan through the axis with the base of the odontoid process shown. A Fielding Type II atlanto-axial rotatory fixation with dislocation of the left atlanto-axial joint anteriorly is present. (b) Axial CT scan at a slightly higher level showed the position of the odontoid process fixed on rotation of the head. (c) Coronal reconstruction at this level confirmed the persistent proximity of the odontoid process to the right lateral mass of the atlas.

Type III: rotatory fixation with more than 5 mm anterior displacement. Both lateral atlantal masses are displaced anteriorly, one more than the other.

Type IV: rotatory fixation with posterior displacement. This is exceedingly rare and can occur only if the dens is absent.

Plain film examination of atlanto-axial rotatory fixation is well established; anteroposterior radiographs reveal shift of the odontoid peg to one side. The diagnosis is confirmed by demonstrating that the atlanto-axial joint is fixed in rotation and that the atlas and the axis move as one. This is shown on open-mouth anteroposterior radiographs of the upper cervical spine taken in neutral and in 15° of rotation to either side to show a persistent proximity of the odontoid peg to the lateral mass of the atlas on the affected side.

Plain film interpretation, as in this case, is often difficult. The problem was demonstrating these complex anatomical structures in a patient who was unable to move her neck to obtain correct radiographic positioning. The value of early diagnosis in relation to outcome has recently been emphasized (Johnson & Fergusson,

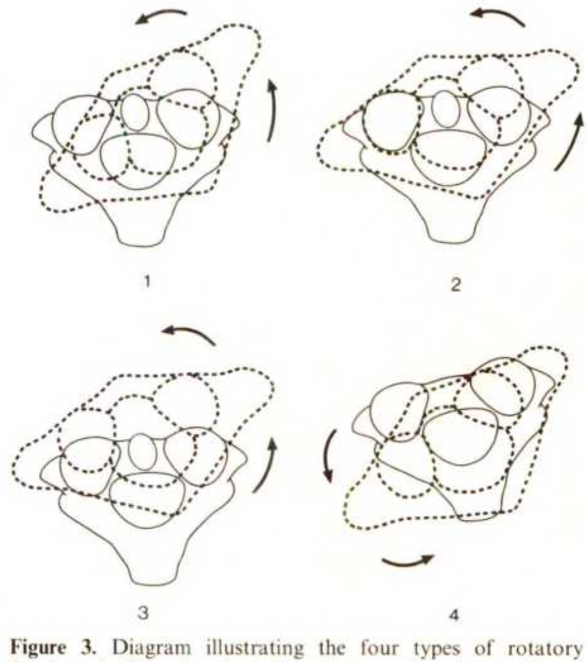

Figure 3. Diagram illustrating the four types of rotatory fixation. 1. Type I: odontoid acting as the pivot with no anterior displacement. 2. Type II: one lateral articular process acting as the pivot with 3–5 mm anterior displacement. 3. Type III: rotatory fixation with more than 5 mm anterior displacement 4. Type IV: odontoid process absent with rotatory fixation and posterior displacement.

1986). Early treatment with a short period of halter traction increases the prospect of successful reduction and early return of function, avoiding subsequent deformity and instability for which cervical fusion may be required.

This case illustrates the difficulty in diagnosing this relatively rare condition and stresses the value of early CT in establishing the diagnosis where plain film interpretation is unclear.

References

CATTELL, H. S. & FILTZER, D. L., 1965. Pseudosubluxation and other normal variations in the cervical spine in children; a study of one hundred and sixty children. *American Journal of Bone and Joint Surgery*, *47A*, 1295–1309.

EL-KHOURY, G. Y., CLARK, C. R. & GRAVETT, A. W., 1984. Acute traumatic rotatory atlanto-axial dislocation in children; a report of three cases. *American Journal of Bone and Joint Surgery*, *66A*, 774–777.

FIELDING, J. W. & HAWKINS, R. J., 1977. Atlanto-axial rotatory fixation (fixed rotatory subluxation of the atlanto-axial joint). *American Journal of Bone and Joint Surgery*, *59A*, 37–44.

HESS, J. H., BRONSTEIN, I. P. & ABELSON, S. M., 1935. Atlanto-axial dislocations unassociated with trauma and secondary to inflammatory foci in the neck. *American Journal of Diseases of Children*, *49*, 1137–1147.

JOHNSTON, D. P. & FERGUSSON, C. M., 1986. Early diagnosis of atlanto-axial rotatory fixation. *British Journal of Bone and Joint Surgery*, *68B*, 698–701.

WORTZMAN, G. & DEWAR, F. P., 1968. Rotatory fixation of the atlanto-axial joint; rotational atlanto-axial subluxation. *Radiology*, *90*, 479–487.

Multifocal central nervous system lesions and retropharyngeal lymphadenopathy on magnetic resonance imaging: an association that suggested progressive multifocal leukoencephalopathy in a patient with acute aphasia

By J. G. Llewelyn, MRCP, *A. R. Valentine, FRCR, C. Bradley, MRCP, K. King, MB, BCh and M. L. P. Gross, MRCP

Departments of Neurological Science and *Radiology, Royal Free Hospital School of Medicine, London

(*Received December 1989 and in revised form April 1990*)

Progressive multifocal leukoencephalopathy (PML) is an uncommon condition associated almost exclusively with impaired host immunity. More recently it has been recognized as a complication of the acquired immunodeficiency syndrome (AIDS), occurring in as many as 3.8% of these patients (Krupp et al, 1985). It may, rarely, be the initial manifestation of primary HIV infection, and in documented cases presents as focal limb weakness, altered mental state, ataxia, visual loss, headache and speech or language disturbance (Berger et al, 1987). We report a case of PML which presented as an acute aphasia, and in whom the diagnosis of an immunodeficient state was suggested by the magnetic resonance imaging (MRI) finding of enlarged retropharyngeal lymph nodes.

Case report

A 45-year-old married man with one child was admitted with an acute aphasia. He had been at work the day prior to admission, and later that evening became aware of difficulty finding words. The following morning his aphasia had progressed and he was admitted to hospital. General examination was unremarkable with no lymphadenopathy detected. Neurological examination revealed an expressive and receptive aphasia, dysgraphia and dyslexia. There was a mild right upper motor neurone facial weakness with normal limb power and symmetrical reflexes, but an extensor plantar response on the right. Serum investigations including white cell differential count were normal. Computed tomography (CT) showed a well defined non-enhancing low density lesion in the left postero-inferior frontal region, involving grey and white matter, but exerting no appreciable mass effect (Fig. 1) Electroencephalogram showed bifrontal delta activity. Cerebrospinal fluid analysis and digital subtraction arteriography were normal.

Despite clinical deterioration, CT brain scan 2 weeks after the first showed very little, if any, progression of the lesion. Magnetic resonance imaging demonstrated an extensive lesion exerting slight but definite mass effect in the left frontal lobe, involving the basal ganglia and corpus callosum. It also revealed other smaller lesions posteriorly in the left cerebral hemisphere and also in the right frontal lobe (Fig. 2). It was also noted that there was a mass in the post-nasal space consistent with adenoidal enlargement (Fig. 3, arrowed) and this latter finding was considered to suggest the possibility of host immunodeficiency. Anti-HIV antibody testing was positive; p24 core antigen titre was negative. Helper (T4): suppressor (T8) lymphocyte ratio was reversed at 0.18. A biopsy taken from the left cerebral cortex showed foci of demyelination with a "snowstorm" appearance in the white matter and grey/white interface, with areas of confluence. Oligodendrocyte nuclei were enlarged, hyperchromatic, with abnormal homogeneous chromatin and some filled with granular material. Bizarre astrocytes were also seen. These appearances were characteristic of PML. Electron microscopy showed uniform viral particles within oligodendrocytes, shown by immunofluorescence to be JC polyoma virus.

Information obtained from a male friend of the patient

Address correspondence to Dr J. G. Llewelyn, University Department of Neurology, King's College Hospital and Institute of Psychiatry, Denmark Hill, London SE5 9RS.

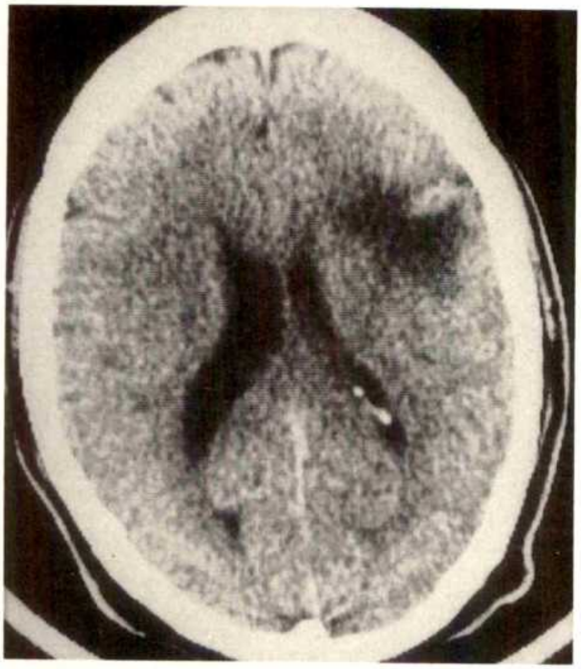

Figure 1. Unenhanced cranial CT. Hypodensity without mass effect in the left posterior frontal region, involving grey and white matter.

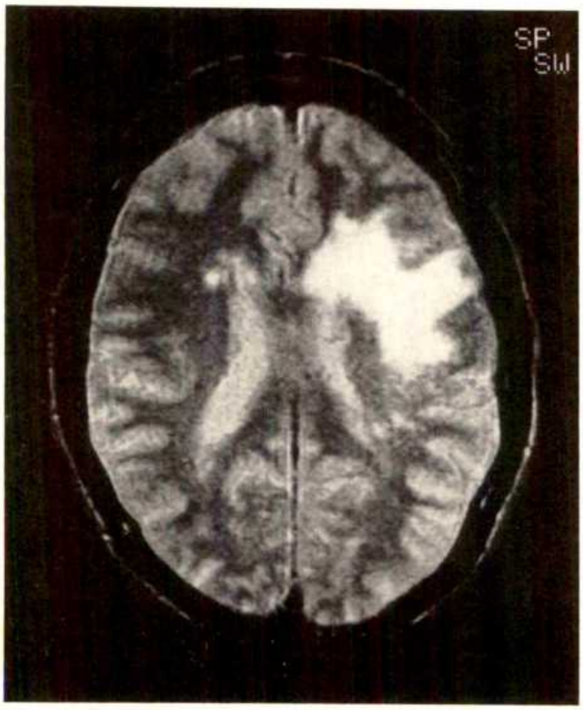

Figure 2. Axial MRI image (T_2-weighted spin echo) reveals multifocal disease.

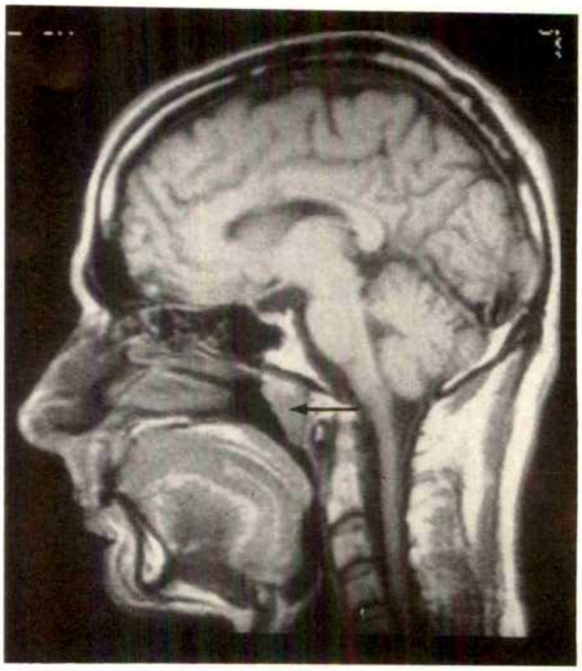

Figure 3. Sagittal MRI demonstrates a mass in the post-nasal space.

revealed a complex situation where both were bisexual, with numerous partners. The patient's wife admitted to her extramarital affairs but was not aware of her husband's sexual inclinations. Treatment with AZT (Zidovudine) was initiated, but the patient developed a leucopenia of 2.9×10^9/l and his clinical condition deteriorated rapidy. He died within 7 weeks of his original presentation.

Discussion

Progressive multifocal leukoencephalopathy occurs in AIDS at a much higher frequency than in other conditions associated with disorder of the immune system (Stoner et al, 1986), and is likely to be encountered with increasing frequency over the next few years. The acute presentation in this case suggested an ischaemic event, and this view was strengthened when CT scanning showed unifocal pathology compatible with infarction. It was only on MRI that the multifocal distribution of lesions was observed. With the exception of a few cases, PML is the result of opportunistic infection of the brain by JC virus.

The possibility that the virus is blood borne has received support following the recent identification of JC virus DNA and capsid antigen in B lymphocytes isolated from the bone marrow and spleen of two patients with PML (Houff et al, 1988).

To our knowledge, acute aphasia has not previously been reported as the initial presentation of HIV infection. Berger et al (1987), in a literature review of AIDS-related PML cases, found that disturbance of speech or language was the initial manifestation of four out of 25 patients (16%) three with dysarthria and one

1990, *The British Journal of Radiology*, *63*, 899–902

case with comprehension difficulties. Aphasia as part of other neurological manifestations was encountered in 14% of cases. The inability of the patient to give a sexual history posed a diagnostic difficulty, and it was the presence of retropharyngeal lymphadenopathy on MRI that raised the possibility of an immunodeficient state. The advantages of MRI over CT scanning in delineating the extent of cortical involvement in known AIDS patients with PML have been previously noted (Guilleux et al, 1986; Levy et al, 1986). Benign tonsillar and adenoidal enlargement has been reported as CT and MRI findings along with other lesions of the head and neck, such as infections and tumours, in AIDS patients (Olsen et al, 1988). We would suggest that, in view of the protean neurological manifestations of AIDS, many of which will be investigated with CT or MRI, scrutiny of the head and neck region for lymph node enlargement or other lesions in that region may alert the radiologist and clinician to the possibility of HIV infection.

Acknowledgments

We thank Dr J. Bayliss who made the initial referral, Dr M. Johnson and the AIDS Counselling Team for their helpful advice and Dr J. E. McLaughlin for reviewing the histology.

References

Berger, J. R., Kaszovitz, B., Donovan Post, J. & Dickinson, G., 1987. Progressive multifocal leukoencephalopathy associated with human immunodeficiency virus infection. A review of the literature with a report of sixteen cases. *Annals of Internal Medicine*, *107*, 78–87.

Guilleux, M. H., Steiner, R. E. & Young, I. R., 1986. MR imaging in progressive multifocal leukoencephalopathy. *American Journal of Neuroradiology*, *7*, 1033–1035.

Houff, S. A., Major, E. O., Katz, D. A., Kufta, C. V., Sever, J. L., Pittaluga, S., Roberts, J. R., Gitt, J. Saini, N. & Lux, W., 1988. Involvement of JC virus-infected mononuclear cells from the bone marrow and spleen in the pathogenesis of progressive multifocal leukoencephalopathy. *New England Journal of Medicine*, *318*, 301–305.

Krupp, L. B., Lipton, R. B., Swerdlow, M. L., Leeds, N. E. & Llena, J. 1985. Progressive multifocal leukoencephalopathy: Clinical and radiographic features. *Annals of Neurology*, *17*, 344–349.

Levy, J. D., Cottingham, K. L., Campbell, R. J., Moore, G. K., Gyorkey, F., Ashizawa, T. & Goldman, A. M., 1986. Progressive multifocal leukoencephalopathy and magnetic resonance imaging. *Annals of Neurology*, *19*, 399–401.

Olsen, W. L., Jeffrey, R. B., Sooy, C. D., Lynch, M. A. & Dillon, W. P., 1988. Lesions of the head and neck in patients with AIDS: CT and MR findings. *American Journal of Roentgenology*, *151*, 758–790.

Stoner, G. L., Ryschewitsch, C. F., Walker, D. L. & Webster, H. D., 1986. JC papovavirus large tumour (T)-antigen expression in brain tissue of acquired immune deficiency syndrome (AIDS) and non-AIDS patients with progressive multifocal leukoencephalopathy. *Proceedings of the National Academy of Sciences USA*, *23*, 2271–2275.

The nidus of an osteoid osteoma mimicking an os supratrochleare dorsale

By *P. Roberts, MA, FRCS, †A. M. Davies, DMRD, FRCR, C. M. Starkie, MRCPath and R. J. Grimer, FRCS, FRCSEd(Orth)

Bone Tumour Treatment Service and †Department of Radiology, Royal Orthopaedic Hospital, Northfield, Birmingham B31 2AP

(*Received February 1990 and in revised form April 1990*)

Osteoid osteomas arising in an intra-articular or para-articular site can present a diagnostic problem, particularly when occurring around the elbow. The adjacent joint can show evidence of synovitis and proliferative arthritis, and on radiographic examination new bone formation may be slight or absent and the nidus invisible (Marcove & Freiberger, 1966; Moreton & Bartlett, 1966; Corbett et al, 1974; Cronemeyer et al, 1981; Clarke et al, 1981). These atypical features can lead to misdiagnosis of this condition. We present a further cause of misinterpretation of osteoid osteomas around the elbow, that of the nidus mimicking an os supratrochleare dorsale.

Case report

A 15-year-old boy was referred with a history of a persistently painful right elbow following a minor injury 12 months earlier. The pain was constant and disturbed his sleep. On physical examination the elbow was found to be swollen with evidence of a joint effusion. Tenderness was maximal on the posterolateral aspect of the distal humerus and movements were restricted. There was a fixed flexion deformity of 20° with futher flexion possible only to 90°. Supination and pronation were unrestricted. Laboratory investigations including erythrocyte sedimentation rate were normal.

Plain radiographs of the elbow demonstrated an effusion and a lamellar periosteal reaction along the posteromedial aspect of the distal humeral metaphysis (Figs 1a,b). Scintigraphy showed markedly increased activity of the distal humerus and elbow joint (Fig. 2). Computed tomography (CT) confirmed the lamellar periosteal reaction and revealed a small cavity within the thickened lateral cortex of the distal humerus (Fig. 3). A radiological diagnosis of an osteoid osteoma was made on the strength of the new bone formation surrounding a cortical cavity. The discrete rounded opacity lying within the olecranon fossa (Figs 1a, 3) was presumed to be a normal variant (os supratrochleare dorsale). Review of the radiographs obtained at the time of the original injury showed a joint effusion with

---

*Author for correspondence.

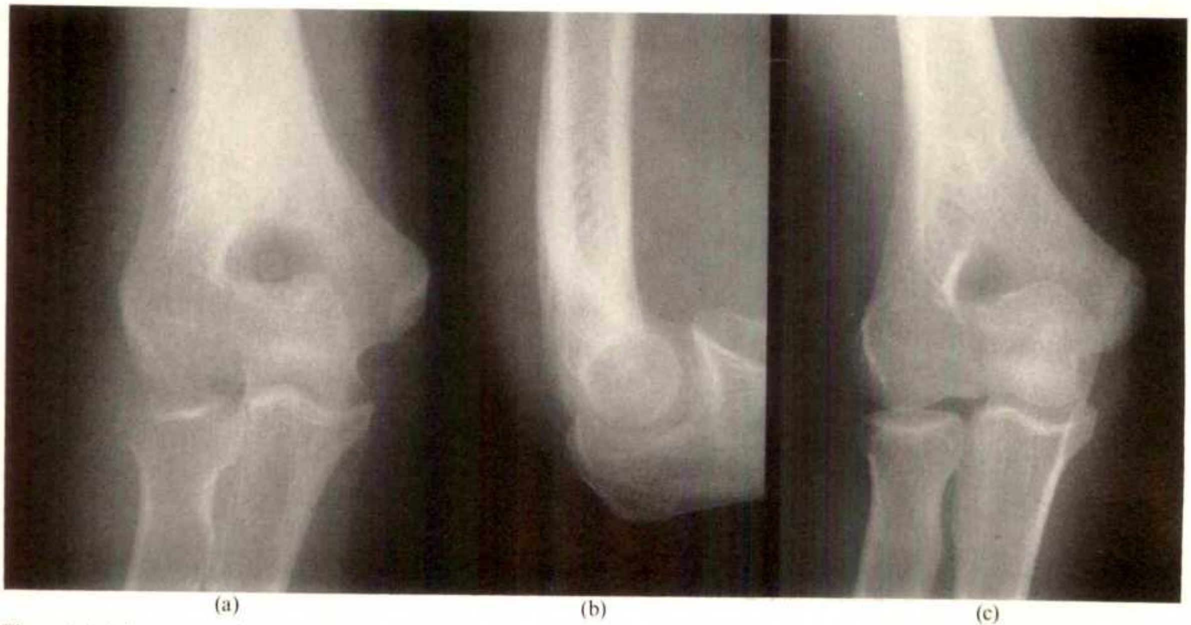
(a) (b) (c)

Figure 1. (a) Anteroposterior radiograph of distal humerus showing lamellar periosteal reaction along the medial metaphysis and an opacity in the olecranon fossa. (b) Lateral radiograph of distal humerus showing a joint effusion and lamellar periosteal reaction of the posterior metaphysis. (c) Anteroposterior radiograph of distal humerus 12 months earlier showing a considerably smaller opacity in the olecranon fossa.

no evidence of a periosteal reaction and the opacity in the olecranon fossa, although present, was considerably smaller (Fig. 1c).

A biopsy was taken from the lateral aspect of the distal humerus, histological examination of which showed pieces of normal lamellar bone and atypical bone. The appearances were consistent with a mature osteoid osteoma but no nidus was seen. The patient's pain persisted unchanged despite a second curettage of the distal humerus 4 months later and, because of the persistent symptoms, the elbow joint was explored.

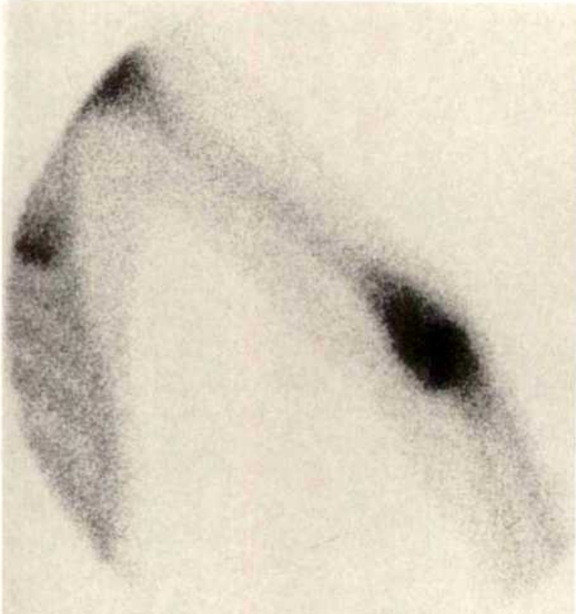
Figure 2. Scintigram of distal humerus with elbow in fixed flexion, showing markedly increased activity in the elbow joint and distal humerus.

There was an effusion in the joint and a very soft piece of bone in the olecranon fossa which was excised. Post-operatively the patient's pain resolved rapidly although the range of movement remained restricted.

Histological examination of the bone from the olecranon fossa showed a typical nidus of osteoid osteoma with surrounding reactive bone (Fig. 4).

Discussion

Less than 3% of all osteoid osteomas occur around the elbow (Mirra, 1989). In this case the history of constant pain, the presence of a persistent joint effusion and the limitation of flexion and extension are consistent with the signs and symptoms previously reported of peri-articular osteoid osteomas around the elbow (Marcove & Freiberger, 1966; Ruggieri et al, 1989). The presence of new bone formation remote from the nidus is typical when the nidus is intra-articular (Cronemeyer et al, 1981; Shifrin & Reynolds, 1971). The scintigraphic appearance of diffuse uptake in the distal humerus and elbow joint is also typical when the nidus is intra-articular. The synovitis is seen as increased activity within the joint whereas the increased uptake remote from the nidus corresponds with the new bone formation in the distal humeral metaphysis (Fig. 2). The cortical cavity revealed on CT (Fig. 3) was initially presumed to be the nidus and the lesion in the olecranon

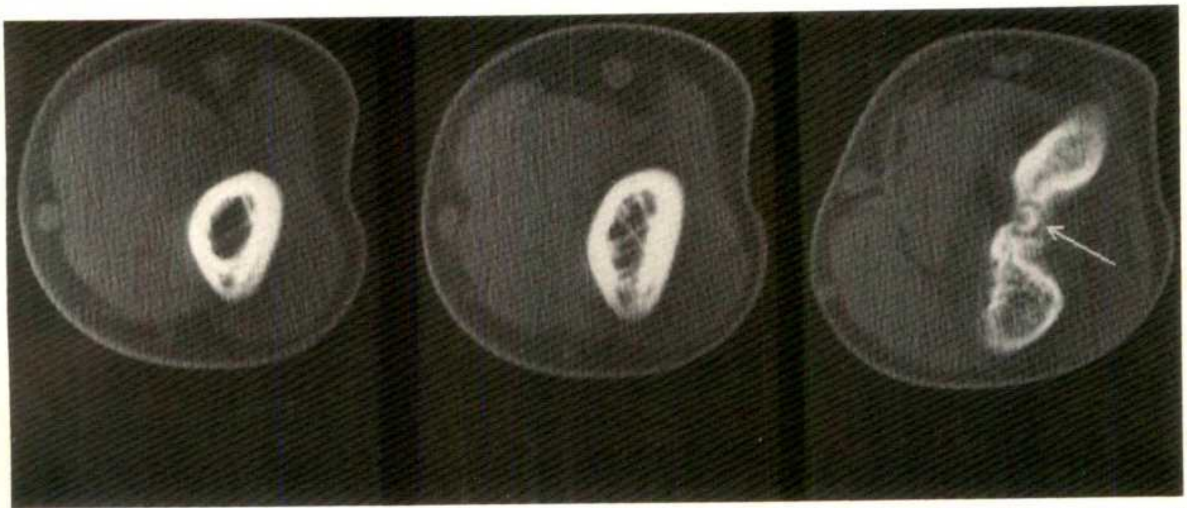

Figure 3. Axial CT of distal humerus showing lamellar periosteal reaction posteromedially with a cavity in the lateral cortex and an ossicle in the olecranon fossa (arrowed).

fossa was thought to be an os supratrochleare dorsale, a well described normal variant (Keats, 1979; Obermann & Loose, 1983). This accessory bone is usually unilateral and is visible on radiographs as a discrete bone of irregular density with a thickened sclerotic rim. It can therefore resemble the nidus of an osteoid osteoma.

Although the radiological diagnosis of osteoid osteoma was correctly made in this case the biopsies were initially taken from the lateral humeral metaphysis in the area of maximal cortical reaction and where the patient was most tender. The nidus was therefore missed and the patient's pain persisted. When the nidus was eventually excised from the olecranon fossa, the pain resolved.

Review of the literature has shown that a nidus of osteoid osteoma in this site is not unique. Marcove and Freiberger (1966) described two cases in which the nidus of an osteoid osteoma arose in olecranon fossa, one of which was also misdiagnosed as an accessory ossicle. As in this case the nidus increased in size considerably over a period of 6 months which would not be expected for an accessory ossicle. Sherman (1947) also described a case in which the nidus arose in the olecranon fossa. In addition, Shifrin and Reynolds (1971) and Rida and Fahmy (1967) have described an osteoid osteoma arising as a discrete lesion in the coronoid fossa.

In summary, osteoid osteomas around the elbow can be difficult to diagnose because the typical radiographic findings of a nidus with adjacent osteosclerosis and a periosteal reaction are often absent. In a young patient with persistent elbow pain and evidence of synovitis, an ossific lesion in the olecranon fossa should be suspected as a nidus of osteoid osteoma rather than an accessory ossicle.

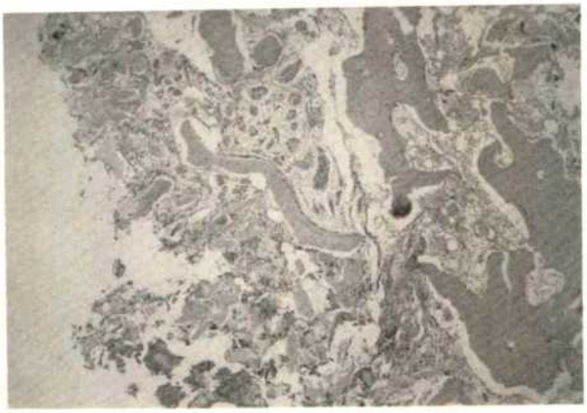

Figure 4. Photomicrograph of excised ossicle showing normal bone trabeculae on right together with smaller spicules of bone, fibroblastic stroma and plump osteroblasts consistent with osteoid osteoma on the left.

References

Clarke, C. R., Ozonoff, M. B. & Drennan, J. C., 1981. Case report 157. *Skeletal Radiology*, *6*, 286–289.

Corbett, J. M., Wilde, A. H., McCormack, L. J. & Evarts, C. M., 1974. Intra-articular osteoid osteoma. A diagnostic problem. *Clinical Orthopaedics and Related Research*, *98*, 225–230.

Cronemeyer, R. L., Kirchmer, N. A., De Smet, A. A. & Neff, J. A., 1981. Intra-articular osteoid osteoma of the humerus simulating synovitis of the elbow. *Journal of Bone and Joint Surgery*, *63-A*, 1172–1174.

Keats, T. E., 1979. *An Atlas of Normal Roentgen Variants That May Simulate Disease* (Yearbook Medical Publishers, Chicago), pp. 251–252.

Marcove, R. C. & Freiberger, R. H., 1966. Osteoid osteoma of the elbow. A diagnostic problem. *Journal of Bone and Joint Surgery*, *48-A*, 1185–1190.

Mirra, M. M., 1989. *Bone Tumours* (Lea & Febiger, Philadelphia), pp. 226–228.

1990, *The British Journal of Radiology*, *63*, 902–904

Moreton, K. S. & Bartlett, L. H., 1966. Benign osteoblastic change resembling osteoid osteoma. Three cases with unusual radiological features. *Journal of Bone and Joint Surgery*, *48-B*, 478–484.

Moser, R. P., Kransdorf, L. T. C., Brower, A. C., Hudson, T., Aoki, J., Berrey, B. H. & Sweet, D. E., 1990. Osteoid osteoma of the elbow. A review of six cases. *Skeletal Radiology*, *19*, 181–186.

Obermann, W. R. & Loose, H. W. C., 1983. The os supratrochleare dorsale: a normal variant that may cause symptoms. *Americal Journal of Roentgenology*, *141*, 123–127.

Rida, A. & Fahmy, A., 1967. Osteoid osteoma of the coronoid fossa of the humerus. A case report. *Egyptian Journal of Orthopaedics*, *2*, 53–61.

Ruggieri, P., Biagini, A., Ferraro, P. & Capanna, R., 1989. Osteoid osteoma of the elbow. A study of twelve cases. *Italian Journal of Orthopaedics and Traumatology*, *15*, 155–163.

Sherman, M. S., 1947. Osteoid osteoma associated with changes in adjacent joint. Report of two cases. *Journal of Bone and Joint Surgery*, *29*, 483–490.

Shifrin, L. Z. & Reynolds, W. A., 1971. Intra-articular osteoid osteoma of the elbow. A case report. *Clinical Orthopaedics and Related Research*, *81*, 126–129.

Note added in proof

Since the submission of our paper, a series of six osteoid osteomas of the elbow has been published (Moser et al, 1990). In none of these cases did the nidus mimic a supratrochlear ossicle.

Radiological diagnosis and management of a solitary tuberculous hepatic abscess

By D. H. Reed, MRCP, FRCR, *A. F. Nash, MRCP and *P. Valabhji, FRCP

Department of *Medicine and Radiology, East Glamorgan General Hospital, Church Village, Pontypridd

(*Received January 1990*)

Tuberculous hepatic abscesses are rare and usually associated with foci of infection in the lung or gastrointestinal tract (Leader, 1952). Primary hepatic abscesses, with no evidence of infection elsewhere, are even less common. To date only 13 cases have been described in the English language literature (Dhekne et al, 1987, Goh et al, 1987, Spiegel & Tuazon, 1984, Stevens & Little, 1987). The diagnosis is often elusive and made at laparotomy or post mortem. This case illustrates that the diagnosis may be made radiologically and then successfully managed by percutaneous drainage.

Case report

A 32-year-old man was admitted with a 4-week history of lethargy, anorexia, weight loss and night sweats. Fourteen years previously a chest radiograph had been taken because of contact with a relative who had pulmonary tuberculosis. The radiograph was normal and he was not followed up.

On examination he was unwell, anaemic and febrile. The right lung base had diminished breath sounds and hepatomegaly was present. The haemoglobin level was 10.5 g/dl and erythrocyte sedimentation rate raised at 100 mm/h. Liver function tests were abnormal with a low albumen (26 g/l) and a raised aspartate transminase (64 IU/l) and alkaline phosphatase (470 IU/l). A Mantoux test was strongly positive but sputum culture was negative. A chest radiograph demonstrated a raised right hemidiaphragm but normal lungs (Fig. 1). Abdominal ultrasound confirmed the hepatomegaly and showed a large hypoechoic area in the superior aspect of the right hepatic lobe. Computed tomography (CT) revealed a 17 cm fluid attenuation, non-enhancing, solitary lesion in the right lobe superior to the level of the porta hepatis (Fig. 2). After excluding hydatid disease serologically, diagnostic aspiration under CT guidance, through a 22 G fine needle, produced watery brown pus containing large numbers of acid-fast bacilli. A 7 French gauge pigtail catheter was inserted percutaneously through an intercostal space in the mid-axillary line, again under CT guidance, and 3200 ml of pus were removed over the next 2 days. Triple anti-tuberculous chemotherapy was started and within 2 days the patient's clinical state improved. Follow-up ultrasound showed the abscess was much smaller in size, though still visible, and the catheter was

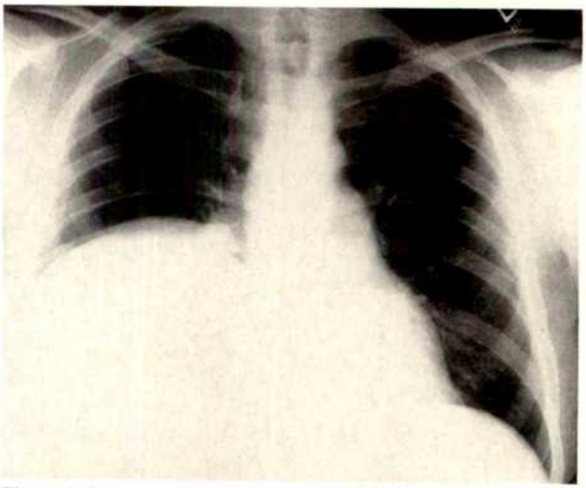

Figure 1. Postero-anterior chest radiograph demonstrating the raised right hemidiaphragm.

---

*Address correspondence to D. H. Reed, Department of Radiology, University Hospital of Wales, Heath Park, Cardiff CF4 4XW.

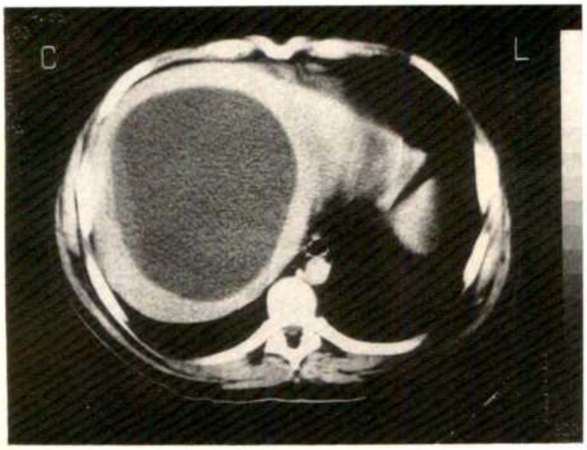

Figure 2. Axial CT with intravenous contrast medium through the upper abdomen.

removed since it had ceased to drain. Two weeks later the patient's condition deteriorated and CT demonstrated a recurrence of the abscess. A second pigtail catheter was inserted and 4300 ml of pus removed over the next 7 days. Patency of the catheter was maintained by flushing through 10 ml of heparinized saline every 24 hours. The catheter was removed when it ceased to drain and serial ultrasound examinations revealed progressive diminuition in size. Eight months later the patient is still on chemotherapy and remains well. A follow-up CT scan demonstated complete healing of the abscess (Fig. 3).

Discussion

Hepatic involvement in tuberculosis may take different forms. First, diffuse infiltration may exist in miliary tuberculosis (Morris, 1930). Secondly, diffuse hepatic disease may exist without pulmonary involvement, so-called primary miliary tuberculosis of the liver (Terry & Gunnar, 1957). Thirdly, focal hepatic disease may occur as solitary or multiple tuberculomata or abscesses. This type is rare (Leader, 1952) and usually exists secondary to pulmonary or gastrointestinal involvement. Occasionally, primary hepatic abscesses may occur, though only 13 cases have been described in the English literature. The diagnosis of this condition may be elusive: only six cases in this series were diagnosed pre-mortem at laparotomy.

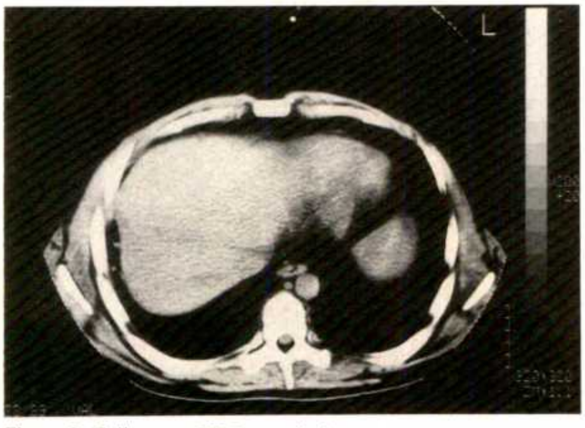

Figure 3. Follow-up CT 8 months later.

The clinical features of fever, right upper quadrant pain, weight loss and hepatomegaly have a low specificity. The description of the radiological features are also variable. The ultrasonographic features were described by Goh et al (1987) as a large, well defined hypoechoic lesion, as in our case. However, the first patient described by Dhekne et al (1987) had a large solid hepatic mass. Spiegel and Tuazon (1984) described a normal liver on ultrasound despite a 6 × 10 cm lesion in the right lobe being removed days later at surgery.

The CT features are also variable: our patient demonstrated a large low attenuation lesion with no visible wall or enhancement. However, ring enhancement has been described by Dhekne et al (1987) and Mustard et al (1986). These differing features on ultrasound and CT may relate to the often indolent natural history of this condition. Local hepatic reaction, capsule formation and the contents of the purulent exudate may depend on the duration of the infection.

Earlier reports stressed the need for surgical exploration and drainage in the diagnosis and management of tuberculous hepatic abscesses (Gracey, 1965; Sherlock, 1985). However, despite the low predictive value of the radiological signs, this case demonstrates how the condition may be successfully managed radiologically using either ultrasound- or CT-guided aspiration or drainage. Initially a narrow gauge needle may be guided into the lesion and pus aspirated, and then a percutaneous catheter may be passed safely into the lesion. Mustard et al (1986) described percutaneous aspiration of a tuberculous liver abscess in a patient with a primary laryngeal infection. They considered necessary three criteria for successful percutaneous drainage: a unilocular collection, a safe access route avoiding other viscera and a route and technique that does not contaminate a previously sterile compartment. If these criteria cannot be met then surgical drainage should be considered. To these criteria should be added the caveat that a microbiological diagnosis must be made. In our patient, Ziehl Neelson staining and microscopy of the aspirate gave the diagnosis. However, microscopy may be negative and a diagnosis only reached after culture. Sometimes, a microbiological diagnosis cannot be reached at all and the diagnosis can only be made on histological examination of the abscess wall (Zipser et al, 1976). Surgery may then be needed to make a diagnosis if biopsy of the abscess wall is not diagnostic, since differentiation from a pyogenic abscess or necrotic tumour is of paramount importance.

Of interest was the recurrence of the liver abscess after the beginning of chemotherapy. The development of a liver abscess after treatment has been described (Gracey, 1965; Mustard et al, 1986). Gracey thought that the capsule of scar tissue around the abscess may prevent antibiotics reaching their target. Certainly, the large size of these lesions may stop a bacteriacidal concentration of agent from reaching the centre of the lesion. Mustard et al (1986) infused isoniazid and rifampicin every 6 hours down the catheter in their patient to overcome this problem. In our patient the first drain was probably removed too soon. The second drain was in place for longer and kept patent with regular flushing of saline. The drain should be removed either when the abscess has disappeared or when it ceases to function. In the latter case, if the patient is still unwell, replacement with a larger drain should be considered.

Image-guided interventional techniques may be used to diagnose and treat tuberculous hepatic abscesses successfully, thus avoiding laparotomy, open drainage or hepatic resection.

Acknowledgments

We would like to thank Dr E. Hicks and Dr C. Davies for their help and advice.

References

DHEKNE, R. D., MOORE, W. H., LONG, S. E. & BARRON, B. J., 1987. Tuberculous pseudotumor of the liver. *Clinical Nuclear Medicine, 12*, 816–819.

GOH, K. L., PATHMANATHAN, R., CHANG, K. W. & WONG, N. W., 1987. Tuberculous liver abscess. *Journal of Tropical Medicine, 90*, 255–257.

GRACEY, L., 1965. Tuberculous abscess of the liver. *British Journal of Surgery, 52*, 442–443.

LEADER, S. A., 1952. Tuberculosis of the liver and gall bladder with abscess formation: a review and case report. *Annals of Internal Medicine, 37*, 594–606.

MORRIS, E., 1930. Tuberculosis of the liver. *American Review of Tuberculosis, 22*, 585–592.

MUSTARD, R. A., MACKENZIE, R. L. & GRAY, R. G., 1986. Percutaneous drainage of a tuberculous liver abscess. *Canadian Journal of Surgery, 29*, 449–450.

SPIEGEL, C. T. & TUAZON, C. U., 1984. Tuberculous liver abscess. *Tubercle, 65*, 127–131.

SHERLOCK, S., 1985. *Diseases of the Liver and Biliary System. 7th edn* (Blackwell, Oxford).

STEVENS, A. & LITTLE, J. M., 1987. Isolated tuberculous hepatic abscess. *Australian and New Zealand Journal of Surgery, 57*, 409–411.

TERRY, R. B. & GUNNAR, R. M., 1957. Primary miliary tuberculosis of the liver. *Journal of the American Medical Association, 164*, 150–157.

ZIPSER, R. D., RAU, E., RICKETTS, R. R. & BEVANS, L. C., 1976. Tuberculous pseudotumours of the liver. *American Journal of Medicine, 61*, 946–950.

1990, *The British Journal of Radiology*, *63*, 905–906

Case of the month

A case of colonic defection

By Rosalind Butterworth, MB ChB, FRCS(Ed), FRCS(Eng) and *H. Adams, MRCP, FRCR

Departments of Surgery and *Radiology, Llandough Hospital, Penarth, Cardiff

(*Received October 1989*)

A 76-year-old woman presented with a 6-month history of left iliac fossa pain, associated with alternating constipation and diarrhoea.

For 30 years she had suffered from severe, generalized osteoarthritis. A left knee arthroplasty had been performed 8 years previously but this subsequently failed. Arthrodesis was therefore undertaken with internal fixation using an intramedullary nail. The nail later fractured and the patient underwent further surgery to the left knee with bone grafting.

At presentation the patient was moderately obese. There was tenderness in the left iliac fossa but abdominal and rectal examinations were otherwise normal.

In view of the presenting symptoms, a colonic neoplasm was suspected. A barium enema was performed (Fig. 1).

What does this show?

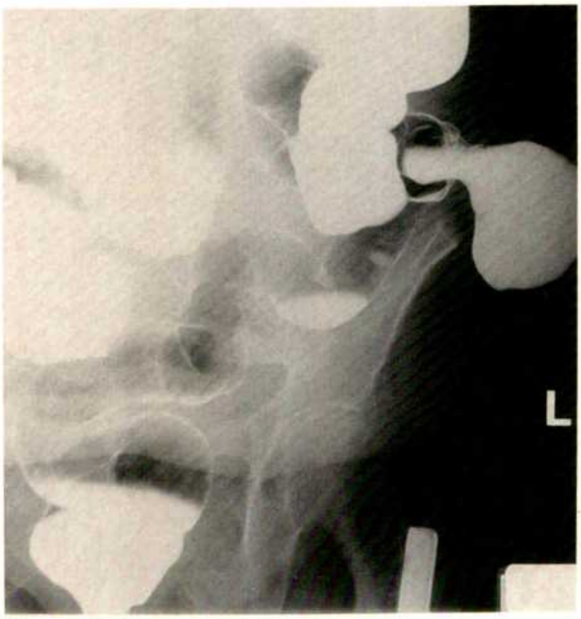

Figure 1. Barium enema of the colon.

Address for correspondence: Dr H. Adams, Department of Radiology, Llandough Hospital, Penarth, S. Glamorgan.

There is no intrinsic colonic abnormality. A bone graft has been taken from the left iliac crest. There is herniation of the descending colon through the resulting defect.

Discussion

Herniation of abdominal viscera through an iliac crest donor site is a rare but recognized complication of bone grafting (Cowley & Anderson, 1983; Kinninmonth & Patel, 1987). Similar herniae have been reported after pelvic trauma or surgical debridement of the iliac crest following osteomyelitis (Lewin & Bradley, 1945; Bosworth, 1955).

In this case computed tomography was performed for further anatomical delineation prior to possible surgery (Fig. 2). The iliac crest defect and the hernial sac containing colon are well demonstrated.

A full thickness bony defect is necessary for herniation of abdominal contents. This complication occurs more commonly if bone is taken from the mid-portion of the iliac crest (Bosworth, 1955). Prevention can be achieved by taking the graft from the anterior or posterior parts of the crest, allowing easier re-attachment of the abdominal wall musculature, or by avoidance of full thickness grafts.

Clinical presentation is usually with a painful swelling related to the bone graft donor site. A cough impulse may be elicited. Symptoms in previously reported cases have developed between 24 days and 15 years after surgery (Cowley & Anderson, 1983). In our case, onset of symptoms occurred almost immediately after bone grafting. The hernia was impalpable owing to the patient's obesity, but once detected fluoroscopically, it could be manually reduced with reproduction of the patient's pain. Strangulation of these herniae has been reported (Challis et al, 1975) and early surgery has been recommended to our patient.

Methods of surgical repair which have been described include soft-tissue repair using a gluteal flap, the insertion of prosthetic material and refashioning of the iliac crest with re-attachment of the abdominal wall musculature (Cowley & Anderson, 1983). No method of repair is reported to have failed.

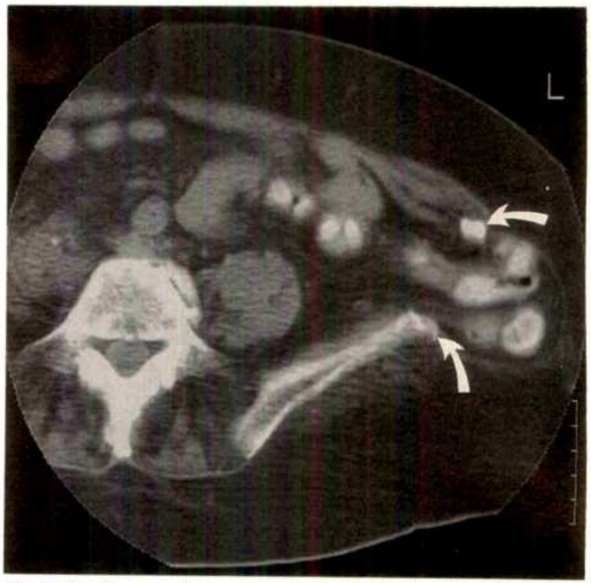

Figure 2. Computed tomography at the level of the iliac crest showing the bony defect (arrows) and hernial sac.

Acknowledgments

We would like to thank Mr D. J. T. Webster and Mr M. H. Young for their permission to report this case.

References

Bosworth, D. M., 1955. Repair of herniae through iliac-crest defects. *The Journal of Bone and Joint Surgery*, *37A*, 1069–1073.

Challis, J. H., Lyttle, J. A. & Stuart, A. E., 1975. Strangulated lumbar hernia and volvulus following removal of the iliac crest bone graft. *Acta Orthopaedica Scandinavica*, *46*, 230–233.

Cowley, S. P. & Anderson, L. D., 1983. Hernias through donor sites for iliac-bone grafts. *The Journal of Bone and Joint Surgery*, *65A*, 1023–1025.

Kinninmonth, A. W. G. & Patel, P., 1987. Herniation through a donor site for iliac bone graft. *Journal of the Royal College of Surgeons of Edinburgh*, *32*, 246.

Lewin, M. L. & Bradley, E. T., 1949. Traumatic iliac hernia with extensive soft tissue loss. *Surgery*, *26*, 601–607.

1990, *The British Journal of Radiology*, *63*, 907–909

Short communication

High resolution, high field magnetic resonance imaging of joints: unexpected features in proton images of cartilage

By P. R. Cole, MSc, *M. K. Jasani, MD, B. Wood, PhD, †A. J. Freemont, MD and §G. A. Morris, DPhil

Biomedical NMR Unit, Departments of †Rheumatology and §Chemistry, University of Manchester, Oxford Road, Manchester M13 9PL and *Ciba-Geigy Pharmaceuticals, Horsham, W. Sussex RH12 4AB

(*Received February 1990*)

Clinical magnetic resonance (MR) imaging at normal resolution is of proven value in the diagnosis of joint disease (Reicher et al, 1985; Ehman et al, 1988). However, prospective studies of conditions such as osteoarthritis are technically more demanding, requiring reliable quantitative assessment of such parameters as cartilage thinning and matrix over-hydration. This report concerns the observation and explanation of some unexpected features in the high field, high resolution imaging of proximal interphalangeal joints *in vivo* (Cole et al, 1989) and of sections of knee joints *in vitro*. The results suggest that high resolution MR images of joints obtained by conventional methods should be interpreted with some caution, but that there may be scope for using some unusual MR properties of cartilage reported below as a probe of joint disease.

Methods

Images and longitudinal spin-echo profiles were obtained using a 3 cm diameter, eight segment birdcage resonator (Hayes et al, 1985; Mackenzie et al, 1988) in a Bruker Biospec system with a 4.7 T, 11 cm horizontal bore magnet. At this field strength the chemical shift between lipid and water signals amounts to some 700 Hz, necessitating the use of chemically selective imaging methods. Multislice spin-echo imaging with chemical selection by gradient reversal (Volk et al, 1987) was used for *in vivo* and *in vitro* imaging, with four contiguous 2.5 mm slices per experiment, gradient strengths of up to 2.3 G/cm, a field of view of 3 cm and a typical resolution of 100×100 μm. One-dimensional spin-echo profiles were obtained using the normal spin-echo imaging sequence to measure the longitudinal proton signal profiles of 7 mm diameter knee cores, with a read gradient of 2.3 G/cm and variable T_E. Transverse slice selection was obtained where necessary using selective inversion pulses in the presence of field gradients.

Results

Figure 1 shows an expanded view of a typical water signal spin echo ($T_E = 40$ ms, $T_R = 3000$ ms) image of the proximal interphalangeal (PIP) joint, in this case of the left middle finger of the first author, measured with the read gradient transverse to the finger and the phase encode gradient longitudinal (reasons for this choice of geometry are discussed below). A number of unexpected features, common to all the normal joints examined in this study, are apparent. Bright wedges are seen at the periphery of the joint; these have long T_1 and T_2 times, and are attributed to highly hydrated synovial tissue. The overall thickness of the cartilage observed is much less than that expected from known anatomy and inferred from microfocal radiography (Buckland-Wright, 1989). Even more disturbing is the appearance of a dark line, approximately 100 μm wide, apparently following the cartilage surfaces. Again, this feature appeared to a greater or lesser extent in all of the normal joint images obtained. A 0.26 T low field high resolution finger image (spin echo, $T_E = 30$ ms) of the first author showed cartilage thickness approaching that expected, but still with the dark line.

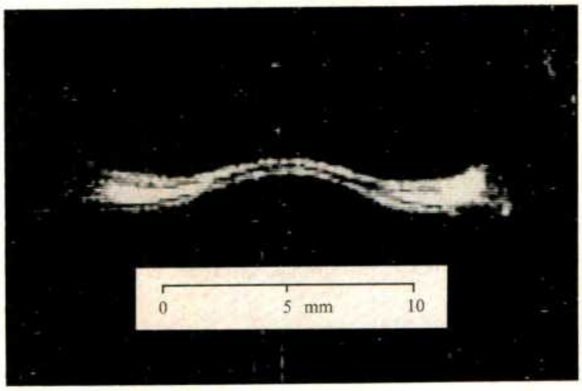

Figure. 1. Spin echo ($T_E = 40$ ms, $T_R = 3000$ ms) chemically-selected water image of a normal PIP joint *in vivo*. The finger is fully extended, with the distal end at the top of the image. A 2.5 mm thick slice, midway through the joint and in the plane of the fingers, is shown.

In order to establish reasons for these unexpected features, a simple *in vitro* model system using freshly excised human cartilage was chosen, consisting of 7 mm diameter, 2 cm long cores through cadaveric knee joints. In this preparation the cartilage and cortical bone

---

Address correspondence to Dr G. A. Morris.

surfaces are approximately planar and the cartilage layers are substantially thicker than in PIP joints, minimizing any systematic image distortions that might be caused by magnetic susceptibility differences between different joint components. Care was taken to ensure that the joint surfaces remained in contact during the experiments. Orientation of the preparation to within a few degrees of the read gradient direction was achieved using sighting images. Cores were imaged (a) using normal slice-selective spin echo methods with chemical selection, (b) using spin echo without slice selection or chemical selection and (c) using a three-dimensional Fourier transform spin echo technique. The features noted above, observed at the limits of resolution in PIP joint images, were seen much more clearly in knee core images obtained in all three techniques. The cartilage width observed was approximately half that expected, and a dark line 500 μm wide was seen following the bearing surface.

Figure 2 shows the T_E dependence of the one-dimensional longitudinal proton spin-echo signal profile of a knee core from a 45-year-old man with no joint diease. No chemical selection or slice selection was used, so the fat signals at the sides of the profile (regions I and III) are displaced by approximately 0.7 mm to the right with respect to the water signals (region II). Reversal of the read gradient caused the outer (fat) features to move to the left in the profile. Application of transverse slice selection resulted in a slight sharpening of the features observed, but the T_E dependence was unchanged.

Discussion

A variety of explanations were considered for the features observed in Fig. 1. Loss of signal owing to long spin-lattice relaxation times was eliminated as an explanation by comparison of images with different recovery times T_R. Reported differences in hydration between different layers of cartilage (Maroudas, 1979) are far too small to account for the large signal changes seen. Anomalies in joint images are sometimes attributed to "chemical shift artefacts", presumably a misnomer for the distortions caused by the difference in magnetic susceptibility between cartilage and bone. These effects depend on the orientation of the read gradient with respect to the cartilage: bone interface. Proximal interphalangeal images obtained using the read gradient along the finger axis show the dark line displaced to one side of the joint or the other, depending on the sign of the read gradient, by an amount comparable to the resolution (100 μm) in the experiments described. The effects may be minimized by placing the phase encode direction along the finger axis and the read gradient across the joint (Wradzilo et al, 1988). The logic here is to ensure that the phase encode gradient, for which the spin echo provides compensation

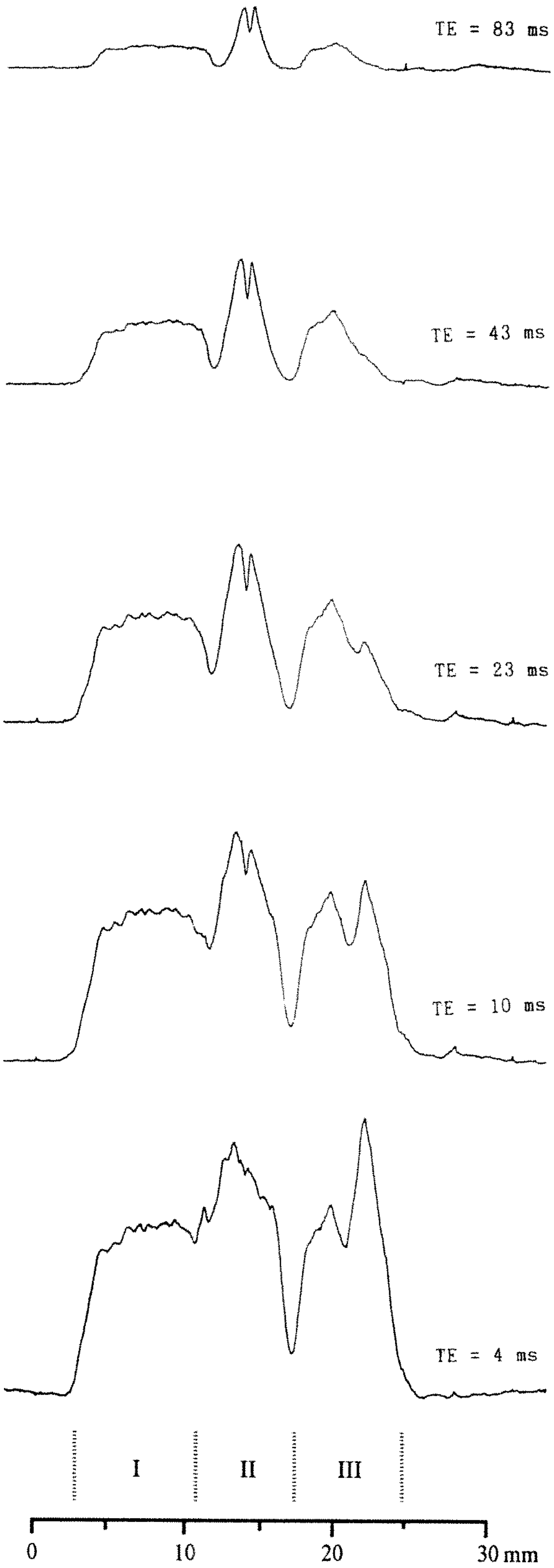

Figure 2. Longitudinal proton signal profiles of a 7 mm diameter knee core; the femoral side appears to the left and the tibial to the right of the profiles. Regions I and III contain proton signals from fat (in trabecular bone), and region II from water (in cartilage).

for any errors in the static magnetic field, lies along the direction of most rapid change in magnetic susceptibility, in this case along the finger. Comparison between images measured with different gradient strengths confirmed that image distortions due to susceptibility effects are rendered negligible by the experimental conditions used for Fig. 1, with the phase encode direction along the finger axis.

The knee core experiments were designed to confirm that susceptibility effects are not to blame for the dark line and lost cartilage signal observed in spin-echo images of PIP joints, and to test the hypothesis that spin-spin relaxation is responsible. Although the features of Fig. 2 are slightly blurred as a result of the difficulty of achieving perfect alignment of the core with respect to the read gradient, they give clear evidence of the origins of the signal loss seen in Fig. 1. The growth of a notch in the cartilage water profile and the gradual thinning of the cartilage profile as T_E is increased from 4 to 83 ms are evident even at 10 ms, and at 40 ms the profile shows a good match with that obtained by taking a cross-section through the spin echo ($T_E=40$ ms, $T_R=3000$ ms) core images (although as expected from the imperfect alignment of the core, the notch in the profile is less deep than that seen in the image). The clear implication is that both the dark line, and the signal loss in cartilage close to cortical bone, have their origin in some type of T_2 relaxation. The observation of thicker cartilage in the low field finger image than in Fig. 1 suggests that the mechanism responsible for the shortened T_2 of water from cartilage layers nearest the bone is field-dependent.

The variation in T_2 observed across cartilage layers in the profiles of Fig. 2 is considerably greater than that encountered within most other tissues, with different components of the cartilage having apparent values of T_2 differing by almost an order of magnitude. Small differences in T_2 between different layers of hip cartilage have been reported previously (Lehner et al, 1989), but this minor variation may mask a much larger range, probably because of the difficulty of achieving sufficient spatial resolution to obtain signals from areas of tissue with homogeneous relaxation properties. The observation that cartilage water T_2 values cover a wide range in man is surprising but not unprecedented; the apparent cartilage T_2 in rabbit is known to fall from tens of milliseconds in the juvenile to less than 5 ms at maturity (Waterton, 1989; Checkley et al, 1989). At this stage it is premature to speculate on the mechanisms involved, but possibilities include water diffusion across local field gradients in regions of calcified cartilage, and exchange between free and tightly bound water.

Several conclusions may be drawn from this study. Proton images of joints at high field are likely to give grossly misleading estimates of cartilage thickness if values of T_E longer than a few milliseconds are employed. The dark line observed under high resolution may be useful in indicating the position of cartilage surfaces. With such a wide range of cartilage spin-spin relaxation properties, it seems very likely that there is scope for using cartilage T_2 measurements to probe articular disease.

Acknowledgments

The Biospec instrument used in this research was funded by the Science and Engineering Research Council and by the University of Manchester. P.R.C. thanks the Isle of Man Government for a research studentship, and Drs D. T. Edmonds and M. A. H. McCausland for helpful discussions. Sha Zhao kindly provided a high resolution low field image of a PIP joint. G.A.M. is grateful to Dr J. C. Waterton for many helpful conversations and for much patient advice; helpful discussions with Prof. M. I. V. Jayson and Dr. J. C. Buckland-Wright are also gratefully acknowledged. The early stages of this project owed much to the energy and enthusiasm of Dr I. S. Mackenzie.

References

Buckland-Wright, J. C., 1989. A new high-definition microfocal X-ray unit. *British Journal of Radiology, 62*, 201–208.

Checkley, D., Johnstone, D., Taylor, K. & Waterton, J. C., 1989. High-resolution imaging of an antigen-induced arthritis in the rabbit knee. *Magnetic Resonance in Medicine, 11*, 221–235.

Cole, P. R., Wood, B., Morris, G. A., Freemont, A. J., Jayson, M. I. V. & Jasani, M. K., 1989. High resolution, chemical shift specific imaging of human interphalangeal joints *in vivo* at 4.7T. *Proceedings of the 8th Annual Meeting, Society for Magnetic Resonance in Medicine, Amsterdam*, 934.

Ehman, R. L., Berquist, T. H. & McLeod, R. A., 1988. MR imaging of the musculoskeletal system: a 5 year appraisal. *Radiology, 166*, 313–320.

Hayes, C. E., Edelstein, W. A., Schenck, J. F., Mueller, O. M. & Eash, M., 1985. An efficient, highly homogeneous r.f. coil for whole-body imaging at 1.5T. *Journal of Magnetic Resonance, 63*, 622–628.

Lehner, K. B & Rechl, H. P., 1989. Normal morphology and degeneration of hyaline articular cartilage in MR imaging. An in vitro study of bovine patellae and human arthritic femoral heads. *Proceedings of the 8th Annual Meeting, Society for Magnetic Resonance in Medicine, Amsterdam*, 308.

Mackenzie, I. S., Cole, P. R., Robinson, E. M. & Wood, B., 1988. A trombone-tuned birdcage resonator for ^{1}H and ^{19}F NMR imaging at 4.7T. *Proceedings of the 7th Annual Meeting, Society for Magnetic Resonance in Medicine, San Francisco*, 856.

Maroudas, A., 1979. Physicochemical properties of articular cartilage. In *Adult Articular Cartilage*, ed. by M. A. R. Freeman (Pitman Medical, Tunbridge Wells), pp. 215–290.

Reicher, M. A., Bassett, L. W. & Gold, R. H., 1985. High-resolution magnetic resonance imaging of the knee joint: pathologic correlations. *American Journal of Roentgenography, 145*, 903–909.

Volk, A., Tiffon, B., Mispelter, J. & Lhoste, J.-M., 1987. Chemical shift specific slice selection. A new method for chemical shift imaging at high field. *Journal of Magnetic Resonance, 71*, 168–174.

Waterton, J. C., 1989. Personal communication.

Wradzilo, W., Schneider, S., Richter, G., Kauffmann, G., Hiltbrand, E. & Gottschlich, K., 1988. Magnetic resonance imaging of the hyaline joint cartilage of the hip. *Proceedings of the 8th Annual Meeting, Society for Magnetic Resonance in Medicine, Amsterdam*, 307.

1990, *The British Journal of Radiology*, *63*, 910–911

Correspondence

(The Editors do not hold themselves responsible for opinions expressed by correspondents)

Major contamination from an iodine-131 therapy patient

THE EDITOR—SIR,

The events surrounding the iodine therapy of a patient with carcinoma of the thyroid have indicated that the normal pattern of uptake and excretion cannot be taken for granted.

Case report

The patient was given 7.4 GBq of I-131 by mouth at approximately 2.00 p.m. on Monday. The level of activity in the patient was assessed by measuring the dose rate at 1 m from the thyroid shortly after the administration and at 24-hour intervals until the following Friday. In normal circumstances, subject to the activity measured on the Friday having fallen to a satisfactory level, the patient would have been discharged at the weekend. Apart from this, the change in activity levels was not followed closely.

On the Friday the activity level in this particular patient had not fallen to a level low enough for him to be discharged. Over the Friday and Saturday, the patient's condition deteriorated. On the Saturday evening the patient was seen by the Radiotherapy SHO on duty and with the agreement of the Radiation Protection Advisor was transferred from the side ward to the main ward so that the nursing staff could monitor his condition more closely. Otherwise precautions against radioactive contamination, *e.g.* the use of a commode and of disposable eating utensils by the patient and the use of plastic aprons and overshoes by the staff, were continued and the one bed next to the patient was closed. The patient's condition continued to deteriorate, he became incontinent and finally died at 3.30 a.m. on the Monday morning.

The duty physicist was called and advised that the patient should be moved to the side ward. At this stage significant levels of contamination were not expected. Two physicists came into the hospital and started monitoring the ward and staff. The activity level in the patient had fallen significantly and the mortuary were advised that the patient could be removed from the side ward and released to the undertakers.

Using a calibrated Mini Instrument Type 5.41 Scintillation Monitor, high levels of contamination were found. Notably the mattress and its cover gave count rates suggesting a contamination level of approximately 20 kBq/cm^2. A cushion on an easy chair gave 400 Bq/cm^2 and two areas of floor, one on the side ward surrounding the patient's bed about 2.5 × 1 m, and another on the main ward between the bed and the easy chair about 0.75 × 0.5 m, gave count rates suggesting a contamination of approximately 5 kBq/cm^2.

A large quantity of cleaning wipes, etc., used for nursing the patient, paper used for mopping up urine and plastic aprons and overshoes had been collected in plastic bags. These showed significant contamination levels; the total activity was estimated as 18 MBq.

The mattress, which was the worst contaminated item, was stored until its activity level had fallen to a level where it could be disposed of to a rubbish tip. The remaining items were sent to the hospital incinerator for burning. Attemps were made to remove the activity from the floor using Decon solution. However, the activity level could not be brought below 1 kBq/cm^2 and the floor areas concerned were therefore covered with vinyl to prevent the spread of contamination.

Measurements on the nursing staff and the physicists who had attended the incident showed significant contamination on the underneath of some of their shoes. This was removed by wiping with swabs soaked in Decon solution. All the staff concerned had taken great care in the wearing of plastic overshoes.

Measurements

The dose rate at 1 m from the thyroid is plotted in Fig. 1. Comparison of the decay of the dose rate with the physical half-life of I-131 and a typical normal pattern of combined physical and biological decay shows that very little of the activity was excreted over the first 4 days. The activity of a blood sample taken for a renal function test after just over 24 hours was found to be more than 31 kBq in 50 μl. Thus it is apparent that most of the activity remained in the patient's body and was not excreted until he became incontinent.

A plastic overshoe was placed over a plastic phantom foot and left in an I-131 solution of 200 kBq in 50 ml for 1 minute, applying firm downward pressure. The overshoe had first been worn to walk 400 m. When the overshoe was removed a contamination level of 70 Bq/cm^2 was found on the phantom foot. Similar measurements repeated with a heavy duty overshoe and with an unworn thinner overshoe left no contamination behind on the foot. Examination of the thinner overshoe showed that abrasion had produced small holes.

Conclusions

In an iodine therapy patient with impaired renal function, activity may remain in the blood or urine pool. It cannot be assumed that there is no contamination hazard after 24 hours unless a measurement of activity (or of dose rate at a fixed distance) confirms that this is so. Special precautions therefore

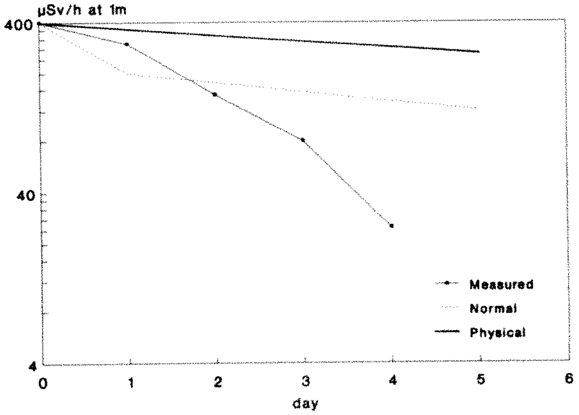

Figure 1. Dose rate at 1 m from the thyroid over time.

need to be taken with ill and incontinent patients who are exceptions to the usual I-131 type.

Single thin overshoes do not provide adequate protection against radioactive contamination. Thick or double overshoes are necessary and these should be changed after each short period of use.

Yours, etc.,
F. J. F. MADDEN
*R. J. AUKETT
*M. Y. EARLY
M. J. DUNN
J. RAMPTON

Department of Radiotherapy & Oncology and
*Department of Medical Physics,
Leicester Royal Infirmary,
Infirmary Square,
Leicester LE1 5WW
(*Received March 1990*)

Temporary enlargement of penumbra on linear accelerators

THE EDITOR—SIR,

We have recently observed that check radiographs produced on some of our linear accelerators have exhibited a greatly enlarged penumbra in the radial (G–T) direction. The effect was however observed only on fast diagnostic film and not on the much slower radiotherapy verification film. The faster film was given a dose of approximately 0.02–0.03 Gy, whereas the slower received a dose in excess of 1.0 Gy. The effect was also found to be restricted to linear accelerators employing 90° beam bending systems with servo-stabilization.

The cause was found to be that in these machines, immediately following the commencement of radiation, the beam is temporarily very unstable in the radial plane, with rapid marked excursions of the corresponding beam edges from the correct positions. This behaviour is however of very short duration, stability being attained after the delivery of the first few monitor units and thus explains why the effect is observable only on check radiographs using fast films and not either on slow films or on the integrated therapy field distribution.

Yours, etc.,
J. B. TUOHY
A. M. MORGAN

Regional Radiotherapy Centre,
Cookridge Hospital,
Leeds LS16 6QB
(*Received April 1990 and in revised form June 1990*)

1990, *The British Journal of Radiology*, *63*, 912–915

Proceedings of the British Institute of Radiology

The repair of radiation damage: molecules to man

Abstracts of papers presented at a BIR work-in-progress meeting held at 36 Portland Place, London W1N 4AT on Friday, 11 May 1990

Repair and misrepair of DNA double-strand breaks in relation to the induction of chromosomal aberrations, by P. E. Bryant

Origins of chromosome structural aberrations, by J. R. K. Savage

Transfection and expression of the *E. coli* nth gene in mammalian cells and its effect on radiation and hydrogen peroxide cytotoxicity, by L. Harrison, M. Skorvaga, A. J. Watson, H. Ahern, R. P. Cunningham, J. H. Hendry and G. P. Margison

The measurement of DNA repair in human tumour cells, by T. J. McMillan, A. Cassoni, J. J. Eady, J. H. Peacock, S. Powell and G. G. Steel

What can gene cloning tell us about the UV-induced DNA repair defect in the human disease, xeroderma pigmentosum, by J. E. Arrand. Abstract not received

DNA double-strand break rejoining by human cell extracts, by P. North, A. Ganesh and J. Thacker

The kinetics of repair for radiation induced sublethal damage in pig skin: evidence for multi-components of repair, by G. J. M. J. van den Aardweg and J. W. Hopewell

Isolation of a radioresistant mutant, obtained from a radiosensitive human neuroblastoma cell line, by J. Russell

Does nicotinamide inhibit repair of radiation damage *in vivo*? by A. Rojas, E. Kjellen and M. C. Joiner

Modelling repair kinetics: extension of the linear-quadratic equation to higher order terms, by M. C. Joiner and P. Nilsson

Repair of radiation damage: overview, by A. Horwich

Repair and misrepair of DNA double-strand breaks in relation to the induction of chromosomal aberrations

P. E. Bryant

Department of Biology and Preclinical Medicine, University of St Andrews, Scotland

It is important to understand the molecular basis for the induction of chromosomal aberrations by radiation, as these appear to occupy a central position in relation to other biological end-points such as mutation, oncogenic transformation and cell death. Evidence suggests that chromosomal aberrations are induced from double-strand breaks (dsb) in DNA of cells. Measurements using the neutral velocity sedimentation technique indicate that, in mammalian cells, dsb are induced linearly with a frequency of about 40/Gy/diploid genome, and that first-order repair occurs with a half-time of 2–4 h. However, other techniques, notably the neutral elution method, indicate a linear-quadratic induction of dsb and a two-component repair kinetic with an initial half-time of some 20–30 min. The mechanisms of repair of dsb in mammalian cells are as yet unknown. However, results indicate that at least two mechanisms may operate: recombination and simple ligation. Chromosomal aberrations can be generated by introducing restriction endonucleases into permeabilized or porated cells, favouring the "breakage-first" hypothesis involving dsb. Blunt-ended dsb are more effective in inducing aberrations than cohesive-ended dsb. With X-rays there is an approximately sevenfold lower frequency of chromosome breaks than dsb, possibly as a result of the mixture of blunt- and cohesive-ended dsb induced by radiation. However, there is a genetically determined rate of conversion of dsb into chromosomal breaks. Repair of dsb appears to be reflected in the rejoining of chromosomal breaks either measured by the premature chromosome condensation (PCC) or G2 assay. Misrepair of dsb, giving rise to exchanges, follows quite different kinetics from those of breaks, suggesting an independent mechanism, different from that for rejoining of breaks.

This work is supported by the Cancer Research Campaign and the Commission of European Communities, Radiation Protection Programme.

Origins of chromosome structural aberrations

John R. K. Savage

MRC Radiobiology Unit, Chilton, Didcot, Oxon OX11 0RD

Structural aberrations, the majority of which involve the interaction between two or more lesions, are thought by many to be manifestations of repair ("misrepair"). The initiating lesions are clearly in DNA, but the plethora of clastogens and the variety of repair systems indicate that no one lesion is always responsible. Repair may work to remove lesions and preclude aberrations, modify lesions to permit aberrations, or the process of repair itself may actually produced aberrations. It is necessary to distinguish between *induction* (the placement of initial lesions) and *production* (the actual establishment of a structural change). These two events are separated in time and many intervening intranuclear events act to sever any simple relationship between them. Irrespective to the type of lesion, interaction requires that two DNA molecules must "touch". This raises two important questions. (a) Where, within the nucleus, is contact made? (b) Does contact precede or follow lesion induction? Current understanding of intra-nuclear architecture conditions our answers to these questions, and leads to the conclusion that probably only a small volume of the chromatin is actually at risk for the production of aberrations. The enormous length of DNA present and the extremely complex and precise packing/condensation of it to form the visible metaphase chromosome means that many aberrations are disguised and often obscured, so that only a proportion are actually registered on score sheets. This cautions against a hasty attempt to equate specific molecular events with observed aberrations.

Transfection and expression of the *E. coli* nth gene in mammalian cells and its effect on radiation and hydrogen peroxide cytotoxicity

L. Harrison, M. Skorvaga, A. J. Watson, *H. Ahern, *R. P. Cunningham, J. H. Hendry and G. P. Margison

PICR, Christie Hospital, Manchester M20 9BX and

**Department of Biological Sciences, University at Albany, New York 12222 USA*

The *E. coli* nth gene encodes endonuclease III which removes ring saturated, fragmented and ring contracted thymine derivatives from irradiated and/or oxidized DNA. The nth gene was ligated into pZipneoSV(X)I and transfected into two cell lines: RJKO (Chinese hamster V79 lung fibroblasts) and xrs7 (radiation sensitive Chinese hamster ovary cells). Following selection with G418, Southern analysis and the polymerization chain reaction, using oligonucleotides homologous to the nth sequence, showed the presence of the nth gene, while western analysis, using an *anti*-endonuclease III rabbit antibody demonstrated the presence of endonuclease III in extracts of two clones of each cell line: 1D and 7D (RJKO origin) and x7nth1 and x7nth6 (xrs7 origin). On gamma irradiation 1D and 7D were found to be more radiosensitive than the parental and vector control cell lines, which had equivalent clonal survival. The x7nth1 was found to be more radioresistant than the parental cell line while x7nth6 had equivalent clonal survival to xrs7. Differences in cell cycle and growth could not explain the radiosensitization of 1D and 7D, but may explain the radioresistance of x7nth1, which was found to have an increased G1 phase and decreased G2/M phase. Following hydrogen peroxide treatment, all clones expressing the nth gene were found to be more resistant than the parental cell lines to the mode one killing of hydrogen peroxide.

The measurement of DNA repair in human tumour cells

Trevor J. McMillan, A. Cassoni, J. J. Eady, J. H. Peacock, S. Powell and G. G. Steel
Radiotherapy Research Unit, Institute of Cancer Research, Cotswold Road, Sutton, Surrey

The repair capacity of human tumour cells has rarely been measured directly, although it has often been assumed to be an important determinant of cellular radiosensitivity. The major problem associated with a study of DNA repair in relation to sensitivity is that the critical lesions have not yet been identified. This study has therefore used three different assays which may assess different facets of repair in order to evaluate the role of repair in the determination of the radiosensitivity of human tumour cells. *Neutral filter elution* has been used to compare four human lung carcinoma cell lines of differing radiosensitivity. Differences in the level of damage induction were found, but even larger differences were seen after low dose rate irradiation during which repair can take place. At low dose rate significant levels of double-strand breaks (dsb) were still detectable after 70 Gy in the sensitive lines but no damage was evident in the two resistant lines. *Viral reactivation* involves the assessment of the repair of Adenovirus 5 which is irradiated prior to infection of the test cells. With this assay, no overall correlation was found between viral reactivation and sensitivity, but highly radiosensitive neuroblastoma cells were less able to repair the virus than radioresistant bladder carcinoma cell lines. *The plasmid reconstitution assay* involves the introduction of double-strand breaks in a specific gene by restriction endonucleases and their subsequent cell-mediated repair. With this technique, it was found that radiosensitive mutants of two human lines were repair deficient but two bladder carcinoma lines of almost identical radiosensitivity had very different abilities to repair plasmids. Thus this measure of repair does not always correlate with radiosensitivity. The three assays used in this study probably measure different aspects of repair. Neutral elution measures rejoining of double-strand breaks while the plasmid reconstitution assay measures the fidelity of the rejoining. The virus reaction also measures fidelity of repair but it probably is dominated by the processing of single-strand breaks. While apparently producing contradictory results in some cases, the use of several assays may provide a more detailed analysis of the repair proficiency of human tumour cells.

DNA double-strand break rejoining by human cell extracts

Phillip North, Anil Ganesh and John Thacker
MRC Radiobiology Unit, Chilton, Didcot, Oxon OX11 0RD

DNA double-strand breaks and their repair are thought to be important for cell survival after exposure to ionizing radiation. Cells from the radiosensitive human disorder ataxia-telangiectasia (A-T) show some characteristics of being defective in DNA-break repair. To examine the efficiency and fidelity of DNA-break rejoining, we have developed an *in vitro* assay using defined DNA molecules. Protein extracts are prepared from cell nuclei and used to treat plasmid DNA containing a model DNA double-strand break (generated by a restriction enzyme) at a specific site in a selectable gene. Rejoining is assessed by agarose gel electrophoresis and Southern analysis, and the fidelity of rejoining by bacterial transformation. We found that extracts from an A-T cell line (AT5BIVA) and a normal cell line (MRC5V1) were equally efficient at rejoining restriction breaks, but some restriction sites were rejoined more efficiently than others, irrespective of the origin of the extract. The fidelity of rejoining was equal for both cell extracts when the efficiency was relatively high, *e.g.* for *Sal*I-broken DNA. When the efficiency of rejoining was low, *e.g.* for *Eco*RI-broken DNA, the A-T cell extract showed a much higher frequency of mis-rejoining compared with the normal cell extract. One interpretation of this result is that the limited cohesiveness of the *Eco*RI-broken ends, relative to those for *Sal*I, affects the rejoining efficiency. This in turn affects the fidelity of rejoining with an A-T extract, presumably because the DNA ends are available to other enzymes. Data for the rejoining of other break sites supported this interpretation. Analysis of the mis-rejoined molecules showed deletions of mainly 20–40 base pairs.

The kinetics of repair for radiation-induced sublethal damage in pig skin: evidence for multi-components of repair

G. J. M. J. van den Aardweg and J. W. Hopewell
CRC Normal Tissue Radiobiology Research Group, Research Institute (University of Oxford), Churchill Hospital, Oxford OX3 7LJ

The clinical use of accelerated fractionation and hyperfractionated irradiation involving multiple fractions per day raises questions as to the kinetics of repair of sublethal radiation damage. The repair of sublethal damage was studied for the epidermis of the pig. Animals were irradiated with β-rays from strontium-90 plaques. Doses were given as 3F (3F/d) or as 4F (2F/d + 2F/d) with interfraction intervals of 5 min–8 h. The incidence of moist desquamation was used as an endpoint to assess the severity of the radiation response and dose–effect curves were fitted to the data by probit analysis. From these curves ED_{50} values ($\pm$SE) were calculated. Analysis of the data with a simple incomplete repair (IR) model, in which first order kinetics was assumed, showed an increase in the half-time $T_{\frac{1}{2}}$ for repair with increasing interfraction interval. For 3F/d, intervals of 0.25 h and 4 h between fractions produced significantly different estimates of $T_{\frac{1}{2}}$ (95% confidence limits) of 0.25

(0.18–0.42)h and 1.33 (0.91–2.41)h, respectively. Combining all data and using this simple IR-model produced estimates of $T_{\frac{1}{2}}$ which were biased depending on the design of the experiment. In an alternative analysis the 3F and 4F results were expressed in terms of the percentage dose unrepaired based on the ED_{50} values for the shorter intervals as compared with those for an interval of 24 h. The variation in the percentage dose unrepaired with respect to the interfraction interval was fitted significantly better by a bi-exponential equation than a mono-exponential equation. The slopes of the two components suggested a fast component and a slow component of repair with $T_{\frac{1}{2}}$ ($\pm$SE) of 8.7 ± 3.0 min and 2.77 ± 0.33 h, respectively. Studies of repair kinetics have also been initiated for clinically relevant doses of 2–3 Gy/fraction using 14 dose fractions and a half tolerance top-up dose of 17 Gy. With doses given as 14F plus a top-up dose and 24 h between the dose fractions the ED_{50} value for moist desquamation was 104.1 ± 4.2 Gy, this was not significantly different from that of 110.9 ± 3.9 Gy for a top-up dose followed by the 14 dose fractions. The data combined gave an ED_{50} of 107.9 ± 2.9 Gy. For 28 fractions, 2F/d and an 8 h interval between dose fractions, a significantly lower ED_{50} of 97.7 ± 2.7 Gy was observed. This indicated that with 8 h between fractions repair was still not complete and that a 10% reduction in total dose was required to achieve a comparable level of effect. After X-irradiation, dermal necrosis was used to assess late damage in the skin. From studies with 12 and 14 fractions given with either 24 h or $\geqslant 48$ h between fractions evidence was obtained that the repair of sublethal damage was incomplete in 24 h in this late responding tissue. The ED_{50} values for dermal necrosis were 4–12% lower using the schedules with 24 h as compared with $\geqslant 48$ h inbetween fractions. This finding has a considerable effect on the interpretation of the applicability of the different models of dose fractionation in studies carried out using this endpoint in pig skin.

Isolation of a radioresistant mutant, obtained from a radiosensitive human neuroblastoma cell line

J. Russell

Department of Radiation Oncology, Belvidere Hospital, Glasgow

Using a radiosensitive human neuroblastoma derived cell line, NB 1, we have obtained by selection with fractionated X-irradiation, a radioresistant variant, XRNB 1. Beginning with an original population of approximately 5×10^6 cells, selection was carried out by once or twice weekly irradiation with doses of 2 Gy. After 15 such treatments, an increase in the radioresistance of the population was noted. Using a clonogenic assay, the parent line displayed a D_0 of 0.8 Gy $\pm$ 0.1 (95% c.l.) and an extrapolation n_0, $n = 1.4 \pm 0.4$. The resistant line had a D_0 of 1.4 ± 0.3, and an extrapolation n_0, $n = 1.0 \pm 0.5$. Further irradiation did not increase the resistance of the population. However, in the absence of selective pressure, resistance was lost by the ninth passage. A similar phenomenon was observed in a subline established from a single cell of XRNB 1 population, suggesting that loss of the resistant phenotype cannot be ascribed to differences in growth rates between the resistant and normal cells, but that the mutation must be unstable. Preliminary results indicate that XRNB 1 cells have a capacity for PLD repair that is absent from the parent cells.

Does nicotinamide inhibit repair of radiation damage *in vivo*?

A. Rojas, E. Kjellen and M. C. Joiner

Cancer Research Campaign, Gray Laboratory, Mount Vernon Hospital, P.O. Box 100, Northwood, Middlesex HA6 2JR

Nicotinamide, the amide derivative of niacin and a structural analogue of 3-aminobenzamide, is thought to inhibit the chromatin-bound enzyme adenosine diphosphate ribosyl transferase (ADPRT). Inhibitors of ADPRT enhance the effect of DNA damaging agents, such as radiation and alkylating drugs, and have been shown to impair potentially and sub-lethal damage repair *in vitro*. We present evidence for a lack of repair inhibition by nicotinamide *in vivo*. The effect on recovery kinetics was investigated in mouse skin using a split-dose of 2×10.5 Gy of X-rays, separated by either 1 or 6 h, followed by graded doses of neutrons. Recovery half-times, determined using the Incomplete Repair model were similar for treatments with and without nicotinamide, indicating that it does not alter the rate of split-dose recovery in skin. The effect on repair capacity was studied by determining the α/β ratio, an inverse measure of the recovery *in vivo*. Inhibition of repair would have the effect of reducing the sensitivity of the tissue to dose-fractionation, and hence increasing the α/β ratio. Single doses, 2, 5 or 10 fractions of X-rays with and without the drug were given, and the isoeffect doses obtained were used to derive the α/β values. The effect of nicotinamide as a function of dose per fraction was also studied by defining the proportion of full-effect curve obtained by giving a single X-ray dose (from 2.5 to 25 Gy) followed by graded doses of neutrons. The α and β parameters were calculated by fitting the underlying effect curve using a linear-quadratic equation. Using these two different experimental designs we detected no change in α/β for skin, indicating that nicotinamide does not alter the sensitivity to dose fractionation in this early reacting tissue.

Modelling repair kinetics: extension of the linear-quadratic equation to higher order terms

M. C. Joiner and P. Nilsson

Gray Laboratory of the Cancer Research Campaign, P.O. Box 100, Mount Vernon Hospital, Northwood, Middlesex HA6 2JR

There is now a large amount of experimental and clinical data indicating that the increase in total dose with fractionation in radiotherapy is modelled well over the dose per fraction range 1–15 Gy by a linear-quadratic (LQ) equation. However, in fractionation studies with acute reactions in mouse skin, at high doses per fraction we have observed that the response is slightly *less* than predicted by LQ. This can be accounted for by subtracting a dose-cubed term in the LQ model to give a linear quadratic cubic (LQC) model, Effect $= \alpha d + \beta d^2 - \gamma d^3$. The difference between the LQ and LQC descriptions is less than a few per cent below 20 Gy, but above this the difference increases rapidly to $\sim 12\%$ by 30 Gy. Although not clinically relevant, this can give fundamental radiobiological information. For example, the LQC model is akin the to Curtis LPL model and α, β and γ values obtained from fitting the LQC model to the skin fractionation data can be compared to derive a ratio of lethal to potentially lethal lesion production as 5%, and a ratio of misrepair to repair half-time as ~ 11. An Incomplete Repair (IR) model can also be derived from an LQC rather than LQ base. For a given rate of *repair* of potentially lethal lesions, the LQC IR model predicts that *recovery* (*i.e.* "shoulder" or Elkind recovery) between two doses takes place slightly slower than predicted by the LQ IR model and this discrepancy is dose per fraction dependent, with slower recovery at higher doses per fraction. The IR model based on an LQC equation, or the Curtis LPL model directly, may therefore be relevant to the description of biological systems where such dose-dependent recovery kinetics have been seen, such as skin.

Repair of radiation damage: overview

Alan Horwich
Academic Unit of Radiotherapy & Oncology, The Royal Marsden Hospital, Downs Road, Sutton, Surrey SM2 5PT

The range of human tumour radiosensitivity can be accounted for by differences in intrinsic cellular radiosensitivity. However, it is not clear whether the level of damage induction or extent of damage repair dominate in determining the observed differences. Although this conference was centred on repair, an important theme was the definition by which biochemical lesion or lesions determine cytotoxicity from radiotherapy. There is considerable evidence correlating DNA double-strand breaks with radiosensitivity. However, a range of types of double-strand breaks can be investigated using restriction endonucleases and, since most radiation-induced double-strand breaks are repaired successfully, it is clear that the quantitation of all double-strand breaks, though an index of radiation damage, may not represent a quantitation of radiation cytotoxicity. The events which lead from double-strand break to chromosome aberration are poorly understood. There is good correlation between radiosensitivity and numbers of residual-strand breaks. There are difficulties in measuring double-strand breaks using velocity sedimentation or neutral elution, especially at clinical radiation doses, since the relatively small number of breaks leaves molecules too large to size accurately. New techniques of pulse field electrophoresis may help to resolve this problem. The technique of premature chromosome condensation provides a measure of chromosome breaks, which may be regarded as the final common endpoint of radiation effects, and, though far removed from damage induction, it may be that residual damage is a better measure of potentially cytotoxic lesions. The methods of measuring double-strand breaks are not necessarily equivalent to one another. The analogy with repair of ultraviolet damage to DNA is stimulating, and elegant molecular biological experiments were described illustrating the identification and cloning of a gene which partially complements the repair defect in xeroderma pigmentosum subgroup D. However, the major step remains of understanding how the gene product functions. Studies were described of the *E. coli* nth gene product, an endonuclease which recognizes radiation-induced thymine damage and causes of single-strand break. The influence of this gene product on mammalian hypersensitivity has been studied following insertion of the nth gene into mammalian cells using a plasmid elector. In most experiments, the gene product did not influence radiation cytotoxicity despite thymine damage being a common form of radiation cytotoxicity. Possibly the single-strand breaks were repaired and thus the change in level of expression of the nth gene was irrelevant. Repair can most simply be measured by studying the kinetics of double-strand break clearance. Other methods of measuring repair were described including reactivation of adeno-virus and reactivation of plasmid genes. Although differences in level of reactivation can be seen in different cell lines, these techniques have been explored in a relatively small number of tumours and, as yet, there is no clear association with radiosensitivity. Although one method of validating an assay of repair would be using cellular models, it is clear from presentation of cellular studies that their kinetics of cellular recovery may be influenced by fraction size, interfraction interval and of course, by choice of mathematical model. A further caveat derives from the presentation of work on a neuroblastoma cell line where induced radiation resistance was not a genetically stable trait. In an applied setting, this field naturally investigates the role of DNA repair inhibitors as radiosensitizers. In general, the effects of these are too small to be clinically useful and nicotinamide did not appear to be an exception to this rule. This conference was attended by molecular biologists, cell and radiobiologists and clinicians, and represented a valuable forum for discussing the problems and clinical potential of this relatively new field of research.

1990, *The British Journal of Radiology*, *63*, 916–918

Book reviews

Endovaginal Ultrasound. By S. R. Goldstein, pp. xviii + 175, 1988 (Alan R. Liss, New York).
ISBN 0-8451-4263-1

Rapid advances in probe technology has lead to exploitation of a number of ultrasound endoprobes. This book explores in depth the use of endovaginal probes beginning with basic ultrasound, physics and instrumentation and a chapter on the method of examination, very necessary even for those experienced in abdominal ultrasound, as this technique is very different in image orientation. Chapters follow on normal pelvic anatomy, pelvic masses and pregnancy, including separate chapters on ectopic pregnancy and a final section on ovulation induction, follicle surveillance and *in vitro* fertilization.

Unlike some of the earlier texts on this subject, which tended to describe uncritically all the possible uses of the technique, this text is written by a group of authors who obviously use the technique extensively and, whilst describing uses that are unlikely to be everyday ones, demonstrate a number of possible uses such as the assessment of the incompetent cervix in the pregnant patient which will be very useful in selected cases.

The text goes into sufficient depth about clinical criteria as is necessary to exemplify the uses of the technique without being over elaborate. The references are very much up to date, with many from 1988 (the year of publication). The quality of production of the text is excellent, although a little more careful proof reading would have eliminated the spelling mistakes amongst the references.

This book can be recommended to all those interested in the technique, which will include radiologists, obstetricians and gynaecologists, although in such a rapidly expanding field it will probably be quickly succeeded by a text with an even more critical appraisal of the uses of the technique.

D. W. Pilling

Neonatal and Pediatric Ultrasonography. Clinics in Diagnostic Ultrasound, No. 24. Ed. by Diane S. Babcock, pp. xii + 275, 1989 (Churchill Livingstone, New York) £37.50.
ISBN 0-443-08606-0

This volume (number 24 in the *Clinics In Diagnostic Ultrasound* series) brings together a distinguished group of specialists in paediatric ultrasound from America and Canada. In 10 chapters, all the important facets of neonatal and paediatric ultrasound are covered with particular emphasis on cranial sonography, but this is adequately balanced by sections on the abdomen, hip and paediatric Doppler application. The chapters on cranial sonography, in particular, provide a good review of current thinking, although it is necessary to skip to the section on Doppler for a complete picture. The section on the infant hip provides a rather individual chapter almost entirely devoid of measurement and much at variance with most other articles on the subject.

Overall, this latest volume keeps up the very high standard of the series, although the mixed polarity of images in the section on the biliary tract is unhelpful, in Europe DMSA is usually used for Di Mercapto Succinic Acid and not Disodium Monomethanearsonate, and the section on ovarian cysts in the neonate could have been expanded to include the recent discussion with regard to the active management of these cysts. Those involved in much paediatric ultrasound will find the whole of this book interesting, and it should also find a place on the shelves of those involved in ultrasound but with less extensive paediatric experience, as it provides a ready reference and extensive bibliography relating to most paediatric ultrasound problems.

D. W. Pilling

Digital Subtraction Imaging in Infants and Children. Ed. by Eric N. Faberer, pp. xii + 193, 1989 (Futura, New York), $42.00.
ISBN 0-87993-340-2

The aim of this monograph is to provide information on the techniques available and the indications for digital subtraction angiography (DSA) in infants and children. The monograph covers the basic physics and general techniques as well as specific chapters on different body systems. The final chapter looks at the future applications of digital imaging.

The chapters on basic physics and techniques are both basic and useful with good explanations, important in understanding digital imaging. The chapters on the cardiac and renal systems are both comprehensive and critical, the former chapter providing functional data as well. The chapters on intra-arterial DSA, DSA of the aorta and great vessels and DSA of the extremeties provide neither adequate text nor a critical overview of the areas covered. The image quality in the chapter on extremeties is of poor quality, whilst in the former two chapters are presented more as an atlas and not in keeping with the remainder of the monograph.

The chapter on the head has a good overview but the images are all rather old. Digital subtraction angiography in interventional radiology of the central nervous system is missing. Interventional work in other areas is covered to some extent in the other chapters.

Every chapter starts with a similar historical review; this becomes somewhat repetitive.

The monography falls somewhere between a textbook and an atlas; the speed of technological developments precludes any book being really up to date, and DSA is one area where this is most obvious.

In a multi-author book it is hard to ensure that every chapter meets the same standards, and such variation is evident in this particular monograph. It is relatively cheap for a radiological textbook and those few departments which carry out paediatric angiography will find a few chapters of value.

I am afaid that the aim of the book, in the terms of providing indications for DSA, is only met in the cardiac and renal sections.

I. Gordon

Cardiac Application of Digital Angiography. Ed. by A. G. Wasserman and A. M. Ross, pp. xii + 311, 1989 (Futura Publishing Company, New York), $53.00.
ISBN 0-87993-332-1

This is a book of 311 pages in the usual format of multi-author chapters under the editorial control of Drs Wasserman and Ross.

The preface sets out the aims of the book and, in summary, these aims are fulfilled by 12 chapters covering all aspects of cardiovascular digital subtraction angiography (DSA).

In the introduction, one quibble is the use of "digitalization" when clearly the authors meant "digitization", one referring to examination by the use of a finger, the other being the computerization of data! Otherwise the introduction covers briefly the history and present and future potential of subtraction angiography.

Chapter 2 discusses the underlying theory of DSA, which it covers reasonably well. The quality of the illustrations is adequate and the bibliography is representative of the early work implementing DSA.

Chapter 3 covers the assessment of ventricular function in some detail, the only omission being a discussion of Fourier techniques. The quality of the images again is adequate, and there is a reasonable bibliography, although none of the European work, principally from Kiel, has been referenced.

Chapter 4 is interesting as it discusses a rather unusual technique of exercise DSA. The results merit close reading; there are no images. Chapter 5 is the sequel to Chapter 4 and discusses atrial pacing as a method of stressing the patient. The images are surprisingly good and the whole technique well presented and referenced.

Chapter 6 discusses quantitation of stenosis in the coronary circulation, providing a useful overview of available techniques, together with an appraisal of limitations imposed by the physics of acquisition. In particular, the bibliography is extensive and the images are of good quality.

Chapter 7 discusses parametric imaging of myocordial flow reserve, which is well described by Dr Vogel; it is a pity that none of his excellent colour images is included, imaging being limited to monochrome only.

Chapter 8 discusses measurement of coronary blood flow using densitometric techniques. A brief history is given and the principles of indicator-dilution curve analysis stated. An interesting overview of mean transit times is also given and should be compared with Chapter 7.

Chapter 9 outlines the value of DSA in the evaluation of coronary angioplasty; the images are of good quality.

Chapter 10 is a collection of cases covering the visualization of the great vessels, bypass grafts, carotid bifurcation and pulmonary circulation. The quality of the images is variable, some being of the highest quality, whilst some are poor.

Chapter 11 is about paediatric applications of DSA and is a pleasure to read, with high quality imaging and a useful discussion of paediatric pathology and how best to image it.

Finally, Chapter 12 covers non-cardiac cardiovascular imaging in a necessarily abbreviated manner, although the major disorders are discussed and well illustrated.

In conclusion, this is yet another book on the uses of DSA; overall it is moderately well illustrated and quite well written. The bibliographies are well worth having for further details. I can recommend it for the non-specialist interested radiologist and possibly also for cardiologists.

G. J. Hunter

Handbook of Cardiovascular and Interventional Radiologic Procedures. By Krishna Kandarpa, pp. xviii + 254, 1989 (Little, Brown & Company, Boston), £16.50.
ISBN 0–316–48255–2

This slim volume will just slip into a man's inside coat pocket (or be lost in a woman's handbag) yet it contains a wealth of practical information that is well presented in concise note-form style. Dr Kandarpa is a radiologist at Harvard Medical School and together with 11 colleagues, predominantly radiologists, they have produced this comprehensive handbook which covers most aspects of vascular and interventional radiology, except for a few specialized areas.

In addition to excellent accounts on angiography, venography and pulmonary angiography, there is a brief section on cardiac angiography. Needles, guidewires and catheters are detailed and there is a section on radiographic equipment and techniques that includes a useful table with injection rates and filming programmes etc. There is a section on drugs with very useful prescribing information as well as a short but excellent account of radiation safety. Non-invasive vascular and radio-nucleide studies are briefly covered and there is an Appendix with several useful diagrams of arterial anatomy.

In the vascular interventional section there are good basic accounts of lower limb angioplasty, renal angioplasty and intra-arterial thrombolysis. Coronary and cardiac angioplasty are rather surprisingly covered yet there are only very brief sections on acute gastro-intestinal bleeding and embolization. The account of IVC filter placement deals exclusively with the Kimray–Greenfield filter which will be of no interest to Europeans. The non-vascular interventional section includes good basic accounts of nephrostomy, biliary drainage, biopsy procedures, abscess drainage and gastrostomy.

The layout of this book is excellent so that it will be easy to look up any procedure and check on all the practical points. The diagrams are clear and on the whole supplement the text well. At the end of each section there are a few selected references.

I think this book would be extremely useful to all radiologists in training as well as any radiologist who does some vascular and interventional work without being wholly committed to it. I would not recommend that X-ray departments and libraries buy this book unless their security is first rate! Radiologists should have their own copy that they can make additional notes on to supplement their practical techniques. Although £18.00 seems a lot for a small book with no X-ray plates, I think it will repay itself with the use that will be made of it.

John Reidy

Diagnostic and Interventional Radiology: A Clinical Manual. By G. M. Gaylord, L. P. Davis and S. R. Baker, pp. xvii + 316, 1989 (W. B. Saunders, London), £17.95.
ISBN 0–7216–2333–6

Diagnostic and Interventional Radiology: A Clinical Manual is a pocket-sized book of 316 pages edited by three American radiologists with contributions from seven others. The stated aim of the authors is to provide a guide to the repertoire of the X-ray department, and how to get the best use from it, for medical students and newly qualified doctors.

The book is arranged in three sections. The first part describes the role of the radiologist and the differing types of X-ray department, and these chapters necessarily have a strong American bias. Together with these go an introduction to radiation physics and a useful chapter on informed consent. Part two is entitled "Diagnostic Modalities" and runs briefly through the major investigations which we have at our disposal.

The bulk of the book is the third part which consists of a series of chapters on the imaging each of the different organ systems. The place of each mode of investigation in the imaging of the various organ systems is discussed with comments on the techniques, patient preparation, pathology and limitations.

This little book contains a great deal of information for someone who has little or no knowledge of the workings of a radiology department, although it is by virtue of its size a little sketchy and generalistic in places. Apart from a few typographical errors, it is very easy to read and, particularly in the third section, gives a very useful overview of the service we have to offer.

Bearing in mind how we like to encourage medical students into the department to follow their patients and to attend meetings, and also how busy housemen have little time to do more than fill in requests on behalf of their seniors, a department would do well to have a few copies to loan out to visitors.

Possibly the most important point the authors make is to emphasize that we, as radiologists, need to be given good clinical information and the best way to do this and get the most out of the X-ray department is to talk to us.

C. E. C. TODD

Breast Imaging: Diagnosis and Morphology of Breast Diseases. By Robert L. Egan, pp. xvi+688, 1988 (W. B. Saunders, Philadelphia), £57.75.
ISBN 0-7216-2320-4

This book encapsulates the vast experience of one of the leading pioneers in the field of mammography. Dr Egan is rather more than an innovator: he is an exceptional communicator, having not only personally taught mammographic techniques and interpretation to many hundreds of radiologists, but also producing over a dozen monographs on the subject. His seminal work at the M. D. Anderson Hospital and Emory University was based on scrupulous radiographic technique, detailed radiological and pathological correlation and extensive statistical analysis.

The first chapter is a historical perspective in which the author emphasizes his own part in convincing sceptics of the role that mammography had to play in the management of breast cancer and in screening. There are chapters on breast self-examination, clinical examination, mammography, ultrasound and other non-radiographic techniques. These latter chapters do not always describe current trends. For instance, the ultrasound chapter describes the water path method in detail with no description of direct contact, real time breast scanning. There is no description of the recent developments in digital imaging techniques. The chapter on localization methods does not include a description of computerized stereotaxis for fine needle aspiration. The bulk of the book consists of a miscellany of topics — really a series of essays — on various mammographic signs, breast pathologies and clinical situations. Statistical data on the author's own experience is always prominent and all chapters are copiously illustrated by radiographic and pathological material. Clinical and pathological aspects are always well interpreted with the radiology but some of the mammographic illustrations are not of the highest quality. Surprisingly, there are some important conditions which are not illustrated, particularly radial scars and fat necrosis. Finally, there are chapters on breast screening and statistical data for breast cancer.

It is not the author's stated intention to produce a complete treatise on the subject. Readers will not find a comprehensive review on mammography with extensive and up-to-date references. What readers will learn is the interpretation of mammographic appearances in terms of the underlying pathology and the clinical context. This book tends to be discursive, at times it is idiosyncratic and pragmatic, but it is always interesting and a mine of information. Those with a particular interest in the radiology of breast disease will find it a companion volume to the more didactic and concise mammographic atlases.

G. H. WHITEHOUSE

Diagnostic Imaging of the Acute Abdomen: A Clinico-Radiologic Approach. By Dieter Beyer and Ulrich Modder (with contributions from others), translated by T. C. Telger, pp. xvi+453, 1988 (Springer-Verlag, Berlin Heidelberg), DM180.00.
ISBN 3-540-17520-2 (Berlin Heidelberg) 0-387-17520-2 (New York)

This well produced, multi-authored book is essentially a question-and-answer aid to diagnosis. The stated aim is to enable clinicians, particularly surgeons, to choose the most appropriate imaging modality to help solve a specific diagnostic problem.

The format is basic, a suspected disease or specific clinical finding being followed by an exhaustive list of potential causes and how they might be investigated radiologically. The authors draw attention to major deficiencies in the various available techniques or to possible areas of confusion arising from radiological findings by highlighting sections of the text. The illustrations and accompanying history and interpretation are excellent. The references are reasonably recent but a number, unfortunately, are in German.

For radiologists, the main value of this book will be to those preparing to sit their Final Fellowship examination.

J. A. GLEESON

BJR

THE BRITISH
JOURNAL
OF RADIOLOGY

Volume 63 Congress Supplement

ucm

Radiology '90

Proceedings of the 48th Annual Congress of The British Institute of Radiology

X-ray Diagnosis • Ultrasound • Interventional Radiology
Radiotherapy • Oncology • Hyperthermia
Nuclear Medicine • Nuclear Magnetic Resonance
Radiation Physics • Radiobiology • Radiation Protection

BJR is published by The British Institute of Radiology BIR

Matrix Compact L moves daylight laser imaging into the 90's with Matrix Imagenet

MATRIX IMAGENET
the 4×4 data traffic controller

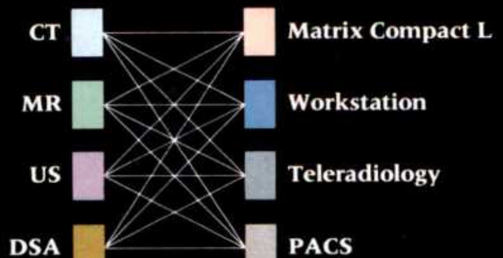

BUILDING UP A MINI NETWORK OF DIAGNOSTIC EQUIPMENT.

Matrix Compact L is a second generation multi-format imaging centre with a fully computer controlled film handling system and processor.

- **INTERFACING The memory built into the Matrix Compact L allows interfacing with almost all other equipment either Digital and/or Analogue signals and will readily accept and differentiate between text graphics and control signals.**
- **EXPANDABILITY Matrix Compact L can be expanded by the use of the Imagenet Unit which allows multiple input with simultaneous acquisition.**
- **EASE OF OPERATION Fully computer controlled with a user friendly menu driven terminal makes the operations of this system relatively simple to operate.**

AGFA Agfa
IMAGE AND VISION

Radiology 90

Harrogate, 11-13 June 1990

The 48th Annual Congress of the British Institute of Radiology incorporating the joint Spring Meeting with the Royal College of Radiologists and the Radiology Section of the Royal Society of Medicine.

The scientific programme is organized by the BIR in scientific collaboration with the American College of Radiology.

As an organization accredited for continuing medical education, The American College of Radiology certifies that this continuing medical educational offering meets the criteria for Category 1 credit for up to 17 hours, providing it is completed as designed.

Published and typeset by
The British Institute of Radiology, London 1990

Phototypeset by Whitefriars Press, Tunbridge Wells, Kent, and printed and
bound in Great Britain by BPCC Wheatons Ltd, Exeter

ORGANIZING COMMITTEES

Congress Committee

Professor C R Hill	BIR President and Chairman
Dr M Gowland	BIR Honorary Secretary
Professor C A Joslin	BIR Vice President
Dr M P Law	Scientific Exhibition Chairman and BIR Honorary Secretary
Dr V R McCready	Scientific Programme Chairman
Dr D S McIntosh	BIR Honorary Treasurer
Dr N J McNally	BIR Vice President and Honorary Editor
Mr G Mountford	MED X RAY Advisor
Ms N van Helfteren	BIR Conference Manager
Miss S M Johnstone	BIR General Secretary (1989)
Mr R Smith	BIR Publications Manager (1989)

Scientific Programme Committee

Dr V R McCready (Chairman)
Dr M Gowland
Professor C R Hill
Professor A Horwich
Professor C A Joslin
Dr I Kerr (RCR)
Dr M P Law
Dr N J McNally
Dr D Nolan (RSM)
Professor B S Worthington
Ms N van Helfteren

Acknowledgments

The BIR acknowledges with gratitude the help and support of the following:
3M UK PLC
Agfa (UK) Ltd
Harrogate Resort Services
Kodak Ltd
Kyowa ME Ltd
May & Baker Pharmaceuticals, Rhone Poulenc Ltd
Mr A M Oxley and team
Radiographers from the Leeds Radiotherapy Teaching Hospital
RAD Magazine, Kingsmoor Publications
Schering Health Care Ltd

CONTENTS

Organizing Committees ii
Acknowledgments ii
Message from the President iv
General Information v
List of MED X RAY Exhibitors vii
BIR Information viii
BIR Publicatons ix

Scientific Programme and Timetable xii
Monday xv
Tuesday xix
Wednesday xxii

Abstracts

Monday Congress 1
Tuesday Congress 37
Wednesday Congress 67

Index to Authors Congress 95

Map Back cover

RADIOLOGY 91

Brighton 2 – 4 May 1991

British Institute of Radiology 49th Annual Conference

incorporating the joint spring Provincial Meeting with the Royal College of Radiologists and Radiology section of the Royal Society of Medicne

Radiology 91 will incorporate all aspects of modern radiology for all those concerned with diagnostic radiology and radiotherapy.

Proffered abstracts are invited for oral and poster presentation and will form a major element of the meeting. Deadline for receipt of abstracts: **30 November 1990**

MESSAGE FROM THE PRESIDENT

Welcome to Radiology 90 and its associated MED X RAY exhibition and social programme.

This programme and abstract booklet has been designed to help you make best use of your time in Harrogate. This year you may notice an increased interdisciplinary structure to the programme, with sessions focusing on problems rather than specialization, and we look forward to hearing your reactions to this approach. You will also see that most sessions open with an invited, often broad-ranging lecture, which is followed by related proffered papers. We also hope that the "teach-in" sessions and special symposia, addressing recent developments in the field, will be of particular interest. As last year we include work-in-progress sessions to allow presentation, with minimum delay, of topical research work.

Be sure to allow plenty of time to visit and meet the exhibitors at MED X RAY. This is Britain's largest technical exhibition devoted to the radiological sciences and will be open for the full three days of the conference.

Best wishes for a rewarding and stimulating meeting in Harrogate.

KIT HILL

GENERAL INFORMATION

Congress Site

Radiology 90 takes place at the International Conference Centre in Harrogate. Plenary lectures are held in the Conference Hall, with all other sessions in the Moat House International Hotel.

MED X RAY technical exhibition and the Scientific Poster Exhibition are also at the International Conference Centre.

Registration

Your delegate's pack contains all relevant tickets (please check these), list of delegates, the MED X RAY handbook and your Congress badge.

Your badge entitles you to admission to all lectures at Radiology 90 and to MED X RAY and *must be worn throughout the Congress.*

Registration Desk Opening Times

The registration desk will be situated in the Foyer of the International Conference Centre and will be open at the following times:

Sunday	4.00 pm – 8.00 pm
Monday	8.00 am – 4.30 pm
Tuesday	8.00 am – 4.30 pm
Wednesday	8.00 am – 2.00 pm

MED X RAY

MED X RAY runs for the three days of the Congress, from Monday 11 June to Friday 13 June, to span the annual meeting of both organisations. MED X RAY is sited in the exhibition halls of the International Conference Centre. The opening times are:

Monday 11 June – Friday 13 June 9.00 am – 5.30 pm.

Full details of the companies exhibiting are given in the MED X RAY handbook.

Messages

Please check the notice board by the registration desk for messages.

Scientific Poster Exhibition

The large scientific poster exhibition is in the Foyer on Level 5 of the International Conference Centre. Opening times are as for the Registration Desk.

BIR posters will be discussed in chaired sessions and a note of the date, time and session of oral presentation will be on the poster. Abstracts are included within the relevant sessions. The BIR poster exhibition includes presentations on the following topics:

Ultrasound
Nuclear Medicine
Interventional Radiology
Nuclear Magnetic Resonance
Computed Tomography
Radiotherapy and Oncology
Radiobiology
Radiological Physics
Radiation Protection

BIR Information Stand

The BIR Stand will be situated close to the Poster Exhibition on Level 5. BIR Council members and staff will be available to discuss any aspect of the Institute's business. We welcome both members and non-members to come and discover the benefits of membership.

Radiology 90 Competition

As last year, the BIR's Industry Committee in conjunction with RAD Magazine have organised a competition for delegates at Radiology 90. Your question sheet is in your delegates pack. Simply answer the questions, collect as many different coloured stickers from MED X RAY as you can and post your answer sheet into the drum to be found in the RAD Magazine Hospitality Lounge. You could win a travel bursary to attend Radiological Meetings worth up to £500.

Telephone

There will be a telephone manned during Congress registration opening hours for urgent messages: Harrogate (0423) 527287 and ask for Radiology 90 Registration Desk.

Refreshments

Tea and coffee points are sited throughout MED X RAY from Monday to Wednesday. Refreshments will be available throughout the day.

Lunch

Light snacks are available on a cash basis from refreshment points in MED X RAY and there are pubs and restaurants within walking distance of the International Conference Centre. There are also licensed bars in the Centre.

Accompanying Persons Programme (admission by ticket only)

It may be possible to accept last-minute bookings for the following at the registration desk. All tours will depart from the Moat House International Hotel by 9.30 am and return by 5.30 pm, except on Wednesday when the tour will return by 3.30 pm.

Monday 11 June, Castle Howard and City of York

Our first outing takes us to one of the most sumptuous family homes in the country. Castle Howard, built in the 18th century, was used as the setting for the television series "Brideshead Revisited" and is set in 1600 acres of parks and gardens. We shall then proceed to York and a guided tour of York Minster, the largest medieval cathedral in Northern Europe. You will then be free to wander at your leisure around the ancient streets of the city, of which the Shambles is the most famous. The Jorvik Viking Museum , with its reconstructions of life in Dark Age York, and the Yorkshire Museum, with some of the finest Dark Age and Medieval treasures discovered in Britain, are particularly recommended for giving you a special flavour of this one-time capital of Northern England.

Tuesday 12 June, Beautiful Yorkshire Dales

Tuesday's excursion takes us on a tour of the beautiful Yorkshire Dales, which includes some of England's richest farming country. The itinerary will take in a visit to a traditional craft workshop, of which there are several in the Dales, a castle and a stately home as well as taking you through some of the Dales' most breathtaking and memorable scenery.

Wednesday 13 June, Ripley Castle Fountaions Abbey and Knaresborough

Ripley Castle has been the Ingilby family home since the 1450s. The Castle is full of reminders of its place in the forefront of history with its ancient gatehouse built to keep out marauding Scots, the library in which "Trooper Jane" Ingilby held Cromwell at gunpoint, and the unique 16th century waggon roof ceiling in the Knight's Chamber. Your guided tour will also take you around Capability Brown's walled gardens. We then go on to the fabulous Fountains Abbey after which we then proceed to the ancient market town of Knaresborough, perched above the gorge of the river Nidd with its cliff-top castle. After lunch you may roam around the town and into the medieval square where the weekly market will be in full swing.

Social Programme (admission by ticket only)

Sunday: *Informal Welcome Gathering 6–8 pm.*
This will be held at the Harrogate International Centre. Meet your fellow delegates, have a drink and pick up your conference folder on Sunday evening so that you can plan your lecture programme in advance.

Monday: *Civic Reception 6.30 – 7.15 pm*
This will be held at the Harrogate International Centre. The Mayor of Harrogate will welcome the delegates at Radiology 90 and the 44th Conference of The College of Radiographers at a cocktail reception. Then, go on to ...

Buffet and Disco 7.30 – 11.00 pm
This will be held at the Royal Baths Assembly Rooms. A joint disco and buffet supper for delegates of both conferences held at the lovely Royal Baths Complex. The buffet and disco will be in separate rooms, so you can talk as well as dance! Price per person £5.

Tuesday: *Annual Dinner 7.30 for 8.00 pm*
This will be held at The Crown Hotel (see map on back cover). There will be free seating so guests can choose their own companions. Black tie/dark suit. Cost including drinks reception and wine £27 per person.

While all information was correct at the time of going to press, we regret that it was impossibe to make changes notified later.

MED X RAY EXHIBITORS

Listed below are the companies booked to exhibit at MED X RAY, the UK's largest exhibition devoted to the radiological sciences. It is held jointly with The College of Radiographers and is open to all delegates at Radiology 90 throughout the Congress. This is the ideal opportunity to view the very latest in equipment and services to the whole industry, and to meet the leading manufacturers to discuss how modern technology can help your concern. Also listed are their stand numbers. Further information can be found in your MED X RAY Catalogue which is in your delegates pack.

72	Agfa Gevaert Ltd (X-ray Division)
56	Appleford Instruments Ltd
19	Arplay SA
20	Atlantic Medical Ltd
67	Bartec Medical Systems Ltd
12	Baron Medical PIMS
33	Bioglan Laboratories Ltd
29	British Nuclear Fuels plc
42a	Cambridge Medical Books
13	Cea (UK) Ltd
21	Compact Communication Centre
50	Corinth Medical Services
58	Courtaulds Structural Composites
46	D C Bayman (Construction) Ltd
28	Data Med Computer Services
74	Dept of Health Supplies Technology Division
7	Diasonics Sonotron Ltd
70	Du Pont (UK) Ltd
23	Dynamic Imaging Ltd
75	E G & G Astrophysics Ltd
62	E Merck Ltd
35	Elscint (GB) Ltd
61	Eschmann Healthcare
5	E-Z-EM Ltd
78	Fuji Photo Film (UK) Ltd
25	Gama International
24	Gammex RMI Ltd
38	Granta Book Exhibitions
84	Henleys Medical Supplies Ltd
15	IGE Medical Systems Ltd
30	Impex Imaging Systems Ltd
33a	ISRRT
71	Kodak Ltd (Health Sciences)
10	Konica (UK) Ltd
60	Kretztechnik (UK) Ltd
17	Lanmark
66	Lynton Commercial Units Ltd
47	MAS Medical Ltd
82	May & Baker Pharmaceuticals (Rhone Poulenc Ltd)
45	Medical X-Ray Supplies Ltd
43	Mediplus Ltd
3	Mediscus Products Ltd
11	Merit Health Systems Ltd
6	Microtel Logic Ltd
32	N E Technology Ltd
39	National Radiological Protection Board
64	Nucletron Trading Ltd
77	Nycomed (UK) Ltd
80	Philips Medical Systems
52	Phoenix Imaging Systems Ltd
55	Photosol Ltd
34	Planmed
42	Polaroid (UK) Ltd
8	Polystan Ltd
41	Postrad
51	Power Silver Engineering
54	Premise Engineering Ltd
87	Provalid
76	Quantel Ltd
4	Radi Medical Systems
2	Radiatron Components Ltd
16	Radiologic Ltd
37	Rapitech UK Ltd
27	Schering Healthcare Ltd
86	Schneider UK
83	Siel Imaging Equipment Ltd
79	Siemens plc
40	Silver Coin Ltd
61	SIMS Medical Distribution
57	Smith & Nephew Pharmaceuticals Ltd
31	The College of Radiographers
73	3M United Kingdom plc
81	Toshiba Medical Systems
53	Varian TEM Ltd
65	Vertec Scientific Ltd
18	Videlcom Ltd
85	Vinten Analytical Systems
63	W S Rothband & Co Ltd
49	Wardray Products Ltd
14	Wessex Medical Ltd
22	Cook Europe Ltd
1	Wisepress Ltd
36	Wise Systems Ltd
59	Wolverson X-Ray & Electro Medical Ltd
48	X-Rite (H Miller Graphics Ltd)
68	Zenith Medical Systems

Listing correct at the time of going to press.

BIR

BRITISH INSTITUTE
OF RADIOLOGY &
RONTGEN SOCIETY

Membership of The British Institute of Radiology is open to everyone concerned with medical radiology. From its inception as the Roentgen Society in 1897, the BIR has grown and developed its vision as a multidisciplinary learned society with the aim of furthering all aspects of radiology and the radiological sciences.

Its primary activities are publishing and scientific meetings, and its excellent library is the best source of radiological literature, both historica and current, in the UK.

BJR
THE BRITIS
JOURNA
OF RADIOLOG

X-ray Diagnosis • Ultrasound • Interventional Radiology
Radiotherapy • Oncology • Hyperthermia
Nuclear Medicine • Nuclear Magnetic Resonance
Radiation Physics • Radiobiology • Radiation Protection

BJR published by The British Institute of Radiology BIR

Based in beautiful premises in London's West End, the BIR has a modern and well equipped lecture theatre with seating for 100, together with conference and catering facilities.

The British Journal of Radiology, distributed monthly to members, is one of the world's foremost radiological journals and publishes original research papers and review articles on the latest clinical and technical developments in all aspects of the radiological sciences. In addition the BIR publishes supplements to the Journal, reports of working parties, proceedings of conferences and practical handbooks. The BIR encourages enquiries from potential authors.

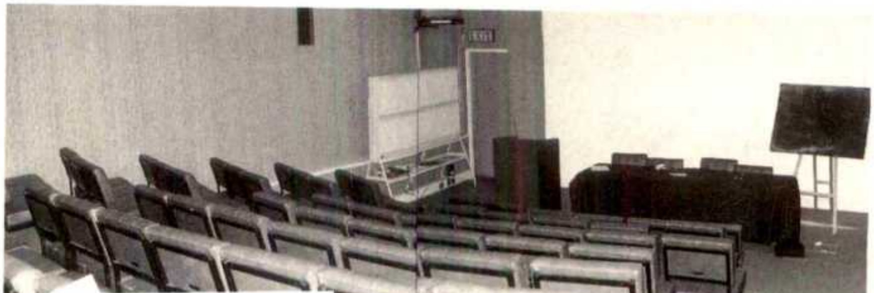

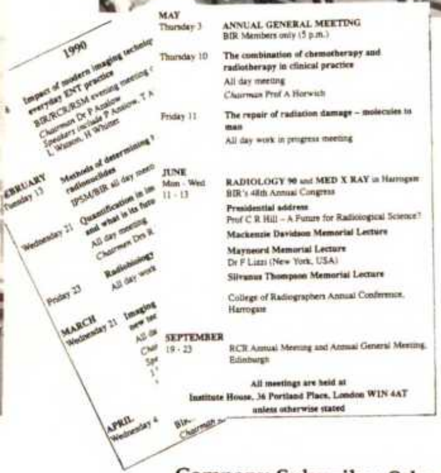
1990

Impact of modern imaging technolog
everyday ENT practice
BIR/RCR/RSM evening meeting
Chairman Dr P Anslow
Speakers include P Anslow, T A
L Watson, H Whiter

EBRUARY
Tuesday 13 Methods of determining
radionuclides
IPSM/BIR all day meeti

Wednesday 21 Quantification in im
and what is its futu
All day meeting
Chairmen Drs R

Friday 23 Radiobiology
All day work

MARCH
Wednesday 21 Imaging
new tec
All da
Chai

APRIL
Wednesday 4 BIR
Chairman

MAY
Thursday 3 **ANNUAL GENERAL MEETING**
BIR Members only (5 p.m.)

Thursday 10 **The combination of chemotherapy and radiotherapy in clinical practice**
All day meeting
Chairman Prof A Horwich

Friday 11 **The repair of radiation damage – molecules to man**
All day work in progress meeting

JUNE
Mon - Wed 11 - 13 **RADIOLOGY 90** and **MED X RAY** in Harrogate
BIR's 48th Annual Congress
Presidential address
Prof C R Hill – A Future for Radiological Science?
Mackenzie Davidson Memorial Lecture
Mayneord Memorial Lecture
Dr F Lizzi (New York, USA)
Silvanus Thompson Memorial Lecture

College of Radiographers Annual Conference, Harrogate

SEPTEMBER
19 - 23 RCR Annual Meeting and Annual General Meeting, Edinburgh

All meetings are held at
Institute House, 36 Portland Place, London W1N 4AT
unless otherwise stated

A significant number of scientific meetings are arranged each year – ranging from small evening meetings to the three day Annual Congress. The meetings are diverse – some are primarily presentations of clinical cases whilst others are presentations of original research papers in sciences associated with radiology. The BIR welcomes the opportunity to host scientific meetings in conjunction with interested organisations.

The British Radiological Library.
BIR Members have the assistance of a professional librarian, accommodation for study, and a lending and photocopying service in addition to a reciprocal arrangment with the RSM library.

Company Subscriber Scheme
In 1988 a Company Subscriber Scheme was launched to foster links between the BIR and Industry. Over 25 companies have joined to date and benefit from advertising concessions, discount on hiring BIR facilities and free membership for two members of staff. The BIR welcomes enquiries from potential subscribers.

The General Secretary will be happy to answer any queries. Please take one of our membership information forms for further details.

The British Institute of Radiology, 36 Portland Place, London W1N 4AT
Tel. 071-580 4085/4189 Fax. 071-255 3209

PUBLICATIONS OF THE BRITISH INSTITUTE OF RADIOLOGY

BJR Supplements:

23. Treatment Simulators, 1989, 48pp., ISBN: 0 905 74919 7	£10.00
22. Megavoltage Radiotherapy 1937-1987, 1988, 158 pp., ISBN: 0 905 74916 2	£28.50
21. Radionuclides in Brachytherapy: Radium and After, 1987, 54 pp., ISBN: 0 905 74915 4	£15.00
20. The Safety of Diagnostic Ultrasound, 1987, 48 pp., ISBN: 0 905 74914 6	£12.00
18. Criteria and Methods for Quality Assurance in Medical X-ray Diagnosis, 1985, 180 pp., ISBN: 0 905 74912 X	£27.50
17. Central Axis Depth Dose Data for use in Radiotherapy This standard work replaces BJR Supplement 11 (1972), 1983, 148 pp., ISBN: 0 905 74911 1	£25.00

Other Publications:

Assurance of Quality in the Diagnostic X-ray Department, 1988, 108 pp., ISBN: 0 905 74917 0	£20.00
Basic Clinical Ultrasound Hylton B Meire and Pat Farrant, 1982 (BIR Teaching Series No 4) 170 pp., ISBN: 0 905 74910 3	£12.50
Special Report 17: High Dose Rate Afterloading in the Treatment of Cancer of the Uterus, 1980, 200 pp., ISBN : 0 905 74907 3	£18.50
Report 18: Technical and Physical Parameters for Quality Assurance in Medical Diagnostic Radiology, 1989, 166 pp., ISBN: 0 905 74918 9	£30.00
Report 19: The Scientific Basis of Modern Radiotherapy, 1989, 142 pp., ISBN: 0 905 74920 0	£30.00
Report 20: Optimization of Image Quality and Patient Exposure in Diagnostic Radiology, 1989, 288 pp., ISBN: 0 905 74921 9	£30.00
Report 21: Risks from Radium and Thorotrast, 1989, 188 pp., ISBN : 0 905 74922 7	£40.00

ORDER FORM

Please order these titles from your local bookseller – or in case of difficulty from:
Butterworths, Borough Green, Sevenoaks,
Kent TN15 8PH

Telephone Orders (0732) 884567
Telex Orders 95678
24-Hour Order Line (0732) 882566

This line gives immediate access at any hour. Orders can be placed over the telephone by using your Butterworths account number or by charging to your credit card account.

Please send me the following titles:

Qty	Title/ISBN	£ Price
	Total £	

Please select preferred method of payment

☐ I enclose remittance for £

☐ Please debit my credit card as follows:

☐ Access/ Mastercard ☐ Barclaycard and other VISA cards ☐ American Express

Card number

Expiry date ________

Signature ________ Date ______

Name ________

Position ________

Address ________

Postcode ______

All prices are subject to change without notice and orders are subject to acceptance by Butterworths head office.

Please allow 28 days for delivery in the UK.

Registered Office: 88 Kingsway, London, WC2B 6AB
Registered in England No 125354

BIR

THE BRITISH INSTITUTE OF RADIOLOGY

MAYNEORD MEMORIAL LECTURE 1991

Nominations for the eighth lectureship, to be delivered at Radiology 91, are invited and should include a curriculum vitae and a clear concise statement of the work on which the lecture is to be based, which must come within the field of interest of the British Institute of Radiology. The Award is made annually to an individual or group of collaborators in recognition of recent or current contributions to the wide and expanding field of radiology. **Self-nominations are welcome.**

Please send nominations to: The President, The British Institute of Radiology, 36 Portland Place, London W1N 4AT by **1 July 1990.**

The seventh Mayneord Memorial Lecture entitled **Conjoint Application of Diagnostic and Therapeutic Ultrasound** will be given by Dr F L Lizzi of the Riverside Research Institute, New York. It will be delivered during the BIR Annual Congress - Radiology 90 - at the Harrogate International Conference Centre on Tuesday 12 June at 12.15 pm. It is open to non-registrants.

3M

The Mayneord Memorial Lecture is financed through the generosity of 3M United Kingdom PLC.

MON	HAREWOOD SUITE	RIPLEY SUITE	BRAMHAM SUITE	CHARTER SUITE
8.45- 9.00	OPENING - Prof C R Hill			
9.00 - 10.15	CENTRAL NERVOUS SYSTEM Invited Review Lecture MRI - Spinal column Prof B S Worthington,Nottingham	RENAL STUDIES Invited Review Lecture Ultrasound in paediatric renal disease Dr R de Bruyn, London	RADIOISOTOPE DIAGNOSIS AND THERAPY IN ONCOLOGY Invited Review Lectures PET in oncology Dr T Jones London Strontium 89 therapy Dr A Laing Oxford	CONSENSUS WORKSHOP: THE ROLE OF RADIOLOGY IN SURVEILLANCE POLICIES
COFFEE IN MED X RAY				
10.45 - 12.00	TRAUMA Invited Review Lecture The radiology of chest trauma Dr A McNeill, Belfast	CARDIOVASCULAR STUDIES	RADIOTHERAPY PAPERS Invited Review Lecture Intraluminal brachytherapy Dr R Stout, Manchester	FOR TESTICULAR TUMOURS Organiser:Dr M Williams, Chairman: Dr A Dixon, Cambridge
12.15 - 1.15	CONGRESS THEATRE MACKENZIE DAVIDSON MEMORIAL LECTURE Prof H H Holm, Sweden			
LUNCH IN MED X RAY				
2.30 - 3.45	SKELETAL STUDIES Invited Review Lectures Current trends in the radiology of joint disease Dr I Watt, Bristol MRI of the knee Dr C W Heron, London	LIVER AND ABDOMINAL STUDIES Invited Review Lecture Liver transplantation - the role of ultrasound Dr J Karani, London	QUALITY ASSURANCE AND PROTECTION	TEACH-IN IN RADIOTHERAPY PLANNING FOR HEAD AND NECK CANCER Dr D Ash, Leeds
TEA IN MED X RAY				
4.15 - 5.30	PAEDIATRIC STUDIES Invited Review Lectures Paediatric isotope studies Dr H Carty Liverpool and Dynamic CT in young children Prof B J Cremin, South Africa	VASCULAR ULTRASOUND STUDIES Invited Review Lecture Colour flow imaging principles Mr G Thirsk, ATL London	ULTRASOUND AND INTERVENTIONAL RADIOLOGY WORK IN PROGRESS PAPERS AND POSTERS	RADIOTHERAPY WORK IN PROGRESS PAPERS AND POSTERS

TUES	HAREWOOD SUITE	RIPLEY SUITE	BRAMHAM SUITE	CHARTER SUITE
9.00 - 10.15	LIVER AND BILIARY SYSTEM Invited Review Lecture Current trends in diagnostic radiology of the liver Prof A Baert, Belgium	CARDIAC STUDIES Invited Review Lectures Pharmacological stress in the diagnosis and management of coronary artery disease Dr R Underwood London and Computer assisted diagnosis of ischaemic heart disease Professor Y Sasaki, Kyoto, Japan	CONSENSUS WORKSHOP: EVALUATION OF SKELETAL METASTASES	ADVANCES IN ONCOLOGY Invited Review Lectures Megavoltage imaging: new methods and applications for radiotherapy Dr W Swindell, Sutton and Conformation therapy Dr A Nahum, London
COFFEE IN MED X RAY				
10.45 - 12.00	CHEST RADIOLOGY Invited Review Lecture Diagnosis of pulmonary embolism Professor P Lavender, London	MAMMOGRAPHY	Organiser Dr M Merrick, Edinburgh	PHYSICS Invited Review Lecture Magnetic resonance spectroscopy - measurements of human tumours Dr M Leach, Sutton
12.15 - 1.15	CONGRESS THEATRE MAYNEORD MEMORIAL LECTURE Prof F Lizzi, New York, USA			
LUNCH IN MED X RAY				
2.30 - 3.45	SMALL BOWEL STUDIES	ULTRASOUND STUDIES Invited Review Lecture Current status of transrectal ultrasound of the prostate Dr G J Griffiths Newport	TEACH-IN INTERPRETATION OF MAMMOGRAMS Organiser: Dr C Parsons, London	ONCOLOGY Invited Review Lecture Modelling for dose fractionation in radiotherapy Dr R Dale, London
TEA IN MED X RAY				
4.15 - 5.30	CONGRESS THEATRE SYLVANUS THOMPSON MEMORIAL LECTURE Prof J Denekamp			

WED	HAREWOOD SUITE	RIPLEY SUITE	BRAMHAM SUITE	CHARTER SUITE
9.00 - 10.15	CONTRAST STUDIES Invited Review Lectures Magnetic resonance imaging contrast studies Dr B Brasch California, U S A and Ultrasound contrast media, Dr R Schlief, Berlin, FRG	DIAGNOSTIC RADIOLOGY WORK IN PROGRESS PAPERS AND POSTERS	ONCOLOGY Invited Review Lecture Diagnosis of soft tissue sarcomas by CT and NMR Dr J Husband, Sutton Clinical applications of SPECT V R McCready, Sutton	RADIOTHERAPY DOSE DISTRIBUTION AND
COFFEE IN MED X RAY				
10.45 - 12.00	INTERVENTIONAL RADIOLOGY	TECHNOLOGY AND OPTIMISATION Invited Review Lecture QUALYS in diagnostic radiology Dr J G B Russell Manchester	ENDOCRINE STUDIES Invited Review Lecture Endocrine tumour localisation Dr S McEwan, Edmonton, Canada	TUMOUR CONTROL PROBABILITY Organiser: Prof G Steel, Sutton
12.15 - 1.15	CONGRESS THEATRE PRESIDENTIAL ADDRESS Prof C R Hill			
LUNCH IN MED X RAY				
2.30 - 3.45	DIGITAL RADIOLOGY	ONCOLOGY Invited Review Lecture Pathology and treatment of soft tissue sarcomas Dr C Harmer, London	TEACH-IN DIAGNOSIS OF HEAD AND NECK DISEASE Drs J Gillespie amd A Gholkar, Salford	QUANTITATIVE BONE STUDIES Invited Review Lecture Bone densitometry I Fogelman
TEA IN MED X RAY				
4.15 - 5.30	CONGRESS THEATRE THE NHS WHITE PAPER BARONESS HOOPER (COR lecture, open to our delegates)			

MONDAY 11 JUNE 9.00–10.15

HAREWOOD SUITE

CENTRAL NERVOUS SYSTEM

Chairman:	Dr V R McCready, Sutton
9.00-9.20 *Invited Review*	**MRI – Disorders of the spinal column; pathophysiological insights and contribution to management** B S Worthington, Nottingham *(p.1)*
9.20-9.23	**Magnetic resonance imaging of vascular abnormalities of the CNS** J M Hawnaur, Manchester *(p. 1)*
9.23-9.35	**Craniospinal magnetic resonance imaging in neurofibromatosis** P M Hughes, Manchester *(p. 2)*
9.35-9.38	**Changes in regional cerebral blood flow of patients with hydrocephalus after CSF shunting: detection by ^{99}Tc^{m}-HMPAO SPECT** B Caner, Ankhara, Turkey *(p. 2)*
9.38-9.50	**Computerised tomography of the brain: does contrast enhancement really help?** M Bernard, Cardiff *(p. 2)*
9.50-10.02	**MRI and RARE-myelography in diagnosis of spinal cord compression due to metastatic disease** E Dinkel, Freiburg, FRG *(p. 3)*
10.02-10.05	**Paranasal sinus abnormalities in patients referred for cranial CT** G Needham, Aberdeen *(p. 3)*
10.05-10.08	**Magnetic resonance angiography of dural sinus thrombosis** T S Padayachee, London *(p. 4)*
10.08-10.15	**Computed tomography in the evaluation of idiopathic pseudotumour of the orbit** M McNicholas, Dublin *(p. 3)*

RIPLEY SUITE

RENAL STUDIES

Chairman:	Dr M C Collins, Sheffield
9.00-9.20 *Invited Review*	**Ultrasound in paediatric renal disease** R de Bruyn, London *(p. 13)*
9.20-9.23	**Ultrasound diagnosis of horseshoe kidney** B Banerjee, Ashton-under-Lyne *(p. 13)*
9.23-9.35	**Contrast clearance: a new method for the measurement of glomerular filtration rate** S C W Brown, Stockport *(p. 13)*
9.35-9.38	**The effect of hydration on the non-ionic intravenous pyelogram** D C F Lloyd, Manchester *(p. 14)*
9.38-9.41	**The most advantageous timing of external ureteric compression during intravenous urography** T H Hughes, London *(p. 14)*
9.41-9.53	**The intravenous urogram: an appropriate use of resources?** J A Clarke, Manchester *(p. 14)*
9.53-9.56	**The role of MRI in the early post transplant kidney** G M Baxter, Glasgow *(p. 14)*
9.56-9.59	**A comparison of renography and IVU for urological assessment of spinal cord injury patients** S G Cooke, Oswestry *(p. 15)*
9.59-10.02	**Magnetic resonance imaging of renal masses** J E Kabala, Bristol *(p. 15)*
10.02-10.14	**^{99}Tc^{m}-MAG3 compared to conventional radiological investigation in paediatric renal tract disease** F E Pickworth, Plymouth *(p. 15)*

BRAMHAM SUITE

RADIOISOTOPE DIAGNOSIS AND THERAPY IN ONCOLOGY

Chairman:	Dr H Carty, Liverpool
9.00-9.20 *Invited Review*	**PET in oncology** T Jones, London *(p. 25)*
9.20-9.40 *Invited Review*	**Strontium-89 therapy** A H Laing, Oxford *(p. 25)*
9.40-9.52	**Dose-response study on thyrotoxic patients undergoing PET and radio-iodine therapy** M A Flower, Sutton *(p. 25)*

CHARTER SUITE

CONSENSUS WORKSHOP: THE ROLE OF RADIOLOGY IN SURVEILLANCE POLICIES FOR TESTICULAR TUMOURS

Organiser:	Dr M P Williams, Plymouth
Chairman:	Dr A K Dixon, Cambridge
Panel:	A Horwich, Sutton R J Johnson, Manchester G Rustin, London M P Williams, Plymouth *(pp. 34–35)*

MONDAY 11 JUNE 10.45 - 12.00

HAREWOOD SUITE

TRAUMA

Chairman: Dr J K Davidson, Glasgow

10.45-11.05 **The radiology of chest trauma**
Invited Review A McNeill, Belfast *(p. 5)*

11.05-11.08 **The significance of multiple posterior urethral false passages following pelvic trauma**
S Garber, London *(p. 5)*

11.08-11.20 **MRI of acute, sub-acute and chronic spinal trauma**
R W Kerslake, Nottingham *(p. 5)*

11.20-11.23 **Real-time sonographic assessment of suspected scaphoid fracture**
W W Gibbon, Manchester *(p. 6)*

11.23-11.26 **Real-time digital contrast enhancement and magnification in the assessment of scaphoid and other wrist injuries**
R Wellings, Birmingham *(p. 6)*

11.26-11.38 **Pitfalls in bone scintigraphy for suspected hip fractures**
J Rees, Cardiff *(p. 6)*

11.38-11.41 **Fractures of the atlas vertebra**
A Sandhu, Adelaide, South Australia *(p. 7)*

11.41-11.44 **An assessment of triage of casualty radiographs by radiographers**
I Renwick, Leeds *(p. 7)*

11.44-11.47 **Computed tomographic assessment of old calcaneal fractures**
S A Bradley, Birmingham *(p. 7)*

11.47-11.59 **3D CT of pelvic fractures**
R L Guy, London *(p. 7)*

BRAMHAM SUITE

RADIOTHERAPY PAPERS

Chairman: Dr D Tait, Sutton

10.45-11.05 **Intraluminal brachytherapy in bronchial carcinoma**
R Stout, Manchester *(p. 16)*

11.05-11.17 **Pelvic insufflation: a method of displacing small bowel during radiotherapy to the pelvis**
A C Hindley, Northampton *(p. 16)*

11.17-11.29 **Use of an electron beam for post mastectomy radiotherapy: 5 year follow-up of 500 cases**
B Magee, Manchester *(p. 17)*

11.29-11.41 **Strategy for the use of highly focussed ultrasound for the non-invasive destruction of deep seated tumours *in vivo***
G R ter Haar, Sutton *(p. 17)*

11.41-11.53 **Radiotherapy for cerebral oligodendroglioma in adults: an analysis of 98 cases and the dose-response relationship**
J Lim, Manchester *(p. 17)*

11.53-11.56 **Visual loss in the irradiated eye—an incidence study of 42 cases**
S F Leung, Shatin, Hong Kong *(p. 18)*

11.56-11.59 **Langerhans Cell Histiocytosis (LCH): its morbidity and mortality**
D Gilligan, Manchester *(p. 18)*

RIPLEY SUITE

CARDIOVASCULAR STUDIES

Chairman: Professor A Hemingway, Sheffield

10.45-10.57 **Early experiences using ^{99}Tc^{m}-MIBI for SPECT imaging of the ischaemic myocardium pre- and post-angioplasty**
C Collins, Dublin *(p. 26)*

10.57-11.00 **Combined exercise ECG and thallium stress testing in suspected coronary artery disease**
C S Romaniuk, Leeds *(p. 26)*

11.00-11.12 **Monoclonal platelet specific antibody imaging in the selection of patients for peripheral arterial thrombolysis**
D C Berridge, Nottingham *(p. 27)*

11.12-11.15 **Misdiagnosis of an atypically located pericardial cyst with a high CT number presenting in a patient with multiple trauma**
K Tung, London *(p. 27)*

11.15-11.18 **CT appearances of abdominal aortic graft infection**
A H Choudhri, London, *(p. 27)*

11.18-11.21 **Spontaneous dissecting aneurysm of the external iliac artery**
A H Choudhri, London *(p. 28)*

11.21-11.24 **MRI assessment of the thoracic aorta following aortic surgery**
G G Hartnell, Bristol *(p. 28)*

11.24-11.36 **A retrospective study of the fate of asymptomatic superficial femoral artery stenoses**
P Murphy, Bristol *(p. 28)*

11.36-11.39 **Evaluation of stenoses by magnetic resonance jet velocity measurement**
P Kilner, London *(p. 29)*

11.39-11.42 **Angiography access through vascular grafts. Is it contraindicated?**
P F Jaques, North Carolina, USA *(p. 29)*

11.42-11.54 **"Malignant" angiodysplasia**
A-M Belli, Sheffield *(p. 29)*

CONGRESS THEATRE

MACKENZIE DAVIDSON MEMORIAL LECTURE (12.15-1.15)

Interventional Ultrasound
H H Holm, University of Copenhagen, Denmark *(p.37)*

MONDAY 11 JUNE 2.30-3.45

HAREWOOD SUITE

SKELETAL STUDIES

2.30-2.50 Current trends in the radiology of joint disease
Invited Review I Watt, Bristol *(p. 8)*

2.50-2.53 Ultrasound and MRI diagnosis of meniscal cysts
A Coral, Michigan, USA *(p. 8)*

2.53-3.05 Comparison of marrow and bone scintigraphy of vascular bone grafts for fermoral head necrosis in 28 patients
I Stewart, Shatin, Hong Kong *(p. 8)*

3.05-3.08 Bilateral wrist arthrography in patients with unilateral symptoms
C S Romaniuk, Leeds *(p. 9)*

3.08-3.11 Assessment of bone scintigraphy in the diagnosis of scaphoid fractures
C J Occleshaw, Sheffield *(p. 9)*

3.11-3.23 Sonographic assessment of medial collateral ligament injuries to the knee
W W Gibbon, Manchester *(p. 9)*

3.23-3.26 Radiological features during and following treatment of spinal tuberculosis
D I Boxer, London *(p. 10)*

3.26-3.29 Symptomatic dorsal defects of the patella
V C Pullicino, Oswestry

3.29-3.41 Is there a familial risk in early disc failure?
B S Worthington, Nottingham *(p. 10)*

3.41-3.44 CT and isotope bone scan appearances of the knee joint following replacement of the anterior cruciate ligament
D I Cooke, Leeds *(p. 11)*

3.45–4.15 Tea

4.15-4.35 MRI of the knee
Invited Review C W Heron, London *(p. 5)*

RIPLEY SUITE

LIVER AND ABDOMINAL STUDIES

Chairman: Dr R Fowler, Leeds

2.30-2.50 Liver transplantation: the role of ultrasound
Invited Review J Karani, London *(p. 19)*

2.50-2.53 A prospective study of colour doppler ultrasound and isotope imaging in the detection of early renal transplant rejection
B J G Dall, Glasgow *(p. 19)*

2.53-2.56 Cholangiography in liver transplantation
P Holland, Birmingham *(p. 19)*

2.56-3.08 Hepatic vein Doppler in the diagnosis of acute liver transplant rejection
R A Coulden, Cambridge *(p. 20)*

3.08-3.11 More complications of intraarterial hepatic perfusion catheters: the radiological appearances of perfusion catheters having migrated outside the hepatic artery
F Regan, London *(p. 20)*

3.11-3.14 Know your physics and avoid a pitfall
P Ignotus, London *(p. 20)*

3.14-3.26 Perfluoroctylbromide (PFOB) as a contrast agent for liver and spleen enhancement in computed tomography
D O'Connell, Dublin *(p. 21)*

3.26-3.29 The recognition of abdominal scars at computed tomography
A K Dixon, Cambridge *(p. 21)*

3.29-3.32 Percutaneous gastrostomy in children
S Peterson, Newcastle under Lyme *(p. 21)*

3.32-3.44 Abdominal CT scanning in AIDS
P C Rowlands, London *(p. 21)*

BRAMHAM SUITE

QUALITY ASSURANCE AND PROTECTION

Chairman: Professor C R Hill, Sutton

2.30-2.42 Use of ionising radiation by non-radiologists
R Keal, Leicester *(p. 30)*

2.42-2.54 Factors affecting the radiation dose to the lens of the eye during cardiac catheterisation procedures
T A Pratt, Manchester *(p. 30)*

2.54-3.06 Evaluation of implementation of guidelines of choice of projection for X-ray examinations to reduce patients' exposure
I P Matthews, Cardiff *(p. 31)*

3.06-3.18 Quality assurance in PACS
R M Dawood, London *(p. 31)*

3.18-3.30 Design and performance of a computerised quality assurance and patient dosimetry system in diagnostic radiology
K Faulkner, Newcastle-upon-Tyne *(p. 31)*

3.30-3.33 The effect of shielding trays on surface absorbed dose outside primary megavoltage radiotherapy beams
A Morgan, Leeds *(p. 32)*

3.33-3.36 The diary of a "rogue" mobile breast screening unit: a chronological Q C record of its eventual demise, aged 19 months
M Pearce, Manchester *(p. 32)*

3.36-3.39 A study of patient dosage and protection in computed tomography. 1. patient dosage, distributions and hygienical evaluation during chest CT scanning
D-Y Qi, Suzhou, China *(p. 32)*

3.39-3.42 A study of patient dosage and protection in computed tomography. 2. patient dosage, distributions and hygienical evaluation during liver CT scanning
D-Y Qi, Suzhou, China *(p. 33)*

3.42-3.45 A study of patient dosage and protection in computed tomography. 3. patient dosage, distributions and hygienical evaluation during lumbar vertebra CT scanning
D-Y Qi, Suzhou, China *(p. 33)*

CHARTER SUITE

TEACH-IN: RADIOTHERAPY PLANNING FOR HEAD AND NECK CANCER

D Ash, Leeds

MONDAY 11 JUNE 4.15–5.30

HAREWOOD SUITE

PAEDIATRIC STUDIES

Chairman: Dr D W Pilling, Liverpool

4.35-4.55 **The role of radionuclides in renal imaging in children — a review**
H Carty, Liverpool *(p.12)*

4.55-5.15 **Dynamic CT in young children (chest and abdomen)**
B J Cremin, South Africa *(p.12)*

RIPLEY SUITE

VASCULAR ULTRASOUND STUDIES

Chairman: Dr W Hately, London

4.15-4.35 **Colour flow imaging principles**
G Thirsk, Letchworth *(p.22)*

4.35-4.47 **Colour Doppler evaluation of prosthetic cardiac valve function after exercise**
C J Occleshaw, Sheffield *(p.22)*

4.47-4.59 **Progress of treated deep venous thromboses: evaluation with colour doppler ultrasound**
G Baxter, Glasgow *(p.23)*

4.59-5.02 **Dextricity and carotid plaque lesion**
P C Njemanze, Owerri, Nigeria *(p.23)*

5.02-5.14 **Duplex scanning and non-invasive impedance analysis to detect the 'at risk' femoro-distal graft**
A M Jones, Bristol *(p.24)*

5.14-5.17 **The value of combined venography: comparison with contrast venography**
B Caner, Ankara, Turkey, *(p. 24)*

5.17-5.29 **The use of duplex derived hyperaemic flow to detect femoro-distal graft related stenoses**
J E Kabala, Bristol *(p.24)*

BRAMHAM SUITE

WORK IN PROGRESS SESSION

CHARTER SUITE

WORK IN PROGRESS SESSION

TUESDAY 12 JUNE 9.00–10.15

HAREWOOD SUITE

LIVER AND BILIARY SYSTEM

Chairman: Dr D Martin, Manchester

9.00-9.20 **Radiology of the liver**
A L Baert, Leuven, Belgium *(p. 37)*

9.20-9.23 **Dynamic contrast enhanced CT scanning in prognostically severe acute pancreatitis**
J M Lavelle, Leicester *(p. 37)*

9.23-9.26 **Corrugation of the common duct during endoscopic retrograde choledocho-pancreatography: a sensitive but non-specific indicator of pancreatico-biliary disease**
H J Fairhurst, Manchester *(p. 38)*

9.26-9.38 **Comparison of cholescintigraphy, ultrasound and ERCP in 55 patients with intrahepatic cholelithiasis**
I Stewart, Shatin, Hong Kong *(p. 38)*

9.38-9.41 **Correlation of staging with survival in patients with cholangiocarcinoma**
J J Donald, London *(p. 38)*

9.41-9.44 **Diagnostic value of cholangiograms in patients with obstructive jaundice**
A H Hasan, Glasgow *(p. 38)*

9.44-9.56 **A strategy for percutaneous removal of multiple intrahepatic calculi**
A Adam, London *(p. 39)*

9.56-9.59 **Percutaneous cholecystostomy in the treatment of acute calculous cholecystitis in high risk patients**
O Chan, London *(p. 39)*

9.59-10.02 **Benign biliary disease: percutaneous endoprosthesis or balloon dilatation?**
A Gillams, London *(p. 40)*

10.02-10.14 **Technical aspects of percutaneous gallstone dissolution with methyl-tert-butyl-ether (MTBE)**
D J Wright, London *(p. 40)*

RIPLEY SUITE

CARDIAC STUDIES

Chairman: Dr G I Verney, Papworth

9.00-9.20 *Invited Review* **Pharmacological stress in the diagnosis and management of coronary artery disease**
S R Underwood, London *(p.47)*

9.20-9.35 **Computer assisted diagnosis of ischemic heart disease: a system development and clinical trials for the interpretation of nuclear images**
Y Sasaki, Kyoto, Japan *(p.48)*

9.35-9.47 **MR measurement of cardiac output using cardiac gated acquisition**
M Tarnawski, London *(p.48)*

9.47-9.59 **Comparison of bulls' eye polar maps and added circumferential profiles for detection of coronary artery disease using ^{99}Tc^{m}-MIBI SPECT**
M Ünlü, Ankara, Turkey *(p. 49)*

9.59-10.11 **Comparison of ultrafast CT and MRI for cardiac diagnosis**
R M MacMillan, Philadelphia, USA *(p. 49)*

BRAMHAM SUITE

CONSENSUS WORKSHOP
EVALUATION OF SKELETAL METASTASES

Organiser and Chairman: M Merrick, Edinburgh

Panel: J S M Beales, Stevenage N Garvie, London, R Leonard, Edinburgh *(p. 56)*

CHARTER SUITE

ADVANCES IN ONCOLOGY

Chairman: Professor C A Joslin, Leeds

9.00-9.20 **Conformal radiotherapy**
Invited Review A E Nahum, Sutton *(p. 57)*

9.20-9.40 **Megavoltage imaging: new methods and applications for radiotherapy**
W Swindell, Sutton *(p. 57)*

9.40-9.43 **Bladder cancer and magnetic resonance imaging**
R A Persad, Bristol *(p. 57)*

9.43-9.46 **Computed tomography in carcinoma of the bladder**
M J Charig, Oxford *(p. 58)*

9.46-9.49 **Localised recurrence of rectosigmoid carcinoma — CT and MR assessment**
C E Williams, Liverpool *(p. 58)*

9.49-9.52 **Post-surgical CT images are not degraded by use of polydioxonone Ligaclips: advantages for follow-up after para-aortic node dissection for metastatic germ cell tumours**
J S K Gelister, London *(p. 58)*

TUESDAY 12 JUNE 10.45-12.00

HAREWOOD SUITE

CHEST RADIOLOGY

Chairman: Dr S J Golding, Oxford

10.45-11.05 Diagnosis of pulmonary embolism
Invited Review J P Lavender, London *(p. 41)*

11.05-11.08 Magnetic resonance anatomical and flow imaging of pulmonary arteries in patients with single lung transplantation
R H Mohiaddin, London *(p. 41)*

11.08-11.20 Pulmonary kaposis sarcoma: a review of the radiographic appearances in the St Mary's Hospital group of patients with the acquired immune deficiency syndrome
M McCarty, London *(p. 42)*

11.20-11.23 CT and ultrasound guided drainage of pleural empyemas and malignant effusion using fine pigtail catheters
C Sampson, Guildford *(p. 42)*

11.23-11.26 Sensitivity of fine needle transthoracic percutaneous needle biopsy (TNAB) versus histologic type, mass size and location of lung carcinoma
C Collins, Dublin *(p. 42)*

11.26-11.38 High-resolution computed tomographic appearances of lymphangioleiomyomatosis
C Prendergast, London *(p. 43)*

11.38-11.41 Pulmonary involvement in systemic lupus erythematosus: evaluation with computed tomography
C M Prendergast, London *(p. 43)*

11.41-11.44 CT density mapping in the assessment of pulmonary emphysema: a technical appraisal
M S Bernard *(p. 43)*

11.44-11.56 MRI scanning of the thorax in patients with active lymphoma
P R Goddard, Bristol *(p. 44)*

11.56-11.59 Thoracic computed tomography: value in respiratory failure secondary to kyphoscoliosis
P Carvalho, London *(p. 44)*

RIPLEY SUITE

MAMMOGRAPHY

10.45-10.57 Mammographic and histological classification of 100 patients requiring biopsy from the Manchester breast screening programme
D A Nicholson, Manchester *(p. 50)*

10.57-11.00 Can magnetic resonance imaging replace axillary lymph node sampling in the management of breast carcinoma: a prospective study
Dr H G Lewis-Jones, Liverpool *(p. 50)*

11.00-11.12 The individual and training in mammographic screening
G E Walker, Nottingham; *(p. 51)*

11.12-11.15 Mammographically demonstrated asymmetrical thickened ducts: a sign of ductal carcinoma *in situ*
A M Wood, Manchester *(p. 51)*

11.15-11.27 Film processing in mammography
A Servomaa, Helsinki, Finland *(p. 51)*

11.27-11.30 Mammographic screening: what do radiologists look for?
A G Gale, Nottingham *(p. 52)*

11.30-11.33 The Nottingham breast marker localisation set
A R M Wilson, Nottingham *(p. 52)*

11.33-11.45 Computer-aided interpretation of mammograms — a feasability study
S M Astley, Manchester *(p. 52)*

CHARTER SUITE

PHYSICS

Chairman: Dr I R Young, London

10.45-11.05 Localisation and quantitation in magnetic
Invited Review **resonance spectroscopy**
M O Leach, Sutton *(p. 60)*

11.05-11.17 Use of field inhomogeneity pulse to correct line shape and broadening spectra in *in vivo* MRS
I R Young, London *(p. 60)*

11.17-11.20 Fat suppression in MRI at low field strength using binomial pulse sequences
C J Baudouin, London *(p. 60)*

11.20-11.23 Motion tagging by spatial modulation
T W Redpath, Coventry *(p. 61)*

11.23-11.26 Receiver coil and sequence choice for optimal renal allograft MR imaging
N R Moore, Cambridge *(p. 61)*

11.26-11.29 *In vivo* measurement of the optical parameters of tumour tissue in man
I Driver, Leeds *(p. 61)*

11.29-11.32 Luminescence measurements on X-ray phosphors
G E Giakoumakis, Ioannina, Greece *(p. 62)*

11.32-11.35 New computer graphics for medicine and science
S Rish, London *(p. 62)*

11.35-11.47 3D microscopic computed tomography
S Webb, Sutton *(p. 62)*

CONGRESS THEATRE

TUESDAY 12 JUNE 12.15-1.15

MAYNEORD MEMORIAL LECTURE

Conjoint application of diagnostic and therapeutic ultrasound
F L Lizzi, New York, USA *(p. 66)*

The Mayneord Memorial Lecture is generously sponsored by 3M UK Plc.

TUESDAY 12 JUNE 2.30 - 3.45

HAREWOOD SUITE

SMALL BOWEL STUDIES

Chairman: Dr J N Glanville, Tadcaster

2.50-3.02 **Plain radiographic and computed tomographic appearances of lesser sac hernias**
F Regan, London *(p. 45)*

3.02-3.14 **Herniography in unexplained groin pain**
M C Collins, Sheffield *(p. 45)*

3.14-3.26 **^{99}Tc^{m}-HMPAO imaging in Crohn's disease of the small bowel**
N Kennan, Cardiff *(p. 45)*

3.26-3.38 **Per-oral pneumocolon in the evaluation of the distal small bowel**
B Patel, Manchester; *(p. 45)*

3.38-3.41 **Hereditary pancreatitis: early ultrasound appearances**
J A Spencer, Oxford *(p. 46)*

3.41-3.44 **Right sided diverticulitis**
P A Gaines, Shatin, Hong Kong *(p. 46)*

3.44-3.47 **Buscopan in radiological procedures — should patients drive afterwards?**
G R J Sissons, Cardiff *(p. 46)*

RIPLEY SUITE

ULTRASOUND STUDIES

Chairman: Dr S. Rimmer, Manchester

2.30-2.50 *Invited Review* **The current status of transrectal ultra sonography in the diagnosis and management of diseases of the prostate**
G J Griffiths, Newport *(p. 53)*

2.50-2.53 **Ultrasound of the post surgical thyroid**
A Ahuja, Shatin, Hong Kong *(p. 53)*

2.53-3.05 **Dynamic scanning in the assessment of intraocular abnormalities**
J A Fielding, Shrewsbury *(p. 53)*

3.05-3.08 **The role of ultrasound in the investigation of the salivary gland**
E J McAteer, Edinburgh *(p. 53)*

3.08-3.11 **The ultrasound features of forty peripheral haemangiomata**
I Stewart, Shatin, Hong Kong *(p. 54)*

3.11-3.23 **Techniques for 3D volume imaging with ultrasound**
J E Gardener, London *(p. 54)*

3.23-3.26 **Umbilical artery Doppler in high risk pregnancy**
P Twining, Nottingham *(p. 54)*

3.26-3.29 **The sonographic features of post-partum thyroiditis**
H Adams, Caerphilly *(p. 55)*

3.29-3.32 **The Venetian blind sign - an unusual ultrasound appearance in uterine fibroleiomyomata**
R J Davies, London *(p. 55)*

3.32-3.44 **Ultrasound markers in chromosomal disease, a retrospective study**
P Twining, Nottingham *(p. 55)*

3.44–3.47 **Ultrasound in the diagnosis of gallstone ileus**
R J Davies, London (visual presentation only) *(p. 55)*

BRAMHAM SUITE

TEACH-IN: INTERPRETATION OF MAMMOGRAMS

C Parsons, London *(p. 56)*

CHARTER SUITE

ONCOLOGY

Chairman: Professor A Horwich, Sutton

2.30-2.50 *Invited Review* **The current status of radiobiological modelling**
R G Dale, London *(p. 63)*

2.50-3.02 ***In vitro* radiosensitivity of human malignant astrocytomas**
J Ramsay, Cambridge *(p. 63)*

3.02-3.14 **Comparison of the biological effects of LDR and HDR radiation on epidermoidal cervix carcinoma cells (Caski cells) and human primary keratinocytes obtained after transfection with human papillomavirus type 16 DNA**
R Schulz-Wendtland, Freiburg, Germany *(p. 63)*

3.14-3.26 **Radiotherapy of lung cancer: evaluation of treatment volume and tumour remission by computed tomography**
T Feyerabend, Wurzburg, FRG *(p. 64)*

3.26-3.29 **The effect of ultrasound on the cytotoxicity of some chemotherapeutic agents**
G R ter Haar, Sutton *(p. 64)*

3.29-3.41 **Radiotherapy, head and neck tumours and cigarette smoking**
C Des Rochers, Northwood *(p. 64)*

3.41-3.44 **The assessment of tunour volume in the management of lung cancer by radiotherapy**
B E Lyn, Northwood *(p. 64)*

3.44 -3.47 **A quantitative method of expressing the radiation sensitivity of the epithelium in the human oral cavity**
T Ljubenov, Sofia, Bulgaria *(p. 65)*

CONGRESS THEATRE

TUESDAY 12 JUNE 4.15-5.30

SILVANUS THOMPSON MEMORIAL LECTURE

Tumour vasculature: a bother or a boon to the cancer therapist
Professor J Denekamp, Northwood *(p.66)*

WEDNESDAY 13 JUNE 9.00-10.15

HAREWOOD SUITE

CONTRAST STUDIES

Chairman: Professor B S Worthington, Nottingham

9.00-9.40 *Invited Review* **Contrast enhanced MRI: Gd-DTPA and beyond**
R Brasch, San Francisco, USA *(p.67)*
This lecture has been generously supported by Schering Health Care, UK

9.40-10.00 *Invited Review* **Contrast agents for diagnostic ultrasound — basic mode of action, state of the development and future prospects**
R Schlief, Berlin, FRG *(p. 67)*

10.00-10.03 **The effect of contrast media on renal vascular resistance (RVR)**
S K Morcos, Sheffield *(p. 68)*

10.03-10.06 **Magnetic resonance imaging with gadolinium-DTPA in the evaluation of bone and soft tissue tumours**
J M Hawnaur, Manchester *(p. 68)*

10.06-10.09 **Oral magnetic particles: a new oral contrast for abdominal MRI. Clinical results**
D Kean, Edinburgh *(p. 68)*

10.09-10.21 **The kinetics of tissue enhancement in intracranial tumours following intravenous Gd DTPA studied by ultra high speed inversion-recovery EPI**
B S Worthington, Nottingham *(p. 69)*

BRAMHAM SUITE

ONCOLOGY

Chairman: Dr A H Laing, Oxford

9.00-9.20 *Invited Review* **The diagnosis of soft tissue sarcomas by CT and NMR**
J Husband, Sutton *(p. 83)*

9.20-9.40 *Invited Review* **Clinical applications of SPECT with special reference to oncology**
V R McCready, Sutton *(p. 84)*

9.40-9.43 **Comparison of CT and MRI in Ewing's sarcoma**
J F C Olliff, Sutton; *(p. 84)*

9.43-9.55 **Wilm's tumour; what changes are seen on CT following chemotherapy?**
Y Y Ng, London *(p. 85)*

9.55-10.07 **Inguinal and iliac node involvement in germ cell tumours of the testis. Implications for radiological investigation and for therapy**
M Mason, Sutton *(p. 85)*

10.07-10.19 **Thin slice computed tomography for assessment of tumours and responses to therapy**
R G Sephton, Melbourne, Australia *(p. 86)*

10.19-10.22 **Paratesticular Rhabdomyosarcoma: radiological appearances of patterns of disease, presentation and relapse**
J E Stutley, Sutton *(p. 86)*

10.22-10.25 **Ultrasound examination of regional lymph nodes: value in staging and follow-up of malignant melanoma**
T Feyerabend, Wurzburg, FRG *(p. 86)*

CHARTER SUITE

SYMPOSIUM: RADIOTHERAPY DOSE DISTRIBUTION AND TUMOUR CONTROL PROBABILITY

Determinants of control probability of experimental tumours
N J McNally, Northwood; *(p. 91)*

Dose response data for local tumour control
D M Tait, Sutton; *(p. 91)*

The radiosensitivity of human tumour cells
G Gordon Steel, Sutton; *(p. 91)*

Influence of dose distribution on local tumour control probability
A E Nahum, Sutton. *(p. 92)*

WEDNESDAY 13 JUNE 10.45-12.00

RIPLEY SUITE

TECHNOLOGY AND OPTIMISATION

Chairman: Dr A E Hugh, Stoke on Trent

10.45-11.15 **QALY's in diagnostic radiology**
J G B Russell, Manchester; *(p. 70)*

11.15-11.18 **A new personal computer based image transfer system: impact on patient management**
J A Spencer, Oxford *(p. 70)*

11.18-11.21 **Memory for radiological appearances: objective evidence for perceptual schemata**
B S Worthington, Nottingham *(p. 70)*

11.21-11.24 **"Reporting in a flash"**
A G Gale, Nottingham *(p. 71)*

11.24-11.27 **Patient expectation and accident and emergency radiology**
E McNally, Harrow *(p. 71)*

11.27-11.30 **Ergonomic assessment of mobile X-ray units**
A G Gale, Nottingham *(p. 71)*

11.30-11.33 **Radiology in developing countries. Three years' experience in Rwanda with a basic radiologic system specifically designed for developing countries**
R Van Tiggelen, Brussels, Belgium *(p. 71)*

11.33-11.36 **Potential savings from improved reporting practices in a radiology department**
I W J Birchall, Bristol *(p. 72)*

11.36-11.48 **Audit of a radiodiagnostic department**
I W J Birchall, Bristol *(p. 72)*

11.48-12.00 **Outpatient angiography in a district general hospital**
R M Evans, London *(p. 72)*

HAREWOOD SUITE

INTERVENTIONAL RADIOLOGY

Chairman: Dr A-M Belli, Sheffield

10.45-10.57 **Percutaneous angioscopy of peripheral and coronary arteries**
M R Rees, Leeds *(p. 76)*

10.57-11.00 **Mechanical recanalisation of peripheral vascular occlusions after guide wire dissection using a metal laser probe**
A-M Belli, Sheffield *(p. 76)*

11.00-11.03 **Technique and complications of direct brachial artery puncture for arteriography**
A F Watkinson, Bristol *(p. 77)*

11.03-11.15 **Dynamic angioplasty in vascular occlusions: patient selection and follow-up results**
M R Rees, Leeds *(p. 77)*

11.15-11.18 **Treatment of chronic coronary artery occlusions with an olive tipped guide wire (Magnum) *versus* terumo guidewire**
M R Rees, Leeds *(p. 77)*

11.18-11.30 **The influence of Nd-YAG laser and dynamic angioplasty devices on platelet reactivity**
A A Gehani, Leeds *(p. 78)*

11.30-11.33 **Percutaneous peripheral laser angioplasty using an ND-YAG laser and sapphire tipped device**
S Ashley, Leeds *(p. 78)*

11.33-11.36 **Is iliac angioplasty indicated for the treatment of critical ischaemia?**
C J Wakely, Bristol *(p. 78)*

11.36-11.39 **Lipiodol assisted ultrasound guided liver biopsies**
P A Gaines, Shatin, Hong Kong *(p. 79)*

11.39-11.51 **Radionuclide limb blood flow measurement in the assessment of balloon angioplasty in peripheral vascular disease**
A Parkin, Leeds *(p. 79)*

BRAMHAM SUITE

ENDOCRINE STUDIES

Chairman: Dr N Garvie, London

10.45-11.05 **Endocrine tunmour localisation**
Invited Review S McEwan, Edmonton, Canada *(p. 87)*

11.05-11.17 **Computed tomography in phaeochromocytoma**
C S Deacon, Manchester *(p. 87)*

11.17-11.29 **The elusive upper parathyroid adenoma on thallium-201/technetium-99m subtraction scintigraphy**
T Y K Chan, London *(p. 87)*

11.29-11.41 **Correlation of the ultrasound and histology of the scintigraphically hot thyroid nodule**
I Stewart, Shatin, Hong Kong *(p. 88)*

11.41-11.53 **High resolution CT of the pituitary in children with growth hormone deficiency**
G Kelly, Manchester; *(p. 88)*

11.53-11.56 **Retroconversion of immature teratoma of the ovary: CT appearances**
E Moskovic, London *(p. 88)*

11.56-11.59 **Low field MRI in the management of high volume testicular teratoma** L Wilkinson, Glasgow; *(p. 89)*

SYMPOSIUM: RADIOTHERAPY DOSE DISTRIBUTION AND TUMOUR CONTROL PROBABILITY

Continued

WEDNESDAY 13 JUNE 2.30-3.45

HAREWOOD SUITE

DIGITAL RADIOLOGY

Chairman:	Professor G Whitehouse, Liverpool
2.30-2.42	**Digital subtraction angiography** S J King, London *(p. 73)*
2.42-2.54	**Digital subtraction imaging of the investigation of the salivary glands** D MacVicar, London *(p. 73)*
2.54-3.06	**DSA of digital ischemia** B P Menanteau, Reims, France *(p. 73)*
3.06-3.18	**Digital fluorography: the first year's experience** D J Lintott, Leeds *(p. 73)*
3.18-3.21	**A review of thermal-processed paper/film hard-copy units in medical imaging** N J Coleman, Leeds *(p. 74)*
3.21-3.33	**A physical assessment of the imaging performance of the DSI digital fluorography system** A R Cowen, Leeds *(p. 74)*
3.33-3.36	**The influence of intravenous DSA in the management of peripheral vascular disease** O Chan, London *(p. 74)*
3.36-3.39	**Real time digital peripheral angiography** S C Ward, Kingston-upon-Hull *(p. 75)*
3.39-3.42	**Early experience with a prototype (2k) projectional digital chest unit: ROC study of simulated lung nodules** D M Hansell, Los Angeles, USA *(p. 75)*

RIPLEY SUITE

ONCOLOGY

Chairman:	Dr W G Jones, Leeds
2.30-3.00 *Invited Review*	**Radiotherapy for soft tissue sarcomas** C L Harmer, London *(p. 80)*
3.00-3.12	**Preliminary results of prospective study of hyperfrarctionated high dose radiotherapy in the management of extremity soft tissue sarcomas** M H Robinson, London *(p. 80)*
3.12-3.24	**Tumour size as a prognosis pactor in carcinoma of cervix: assessment by transrectal ultrasound** J P Logue, Manchester *(p. 80)*
3.24-3.36	**Comparison of the Ho's and the UICC/AJC stage classifications for NPC** P Teo, Shatin, Hong Kong *(p. 81)*
3.36-3.39	**Cranial nerve involvement by nasopharyngeal carcinoma: response to treatment and clinical significance** S Y Ts'ao, Shatin, Hong Kong *(p. 81)*
3.39-3.42	**Concomitant chem/radiotherapy for advanced carcinoma of the head and neck** C H Macmillan, Nottingham *(p. 82)*
3.42-3.45	**Odorous symptoms during irradiation of the olfactory system** S M Sagar, London *(p. 82)*

BRAMHAM SUITE

TEACH-IN:
DIAGNOSIS OF HEAD AND NECK DISEASE

J E Gillespie, A Gholkar, Salford *(p. 90)*

CHARTER SUITE

QUANTITIVE BONE STUDIES

Chairman:	Dr I Fogelman, London
2.30-2.50 *Invited Review*	**Bone densitometry** I Fogelman, London *(p. 93)*
2.50-3.02	**Quantitative bone mass measurement — techniques and correlations** J E Adams, Manchester *(p. 93)*
3.02-3.13	**Dual energy quantitative computed tomography (DEQCT) for measurement of vertebral trabecular bone composition** R Whitehouse, Manchester *(p. 94)*
3.13-3.25	**An *in vitro* study of ultrasonic attenuation in bone** J A Evans, Leeds *(p. 94)*

Scientific Programme Abstracts

Monday 11 June

Harewood Suite

Central Nervous System (9.00–10.15)

MRI disorders of the spinal column; pathophysiological insights and contribution to management

B.S.Worthington
Department of Radiology, University Hospital, Nottingham NG7 2UH

The development of surface coil imaging of the spinal column which permits high-quality thin-section studies without planar restriction has led to MRI becoming the preferred method of addressing many types of clinical problems, especially those based on disc pathology. It has become apparent that MRI is a valuable research tool for studying fundamental questions relating to the pathophysiology and natural history of several conditions involving the spinal column. The pathophysiology of disc degeneration, which is part of normal senescence, is complex and incompletely understood. It is associated with reduction in signal from the central portion of the disc on T_2-weighted images which correlates closely with discographic evidence of disc degeneration. The high incidence of premature disc degeneration in adolescents with disc protrusion suggests a possible underlying diathesis in some individuals. The increased prevalence of disc degeneration in the disc below a neural arch defect in spondylolysis suggests that disc failure is potentiated by mechanical stress. In Scheuermann's kyphosis also, loss of nuclear signal at multiple levels is probably secondary to repetitive microtrauma to the discovertebral junction. Studies in an animal model have demonstrated the evolution of changes which occur in disc space infection and emphasize the value of the technique in early diagnosis and the recognition of extension into the extradural space.

Magnetic resonance imaging of vascular abnormalities of the CNS

H. M. Hawnaur, J. P. R. Jenkins and I. Isherwood
Department of Diagnostic Radiology, University of Manchester, Manchester M13 9PT

Magnetic Resonance (MR) findings in vascular malformations and aneurysms of the brain and spine are reviewed with particular reference to the role of gadolinium-DTPA (Gd-DTPA).Thirty-five patients (F=21, M=14, age 27–75 years) were scanned on a 0.26T superconducting magnet system. Spin echo and partial saturation recovery sequences (SE560–2000/26-120; PSR500/18) were obtained in various planes using head or spine surface coils. In 24 patients, T_1-weighted sequences were repeated after Gd-DTPA. Eighteen patients had a intracranial arteriovenous malformation (AVM) and 10 had spinal AVMs. On MR, patent vessels showed signal void, and haemorrhage and infarction were identified but calcification was not always apparent. Increased signal intensity was observed within some AVMs after Gd-DTPA but generally enhancement was minimal. Spinal dural AVMs were associated with cord expansion, abnormal signal intensity and diffuse enhancement following Gd-DTPA, more intense on delayed scans. Patients with intramedullary AVMs tended to present acutely with signs of haemorrhage on MR and no enhancement after Gd-DTPA. Seven patients with aneurysms were studied, six with giant cerebral aneurysms (GCA). MR findings included signal void in the patent lumen, with surrounding laminated thrombus, evidence of haemorrhage and peri-aneurysmal oedema. Slight peri-aneurysmal parenchymal enhancement occurred in patients given Gd-DTPA. Vascular malformations have a specific appearance on MR which can also demonstrate their effect on brain or spine. The use of Gd-DTPA does not increase the diagnostic information obtained.

Craniospinal magnetic resonance imaging in neurofibromatosis

P. M. Hughes, J. M. Hawnaur, J. P. R. Jenkins and I. Isherwood
Department of Diagnostic Radiology, University of Manchester, Manchester M13 9PT

The role of craniospinal Magnetic Resonance Imaging (MRI) in patients with neurofibromatosis (NF) and neurological symptoms has been reviewed. Seventeen patients (M=12, F=5; age range 9-75 years) were studied on a 0.26T superconducting magnet system using a variety of T_1- and T_2-weighted sequences (spin echo 500–2000/26–120; partial saturation recovery 500/18). In eight patients the T_1-weighted sequences were repeated following 0.1 mmol gadolinium-DTPA (Gd-DTPA) per kg body weight. Cranial imaging revealed at least two lesions in five out of nine patients studied, including two cerebellar gliomas, three areas of grey matter heterotopia, two optic gliomas, three acoustic neuromas (bilateral in one) and multiple meningiomas in two. Gd-DTPA improved identification of intrameatal acoustic neuromas, meningiomas and cerebellar gliomas. Spinal imaging in 10 patients demonstrated neurofibromas to be isointense with neural tissue on T_1-weighted sequences. All enhanced following Gd-DTPA improving conspicuity of lesions. On T_2-weighted sequences neurofibromas demonstrated high signal with a heterogenous low signal centre to most lesions greater than 3 cm diameter. Gd-DTPA improved identification of small intradural tumours. MRI demonstrated extent of craniospinal involvement in NF, frequently identifying asymptomatic tumours. Gd-DTPA improved conspicuity of small lesions. MRI may be a useful screening technique in families with central NF.

Changes in regional cerebral blood flow of patients with hydrocephalus after CSF shunting: detection by ^{99}Tc^{m}-HMPAO SPECT

B. Caner, H. Caner, H. Turul, O. E. Ozcan, G. Erbengi and C. Bekdik
Departments of Nuclear Medicine and Neurosurgery, Hacettepe University School of Medicine, Ankara 06100, Turkey

Obstruction of the cerebrospinal fluid (CSF) pathways decreases regional cerebral blood flow (rCBF). It was demonstrated by experiments that shunting of CSF from ventricles increased rCBF if hydrocephalus was present for less than 8 weeks. But there was no clinical study confirming this finding. Therefore this study was designed to evaluate the effect of shunting on rCBF in patients with different durations of high-pressure hydrocephalus. Fifteen patients (eight male, seven female, age range 1 week–56 years) underwent CT and ^{99}Tc^{m}-HMPAO SPECT examination before and after shunting. The patients were divided into three groups according to the post-operative scintigraphic finding (see Table). Pre- and post-operative quantitative analysis of rCBF for each lobe was done by taking the cerebellum as a reference region. A diffuse increase in rCBF, predominantly in the frontal region, was noticed post-operatively in Groups A (marked) and B (moderate) but not in Group C. It is suggested that although the dilated ventricles became smaller post-operatively regardless of the duration, no improvement in rCBF was detected if hydrocephalus was present for more than 12 weeks.

	Group A (*n*=6)	Group B (*n*=4)	Group C (*n*=5)
Increase in rCBF (%) (Mean of all lobes)	15.5±3.5	10.25±9.1	1.19±1.2
Mean duration of hydrocephalus (weeks)	5±0.5	8±1	≥12
Decrease in ventricle size (on CT)	+	+	+

Computerized tomography of the brain: does contrast enhancement really help?

M. S. Bernard, H. Adams and M. D. Hourihan
Department of Radiology, University Hospital of Wales, Heath Park, Cardiff CF4 4XN

Established policies regarding the use of intravenous contrast in Computerised Tomography (CT) of the brain are largely based on experience with early scanners. Given the high resolution of current generation scanners, we have conducted a prospective study to reassess the contribution of intravenous contrast to the final diagnosis in cranial CT. Three hundred patients who required intravenous contrast during routine axial cranial CT were included in the study. Two hundred and twelve patients presented with symptoms or signs suggesting focal intracranial pathology and 88 with non-focal features. A total of 110 post-contrast scans were abnormal. The differential diagnosis was altered in 15 patients following contrast enhancement, 13 of whom presented with focal features. In 3 patients with normal plain scans abnormalities were only seen after contrast. In a further 15 patients contrast enhancement increased the certainty of the diagnosis made on the uncontrasted scan. Despite the improvements of current CT scanners, we feel that intravenous contrast enhancement alters the differential diagnosis and the degree of confidence in sufficient patients to justify its continued widespread use.

Computed tomography in the evaluation of idiopathic pseudotumour of the orbit

M. J. McNicholas, W. J. Power and J. G. Griffin
Department of Diagnostic Imaging, St Vincent's Hospital, Elm Park, Dublin 4

Orbital pseudotumour is an inflammatory process for which no identifiable cause can be found. Certain features on computed tomography (CT), together with a classical clinical picture, can allow a specific diagnosis to be made. We examined 13 patients with inflammatory orbital pseudotumour using CT. The CT appearances were correlated with clinical presentation and with response to treatment. Proptosis and diplopia were found with all varieties of CT appearance. Visual loss was associated with direct involvement of the optic nerve. The Tolosa Hunt Syndrome was found with lesions related to the superior orbital fissure. Biopsy may worsen the clinical course of this disease. In several cases the typical CT appearances combined with the clinical presentation obviated the need for biopsy. CT was helpful in predicting response to treatment. Patients with lesions confined to the lacrimal gland or extraocular muscles, or those with an inflammatory mass of less than 1 cm, had a rapid and sustained response to oral steroids. Those with a larger mass, diffuse disease or involvement of the sclera had a poor response to steroid treatment and required immunosuppressants. Patients with involvement of the optic nerve suffered permanent visual loss. We present our findings in these patients with idiopathic orbital pseudotumour.

MRI and RARE myelography in diagnosis of spinal cord compression due to metastatic disease

E. Dinkel, S. Landwehrmann, D. Ott, A. Mundinger and H. Friedburg
Department of Radiology, University Clinics, D 78 Freiburg, West Germany

Fifty-two patients with known malignancies outside the central nervous system had magnetic resonance imaging (MRI) of the spine for the investigation of possible metastatic compression of the spinal cord and cauda equina. T_1-weighted sagittal sections of the spine and additionally rapid acquisition with relaxation enhancement (RARE) hydrography were performed using a whole-body MRI system operating at a field strength of 0.23 Tesla, corresponding to 10 MHz proton resonance frequency. RARE hydrography yields T_2-weighted aqueous fluid-specific images within a few seconds and offers a rapid non-tomographic approach to MR myelography. Plain radiography of the spine did not contribute to the diagnosis of tumour extension. CT proved accurate in diagnosis of osteolytic lesions, especially of the vertebral arch and articular processes. MRI results were compared with neurosurgical findings and histological examinations of the spinal or epidural lesion in 27 patients. Sensitivity of RARE myelography for metastatic compression of the spinal cord or cauda equina was 100%. RARE myelography thus provides a rapid and sensitive diagnosis of complete or partial block of the spinal canal and may substitute for myelography in the preoperative work-up.

Paranasal sinus abnormalities in patients referred for cranial CT

G. Needham and A. F. MacDonald
Neuroradiology Department, Department of Diagnostic Radiology, Aberdeen Royal Infirmary, Aberdeen

Paranasal sinus (PNS) disease is an area of confusion both in ENT practice and for us as radiologists. Both clinical and radiological diagnoses are dependent on identifying maxillary or frontal disease. Recently the importance of the ethmoid sinuses in relation to the pathogenesis and treatment of maxillary and frontal sinus disease has been recognized. CT is superior to standard PNS radiography in demonstrating the ethmoid sinuses. We have performed a prospective analysis of the PNS of 235 patients with non-sinus-related problems who were referred for cranial CT, in an attempt to identify the patterns of disease in this population. This was not an asymptomatic population and patients fell into one of four groups (see Table). Of patients with CT demonstrable disease, 47% had involvement of the anterior ethmoid sinuses. The results of our study have shown that sinus occurs in 26% of patients referred for cranial CT for non-sinus-related problems, and that a clinical history of sinus disease is a poor indicator of the presence of sinus disease. The implication of these results is discussed, with particular reference to our ENT collaboration and new techniques in endoscopic surgical treatment.

Group 1	PNS symptoms/no CT-demonstrable PNS disease	78 (33.2%)
Group 2	PNS symptoms/CT-demonstrable PNS disease	43 (18.3%)
Group 3	No PNS symptoms/CT-demonstrable PNS disease	18 (7.7%)
Group 4	No PNS symptoms/no CT-demonstrable PNS disease	94 (40%)

Magnetic resonance angiography of dural sinus thrombosis

T. S. Padayachee, M. Tarnawski, M. J. Graves, P. E. Graves, M. G. Taylor, J. B. Bingham, A. C. F. Colchester and T. Cox
Division of Radiological Sciences, UMDS, Guy's Hospital, London SE1 9RT

Magnetic resonance imaging (MRI) has been recommended in the detection of dural sinus thrombosis. The presence of high signal in the sinuses, instead of the normal flow void, is a reliable indicator of thrombosis. Demonstration of flow obstruction, however, has relied upon conventional X-ray angiographic techniques. We describe MR venous angiography to augment MR assessment of dural sinus thrombosis. Cerebral venograms were produced in volunteers (six) and patients (three), using the inflow technique. This is based upon the flow-related enhancement obtained with short-TR velocity-compensated field–echo pulse sequences and provides a high contrast between moving blood and stationary tissue. A stack 50 x 2 mm slices were acquired using a 2D multislice sequence. A presaturation slab positioned proximal to the imaging region allows suppression of arterial flow. The data were reformatted and a maximum intensity ray tracing algorithm applied to produce an angiographic projection; combining projections with different viewing angles in a cine sequence provided an impression of the 3D nature of the vasculature (ANALYZE, BRU, Mayo Foundation). The flow images demonstrate the sagittal, straight and transverse sinuses in normal subjects. In patients with dural sinus thrombosis the absence of flow in the sinuses was demonstrated. In one patient, follow-up MR angiography demonstrated the gradual return of flow to the sinuses over a few weeks in response to anticoagulant therapy. Combined MR imaging and angiography enables a more complete assessment of dural sinus thrombosis. It does not require ionizing radiation, contrast media or vessel puncture and may be the imaging modality of choice for assessing this condition.

Notes

Trauma (10.45–12.00)

The radiology of chest trauma

A. McNeill
Radiology Department, Royal Victoria Hospital, Belfast BT12 6BA

Experience of chest trauma in Northern Ireland is somewhat unique within the United Kingdom, owing to our continuing civil unrest. Over 300 cases of major thoracic trauma have been treated in the Regional Thoracic Surgical Unit since 1982. Many patients have multiple injuries affecting more than one system, therefore initial assessment by an experienced clinician is vital. The role of the radiologist is important but must be secondary to good clinical assessment and resuscitation. In the acute situation time often permits only limited radiography. This is usually a supine AP film which can be difficult to interpret. Variation due to technique must be recognized. Cases are discussed with special reference to assessment of the initial plain radiograph and the necessity for further radiology. Late developments and complications are addressed, as well as chest complications of trauma to other areas, such as the abdomen and cranium.

The significance of multiple posterior urethral false passages following pelvic trauma

S. J. Garber, D. Rickards and *R. Turner-Warwick
*Departments of Radiology and *Urology, Middlesex Hospital, London W1N 8AA*

Ten per cent of pelvic fractures are associated with urethral trauma, which can result in complete disruption to stricturing of the posterior urethra. Pre-operative imaging provides information on the site and extent of pathology, the competence of the sphincter mechanisms and whether there are false passages. Ten cases are presented. All had urethral pathology due to trauma, and attempted primary repair of a defect or dilatation of a stricture, and were referred with supra-pubic catheters *in situ*. Pre-urethroplasty work-up included combined cystography and retrograde urethrography. In seven out of 10 patients, two bladder necks associated with false passages were identified and in the other three, multiple bladder necks. Urethral defects involving the distal sphincter mechanism were identified in five. In all patients, the true posterior urethra could be distinguished by recognition of the verumontanum and residual bladder neck sphincter activity. Before reconstructive surgery it is important to depict urethral anatomy accurately following trauma. This presentation stresses the salient points in identifying the true posterior urethra in 10 patients in whom the distal sphincter mechanism has been compromised.

MRI of acute, sub-acute and chronic spinal trauma

R. W. Kerslake, T. Jaspan and B. S. Worthington
Department of Radiology, University Hospital, Nottingham NG7 2UH

MR imaging was performed in 90 patients with a history of spinal trauma; in 40, injury had occurred in the previous 6 months (acute); in the remainder from between 6 months and one year (sub-acute), and up to 40 years (chronic). In the acute group abnormalities were shown in the extraspinal soft tissues, the vertebral column including the intervertebral discs and within the spinal canal in 38%, 62% and 55% respectively. Ten cases showed abnormality in all three regions and 10 no abnormality. Many of the findings such as acute disc herniation have significant management implications. In the sub-acute and chronic groups extraspinal soft-tissue abnormalities were present in only eight cases (16%) and six of these were a result of previous surgery. The vertebral column was abnormal in 82% and the cord showed areas of abnormal signal or morphology in 50%. Of these there were 10 cases of syringohydromyelia (which was never seen within 6 months of injury): five with isolated cord compression, eight with cord atrophy and five with changes consistent with cystic myelomalacia. The underlying pathophysiology of abnormal cord morphology and signal intensity, which is seen in both the acute and chronic stages, is incompletely understood. The morphological appearance of syringohydromyelic cavities, which is usually different above and below the level of injury, is possibly related to alterations in CSF flow secondary to focal canal stenosis.

Real-time sonographic assessment of suspected scaphoid fracture

W. W. Gibbon and A. N. Khan
Department of Diagnostic Radiology, North Manchester General Hospital, Crumpsall, Manchester M8 6RB

The common clinical problem of the correct management for patients with suspected scaphoid fracture in the presence of normal carpal radiography remains unclear. The radial artery traverses the anatomical snuff-box in close proximity to the scaphoid, separated only by a thin layer of synovial fluid, synovium and wrist joint capsule/radial collateral ligament. Consequently if the scaphoid-radial artery distance is increased it must be because of a joint effusion/haemarthrosis, synovitis or capsule/collateral ligament injury. Both radial artery and carpal bone contours are clearly seen on ultrasound. We now present our preliminary findings on the use of real-time ultrasound in the assessment of suspected scaphoid fracture. An initial volunteer normal/asymptomatic control group (17 women, three men; age range 22–61 years, mean 29.0 years) was examined sonographically comparing the scaphoid-radial artery distance for both wrists. Values ranged from 2.2 to 4.0 mm (mean 2.93 mm) with a variation between limbs ranging from 0.0 to 0.8 mm (mean 0.25 mm). In our study group we examined 18 patients with clinically suspected scaphoid fractures. The nine patients with normal scans all failed to show evidence of bony injury at follow-up. In the nine patients with scaphoid-radial artery distances outside the normal range, two patients had old scaphoid fractures, one a new fracture at the scaphoid waist and one a bony avulsion of the distal pole of scaphoid-radial collateral ligament. Further studies are required to provide a conclusive statistical correlation.

Real-time digital contrast enhancement and magnification in the assessment of scaphoid and other wrist injuries

R. Wellings, E. Morris, J. Fowler, R. A. Manns and A. M. Davies
Department of Radiology, The General Hospital, Birmingham B4 6NH

A study was conducted on the value of a commercially available desk-top digital contrast enhancer-magnifier (DETECT system) in a series of 550 patients presenting with an acute wrist injury. Four radiologists, of varying experience, independently reviewed the radiographs on a conventional lightbox and subsequently with the "digitizer". Statistical analysis was performed on the collated observations. In the scaphoid series (350 cases) the performance of the two more experienced radiologists was marginally better with the digitizer whereas the less experienced radiologists performed slightly worse. Overall the digitizer improved the confidence of the radiologists in correctly diagnosing the presence of a scaphoid fracture but for the less experienced radiologists this was at the expense of identifying normality. In the wrist series (200 cases) the use of the digitizer resulted in a minor increase in the true positive and decrease in the false negative observations but this was offset by a concomitant minor increase in the false positive and decrease in the true negative categories. Evaluation of the soft-tissue planes around the wrist joint showed a limited value in the identification of a scaphoid fracture with an overall positive predictive value of 0.26. Correlation of soft-tissue changes and the presence or absence of a scaphoid fracture was slightly worse with the digitizer. Possible causes for the apparently poorer performance of the digitizer are discussed as well as the relative merits and potential value of the unit.

Pitfalls in bone scintigraphy for suspected hip fracture

J. Rees, G. V. Thomas and L. A. Williams
Department of Radiology, Cardiff Royal Infirmary, Cardiff CF2 1SZ

^{99}Tc^{m}-MDP bone scintigraphy has been advocated as a highly sensitive and specific method of identifying "occult" fractures of the hip in elderly patients who present with an acutely painful hip, and normal plain radiographs. Previous studies have shown bone scintigraphy to be totally reliable in the identification of these fractures, there being no false-positive or false-negative results. However, continued experience has highlighted several diagnostic difficulties and pitfalls. In a review of 2617 patients who were admitted with a suspected fractured neck of femur over a period of 5 years, 213 had no detectable fracture on plain radiographs, and were subsequently investigated by bone scintigraphy. Normal scans were obtained in 127 cases (60%). Of the remaining 86 cases, 82 (38%) were reported to show fractures of the proximal femur, three showed pubic ramus fractures, and one acetabular fracture was demonstrated. Review and follow-up have identified several false-positive and two false-negative scans. The various factors accounting for these errors are considered, and the clinical implications discussed. Bone scintigraphy remains a very useful test for detecting occult fractures of the hip and surrounding skeleton, but careful analysis should be made within the context of the clinical findings and plain radiographs in order to avoid the diagnostic pitfalls of this investigation.

Fractures of the atlas vertebra

A. Sandhu, J. L. Fowler and R. D. Fraser
Departments of Radiology and Spinal Injury, Royal Adelaide Hospital, North Terrace, Adelaide, South Australia 5000

A total of 52 cases of atlas fractures were admitted to the Spinal Injury Unit over a 14-year period. Two groups are apparent, which differ in age, presentation, mechanism of injury, radiology and treatment given. Patients with Jefferson fractures were on average 42 years of age and the radiology, including CT, is presented. Correlation of the radiology initially, during traction and follow-up is discussed. Cases of posterior arch fractures were on average 17 years older, and had marked degenerative changes in the mid to distal cervical spine fracture. Injury in the elderly was often after minor trauma.

An assessment of triage of casualty radiographs by radiographers

I. Renwick, W. P. Butt and B. Steele
Department of Diagnostic Radiology, St James's University Hospital, Leeds LS9 7TF

A study has been undertaken to assess the ability of radiographers in a busy accident and emergency department to triage patients on the basis of their radiographs. A total of 3000 patients have been studied. The radiographers performing the radiographs were offered a choice of four categories in their assessment: normal, abnormal, insignificantly abnormal, or further advice required. Their choice was compared with an assessment made by the radiologist reporting the film (from the categories normal, abnormal, insignificantly abnormal). The assessments were made independently. The results are presented. With ever-increasing demands on radiologists' time, these results could point a way towards reducing errors in radiographic interpretation by unsupervised junior casualty staff. An extension of the study is planned with larger patient numbers, and subsequently an assessment of formal reporting by radiographers.

Computed tomographic assessment of old calcaneal fractures

S. A. Bradley, A. M. Davies and K. M. Porter
Departments of Radiology and Trauma Surgery, Birmingham Accident Hospital, Birmingham B15 1NA

There is limited consensus as to the most appropriate treatment for the acute calcaneal fracture, and a large proportion of patients may be left with long-term disability and pain. In this prospective study high-resolution CT in axial and coronal planes was performed in 61 patients with 71 old calcaneal fractures. The series comprised 45 men and 16 women with an age range of 12 to 83 years (mean 49.7 years). The time interval between the occurrence of the fracture and the CT examination ranged from 6 to 300 months (mean 32.2 months). The CT images on both bone and soft-tissue window settings were assessed for fracture healing, secondary degenerative changes, alterations in calcaneal configuration and abnormalities of the adjacent tendon. Of the 49 intra-articular fractures, flattening of the calcaneum was revealed in 92%, osteoarthrosis of the posterior subtalar joint in 90%, lateral spur formation in 75%, intra-articular loose bodies in 26.5% and involvement of the calcaneo-cuboid joint in 35% of cases. Peroneal tendon abnormalities were identified in 75% of cases, with subluxation or dislocation of the tendons in 49%. Medial tendon abnormality was revealed in 18.4% of cases. These findings are correlated with the patients' current clinical conditions, and the relative merits of measuring the calcaneal height, heel-valgus and sustentacular angles and medial offset of the talar head from the CT examinations are discussed.

3D-CT of pelvic fractures

R. L. Guy, P. A. Butler-Manuel, R. N. Brueton and F. W. Heatley
Departments of Radiology and Orthopaedics, St Thomas' Hospital, London SE1 7EH

Pelvic and acetabular fractures often occur in young patients and accurate open reduction with internal fixation now offers the chance of achieving a better long-term result by reducing subsequent degenerative changes. Pre-operative planning with detailed knowledge of the three dimensional anatomy of these fractures is vital to ensure the best possible outcome. Current methods of evaluation include Judet views and axial CT scanning. The aim of this study was to assess whether 3D CT reconstruction improves pre-operative planning. Seven patients have been investigated, three transverse acetabular fractures with separation of a posterior fragment, two two-column fractures, a bilateral sacroiliac dislocation and a bilateral sacral fracture with diastasis of the pubic symphysis. Plain radiography with Judet views and axial CT scans with 3D reconstruction were performed in all cases. The scans were performed on a Somatom DR H scanner and the 3D reconstructions were made using a surface imaging technique utilizing the scanner's own computer. 3D CT reconstructions were helpful in all cases. The complex anatomy of the pelvic fractures, in particular the precise relationships of all the fragments, was clearly demonstrated. Although the three imaging techniques are complementary, 3D CT presents the information in a more readily interpretable form, facilitating pre-operative planning.

Skeletal Studies (2.30–3.45)

Current trends in the radiology of joint disease.

I. Watt
Department of Radiology, Bristol Royal Infirmary, Bristol BS2 8HW

Abstract not received.

Ultrasound and MRI diagnosis of meniscal cysts

A. Coral, M. van Holsbeeck, R. S. Adler and K. A. Buckwalter
Department of Radiology, University of Michigan Hospitals, Ann Arbor, Michigan 48109, USA

Cystic change in a degenerate meniscus occurs in 2.5% of medial and 22.2% of lateral menisci and is usually confined within the fibrocartilage. Occasionally, the cyst can enlarge and migrate and present as a mass around the knee. Recent evidence indicates that there is always an associated tear of the underlying meniscus, most often a horizontal linear or serpentine cleavage tear. The hypothesis is that synovial fluid is forced along the tear and into the cyst, causing enlargement. The diagnosis is often missed by arthrography and arthroscopy. We present three cases of meniscal cyst (two lateral and one medial) diagnosed by ultrasound and MRI. On ultrasound the cysts were generally hypoechoic but contained focal areas of highly echogenic material presumed to be debris, and also internal septa. On MRI the cysts were of low intensity, similar to that of muscle on, T_1-weighted images, and very intense on heavily T_2-weighted images, indicating a high water content. Ultrasound showed an abnormal meniscus in the two cases of lateral meniscus; and MRI demonstrated clearly the torn meniscus and its continuity with the cyst in all three cases. While it is possible to make the diagnosis using both imaging methods, MRI gave more useful and complete information than ultrasound.

Comparison of marrow and bone scintigraphy of vascular bone grafts for femoral head necrosis in 28 patients

I. Stewart, K. C. Ho, Y. K. Leung, P. C. Leung and C. Metreweli
Departments of Diagnostic Radiology and Organ Imaging, and Orthopaedics, Prince of Wales Hospital, Chinese University of Hong Kong, Shatin, New Territories, Hong Kong

We compared marrow with bone scintigraphy in 28 patients with femoral head avascular necrosis due to trauma or idiopathic causes. All had vascular bone grafts. The demonstration of vascular bone graft viability in the early post-operative period is bedevilled by intense tracer uptake in surrounding bone and soft tissues. Viable bone graft contains marrow while the femoral head and non-viable graft are avascular. Scintigraphy was performed pre-operatively in the majority and post-operatively in all. Marrow scintigraphy was performed using 370 MBq (10 mCi) tin colloid. Three-phase bone scintigraphy was performed using 555 MBq (15 mCi) diphosphonate. Differentiation of viable from non-viable graft in the post-operative bone scintigram was impossible. However, marrow scintigraphy frequently showed a viable graft despite the drawbacks of marrow scintigraphy such as deficient marrow, poor tracer uptake, high blood pool activity and orthopaedic ironmongery. Marrow scintigraphy is superior to bone scintigraphy in demonstrating viability of vascular bone grafts.

Bilateral wrist arthrography in patients with unilateral symptoms

C. S. Romaniuk, W. P. Butt and A. Coral
Department of Radiology, St James' University Hospital, Leeds LS9 7TF

Bilateral tricompartmental wrist arthrograms have been performed in 13 patients with unilateral symptoms to assess the incidence of abnormal findings in the symptomatic and asymptomatic wrist. The midcarpal, distal radio-ulnar and radiocarpal joints were injected separately with a mixture of ioxoglate 320 and lignocaine. Arthrography was normal in 5/13 symptomatic wrists. Abnormalities in the remaining eight included one partial and four complete tears of the triangular fibrocartilage complex (TFCC), two lunotriquetral ligament tears, two scapholunate tears and five other abnormal joint communications. One lunotriquetral ligament tear in a patient with probable inflammatory disease was not thought clinically significant. In 13 asymptomatic wrists there were 4 (31%) with abnormalities. There were two tears of the TFCC, 1 scapholunate tear, and 4 other abnormal joint communications. Absence of lignocaine-induced pain relief suggested extra-articular causes of symptoms in 3 wrists, 2 of which had arthrographic abnormalities. This study shows that triple-compartment wrist arthrography may demonstrate tears in asymptomatic wrists, and therefore care must be taken in interpreting any positive findings in a painful wrist.

Assessment of bone scintigraphy in the diagnosis of scaphoid fractures

C. J. Occleshaw, N. A. Barrington and J. Williams
Department of Diagnostic Radiology, Royal Hallamshire and Northern General Hospitals, Sheffield

Plain film radiography in the diagnosis of scaphoid fractures is known to be unsatisfactory, with a significant false-negative rate, even in experienced hands. Bone scintigraphy is used for this purpose in our centre on patients in whom fracture has been assessed clinically but not demonstrated on plain radiographs either at presentation or 10 days post-trauma. We have compared results of bone scintigraphy and plain radiography in 100 such cases retrospectively. Radiographs were reported "blind" by a consultant bone radiologist (N.A.B.) as were the scintigraphic images. In 25 patients, fractures were shown on scintigraphy which were not seen on radiography. Eight patients with at least one radiograph assessed as suspicious of, but not diagnostic of, fracture had the diagnosis refuted by scintigraphy. Follow-up radiography on some patients showed that most fractures diagnosed on scintigraphy did not become visible subsequently. The results show that bone scintigraphy adds diagnostically significant information in 33% of patients studied. These results, and comparisons with previous studies, are discussed, and examples of potential pitfalls in the interpretation of scintigraphic images are shown.

Sonographic assessment of medial collateral ligament injuries to the knee

W. W. Gibbon and H. Mamtora
Department of Diagnostic Radiology, Salford Royal Hospital, Salford, Manchester M60 9EP

High-resolution real-time diagnostic ultrasound has found increasing use in the evaluation of acute and chronic soft tissue injuries. Sonography is able to distinguish the deep and superficial static and dynamic medial supporting structures of the knee. We now present our findings in 17 patients with clinically suspected isolated medial stabilizer injuries (Grades I and II sprains) to the knee. In five patients there was sonographically demonstrable calcification in the region of the medial capsular attachment to the medial femoral condyle, *i.e.* Pellegrini–Steida type lesion. The high incidence of these lesions probably reflects the referral process for our study. We discuss the possible patho-physiological mechanism for such phenomena, based on our sonographic findings. We were able to localize the precise anatomical site and extent of collateral ligament ruptures and avulsions in seven cases. In the remaining five patients, ultrasound was able to diagnose a medial meniscal tear and osteoarthritic changes not fully appreciated on plain radiography and in a third patient, a loose body within the medial femoral recess previously misdiagnosed as a Pellegrini–Steida lesion on plain radiographs. The remaining two patients were sonographically normal except for mild joint effusions and may represent meniscal injuries, although the exact diagnosis is unclear. We conclude by discussing the clinical relevance of ultrasound in the management of knee injuries.

Radiological features during and following treatment of spinal tuberculosis

D. I. Boxer, *C. Pratt, A. L. Hine and *M. McNichol
*Departments of Radiology and *Thoracic Medicine, Central Middlesex Hospital, London NW10 7NS*

Following the advent of effective chemotherapy, the incidence and morbidity of spinal tuberculosis has improved dramatically. Response is measured with a combination of clinical and radiological features. We have reviewed 28 cases of vertebral tuberculosis to document the sequence of radiological changes following treatment. Bone destruction was demonstrated in 24 cases at presentation, being delayed in the remainder for up to 3 months. Destruction progressed whilst on treatment for an average of 6.5 months, progressive vertebral collapse continued for up to 14 months. Only three patients showed evidence of vertebral height recovery. Disc height was reduced in 20. Vertebral fusion occurred in 75% of these, the onset varying between 3 weeks and 27 months. A paraspinal soft-tissue mass was present in 75% of those with cervical or thoracic disease. The mass enlarged in most cases, for up to 5 months. Complete resolution took between 3 and 24 months. Osteosclerosis was present at onset in 13 cases and developed in a further 12, always within 5 months. Maximal sclerosis occurred at up to 14 months. Bone density returned to normal in 11 cases, taking up to 59 months. It is important for the radiologist to appreciate the varied radiological response to successful treatment of spinal tuberculosis.

Symptomatic dorsal defects of the patella

V. C. Pullicino, D. Kinsella, L. B. Williams and I. W. McCall
Department of Radiology, Robert Jones and Agnes Hunt Orthopaedic Hospital, Oswestry, Shropshire SY10 7AG

"Dorsal defect of the patella" involves the supero-lateral portion of the patella, is deemed incidental and of no clinical significance. The plain radiographic appearances are similar to the centrally located "osteochondritis dissecans" which needs further evaluation and treatment. Eighteen patients with a combination of anterior knee pain and a subarticular patellar defect have been prospectively studied utilizing plain radiography, double contrast arthrography, CT and scintigraphy. The clinical and radiological features in symptomatic dorsal defects of the patella are compared with those of osteochondritis dissecans. Double-contrast CT arthrography in 10 patients with dorsal defects of the patella revealed significant abnormalities in the overlying articular cartilage which were confirmed arthroscopically. These were scintigraphically active and associated with abnormal patellar tracking. Osteochondritis dissecans cases showed similar scintigraphic and CT arthrographic findings, with retention of the functional patello-femoral relationship. The results suggest that the dorsal defect should not be dismissed as an innocent finding in symptomatic cases, and requires further radiological investigation. The distinction drawn between the dorsal defect and osteochondritis dissecans of the patella is questioned and the aetiological role and therapeutic implications of patellar tracking abnormalities are discussed.

Is there a familial link in early disc failure?

B. S. Worthington, *A. D. North, *P. Wilde, R. W. Kerslake and *R. C. Mulholland
*Departments of Radiology and *Orthopaedic and Accident Surgery, University Hospital, Nottingham NG7 2UH*

Adolescent disc failure, whilst rare, is frequently associated with multiple-level disc abnormalities, suggesting an underlying diathesis. The present study investigates the possibility of a familial factor in early disc failure. MR scanning of the lumbar spine was carried out in the sagittal plane on 45 first-degree relatives of 15 patients with adolescent disc herniation. An assessment was made of the signal returned from the central part of each disc on the STIR sequence and allocated a score on a scale of 0–4 (0=normal signal, 4= complete loss of signal). The results were compared with those from the same number of age- and sex-matched controls. Comparison of the two groups of scores was made using the Mann–Whitney *U* test for non-parametric data. As expected the L4-5 and S-1 discs scored the highest, these being the commonest levels to undergo degeneration. The first-degree relatives of the patients had a level of disc degeneration which was significantly greater than that of the control group; this difference was more pronounced in the caudal discs. We conclude that in some individuals the predisposition to early disc failure may have a familial component.

CT and isotope bone scan appearances of the knee joint following replacement of the anterior cruciate ligament

D. I. Cooke, P. J. R. Robinson, S. J. O. Ostlere, G. K. Sefton, B. B. Seedhom and A. C. Swann
Department of Radiology, St James' University Hospital, Leeds LS9 7TF

This poster illustrates the appearance of the knee joint following the insertion of an open-weave polyester prosthetic ligament. The prosthesis replaces the native anterior cruciate ligament and extends from the medial tibial condyle to the lateral femoral condyle, running within a surgically constructed endosteal tunnel. The ligament is anchored at either end by a bone plug which fits inside the stocking-like ligament. The plug is, in fact, the core of bone produced by formation of the tunnel. Scans of the knee were obtained following injection of $^{99}Tc^{m}$-MDP. Five patients, all of whom had a successful surgical result, were studied post-operatively. The static isotope scan shows varying degrees of increased activity in the tibial plateau and femoral condyles. The activity mirrors the osteochondral junction around the articular margins of femur and tibia. It is not at present known what pathological process this represents. One patient had marked isotope uptake in the tibial canal. CT scanning shows marked bony bridging between the plug and canal. CT scans were obtained on all patients; they show well corticated endosteal tunnels with varying degrees of bridging between tunnel and plug.

Notes

MRI of the Knee (4.15–4.35)

MRI of the knee

C. W. Heron
Radiology Department, St George's Hospital, London SW17 0QT

MRI is firmly established as the technique of choice of the non-invasive evaluation of disorders of the knee. In places where MRI is widely available it has replaced arthrography and reduced the indications for diagnostic arthroscopy. Imaging may be performed using conventional T_1- and T_2-weighted pulse sequences but volume gradient echo techniques reduce examination times and improve resolution. MRI enables the accurate assessment of all degrees of meniscal degeneration. An area of high signal intensity extending to an articular margin indicates a tear, whereas intrameniscal high signal indicates degenerative change. The integrity of the cruciate and collateral ligaments may be assessed using MRI. A tear is diagnosed when there is failure to visualize the ligament on thin contiguous sections, or an area of high signal intensity fluid crosses the ligament on T_2-weighted images. In the investigation of disorders involving hyaline cartilage MRI accurately assesses both thickness and integrity. The complete spectrum of disorders of the knee may be investigated using MRI, but familiarity with normal variants is essential in order to avoid errors in interpretation. As a result of undergoing MRI some patients may be saved surgical intervention whereas others may be able to benefit earlier from operations which are indicated.

Notes

Paediatric Studies (4.35–5.15)

The role of radionuclides in renal imaging in children: a review

H. Carty
X-Ray Department, The Royal Liverpool Children's Hospital, Alder Hey, Liverpool L12 2AP

While there is now a general appreciation of the differing roles of static renal imaging and functional studies in adults, there is still uncertainty, particularly among paediatricians, as to the most appropriate radionuclide imaging study in children with renal problems. The indications for each study, its timing, its advantages and disadvantages, are reviewed in relation to the clinical problems of infection, obstruction, dilatation and trauma. The place of radionuclide cystography is discussed. The role of radionuclide imaging in the management of renal disease in childhood is presented in relation to other imaging techniques.

Dynamic CT in young children (chest and abdomen)

B. J. Cremin
Department of Radiology, Red Cross Children's Hospital, Rondebosch 7700, Cape Town, South Africa

Abstract not received.

Ripley Suite

Renal Studies (9.00–10.15)

Ultrasound in paediatric renal disease

R. de Bruyn
Department of Paediatric Radiology, Hospital for Sick Children, Great Ormond Street, London WC1N 3JH

The prenatal ultrasound diagnosis of congenital urological abnormalities is now well established, with an incidence of approximately 1500 pregnancies nationally. The role of prenatal ultrasound lies in identifying severely affected fetuses, and, perhaps more importantly, in identifying fetuses requiring further investigation postnatally which would otherwise pass undetected. Over an 8-year period 286 neonates with an antenatal diagnosis of hydronephrosis have been referred to the Hospital for Sick Children. The ultimate diagnosis has broadly fallen into six groups: pelvi-ureteric junction obstruction, mega-ureter, vesico-ureteric reflux, multicystic kidney, posterior valves and duplex systems. The ultrasound diagnosis is reviewed, together with current thinking and trends in postnatal management.

Ultrasound diagnosis of horseshoe kidney

B. Banerjee and I. Brett
Department of Diagnostic Radiology, Tameside General Hospital, Ashton-under-Lyne, Lancashire OL6 9RW

In recent years, ultrasound has replaced intravenous pyelogram (IVP) as the primary imaging method in several renal tract disorders. However, several congenital malformations of kidneys, including horseshoe kidney, which are readily diagnosed by IVP may evade detection by routine ultrasonic examination. Sonographic diagnosis of horseshoe kidneys depends on the demonstration of an isthmus of renal tissue situated in front of the great vessels in the upper abdomen connecting the lower poles of the kidneys. In a number of cases, the bridge of renal tissue may be replaced by a fibrous band which may not be demonstrated by ultrasound, or this tissue may be misdiagnosed as lymph nodes or pancreatic tissue. We report ultrasonic findings in a series of 11 patients with horseshoe kidneys, confirmed by IVP examinations. In seven patients isthmus of renal tissue was demonstrated by US but in all 11 cases, the renal outlines appeared "inverted triangular" or "inverted pyriform" in shape, instead of normal ovoid or reniform outline. Detection of "inverted triangular" or "inverted pyriform" shape of the kidneys should raise suspicion of horseshoe kidney. The mid-line of the upper abdomen should then be meticulously scanned for detection of isthmus of renal tissue. If negative, IVP should be carried out.

Contrast clearance: a new method for the measurement of glomerular filtration rate

S. C. W. Brown and P. H. O'Reilly
Department of Urology, Stepping Hill Hospital, Stockport, Cheshire SK2 7JE

The clearance of standard iodinated contrast media can be measured during contrast examinations using an X-ray fluorescence technique. We present an evaluation of this new, simple and potentially accurate method for the measurement of glomerular filtration rate (GFR). To test accuracy and reproducibility, repeat analysis of 12 standard iodine solutions was performed throughout the study period. Iohexol clearance was compared with inulin and Tc-DTPA clearances using both classical renal and single injection plasma clearance methods. An overall 2% variation in iodine concentration measurement was observed over the working range. The classical renal clearances of inulin and iohexol compared favourably (r=0.99; mean difference 2.6 ml/min). Single-injection contrast clearance correlated closely with single-injection ^{99}Tc^{m}-DTPA clearance (r=0.97: mean ratio 0.98), as did a single-sample single-injection method, the simplest for clinical purposes (r=0.94, mean ratio 1.02). Contrast clearance is a simple and accurate method for the determination of GFR. This may be performed alone or in conjunction with urography to make a truly functional examination.

The effect of hydration on the non-ionic intravenous pyelogram

D. C. F. Lloyd and A. J. Maxwell
Department of Diagnostic Radiology, University Hospital of South Manchester, Manchester M20 8LR

Sixty-one patients undergoing intravenous urography with non-ionic contrast medium (iohexol 350 mg/ml) were included in this prospective study designed to assess the effect of hydration on pelvicalyceal distension and pyelogram density. Patients were allocated randomly to one of two groups. The first group was instructed to take no fluids for 6 hours prior to the examination, the second group was given no instructions regarding fluid intake, and received 300 ml of water orally 5–10 min before the examination. Abdominal compression was not employed. The radiographs produced were assessed by an experienced observer (A.J.M.) who was unaware of the state of hydration. No significant difference in the degree of pelvicalyceal or ureteric distension was demonstrated between the two groups. However, the density of the pyelogram was significantly poorer in the hydrated than the fluid restricted group ($p \leq 0.005$). We conclude that when using non-ionic contrast medium prior fluid restriction remains an important part of the technique.

The most advantageous timing of external ureteric compression during intravenous urography

T. H. Hughes and A. Hine
Department of Radiology, Central Middlesex Hospital, Acton Lane, Park Royal, London NW10 7NS

The objective of this study was to ascertain the most advantageous timing during an intravenous urogram, to apply external ureteric compression, so as to gain the greatest calyceal distension. This was a prospective randomized trial of 60 patients, divided into three equal groups, having compression applied: immediately after injection, at 5 minutes and after the 5-minute film had been viewed. Patients with the usual exclusion criteria for compression were not included in the study. A statistically significant improvement in the calyceal distension occurred when the ureteric compression was applied at 5 minutes compared with compression applied after the 5-minute film had been viewed. No improvement in distension was seen when the compression was applied immediately after injection. We recommend that, except in patients with the usual exclusion criteria, external ureteric compression should be applied immediately after the 5-minute film has been taken to achieve optimal calyceal distension.

The intravenous urogram: an appropriate use of resources?

J. A. Clarke and J. E. Adams
Department of Diagnostic Radiology, Manchester Royal Infirmary and University of Manchester, Manchester M13 9PT

The demand for radiological services continues to increase and critical analysis of current radiological practice is necessary to ensure that limited resources are used effectively. This study was designed to investigate the use of intravenous urography (IVU) in a large teaching hospital. The request cards of 643 IVUs performed during a 6-month period were reviewed retrospectively. Details concerning (a) the source of referral, (b) clinical indication for IVU and (c) presence of a significant abnormality on the IVU were abstracted. Note was also made of the number of chest radiographs requested with the IVU, and any abnormality demonstrated. Relevant abnormalities were demonstrated in 16.5% of the IVUs analysed. An IVU is essential in the investigation of haematuria, loin pain and known urothelial tumours. Its use is not always appropriate in other conditions including prostatism, urinary tract infections, testicular complaints and non-specific abdominal pain. It was estimated that at least 54% of IVUs were probably unnecessary. If more appropriate use of the IVU could be established by implementation of guidelines drawn up in conjunction with clinical colleagues, savings of £32 000 per annum could be achieved. However, as alternative investigations (ultrasound, radionuclide renogram, etc) may be required, not all these savings would be realized. Chest radiographs were requested and performed in 30% of the patients, but a significant abnormality was present in less than 1%. An additional saving of £2000 could be made if the practice of performing "routine" chest radiographs with IVUs was abandoned. With more selective and appropriate use of IVUs, not only could financial savings be made, but exposure of patients to potential reactions to IV contrast medium and unnecessary ionizing radiation could be reduced.

The role of MRI in the early post transplant kidney

G. M. Baxter, G. McCreath, P. Morley, E. McGregor and M. Akyol
Department of Radiology, Southern General Hospital, Glasgow G51 and Department of Renal Medicine, Western Infirmary, Glasgow G11

The search for an accurate imaging modality to diagnose renal allograft rejection has intensified in recent years. In view of this we report on a recent prospective study of 20 patients (25 cases) assessing the role of MRI in the diagnosis of acute rejection. All patients included in this study were within 3 months of transplantation and had either primary non-function or secondary dysfunction. Obstruction and urinary tract infection had been previously excluded. Twenty-five ultrasonic scans, 20 of them with Doppler, were also performed, and these results compared with the MRI findings. MRI examination was carried out using a 0.15 Tesla resistive magnet. Both TE40 (T_1-weighted) and TE80 (T_2-weighted) sequences were performed. The diagnosis of acute renal allograft rejection was based on loss of corticomedullary differentiation and/or poor vascular supply. The final diagnoses, which included acute rejection, ATN and cyclosporin toxicity, were based on a combination of clinical review, cyclosporin levels and histology. Both MRI and ultrasound correctly identified the diagnosis in 70% of cases, but preliminary results suggest Doppler US may be superior to either.

A comparison of renography and IVU for urological assessment of spinal cord injury patients

S. G. Cooke, *W. El Masri, †M. Haddaway, V. C. Pullicino and I. W. McCall

*Departments of Radiology, †Physics and *Orthopaedics, Robert Jones and Agnes Hunt Orthopaedic Hospital, Oswestry, Shropshire SY10 7AG*

Genito-urinary complications are the principal cause of morbidity in spinal cord injury patients. Prevention of these complications with preservation of renal function is a fundamental goal of management. This requires repeated patient assessment, conventionally using urography to image the renal tract. We have compared the results of IVU and radionuclide renography in the assessment of 33 patients with spinal cord injury. After initial assessment by both methods, cases were followed up for up to 6 years by conventional means. The upper renal tracts were shown by both methods to be normal in 18 and abnormal in eight patients. Important abnormalities (calculi and diverticula) were diagnosed by IVU only in six cases. Seven patients had abnormal renography but normal IVU, three of whom subsequently developed abnormalities. No subsequent abnormality developed following normal renogram and IVU. We conclude that renography combined with kidney, ureter and bladder offers a suitable interim method for the assessment of spinal cord injury patients after initial IVU. This has the advantage of lower cost and radiation burden.

Magnetic resonance imaging of renal masses

J. E. Kabala, J. B. Penry and D. Chadwick

Department of Radiodiagnosis, Southmead Hospital, Bristol BS10 5NB

Investigation of renal masses with magnetic resonance imaging (MRI) is being studied. Thirteen cases have been examined to date: two hamartomas, one transitional cell carcinoma, one renal vein thrombosis and nine renal cell carcinomas. MRI (coronal: TR 860 ms, TE 26 ms; transverse: TR 860 ms, TE 26 ms and TR 1900 ms, TE 30 ms, T_1 100 ms) accurately demonstrates the inferior vena cava (IVC) in all cases, delineating the full extent of thrombus and/or tumour invasion. In patients with renal cell carcinoma, CT suggested IVC invasion in four cases. MRI confirmed this in three (with more acute delineation); in the fourth MRI showed the IVC to be compressed but patent. MRI demonstrated invasion beyond perinephric fat in five cases; in one MRI and CT appear to have overstaged the disease compared with surgery. In one other, involvement of multiple vertebral bodies was not demonstrated on CT. In four patients MRI, in agreement with surgery, showed no invasion beyond perinephric fat. In one CT had suggested possible hepatic invasion. In conclusion, MRI accurately stages renal cell carcinoma, especially with respect to vascular and bone involvement. It is at least as accurate as CT for assessment of local invasion, rendering CT unnecessary where MRI is available.

^{99}Tc^{m}-MAG3 compared to conventional radiological investigation in paediatric renal tract disease

F. E. Pickworth and G. C. Vivian

Department of Nuclear Medicine, Derriford Hospital, Plymouth PL6 8DH

Our experience of ^{99}Tc^{m}-mercapto-acetyl-triglycine (^{99}Tc^{m}-MAG3), a new Hippuran substitute for renography and indirect micturating cystography (iMCUG), in the investigation of 75 infants and children with renal tract disease is reported. A retrospective analysis of clinical details and radiological investigations was made, comparing ^{99}Tc^{m}-MAG3 results with those of other investigations. Sixty-one patients had ultrasonic scanning, 31 conventional MCUG, 30 intravenous urograms (IVU) and 27 ^{99}Tc^{m}-DMSA scans. Referrals were for: investigation of urinary tract infections (UTI) (39); surgical assessment (17); investigation for antenatally diagnosed renal tract disease (11); multiple congenital defects (4); screening asymptomatic patients (2); and loin pain (2). Twelve patients had concurrent ^{99}Tc^{m}-DMSA scans with 6 scarred kidneys, four of which were identified on ^{99}Tc^{m}-MAG3 parenchymal images, and in two differential renal function was reduced by more than 10%. The latter two criteria, when taken together with reflux as demonstrated by iMCUG, gave a sensitivity for renal scarring in the UTI group of 92% and specificity 85%, compared to 50% and 86% respectively for ultrasound alone. All significant lesions identified by ultrasound and IVU in all groups were also identified by ^{99}Tc^{m}-MAG3. ^{99}Tc^{m}-MAG3 gave more information than any other single imaging modality, is safe and sensitive for the investigation of childhood renal tract disease and may reduce the need for other investigations with higher radiation doses.

Bramham Suite

Radiotherapy Papers (10.45–12.00)

Intraluminal brachytherapy in bronchial carcinoma

R. Stout, P. V. Barber, P. A. Burt, B. R. O'Driscoll and M. Notley
Departments of Radiotherapy and Thoracic Medicine, The Christie Hospital and Holt Radium Institute, and Wythenshawe Hospital, Withington, Manchester M20 9BX

External beam radiotherapy is the established treatment for the relief of respiratory symptoms in patients with inoperable non-small-cell bronchial carcinoma. Although beneficial, it usually produces a temporary oesophagitis and permanent lung fibrosis. Endobronchial brachytherapy is attractive because it can spare the surrounding normal tissues from the early and late effects of radiation. It has never gained widespread acceptance because of the significant complications associated with interstitial implantation and the long treatment times and radiation protection problems inherent in low-dose-rate intraluminal therapy. The development of high-dose-rate remote afterloading equipment using a miniature high-activity source has now solved the problems of endobronchial irradiation. Treatment is given to patients admitted for the day, using fibreoptic bronchoscopy under local anesthesia to identify the tumour and position the intraluminal applicator. A miniature (1.1 mm diameter) 10 Ci iridium source is remotely despatched along the applicator using the high-dose-rate Micro Selectron. 15 Gy is prescribed at 10 mm from the source and treatment delivered in 10–20 min. Our pilot study of 150 patients has demonstrated that durable palliation can be achieved when intraluminal irradiation is used alone as the primary treatment. Cough improved in almost 60%, breathlessness in 70% and haemoptysis in 90%. Re-expansion of pulmonary collapse was obtained in almost 50%. No significant morbidity was observed. Intraluminal radiotherapy is now a simple, safe and effective palliative for selected patients with inoperable lung cancer, achieving results comparable to conventional X-ray therapy with less morbidity.

Pelvic insufflation: a method of displacing small bowel during radiotherapy to the pelvis

A. C. Hindley and P. H. Cole
Department of Radiotherapy, Northampton General Hospital, Northampton

Failure to cure common gynaecological and urological malignancies is frequently due to recurrence confined to the pelvis. Increasing the dose of conventional radiotherapy leads to a greater incidence of small bowel damage. We have attempted to overcome this by introducing gas into the peritoneal cavity to displace small bowel from the pelvic radiation field immediately prior to radiotherapy in five patients with advanced cervical carcinoma. Three litres of nitrous oxide is introduced into the pelvis over 3 min via an implanted Tenckhoff cannula, with the patient tilted head down to force the gas to rise into the pelvis, displacing the bowel downwards. Conventional radiotherapy is given with the patient on a 15° polystyrene slope to maintain displacement. Deflation occurs over 60–90 minutes. Displacement of the bowel is assessed by weekly simulator films with barium. Reproducible displacement of the small bowel was achieved with minimal discomfort during the procedure. Acute radiation reactions were mild. Only 10 min of additional staff time was required per day, with no increase in setting-up time. Dosimetry is discussed.

Use of an electron beam for post-mastectomy radiotherapy: 5-year follow-up of 500 cases

B. J. Magee, G. G. Ribeiro and R. Swindell
Department of Radiotherapy, The Christie Hospital and Holt Radium Institute, Withington, Manchester M20 9BX

From 1982 onwards, the standard method of regional radiotherapy post-mastectomy at this institute has used a single electron field of fixed energy (8 MeV) to irradiate the chest wall, matched to a single megavoltage field (4 or 8 MV) irradiating the nodal areas in the axilla and supraclavicular fossa. (A separate parasternal field was *not* used). All 500 cases treated in 1982 and 1983 with this method were reviewed (median follow-up 59 months), 422 referred directly post-mastectomy and 78 for local recurrence after previous mastectomy. Of these, 42 were treated palliatively, and 458 with radical intent. In radical cases the given dose in both fields was 40 Gy in 15 fractions in 3 weeks. At 5 years the overall survival (n=458) was 51% and the local recurrence rates by site and UICC stage were as follows: chest wall: all 18%, Stage I 4%, Stage II 13%, Stage III 26%, recurrent cases 21%; axillary recurrences: all 20%, Stage I 4%, Stage II 10%, Stage III 22%, recurrent cases 39%; supraclavicular recurrences: all 9%. Only one patient of the 500 treated had a parasternal recurrence. Late effects included telangiectasia in the electron field and asymptomatic apical lung fibrosis in the photon field. There was no match line fibrosis.

Strategy for the use of highly focussed ultrasound for the non-invasive destruction of deep seated tumours *in vivo*

G. R. ter Haar, I. Rivens, R. L. Clarke and C. R. Hill
Department of Physics, Institute of Cancer Research, The Royal Marsden Hospital, Sutton SM2 5PT

Highly focussed beams of ultrasound of sufficiently high intensity may be used for the selective destruction of tissue volumes at depth in tissue, without damage to overlying regions (ter Haar et al, 1989). We are investigating this technique for the non-invasive treatment of discrete liver and bladder tumours. A system has been designed and built that enables the focus of an ultrasonic beam to be moved around any given point in tissue in a controlled fashion, and thus to destroy a predetermined tissue volume. This system has been successfully tested both in pig's liver *in vitro* and in pig thigh muscle *in vivo*. In pig's thigh, a cube of tissue 2 cm x 3 cm x 1 cm lying 7 cm below the skin surface was successfully destroyed. Simultaneous diagnostic ultrasound imaging allows visualization of the damaged tissue volume in real-time. Tissue volumes that are ellipsoid in shape (1.5 cm x 5 mm) are damaged at each focal position of the beam. The strategy for damaging larger tissue volumes will be discussed in terms of exposure times (commonly 1–20 s), proximity of adjacent lesions and the planning of the positions in which successive lesions should be placed, since the presence of a lesion may alter the tissue acoustic properties and thus the exposure conditions for adjacent lesions.

Reference

TER HAAR, G. R., SINNET, D., RIVENS, I., 1989. High intensity focused ultrasound — a surgical technique for the treatment of discrete liver tumours. *Physics in Medicine and Biology, 34,* 1743–1750.

Radiotherapy for cerebral oligodendroglioma in adults: an analysis of 98 cases and the dose-reponse relationship

J. Lim and M. L. Sutton
Department of Radiotherapy, Christie Hospital and Holt Radium Institute, Manchester M20 9BX

Ninety-eight adults aged 16–69 years received megavoltage cranial irradiation for oligodendroglioma at the Christie Hospital between 1965–88. The influence of radiotherapy on local control and survival, and the dose-response relationship, were analysed. Patient characteristics (age, sex, condition, mode and duration of presentation), site of disease, surgical technique, duration of delay to radiotherapy, and irradiation technique were examined for prognostic significance. The fractionation schedule employed and the Karnofsky Performance (KP) score before starting radiotherapy were the only factors which influenced outcome. After a median follow-up of 48 months, the best results were obtained in a group of 38 patients with a KP score of 80 and over who received 37.5–42.5 Gy in 16–18 fractions: in this group, 68% survived 5 years and 33% survived 10 years. The results obtained for the whole group were 39% at 5 years and 19% at 10 years. The median time to recurrence after radiotherapy was 44 months and all patients whose disease recurred died within 38 months. The literature was reviewed and comparisons with our results are discussed. We conclude that optimally fractionated radiotherapy to brain tolerance is beneficial as it improved the overall and relapse-free survival.

Visual loss in the irradiated eye — an incidence study of 42 cases

S. F. Leung and S. Y. Ts'ao
Department of Clinical Radiology, Prince of Wales Hospital, Shatin, Hong Kong

Forty-two patients with locally-advanced nasopharyngeal carcinoma were treated with a radiotherapy plan which involved sacrificing one of the eyes. The globe, the optic nerve and part of the lacrimal gland were included in the high dose zone. The dose–fractionation was either 60 Gy/26 fractions/6 weeks or 66 Gy/33 fractions/6.5 weeks. The actuarial risks of severe visual loss in the irradiation eye at 1 year, 2 years and 3 years after radiotherapy were 4%, 15% and 30%, respectively.

Langerhans cell histiocytosis (LCH): its morbidity and mortality

D. Gilligan, A. C. Robinson, H. R. Gattamaneni and P. Morris Jones
Department of Paediatric Oncology, Christie Hospital and Holt Radium Institute, Withington, Manchester M20 9BX

The morbidity resulting from LCH and its treatment is poorly defined. We evaluated outcome in 59 patients treated at the Christie Hospital and Royal Manchester Children's Hospital between 1944 and 1987. Median follow-up was 76 months. Sixty-nine bone lesions were irradiated in 48 patients and 67 responded. Hypothalamic pituitary axis irradiation did not reverse diabetes insipidus (DI) in the four patients treated. In 7/9 cases treated, extraskeletal lesions responded to local irradiation. There was no relation between dose and outcome. Cytotoxics were successful in arresting extraskeletal pathology in 10/23 patients. Five patients have residual skeletal deformity, two had received irradiation. All 12 patients with DI require DDAVP and one has growth hormone deficiency. Persistent oral LCH has resulted in dental morbidity in one child; another has recurrent soft tissue disease in the infratemporal area. Both had irradiation. No patients with skeletal pathology alone died; 10 with extraskeletal manifestations succumbed to progressive disease, and there was one intercurrent death. Overall 5-year survival is 80%. Three patients have had successful pregnancies. No second malignancies have occurred. We conclude: (1) major soft-tissue/skeletal defects are uncommon in long term survivors; (2) regular endocrine assessment is required; (3) optimal management of extraskeletal LCH needs defining.

Notes

Ripley Suite

Liver and Abdominal Studies (2.30–3.45)

Liver transplantation: the role of ultrasound

J. Karani
Department of Radiology, King's College Hospital, London SE5 9RS

Orthotopic liver transplantation is now an accepted treatment for end-stage liver cell failure. The combined programme in King's College Hospital and Addenbrooke's Hospital, Cambridge has now carried out 600 transplants. Radiology has played a crucial part in the development of the programme, and in the improved survival rate achieved, through its role in judicious patient selection, and also in early detection and treatment of complications following liver grafting. Ultrasound is important in assessment of complications related to the biliary tract and peri-hepatic collections. The operation requires a series of complex vascular anastomoses. Early occlusion of these, particularly of the hepatic artery, may have catastrophic clinical consequences, with graft infarction necessitating re-transplantation. If occurring late, graft sepsis and biliary leaks or strictures may be the clinical sequelae. Doppler ultrasound therefore plays an important role in evaluation of continuing vascular flow. To date, results of ultrasound in the diagnosis of rejection are disappointing. The role of ultrasound will be fully explored, indicating how it is integrated into the overall radiological treatment of liver transplantation.

A prospective study of colour Doppler ultrasound and isotope imaging in the detection of early renal transplant rejection.

B. J. G. Dall, G. J. Gillen, B. J. R. Junor, J. D. Briggs, C. Muir and P. Morley
Departments of Radiology, Nuclear Medicine and Renal Medicine, Western Infirmary, Glasgow G11 6NT

A prospective study of 46 renal transplant recipients (211 examinations) comparing colour Doppler ultrasound and isotope imaging in the diagnosis of acute transplant rejection was performed over a 5-month period. All patients had both examinations within two days of transplantation and further examinations as dictated by the clinical course. In 19 patients who had serial scans, 12 episodes of acute rejection were identified by definite histological changes on biopsy. Of these 12, 10 were identified as abnormal by a pulsatility index (ratio of peak systolic flow minus minimum diastolic flow divided by mean flow) greater than 1.5 and seven out of 12 were identified by isotope imaging. Four of the five false-negative isotope studies were probably related to the absence of a satisfactory baseline study. Doppler examination appeared to be particularly useful in the early post-transplant period when the kidney is poorly perfused, leading to difficulties in interpreting the isotope results. In conclusion, Doppler examination and isotope imaging are valuable and complementary techniques for the detection of early complications following renal transplantation.

Cholangiography in liver transplantation

P. Holland and E. Morris
Department of Diagnostic Imaging, Queen Elizabeth Hospital, Edgbaston, Birmingham

Cholangiography is an important part of the post-operative assessment of patients who have undergone liver transplantation. In our centre, more than 315 liver transplants have been performed since 1982. We have reviewed over 250 of these patients, assessing the T-tube cholangiograms, percutaneous transhepatic cholangiograms and endoscopic retrograde cholangiograms. The normal appearances of the various biliary reconstructive procedures are demonstrated. Some 30% had no biliary tract evaluation because they died soon after the operation. In the remainder, more than 550 cholangiograms were reviewed, together with any biliary interventional procedures undertaken. The commonest complications were biliary leakage (17.5%) and stricture formation with or without significant obstruction (10.5%). In many cases, the two complications were related. T-tube migration occurred in 2.7%. Other complications, including sludge and stone formation, accounted for 3%. Biliary interventional procedures were performed in a number of patients, including balloon dilatation of strictures, biliary drainage, debris removal using a balloon catheter and stent insertion. The relationship between biliary tract changes seen at cholangiography following transplantation and other post-operative complications, particularly hepatic artery occlusion, rejection and abscess formation, is discussed.

Hepatic vein Doppler in the diagnosis of acute liver transplant rejection

R. A. Coulden, P. D. Britton, *G. Noble-Jamieson and P. Farman
*Departments of Radiology and *Paediatrics,*
Addenbrooke's Hospital, Cambridge CB2 2QQ

Doppler examination of the hepatic artery and portal vein following liver transplantation is widely described. Although of great value in the diagnosis of acute vascular complications, it has played no part in the detection of rejection. In the normal liver, Doppler ultrasound of the hepatic veins gives a pulsatile waveform. There is anecdotal evidence that this pulsatility is lost in liver disease. We have explored the use of this observation in the assessment of acute liver transplant rejection. Thirty-seven liver transplants in 31 patients (aged 1–20 years) were studied for up to four weeks after transplantation. Routine ultrasound and Doppler examinations of the transplanted liver and hepatic vessels were performed within the first 48 hours and then at 2–3 day intervals. There were 23 biopsy-proved rejection episodes. Eighteen of these were correctly diagnosed before biopsy by a reduction in hepatic vein pulsatility. The five missed periods of rejection occurred in patients in whom the waveform was already severely damped by peri-operative ischaemia or preservation injury. There were no cases of proved rejection with normal hepatic vein Doppler traces. Most importantly, the changes in pulsatility may precede clinical or biochemical evidence of rejection by up to 36 hours. The earlier diagnosis of rejection enables treatment to be started sooner, improving the possibility of graft survival.

More complications of intra-arterial hepatic perfusion catheters: the radiological appearances of perfusion catheters which migrated outside the hepatic artery

F. Regan and T. Tran
Department of Radiology, St Mary's Hospital, London W2 1NY

Direct infusion of chemotherapeutic agents into the hepatic arterial system has become a popular method of treatment of unresectable liver metastatic disease. The method involves placing a cannula at open operation with its tip within the hepatic artery and its end connected to a subcutaneous porte (Porte Cath TM) through which direct injection of cytotoxic agents can be made. This method has become an effective alternative to systemic chemotherapy as it has a lower incidence of systemic side effects than other routes of administration, and better patient compliance. However, it is not without side effects, both local and systemic, some of which are potentially life-threatening. Side effects already described include a chemically induced hepatitis, gastric and duodenal mucosal damage, small bowel perforations and biliary strictures. Factors postulated in the development of these complications include ischaemia induced at the initial operation to place the catheter, a chemical arteriolitis, and direct mucosal irritation by the catheter. We present three cases of catheter migration out of the artery into surrounding structures, caused presumably by a combination of the above factors. We present the radiological appearances of these complications, including CT and ultrasound, and show the importance of radiology in diagnosing these complications.

Know your physics and avoid a pitfall

P. Ignotus, F. A. Sandrasagra, E. J. Adam and A. E. A. Joseph
Department of Diagnostic Radiology, St George's Hospital, London SW17 0QT

Posterior echo enhancement is rightly considered to be a reliable indicator of a fluid-filled lesion. This is because the fluid attenuates the ultrasound beam much less than the surrounding tissue, so echoes deep to this fluid-filled lesion are enhanced. This appearance may also be observed when two areas of soft tissue of markedly different attenuation values lie side by side. Fatty liver attenuates the liver more than normal liver or soft tissue; therefore a metastasis within fatty liver will show posterior echo enhancement compared to the neighbouring tissue. We show examples of these phenomena, together with similar appearances produced by intra-hepatic abscesses. We discuss practical ways of recognizing this and differentiating the two, and demonstrate that an understanding of physics helps in the interpretation of images and in avoiding pitfalls.

Notes

Perfluorooctylbromide (PFOB) as a contrast agent for liver and spleen enhancement in computed tomography

D. O'Connell, M. Behan, D. Carney and R. Mattrey
Department of Radiology, Mater Misericordiae Hospital, Dublin 7

Perfluorooctylbromide (PFOB) 100% emulsion is a radio-opaque fluorocarbon which is taken up by the liver and spleen when given intravenously. A trial of PFOB was carried out on 18 patients with malignancy and distal metastases, using doses ranging from 0.5 g/kg to 3.0 g/kg. Enhancement of liver up to 29 HU, spleen up to 318 HU and blood pool up to 55 HU was achieved, using 96 kV. Except for rim enhancement in two cases, there was no detectable enhancement of primary or metastatic tumours. PFOB increased the visibility of liver metastases and revealed smaller metastases less than 1 cm in diameter not visible prior to contrast injection. Scans taken at 24 hours after contrast medium showed improved definition of metastases but because enhancement of veins was absent, interpretation was more difficult. A rapid fall in blood pool enhancement was attributed to strong splenic sequestration of emulsion following infusion of contrast. PFOB is a significant improvement on existing contrast media, because it gives more prolonged blood pool enhancement, and is selectively taken up by the liver and spleen.

The recognition of abdominal scars at computed tomography

J. M. Somers, M. Deal, *S. G. Pollard and A. K. Dixon
*Departments of Radiology and *Surgery, Addenbrooke's Hospital and University of Cambridge, Cambridge CB2 2QQ*

Accurate knowledge about previous surgical procedures is of paramount importance when reporting computed tomographic (CT) studies of the abdomen. Sadly, the referring clinician does not always provide this information along with the clinical details. It might be argued that careful scrutiny of the images should reveal scars in the anterior abdominal wall and other effects of surgery. To test this hypothesis, we have studied 50 consecutive patients undergoing CT of the abdomen and pelvis. The radiologist performing the CT study examined the patient's abdomen for scars and established the nature of any previous surgery by discussion with the patient. A second radiologist, who was unaware of the patient's clinical details, reviewed the CT images at the console and predicted whether there had been any previous surgery. These predictions proved inaccurate; only 60% of scars were recognized. Although the absence of major organs was reliably reported, even large paramedian scars were missed. Most of the Pfannenstiel's incisions were missed, despite recognition of an absent uterus. Old scars were missed more frequently than recent scars. The results re-emphasize that accurate clinical details, including those of previous surgery, are necessary when interpreting abdominal CT.

Percutaneous gastrostomy in children

S. Peterson and D. J. West
Department of Radiology, City General Hospital, Newcastle under Lyme ST4 6QG

Percutaneous gastrostomy is now an accepted alternative to surgical gastrostomy. Our experience with percutaneous gastrostomy in adults, in whom we found it a simple, effective, safe and well tolerated procedure, led us to explore its value in children with various nutritional problems. We have used the technique now on six children, five with cystic fibrosis and one with presumed Behçets disease. All procedures were performed under local anaesthesia and intravenous sedation. The day before, a cup of barium was given to outline the colon. Buscopan 20 mg IV was given to paralyse the stomach. The stomach was inflated with air either via an endoscope or NG tube. The stomach was fixed to the anterior abdominal wall using one T-fastener. Direct puncture of the anterior gastric wall with a Seldinger needle was followed by guide-wire insertion and dilatation to accept a thin-wall catheter, *e.g.* Freka, which was left in the stomach or directed into the proximal jejunum. The procedure has been well tolerated by all the children and there have been no complications. Dramatic improvements on the centile weight charts have been recorded. We conclude that percutaneous gastrostomy is a safe technique which can significantly improve nutrition in children with GI disorders like cystic fibrosis.

Abdominal CT scanning in AIDS

P. C. Rowlands, M. McCarty and K. P. Gill
Department of Radiology, St Mary's Hospital, London W2 1NY

Abdominal CT scans were carried out in 35 patients with AIDS. Twenty scans (57%) were abnormal. Several patterns of abnormality were noted. *Mesenteric/para-aortic lymphadenopathy:* this was usually a result of lymphoma or atypical mycobacterial infection; occasionally the appearance results from Kaposi's sarcoma; *focal liver lesions*: these were again a result of mycobacterial infection or lymphoma; *biliary abnormalities*, owing to cryptosporidial infiltration. Ultrasound examinations and biopsies were performed in the majority of patients. Correlation with CT findings is presented.

Vascular Ultrasound Studies (4.15–5.30)

Colour flow imaging principles

G. Thirsk
ATL UK Limited, Arden Press House, Letchworth SG6 1LH

The visualization of blood flow using colour flow imaging systems may provide useful diagnostic information that cannot be acquired as easily by other techniques. However, in order to make best use of this diagnostic information, it is necessary to consider the fundamental principles of the technique and its limitations. Colour flow imaging systems utilize a pulsed Doppler technique to determine the velocity of flow, and are therefore subject to the same limitations. Pulse pair co-variance estimation is used to analyse the Doppler signal, rather than the slower FFT analysis, because of the large number of velocity determinations required in the construction of a colour flow image. This method, which estimates instantaneous mean velocity, variance of the mean and the direction of flow, introduces additional limitations. Shades of red and blue are used to code for the flow direction towards or away from the transducer, respectively. Increasing velocities are coded as increasing intensity of colour and the variance of the mean velocity estimate, which represents flow disturbance, is coded by mixing green into the colour spectrum.

Colour Doppler evaluation of prosthetic cardiac valve function after exercise

C. J. Occleshaw, S. Tennant, A. Hampshaw and D. R. Naik
Department of Radiology, Northern General Hospital, Sheffield S5 7AU

Early prosthetic valve dysfunction can be diagnosed by Doppler echocardiography. The sensitivity of this technique is increased by performing studies after exercise, yet there are few studies assessing the residual gradients across normal prosthetic valves in this situation. In a prospective study we have carried out colour Doppler examinations in the post-operative period on patients undergoing valve replacement. A variety of aortic and mitral prostheses were studied, both before and after exercise. Eighty-six valves were studied in all, and the examination technique is described. Residual gradients vary with the type of valve used and figures for various types of prosthesis are presented. One previous study has found significant increases in pressure gradients across mitral prosthetic valves with exercise but we have found no significant change in residual gradient or peak flow velocity for any one of the types of prosthesis studied, in either aortic or mitral position. Any significant observed increase in these values on exercise almost certainly represents true dysfunction of the prosthesis.

Notes

Progress of treated deep venous thromboses: evaluation with colour Doppler ultrasound

G. M. Baxter, P. Duffy and S. MacKechnie
Department of Radiology, Western Infirmary, Glasgow G11

Colour Doppler ultrasound has recently been shown to be an accurate imaging modality in the diagnosis of lower-limb venous occlusive disease. Being a safe and non-invasive technique it affords the potential advantage of monitoring patient response to treatment. Twenty-five patients with lower-limb venous thrombosis, diagnosed both on venography and colour Doppler examination, were re-scanned at intervals of 1, 3, and 6 months. Flow characteristics both spontaneous and augmented with distal compression, were observed. Intraluminal echogenicity, partial recanalisation of thrombus, vein distensibility and collateral circulation were also assessed. The relationship of these findings to the treatment time was noted. Post-phlebitic changes, which are discussed, appeared to persist in the vast majority of cases. Awareness of these changes may help avoid misdiagnosing chronic post-phlebitic change as acute deep venous thrombosis.

Dextricity and carotid plaque lesion

P. C. Njemanze, *W. M. McKinney, *W. G. Ferrell, *G. Evans and *C. Taylor
*Non-Invasive Flow Laboratory, Chidicon Medical Center, PO Box 302 Owerri, Imo State, Nigeria and *Department of Neurology, Department of Health Sciences, Bowman Gray School of Medicine, Winston-Salem, 27103 NC, USA*

The relationship of handedness to the size and spread of carotid plaque lesions was evaluated using B-mode real-time ultrasound studies in 80 patients. Eight were left-handed and 72 were right-handed. Most left-handers (75%) had more carotid plaque lesion in the left carotid arteries, most right-handers (75%) in the right. The odds of having more plaque on the side ipsilateral to handedness were more than nine times greater than the odds of having more plaque lesion on the opposite side ($p=0.001$); after controlling for age, sex, race, hypertension and smoking. The results are discussed with reference to changes in cerebral blood flow.

Duplex scanning and non-invasive impedance analysis to detect the "at-risk" femoro-distal graft

A. M. Jones, M. G. Wyatt, G. Hartnell and M. Horrocks
Department of Radiodiagnosis and Vascular Studies Unit, Bristol Royal Infirmary, Bristol BS2 8HW

Computer-assisted impedance analysis is a new technique, which may help identify "at-risk" femoro-distal grafts prior to failure. Pulsatile pressure and flow within the graft are determined non-invasively. Transfer analysis is performed on the paired pressure/flow signals and an impedance score derived. Fifty patients with functioning, non-reversed femoro-distal vein grafts were studied. Each graft was assessed using duplex scanning, impedance analysis and intra-arterial digital subtraction arteriography. Grafts were defined as "at-risk" (22) or control (28), dependent upon arteriographic evidence of graft or run-off stenoses over 50%. Duplex scanning successfully predicted all seven proximal/mid-graft stenoses, but only four of 16 distal graft/run-off lesions. Impedance scores were significantly increased in the "at-risk" grafts (0.58 + [0.43–0.72]*), when compared with the control grafts (0.34 + [0.30–0.38]*). An impedance score of over 0.45 was able to predict stenoses over 50% with a sensitivity, specificity and predictive value of 87%, 96% and 93% respectively. Duplex scanning is an excellent technique for the detection of proximal/mid-graft stenoses. When the stenosis is at, or below, the level of the knee, impedance studies have the advantage. These results are reproducible and show that the non-invasive measurement of limb impedance has a role in the detection of "at-risk" femoro-distal grafts.

*Means + 95% confidence intervals, $p<0.001$ Mann–Whitney *U* test

The value of combined venography: comparison with contrast venography

B. Caner, M. Özmen, A. Dincer, O. Kapucu, S. Naldoken, G. Erbengi and C. F. Bekdik
Radiology and Nuclear Medicine Departments, Hacettepe University, School of Medicine, Ankara 06100, Turkey

This study was performed to validate the combined study of flow radionuclide venography (FRV) with subsequent $^{99}\text{Tc}^{\text{m}}$ RBC blood pool venography (BRV) for the detection of deep vein thrombosis (DVT). FRV was performed by using three separate doses of large $^{99}\text{Tc}^{\text{m}}$04- bolus (6–10 ml) injection. Findings of 32 patients with suspected DVT of lower extremities ($n = 52$) were compared with those of corresponding contrast venography (CV) serving as a reference method. Our findings were as follows:

	CV and FRV		CV and BRV		CV and FRV + BRV	
Vein	Agree	Disagree	Agree	Disagree	Agree	Disagree
Iliac	98%	2%	98%	2%	98%	2%
Femoral	96%	4%	71%	29%	96%	4%
Calf	67%	33%	60%	40%	73%	27%

In 7.6% extremities, collaterals not demonstrated by CV were seen by only FRV. Although radionuclides were injected into a relatively large volume, all the calf veins could not be filled even when they were completely patent. Conclusions: (1) although a combined study of FRV with BRV improved the diagnostic value of radionuclide venography for the detection of DVT in calf veins, CV is a mainstay in this region unless it is contraindicated, and (2) CV can be replaced by FRV without combination with BRV for the detection of DVT in femoral and iliac veins.

Notes

The use of duplex derived hyperaemic flow to detect femoro-distal graft related stenoses

J. E. Kabala, M. G. Wyatt, G. Hartnell and M. Horrocks
Department of Radiodiagnosis and Vascular Studies Unit, Bristol Royal Infirmary, Bristol BS2 8HW

The identification of "at-risk" femoro-distal grafts has been investigated in 40 patients using duplex derived volume flow. Two hyperaemic stress tests (I: an occlusive cuff 50 mm Hg above systolic pressure for 2 minutes; II: active ankle flexion for 2 minutes) were assessed and the results expressed as the mean percentage rise from the resting value + 95% confidence interval. Grafts were defined as "at-risk" or control, depending on the presence or absence of graft or run-off stenoses greater than 50% following intra-arterial digital subtraction arteriography.

	Controls	"At-risk"
Number of patients	22	18
Mean resting flow (Q)	122 + (87–57)	161 + (115–207)
Test I (% rise Q)	647 + (343–950)	169 + (85–253)**
Test II (% rise Q)	434 + (51–816)	149 + (60–238)*

Whereas resting flows were similar, there was a significant difference between the groups following both hyperaemic tests. A hyperaemic flow increase of greater than 200% was able to predict "at-risk" grafts with a sensitivity and specificity of 100% and 78% for Test I and 53% and 53% for Test II respectively. These results show that duplex derived volume flows are only predictive of "at-risk" grafts following the use of a hyperaemic test. The 2-minute cuff hyperaemic test is superior to active ankle flexion; it is simple to apply and can help to identify "at-risk" grafts before they fail.

*$p < 0.05$; **$p < 0.001$ (Mann–Whitney U test).

Bramham Suite

Radioisotope Diagnosis and Therapy in Oncology (9.00–10.15)

PET in oncology

T. Jones and *C. B. Wilson
*MRC Cyclotron Unit and *Department of Clinical Oncology, Hammersmith Hospital, Du Cane Road, London W12 0HS*

Current positron emission Tomographic (PET) scanners provide in practice a voxel spatial resolution of approximately 8 mm FWHM within a 10.5 cm section through the body. The recorded tomographic data can be corrected for tissue attenuation to provide quantitative values of regional tissue concentrations of positron-emitting radionuclides. The use of this spatial and quantitative accuracy to follow the uptake and time course of tracer molecules, labelled with positron emitters such as oxygen-15, carbon-11 and fluorine-18, allows entities of regional tissue physiology, biochemistry, pharmokinetics and targeting to be measured. This paper reviews the clinical oncological research studies currently being undertaken internationally with PET. These include measurements of tumour; blood flow ($H_2{}^{15}O$, energy metabolism ($^{15}O_2$ and ^{18}FDG), protein synthesis (^{11}C-methionine), proliferation (^{11}C-thymidine), drug deposition (^{18}F-uracil, ^{18}F-misonidazole, ^{11}C-BCNU), receptor activity (^{18}F-oestrodiol and ^{11}C-raclopride), antibody targeting (^{124}I-MCA).

Strontium-89 therapy

A. H. Laing
Department of Radiotherapy and Oncology, Churchill Hospital, Headington, Oxford OX3 7LJ

Strontium-89 is a pure beta-emitter (maximum beta energy 1.4 MeV) with a half-life of 51 days. It localizes preferentially adjacent to metastatic deposits, being retained at these sites much longer than in normal bone. A number of studies have assessed its potential to control pain in skeletal metastases. The majority of patients had carcinoma of the prostate and had failed conventional therapies. Assessment was made at 12 weeks by a scoring system taking into account general condition, mobility, analgesics required and level of pain. In the British study an attempt was made to obtain a dose response but no additional benefit was seen with doses larger than 1.5 MBq/kg. A total of 131 patients were entered into this study: 75% showed improvement (21% dramatic, 32% substantial and 21% some improvement). Benefit was obtained in 10–20 days and lasted for 6 months on average. There was a suggestion that patients with fewer metastases do better, but patients obtained benefit even with very extensive disease. Apart from a few cases, in which a flare of pain was experienced shortly after injection, the only toxicity was bone marrow depression. Repeat doses of ^{89}Sr can be administered with further pain relief. It is possible to give ^{89}Sr after failure of hemi-body irradiation. Randomized studies are being undertaken comparing ^{89}Sr with external radiotherapy, both limited-field and hemi-body.

Dose-response study on thyrotoxic patients undergoing PET and radioiodine therapy

M. A. Flower, A. Al-Saadi, V. R. McCready, C. L. Harmer, B. Pratt, B. Cronin, J. Mundy and R. J. Ott
Departments of Physics, Nuclear Medicine and Radiotherapy, The Royal Marsden Hospital, Sutton SM2 5PT

With the acknowledged problems in assessing thyroid mass and hence radiation dose, our policy has been to give 75 MBq ^{131}I at 6-monthly intervals to patients with Graves' disease until they become euthyroid. Recently 35 patients have had their functioning thyroid mass determined from a ^{124}I PET scan, and the radiation dose to the thyroid has been calculated. The clinical response of these 35 patients has been assessed at 6-monthly intervals. The results show that patients who receive a low dose (<20 Gy) at their first treatment have a high probability (64%) of still being toxic at 18 months, independent of the number of extra treatments. In contrast, patients who receive higher doses (>40 Gy) at their first treatment have a high probability (90%) of control at 18 months. A dose of over 40 Gy needs to be delivered to minimize the chances of remaining toxic after a single treatment with radioiodine. A dose of over 60 Gy involves a 40% probability of becoming hypothyroid. In future, a PET tracer study will be performed prior to radioiodine therapy to enable a prescribed thyroid dose of 50 Gy to be delivered to patients with Graves' disease. Further ^{131}I therapy will only be considered if patients are still toxic at 12 months.

Ripley Suite

Cardiovascular Studies (10.45–12.00)

Early experiences using $^{99}Tc^{m}$-MIBI for SPECT imaging of the ischaemic myocardium pre- and post-angioplasty

C. D. Collins, D. J. Dowsett, D. Sugrue and J. T. Ennis
Department of Nuclear Medicine, Mater Misericordiae Hospital, Eccles Street, Dublin 7

Methoxyisobutyl isonitrile (MIBI), a lipophilic compound, is becoming the preferred agent for myocardial imaging. The sensitivity of $^{99}Tc^{m}$-MIBI for detecting regional perfusion defects in patients with known coronary artery stenosis was investigated by selecting 20 patients who had stenoses of varying severity in the right coronary, left circumflex and left anterior descending arteries. The aim was to demonstrate the improvement in myocardial perfusion following angioplasty. All patients were examined using $^{99}Tc^{m}$-MIBI before and after angioplasty and the results correlated with cine-angiography and the clinical status of the patient. Various techniques were explored to obtain optimum image quality. These included: (1) 180° or 360° rotation, (2) preparation and labelling of agent, (3) preparation of patient for stress/rest protocol and (4) image display. Good correlation was present between cine-angiography and $^{99}Tc^{m}$-MIBI. It is of particular use in those cases where differentiation of myocardial ischaemia from other causes of retrosternal chest pain is difficult. It also allows prompt diagnosis of early re-stenosis without resorting to immediate angiography. The major drawback of $^{99}Tc^{m}$-MIBI is its cost. Two methods of reducing this are outlined.

Combined exercise ECG and thallium stress testing in suspected coronary artery disease

C. S. Romaniuk and M. R. Rees
Departments of Radiology and Nuclear Imaging, Killingbeck Regional Cardiothoracic Centre, Leeds LS14 6UQ

A combined exercise ECG and thallium test is described. This was performed using a treadmill and standard protocols, with 12-lead ECG monitoring. At the end-point the patient was injected with 80 MBq thallous chloride. The heart was imaged immediately and at 4 hours to assess resting perfusion. Each left ventricular image was divided into three segments and scored. ECG stress tests were scored as positive, negative or borderline. *Results:* in 105 consecutive patients with suspected coronary artery disease there was close agreement between positive exercise tests (32) and positive thallium scans (30). Where the exercise test was negative (50), there were a significant number of positive scans (27) as well as borderline positive scans (9). These exceeded the number of negative scans (13). Patients with equivocal exercise tests (23) had positive (13) and negative (10) scans. Although the sensitivity and specificity of each test in this group of patients is not known, to date it has been found that nine patients with negative exercise tests and positive thallium scans have definite evidence of coronary disease. These results suggest that the combined exercise test and thallium scan have a high predictive value for coronary disease when both tests are positive, and that exercise testing alone underestimates the presence of coronary disease.

Notes

Monoclonal platelet specific antibody imaging in the selection of patients for peripheral arterial thrombolysis

D. C. Berridge, M. L. Wastie, A. C. Perkins, M. Frier and R. H. S. Gregson
Department of Medical Physics, University Hospital, Nottingham NG7 2UH

Arterial occlusion may be treated by intra-arterial thrombolysis, so avoiding major arterial surgery. However, for satisfactory results the thrombosis should be of recent origin and if it is of more than four weeks' duration the success rate falls. Clinical history alone is unreliable, as there may be pre-existing arterial disease, and the patients often learn to live within their disability. In recent arterial thrombosis, platelet deposition occurs which can be detected by imaging with ^{111}In labelled platelet specific antibody (^{111}In P256 Fab'). Thirteen patients with a clinical diagnosis of acute or subacute peripheral arterial thrombosis had a platelet antibody study prior to angiography and intra-arterial thrombolysis. Six patients had positive focal uptake, all were successfully lysed and 5 remained patent at 30 days. Seven patients had negative images. Six were initially lysed following thrombolytic therapy but four rethrombosed, usually on withdrawing the catheter. Only two remained patent at 30 days, one of whom was receiving drugs with some antiplatelet effects which may have interfered with deposition. This study suggests that this antibody may help to detect sites of recent arterial thrombosis and define those patients most likely to benefit from intra-arterial thrombolysis.

Misdiagnosis of an atypically located pericardial cyst with a high CT number presenting in a patient with multiple trauma

K. T. Tung and O. Chan
Department of Radiology, St Thomas' Hospital, London SE1 7EH

Pericardial cysts are estimated to occur in 1/100 000 of the general population. They are usually an incidental finding on chest radiographs and show a rounded, well defined homogenous mass in the cardiophrenic angles, and in this classical site they seldom cause any diagnostic difficulty. However, in 8% of cases, they occur in an atypical site and can then be a diagnostic problem. CT is usually very helpful in these circumstances, showing a homogeneous cystic mass in continuity with the pericardium. A change in size or shape of the cyst may be seen with breathing or with the patient in the prone position. The contents of the pericardial cyst typically have a density of 5–25 HU. Very rarely, pericardial cysts can have a high CT number and this is often interpreted as a solid mediastinal tumour. We present a 17-year-old man involved in a road traffic accident who sustained major chest trauma but who unfortunately had an atypically sited pericardial cyst with a high CT number; this led to a misdiagnosis and the patient had a thoracotomy. At surgery he was found to have a cystic mass in the mediastinum containing clear yellow fluid. This was excised and was confirmed to be a pericardial cyst histologically.

CT appearances of abdominal aortic graft infection

A. H. Choudhri, T. Tran, C. J. Barber, F. Regan and A. Al-Kutoubi
Department of Radiology, St Mary's Hospital, London W2 1NY

Prosthetic grafting of the abdominal aorta for aneurysmal or atherosclerotic disease is a relatively commonplace procedure with low mortality and morbidity rates. However, complications such as haemorrhage, anastomotic pseudoaneurysm formation, graft-enteric fistulae and graft occlusion may occur. Graft infection is one of the less common but more serious complications. Although it is important to recognize and manage this situation from an early stage, it is a difficult diagnosis to make clinically. Computed tomography is frequently performed to detect and evaluate the extent of graft infection. Accurate diagnosis of graft infection on CT requires a thorough knowledge of the normal post-operative appearance, which depends on the type of surgery employed. The clinical and CT findings in 22 patients with proven aortic graft infection, along with the normal appearances of various types of graft procedures, are presented. The role of complementary investigations is discussed.

Notes

Spontaneous dissecting aneurysm of the external iliac artery

T. Tran, A. H. Choudhri, M. McCarty, F. Regan and A. Al-Kutoubi
Department of Radiology, St Mary's Hospital, London W2 1NY

Primary dissecting aneurysms of the peripheral arteries are rare, as opposed to extensions from aortic dissection, which are relatively common. Significant atheromatous changes in the affected artery are unusual, with risk factors including hypertension, trauma, fibromuscular dysplasia and medial degeneration of the arterial wall. To our knowledge, only one case of spontaneous dissection of the external iliac artery has been reported previously. We present three cases of spontaneous dissection of the external iliac artery, each with discrete but characteristic angiographic features of dissection. The pathological and haemodynamic factors governing the various angiographic appearances are discussed. Dissecting aneurysm of the iliac artery should be borne in mind as a cause for acute unilateral limb ischaemia, particularly in the young or those with the appropriate risk factors.

MRI assessment of the thoracic aorta following aortic surgery

G. Hartnell, J. D. Wisheart, R. P. H. Wilde and P. R. Goddard
Departments of Radiology and Cardiac Surgery, Bristol Royal Infirmary, Bristol BS2 8HW

Thoracic aortic MRI has been shown to be a particularly accurate method for demonstrating a variety of abnormalities. MRI has been advocated as a routine investigation following thoracic aortic surgery as it has been reported to demonstrate unexpected complications. We report experience which does not favour this policy. Twenty-four patients who had undergone surgery involving the thoracic aorta were examined on a 0.5 Tesla MRI scanner using ECG gated spin-echo sequences. Ten of these patients were investigated as a result of the development of new signs following surgery. The remaining 14 patients were examined either as a routine follow-up or to investigate non-specific symptoms in the absence of any change in clinical findings. In the group with new signs, significant abnormalities were demonstrated by MRI. In the 14 patients with no new signs, no significant abnormalities were demonstrated. The availability of MRI is limited. Our results indicate that if there are objective signs of deterioration following surgery involving the thoracic aorta, then MRI is worthwhile. In the absence of objective signs of deterioration, routine scanning is unlikely to demonstrate any important abnormalities which would affect management.

A retrospective study of the fate of asymptomatic superficial femoral artery stenoses

P. Murphy, W. D. Jeans, M. Horrocks and R. Baird
Department of Radiodiagnosis, Bristol Royal Infirmary, Bristol, BS2 8HW

Balloon dilatation is not currently offered to patients with asymptomatic SFA stenosis. Though it would seem reasonable not to perform an angioplasty on an asymptomatic lesion, many of us performing transfemoral arteriograms note stenoses in asymptomatic limbs which on radiological criteria would seem very suitable for dilatation. There has been no real assessment of these lesions in the literature, and with this in mind, we performed a retrospective study of patients who had transfemoral arteriography between January 1986 and June 1988. Of 521 peripheral arteriograms there were 36 asymptomatic SFA stenoses. We reviewed these patients and followed them up for between 1 and 5 years (average 2 years). Of a total of 36 asymptomatic stenoses, 22 remained asymptomatic but 14 became symptomatic, on average within 2 years, the earliest at 3 months, the latest at 5 years. Symptoms were split evenly between claudication and rest pain or ischaemic change. Of the 14 patients, three later had a balloon angioplasty, two had femoral popliteal grafts, one had a sympathectomy and four required no intervention. There were, however, two patients who came to amputation. This study looked at predisposing factors such as the brachial to ankle index, diabetes mellitus, age and smoking. We concluded that approximately one third of asymptomatic superficial femoral artery stenoses will become symptomatic within 2 years. The predisposing factors to developing symptoms appear to be a brachial to ankle index of less than 0.9% and diabetes. It would appear from our study that the fact that a superficial femoral artery stenosis is asymptomatic is no reason for complacency and no guarantee that a limb-threatening situation may not develop in the future. We have now started a prospective trial to assess these lesions.

Evaluation of stenoses by magnetic resonance jet velocity measurement

P. J. Kilner, D. N. Firmin, R. H. Mohiaddin, S. R. Underwood, R. S. O. Rees and D. B. Longmore
Magnetic Resonance Unit, The National Heart and Chest Hospitals, London SW3 6NN

To minimize the problem of signal loss from turbulent fluid which has hitherto precluded magnetic resonance measurement of post-stenotic jet velocities, we shortened the echo time (TE) of the field even-echo rephasing (FEER) velocity mapping sequence from 14 to 6 and 3.6 ms. Rotating disc and stenotic flow phantoms were used for *in vitro* trials, demonstrating that the 3.6 ms sequence allows MR measurement of jet velocities up to 6m/s with accuracy similar to that of continuous-wave Doppler used under optimal conditions. *In vivo* MR jet velocity measurements were made in 39 patients. Diagnoses were: partially obstructed ventriculo-pulmonary conduit (20), pulmonary, aortic and mitral valve stenoses (10), aortic coarctation (8) and Fontan procedure (2) Continuous-wave Doppler velocity measurements, available in 20 cases, correlated will with MR measurements. Catheter pressure gradient measurements (11 cases) correlated moderately well with gradients estimated, using the modified Bernoulli equation, from either MR or Doppler velocities. Fast echo MR velocity mapping is likely to have considerable importance as a non-invasive means for locating and evaluating stenoses, particularly at sites inaccessible to ultrasound, but the potential for error due to malalignment, signal loss, phase wrap and partial volume effects must be recognized and avoided.

Angiography access through vascular grafts. Is it contraindicated?

P. F. Jaques and M. A. Mauro
Department of Radiology, University of North Carolina School of Medicine, Chapel Hill, NC 27599, USA

Recent surgical literature suggests that synthetic inflow grafts to the common femoral artery contraindicate subsequent transfemoral arteriography. Many patients who have undergone inflow graft procedures will require subsequent arteriographic evaluation to evaluate the graft post-operatively, and more commonly to evaluate and treat the more distal extremity vasculature for continuing peripheral vascular disease. The purpose of this review is to compare the relative safety of transfemoral arteriography through synthetic grafts versus the alternative transbrachial approach. A review of a computer database extending over a nine year period identified 87 patients who underwent 114 arteriographic procedures where vascular access was obtained by either the brachial approach or a transfemoral approach through a synthetic graft. Twenty patients had multiple procedures. The ages ranged from 38–86 years and there were 61 men and 27 women. There were 46 transfemoral graft and 68 transbrachial procedures. Only complications relating to vascular access were included in the review. Complications were divided into major and minor categories. A major complication required either blood transfusion or operative intervention. All other complications were considered minor and included haematomas, pain, vasovagal episodes, numbness and temporary coolness or decreased pulses. Of the 46 transfemoral graft procedures, there were 12 (26%) minor and three (6.5%) major complications. Of the 68 transbrachial procedures there were 27 (39.7%) minor and two (2.9%) major complications. These differences were not statistically significant and clearly show no increased procedural morbidity related to transfemoral graft punctures. These data suggest that there is no significant difference in procedural complications between transfemoral graft punctures and transbrachial approaches. The transfemoral approach can continue to be used for vascular access in patients with synthetic grafts in the groin.

"Malignant" angiodysplasia

A-M. Belli and A. P. Hemingway
Academic Department of Radiology, Royal Hallamshire Hospital, Sheffield S10 2JF

Angiodysplasia, a condition of unknown aetiology consisting of microvascular abnormalities in the mucosa and submucosa, predominantly affects the caecum and ascending colon and is associated with either acute or chronic intestinal haemorrhage. Angiodysplasia is diagnosed by selective visceral angiography and/or colonoscopy, but it cannot be detected on barium enema or by the naked eye at laparotomy. The characteristic features seen on superior mesenteric arteriography include vascular tufts on the antimesenteric border of the bowel in the arterial phase, an early-filling draining vein and a slowly emptying, dilated intramural vein. However, these features are not pathognomonic and can be demonstrated in other conditions including inflammatory bowel disease and malignancy. We report four patients in whom angiography revealed features suggestive of angiodysplasia but in whom malignancy was present. In three cases the lesion was a primary carcinoma and in one a metastasis. Retrospective review of the barium studies revealed the tumour in three cases; the fourth patient was known to have a teratoma with lymph-node metastases. In all cases the angiographic appearance was indistinguishable from angiodysplasia. This stresses the importance of viewing the caecum and right colon either at colonoscopy or double-contrast barium enema before the diagnosis of angiodysplasia is accepted, particularly if conservative management is to be adopted.

Bramham Suite

Quality Assurance and Protection (2.30–3.45)

Use of ionizing radiation by non-radiologists

R. Keal and C. Reek
X-Ray Department, Groby Road Hospital, Leicester LE3 9QE

The Ionizing Radiation Regulations 1988 state that all individuals who clinically or physically direct the exposure of patients to ionizing radiation are required to have attended an approved course in radiation protection. We have conducted a survey of hospital doctors in Leicester to identify those groups that use ionizing radiation and need appropriate training to comply with the regulations. A questionnaire was also included with the survey to establish the base-line knowledge of radiation physics amongst non-radiologists. The survey and questionnaire were sent to all hospital doctors in Leicester of registrar grade and above. The main groups using X-ray screening were general and vascular surgeons, anaesthetists and physicians with an interest in thoracic medicine and cardiology. The great majority of these doctors had not received any training in radiation protection but nearly all were willing to attend a suitable course. Knowledge of radiation physics and protection varied widely amongst the respondents with a significant percentage making fundamental basic errors. The detailed results are discussed, together with proposals for future training in radiation protection.

Factors affecting the radiation dose to the lens of the eye during cardiac catheterization procedures

T. A. Pratt and A. J. Shaw
Regional Department of Medical Physics and Bioengineering, Christie Hospital and Holt Radium Institute, Manchester M20 9BX

Concern has been expressed about the relatively high radiation doses to the lens of the eye received by the operator during cardiac catheterization studies. Under high workload conditions and without adequate protective measures, the operator may exceed the "classification level" for the lens of the eye. A study was undertaken to assess the occupational doses received by cardiologists, to examine the factors that affect the individual's eye dose and to find a practical relationship between occupational doses and workload. Nineteen cardiologists at three centres were studied. During the study each cardiologist was provided with forehead dosemeters by individual centres and their workload was recorded. Full equipment performance measurements were performed on the five X-ray units. One centre recorded data from a Diamentor for each operator and this has been compared with the individual's eye dose, to assess its usefulness as an indicator of total workload and to compare the techniques used. Scatter experiments using a phantom were performed to compare operator eye doses during typical fluoroscopy and cineangiography exposures for each unit. Some unexpected variations in eye dose due to equipment type, dose rate, individual operator's workload, technique and experience were noted. The results are presented and discussed.

Notes

Evaluation of implementation of guidelines of choice of projection for X-ray examinations to reduce patients' exposure

I. P. Matthews and D. Yates
Department of Epidemiology and Community Medicine, University of Wales College of Medicine, Heath Park, Cardiff CF4 4XN

An observational study of radiographic practice carried out from 1983-86 throughout Wales has revealed a wide interdepartmental variation in patients' exposure for the same type of examination. The variations in the number of projections and their associated film sizes for a particular type of examination have been shown to be a significant determinant in this variation. Currently, a multicentre evaluation of implementation of guidelines of choice of projection relating to 11 frequently performed procedures is revealing useful information with regard to (a) the compliance with the guidelines; (b) acceptability of the guidelines to radiologists and radiographers (*e.g.* ensuring that guidelines result in adequate information); (c)clinical exceptions to the guidelines (additional to those already specified). These guidelines, if successfully implemented, would have important implications for prevention of radiogenic cancers attributable to current use of diagnostic radiology in the UK. In the light of the results of this evaluation, the prospects of implementing guidelines nationally will be discussed.

Quality assurance in PACS

R. M. Dawood, J. O. M. C. Craig, J. H. Highman, A. Todd-Pokropek and A. W. Porter
Department of Radiology, St Mary's Hospital, London W2 1NY

Current methods of quality assurance (QA) have taken years to develop and refine. Though sometimes regarded as a tedious chore, QA remains an inescapable necessity for every modern film-based X-ray department that aspires to provide a good service. The arrival of new digital technology brings new and unfamiliar problems of QA that have so far received little attention, but that have important practical consequences for the day-to-day viability of such systems. We have examined the problems of setting up and monitoring the performance of TV display systems — for physical parameters such as phosphor characteristics, flicker, jitter, spatial and contrast resolution, temporal uniformity, spatial uniformity, spatial distortion, signal-to-noise ratio, dynamic range and interference from other equipment. We have also had to monitor the performance of film digitizers. Computed radiography produces images of consistent appearance over a much wider exposure range than conventional film: QA provision for such systems must include patient dosimetry. QA is the responsibility of individual departments, and will inevitably remain so. With as many as 30–40 UK centres currently examining the prospects for introducing PACS, it is important that the need for adequate QA should be recognized and allowed for.

Design and performance of a computerized quality assurance and patient dosimetry system in diagnostic radiology

C-L. Chapple and K. Faulkner
Regional Medical Physics Department, Newcastle General Hospital, Newcastle upon Tyne NE4 6BE

A system has been developed to undertake automatic quality assurance and dosimetry for diagnostic radiology examinations. A microcomputer has been interfaced to a microprocessor-controlled generator, and this allows tube and generator parameters to be measured for each exposure, and compared to nominal settings. Patient and examination details are entered by the operator, and exposure-area product and field size are automatically monitored for each radiographic exposure. The data collected, together with data already stored in the computer memory, are used to calculate the energy imparted to the patient, and individual organ doses. A laboratory study has been undertaken to investigate the accuracy and reproducibility of the measurements and calculations made by the automated system. Concurrent measurements of quality assurance parameters were made using standard techniques, and doses were measured using a RANDO anthropomorphic phantom and thermoluminescent dosimeters. The results of the study show that the automated system can measure exposure parameters with accuracy comparable to that of standard techniques, and that it is suitable for performing on-line dosimetry.

The effect of shielding trays on surface absorbed dose outside primary megavoltage radiotherapy beams.

A. Morgan
Medical Physics Department, Regional Radiotherapy Centre, Cookridge Hospital, Leeds LS16 6QB

Shielding trays are commonly used in radiotherapy. Their purpose is to hold lead blocks within the primary radiation beam in order to reduce the dose to specified normal tissues. However, the presence of a shielding tray produces scattered radiation which significantly increases the surface dose outside the primary beam, relative to an unleaded field. Surface doses of 14% of the dose maximum on the central axis of the beam have been recorded 5 cm outside the primary beam with a shielding tray in position. A series of measurements has been performed on various Perspex shielding trays used in this centre to determine (1) the magnitude of the effect and its variation with field size; (2) the quality of the scattered radiation; (3) the variation of (1) and (2) with primary beam energy. Results of the above measurements are presented and methods of reducing the amount of scatter by suitable lead tray design and local patient shielding are discussed.

The diary of a "rogue" mobile breast screening unit: a chronological QC record of its eventual demise, aged 19 months

M. Pearce, A. G. Brennan, T. M. Howard and D. L. Asbury
Manchester Breast Screening Service, Nightingale Centre, Withington Hospital, West Didsbury, Manchester M20 0PT

A mobile breast screening unit without on-board processing was delivered and commissioned in May 1988, after some minor faults had been satisfactorily rectified by the manufacturers. Problems in the operation of the AEC soon became apparent. During clinical use, these included poor repeatability, poor reproducibility, premature termination of exposure and refusal to expose. These were attributable to unstable environmental conditions and poor AEC design. They occasionally resulted in daily variations in density of −0.56 D (maximum) and variations during the day of +0.49 D (maximum) and also adversely affected reject rates. Results are presented to illustrate the nature and progression of the problems, the staff's corrective action and the manufacturers' response. The problems helped to test all aspects of the QA programme from the performance of simple QC tests to the data records and the necessity of good management, communication and physics support. The results also indicate that good QA cannot compensate for poor inherent performance. The unit was finally replaced in January 1990 by the manufacturers, having screened approximately 10600 women in 19 months.

A study of patient dosage and protection in computed tomography. 1. Patient dosage, distributions and hygienic evaluation during chest CT scanning.

D-Y. Qi, *D-H. Feng and *S-J. Li
*Department of Public Health, The Third Military Medical University, Chongqing, and *Department of Radiation Medicine, Suzhou Medical College, Suzhou, People's Republic of China*

In large X-ray departments, whole-body computed tomography is now the rule rather than the exception and more uses are being found for the particular way it can record anatomical structures. A knowledge of the patient dose, and the dose distribution during different investigations, is very important and essential in minimizing patient dose, ensuring that sensitive areas are not over-exposed and estimating the patient risk. Chest CT scanning was 18.2% of torso scanning in all of CT-examined 5776 patients in the Suzhou area in 1987. Fifteen patient dosages were measured using LiF thermoluminescent dosemeters in Hitachi CT-W500 scanning under perfect clinical conditions. The mean surface exposure in direct view of the beam was 2.98 R. Distributions of patient surface dose have been studied. The patient main organ/tissue absorbed dose and the effective dose equivalent during average 20-slice CT chest scanning have been obtained by use of the phantom simulation irradiation experiments (Table). CT chest scanning was compared with regular radiographic chest examinations from the saftey aspect.

Organ/tissue absorbed dose and effective dose equivalent in chest scanning

Organ/ tissue	W_T		Average surface exposure (R)	Absorbed dose (mGy)	Effective dose equivalent (mSv)
	M	F			
Thyroid	0.04	0.03	0.1643	1.0357	
Breast	—	0.26	2.9792	24.528	
Lung	0.14	0.10	2.9792	23.175	
Ovary	—	0.21	0.0400	0.3590	M: 6.4857
Testes	0.29	—	0.0180	0.1512	F: 11.468
Bone marrow	0.18	0.13	—	6.4704	
Other	0.35	0.27	—	5.6878	

A study of patient dosage and protection in computed tomography. 2. Patient dosage, distributions and hygienic evaluation during liver CT scanning

D-Y. Qi, *S-J. Li and *D-H. Feng
*Department of Public Health, The Third Military Medical University, Chonqing, and *Department of Radiation Medicine, Suzhou Medical College, Suzhou, People's Republic of China*

In all the 5776 patients in the Suzhou area examined by CT in 1987, the most frequently scanned organ of the body was the liver (41.9%), but specific studies on the patient dose are still very rare. Twelve patient dosages were measured using LiF thermoluminescent dosemeters in Hitachi CT-W500 scanning under perfect clinical conditions. The mean surface exposure in direct view of the beam was 2.6 R. Distributions of patient surface dose have been studied by fitting scattered radiation distribution curve equations. The patient main organ/tissue absorbed dose and the effective dose equivalent during average 12-slice scanning have been achieved using the phantom simulation irradiation experiments. The safety was also evaluated.

Organ/tissue absorbed dose and effective dose equivalent in liver CT scanning

Organ/ tissue	W_T M	W_T F	Average surface exposure (R)	Absorbed dose (mGy)	Effective dose equivalent (mSv)
Thyroid	0.04	0.03	0.0236	0.1488	
Breast	—	0.26	0.2627	2.1628	
Lung	0.14	0.10	0.5768	4.4869	
Ovary	—	0.21	0.0821	0.7369	M: 4.7795
Testes	0.29	—	0.0137	0.1159	F: 4.3079
Bone marrow	0.18	0.13	—	3.8749	
Other	0.35	0.27	—	9.7552	

A study of patient dosage and protection in computed tomography. 3. Patient dosage, distributions and safety evaluation during lumbar vertebra CT scanning

D-Y. Qi, *S-J. Li and *D-H. Feng
*Department of Public Health, The Third Military Medical University, Chongqing, and *Department of Radiation Medicine, Suzhou Medical College, Suzhou, People's Republic of China*

Lumbar vertebra CT scanning comprised 22.6% of body CT examinations in all of the 5776 patients in Suzhou examined by CT in 1987, especially with greater mA, longer scanning time and younger patients than in the other CT examinations, but the specific studies on the patient dose are still very rare. A method for standardized patient dosage measurement in Hitachi CT-W500 lumbar vertebra scanning under perfect clinical conditions has been established. The mean surface exposure in direct view of the beam was 5.75 R. Distributions of patient surface scattered dose have been studied by fitting curve equations. The patient main organ/tissue absorbed dose and the effective dose equivalent during average 7-slice scanning have been achieved using the phantom simulation experiments. Some further suggestions have been given.

Organ/tissue absorbed dose and effective dose equivalent in lumbar vertebra CT scanning

Organ/ tissue	W_T M	W_T F	Average surface exposure (R)	Absorbed dose (mGy)	Effective dose equivalent (mSv)
Thyroid	0.04	0.03	—	—	
Breast	—	0.26	0.0281	0.2313	
Lung	0.14	0.10	0.0234	0.1820	
Ovary	—	0.21	0.4616	4.1433	M: 1.2286
Testes	0.29	—	0.1002	0.8418	F: 1.6656
Bone marrow	0.18	0.13	—	2.5540	
Other	0.35	0.27		1.4266	

Charter Suite

The Role of Radiology in Surveillance Policies for Testicular Tumours (9.00–12.00)

Organizer: Dr M. P. Williams, Plymouth
Chairman: Dr A. K. Dixon, Cambridge
Panel: A. Horwich, Sutton; R. J. Johnson, Manchester; G. Rustin, London; M. P. Williams, Plymouth

Surveillance policies for testicular tumours

M. P. Williams
Department of Radiology, Freedom Fields Hospital, Plymouth PL4 7JJ

In order to run a surveillance policy it is essential to understand the pattern and time scale of metastases from testicular tumours and the strengths and weakness of the techniques to be employed. A review of 147 patients with non-seminomatous germ cell tumours of the testis on surveillance showed relapse in 37 (25%). CT scanning demonstrated relapse in 28, serum markers in 25, chest radiographs in eight, lymphography follow-up in five and marker relapse only in eight. No patient had a diagnosis of relapse based solely on lymphography and only one patient had a positive lymphangiogram with a negative abdominal CT scan. When the study was extended for a further 12 months, 47 out of a total of 168 patients relapsed, 83% in the first year, 9% in the second year, 6% in the third and 1% in the fourth. Maximum surveillance effort must be made in the first 12 months on patients with non-seminomatous germ cell tumours. All patients with abdominal relapses had involved nodes between the level of the renal hala and the aortic bifurcation. Scanning techniques should thus pay most attention to this area. In this study, employing CT at 2–3 monthly intervals during the first year, over 90% of the relapses detected fell within the Medical Research Council "good prognosis" group.

Surveillance policies for testicular tumours

A. Horwich
Radiotherapy Unit, The Royal Marsden Hospital, Downs Road, Sutton, Surrey SM2 5PT

With the development of effective chemotherapy for metastatic disease it has become practicable to consider surveillance for Stage I testicular tumours to replace routine adjuvant therapy. At the Royal Marsden Hospital, surveillance of Stage I non-seminoma was initiated in 1979 and more than 200 patients have now been followed up. Approximately 26% of patients have subclinical metastases at the time of their initial staging and that pattern of relapse is very predominantly within the first 2 years after orchidectomy. Furthermore, detailed examination of the histology of the primary tumour indicated groups at higher or lower risk of recurrence. Subsequently, the management policy of surveillance has been analysed in a multicentre setting. The Medical Research Council Testicular Tumour Working Party performed a 10-centre retrospective analysis of surveillance in 259 patients (Freedman et al, 1987). This confirmed the safety of surveillance since only three patients died of progressive teratoma; 28% relapsed and again histology was useful in determining the risk of recurrence. The important histological features discerned on multivariate analyses were vascular invasion, lymphatic invasion, undifferentiated cells and absence of yolk sac elements. If three or four of these factors were present, then the risk of recurrence was 58%.

This prognostic index was tested in a prospective surveillance study, was validated and has now provided a basis for studying adjuvant chemotherapy in patients with a high risk of recurrence while the remainder may be candidates for less intensive surveillance. In Stage I testicular non-seminoma, surveillance therefore provides an excellent alternative to either adjuvant retroperitoneal irradiation or to retroperitoneal lymphadenectomy. Since all early stage patients have an excellent overall prognosis, the important issue on which management decisions are based, is the morbidity of treatment alternatives. Surveillance minimizes specific anticancer treatments in that 70% of patients need no treatment following orchidectomy; however, surveillance must be conducted rigorously as an active policy rather than by clinical neglect. The policy must be designed to detect recurrences at an early stage when chemotherapy can be both curative and of low toxicity. This is aided by the sensitivity of current radiological techniques but also by the presence of sensitive and specific serum tumour markers. Research on surveillance should define the optimal programme to ensure clinical safety and economic use of resources. Surveillance in Stage I seminoma has been explored on a much more limited scale. The rationale for this investigation is the avoidance of the side effects of the standard management of Stage I seminoma, namely retroperitoneal irradiation: acute nausea/vomiting, a low risk of peptic ulceration and possible risk of late malignancy. The surveillance policy differs from that in Stage I non-seminoma because of the indolent course of the disease and because of the absence of a sensitive serum tumour marker. The RMH surveillance policy includes initial lymphography and CT scanning of thorax and abdomen. Follow-up includes both postero-anterior and oblique abdominal films for as long as lymphographic contrast media remains, and is continued for 5 years post-orchidectomy with abdominal CT scan each year. Of 113 patients registered on surveillance at the RMH between 1983 and 1988, the median follow-up is 33 months and the actuarial probability of remaining relapse-free at 3 years is 85%. Relapses have been seen up to 3 years, and relatively few patients have been followed for more than 4 years. Relapses are mainly in para-aortic nodes (14/15 recurrences). Two of these patients developed masses more than 5 cm in diameter before recurrence was discovered. Four patients have developed second relapses in the mediastinum and these may represent a consequence of delayed treatment of abdominal disease. The policy appears safe in that no patient has died of seminoma and all patients are currently in remission. However, surveillance in Stage I seminoma is labour-intensive and stressful both for clinician and patient, and in view of the excellent results of radiotherapy, it is felt that surveillance should only be continued in a research setting pending further evaluation.

Reference

Freedman et al (for MRC Testicular Tumour Working Party), 1987. *Lancet, ii*, 294–297.

Teach-in: Radiotherapy Planning for Head and Neck Cancers (2.30–3.45)

D. V. Ash
Cookridge Hospital, Leeds LS16 6QB

Abstract not received.

Congress Theatre

MacKenzie Davidson Memorial Lecture (12.15–1.15)

Interventional Ultrasound

H. H. Holm
Department of Ultrasound and Urology, Herlev Hospital, University of Copenhagen, DK-2730 Herlev Denmark

Since ultrasound scanning is the most convenient, rapid and precise method to guide a puncture needle, interventional ultrasound plays an increasingly important role in the management of more and more patients. "Material" in its broadest sense can be removed from the body or deposited into the body for diagnostic as well as for therapeutic reasons. The result is a large and increasing number of applications of which the most important and newest will be reviewed. The various ultrasonically guided biopsy techniques are described as well as some of their abdominal and extra-abdominal applications. Ultrasonically-guided access to tubular structures such as antegrade pyelography, PTC, pancreatography and central venous catheter placement are mentioned. Placement of nephrostomy catheters and treatment of abdominal and extra-abdominal abscesses as well as pancreatic pseudocysts are described. Various methods for ultrasonically guided tissue destruction (*e.g.* of prostatic cancer, liver tumours, parathyroid adenomas and coeliac plexus block) are presented. They include, for example, alcohol, radioactive seeds and Nd-YAG laser hyperthermia. The risk of interventional ultrasound is discussed. It is concluded that interventional ultrasound is an extremely valuable diagnostic and therapeutic tool which spares many patients much more traumatic procedures, that patient management today in many cases rests on a more firm basis than prior to the introduction of interventional ultrasound, that the future undoubtedly will bring many new applications of the technique, and that, like most other procedures, it carries a risk which, however, is remarkably low.

Notes

Tuesday 12 June

Harewood Suite

Liver and Biliary System (9.00–10.15)

Radiology of the liver

A. L. Baert and G. Marchal
Department of Radiology, University Hospital K. U. L., Gasthuisberg, Leuven 3000, Belgium

During the last decade the number of imaging modalities for the study of liver disease has been constantly growing: nuclear medicine, angiography, US, CT and more recently MRI have become part of the diagnostic modalities available in most large hospitals. *Focal liver lesions:* ultrasound has proved highly sensitive for detecting focal liver lesions, but will only rarely allow differential diagnosis. The value of CT in the detection of small lesions (1 cm or less) is hampered by technical factors such as the level of breath-holding and slice thickness. CECT performed during the portal phase after superior mesenteric artery injection is however actually the most sensitive method for detection of metastatic liver disease. The detection rate of focal liver lesions at high field strength MRI is equal or superior to CT. The results can be improved by IV superparamagnetic iron oxide (ferrite) injection. An MRI differential diagnosis of liver tumours is mainly based on signal intensity but also on morphological features. Large comparative studies are however still needed to assess the value of MRI in this regard as compared with CECT. Ultrasound and MRI are particularly helpful in defining hepatic anatomy prior to surgery because of the excellent visualization of the hepatic veins and the possibility of multiplanar imaging. ^{99}Tc^{m} labelled red blood cell studies are successful in differentiating haemangioma from other focal liver lesions. If surgical treatment of focal liver lesions is considered, angiography is still necessary for precise demonstration of arterial anatomy. On the contrary, intra-arterial injection of oily iodine contrast medium (lipiodol) is not accurate in the detection of secondary tumours in patients with hepatocellular carcinoma, as it accumulates in cavernous haemangioma. Frequently, the combined intra-arterial administration of lipiodol and chemotherapeutic agents is tested in some centres but its efficiency remains to be proven. *Diffuse parenchymal disease:* ultrasound and CT are both well suited for the diagnosis of diffuse or focal hepatic steatosis or changes produced by hepatitis and cirrhosis. Haemochromatosis can be proven both by CT and MRI. Both haemochromatosis and steatosis are however best qualified by CT. The correct choice and appropriate use of these techniques should not only consider sensitivity and specificity but also cost, accessibility, invasiveness and last but not least therapeutic consequences.

Dynamic contrast enhanced CT scanning in prognostically severe acute pancreatitis

J. M. Lavelle, *N. J. M. London, *T. Leese, *K. West and †D. C. James
*Departments of Radiology, *Surgery and †Pathology, Leicester Royal Infirmary, Leicester LE1 5WW*

Bolus contrast-enhanced CT demonstrates areas of non-enhancement in the pancreas which are postulated to represent necrosis. Early surgery in infected necrosis is reported to reduce mortality. In a prospective trial we perform dynamic contrast-enhanced scans on patients predicted severe by biochemical criteria (three or more adverse Glasgow criteria), or having CRP on Day $3 > 0.15$ g/l or a WCC$>15 \times 10^9$ on Day 7. CT-guided fine needle aspiration is performed on non-enhancing areas for cytological and bacteriological examination. To date 43 patients have been scanned and our findings are: (1) these selection criteria are useful, all patients with a severe outcome qualified for a scan; (2) cytology revealed amorphous debris compatible with necrosis; (3) the extent of CT necrosis is not always related to severity; some cases with extensive necrosis recovered early; (4) in three cases pseudocysts developed at the site of necrosis; (5) repeat scans at 6 weeks show persisting non-enhancement and in one case ERP demonstrated cut-off of the pancreatic duct at the junction between normally enhancing and necrotic pancreas; (6) infected necrosis in our experience is uniformly fatal and this group of patients is more likely to benefit from early surgery.

Corrugation of the common duct during endoscopic retrograde choledochopancreatography: a sensitive but non-specific indicator of pancreatico-biliary disease

P. M. Hughes, D. F. Martin and H. J. Fairhurst
Department of Diagnostic Radiology, University Hospital of South Manchester, Nell Lane, Manchester M20

Review of 435 endoscopic retrograde choledochopancreatograms (ERCP) has identified a group of 54 patients demonstrating a feature we have termed corrugation. The ERCPs were evaluated to determine the degree of common duct filling, the presence of pathological abnormality, the extent of corrugation and its persistence on repeat examination in order to determine its sensitivity and specificity as a diagnostic sign. Fifty (93%) of the ERCPs with evidence of corrugation demonstrated biliary or pancreatic abnormality. Common duct stones were identified in 36 cases, pancreatic or cholangiocarcinomas in 12, while one demonstrated an impacted stone in Hartmann's pouch and another a dilated common duct and periampullary diverticulum. The four remaining cases with corrugation but no radiological abnormality at ERCP had biochemical and ultrasonic evidence of acute pancreatitis. Of 16 repeat ERCPs, 15 again showed corrugation. While accepting that ERCP examinations are performed on a selective population, common duct corrugation — a sign not previously described to the authors' knowledge — appears a sensitive but non-specific indicator of pancreatico-biliary disease.

Comparison of cholescintigraphy, ultrasound and ERCP in 55 patients with intrahepatic cholelithiasis

I. Stewart, K. C. Ho, J. Leung and C. Metreweli
Departments of Diagnostic Radiology and Organ Imaging, and Medicine, Prince of Wales Hospital, Chinese University of Hong Kong, Shatin, New Territories, Hong Kong

Intrahepatic cholelithiasis causes duct dilation, stricture formation and hepatic parenchymal atrophy. Patients frequently present with acute cholangitis. The aim of this study was to compare the additional functional information provided by cholescintigraphy with the morphological information provided by ultrasound and ERCP. Fifty-five patients had cholescintigraphy (1.85 MBq (5 mCi) EHIDA), ultrasound and ERCP on admission. Nasobiliary drains were inserted at ERCP when indicated. Analysis of the five phases of cholescintigraphy (perfusion, hepatocyte, excretion, CBD/small bowel and gall bladder) provided significant additional information regarding the presence of intrahepatic cholelithiasis, duct dilatation, abscess formation and parenchymal hypofunction, not available from ultrasonic or endoscopic examination. The addition of cholescintigraphy materially benefits the management of the acute and chronic phases of intrahepatic cholelithiasis.

Correlation of staging with survival in patients with cholangiocarcinoma

J. J. Donald, S. J. Garber, *A. C. Smith and W. R. Lees
*Departments of Radiology and *Gastroenterology, The Middlesex Hospital, London W1N 8AA*

Cholangiocarcinoma is rare and carries a poor prognosis. Knowledge of the distribution of the tumour is essential to successful treatment either by palliative stenting or surgery. In a prospective study 31 patients with an ultrasound diagnosis of cholangiocarcinoma underwent endoscopic retrograde cholangiopancreatography (ERCP). Diagnosis was confirmed by clinical follow-up. The tumour was extrahepatic in 12 cases (39%) and situated at the hilum in 19 (61%). The maximum tumour dimension varied from 10 mm to 89 mm with a mean of 38 mm. Of the tumours, 58% had irregular margins and 71% were homogenous in echo pattern. The tumour echogenicity was less than that of the liver in 42%, equal in 42% and increased in 16%. Doppler signals were detected in the tumour in only four patients and there was evidence of portal vein involvement in five cases. Regional lymphadenopathy was seen in 58% and liver metastases in 10%. The ERCP findings agreed precisely with ultrasonography in 56% of cases and estimated greater tumour extent in 22%. In two patients the final diagnosis was gallstones. There were four ERCP failures. Ultrasonography is an accurate diagnostic method which maps the biliary tree and provides information on tumour load, important in planning treatment. The relation of these factors to survival is discussed.

Diagnostic value of cholangiograms in patients with obstructive jaundice

A. H. Hasan, B. Moule and D. C. Carter
Department of Radiology, Glasgow Royal Infirmary, Glasgow G31 2ER

The cholangiograms (PTC and ERCP) of 147 patients with surgical obstructive jaundice, who had a final diagnosis based on operative findings, biopsy, autopsy or endoscopy, were evaluated to assess their diagnostic value in different surgical conditions; and the liver-function tests were then correlated. The sensitivity and specificity of the cholangiograms in differentiating between benign and malignant conditions were 84% and 86% respectively; 86% and 93% for the diagnosis of choledocholithiasis, and 48% and 71% for the diagnosis of benign non-calculous conditions. A significantly higher value of the total serum bilirubin level and a larger transverse diameter of the gallbladder (GB) were recorded in patients with malignant obstruction. However, there were no statistically significant differences between the groups regarding the maximum diameters of the intrahepatic ducts (IHD), common hepatic duct (CHD) and common bile duct (CBD), nor in terms of the serum alkaline phosphatase concentration. The study concludes that: (1) direct cholangiography still plays an important role in diagnosis of different surgical conditions; (2) the diameters of the IHD, CHD, CBD and GB alone (*e.g.* measured by ultrasound) cannot reliably differentiate benign and malignant conditions; however, small shrunken GB makes diagnosis of a malignant obstruction very unlikely; and finally, (3) in the absence of a history of biliary surgery or the usual cholangiographic features of calculous obstruction, any complete or near-complete obstruction in the biliary system must be highly suspicious for malignant condition regardless of the cholangiographic appearances.

A strategy for percutaneous removal of multiple intrahepatic calculi

A. Adam, M. N. Chetty, E. Y. C. Yeung and I. S. Benjamin
Department of Diagnostic Radiology, Hammersmith Hospital, Du Cane Road, London W12 0HS

The removal of multiple intrahepatic biliary calculi can present formidable problems especially following hepaticojejunostomy. We have treated eight patients with this condition, six of whom had benign hepaticojejunostomy strictures and two retained calculi following cholecystectomy. In patients with strictures a Roux loop was fixed subcutaneously at the time of surgery and marked with metallic clips. It was used later by the radiologist for retrograde access to the biliary tree. A combination of saline irrigation, Dormia-type baskets and occlusion balloons was used to clear the biliary tree of calculi. Occlusion balloons proved particularly useful in dealing with small calculi in distal ducts. The strictures were dilated and in two cases Gianturco self-expandable metallic stents were inserted. In five patients all of the calculi were successfully retrieved. In the remaining three complete removal was not possible but subsequent clinical management was made much easier following radiological intervention. There were three cases of post-procedure cholangitis. The patients have remained symptom-free for a median period of 16 months (mean 12.4 months). Two patients developed recurrent stones after 27 months and 6 months respectively and were successfully treated again. The strategy described appears successful in dealing with the majority of complex patients with intrahepatic calculi.

Percutaneous cholecystostomy in the treatment of acute calculous cholecystitis in high-risk patients

O. Chan, M. Sen, T. Y. K. Chan, E. Loveday and R. J. Nicholls
Departments of Radiology and Surgery, St Thomas' Hospital, London SE1 7EH

Surgical cholecystostomy is regarded as the safest operative method for the treatment of acute cholecystitis, with an operative mortality of 0.5%. However, in the emergency situation and in high-risk patients, the mortality rate can rise as high as 15%. Percutaneous cholecystostomy (PC), when performed in patients undergoing lithotripsy or dissolution therapy or as part of percutaneous stone extraction in the treatment of gallstones, is a difficult procedure and requires both skill and experience. However, when PC is performed in patients with either calculous or acalculous cholecystitis, it is a relatively simple and safe procedure which is performed under local anaesthetic. Whereas PC is now the accepted treatment in acalculous cholecystitis, it has not gained widespread approval in the treatment of calculous cholecystitis, not even in high-risk patients. We present three elderly patients with calculous cholecystitis who failed to settle on conservative treatment; two were considered high-risk and one refused surgery initially. All three patients had PCs with immediate relief of pain with rapid resolution of all symptoms and signs. Two had elective cholecystectomies 3 and 7 months after the PC. The third patient refused surgery and has remained asymptomatic for 1 year. PC is simple and safe and can be life-saving and should be considered as an alternative method of treatment in the management of acute calculous cholecystitis, in particular in elderly and high-risk patients. Elective surgery in these groups of patients should only be offered to those who remain symptomatic.

Benign biliary disease: percutaneous endoprosthesis or balloon dilatation?

A. Gillams, *S. Mathur, W. Taylor, *J. S. Dooley and R. Dick
*Departments of Radiology and *Medicine, The Royal Free Hospital and School of Medicine, London NW3*

When surgery is not considered appropriate, and when an endoscopic approach is not possible, patients with symptomatic benign biliary strictures provide a therapeutic dilemma. We have treated 21 such patients, (11 female, 10 male) with a mean age of 55 years (range 23–78), with either percutaneous insertion of an endoprosthesis (PE) or percutaneous balloon dilatation (PD). Twenty patients had postoperative strictures and of these 16 followed cholecystectomy. One patient had primary sclerosing cholangitis. In 17 of the patients a total of 32 corrective biliary operations had been performed. The indication for the percutaneous procedure was recurrent cholangitis with or without janudice. The mean bilirubin before the procedure was 76 μmol/l [range 5–576 (normal < 17 μmol/l)]. Ten patients had PD, 11 PE (six Teflon endoprostheses and five metal). Four patients in each group developed early complications (*i.e.* less than 24 h after the procedure). The median asymptomatic period following the procedure was PD 11.5 months (range 3–43), PE 11 months (range 5–96). A further procedure (or surgery) for recurrent symptoms was necessary in PD 5/10 and PE 4/11 at a median of 12 and 14 months respectively. All five PD patients who have not required further intervention are asymptomatic at median follow-up of 14 months. Patients in both groups achieved a valuable period of biliary drainage. However 43% needed a further procedure 3 months to 5 years later. Despite recent advances, these data do not suggest that PD is better than or worse than PE

Technical aspects of percutaneous gallstone dissolution with methyl-tert-butyl-ether (MTBE)

D. J. Wright, J. P. M. Ellul, R. H. Dowling and A. M. Keightley
Departments of Radiology and Gastroenterology, Guy's Hospital, London SE1 9RT

Cholesterol gallstones in a functioning gallbladder can be treated by percutaneous cholecystostomy and infusion of MTBE. We report on our initial experience in 14 patients, emphasizing technical aspects of catheter placement and manipulation during MTBE dissolution. Difficulties in catheterization were related to insufficient analgesia, resistance of the gallbladder wall, gallbladder mobility and invagination of the gallbladder wall. Failure in catheterization was associated with intro-peritoneal biliary leakage. Semi-urgent cholecystectomy in two patients resulted and elective cholecystectomy in a third. A further problem that we encountered was extrusion of the pigtail catheter, during MTBE infusion, as a result of respiratory movement (two patients). This was overcome by using a longer (70 cm) catheter and coiling it in the gallbladder. Maximal stone dissolution occurs within the pigtail of the catheter where MTBE concentration is greatest. Manipulation of the catheter during dissolution is therefore desirable to ensure that stones remain in an optimal position. We found that various refinements of technique were required during the initial learning period before technical success could be reliably achieved.

Notes

Chest Radiology (10.45–12.00)

Diagnosis of pulmonary embolism

J. P. Lavender
Department of Diagnostic Radiology, Royal Postgraduate Medical School, Hammersmith Hospital, Du Cane Road, London W12 0NN

The diagnosis of pulmonary embolism remains a widespread problem. Both clinical assessment and the chest radiograph are inaccurate and therefore the patients undergoing further investigation represent a small proportion of the real incidence in a hospital population. Ventilation perfusion imaging has a high accuracy where the perfusion defects are large or multiple, but where they are sub-segmental, correlation with positive angiography falls to non-diagnostic levels, probably due to poor resolution for both sets of images. An alternative approach is the identification of patients at risk by localizing venous thrombus by ultrasound or radioactive tracer. Prospective imaging of venous thrombus in post-operative patients can be performed using a radiolabelled monoclonal antibody with high affinity for platelets (Greenspan et al, 1982; Lavender et al, 1988). This tracer can be used to look at the natural history of post-operative thrombus and also allows imaging of the clot in the pulmonary artery. Data based on 30 post-operative patients imaged in this way showed a greater than 50% incidence of thrombus, mainly in calf veins, with a 20% incidence of pulmonary emboli most of which could be visualized with this tracer. Direct methods of identifying both peripheral and central thrombus seem to offer the way forward in dealing with the widespread clinical problem of thromboembolic disease.

References

Greenspan R.H., Ravin, C. E., Polansky, S. M. & McCoud, T. C., 1982. Accuracy of the chest radiograph in diagnosis of pulmonary embolism. *Investigative Radiology, 17,* 539–543.

Lavender J. P., Stuttle, A. W. J., Peters, A. M., O'Donnell, C. J., Davies, G. J., Harrison, R. & Hogg, N., 1988. *In vivo* studies with an anti-platelet monoclonal antibody; P256. *Nuclear Medicine Communications, 9,* 817–822.

Stuttle A. W. J., Klosok, J., Peters, A. M. & Lavender, J. P., 1989. Sequential imaging of post-operative thrombus In-III-labelled platelet-specific monoclonal antibody P256. *British Journal of Radiology, 62,* 963–969.

Magnetic Resonance anatomical and flow imaging of pulmonary arteries in patients with single lung transplantation

R. H. Mohiaddin, R. Paz, S. Theodoropoulos,
D. B. Longmore and M. Yacoub
Magnetic Resonance Unit, National Heart and Chest Hospitals, 30 Britten Street, London SW3 6NN

Magnetic resonance imaging has been used to study pulmonary arterial anatomy and to measure pulmonary arterial blood flow in patients with single lung transplantation. Nine patients and nine controls matched for age and sex were studied. The anatomy of the main pulmonary artery and its main branches, as well as the site of arterial anastomoses, were identified and their diameters measured. There were no significant differences in diameters of these vessels between the patients and their controls. Arterial blood flows to the transplanted lung were 2.07±0.45 l/min/m^2 in the group with right side transplantation and 2.43±0.60 l/min/m^2 in the left sided group compared with (1.22±0.22) l/min/m^2 and (1.27 ±0.41) l/min/m^2 in the control group respectively. The ratio of blood flow in the transplanted and the native lungs in all patients studied was 2.8±0.83 : 1. The flow profile in the artery of the transplanted lung shows a wide forward flow during systole and most of diastole, while that of the native lung shows a narrow early systolic peak and a reverse flow in most of diastole. This differential flow and its pattern are most likely to be related to the relative resistance in the native and transplanted lung and could well be a good index for monitoring and follow-up of patients with lung transplantation.

Pulmonary Kaposi's sarcoma; a review of the radiographic appearances in the St Mary's Hospital group of patients with the Acquired Immune Deficiency Syndrome

M. McCarty, D. A. Cunningham, F. Moss and R. Jenkins
Department of Radiology, St Mary's Hospital, London W2 1NY

In patients with the Acquired Immune Deficiency Syndrome (AIDS), Kaposi's sarcoma causes significant morbidity and mortality. Although skin involvement is the most common manifestation, the disease is systemic, particularly affecting the lungs and gastrointestinal tract. Lung involvement should be suspected when the chest radiograph demonstrates nodular infiltrates, pleural effusions or lymphadenopathy. In some cases, consolidation repeatedly occurs in a particular segment due to a partially obstructing endobronchial lesion. Of 360 AIDS patients seen at St Mary's, 29 have had bronchoscopically proven Kaposi's sarcoma. We present the radiographic appearances in this group.

CT and ultrasound-guided drainage of pleural empyemas and malignant effusion using fine pigtail catheters

C. Sampson, T. J. Bloomberg and W. McAllister
Department of Radiology, The Royal Surrey County Hospital, Guildford, Surrey GU2 5XX

Drainage of pleural collections is usually performed using Argyle chest drains or repeated aspirations. We describe a series of 34 cases (26 empyemas and seven malignant effusions) in which the collections were drained by CT or ultrasound insertion of a pigtail catheter. A 7 F catheter was used in adults and a 5 F or 6 F one in children. Drainage was by a closed system into a plastic drainage bag and thick collections of pus were irrigated with normal saline. Three cases of multiloculated empyema were treated by the simultaneous insertion of two catheters. In only one case (malignant effusion) was catheter replacement necessary because it became blocked. Three empyema cases which were slow to resolve were managed as outpatients. In one of these a broncho-pleural fistula which required surgical treatment was later demonstrated. Two other cases required surgery due to the persistence of the cavity. No complications of the procedure occurred and no infection developed at the catheter site. We conclude that radiologically-guided fine catheter drainage of pleural collections is a safe and effective method and that drainage by large chest drains or repeated aspirations is unnecessary.

Sensitivity of fine needle transthoracic percutaneous needle biopsy (TNAB) versus histological type, mass size and location of lung carcinoma

C. D. Collins and E. Breatnach
Department of Radiology, Mater Misericordiae Hospital, Eccles Street, Dublin 7

Though TNAB is a well established method for obtaining malignant pathological confirmation of lung carcinoma, in the literature an overall non-diagnostic rate of 15–20% is quoted. To investigate possible negative influences on biopsy rate, we have analysed results of TNAB vs cell type, mass size and location in 129 patients with bronchogenic carcinoma. Overall, TNAB was successful in 89% of cases. Sensitivity was best for small-cell carcinomas (100%) where therapeutic implications are greatest in non-resectable disease, and it was least for squamous cell tumours (72%). Non-diagnostic aspirates occurred in seven of 60 masses over 3 cm in size and in three of 29 masses over 6 cm. Twenty-eight of 30 central tumours showed positive histology vs 77 of 89 peripheral lesions. The negative influence of these variables in our patients was less than figures quoted for trans-bronchial biopsy. We conclude that cell type, tumour site or size (when over 3 cm) do not represent major determinants of yield for TNAB. If low sensitivities are achieved with this technique, they result from other factors. These results are elaborated and discussed.

High-resolution computed tomographic appearances of lymphangioleiomyomatosis

D. M. Hansell, D. R. Aberle, C. M. Prendergast and E. Moskovic
Department of Radiology, Brompton Hospital, London SW3 6HP

Lymphangioleiomyomatosis is a rare condition characterized histologically by proliferation of smooth muscle throughout the lung. The chest radiographs and CT scans of 10 patients with pathologically proven disease were compared. Correlation was also made with lung function tests when available. Chest radiography demonstrated lungs with normal to increased volume with a diffuse fine reticular pattern interspersed with cystic air spaces. CT revealed uniform replacement of the lung with cysts of varying size from 2–30 mm in diameter. The cysts were extremely thin-walled and were evenly distributed throughout all lobes with no central or peripheral predominance. The degree of cystic change in the lung parenchyma visible on CT was much greater than that visible on chest radiographs. In one case with a normal chest radiograph there were definite cystic changes on the concurrent CT scan. There was good correlation between the extent of parenchyma judged to be involved on CT scans and lung function tests. Lymphangioleiomyomatosis has a distinctive cystic appearance on CT. Although not unique, the CT morphology and uniform distribution of abnormality frequently permit differentiation from other cystic conditions of the lung.

Pulmonary involvement in systemic lupus erythematosus: evaluation with computed tomography

C. M. Prendergast, D. M. Hansell and M. B. Rubens
Department of Radiology, Brompton Hospital, London SW3 6HP

High-resolution CT of the chest has an established role in the assessment and monitoring of diffuse diseases of the lung parenchyma. As yet there has been no description in the literature of the appearances of lung involvement in systemic lupus erythematosus (SLE) on high-resolution CT. In SLE the pleura, lung parenchyma, pulmonary vasculature and diaphragm may be involved. The resulting changes reflected on conventional chest radiography include recurrent pleural effusions, subsegmental collapse, areas of consolidation and shrinking lung syndrome. We have reviewed our patients with SLE who have had high-resolution CT of the thorax over the past six years. All patients fulfilled the criteria of the American Association of Rheumatologists in establishing the diagnosis. In over 80% of cases there was evidence of pleural disease, either pleural thickening or small pleural effusions. Linear, band-like opacities were the next most common abnormality. These tended to be both peripheral and basal in distribution. Another frequent manifestation was small areas of consolidation and poorly defined areas of increased parenchymal density, visible in up to 60% of patients. The pathological explanation for these appearances needs further clarification since it remains uncertain whether they represent areas of lupus pneumonitis, infarction due to vasculitis, or intercurrent infection.

CT density mapping in the assessment of pulmonary emphysema: a technical appraisal

M. S. Bernard and H. Adams
Department of Radiology, Llandough Hospital, Penarth CF6 1XX

Many modern CT scanners have post-processing facilities which allow pixels within a selected density range to be highlighted. It has recently been suggested that using this technique to highlight regions of low CT density (–900H to –1000H) can accurately locate and quantitate areas of pulmonary emphysema ("lung density mapping"). This method was evaluated in 17 subjects who had no evidence of structural lung disease on full respiratory function testing. CT technique was standardized. In sections obtained at the level of the carina, mean CT density varied from –770H to –875H (overall mean –817H). The percentage cross-sectional area in the range –900H to –1000H varied from 0.6% to 58% (mean 15.3%). In two further groups of subjects the influence of CT slice thickness and intravenous contrast administration on the lung density map was evaluated. The use of narrower collimation led to a significant increase in mean cross-sectional area within the low density range ($p < 0.05$). The use of intravenous contrast medium led to a significant reduction in cross-sectional area within this range ($p < 0.01$). There is considerable variation in the lung density map of normal individuals. The method is also dependent on radiographic technique. The potential usefulness and limitations of CT lung density mapping in the assessment of lung disease are discussed.

MRI scanning of the thorax in patients with active lymphoma

P. R. Goddard, M. Cobby, A. Case, G. Hartnell and P. Murphy
Department of Radiology, Bristol Royal Infirmary, Bristol BS2 8HW

The magnetic resonance imaging (MRI) findings are presented of 27 patients with lymphoma affecting the thorax (20 Hodgkin's, 7 NHL). Scanning was undertaken using a Picker Vista 0.5T MRI Scanner. T_1-weighted spin–echo coronal and transverse scans with corresponding STIR (short tau inversion recovery) scans were the most commonly employed sequences and proved efficacious in demonstrating pathology in the chest and mediastinum. Sagittal scans were useful for the thoracic spine. Abnormalities were shown in the mediastinum (15), perocardium (7), chest wall (5), pleura (4) and bone marrow (11). MRI was able to demonstrate mediastinal nodes, invasion of vascular structures and bone marrow involvement when not visible by CT. More surprisingly, MRI was also able to clearly show intrapulmonary nodules. MRI will have an important role in the staging and follow-up of patients with lymphoma.

Thoracic computed tomography: value in respiratory failure secondary to kyphoscoliosis

P. Carvalho and D. Carr
Department of Radiology, Brompton Hospital, London SW3 6HP

The chest radiographs of patients with a kyphoscoliosis severe enough to cause respiratory failure are often difficult to interpret because the spine and mediastinal structures overlie lung. In order to establish whether CT would be helpful in this situation, thoracic CT was performed prospectively on 10 patients. Informed consent was obtained from all. We confirmed that the plain chest radiograph is a particularly insensitive investigation in such patients, and was potentially misleading in several. Relatively gross pathology, such as right lower lobe collapse, was not visible on the chest radiograph, even in retrospect. Pulmonary artery size was also difficult to assess on the chest radiographs of several patients. In no patient did the abnormal thoracic structure prevent entry into the gantry nor scanning. CT was able to confirm or exclude pulmonary consolidation in patients with an acute exacerbation of their respiratory failure. CT was also able to determine pulmonary artery size. In conclusion, plain chest radiography can be misleading in patients with a severe thoracic kyphoscoliosis; CT is feasible, and can reveal gross pathology not visible on the chest radiograph.

Notes

Small Bowel Studies (2.50–3.45)

Plain radiographic and CT appearances of lesser sac hernias

T. Tran and F. Regan
Department of Radiology, St Mary's Hospital, London W2 1NY

Internal hernias are rare, accounting for only 1% of all intraperitoneal causes of intestinal obstruction. Internal hernias through the lesser sac occur (in decreasing frequency) through the foramen of Winslow, the transverse mesocolon, the greater omentum and the lesser omentum. Foramen of Winslow hernias account for 8% of all internal hernias. Internal hernias through the gastro-hepatic omentum are extremely rare and to our knowledge only one case has been described. We have encountered three cases of lesser sac hernia, two via the foramen of Winslow and one via the gastro-hepatic omentum. Plain abdominal radiographs of all three cases are presented as well as the CT appearances of the gastro-hepatic omental hernia. We show that CT can differentiate between gastro-hepatic and foramen of Winslow hernias and that careful scrutiny of the CT and plain films can lead to a preoperative diagnosis.

Herniography in unexplained groin pain

M. C. Collins and W. Morris-Jones
Department of Radiology, Royal Hallamshire Hospital, Sheffield S10 2JF

Sixty patients complaining of groin pain where no clinical abnormality was found were investigated using herniography, a simple outpatient procedure with a very low complication rate, in which non-ionic water-soluble contrast medium is injected directly into the peritoneal cavity using a 20-gauge needle. Radiographs are obtained in the prone, erect and oblique positions. The examination and interpretation of the radiographs are described. Herniography may detect hernial sacs not obvious clinically. Alternatively, the absence of hernial sac on herniography avoids needless groin exploratory surgery. The results and complication rates in the first 60 patients are described and the relationship between this investigation and the eventual clinical outcome detailed. A future role for herniography in the investigation of unexplained groin pain is discussed.

^{99}Tc^{m}-HMPAO imaging in Crohn's disease of the small bowel

N. Kennan, P. Facey, J. Jones, J. Rhodes and M. Hayward
Department of Radiology, University Hospital of Wales, Cardiff CF4 4XW

Radioisotope techniques using labelled leucocytes provide a relatively non-invasive means of determining the site and extent of disease activity in inflammatory bowel disorders, including Crohn's disease. Newer techniques use white cells labelled *in vitro* with 99m-technetiumhexamethyl propylene amine oxime (Tc-HMPAO)(Amersham). We report our initial experience using ^{99}Tc^{m}-HMPAO-labelled leucocytes in 14 patients with known small bowel Crohn's disease. Eleven patients had comparable barium studies, *i.e.* performed within a year of the scan and with no intervening surgery. There was good correlation in nine as to the site and extent of disease. In one, the scan confirmed active disease when a small bowel enema suggested only deformity due to scarring. In a second, the technetium scan failed to show total colonic involvement demonstrated on barium studies. Of the remaining three patients, two were clinically well, one of whom had an abnormal scan. Perianal disease could not be visualized in the third. These early results show good correlation with barium studies and clinical evaluation and suggest this may be a useful and sensitive alternative method of imaging these patients.

Per-oral pneumocolon in the evaluation of the distal small bowel

B. Patel, D. F. Martin and A. J. Maxwell
Department of Radiology, Hope Hospital, Salford M6 8HD and University Hospital of South Manchester, West Didsbury, Manchester M20

Although the small bowel enema is widely regarded as the 'gold standard' for examination of the small bowel, the small bowel meal (SBM) remains the most commonly performed procedure. The peroral pneumocolon examination (POPC) allows double-contrast images of the terminal ileum to be obtained by insufflating air through a rectal tube when orally ingested barium reaches the right colon. The technique offers the possibility of improving the sensitivity of the standard SBM by (1) distending the distal small bowel, and (2) improving mucosal detail with double rather than single-contrast images. We have performed POPCs on 30 patients referred for SBMs. Standard views of the ileum were obtained before and after air insufflation. Blind comparison was made between the pre- and post-insufflation images, assessing maximum ileal distension, quality of the demonstration of the ileum, and degree of confidence of normality and abnormality. Air reflux was achieved in 23/30 cases (77%). Many patients found air insufflation uncomfortable, despite routine administration of intravenous glucagon. Although in most cases the distal ileum was better distended following insufflation, the certainty with which the observer felt pathology could be diagnosed or excluded was not significantly altered. In three patients who had previously undergone ileo-caecal resections for Crohn's disease, easy air reflux into the ileum occurred, allowing excellent demonstration of recurrent disease at the anastomosis. It is concluded that the POPC is not helpful as a routine technique for small bowel examination, but may be useful in patients who have had previous ileo-caecal resection.

Hereditary pancreatitis: early ultrasound appearances

J. A. Spencer, D. R. M. Lindsell and *D. Isaacs
*Departments of Radiology and *Paediatrics, John Radcliffe Hospital, Oxford OX3 9DU*

Hereditary pancreatitis (HP) is a rare familial condition first described in 1952 which may present with acute abdominal pain in childhood. The radiological findings in a family with HP are presented. The radiological hallmark of HP is the extensive pancreatic calcification and the frequent and large pancreatic duct calculi. These have been reported as early as the second decade, more commonly in the third. The early ultrasound (US) features have not been previously described. The US appearances at acute presentation in a 2-year old boy and over a 3-year follow-up are shown. We demonstrate that progressive duct dilatation and other features of chronic pancreatitis can be appreciated on US in the absence of pancreatic calculi or calcification. The adult US features are illustrated. US is of value in the diagnosis and screening of family members as well as in following the clinical course and complications of affected individuals. The aetiology of HP remains unclear but early US appearances indicate that progressive pancreatic duct dilatation precedes the development of the characteristic pancreatic calculi and calcifications.

Right-sided diverticulitis

P. A. Gaines, A. Sharma, M. Arnold, M. Lin and C. Metreweli
Department of Diagnostic Radiology and Organ Imaging, Prince of Wales Hospital, Shatin, New Territories, Hong Kong

Purely right-sided diverticulosis is rare in the West but accounts for approximately 68–76% of cases of diverticulosis in the Far East. Consequently right-sided diverticulitis is seen more commonly than in the West. We studied 604 consecutive barium enemas and the pathology, radiology and clinical details of the last 34 cases of diverticulitis, which are presented. None of the patients went to theatre with the correct diagnosis. All but one were considered to have appendicitis and the remaining patient, who had previously had an appendectomy, was thought to have a perforated caecum. Discriminating features that aid a successful preoperative diagnosis of right-sided diverticulitis are: (1) a relatively longer history than appendicitis; (2) a relative lack of constitutional symptoms; (3) the age of the patient; (4) an awareness of the high frequency of right-sided diverticulosis in SE Asian patients.

Buscopan in radiological procedures — should patients drive afterwards?

G. R. J. Sissons
Department of Diagnostic Radiology, University Hospital of Wales, Heath Park, Cardiff CF4 4XN

Buscopan (hyoscine-n-butyl bromide, HBB) is a smooth muscle relaxant regularly used in radiological and endoscopic procedures. One unwanted effect is temporary impairment of visual accommodation. Near and distance vision has been assessed in 100 patients undergoing barium meal and barium enema studies. Visual testing was performed prior to the examination and repeated immediately before leaving the X-ray department. Completed data were obtained in 90 patients. Of these, 37 were given a conventional 20 mg intravenous dose of HBB, 37 were given glucagon and 16 received no drug. No patient showed any impairment of distance vision. Minor abnormalities of near vision were observed in five patients, all of whom had been given HBB, were aged 50 years or under and had been re-tested 12–21 minutes after administration of the drug. It is suggested that the degree of visual impairment observed is not sufficient to impair driving ability and that patients need not be advised to delay their departure on this account. However, an explanation regarding possible changes in near vision is considered appropriate. The other ocular effects of HBB are also discussed.

Ripley Suite

Cardiac Studies (9.00–10.15)

Pharmacological stress in the diagnosis and management of coronary artery disease

S. R. Underwood, D. J. Pennell, R. S. O. Rees and D. B. Longmore
Magnetic Resonance Unit, National Heart and Lung Institute, London SW3 6LY

Some form of stress is essential to the functional assessment of coronary artery disease using non-invasive imaging techniques and dynamic exercise is widely used even though exercise tolerance may not be limited by cardiovascular symptoms. Pharmacological stress is an attractive alternative or adjunct, and dipyridamole has been used successfully with thallium-201 myocardial perfusion imaging despite the fact thats its method of action is poorly understood. It is a powerful coronary arterial dilator and defects of ^{201}Tl uptake occur because of the impaired flow reserve of diseased arteries which leads to a differential delivery to the territories served by diseased and by normal arteries. When given intravenously, it can also cause ischaemia, and possible mechanisms for ischaemia in the face of coronary dilatation include a pressure drop across a stenosis with high flow and a stealing of flow by arteries supplying collateral vessels. In order to investigate the relative importance of these mechanisms, we have compared ^{201}Tl emission tomograms acquired following intravenous dipyridamole with cine MR tomograms acquired under the same conditions in 40 patients with coronary artery disease. Defects of ^{201}Tl uptake were seen in all patients but new wall motion abnormalities were induced in only 60%, indicating true ischaemia in these patients. The patients with ischaemia had more extensive ^{201}Tl defects and more severe coronary artery disease, and were more likely to experience chest pain during the infusion. In a number of patients, alterations in MR signal were seen within the ischaemic myocardium and this is likely to represent alterations in blood content. Forty patients have also heen studied using intravenous dobutamine. This is also a coronary dilator, but is main action is to increase blood pressure, heart rate and contractility. Myocardial blood supply is therefore reduced and demand is increased. In all patients, both defects of ^{201}Tl uptake and of regional wall motion were observed. No adverse side effects were encountered other than chest pain, and most patients preferred the pharmacological stress to dynamic exercise. Dobutamine infusion therefore appears to be an ideal form of stress for MRI and the potential of MRI and spectroscopy in patients with coronary artery disease is obvious. The findings also throw new light upon the mechanism of action of dipyridamole when used during ^{201}Tl imaging.

Notes

Computer-assisted diagnosis of ischaemic heart disease: a system development and clinical trials for the interpretation of nuclear images

Y. Sasaki, M. Tateno, T. Iizuka and M. Horino
Department of Nuclear Medicine, The 2nd Department of Internal Medicine, Gunma University School of Medicine and Shimazu Corporation, Maebashi and Kyoto, Japan

Nuclear medicine procedures are applications of tracer technology to medicine, used for evaluation of tissue functions. Quantitative analysis and imaging of regional organ functions have been combined by the aid of computer systems since late 1960s. Image processing in nuclear medicine has been widely used in the study of heart diseases. In order to achieve efficient operation of routine nuclear medicine procedures, image processing computers in nuclear medicine were linked to the hospital information system (HIS). The third computer system was added, which is used for reporting the results of the studies and to construct a relational data base. Furthermore, artificial intelligence (AI) function was developed to support image interpretation and reporting. The system was applied to cardiac studies such as ^{201}T1 myocardial scintigraphy and ECG-gated cardiac blood pool scintigraphy (MUGA) for the diagnosis of ischaemic heart disease (IHS). The purpose of this presentation is to describe the whole scope of our computer-aided system for the diagnosis of IHS. The emphasis is put on the AI system for the interpretation of bull's eye display and MUGA. The bull's eye display of SPECT is transferred to the data base of the patient information management system (PM). When inference request is made, the feature extraction program extracts information on the extent, severity and localization of decreased count rates, comparing the data pixel by pixel with that obtained from seven normal controls. The inference engine is activated to determine the presence of focal defects, utilizing diagnostic rules in the knowledge base. The results are sent back to PM and reported, with the probability of assurance. Initial clinical trials on 58 patients revealed good agreement between nuclear physicians (NP) and AI. The system is useful, as it enables efficient implementation of nuclear medicine procedures and also provides NP with complementary and supportive information for interpreting and reporting nuclear medicine images.

MR measurement of cardiac output using cardiac-gated acquisition

M. Tarnawski, T. S. Padayachee, M. J. Graves and P. E. Graves
Division of Radiological Sciences, UMDS, Guy's Hospital, London SE1 9RT

MRI can be used to provide quantitative velocity and flow information by using phase difference pulse sequences. We have applied a cardiac-gated flow-adjusted gradients (FLAG) pulse sequence to measure time-averaged flow in the ascending aorta and pulmonary artery of healthy volunteers. Data acquisition was performed on a 1.5T whole body system (Philips, Gyroscan). A minimum trigger delay of 8 ms was used for the first image with successive images obtained at 34 ms intervals. The number of images acquired was typically 17–20, which covered the systolic and most of the diastolic phase. The sequence used an rf flip angle of 45°, TE = 17 ms, a 256^2 data matrix and 1 signal average giving a scan time of 7-8 min. The images were analysed using a quantitative flow analysis program (Sun 3 Workstation). The region of interest was defined from the velocity-compensated modulus image and then used on the phase image for calculation of the area and average velocity. Each image yielded an instantaneous flow value. Flow values from the complete set of images were integrated to give the time-averaged flow. The results indicate that signal loss during the decelerative phase of systole leads to an underestimation of flow, particularly in the ascending aorta. This can be explained by both spatial and temporal averaging of the data due to voxel size and relatively long TE. The implications of the above for *in vivo* flow measurement using the cardiac-gated FLAG method are discussed.

Comparison of bull's eye polar maps and added circumferential profiles of detection of coronary artery disease using ^{99}Tc^{m} MIBI SPECT

M. Ünlü, B. Erbas, T. Aras, *F. Özmen, C. F. Bekdik and G. Erbengi
*Departments of Nuclear Medicine and *Cardiology, Hacettepe University Medical Faculty, Ankara 06100, Turkey*

In the diagnosis of coronary artery disease (CAD), two quantitative methods for the evaluation of ^{99}Tc^{m} methoxy isobutyl isonitryl (MIBI) myocardial perfusion SPECT studies, bull's eye polar maps (BL) and added circumferential profiles (ACP) were assessed for their diagnostic values and compared with qualitative visual evaluations (VE) and coronary angiography results (CA), in 11 normals (six men, five women, mean age: 44±5) and 24 patients with CAD (20 men, four women, mean age: 50±9) whose CA demonstrated 50% or greater stenosis in one or more coronary arteries. Tomographic studies were performed using 180°, 6°, 30 inch data sampling technique for exercise and rest in two different days. ^{99}Tc^{m} MIBI percentage uptake values were obtained from apical, mid and basal parts of five myocardial segments which were determined according to the supplying coronary arteries. Percentage uptake values of normals were taken as references, considering gender differences. The following results were obtained:

CA	*n*	VE (%)	BL (%)	ACP (%)	
3 vessel	10	76	96	93	sens.
2 vessel	4	50	75	87	sens.
		75	75	75	spec.
1 vessel	10	80	90	90	sens.
		68	75	80	spec.

CA	*n*	VE	BL	ACP
LAD	21	20 (95%)	21 (100%)	21(100%)
LCX	12	3 (25%)	9 (75%)	10 (83%)
RCA	15	11 (73%)	13 (86%)	12 (80%)
Total	48	34 (71%)	43 (90%)	43 (90%)

	Sensitivity (%)	Specificity (%)	Accuracy(%)
VE	74	69	72
BL	90	75	85
ACP	91	79	87

In conclusion, between two quantitative methods no statistically significant difference was observed. But both methods are found more sensitive in the diagnosis of three vessel CAD patients and in the detection of LCX lesions than VE. Moreover, with BL and ACP analysis false positive results were less frequently encountered.

Comparison of ultrafast CT and MRI for cardiac diagnosis

R. M. MacMillan, M. R. Rees, J. Ivanoff and M. E. Haskin
Departments of Cardiology and Radiology, Hahnemann University Hospital, Philadelphia, PA 19102, USA

Ultrafast CT using an Imatron C-100 scanner and MRI using a GE 1.5 T Signa scanner can acquire images of the heart and great vessels with excellent spatial and temporal resolution. Image acquisition time is 50 ms for CT and 33 ms for MRI. Slice thickness is 8 mm for CT and 3, 5 or 10 mm for MRI. Eight contiguous slices can be acquired in 220 ms (CT), while cine MRI requires gated acquisition times of 256 divided by heart rate per pair of slices. CT has limited slicing planes based on table positioning while MRI can scan in any plane. Advantages of MRI are: no radiographic contrast is required; no X-irradiation is used; totally non-invasive. Advantages of CT are: no gating required; short multislice acquisition times; can be performed with irregular cardiac rhythm; safe for pacemakers and other implanted devices. CT and MRI can evaluate atrial and ventricular cavity dimensions, ventricular volumes, mass and wall motion, pericardium, hypertrophic cardiomyopathy, congenital heart disease, extra- or intra-cardiac tumours, cardiac valves, aortocoronary bypass patency and aortic aneurysms. The normal and pathological anatomy of similar cases shown by both techniques is contrasted and compared, and the physiological data derived is discussed, with advantages and disadvantages of each.

Mammography (10.45–12.00)

Mammographic and histological classification of 100 patients requiring biopsy from the Manchester Breast Screening Programme

D. A. Nicholson, C. R. M. Boggis, J. P. R. Jenkins, D. L. Asbury and G. H. Hartley
Breast Screening Unit, Department of Radiology, University Hospital of South Manchester, West Didsbury, Manchester M20

The mammograms and histology of the first 100 patients from the Manchester breast screening programme who have undergone excision biopsy were reviewed retrospectively. All patients underwent excision biopsy or wide local excision, 46 after needle localization. The radiological features in terms of mass type, size, location, density, clarity of margin, spiculation, microcalcification, architectural distortion and skin thickening were assessed independently of the final histological diagnosis. In the 100 patients, 56 had a radiological mass (15 with associated microcalcification), 38 showed microcalcification alone, the remaining 6 showed spiculation or architectural distortion. Forty-nine cases (age range 50–79 years, mean 60.8 years) proved malignant (39 ductal and 10 lobular carcinomas), 46 were benign (age range 50–65 years, mean 56.1 years). Five showed borderline histology, three with atypical ductal hyperplasia and two lobular carcinomas *in situ*. Of the 49 malignancies, 36 had clinically palpable masses (range 10–80 mm), with only 13 requiring needle localization. Pre-operative radiological assessment was reliable, with 41 of the 49 being graded as suspicious or malignant. Of the 46 benign cases, only 17 had clinically palpable masses, 29 requiring needle localization, mainly for microcalcification. The majority (28 patients) were radiologically uncertain. The ratio to benign to malignant biopsies performed is less than that predicted by the Forrest recommendations. The radiological features of benign and malignant lesions are discussed with reference to the implications regarding surgery and radiotherapy.

Can magnetic resonance imaging replace axillary lymph node sampling in the management of breast carcinoma? A prospective study

H. G. Lewis-Jones, M. Newstead, S. J. Leinster and G. H. Whitehouse
Magnetic Resonance Research Centre, University of Liverpool, PO Box 147, Liverpool L69 3BX

The aim of this study was to compare the efficacy of surgical axillary lymph node sampling with Magnetic Resonance Imaging (MRI) of the axilla. Forty patients with biopsy-proven breast carcinoma were studied by MRI prior to surgery. Images were obtained in the axial and coronal planes using T_1- and T_2-weighted sequences. All the patients proceeded to either lumpectomy or patey mastectomy combined with axillary nodal sampling. The results of MRI were then compared with pathological findings. MRI was 100% accurate in identifying lymph node involvement in nodes greater than 10 mm in size although no cases of reactive adenopathy were present in this group. Of the remaining cases, masses less than 10 mm in size were shown in 23 cases. In 14 of these, multiplanar imaging showed vessels to be the cause of the defects, but in the remaining nine the appearances could only be attributed to non-enlarged nodes. Unfortunately chemical shift artefact obscured all tissue characterization information in the normal-sized lymph nodes and we could not therefore differentiate the four cases with microscopic evidence of tumour. Nevertheless, a protocol for MR investigation and interpretation is proposed, which could significantly reduce the number of patients who would require sampling, yet retain overall accuracy. We also report preliminary results of surface coil studies.

The individual and training in mammographic screening

G. E. Walker, A. G. Gale, *E. J. Roebuck, *A. R. M. Wilson and B. S. Worthington
*Division of Radiology and *Breast Screening Training Centre, University and City Hospitals, Nottingham NG7 2UH*

Breast cancer screening raises the questions of how best to train radiologists for the task and how appropriate is the training for each individual? During a 2-year period (1988–1989), approximately 75 radiologists attended the multidisciplinary training course in mammographic screening at Nottingham. As part of this course their film-reading ability was studied by reporting on a set of 100 screening mammograms in order to obtain a baseline performance measure. Variations in this were found as, although all participants were qualified radiologists, their experience of mammography varied from none at all to some symptomatic work. Tests of aptitude and personality assessments were also administered. Those radiologists who underwent a period of further specialist training were again asked to read the same test films. Signal detection theory was then applied to the results of both sessions, producing ROC curves for each individual. Improvements in performance were examined and correlated with the psychological test scores. Reasons for variability in the individuals' film reading performance are discussed and related to the training offered.

Mammographically demonstrated asymmetrical thickened ducts: a sign of ductal carcinoma *in situ*

A. M. Wood, C. R. M. Boggis, D. L. Asbury and G. H. Hartley
Department of Radiology, Withington Hospital, Manchester M20 0PT

Asymmetrical glandular appearance on mammography always necessitates further evaluation. Additionally, a prominent duct pattern to the gland tissue has been associated with an increased risk of breast carcinoma. We present four cases where mammography demonstrated an area of thickened duct-like structures, broader than equivalent structures elsewhere in the same breast or in the contralateral breast. None of these areas was primarily subareolar and all were ultimately associated with mixed calcifications. Histological findings following surgical biopsy showed extensive ductal carcinoma *in situ* (DCIS) in three patients. The fourth patient's mammographic abnormality progressed over three years from the features summarized above to a mammographically malignant mass. After surgical removal, this was found to be invasive duct carcinoma. We think that this type of asymmetrical thickened duct pattern should alert the radiologist to the possible presence of extensive DCIS. Thus DCIS may be diagnosed more confidently, rather than found serendipitously at a breast biopsy instigated by the radiologist for equivocal radiological findings. Any increase in the confidence levels of diagnosis of early malignant breast disease in the context of our national breast cancer screening programme would be beneficial.

Film processing in mammography

A. Servomaa, M. Tapiovaara and *K. Ceder
*Finnish Centre for Radiation and Nuclear Safety, and *Helsinki University Central Hospital, Helsinki, Finland*

Optimized film processing is an important factor for image quality and breast dose in mammography. Film processing in mammography has been studied sensitometrically by varying developer temperature between 31° C and 36° C and processing time between 90 s and 240 s. Measurements were made for four brands of mammographic film and two brands of processing chemical. Contrast, relative speed, base plus fog and maximum optical density were analysed. The results show that contrast, relative speed and maximum density increase with developer temperature or processing time, but the increase owing to processing time is more significant. The toe region contrast does not behave like the other contrast indexes; the maximum is reached with long processing time and low developer temperature. Film speed varied by a factor of four within the range of processing conditions studied.

Notes

Mammographic screening: what do radiologists look for?

A. G. Gale, G. E. Walker, *E. J. Roebuck, *A. R. M. Wilson and B. S. Worthington
*Division of Radiology and *Breast Screening Training Centre, University and City Hospitals, Nottingham NG7 2UH*

Elucidating which mammographic areas have actually been visually examined in detail and which have not is a key factor in understanding the difficulties and source of errors made by individual radiologists during training for breast cancer screening. Consequently the visual search strategies of radiologists were recorded as they inspected the same test set of screening mammograms. Experts first read the films and reported on the presence of abnormalities as well as other key radiological features. Radiologists in training at the Nottingham Breast Screening Training Centre also performed the same task. The eye movement data from both groups were analysed for overall research strategy, mammographic areas examined and the amount of time spent attending to specific areas. This information was then related to the trainees' performance in reporting the films and identifying features. Variations between the trainees and the experts are considered. The data are also discussed with regard to understanding the processes underlying errors and in relation to training.

The Nottingham breast marker localization set

A. R. M. Wilson, I. O. Ellis, E. J. Roebuck and R. W. Blamey
Breast Screening Training Centre, Nottingham City Hospital, Nottingham NG5 1PB

Breast cancer screening has resulted in a large increase in the number of impalpable breast lesions requiring marker localization prior to open biopsy. As well as enabling the surgeon to accurately locate an impalpable lesion, marker localization should allow the surgeon to achieve the best possible cosmetic result. In our experience none of the marker techniques or equipment available are ideal for these purposes. The dye and carbon particle techniques often require the surgeon to excise a larger specimen than necessary. Hooks or curved fine wires are too easily displaced and are difficult to find within the breast at surgery. The Reidy X wire has solved these problems but may interfere with accurate pathological assessment of the excised specimen. In conjunction with Mediplus Ltd, the Nottingham breast team has developed a breast marker localization set which can be easily and accurately placed, may be left in situ without fear of displacement, is comfortable for the patient, can be easily located within the breast at surgery and can be removed from the biopsy specimen without need to dissect the specimen. We describe this new marker wire and outline its use in achieving accurate breast lesion localization.

Computer-aided interpretation of screening mammograms: a feasibility study

S. M. Astley, C. R. M. Boggis, J. P. R. Jenkins, D. L. Asbury and C. J. Taylor
Department of Medical Biophysics and Manchester Breast Screening Service, University of Manchester, Manchester M13 9PT

Systematic mammographic analysis methods are employed by radiologists; however, significant observer variability exists and high error rates have been reported. We have investigated the feasibility of using computer-based image analysis methods to improve the accuracy and objectivity of mammographic interpretation. Computer-based image analysis techniques were developed for the detection of mammographic abnormalities, including spiculation, mass lesions, asymmetry and microcalcifications. A pilot study was also undertaken, investigating the effects of digitization and feature enhancement of radiologists' performance in interpreting mammograms with subtle abnormalities. Three radiologists independently reviewed previously unseen mammograms of 12 patients without clinical information. Prior training, using a different set of self-selected mammograms, was provided. Results show that interactive enhancement of digitized mammograms can increase diagnostic confidence, although difficulties were encountered in defining microcalcification. Methods for detecting mammographic abnormalities show potential, but require further rigorous assessment. Possible applications of this technology to mammographic screening include detection of specific radiological signs and the provision of reproducible, quantitative information about suspicious regions.

Notes

Ultrasound Studies (2.30–3.45)

The current status of transrectal ultrasonography in the diagnosis and management of diseases of the prostate

G. J. Griffiths
Radiology Department, Royal Gwent/St Woolos Hospitals, Newport, Gwent NP9 2UB

There is a need in clinical urology for an objective imaging technique which might be applied to the prostate. Transrectal Ultrasonography (TRUS) provides a simple, safe method of assessing the prostate gland. Serial examinations have been performed on over 8000 patients with malignant and benign prostatic disease. The extent of the disease, including involvement of the periprostatic structures, has also been determined. The correlation of TRUS, microradiography and histopathology of matching slices of the cadaver prostate is used to support the interpretation of the ultrasonic features of normal and pathological states. The importance of assessing the seminal vesicles and ejaculatory ducts is also discussed. The significance of calcification in benign and malignant disease has also been evaluated. The ultrasonic volume of the prostate gland has been compared with the actual volume of the cadaver gland and the volume determined by digital rectal examination. The aims and objectives of this review are to demonstrate the value of TRUS in the diagnosis and management of patients with prostatic cancer, benign hyperplasia and prostatic inflammation. Other clinical applications such as ultrasound guided biopsy and aspiration techniques are also discussed. The importance of the size of the primary tumour in prostatic cancer in relation to prognosis is emphasized and this opens an exciting area for TRUS.

Ultrasound of the post surgical thyroid

A. Ahuja, K. Ng, I. Birchall and C. Metreweli
Department of Diagnostic Radiology and Organ Imaging, Prince of Wales Hospital, Chinese University of Hong Kong, Shatin, New Territories, Hong Kong

We present the ultrasound appearances of the post thyroidectomy neck which have not been described previously. The type of thyroidectomy (hemi, partial, subtotal or total) and presurgery pathology influence the post-operative appearance. Patients are examined with an SDU 7000 7.5 mHz static B-scan to produce multiple axial and sagittal slices. Our results show that ultrasound of the thyroid reveals differences in shape and texture from the normal which must not be confused with recurrence or malignancy, in particular the superior pole hypoechogenic clusters of total thyroidectomy. Frequently there are discrepancies between the ultrasound appearances and the surgical record, with ultrasound showing less of the gland removed than the surgeon described. The object of this paper is to present these various appearances to the radiologist unfamiliar with the post-operative thyroid.

Dynamic scanning in the assessment of intraocular abnormalities

J. A. Fielding
Department of Radiology, Royal Shrewsbury Hospital (North), Mytton Oak Road, Shrewsbury, Shropshire SY3 8BR

Most radiologists have access to currently available sector scanners, whose small-parts probes are eminently suitable for eye scanning. Dynamic scanning is carried out when the patient moves the eyes from side to side, which induces movements in pathological intraocular structures. Observation of these movements is of value, both in making the diagnosis, and in assessing surgical approach. The technique is of particular value when the light-conducting media of the eye are opaque to direct opthalmoscopy, for example in the presence of cataract or haemorrhage. Knowledge of the anatomy of the coats of the eye, the vitreous, and the internal attachments of intraocular structures is of great relevance when observing intraocular movements during dynamic scanning. The type of motion exhibited by some structures may be the only clue to diagnosis, and furthermore, mobility or fixity of detachments are good indicators of surgical prognosis. Although scanning the eye at rest yields useful information, vitreous detachment may mimic RD, retrogyaloid haemorrhage may mimic subretinal haemorrhage, and haemorrhage itself may mimic a choroidal tumour. Dynamic testing demonstrates the typical motion of the detached vitreous gel mass, as an elastic body, whereas the detached retina undulates as a membrane. Examples of a range of conditions are presented, amassed over the 7 years' existence of the eye scanning service, demonstrating the value of this simple technique.

The role of ultrasound in the investigation of the salivary gland

E. J. McAteer, M. Chapman and P. L. Allan
Department of Radiology, Royal Infirmary, Edinburgh EH3 9YW

Sialography has several disadvantages including: difficulty gaining access, the time consumed and the high false negative rate (up to 20% for tumours). Forty-five patients who presented with symptoms of salivary gland diseases studied using real-time ultrasound with a 5 mHz linear array transducer (Acuson). The normal ultrasound anatomy and relationships of the parotid and submandibular glands were defined. Each subject had sialography performed and the two methods compared. Using ultrasound, eight cases of calculous disease of the submandibular gland were diagnosed: six cases were confirmed by sialography, two had failed sialography and one case was demonstrated on sialography but not demonstrated by ultrasound. The ultrasonic appearances of sialiectasis were shown in 12 cases, 11 of which were confirmed using sialography.

Four subjects with masses in the parotid gland were assessed with ultrasound; all subjects had normal sialography. The ultrasonic appearances of the mass lesions were demonstrated, involvement of surrounding structures assessed and correlated with pathological findings. Ultrasound is a rapid method of assessing the salivary glands. It is relatively inexpensive, and surrounding structures and the other salivary glands can be imaged. It is as sensitive as sialography for calculous disease and sialectasis; and very sensitive in the diagnosis of mass lesions.

The ultrasound features of 40 peripheral haemangiomas

I. Stewart, M. Bradley, K. C. Ho, W. King and C. Metreweli
Departments of Diagnostic Radiology and Organ Imaging and Surgery, Prince of Wales Hospital, Chinese University of Hong Kong, Shatin, New Territories, Hong Kong

Liver haemangiomas are common and the ultrasound features well known; peripheral haemangiomas are rare and the ultrasound features not well known. We describe the ultrasound findings of 40 patients with peripheral haemangiomas, all confirmed by $^{99}Tc^{m}$ RBC scintigraphy. Ultrasound was performed with an Aloka SSD 650 3.5 and 5 mHz convex probes. Scintigraphy was performed with a semi *in vitro* method using 15 mCi of Tc pertechnetate. Forty patients were examined: 10 had head and neck haemangiomas including five parotid haemangiomas; six had upper-limb and 24 lower-limb haemangiomas. All haemangiomas were demonstrated with ultrasound. The majority of limb lesions were intramuscular. The haemangiomas showed a wide spectrum of echo features: only two features were constant, namely disruption of the normal anatomy and poor edge definition. The diagnosis of peripheral haemangiomas can only be suspected with ultrasound. Confirmation of the vascular nature of the lesion is required before invasive methods are attempted.

Techniques for 3D volume imaging with ultrasound

J. E. Gardener and W. R. Lees
Medical Physics and Radiology Departments, University College and Middlesex Medical School, London WC1

There has recently been considerable interest in the presentation of views of 3D sets of section images, typically from CT and MRI studies and more recently in sonography, where slow reconstruction methods may appear unsatisfactory compared with normal clinical techniques. We have developed a system based on high-speed, low-cost transputer technology, which provides for very rapid interactive manipulation of a 3D scan set. Video data is acquired and stored at near real-time rates, providing for a simple and low cost add-on to most types of scanner. Once acquired, the 3D array of data may be immediately displayed by rapid interactive positioning of a "view section" through the data volume, in a manner similar to, but much more flexible than, normal sonography techniques, at rates of up to five frames/s. The system can also generate a range of views not available to the normal scanner, for example: as a curved section; a density projection; a shaded surface extracted from the data; or other processed formats. An immediate benefit results from the storing of complete volume information for subsequent diagnostic review or for surgical planning. Other applications include generation of novel or "inaccessible" views to resolve questions about complex structures, and quantitative measurements in 3D. We have used the system for a range of clinical investigations including endoscopic studies of the oesophagus and rectum using a standard rotating endoscopic transducer, *e.g.* to help assess tumour extent and penetration. It has also been used with a new ultrasound angioscopy system to make intravascular measurements of atherosclerotic plaque. The system can produce a standard video output, which may be recorded on videotape (examples shown).

Umbilical artery Doppler in high risk pregnancy: relationship to outcome

P. Twining, J. Swallow and E. Lewin
Department of Radiology, University Hospital, Queen's Medical Centre, Nottingham NG7 2UH

Over a 12-month period systolic/diastolic ratios of umbilical artery blood flow were obtained in 119 high-risk pregnancies. The main indications for a Doppler study were: suspected or documented growth retardation, pregnancy induced hypertension and reduced fetal movements. Systolic/diastolic ratios were classified into four groups: I. normal; II. a raised ratio which subsequently returned to normal; III. raised systolic/diastolic ratio but positive diastolic flow; IV. absent end diastolic flow. Patients with absent end diastolic flow had significantly higher Caesarean section rates, and Caesarean section for fetal distress was five times higher. Fetuses with absent end diastolic flow were delivered at an earlier gestational age (33.6 weeks), had lower birth weight (1.68 kg) and spent more time on the Special Care Baby Unit (15.4 days) than fetuses with normal ratios (38.6 weeks, 2.7 kg and 1.2 days, respectively). Patients with raised ratios but positive diastolic flow were delivered of babies with intermediate values for gestational age at delivery (37.6 weeks), birth weight (2.2 kg) and Special Care Baby Unit stay (6.2 days). In conclusion, we feel that umbilical artery Doppler is a useful parameter in monitoring high-risk pregnancies. Abnormal Doppler ratios are associated with an adverse outcome.

The sonographic features of post-partum thyroiditis

H. Adams, M. C. Jones, S. Othman, C. J. Richards and J. H. Lazarus
Departments of Radiology and Obstetrics, Caerphilly District Miner's Hospital, Caerphilly, and Department of Medicine, UWCM, Cardiff

During the post-partum period there is an increased incidence of acute auto-immune thyroiditis in women with anti-thyroid auto-antibodies. This study was designed to determine the sonographic appearances and volumetric changes in thyroids of patients with post-partum thyroiditis (PPT). Thyroid ultrasound was performed in 85 women between 15 and 25 weeks post-partum using either a 5 MHz sector scanner with stand-off gel or a 7.5 MHz linear array. Patients were divided into three groups according to thyroid status: Group 1, (23) patients with PPT; Group 2, (28) patients with thyroid auto-antibodies but no biochemical evidence of PPT; Group 3, (34) age-matched controls. Mean thyroid volume in PPT patients (20.0 ml ± 2.1 ml (SE)) was significantly greater than the mean volume in both Group 2 (13.5 ml ± 0.94 ml, $p<0.01$) and Group 3 (10.6 ml ± 0.67 ml, $p<0.001$). Mean volume was significantly greater in Group 2 than Group 3 ($p<0.02$). The characteristic sonographic appearance in PPT was focal or generalized decrease in thyroid echogenicity and this was present in 22/23 patients (96%) with PPT, 11/28 (39%) in Group 2 and 0/34 in Group 3. Thyroid ultrasound demonstrates significant morphological changes in patients with PPT. Thyroid damage can also occur in antibody-positive patients in the absence of thyroid dysfunction. Sonography may have a useful role in the evaluation of antibody-positive patients during the post-partum period.

The Venetian blind sign — an unusual ultrasound appearance in uterine fibroleiomyomas

R. J. Davies and A. E. A. Joseph
Department of Diagnostic Radiology, St George's Hospital, London SW17 0QT

Uterine fibroids occur in up to 40% of women over 35 years of age and ultrasound is generally regarded as the most accurate means of diagnosis. A variety of ultrasonic appearances area seen, however, and some of these may cause diagnostic difficulties by simulating other pelvic conditions. The Venetian blind sign — a pattern of alternating acoustic shadows and through transmission — is an unusual appearance of a fibroid that may occur and be confused with an ovarian dermoid. The Venetian blind appearance is also known to occur in other situations such as in the liver in hepatoma, and ultrasound/pathological correlation in these conditions is presented.

Ultrasound markers in chromosomal disease: a retrospective study

P. Twining and J. Zuccollo
Departments of Radiology and Histopathology, University Hospital, Queen's Medical Centre, Nottingham NG7 2UH

Over a 12-month period 24 pregnancies were complicated by a chromosomal abnormality. Antenatal and postnatal scans were reviewed and post-mortem specimens were also assessed for potential ultrasound markers. All four cases of Turner's syndromes demonstrated a cystic hygroma and two cases also showed hydrops. In the two cases of Trisomy-13, holoprosencephaly with midline facial clefting, polydactyl and growth retardation were seen. In the three cases of Trisomy-18, diaphragmatic hernia and abnormalities of the extremities were common findings. Choroid plexus cysts, growth retardation and cardiac anomalies were also demonstrated. In the 14 cases of Trisomy-21 the main abnormalities were cardiac. There were three atrioventricular canal defects, one hypoplastic left heart syndrome and one small ventriculo-septal defect associated with duodenal atresia and choroid plexus cysts. In the single cases of triploidy 69xxx, the most marked finding was a large hydropic placenta. From the antenatal scans, only eight cases of chromosomal disease were suspected. However the routine assessment of cardiac structures at 18 weeks' gestation should detect more cases of Down's syndrome. The presence of choroid plexus cysts, diaphragmatic hernia and growth retardation should prompt assessment of the extremities for markers of Trisomy-18 and 13. The ultrasound markers of chromosomal disease are demonstrated with pathological correlations.

Ultrasound in the diagnosis of gallstone ileus

R. J. Davies, F. A. Sandrasagra, A. E. A. Joseph and P. Ignotus
Department of Diagnostic Radiology, St George's Hospital, London SW17 0QT

Gallstone ileus accounts for up to 25% of al non-malignant causes of small bowel obstruction in those over 65 years of age and is readily treatable. The diagnosis is often a difficult one, however, and the characteristic plain radiographic features are present in only one third of cases. Recent studies have shown that ultrasound can be useful and demonstrate small bowel obstruction, pneumobilia, and ectopic gallstones which clinches the diagnosis in the absence of plain radiographic features. We present two patients from our unit in whom gallstone ileus was diagnosed by ultrasound alone. A third patient with identical ultrasonic features was found to have distal small intestinal obstruction caused by adhesions around a calcified mesenteric lymph node. Ultrasound is useful in the diagnosis of gallstone ileus when the plain abdominal radiographs are inconclusive.

Bramham Suite

Evaluation of Skeletal Metastases (9.00–12.00)

Organizer and Chairman: Dr M. Merrick, Edinburgh
Panel: J. S. M. Beales, Stevenage; N. Garvie, London; R. Leonard, Edinburgh

A practising clinical oncologist, a general radiologist and a nuclear medicine specialist review the clinical role of bone scintigraphy in lung, breast, prostate and bladder cancer and in the lymphomas. Each disease is considered separately and in depth. The panel, with the participation of the audience, attempts to come to a consensus defining the most effective use of skeletal investigations of these conditions.

Notes

Teach-in: Interpretation of Mammograms (2.30–3.45)

Organizer: Dr C. Parsons, London

The session concentrates on the implicationss of normal variants and abnormalities seen on mammograms. The essential questions are: (1) What, if anything, do you do once an "abnormality" has been observed? (2) Why are the patients managed as they are? (3) How well does the natural history of breast disease support current practice? The topics discussed include: asymmetric breast density, opacities due to overlapping normal structures, solitary smooth round opacities, fibrocystic change, ductal and lobular carcinoma *in situ*, the various apppearances of infiltrating cancers, assessing response to primary medical treatment, specimen and localization procedures.

Charter Suite

Advances in Oncology (9.00–10.15)

Conformal radiotherapy

A. E. Nahum
Joint Department of Physics, Royal Marsden Hospital and Institute of Cancer Research, Sutton, Surrey SM2 5PT

Improvements in the local control of tumours in a significant number of patients could be achieved by increasing the dose to the tumour. However, tumour dose is frequently limited by the tolerance of normal tissues to radiation damage, which is in turn related to the volume of normal tissue irradiated. CT shows that the tumour or target volume is generally an irregularly-shaped 3D volume which is much smaller than the box-shaped high-dose volumes (HVLs) usually prescribed. Conformal therapy aims to shape the HVL to conform to that of the target volume, thereby reducing the volume of normal tissues irradiated. The different ways of shaping the high-dose volume are discussed: custom blocking, the multi-leaf collimator (MLC), non-uniform beams and dynamic therapy. Impressive results can be achieved but at the expense of simplicity. The MLC appears to offer the most practical way of improving conformity and hence increasing local control rates, particularly for pelvic tumours.

Notes

Megavoltage imaging: New methods and applications for radiotherapy

W. Swindell and P. M. Evans
Department of Physics, The Royal Marsden Hospital, Sutton, Surrey SM2 5PT

Herman Suit (1982) proved theoretically that cancer patients could benefit from significant and worthwhile gains in survival if treatment methods could be modified to improve local control rates. Kinzie et al (1982) confirmed this prediction, in a particular case of radiotherapy treatment, with a retrospective study of 98 patients with Hodgkin's disease. There is a strong incentive to realise these potential gains on a wider basis and conformation therapy is widely held to offer an excellent chance of accomplishing this. In conformation radiotherapy the high dose margins are narrowed and shaped to make the treatment volume conform as closely as possible to the target volume. It has the potential to improve the local control rate because less normal tissue is involved and higher doses can therefore be applied to the target. However, great care must be taken when positioning the patient on the treatment machine to ensure that the target volume (which is referenced to the patient) is correctly positioned relative to the treatment volume (which is referenced to the machine). The traditional method of verifying the position of the patient involves the use of photographic film but there is now an increasing interest in digital imaging techniques which have many advantages over film, especially in the context of high-precision treatment. Several centres around the world have been developing new methods for imaging, using the treatment beam as the source of imaging radiation, and as as result, commercial versions of megavoltage imaging systems are beginning to appear. The technical aspects of these imaging methods are reviewed and the merits of these systems relative to film discussed. Examples of clinical images and their applications are shown.

References

Kinzie, J. J., Hanks, G. E., Maclean, C. J. & Kramer, S., 1982. Patterns of care study: Hodgkin's disease relapse rates and adequacy portals. *Cancer*, 2223.

Suit, H., 1982. *Cancer*, *50*, 1227–1234.

Bladder cancer and magnetic resonance imaging

R. A. Persad, D. A. Gillatt, J. B. Penry and J. C. Gingell
Department of Urology, Southmead Hospital and Bristol Royal Infirmary, Bristol BS2 8HW

The accurate staging of transitional cell carcinoma (TCC) of the bladder is essential in order to offer the correct treatment to patients with the condition. In particular, the detection of invasion into the muscle layers or into adjacent organs will affect both prognosis and the treatment available. The value of Magnetic Resonance Imaging (MRI) for staging bladder cancer has been studied. Thirty-six patients with a diagnosis of TCC of the bladder were studied. In each case MRI scans were obtained in three dimensions — sagittal, coronal and transverse — on a Picker Vista 2 500 0.5 Tesla scanner. The spin sequences used included T_1-, T_2-weighted and STIR (short tau inversion recovery). Clinicopathological data were obtained in each patient and included clinical stage, tumour grade and pathological stage. Pathological stage was assessed by examination of tissue obtained at transurethral resection (*n*=30) or cystectomy (*n*=17). In 22 cases the tumour was pTa or pT1 (non-invasive), in 15 pT2 or pT3 (muscle invasion) and in 10 pT4 (invasion through the bladder wall). In 41 cases the MRI scan agreed with the clinicopathological staging, in four cases the MRI scan understaged and in two overstaged the disease. MRI offers an accurate method of imaging TCC that has extended beyond the wall of the bladder. There are a significant number of both false positives and false negatives, the main problem being the differentiation of non-invasive from muscle-invasive disease. The use of a contrast agent (gadolinium-DTPA) to improve the results of imaging is also discussed.

Computed tomography in carcinoma of the bladder

M. J. Charig and S. J. Golding
Regional CT Unit and University Department of Radiology, Churchill Hospital, Oxford OX3 7LJ

A study was undertaken to determine the role of computed tomography in the management of carcinoma of the bladder in a general oncology service in which only CT referrals relevant to clinical management were accepted. Two hundred and sixty-eight patients underwent 490 examinations between 1982 and 1989. Two hundred and twenty-two (45%) examinations were carried out for staging purposes and 205 (42%) were for CT-assisted radiotherapy planning. Examinations to monitor therapy and to detect recurrence were less common — 24 and 19 (5% and 4%), respectively. Nine (2%) were assessments prior to cystectomy. Enlarged lymph nodes were detected in 26 (5.3%) patients and were noted above the aortic bifurcation in only seven (1.4%). In no case was abdominal lymphadenopathy present without pelvic lymphadenopathy. These results have implications in the planning of examinations, and in the allocation of appointments for CT in patients with carcinoma of the bladder.

Localized recurrence of rectosigmoid carcinoma: CT and MR assessment

C. E. Williams, S. R. Smith and H. G. Lewis-Jones
Department of Radiodiagnosis and Magnetic Resonance Research Centre, University of Liverpool, Liverpool L69 3BX

Twenty patients with suspected local recurrence of rectosigmoid carcinoma were examined by CT (GE 9800) and MR (1.5T GE Signa system) to determine the value of MR and to compare the results. Spin–echo pulse sequences were obtained in the axial and, in some cases, sagittal planes within the pelvis. In 12 patients the demonstrated lesions were confirmed histologically and eight were followed up clinically (four with repeat imaging) up to 14 months. There was tumour recurrence in 15 cases and no recurrence in five. The sensitivities of CT and MR were both 87%, while the specificity of MR was 60% as compared to 40% for CT, with an overall accuracy of 80% for MR and 75% for CT. It is concluded that MR lacks specificity but it may have a role in selective cases. The methods, results and illustrative cases are presented and discussed.

Post-surgical CT images are not degraded by use of polydioxonone Ligaclips: advantages for follow-up after para-aortic node dissection for metastatic germ cell tumours

J. S. K. Gelister, D. P. Dearnaley, A. Horwich, W. F. Hendry and *D. M. King
*Departments of Urology and *Radiology, Royal Marsden Hospital, London SW3 6JJ*

Relapse has occurred in 51 of 205 patients with metastatic germ cell tumours treated with chemotherapy and para-aortic node dissection (PAND). The identification`of site(s) of recurrent disease influences treatment and is dependent on accurate CT. While we have found the routine use of stainless steel Ligaclips facilitates PAND, they cause significant CT image degradation and thus interfere with the interpretation of post-surgical CT scans. We have therefore studied the use of absorbable polydioxonone (PDS) Ligaclips during PAND in 10 consecutive patients. CT was performed pre-operatively in both the early (2 weeks) and later (3–6 months) post-operative periods. PDS Ligaclips were easily visible on all early post-operative scans but only faintly visible on six of the later scans, in keeping with absorption. In none of the early or later post-operative scans were PDS Ligaclips associated with any image degradation, thus facilitating radiological interpretation. No complication associated with the use of PDS Ligaclips was encountered. This study shows that PDS Ligaclips, unlike conventional Ligaclips, do not prejudice the interpretation of post-surgical CT scans. Their use increases the sensitivity for the early identification of recurrence following PAND, and can also be recommended for any operation where post-surgical imaging is important.

Notes

Physics (10.45–12.00)

Localization and quantitation in magnetic resonance spectroscropy

M. O. Leach
Joint Department of Physics, Royal Marsden Hospital and Institute of Cancer Research, Sutton, Surrey SM2 5PT

Nuclear magnetic resonance spectroscopy provides a "window" into the body that allows tissue biochemistry and metabolism to be monitored non-invasively. The technique is currently at an early stage in its clinical application, but is already showing promise in a variety of fields. This paper addresses applications in oncology, where the requirements for accurate localization, to acquire signal specific to particular tissues, as well as for signal quantification, to allow individual metabolite signals to be followed with disease progression and treatment, are particularly demanding. Research projects employing NMR spectroscopy in oncology are principally directed at investigating whether NMR spectra provide information of value in differential diagnosis, in monitoring the efficacy of therapeutic regimes, in monitoring the behaviour and distribution of therapeutic agents and in providing insight into the effects of therapy in the patient. The major methods of signal localization employed in NMR spectroscopy are reviewed, together with clinical examples, with particular regard to the demands of the range of applications in oncology. The importance of metabolite quantification in this field is discussed, together with methodology and practical limitations.

Use of field inhomogeneity pulse to correct line shape and broadening spectra in *in vivo* MRS

I. R. Young, *D. R. Page and D. J. Bryant
*NMR Unit, Hammersmith Hospital, Du Cane Road, London W12 0RS, and *IBM Research Laboratories, Winchester, Hants*

Phase images which map field derivations (and which are a by-product of susceptibility mapping (Cox et al, 1986)) potentially provide a means of measuring line-shape and broadening effects in *in vivo* spectroscopy (MRS). We have acquired such maps of regions from which spectra are also measured and evaluated. The field maps are obtained at much higher spatial resolution than the spectra (typically at least 100 times), and the data is plotted in histogram form. This provides a weighted distribution of field against deviation, and allows a direct evaluation of the effective value of T_2^*, using the relationship $1/T_2^* = 1/T_2 + \gamma\delta B_0$. This permits a direct measure of the effective line broadening. The histogram also provides information about the deformation of the ideal Lorentzian line by the field pattern, and its use as a convolution function for simple phantom experiments is demonstrated. The method has been applied to proton spectra of phantoms where line shapes and broadening are known, to determine the terms expected and make adjustments to those obtained. *In vivo* results can be corrected in the same way, which is theoretically a preferable way of minimizing artefacts due to field inhomogeneity, since it determines the correction functions to be applied from actual measurement. Additional experimental time is needed, however, to map the regions from which spectra are to be recovered with adequate spatial resolution.

Reference

I. J. Cox et al, 1986, *Journal of Magnetic Resonance*, *70*, 163–168.

Fat suppression in MRI at low field strength using binomial pulse sequences

C. J. Baudouin, D. J. Bryant and I. R. Young
NMR Unit, Hammersmith Hospital, Du Cane Road, London W12 0HS

Suppression of the signal from fat is useful in several situations in MRI. The STIR sequence is frequently used but is not selective for lipid and is not highly T_1-weighted. A different approach involves selective excitation of fat or water and such sequences can be highly T_1-weighted to provide high sensitivity to contrast enhancement. This approach has been used at high field, but not previously at low field. We have investigated two fat suppression sequences using binomial pulses at 0.15 Tesla: (1) spin echo sequences employing a 121 90° pulse optimized to excite water; (2) a binomial 180° pulse to excite fat followed at time TI by a 90° pulse with spin echo data collect. As in a STIR sequence TI is adjusted so fat has relaxed to the null point. Images have been obtained of the limbs and pelves of volunteers and patients, showing that binomial pulse sequences for fat suppression can be applied at low field strength. However, particularly in regions with large cross-sectional areas, artefacts are more common than with the STIR sequence. A potential application of binomial sequences is to allow visualization of signal alteration due to paramagnetic contrast agents while suppressing the signal from fat.

Motion tagging by spatial modulation

T. W. Redpath
Department of Clinical Physics, Walsgrave Hospital, Coventry CV2 2DX

Spatial modulation of magnetization can be achieved by applying two non-selective rf pulses, separated by a short-gradient pulse, before a conventional sequence, resulting in the superimposition of a regular pattern of stripes on the image (Axel & Dougherty, 1989). The local displacement of stripes reflects the motion of that tissue in the interval between the non-selective rf pulses and the time of signal observation. Application of the technique to T_2-weighted images of the cervical spine provides a straightforward method of mapping pulsatile CSF flow around the cord and brain-stem, provided the images are cardiac-gated. Stripe separations of 6 mm, with echo times of 100 ms, show maximum displacements of the order of 3 mm, corresponding to an average velocity of 3 cm/s, in the interval 150–250 ms after the R-wave. This is in agreement with values measured using an MRI phase-encoding technique (Ridgeway et al, 1987). In its simplest form, spatial modulation superimposes a sinusoidal intensity variation across the whole field of view. Application of a series of rf pulses of different amplitudes can be used to sharpen up stripe edges, in a manner akin to Fourier series analysis of square waves. As an extension to the methods outlined by Axel and Dougherty, a method of producing stripes of variable width, shape and spacing within chosen spatial limits, is described.

References

Axel, L. & Dougherty, L., 1989. MR imaging of motion with spatial modulation of magnetization. *Radiology*, *171*, 841–845.

Ridgeway, J. P., Turnbull, L. W. & Smith, M. A., 1987. Demonstration of pulsatile cerebrospinal fluid flow using magnetic resonance phase imaging. *British Journal of Radiology*, *60*, 423–427.

Receiver coil and sequence choice for optimal renal allograft MR imaging

N. R. Moore, A. K. Dixon, D. B. Evans, C. E. L. Freer, L. D. Hall and C. Sims
Departments of Renal Medicine and Medicinal Chemistry, Addenbrooke's Hospital and Cambridge University, Cambridge CB2 2QQ

Loss of cortico-medullary differentiation (CMD) in renal allografts as shown by magnetic resonance (MR) imaging is indicative of rejection, acute tubular necrosis or other major insult. Because of the rapid advances in MR technology, we have examined 23 patients to determine the optimal receiver and pulse sequence to demonstrate the CMD on a high field system. Fifty-eight imaging sequences were performed, 27 using the body transmit/receive resonator and 31 using a variety of surface receiver coils (spine coil, "knee" coil, "TMJ" coil) either placed directly on the skin or mounted on a special holder. Sequences included multislice dual-echo transverse (TR=2000 ms, TE=20/80 ms), T_1-weighted oblique coronal (700/26), inversion recovery coronal (2000/600/30) STIR coronal (2000/100/30) and gradient-recalled echo coronal (300/13/30° flip angle) techniques. CMD, assessed qualitatively on a scale 0–3 (not visible, just visible, well seen, very well seen), was best demonstrated by thin (5 mm) T_1-weighted oblique coronal sequences using a surface receiver coil mounted on a special coil holder. The TMJ coil proved better than the knee coil provided the kidney was superficial and not very large.

In vivo measurement of the optical parameters of tumour tissue in man

I. Driver, *C. P. Lowdell and *D. V. Ash
*Departments of Medical Physics and *Radiotherapy, University of Leeds, Leeds LS1 3EX*

Photodynamic therapy (PDT) is a new treatment modality which, although now at an experimental stage, may be suitable for many forms of malignant disease. In PDT, visible light (630 nm) is used to activate a photosensitizing agent present in the tumour following its systemic introduction 48–72 hours earlier. Successful treatment requires sufficient quantities of both drug and light to be present throughout the target volume. The light distribution within a treatment volume is determined by the source geometry (*e.g.* superficial or interstitial illumination) and the optical interaction coefficients of the irradiated tissue. We have measured the energy fluence rate at various points within tumours undergoing irradiation with 630 nm light for PDT for several source geometries. The relative positions of source and detector fibres were determined using CT scanning techniques. The results of these measurements were then applied to solutions of the diffusion theory which allowed the determination of the absorption coefficient ($\Sigma_a = 38.4 \pm 6.9\ \mathrm{m}^{-1}$), the reduced scattering coefficient ($\Sigma_s' = 401 \pm 32.5\ \mathrm{m}^{-1}$), the effective attenuation coefficient ($\Sigma_{eff} = 230 \pm 14\ \mathrm{m}^{-1}$) and a coefficient which relates to a surface irradiance to the energy fluence at depth (k' = 0.5). Knowledge of these parameters allows the transmission of light through tissue to be predicted and hence the optical dosimetry of subsequent treatments to be planned more effectively.

Luminescence measurements on X-ray phosphors

G. E. Giakoumakis, C. D. Nomicos and E. N. Yiakoumakis
Physics Department, University of Ioannina, PO Box 1186 - 451 10 Ioannina, Greece

We present the latest results on the luminescence properties of a number of X-ray phosphors and discuss various problems related to the experimental estimation of these properties, including the efficiency and the resolution of the screens, the matching factors between phosphors and photocathodes and the dependence of the luminescence on the various screens and X-ray beam parameters. A report is also given on the methodology and conditions under which the luminescence properties of the phosphor are evaluated, as well as the possible errors arising during such evaluations. Comparative results are presented for excitation in transmission and in reflection. Experimental results are presented for the luminescence of a number of phosphor materials already in use and/or under investigation for X-ray intensifying screens. These results are discussed and explained on the basis of theoretical models (considering either a uniform screen or a granular one) and analytical formulae are derived permitting the theoretical calculation of the luminescence efficiency of the screens. In all cases the agreement between the theoretical and the experimental results proves to be very good.

New computer graphics for medicine and science

S. Rish and *S. J. N. Daniell
*Computer Services Department and *Department of Diagnostic Radiology, St Bartholomew's Medical College and Hospital, London EC1A 7BE*

Medical graphics requirements are different from those for business applications of graphics. We present a computer software package which offers not only the standard facilities but also medically-orientated features not found in business applications software. User friendliness has been enhanced to make the system easily used by anyone with minimal training. The program runs on widely available personal computers. Text and graphics are entered directly onto screen and manipulated using a mouse and a series of menus. In addition, images from computed tomography, ultrasound, magnetic resonance and high-resolution video cameras can be captured, modified and annotated. The most effective layout can be chosen by making instantaneous changes to size, position, spacing, colours, etc. Slides or negatives, in colour or black and white, are produced using a desktop film recorder with a resolution of 4096 x 2730 lines and an almost infinite range of colours. Output can also be plotted or laser-printed. Computer generation of artwork allows an image to be rapidly designed, displayed and altered to achieve maximal effect. This new software gives advantages over other current programs for medical and scientific users.

3D microscopic computed tomography

S. Webb, E. J. Morton, *J. E. Bateman, †L. J. Clarke and †C. G. Shelton
*Joint Department of Physics, Institute of Cancer Research and Royal Marsden Hospital, Sutton, Surrey, *SERC Rutherford Appleton Laboratory, Chilton, Oxon OX11 0QX and †Thornton Research Centre (Shell Research Ltd), Chester CH1 3SH*

X-ray microscopy allows non-destructive study of small (micron-size) structures. Digital capture of X-ray projection images allows further possibilities for image processing and tomography. We have combined a microfocal X-ray generator with a multi-step avalanche/multiwire proportional counter to produce a digital X-ray microscope with around 10-micron spatial resolution at the highest magnification. Samples were placed on a rotating goniometer arranged between source and detector with typical magnifications of 5–30. Projection data taken at multiple orientations have been reconstructed using cone-beam convolution-and-back-projection methods into 3D tomographic datasets with cubic voxels of typical dimensions 100 microns with currently available computer storage and speed. Experimental data-taking with the tomographic microscope is fully automatic under computer control. The tube can operate at up to 30 keV/0.1 mA. With present limitations of detector efficiency (5% at 5 keV) experimental acquisition of views at 90 orientations takes 2–3 h and limits application to *in vitro* samples. We have successfully imaged tomographically: assorted seeds, grasses, dead insects and (in a non-biological context) industrial foams (examples are shown). Present effort is being concentrated on upgrading the equipment enabling the use of higher kVp (requiring a more efficient detector) and opening up the possibility of microtomography for more radio-opaque samples. In paticular such a technique could: (1) allow investigation of the 3D architecture of breast excision samples; (2) allow *in vivo* imaging of tumours in small rodents, assisting studies of tumour growth or regression from radio- or chemotherapy without animal sacrifice.

Oncology (2.30–3.45)

The current status of radiobiological modelling

R. G. Dale
Department of Radiation Physics, Charing Cross Hospital, London W6 8RF

The linear-quadratic (LQ) model possesses greater versatility than its predecessors as it shows more clearly that biological effect is not linearly related to radiation dose. The model demonstrates that the effectiveness of a given treatment type is strongly dependent on the irradiation conditions, and on a number of tissue-specific parameters. Since these parameters are generally different between tumours and dose-limiting tissues the LQ model, when backed by reliable experimental data, indicates the possibility of prospectively designing better treatments. Although much attention has been devoted to investigating the implications of the model for fractionated therapy, it also has value for analysing other types of radiotherapy, and may be used to assess continuous low-dose-rate treatments, treatments with decaying sources, and biologically-targetted radiotherapy. Whilst the LQ model must remain a much-simplified mathematical description of the many radiobiological factors which are of importance in clinical radiotherapy, its sensible application opens up a number of new avenues of evolution of radiotherapy techniques in the future.

In vitro radiosensitivity of human malignant astrocytomas

J. Ramsay, S. Stenning and N. M. Bleehen
University Department and MRC Unit of Clinical Oncology and Radiotherapeutics, Addenbrooke's Hospital, Cambridge CB2 4DH

Patients with malignant astrocytomas have a bad prognosis, and while radiotherapy will significantly increase survival, the tumours are generally considered to be radioresistant. Experiments have been performed to determine radiosensitivity as measured by surviving fraction to 2 Gray (SF 2 Gy) in short-term cultures established from 19 biopsies obtained from the patients at the time of neurosurgery. Results were compared with chemosensitivity measurements and the data were assessed for prognostic importance. Radiation response of cells was determined using a standard clonogenic assay and a rapid colorimetic assay (MTT Assay). There was considerable heterogeneity of response between the individual cultures, with the MTT assay giving values of SF 2 Gy from 0.32 to 0.86 (mean 0.56) and for the clonogenic assay 0.12 to 0.60 (mean 0.41). In each pair of readings the MTT SF was higher and the mean difference is significant ($p < 0.001$). However as a qualitative assessment of sensitivity/resistance the two methods showed a reasonable degree of correlation. Response of the cultures to CCNU and cisplatin as determined by the MTT assay also showed considerable heterogeneity, with the drug dose required to reduce the optical density by 50% (ID50) ranging from 4.5 µg/ml to 32 µg/ml for CCNU and 0.01 µg/ml to 11 µg/ml for cisplatin. There was no significant correlation between chemosensitivity and radiosensitivity, although there was a trend towards higher ID50s being associated with lower SF 2 Gy. Of the 19 patients tested, 18 received radical radiotherapy and six patients also received chemotherapy. Patients with more resistant tumours (SF > 0.5) had a shorter median survival time, but more patients are required to determine if *in vitro* radiation response is useful as a prognostic indicator in this group of tumours.

Comparison of the biological effects of LDR and HDR radiation on epidermoidal cervix carcinoma cells (Caski cells) and human primary keratinocytes obtained after transfection with human papillomavirus type 16 DNA

R. Schulz-Wendtland, M. Bauer, U. Mohrmann, G. Beuthner, T. Bauknecht and M. Durst
Department of Gynaecological Radiology, Radiological Centre of the University of Freiburg, Hugstetter Str. 55, 7800 Freiburg, West Germany

To compare the biological effectivity of HDR and LDR brachytherapy, we carried out experiments on epidermoidal cervix carcinoma cells (Caski cells) and human primary keratinocytes obtained after transfection with human papillomavirus type 16 DNA, varying the dose rate (27cGy/h–8000cGy/h), the dose (1–100 Gy) and fractioning (protracted, 3, 6, 12 and 18 fractions). The results demonstrate that the LDR therapy can be compensated by the HDR therapy with the same therapeutic range if fractioning is high enough.

Radiotherapy of lung cancer: evaluation of treatment volume and tumour remission by computed tomography (CT)

Th. Feyerabend, R. Schmitt, E. Richter and W. Bohndorf
Department of Radiation Oncology, Würzburg University Hospitals, 9700 Würzburg, West Germany

Four hundred and thirty four CT examinations of 133 patients with histologically proven bronchogenic carcinoma (22/133 with small cell lung cancer) were analysed before and after radiotherapy. The three main results are as follows. (1) For the determination of treatment volume, conventional X-ray simulator methods are inferior to CT-aided planning. We found that changes of the treatment volume were necessary in 50%, and in 22% the changes were crucial, especially in non-small-cell lung cancer. (2) Based upon the tumour volumes calculated by CT, the response rate (partial and complete remission after radiotherapy) of the primary could be evaluated: it was more than 70%. The rates of complete regression of the primary were 45% (non-small-cell carcinoma) and 67% (small-cell carcinoma). (3) 1–3 months and 4-9 months after irradiation the rates of complete remissions were 19% and 62%, respectively. Hence, the evaluation of treatment results earlier than 3 months after radiotherapy may lead to incorrect conclusions concerning tumour response.

The effect of ultrasound on the cytotoxicity of some chemotherapeutic agents

G. R. ter Haar and P. Loverock
Department of Physics, Institute of Cancer Research, The Royal Marsden Hospital, Sutton SM2 5PT

We have demonstrated that continuous-wave ultrasound (2.6MHz, 2.3Wcm^{-2}) can considerably enhance the cytotoxic effect of adriamycin on V79 cells maintained in suspension cultures at physiologically normal temperatures. Flow cytometric studies have shown that this effect can in part be explained by an increased intracellular concentration of adriamycin. Similar studies have been carried out to investigate the effect of ultrasound exposures on the cytotoxicity of other chemotherapeutic agents at temperatures in the range 37°C–43°C. Drugs studied include daunomycin, melphalan, chlorambucil and procaine hydrochloride. The toxicity of melphalan is unaffected by ultrasound at any of the temperatures studied. The combination of ultrasound and procaine hydrochloride is more toxic at 43°C than is either agent alone at that temperature, whereas at 37°C no cell killing occurs. Ultrasound enhances the toxicity of daunomycin at 37°C but has no effect on chlorambucil toxicity at this temperature. These and other results are discussed in detail.

Radiotherapy, head and neck tumours and cigarette smoking

C. Des Rochers, R. Beare, T. Rugg, M. I. Saunders and S. Dische
Marie Curie Research Wing, Mount Vernon Hospital, Northwood, Middlesex HA6 2RN

Acute reactions in the mucosa of patients treated for head and neck tumours are influenced in severity by the schedule of radiotherapy and also by host factors which may include cigarette smoking. In a survey of the pattern of cigarette smoking of 41 patients receiving continuous hyperfractionated accelerated radiotherapy (CHART), a significant correlation was shown between persistence of smoking and the duration of mucositis ($p = 0.014$). There was also a correlation with the volume of mucosa irradiated ($p = 0.025$), but both appeared independent factors. It is important to encourage patients to stop smoking altogether prior to radiotherapy in order to minimize mucositis; however, many patients are very resistant. The services available to help patients give up the smoking habit are reviewed and experience gained at Mount Vernon in counselling patients prior to radiotherapy described.

The assessment of tumour volume in the management of lung cancer by radiotherapy

B. E. Lyn, A. W. Ayoub, M. I. Saunders and S. Dische
Marie Curie Research Wing, Mount Vernon Hospital, Northwood, Middlesex HA6 2RN

In the treatment of lung cancer the tumour volume may be correlated with prognosis, and a comparison of volumes before and after treatment is also used to estimate the extent of response to treatment. In clinical practice tumour volume is usually estimated by the product of two diameters of the tumour image on chest X-ray. However, with CT a more accurate assessment of tumour volume may be obtained by using appropriate software and knowledge of the CT slice thickness and the number of slices on which the tumour is visible. Between January 1985 and November 1988 62 patients with locally advanced non-small-cell lung cancer were treated in the pilot study of continuous, hyperfractionated, accelerated radiotherapy (CHART) at Mount Vernon Hospital. From CT scans performed before and after treatment, tumour volumes have been calculated. The volumes have been compared with "volumes" calculated by multiples of two diameters on CT slices and chest radiographs. Initial volume and complete regression determined either by CT or by chest X-ray have been correlated with outcome.

A quantitative method of expressing the radiation sensitivity of the epithelium in the human oral cavity

T. Ljubenov
Department of Radiotherapy, National Oncological Centre, Medical Academy — 2nd Base, 1527 Sofia, Bulgaria

We have followed up 141 patients with tumours in three sites (97 carcinomas of the epipharyngeal cavity, 33 of the tonsils and 11 of the tongue base), in which the correlation between the epithelium of the oral cavity and the irradiated volume varies with a conventional course of fractionation 5 x 2.0 Gy weekly up to 60–65 Gy total dose for 6–7 weeks of telegammatherapy. In our attempt to find more general regularities and a quantitative expression of dependence between "dose — first radiation reaction of epithelium" and the time for healing, we adapted Kirk's formula for cumulative radiation effect (CRE) in out study of radioepithelitis and have found certain quantitative regularities. The epipharyngeal carcinomas are divided into two groups: with early radiosensitivity the interruption begins toward 5.0–6.0 Gy (days 0.11) of the CRE, with more days for the dying down of the epithelitis; and with later radiosensitivity, this starts after the interval of 11.0 Gy (days 0.11) and with fewer days for the fading away of the radioeipthelitis. For the epipharynx the age fluctuations are greater after 11.0–12.0 Gy (days 0.11) for an average age of 30–35 years, while with the base-of-the-tongue patients they are greater at 8. 0–11. 0 Gy (days 0.11) at an average of 60–80 years.

Notes

Congress Theatre

Mayneord Memorial Lecture (12.15–1.15)

This lecture is financed through the generosity of 3M UK plc

Conjoint application of diagnostic and therapeutic ultrasound

F. L. Lizzi
Biomedical Engineering, Riverside Research Institute,
330 West 42nd Street, New York, NY 10036, USA

New diagnostic ultrasound techniques are permitting more precise quantification of tissue microstructure in terms of the sizes, concentrations and mechanical properties of tissue elements. In ophthalmology, this information is improving diagnosis, selection of appropriate therapy, and monitoring of treatment responses. We have found that such tissue characterization information is especially important for planning and monitoring therapeutic ultrasound treatments of intraocular tumours. These treatments employ precisely focussed, high-intensity ultrasound for short-term ablation or longer-term hyperthermia. This presentation reviews the theory and practical application of tissue characterization techniques we are using for several organs; it includes recent simulations that incorporate acoustic micrograms. The theoretical model and clinical instrumentation we have developed for ophthalmic therapeutic ultrasound are discussed. Lastly, we show how our diagnostic and therapeutic results are combined, using three-dimensional computer graphics simulations to plan therapy sessions and monitor alterations induced within tumours. Preliminary three-dimensional results for other body structures (*e.g.* superficial blood vessels) are also presented.

Sylvanus Thompson Memorial Lecture (4.15–5.15)

Tumour vasculature: a bother or a boon to the cancer therapist

Juliana Denekamp
CRC Gray Laboratory, Mount Vernon Hospital,
Northwood, Middlesex HA6 2JR

The poor vascular supply to solid tumours has long been recognized as a common feature. It has given rise to concern about hypoxic radioresistance and poor drug delivery. Much attention has been focused on methods of improving the blood supply during treatment, or of increasing the supply of oxygen and other blood borne substances. Recently, however, several lines of work have emerged in which it appears that neovasculature may be a possible target for tumour attack. The most obvious example is interventive radiology, with deliberate occlusion of major vessels. Interfering with tumour angiogenesis factors has also been shown by Folkman and his colleagues to be a promising avenue. Hyperthermia appears to be more effective on cells deprived of oxygen and other nutrients which exist at low pH, *i.e.* features resulting from the poor blood supply. In addition, tumour vascular collapse can be induced by small temperature elevations, *e.g.* 42.5°C for 30 minutes, which would cause increased flow in normal vessels. Almost a decade ago we proposed that cytotoxic drugs could be targeted at proliferating endothelium because the endothelial turnover is 50–100 times higher than in normal vessels. Since then it has become apparent that the biochemical features of immature endothelium may also influence the possibilities of causing localized vascular collapse or occlusion, or the activation of prodrugs. Vascular effects may already be an important component in the tumour response to many existing and novel forms of therapy. These include hyperthermia, photodynamic therapy, biological response modifiers and certain cytotoxic drugs. Because these effects have been largely ignored, no attempt has been made to optimize them. The potential avalanche effect, in which ischaemic death of thousands of cells can occur for each vessel that is occluded, should not be lightly discarded. Studies of neovascular pathology, including structure and function, physiology and morphology, endothelial proliferation and differentiation and haemodynamic properties must all be brought together with this common aim.

Wednesday 13 June

Harewood Suite

Contrast Studies (9.00–10.15)

Contrast-enhanced MRI: Gd-DTPA and beyond

R. C. Brasch
Contrast Media Laboratory, Department of Radiology, University of California San Francisco, San Francisco, CA 94143-0628, USA

The requirement for contrast enhancement in magnetic resonance imaging is emerging as the capabilities and, more importantly, the limitations of the modality are revealed. MR parameters of normal tissues and diseased tissues overlap. Also abnormalities, when identified, lack aetiological specificity. Contrast media, by providing functional information and clues to specificity, can impact positively upon the diagnostic value of the MR examination. The most successful approach to the development of MR contrast media has been to chemically manipulate the MR tissue intensity by instilling relatively small amounts of paramagnetic or superparamagnetic substances that reduce tissue relaxation times; intensities can be made to either increase or decrease from baseline values. Depending on the biodistribution of the agent, it has been possible to enhance abnormalities of blood-brain barrier integrity, renal excretion, inflammatory foci, neoplasms, the functional reticuloendothelial mass, lymph nodes and the blood pool. Much attention has focused on dimeglumine Gd-DTPA (gadolinium diethylaminetriaminepentaacetic acid), the first MRI contrast agent to have been used widely in clinical practice. Accumulated experience indicates that Gd-DTPA is effective for enhancement of blood-brain barrier defects, renal excretory capacity, inflammatory lesions and certain tumours, which are all well known applications for radiographic ECF contrast media. The 0.1 mmole/kg clinical dose (approximately 14 ml) of Gd-DTPA is 1/100 of the LD_{50} dose in rats, and presents a high safety index. Clinical safety is further evidenced by a very low frequency of relatively minor side effects in patients such as nausea and headache. There is no evidence of measurable dissociation of gadolinium from the DTPA chelate in patients. Demonstrated applications of ECF contrast media include enhancement of lesions in the brain and spinal cord, improved identification of carcinomas in the breast, definition of renal functional impairment, and differentiation of scar and recurrent disc disease in the post-operative spine.

Acknowledgement
This lecture has been generously supported by Schering Healthcare.

Contrast agents for diagnostic ultrasound: basic mode of action, state of the development and future prospects

R. Schlief, E. Cramer and H. P. Niendorf
Clinical Research and Development Diagnostics, Schering AG Berlin, D-1000 Berlin 65, West Germany

Whereas radiodiagnosis and magnetic resonance tomography (MRT) are based on interaction between electromagnetic waves and single molecules, diagnostic ultrasound is based on interactions between mechanical-elastic waves and the body tissue. This fundamentally different type of interaction led to new kinds of contrast media (CM). The known developments of ultrasound CM are based on small bubbles of air (microbubbles) which do not diffuse in the body water like X-ray CM or MRT CM, but remain within the vascular system ("blood-pool agent"). However, all known agents exhibit limited intravascular stability from a few seconds up to a few minutes. Three types of CM are in clinical use or under development: "microbubble foam" prepared immediately before injection, fixed air-filled spheres of sonicated human albumin, and microbubble-containing saccharide-microparticle suspensions (SH U 454 and SH U 508) which are prepared before injection from two components. Most advanced is the clinical development of SH U 454. More than 1600 patients have so far been investigated in the main indications of echocardiography, venous haemodynamics and Fallopian tube imaging. Clinical trials have demonstrated good tolerance and reproducible, dose-dependent echo enhancement. Although chemically almost identical to SH U 454, minor changes to the formulation of SH U 508 have led to prolonged intravascular stability and echo-enhancement of the left heart chambers and arterial vessels after intravenous injection ("transpulmonary CM"). A first clinical trial in contrast-echocardiography which has just been completed shows reproducible left heart opacification lasting dose-dependently for a few minutes and good tolerance of the SH U 508 injections. Ultrasound contrast agents, particularly those with improved intravascular stability, are expected to extend the capability of diagnostic ultrasound, *e.g.* in the broad spectrum of vascular imaging, transcranial Doppler, tumour delineation, tissue-/tumour-perfusion, urology and gynaecology.

The effect of contrast media on renal vascular resistance (RVR)

A. A. El Sayed, J. L. Haylor, *A. M. El Nahas and †S. K. Morcos
*Departments of Pharmacology, *Nephrology and †Radiodiagnosis, University of Sheffield and Northern General Hospital, Sheffield S5 7AU*

In vivo studies in experimental animals have so far failed to dissociate the systemic effect of water-soluble contrast media (WSCM) from their direct renal effect. We have designed a new experimental approach relying on a constant-pressure recirculating model of the isolated perfused rat kidney (IPRK) to study the direct effect of Niopam 340, Omnipaque 350, Hexabrix 320, Ultravist 370, Urografin 325, Sodium Uromiro 300 and Conray 420 on the renal vascular resistance (RVR). Four kidneys of adult male Wistar rats were used to examine the effect of 10 ml of each contrast agent. Four kidneys perfused only with the physiological solution "Krebs-Henseleit with 6.7% albumin" formed a control group. All the WSCM used in this study produced changes in RVR. The high osmolar agents induced a biphasic response: a transient decrease followed by a more sustained increase in RVR; whereas the low osmolar ones produced only an increase in RVR. No change in RVR was observed in the control group throughout the experimental period (50 minutes). The increase in RVR was significant with all the WSCM and the extent of this response ranged from 20% ($p < 0.01$) observed with Niopam 340 (681 mosml/kg) and Urografin 325 (1650 mosml/kg) to a maximum of 35% ($p < 0.001$) observed with Conray 420 (2500 mosml/kg) and Hexabrix 320 (580 mosml/kg). These observations show that WSCM can exert a direct effect on RVR in the rat and that such effect is not solely dependent on the osmolality of the medium tested but may also be affected by its chemical composition.

Magnetic resonance imaging with gadolinium-DTPA in the evaluation of bone and soft tissue tumours

J. M. Hawnaur, J. P. R. Jenkins and I. Isherwood
Department of Diagnostic Radiology, University of Manchester, Manchester M13 9PT

Magnetic Resonance (MR) imaging is a proven technique for the evaluation of bone and soft tissue tumours. Gadolinium-DTPA (Gd-DTPA) increases signal intensity of pathological tissue on T_1-weighted sequences by shortening T_1 relaxation time. The aim of this study was to assess whether Gd-DTPA improves definition and characterization of bone and soft tissue abnormalities compared with unenhanced MR imaging. 39 MR examinations were performed in 34 patients (M=14, F=20, age 13–75 years) using a 0.26T superconducting magnet system. Spin echo and partial saturation recovery sequences (SE740–1500/40–80, PSR500/18) were used with 5–10 mm section thickness. The T_1-weighted sequences were repeated following 0.1 mmol Gd-DTPA per kg body weight. Benign bone lesions showed little change in signal intensity after Gd-DTPA but bone sarcomas and lymphoma enhanced markedly. Cortical permeation and intramuscular extension of tumour were well shown on both T_2-weighted and post-Gd-DTPA T_1-weighted scans. Intramedullary extent of tumour and the interface of extraosseous tumour with fat was most clearly defined on pre-contrast T_1-weighted scans. In the soft tissues, benign tumours generally enhanced less than sarcomas or inflammatory lesions. Tumour definition within muscle improved on T_1-weighted scans psot-Gd-DTPA but contrast with fat decreased. Unenhanced T_1-weighted sequences therefore remain necessary in MR staging protocols. In lesions which enhance, post-Gd-DTPA T_1-weighted sequences can achieve a level of contrast between tumour and muscle similar to that of T_2-weighted sequences. Omission of the T_2-weighted sequence, however, can lead to difficulty in detecting benign tumours and in characterizing tissues.

Oral magnetic particles: a new oral contrast for abdominal MRI. Clinical results

D. Kean, L. W. Turnbull, A. Blane, D. C. Carter, H. McRitchie, A. Parker and J. J. K. Best
Departments of Medical Radiology, Clinical Surgery and Medicine, University of Edinburgh, Edinburgh EH3 9YW

Preliminary results using an oral medium based on a magnetite preparation (Nycomed, Oslo) were presented last year (Kean et al, 1989) which indicated that the agent showed considerable promise and provided good delineation of bowel, particularly in the upper abdomen. A Phase 2 study has recently been completed. This concentrated on the applications of the contrast medium in patients with suspected pancreatic pathology, but in addition several patients with lymphoma were examined. In patients with pancreatic disease, the agent helped to delineate the normal pancreas and was particularly useful in showing the extent of collections associated with pancreatitis, which were often difficult to distinguish in images obtained without it. T_1-weighted images were found to be the most useful and no significant image artefacts were produced by the contrast medium in any imaging plane or pulse sequence. 350 ml of contrast agent at a concentration of 0.1 g/l was sufficient to opacify the upper small bowel and colon. Pancreatic patients were examined immediately after ingesting the agent but those with lymphomas were examined 1 h after ingestion. In the lymphoma patients, the contrast was useful in delineating small bowel loops in the upper abdomen, and allowed confident identification of small para-aortic lymph nodes. In summary therefore, this new oral contrast agent appears to outline the bowel adequately and can be recommended for routine use in abdominal magnetic resonance imaging.

Notes

Reference

KEAN, D. et al, 1989. Oral magnetic particles: a new oral contrast agent for abdominal magnetic resonance imaging. *Proceedings of the 47th Annual Congress of the British Institute of Radiology, 1989* (British Institute of Radiology, London).

The kinetics of tissue enhancement in intracranial tumours following intravenous Gd-DTPA studied by ultra-high-speed inversion-recovery EPI

*B. S. Worthington, M. K. Stehling, †P. Bullock, †J. L. Firth, R. J. Ordidge, R. Coxon, A. M. Blamire, P. Gibbs and P. Mansfield
*Departments of Physics, *Radiology and †Neurosurgery, University of Nottingham, Nottingham NG7 2RD*

The overall effects of intravenous Gd-DTPA on tissue signal in intracranial tumours are complex, depending on dosage, time of administration, pulse sequence and tissue type. High-speed EPI permits the kinetics of tissue enhancement to be analysed for the first time. The IR-MBEST technique combines the advantages of T_1 contrast with image acquisition times of less than 1 second. Signal nulling of the tissue of interest before a bolus injection of Gd-DTPA (0.1 nmol/kg) maximizes sensitivity to T_1 shortening. The amount of blood flow to a tissue and the richness of its vascular bed dictate the "wash in" phase and are major determinants of the "wash out" phase. The rate and amount of contrast medium accumulating in the extracellular space are determined by the degree of breakdown of the blood brain barrier. Dynamic scanning has been shown to be a valuable adjunct to a morphological study of tumours, providing an assessment of vascularity which is important in planning resection; it demonstrates areas with maximal breakdown of the blood brain barrier most suitable for stereotactic biopsy, and the temporal profile of enhancement may allow discrimination between different tumour types and assessment of the malignant potential of a single type.

Ripley Suite

Technology and Optimization (10.45–12.00)

QALYs in diagnostic radiology

J. G. B. Russell
Department of Radiology, St Mary's Hospital,
Manchester M13 0JH

We are all anxious to value the benefits of diagnostic radiology so as properly to plan pathways in the management of diagnostic problems. A large number of variable appear when costings are attempted. Some of these are the cost of the investigation, the cost of subsequent treatment, the cost of alternative methods of diagnosis, the value of a human life, the discounting of a harm which only appears after many years, the value of reassurance, and the value of the making of diagnoses. The valuation of a QALY (or quality-adjusted life-year) is used to indicate priorities in different possibilities of health spending. A QALY can represent one year of extended life, or proportionally, a period of reduced disability. The disability is graded so that for example, a person unable to undertake any paid employment with severe mental distress is rated at a loss of 0.3 (healthy = 1, dead = 0). Thus if such a person's health is improved to normal for 10 years, three QALYs are scored. Because of the variables noted above, QALYs are not suitable for general use in diagnostic radiology, but can be used to compare population screening methods: for instance, population screening for breast cancer or abdominal aortic aneurysm. It is found that the aneurysm screening gives better value than breast screening.

A new personal computer based image transfer system: impact on patient management

J. A. Spencer, P. L. Anslow, A. J. Molyneux, C. S. Barker and D. B. Dobson
Section of Neuroradiology, Radcliffe Infirmary, Oxford OX2 6HE

The value of a new personal computer based image transfer and storage system in a regional neuroradiology department is described. The immediate impact on patient management was analysed prospectively for 149 CT scans transferred over 4 months. Sixty-eight scans were of acute neurosurgical referrals from six linked District General Hospitals; seven were follow-up scans; 50 scans were from radiologists in these hospitals seeking specialist advice from a neuroradiologist; 23 scans were sent to the homes of the neuroradiologists for primary opinions on patients in the base hospital. Overall 56 scans (37.6%) were transferred outside normal working hours. For the acute neurosurgical patients, in 55 cases (80.9%) a significant change in management occurred, principally prevention of transfer when no neurosurgically correctable lesion was present (42.6%) or arrangement of interval transfer for further investigation. Of scans transferred for a radiological opinion, in 38 cases (52.1%) a significant change in diagnosis or management results: 56% of second opinions, 43.4% of primary opinions. The use of the system steadily increased during the period of the study, and is currently two to three cases daily. We believe it offers invaluable assistance to both radiologists and clinicians and has had a major impact on patient management.

Memory for radiological appearances; objective evidence for perceptual schemata

B. S. Worthington, A. G. Gale and F. Johnson
Department of Radiology, University Hospital,
Nottingham NG7 2UH

Our memory of a particular radiological appearance probably does not resemble a photographic copy but is rather a reconstruction or "schema" derived from stored information, which records the spatial relationships within the image and also reflects a number of stored propositions which contain our prior interpretation of the image. The following experiment provides objective evidence for the existence of such schemata and of our ability to manipulate them in problem solving. Fourteen patients were shown at random an AP view of either a left or a right knee at different orientations taken from 45° steps around a circle. Whilst the same array of features is present at all stimulus orientations the reaction time to identify which had been presented was different for each position. One group produced the fastest correct recognition times with the conventional upright radiographic film, while for a few individuals the reverse was the case. These results imply that an internal representation of the knee or schema is rotated into congruence with the perceived image prior to interpretation. The rates of rotation found varied from 200°/s to 415°/s with a mean value of 323°/s.

"Reporting in a flash"

A. G. Gale, J. Vernon, * K. Millar and B. S. Worthington
*Departments of Radiology and * Behavioural Science, University Hospital, Nottingham NG7 2UH*

Three groups of subjects — radiologists, radiographers and medical students — each viewed 100 chest radiographs, 50 of which contained abnormalities under 3 different conditions: firstly, with a 200 ms tachistoscopic exposure; secondly, with a 200 ms tachistoscopic exposure followed by the presentation of a visual noise mask to eliminate any after-image; and thirdly, viewing for an unlimited time. The subject's response to each film was given on a 5-point rating scale and an ROC curve was plotted for each subject under the three different viewing conditions. The performance of the radiologists and radiographers was significantly better than that of the students. There was very little difference in the results for each of the three groups under the different viewing conditions. These results emphasize the importance of a well-developed schema in interpreting radiographs and the great significance of peripheral vision in preliminary assessment of a film and in directing subsequent fixations. Furthermore, the findings indicate that earlier work has underestimated the amount of information which can be assimilated in a single fixation.

Patient expectation and accident and emergency radiology

E. McNally, G. de Lacey, T. Welch and P. Lovell
Departments of Radiology and Accident and Emergency, Northwick Park Hospital, Harrow, Middlesex HA1 3UJ

Five hundred patients who were not referred for radiology following a head or ankle injury were sent a questionnaire. 53% of the responders had expected an X-ray examination (Group 1). Important differences are shown between these patients and those who did not expect radiography (Group 2). These included: a higher level of disappointment (75% vs 0%) and more critical comments (83% vs 17%) and, following head injury, a longer mean recovery time (15 days vs 4 days). But there were very large differences in duration between age groups. For example, for those in their teens, symptom duration was nine times longer for Group 1. This could well have important educational implications. Initial analysis suggests that the overall severity of head injury was not any different between the two groups, and follow-up has shown that no important abnormality had been missed by excluding radiography. These results have implications for all casualty departments, and perhaps particularly for those who introduce guidelines which subsequently produce a reduction in X-ray examinations. Some strategies (mainly to improve communication skills) which might reduce the overall level of patient dissatisfaction are proposed.

Ergonomic assessment of mobile X-ray units

F. F. Jehu, A. G. Gale, B. S. Worthington
Division of Radiology, University Hospital, Nottingham NG7 2UH

Four currently available mobile X-ray units were examined with regard to operator ease of use. The criteria on which performance of the equipment was judged included operator comfort, safety, speed with which the equipment could effectively be used and the health and safety of the operator. Consideration was also given to cognitive aspects of the tasks involved. Three separate approaches to the evaluation were undertaken; 160 questionnaires were distributed to experienced radiographer users, participative discussion groups and user trials. In the latter, naive users were videotaped as they carried out two surrogate radiographic examinations using two of the units, and then retrospective protocol analysis was applied to the users' commentary as they watched their video record. Analysis of quantitative and qualitative data revealed areas of significant design inadequacy in all of the mobiles. These mainly concerned difficulties with unit manoeuvrability and X-ray tube movement.

Radiology in developing countries. Three years experience in Rwanda with a basic radiology system specifically designed for developing countries.

R. van Tiggelen and M. Freson
Radiology Department, Akademisch Ziekenhuis, Vrije Universiteit Brussel, 1090 Brussels, Belgium

We describe our experience of a radiographic system that we have specifically designed for developing countries (or military use) and used for three years in a small hospital in Rwanda. The Basic Radiologic System (BRS) consists of a mobile and detachable X-ray examination unit for radiography combined with a panel-type fluoroscopic intensifier and eventually completed by a linear echograph. This equipment fulfils the requirements of developing countries as well as disaster situations (either traumatic or infectious) outside the third world. In particular, the versability and the modularity of the system are emphasized. We review the efficacy of the system for abnormal disease (often parasitic or gynaecological, as well as for major current pathology.

Potential savings from improved reporting practices in a radiology department

I. W. J. Birchall, S. G. Cooke, R. Sherborne and G. Chilvers
Department of Radiodiagnosis, Bristol Royal Infirmary, Bristol BS2 8HW

62% of the imaging investigations of our department are those of Körner group A. A study has been undertaken to quantify the benefits of modification of the work patterns of such reporting. Two radiologists each reported 50 randomized Körner A investigations either in a quiet room or while in a reporting area centrally within a working suite. In the quiet room, the current and any related past films had been mounted on a film alternator by a clerk. Each radiologist then crossed over films and reporting conditions to provide internal control. Time spent reporting films was reduced by 49-56% if reported in quiet surroundings. Time spent typing the reports from quiet surroundings was reduced by 10%. The cost of clerical assistance was outweighed by the financial savings thereby incurred.

Audit of a radiodiagnostic department: a pilot study of the Bristol Royal Infirmary

I. W. J. Birchall, P. G. Cook and W. D. Jeans
Department of Radiodiagnosis, Bristol Royal Infirmary, Bristol BS2 8HW

To improve any service, it is necessary to identify areas of suboptimal performance and to provide a baseline against which improvements can be measured. Quantification of such material in a medical setting is difficult but in this pilot study, the "quality" of the request card, radiography, radiological report and film bag/report folder have been chosen as markers to provide indices of clinician input, and the performance of radiographic, radiological, secretarial and clerical groups of departmental staff. Twenty-five parameters of quality have been identified from these marker areas, using the investigation of 1 patient/week taken from each of 10 Körner groups in a 10-week period. The data were audited, numerically encoded and analysed. A system was developed which scored the assessment for each item of the process monitored as -1, 0 or +1. For each item a total index was obtained by adding all the scores and calculating this as a percentage of the total possible score. Arbitrary minimum satisfactory levels were set for positive and negative indices. In this way, areas of suboptimal as well as unforeseen areas of good performance from each staff group have been identified. The benefits of such work and problems incurred in the design of such a project are discussed.

Outpatient angiography in a district general hospital

R. M. Evans, K. M. Mourad and B. J. Pardy
Department of Radiology, Newham General Hospital, Plaistow, London E13 8SL

Outpatient angiography in patients with peripheral vascular disease can be a safe and cost-effective procedure. We report on 50 patients who were being investigated for peripheral vascular disease, who underwent angiography via the femoral arterial approach. We outline our patient selection protocol, techniques and post-procedure care. Doppler pulse pressure ratios were used to monitor the patients pre- and post-angiography. Their use and efficacy in detecting possible complications are discussed. No patient had a significant complication of the procedure and the technique was tolerated well, which compares favourably with previous work performed abroad. Our study shows that femoral angiography performed on a day-care basis is a safe and cost-effective technique. The financial savings are significant, and in today's health care climate it is a technique which could be practised more widely.

Notes

Harewood Suite

Digital Radiology (2.30–3.45)

Digital subtraction dacryocystography

S. J. King and S. F. Haigh
Department of Diagnostic Radiology, King's College Hospital, Denmark Hill, London SE5 9RS

Imaging of the lacrimal system by conventional dacryocystography can be unsatisfactory. A technique of digital subtraction dacryocystography (DSDCG) is described. Twenty-one patients presenting clinically with obstructive epiphora were investigated with DSDCG. We found that the technique is simple to perform, is accepted well by patients and provides diagnostic images with improved demonstration of the proximal lacrimal system over conventional dacryocystography. DSDCG produces diagnostic images on a single radiographic projection, delivering a reduced radiation dose to the orbit without the need for lead eye shields. There has been complete correlation between surgical and radiological findings in patients diagnosed as having lacrimal duct obstruction on DSDCG referred for dacryorhinostomy

Digital subtraction imaging of the investigation of the salivary glands

D. MacVicar, G. Tiller and A. Moody
Department of Diagnostic Radiology, St George's Hospital, London SW17 0QT

Contrast sialography is an established technique in the delineation of the duct system of the salivary glands. In recent years ultrasound and computerized tomography have played an increasing part in the investigation of pathology of the salivary gland parenchyma. Digital subtraction imaging (DSI) represents a refinement of existing techniques which can elegantly demonstrate ductal and glandular disease. The principal advantages of the procedure are its speed and technical ease. The patient can be screened into the ideal position, and imaging during injection of contrast agent confirms accurate positioning of the cannula. An appropriate imaging sequence allows all phases of ductal filling to be visualized on a single injection. Digital subtraction of bony structures may reduce the need for multiple projections, and results in images of excellent quality. Digital subtraction sialography is fast and easy to perform; it involves no increase in radiation exposure or patient discomfort. The technique is described in detail and a range of common pathologies illustrated. In our experience, DSI of the salivary glands is the technique of choice, where it is available, and can easily be incorporated into the timetable of a busy DSI department.

DSA of digital ischaemia

B. Menanteau, C. Marcus, L. M. Caquot, V. Ladam and F. Gausserand
Department of Diagnostic Radiology, Robert Debré Hospital, 51092 Reims, France

We report on a prospective study of digital subtraction angiography (DSA) in 32 patients presenting with digital ischaemia. Direct brachial puncture was performed in 26 cases. We injected low-osmolality contrast material (Hexabrix 160) at a rate of 5 ml/s for a total of 20 ml for each injection. Nine prostaglandin E_1 angiograms were obtained to get good peripheral filling, particularly in patients presenting with vasospastic disorders. In this series, owing to instant magnification, we were able to differentiate small emboli, atherosclerosis, Buerger disease, collagen vascular diseases and other entities affecting the arteries of the hand. Since the injection of low-osmolality contrast material is painless, DSA confirmation of digital ischaemia is available on an outpatient basis, without any premedication.

Digital fluorography: the first year's experience

D. J. Lintott, P. M. Chennells and R. C. Fowler
Department of Diagnostic Radiology, The General Infirmary, Leeds LS1 3EX

In April 1989 a 1024 x 1024 digital fluorographic unit with on-line computer enhancement of images (Philips DSI) was installed at the General Infirmary at Leeds. This was the first installation of its kind in the world outside the Netherlands and uses image processing algorithms developed by the Department of Medical Physics at the University of Leeds. Field sizes of 14, 10 and 6 inches are used and computer enhanced images are available for immediate review in either single or multiple formats. In the first year since installation over 900 upper gastrointestinal barium studies, mainly double contrast barium meals, and 400 ERCP examinations, over half of them therapeutic procedures (Sphincterotomies, stone extractions, endoprosthesis placements) will have been performed in addition to over 100 other spot film contrast examinations. An evaluation of digital fluorography is presented with special reference to image quality and ergonomics. The high definition monitor and immediate image review facility permit confident diagnosis at the time of examination. Additional views can be obtained whilst optimal examination conditions persist. Ergonomic analysis of barium meals has shown 31% reduction in examination time, 49% reduction in patient waiting time and 45% reduction in patient dosage compared with conventional fluorography.

A review of thermal-processed paper/film hard-copy units in medical imaging

N. J. Coleman
Medical Physics Department (FAXIL), The General Infirmary, Leeds LS1 3EX

Thermal hard-copy units can provide quickly-available, low-cost images and several different types have been evaluated on behalf of the Department of Health. These utilized either a thermal-head print unit or laser printing with subsequent thermal development of the image. The media were paper or film specific to each imager. Appropriate test images were produced for the measurement of image geometry, unsharpness and grey-scale characteristics. Geometric distortion was not found to be significant either horizontally or vertically (the latter relating to the paper transport mechanism). Unsharpness was determined in the thermal-head units by the physical spacing of the thermal elements, from 6 to 11.8 dots per mm. The laser-printed images had a maximum resolution of 10 pixels per mm. Spurious artefacts were sometimes produced when imaging bar-patterns of particular spatial frequencies. Grey-scale levels ranged from 16–128 for the thermal-head imagers, with 256 for the laser printer. The grey-scale characteristics (with optimally adjusted Brightness and Contrast controls), showed considerable variations in linearity between the units. For some clinical images however, overall linearity was less important than the localized gradient for discriminating diagnostically-significant details.

A physical assessment of the imaging performance of the DSI digital fluorography system

A. R. Cowen and A. Workman
Medical Physics Department (FAXIL), The General Infirmary, Leeds LS1 3EX

We have carried out a physical assessment of the imaging performance of a DSI digital fluorography system. To support this project we have developed a set of X-ray test objects matched to the imaging characteristics of the DSI unit (parameters measured include signal-to-noise ratio, contrast sensitivity, dynamic range, geometry and MTF). The DSI was installed in the Diagnostic Radiology Department to provide a routine clinical service in a number of R & F examinations. Physical analysis of the test image data was performed off-line in the FAXIL laboratory using a PC-based image processing workstation. Aspects of the DSI performance evaluated include: radiation exposure calibration, subjective and objective measurement of image quality, image acquisition protocols, image processing and display facilities, video (cf laser) hard-copy media, image storage capacity, user interface and ergonomics. Results from the DSI are compared with those produced by conventional (film-based) R & F systems, and techniques which have been developed to optimize DSI image quality in clinical service are discussed.

Acknowledgments
The Supplies Technology Division of the Department of Health and Yorkshire Regional Health Authority, who support this project.

The influence of intravenous DSA in the management of peripheral vascular disease

O. Chan, N. M. Wilson, M. Lea Thomas and N. L. Browse
Department of Radiology and Surgical Unit, St Thomas' Hospital, London SE1 7EH

A retrospective study of all patients who had a digital subtraction angiogram (IV DSA) in 1987, was carried out to assess the way in which IV DSA has replaced conventional angiography in the investigation of peripheral vascular disease (PVD). 155 patients underwent IV DSA, 140 had PVD and 15 had abdominal aneurysms. In addition, 71 patients had conventional arteriography and were not investigated by IV DSA. The distribution of PVD was aorto-iliac (AI) 36 (26%), femoro-popliteal-distal (FD) 68 (48%) and mixed AI and FD, 36 (26%). IV DSA was sufficient for the management (ie diagnosis and surgical treatment) in 95% of AI disease, 72% of FD disease and 94% of mixed disease. IV DSA was the only investigation needed in 117 of 140 patients (84%) and in 68 of 72 patients (93%) with AI disease. Although IV DSA was less accurate in defining distal disease, it was sufficient in the management of 94% of those with mixed disease because the proximal disease was treated first. Furthermore, unsatisfactory definition of distal run-off only required a simple femoral angiogram. Conventional angiography was performed in 101 patients investigated for PVD in 1987, compared to 200 in 1982, before IV DSA was introduced, even though more patients with mild claudication are now studied to assess their suitability for angioplasty. IV DSA has, therefore, significantly reduced the requirement of conventional angiography in the investigation of patients with PVD, thus avoiding hospital admission and reducing cost and morbidity.

Harewood Suite

Real-time digital peripheral angiography

S. C. Ward and J. F. Dyet

Department of Radiology, Hull Royal Infirmary, Kingston-upon-Hull HU3 2JZ

A new technique for performing peripheral angiography, utilizing real-time pulsed digital imaging, is described. The equipment used is a Philips Digital Cardiac Imaging System, operated via an Optimus M200 console. The patient lies supine on a fully floating table top, with an absorption wedge and bolus bag between his legs to reduce flare. The common femoral artery is cannulated using standard Seldinger technique, and a 4.5F catheter is introduced into the lower aorta. A pump injector is loaded with 60 ml of either Ioxaglate 320 or Iopromide 300, according to allergic history. Digital acquisition is commenced at the lower aorta and the contrast agent is injected. The table is moved to follow the contrast column as it passes down the legs. Information is acquired at 12.5 frames/s onto a 512 x 512 matrix. Repeat runs, oblique views, or subtraction sequences may be performed, but are rarely required. Selected images are transferred to hard copy using a DuPont Opti Imager. The software allows for post-processing of the images and severity of stenoses may be calculated. The technique is quick and straightforward and provides a rapid method for accurate assessment of the peripheral arterial tree.

Early experience with a prototype (2K) projectional digital chest unit: ROC study of simulated lung nodules

D. M. Hansell, D. R. Aberle, A. S. Hayrapetian, K. Brown and H. K. Huang

Image Processing Laboratories and Division of Thoracic Imaging, University of California, Los Angeles, USA

A Konica KDD dedicated digital chest unit has been in use in the Department of Radiological Sciences for the last 12 months. This unit generates high-resolution images of 2048 x 2462 x 10 bits which can be viewed either on 2048-line interactive monitors or as hard copy from a laser film printer. With the proposed implementation of totally digital radiography in the Division of Thoracic Imaging at UCLA, the Konica KDD was formally compared with a conventional chest unit. Using receiver operating characteristic (ROC) analysis, we compared observer performance using conventional analogue film and digitally acquired 2K images (on both interactive monitors and hard copy film) for the detection of simulated pulmonary nodules projected on an anthropomorphic chest phantom. For each display condition there were 46 images of solitary nodules with various degrees of conspicuity: high surrounding contrast (n=18), low surrounding contrast (n=19) and no nodule (n=9). In each case four observers recorded the presence or absence of a nodule using a six-point confidence scale. Diagnostic accuracy was similar for analogue film and 2K digitally acquired hard copy. Accuracy of diagnosis in the detection of simulated pulmonary nodules tended to be slightly better with the interactive video display than with digital hard copy.

Notes

Interventional Radiology (10.45–12.00)

Percutaneous angioscopy of peripheral and coronary arteries

M. R. Rees, A. A. Gehani, S. Ashley and S. Brooks
Departments of Radiology and Cardiology, Killingbeck Hospital, Leeds LS14 6UQ

Using a variety of flexible fibreoptic endoscopes, 64 separate angioscopic examinations were carried out percutaneously on 23 patients with peripheral vascular disease before and after interventional treatment. Arteries examined were tibial, (2), iliac (3) femoral and popliteal (22). Ten patients underwent laser angioplasty with a sapphire tip modified ND-YAG laser, eight underwent Kensey dynamic angioplasty and five, balloon angioplasty. Tibial angioscopy was achieved using an 0.5 mm angioscope; the other arteries were examined with either a steerable 2.2 mm angioscope or 1.4 or 1.8 mm non-steerable systems. Best results were achieved with a new integrated angioscopic system (Olympus AF system) which consists of a fully immersible angioscope directly connected to a camera system without an eyepiece. A reduction in volume of fluid perfusate was achieved by the use of an angled guiding catheter system (Cordis Corp.) which allowed for placing of the angioscope at the site of interest, and limited steerability. This guiding catheter system introduces the possibility of carrying out therapeutic procedures under angioscopic guidance. Seven coronary examinations were carried out percutaneously with either a 0.5 mm angioscope (4) or a 1.4 mm angioscope (3). The larger angioscope proved more successful in allowing for adequate endoluminal coronary imaging. Both peripheral and coronary angioscopy provided information on the endoluminal appearances that was not appreciated angiographically.

Mechanical recanalisation of peripheral vascular occlusions after guide wire dissection using a metal laser probe.

A-M. Belli, A. E. Procter and D. C. Cumberland
Department of Radiology, Northern General Hospital, Sheffield S5 7AU

Subintimal passage of the guidewire during attempted recanalisation of peripheral vascular occlusions often presages failure. We have successfully recanalized the true lumen in some such cases by using only the mechanical properties of the thermal laser probe. In 14 cases (12 femoro-popliteal, two iliac) where the guidewire had passed subintimally, all attempts to recanalize the lumen with various guidewires and catheters failed. Prior to abandoning the procedure, the laser probe was used without laser energy, and successfully recanalized the lumen in all but two cases (10 femoro-popliteal, two iliac). In one of the iliac occlusions we did not proceed to balloon dilatation for fear of iliac rupture. Follow-up has ranged from 2 to 48 months (mean 11 months). Eight out of the 11 cases who underwent balloon dilatation remain patent clinically. Two have recurred, one at 6 months and the other at 10 months. One was lost to follow-up. The use of the laser probe as a mechanical tool to "rescue" failed conventional recanalization owing to dissection has not previously been reported. We presume that the configuration of the probe allows re-entry of the lumen by finding the correct tissue plane. We believe this to be a useful technique and the development of a wire or catheter with similar mechanical properties would be both helpful and less costly.

Technique and complications of direct brachial artery puncture for arteriography

A. F. Watkinson and G. Hartnell
Department of Radiodiagnosis, Bristol Royal Infirmary, Bristol BS2 8HW

Direct brachial artery puncture is being used increasingly for arterial access in day-case patients and patients with severe aorto-iliac disease. In expert hands low complication rates are reported, but the risks of brachial artery puncture may be higher when performed by less experienced operators. Over a 2-year period 49 direct brachial punctures were performed for arteriography. In 27 cases the catheter was inserted directly over a guidewire while in 22 cases an introducer sheath was used. Significant complications requiring active treatment or surgical intervention occurred in three cases where direct catheter insertion was used. There were no complications when an introducer sheath was used. Causes of complications, and aspects of puncture technique to reduce the risk of them, are discussed and illustrated. Direct arterial introduction of catheters into the brachial artery can be associated with an unacceptable incidence of complications, and the risk is reduced by the use of an introducer sheath.

Dynamic angioplasty in vascular occlusions: patient selection and follow-up results

M. R. Rees, A. A. Gehani, S. Ashley and S. G. Brooks
Departments of Radiology and Cardiology, Killingbeck Hospital, Leeds LS14 6UQ

Twenty-one male patients with occlusive vascular disease (aged 55–76) were treated with Kensey dynamic angioplasty after the failure of conventional balloon and guidewire methods. Seventeen of these patients had discrete occlusions with a visible distal vessel from collateral run-off (three iliac and 14 femoral/popliteal lesions, length 3–18 cm); 12 of these had successful procedures. In the five unsuccessful cases there were three dissections, one perforation and one failure to cross the lesion. There were 2/12 reocclusions after 3 months, and angiography at 6 months revealed 5/7 patent arteries with one patient having a small false aneurysm. Average ankle brachial index (ABI) for the successfully treated group at 3 months was 0.8 ± 0.042 (n=9) compared to the pre-Kensey average ABI = 0.61 ± 0.04. (n=12, $p > 0.05$). Average isotope limb blood flow at 3 months was 7.76 ml/100 g tissue/min (n=8) compared to 4.6 ml/100 g tissue/min before treatment. Percutaneous angioscopy of the two reocclusions revealed a primarily thrombotic lesion with some atheroma. In four patients treated with femoro-popliteal occlusions there was no popliteal run-off. Only one of these cases was successful, the other three resulted in dissections. The successful case reoccluded after 48 h. We conclude that the Kensey catheter can be used successfully in totally occluded vessels provided there is adequate distal run-off.

Treatment of chronic coronary artery occlusions with an olive-tipped guide wire (Magnum) or a Terumo guidewire

M. R. Rees and A. A. Gehani
Departments of Radiology and Cardiology, Killingbeck Hospital, Leeds LS14 6UQ

Four women and one man with chronic right coronary artery occlusions were treated either with an olive-tipped 0.22 thou. inch guidewire and balloon system (Magnum, Schneider) (four cases) or with an 0.35 thou. inch hydrophyllic guidewire (Radiofocus guidewire, Terumo). The length of occlusion was 2–4 cm and all occlusions were treated in the proximal right coronary artery. In all three cases treated with the Magnum wire, the wire failed to cross the occlusion; in one case the procedure was discontinued because manipulation of the wire and guiding catheter after an unsuccessful attempt to re-cross the lesion resulted in dissection of the coronary osteum. In the other two cases the occlusion was successfully crossed using the Terumo wire. In these cases, balloon angioplasty was carried out by guiding an 0.14 wire down the track created by the Terumo wire. Follow-up angiography demonstrated a patent lumen with a dissection in the area of the previous occlusion. Both patients experienced relief from angina. Two more patients were treated with the Terumo wire without prior attempt to cross the lesion with the Magnum wire. These lesions were also successfully crossed with the Terumo wire followed by balloon angioplasty resulting in a patent lumen. We conclude, from our limited series of patients, that the Terumo wire is more effective than the Magnum wire in re-opening chronic coronary occlusions.

The influence of Nd-YAG laser and dynamic angioplasty devices on platelet reactivity

A. A. Gehani, A. B. Latif, S. Ashley, S. G. Brooks and M. R. Rees
Cardiac Research Unit, Killingbeck Hospital, Leeds LS14 6UQ

The interaction of laser and dynamic angioplasty devices with arterial wall is the focus of many studies; however, their effects on surrounding blood are largely unknown. We investigated the influence of a dynamic angioplasty catheter with a fast rotating tip, the Kensey catheter (KC), and CW Nd-YAG laser (with sapphire tip) on platelet function. Blood from healthy volunteers was citrated and divided into 5 ml samples of whole blood (WB) or platelet-rich-plasma (PRP). These were exposed to Nd-YAG laser pulses of 10, 25, 50 or 100 Joules. Similar samples were exposed to KC rotating at 20, 40 or 80 thousand RPM, for 30 or 60 s. Control samples were exposed to the appropriate device without activation. Platelet Count (PC), Platelet Aggregate Ratio (PAR) and Platelet Aggregation to collagen in WB and PRP were obtained in all samples. KC caused inhibition of aggregation in WB and PRP proportional to speed and duration ($p<0.001$). A similar effect was obtained with laser energies over 25 Joules ($p < 0.001$), lower energies potentiated aggregation ($p < 0.01$). There was no change in PC or PAR to account for either phenomenon. Transmission electron microscopy showed no significant platelet disruption or release of granules. We conclude that exposure to these angioplasty devices inhibits *in vitro* platelet aggregation, without apparent loss of the integrity of platelet structure. This phenomenon and its clinical implication justify further study.

Percutaneous peripheral laser angioplasty using an Nd-YAG laser and sapphire-tipped device

S. Ashley, A. A. Gehani, S. G. Brooks, R. C. Kester, A. Parkin and M. R. Rees
Cardiac Research Unit, Killingbeck Hospital, Leeds LS14 6UQ

A multipurpose continuous wave Nd-YAG laser (Surgical Laser Technologies) coupled to an optical catheter with a transparent sapphire contact probe, has been used to recanalize 25 total femoro-popliteal occlusions in 20 patients with severe claudication (17), rest pain (three) and ulceration (two). These occlusions were 3–35 cm in length (median 8 cm), and resistant to conventional angioplasty. Recanalization was successfully achieved in 20 lesions (80%) and the resulting channel improved by balloon dilatation. In these patients the mean ankle-brachial Doppler pressure index (ABI) rose from 0.51 ± 0.06 to 0.81 ± 0.05 ($p<0.001$). There was one reocclusion within 72 h, four lesions reoccluded within 2 weeks, one at 1 month, and one at 6 months. Therefore during a median follow-up period of 3 months (range 1–7 months), 13 treated vessels remain patent with symptomatic relief (clinical success 65%). Measurement of limb blood flow (LBF) in these patients, using an isotope and gamma camera, demonstrated a rise from 4.2 ± 0.6 (before) to 9.0 ± 0.9 ml/100 ml tissue/min (1 month after) ($p < 0.001$, normal = 10). The five technical failures were either due to vessel dissection without re-entry (3), or perforation (2). However, there was no requirement for acute surgical intervention in either primary failures or reocclusions. Furthermore, there was no significant deterioration in the patient's symptoms, ABI, or isotope LBF following failed laser angioplasty. In conclusion, this general-purpose laser system is safe and effective for percutaneous recanalisation of peripheral occlusions. Results of longer follow-up are awaited.

Is iliac angioplasty indicated for the treatment of critical ischaemia?

C. J. Wakely, M. G. Wyatt, G. Hartnell and M. Horrocks
Department of Radiodiagnosis and Vascular Studies Unit, Bristol Royal Infirmary, Bristol BS2 8HW

During an 8-year period (1981–1988), 49 iliac angioplasties were performed in 45 patients with critical ischaemia (M:F=34:12, median age 67 years, range 43–85 years). A successful dilatation with clinical improvement was evident in 24 cases (Group I); in 25, the initial angioplasty was unsuccessful (Group II). There was no significant difference in the presenting symptoms or superficial femoral artery patency rates between the two groups. Despite the 24 initial successes in Group I, eight limbs (33%) required a further procedure for disease progression (six surgical, two angioplasty). At 30 days, clinical improvement was noted in 17 limbs; four limbs (17%) had been amputated and three patients (13%) died. In Group II, significantly more limbs required urgent surgery (17) or repeat dilatation (four) ($p<0.001$, χ^2 +Yates' correction). There was also a significantly reduced 30-day success rate within this group ($p < 0.005$, χ^2 + Yates' correction), with clinical improvement noted in only seven limbs (28%). Seven major amputations were required and four patients died. This study confirms the poor results of iliac angioplasty in the presence of critical ischaemia. In 55% of limbs the superficial femoral artery was completely occluded and iliac angioplasty was not able to improve the inflow sufficiently to allow symptomatic relief. Furthermore, operative intervention for failed angioplasty was associated with a significantly reduced success rate, and appreciable morbidity and mortality.

Lipiodol-assisted ultrasound guided liver biopsies

P. A. Gaines, M. Arnold and C. Metreweli
Department of Diagnostic Radiology and Organ Imaging, Prince of Wales Hospital, Shatin, New Territories, Hong Kong

Computerized tomography (CT) of the liver following the administration of Lipiodol into the hepatic artery is a widely used technique for staging hepatomas. Unfortunately both benign and malignant lesions accumulate Lipiodol. We see four new hepatomas each week in this department and only a very small proportion are operable. If the patient is considered suitable for surgery following initial ultrasound (US) staging, angiography with Lipiodol and subsequent CT are undertaken. A nodule that contraindicates surgery requires histological confirmation of malignancy. The biopsy of small hepatic lesions using CT is difficult. The intention of this work is to determine if lesions containing Lipiodol can be visualized and subsequently biopsied using US. Correlation with CT in seven patients, and the use of an original staining technique that allows Lipiodol to be seen on histological sections, have demonstrated that Lipiodol can be visualized using US. We have biopsied focal lesions that were not apparent on the initial US in five patients, and directly injected contrast medium into a suspected 4 mm haemangioma under US guidance. Using this technique, two patients were considered suitable for surgery who had previously been thought to be inoperable. The staging was confirmed to be correct at surgery. We also demonstrate Lipiodol accumulation by haemangiomas and regenerating nodules.

Notes

Radionuclide limb blood flow measurement in the assessment of balloon angioplasty in peripheral vascular disease

A. Parkin, D. Martinez, P. J. R. Robinson, R. C. Kester, P. J. Thorley, K. Sheard and M. R. Rees
Department of Medical Physics, Surgery and Radiology, St James' University Hospital and Killingbeck Hospital, Leeds

A group of 25 patients underwent 28 balloon angioplasty procedures on stenotic lesions of the iliac, femoral or popliteal arteries. The extent of their disease was assessed clinically, angiographically and by radionuclide limb blood flow measurements (Parkin et al, 1986). The mean pretreatment flow below the knee in the affected leg was 5.1 + 2.5 ml/100 ml tissue/min (normal range 10–20 ml/100 ml/min). In 18 patients who showed a significant clinical improvement, limb blood flow increased by 54% after treatment. In seven patients who showed no clinical improvement, the flow was unchanged. Radionuclide limb blood flow measurement provides an objective measurement of treatment response following balloon angioplasty.

Reference

Parkin, A., Robinson, P. J., Wiggins, P. A., Leveson, S. H., Salter, M. C. P., Matthews, H. N. D. & Ware, F. M., 1986. Measurement of limb blood flow using technetium-labelled red cells. *British Journal of Radiology*, *59*, 493–497.

Ripley Suite

Oncology (2.30–3.45)

Radiotherapy for soft tissue sarcomas

C. L. Harmer, E. Wiltshaw and J. M. Thomas
Sarcoma Unit, The Royal Marsden Hospital, London SW3 6JJ

The optimal treatment for soft tissue sarcomas is wide surgical resection. Such optimal surgery will be followed by local recurrence in 40 to 60% of patients unless radiotherapy is also given. At some anatomical sites, and for very large tumours, enucleation is the most that can be achieved, and this will be followed by recurrence in 90% of patients without radiotherapy. Even radical surgery is associated with 28% risk of recurrence without additional treatment (following amputation, only 8%). Radiotherapy is, therefore, usually required except for low-grade tumours where good margins of clearance have been achieved in all three planes. For non-metastatic extremity soft-tissue sarcoma, the 5-year local control and disease-free survival rates for previously untreated patients are 87% and 74% respectively. The control rates at other sites are less favourable, although even where no surgery is possible, about one-third of patients will be controlled by radiotherapy alone. High-dose large volume irradiation is mandatory and, to avoid significant morbidity, meticulous attention to planning is essential, using a shrinking field technique. All patients must be seen in consultation with the surgeon, preferably pre-operatively. Pre-operative radiotherapy can render an initially inoperable tumour removable, although there is no apparent radiobiological advantage in routinely delivering radiation before surgery. Methods of increasing the effectiveness of radiotherapy have yet to meet with success.

Preliminary results of prospective study of hyperfractionated high dose radiotherapy in the management of extremity soft tissue sarcomas

M. H. Robinson, A. Cassoni, C. L. Harmer, J. M. Thomas and G. Westbury
Sarcoma Unit, The Royal Marsden Hospital, London SW3 6JJ

The RMH Sarcoma Unit manages adult extremity soft tissue sarcoma by limb conservation where feasible. Wide surgical resection is usually combined with large-volume post-operative radiotherapy to 60 Gy in 30 fractions in two phases. Where the tumour is inoperable at presentation, 50 Gy in 25 fractions is given pre-operatively. We have previously reported 85% 5-year local control with this policy. In an effort to improve these results with higher doses of XRT, 29 patients (15 male, 14 female, median age 60, range 20–84) have been entered in a prospective hyperfractionation study using 1.25 Gy fractions twice daily with 6 hours' gap, to a dose of 62.5 Gy/5 weeks pre-operatively or 75 Gy/6 weeks post-operatively. Fifteen tumours were situated in the thigh, eight in the lower leg, two in the ankle/foot and one each in the knee, buttock, elbow and forearm. Twenty-three were high-grade, one intermediate and five low-grade. Mean tumour size was 13 cm. Fourteen patients were treated pre-operatively, 10 post-operatively and five without surgery. Only six patients had "adequate" surgical excision. 19/29 received 75 Gy, and only two patients have not completed the planned treatment due to severe acute effects. Only two patients had field length < 25 cm and four were >40 cm. At a median follow-up of 1 year 18/29 are disease free, seven have died, four are alive with disease. There has been one local failure. Peak early reactions (Grade 3) occurred at about 5 weeks but occasionally persisted to 9 weeks. Although too early for full assessment of late damage there have been four wound breakdowns requiring surgical intervention, and the indications are that 75 Gy/60 fractions produce greater late damage in soft tissue than 60 Gy/30 fractions.

Tumour size as a prognosis factor in carcinoma of cervix: assessment by transrectal ultrasound (TRUS)

B. J. Magee, J. P. Logue, *D. McHugh and †R. Swindell
*Departments of Radiotherapy and Oncology, *Medical Physics and †Medical Statistics, Christie Hospital, Manchester, M20 9BX*

Transrectal Ultrasound (TRUS) was used to measure tumour size in patients with carcinoma of the cervix, and to assess its prognostic significance. All patients were conventionally staged and at the time of EUA TRUS was conducted by an independent assessor; the tumour maximum transverse diameter was recorded. All patients were treated by radiotherapy; clinical management was not influenced by TRUS findings. Eighty-one patients were studied. F. I. G. O. stages were: IB 34 patients, IIA 7, IIB 31, IIA 2 and IIIB 7 patients. Mean tumour size by stage were: IB 37 mm, IIA 37 mm, IIB 49 mm, IIIA 42 mm, IIIB 50 mm. There was a significant correlation between size and stage ($p = 0.0001$). With a median follow-up of 18 months, there have been 16 relapses. The relapse rates by stage were: IB 10%, IIA 17%, IIB 22%, IIIA 0%, IIIB 35%, (p = N.S.). There was however, a significant difference in relapse rate by size. At median follow-up, the relapse rates for the size groupings were: <30 mm, 0%; $>30<40$ mm, 11%; $>40<50$, 22%; >50, 38% ($p = 0.03$). Despite the small number of patients and short follow-up, tumour size as measured by TRUS appears to predict relapse. We are now comparing clinical staging, TRUS and MRI.

Comparison of the Ho's and the UICC/AJC stage classifications for NPC

P. Teo, S. F. Leung, S. Y. Ts'ao, W. Foo and P. Yu
Department of Clinical Oncology, Prince of Wales Hospital, Shatin, New Territories, Hong Kong

From 1985 to 1987, 570 nasopharyngeal carcinomas (NPC) were treated with radical radiotherapy. They were prospectively staged according to the Ho's classification. However, on presentation, the size, number, mobility and laterality of the cervical lymph nodal metastases were recorded and from this computer database, accurate retrospective staging according to both the UICC and the AJC classifications was possible. The UICC and the AJC classifications are identical in the overall staging for each patient, and they were considered together and compared with the Ho's classification. The Ho's classification is superior to the UICC/AJC classifications in predicting prognosis and it has a more even distribution of numbers of patients among the stages. There have been highly significant differences in the actuarial survival (ASR), disease-free survival (DFS) and actuarial free-from-distant-metastasis rate (DM) among the Ho's stages but not among the UICC/AJC stages. In the UICC/AJC classifications, over 400 patients fell into Stage IV, which included N2 and N3, T4 and M1, as if they shared the same prognosis. A significant difference in prognosis among these subgroups has been demonstrated, however, in the present study. Concerning tumours confined to the nasopharynx, those involving one site had a local recurrence rate similar to those involving more than one site (UICC/AJC T1 vs T2). This justified the combination of the two into a single T-stage (Ho's T1).

Cranial nerve involvement by nasopharyngeal carcinoma: response to treatment and clinical significance

S. F. Leung, S. Y. Ts'ao, P. Tao and W. Foo
Department of Clinical Radiology, Prince of Wales Hospital, Shatin, New Territories, Hong Kong

The incidence of cranial nerve involvement in a group of 564 patients with nasopharyngeal carcinoma treated in the Prince of Wales Hospital was 12%. The fifth and sixth cranial nerves were the most commonly involved. Fifty-nine patients were evaluable for response of neurological deficit to radical radiotherapy to a dose equivalent to 60 Gy/24 fr/6 weeks. 44% (26/59) of the patients with cranial nerve involvement had complete neurological recovery at a median follow-up time of 18 months after radiotherapy. The cranial nerve response, however, was not a significant predictor of local tumour control. Sixteen of the 59 patients were also given neoadjuvant chemotherapy before radiotherapy, with two patients achieving complete neurological recovery before radiotherapy. The difference in the rate of recovery may be related to the duration of tumour involvement, which in turn is regarded as being related to the distance away from the nasopharynx. As a significant number recovered completely, the potential for recovery of such peripheral nerves is remarkable.

Concomitant chemo/radiotherapy for advanced carcinoma of the head and neck

C. H. Macmillan, K. Carrick, P. J. Bradley and D. A. L. Morgan
Department of Clinical Oncology, The General Hospital, Nottingham NG1 6HA

Twenty-two patients with advanced head and neck cancer received chemotherapy during the first week of irradiation. Seventeen had Stage IV disease; four Stage III; and one Stage II. Age ranged from 21–73 years (median 60). Tumours involved: oral cavity, six; nasopharynx, five; oropharynx, five; secondary node from unknown primary, three; hypopharynx, two; paranasal sinus, one. Radiotherapy was delivered as 2 Gy per day 5 days a week (total dose 50–70 Gy, mean 60 Gy). A continuous intravenous infusion of 5-fluorouracil, 1 g/m^2/24 h started 3 h prior to radiotherapy and continued for 5 days; mitomycin C 14 mg/m^2 was given IV on Day 3. Chemotherapy was well tolerated. Radiotherapy was interrupted in four patients owing to mucosal reaction. Three patients did not receive the dose of radiotherapy intended; one developed necrosis of the hard palate (since healed), one a severe mucositis, and one known to have alcoholic cirrhosis developed a neutropenic infection and died of tumour haemorrhage. One other episode of neutropenic infection occurred. All five patients with nasopharyngeal carcinoma are disease-free. The 17 other patients have an actuarial 2-year survival of 42% (25% disease-free survival). The combination of 5-fluorouracil and mitomycin with radiotherapy is well tolerated and requires further evaluation. We do not recommend its use for patients with abnormal liver function.

Notes

Odorous symptoms during irradiation of the olfactory system

S. M. Sagar and R. J. Thomas
Department of Radiotherapy and Oncology, The Middlesex Hospital, London W1N 8AA

During irradiation of volumes which incorporate the olfactory system, a proportion of patients have complained of a pungent smell. A retrospective study was designed to determine the prevalence of this side-effect. A questionnaire about olfactory symptoms occurring during irradiation was sent to 40 patients whose treatment volumes included the olfactory area. A control group treated away from the head and neck region completed the same questionnaire. Twenty-five patients replied. The regions irradiated were: whole brain (four); pituitary fossa/suprasella (eight); nasopharynx (seven); maxillary antrum (six) and frontal lobe (one). Overall, 60% of patients experienced odorous symptoms during irradiation. The greatest proportion occurred in patients receiving irradiation to the whole brain (75%) and nasopharynx (71%). None of the controls experienced odour. Their description of the odour was unpleasant and consistent with ozone. The radiochemical formation of ozone is well established and its stimulation of the irradiated olfactory receptors in animals has previously been described, but this side-effect of irradiation in humans is apparently not documented. We suggest that patients administered irradiation to volumes which include the olfactory sensory system should be forewarned and reassured before odorous symptoms occur.

Bramham Suite

Oncology (9.00–10.15)

The diagnosis of soft tissue sarcomas by CT and NMR

J. E. S. Husband, M. P. Williams and E. Wylie
Department of Diagnostic Radiology, The Royal Marsden Hospital, Sutton SM2 5PT

Soft tissue sarcomas are rare tumours accounting for less than 1% of all malignant tumours. The principal treatment is surgical resection, but chemotherapy and radiotherapy play an important role. These treatment regimes require precise delineation of tumour extent, and until recently CT has been the mainstay of radiological staging. MRI provides excellent soft tissue contrast as well as multiplanar images, and both of these facilities are a major advantage in the evaluation of soft tissue sarcomas. We have undertaken MR examinations in 82 patients with soft tissue sarcomas in an attempt to evaluate its role in management at the time of diagnosis, during follow-up and when relapse is suspected. The majority of our patients also underwent CT examinations for comparative purposes. Overall our results have shown that MR delineates tumour extent more precisely than CT, but in the group of patients studied pre-operatively there was no significant difference between the two techniques with regard to the presence or absence of neurovascular invasion, adjacent muscle involvement or attachment to skin. CT demonstrates cortical bone erosion better than MR. In evaluation of post-operative patients MR not only shows reduction in tumour size more precisely than CT, but may also reveal changes in signal intensity within the mass. MR and CT are probably equally accurate in the detection of recurrent disease, although the high contrast between tumour and adjacent muscle on T_2-weighted images gives a higher credibility to magnetic resonance imaging.

Notes

Clinical applications of SPECT with special reference to Oncology

V. Ralph McCready
Department of Nuclear Medicine and Ultrasound, Royal Marsden Hospital, Sutton, Surrey SM2 5PT

Recently developments in equipment and radiopharmaceuticals have occurred which have greatly enhanced the value of SPECT in clinical practice. The result has been a great improvement in the clinical images from tomographic examinations which are now available in seconds after the acquisition has been completed. However, these results can only be obtained with the application of good quality control and the correct use of filters to match the clinical situation (Yanch et al, 1988). In the brain SPECT is used mainly for the study of perfusion using HM-PAO. The group at the Royal Marsden Hospital have documented the patterns of perfusion in brain tumours and the changes in perfusion of brain tumours as radiotherapy and chemotherapy produces a response (Babich et al, 1988). However, the perfusion pattern so far has not proved to be a good predictor of response to therapy.In the thyroid gland, SPECT has been used to provide data on radiation dosimetry to correlate the clinical effect of radioiodine therapy with the dose delivered (Webb et al, 1986). Results so far show that the optimum dose to render patients with thyrotoxicosis euthyroid within one year is about 50 Gray. A similar study of dosimetry in carcinoma of the thyroid should help to reduce unnecessary irradiation.In lung tumours perfusion studies with Tc99m HM-PAO have shown large areas with under perfusion which presumably influence the oxygenation and accessibility of chemotherapeutic agents explaining at least in part the poor response rates (Rowell et al,1989). Currently quantitative SPECT is being used to study the effect of vasoactive drugs on lung perfusion. Hydralazine has been shown to improve lung tumour perfusion by 30%. This may prove to be of value in improving the uptake of diagnostic and therapeutic agents. Studies with emission tomography and Gallium 67 are proving useful in the elucidation of masses near the hilum due to the lymphomas. This technique has proved to be particularly useful in evaluating masses seen on X ray after therapy. In the liver SPECT has improved the detection rate for space occupying lesions. It has been shown that improved contrast can be achieved by using 180 degree rotation centred around the right side of the patient (Ott et al, 1983). SPECT has proved useful for demonstrating the vascularity of haemangiomas - a difficult differential diagnosis for ultrasound where a single lesion can mimic early metastatic involvement. Parenchymal lesiosn of the kidney can be imaged more clearly using SPECT especially during and after infections. The results are complementary to ultrasound where scarring may be difficult to image. Although bone scintigraphy can detect abnormalities long before plain X rays, the use of SPECT can improve the visualisation of abnormalities especially in the deeper areas of the body. These include the lumbar spine, pelvis and maxillofacial region. Techniques where the lesion background ratio can be low such as in antibody imaging and white cell scintigraphy for infection can be greatly improved by using SPECT. Lesions which are barely visible on planar imaging can be seen clearly on the SPECT study. Similarly in miBG studies the lesions are more obvious using SPECT and in addition radiation dosimetry studies can be performed more accurately predicting which tumours are likely to respond to radioiodine therapy (Hinton et al, 1987).

References

Babich, J. W., Keeling, F., Flower, M. A., Whitton, A., Fielding, S., Fullbrook, A., Ott, R. J. & McCready, V. R., 1988. *Nuclear Medicine, 14* ,39-44.

Hinton, P. J., Fielding, S. L., Moyes, J. ,Meller, S. T. & McCready, V. R., 1987. *Proceedings of the European Association of Nuclear Medicine Congress, Budapest.*

Ott, R. J., Flower, M. A., Khan, O., Kalarai, T., Webb, S., Leach, M. O. & McCready, V. R., 1983. A comparison between 180° and 360° data reconstruction in single photon emission computed tomography of the liver and spleen. *British Journal of Radiology, 56*, 931–937.

Rowell, N. P., McCready, V. R., Tait, D., Flower, M. A., Cronin, B., Adams, G. E. & Horwich, A., 1989. *British Journal of Cancer, 59*, 135–141.

Webb, S., Flower, M. A., Ott, R. J., Broderick, M. D., Long, A. P., Sutton, B. & McCready, V. R., 1986. Single photon emission computed tomography imaging and volume estimation of the thyroid using a fan-beam geometry. *British Journal of Radiology, 59*, 951–955.

Yanch, J.C., Irvine, A.T., Webb, S. & Flower, M. A., 1988. Deconvolution of emission tomographic data: a clinical evaluation. *British Journal of Radiology, 61*, 221–225.

Comparison of CT and MRI in Ewing's sarcoma

J. F. C. Olliff, C. R. Pinkerton, G. R. Cherryman, M. P. Williams, J. E. S. Husband and J. Pringle
Department of Diagnostic Radiology, The Royal Marsden Hospital, Sutton SM2 5PT

A prospective comparison was made of the CT and MR examinations of 11 patients with Ewing's sarcoma. Eight patients subsequently underwent surgery and this histology was correlated with the diagnostic imaging. One patient had further surgery for suspected recurrence. Sites of disease were rib (three), pelvis (three), tibia (three) and humerus (two). Assessments were made: pre-treatment (five), during/after treatment (11), pre-operatively (six), pre-operatively MR only (two). We assessed the extent of soft tissue and marrow disease, the relationship of disease to the joint/epiphyseal plate, the presence of cortical breakthrough and response to treatment. There was concordance between the two techniques in: 57% (soft tissue disease), 50% (marrow disease), 50% (relationship to joint), 100% (cortical breakthrough), 75% (response to treatment). Histological correlation showed MR to be superior to CT in assessing relationship of tumour to joint (50%). CT and MR both overestimated the extent of soft tissue and marrow disease in one patient each. High signal on T_2-weighted images did not always indicate active disease. We conclude that MRI is better than CT for the assessment of the relationship of tumour to adjacent joint. Very high signal on T_2-weighted images is often due to necrosis or it may be due to vascular new bone formation. CT and MR may overestimate soft tissue and marrow disease.

Wilms' tumour; what changes are seen on CT following chemotherapy?

Y. Y. Ng, M. A. Hall-Craggs and C. Dicks-Mireaux
Department of Radiology, Hospital for Sick Children, Great Ormond Street, London W1N 3JH

Aim. Pre-operative chemotherapy is used in this institution for all patients with inoperable, and some with large, Wilms' tumours (WT) to improve surgical operability and morbidity. The CT appearances of chemotherapy-induced changes in WT have not been described. We have analysed CT examinations of children undergoing preoperative chemotherapy to assess the effects of treatment. *Method.* Enhanced abdominal CTs of 18 patients (aged 11 months–9 years) performed at presentation and following a course of chemotherapy, were reviewed. Disease was staged, tumour appearances were documented and comparison made with surgical and pathological findings at delayed operation. *Results.* Tumour size reduction of 52–99% occurred in 17/18 patients. Poor clinical response to chemotherapy occurred in one child, where the tumour size decreased by only 26%. Disease relapse was associated with an 84% increase in tumour size in one patient. Cystic changes developed in 14/18 tumours and increased calcification in 11/18. Radiologically assessed tumour stage reduced in 13 patients following chemotherapy, in most cases due to regression of hepatic involvement by the tumour. The accuracy of radiological and surgical staging is compared. *Conclusion.* This study demonstrates reduction of tumour size and radiologically-assessed disease stage in the majority of patients undergoing preoperative chemotherapy, and confirms the potential benefits to the surgical management of WT.

Inguinal and iliac lymph node involvement in germ cell tumours of the testis. Implications for radiological investigation and for therapy

M. Mason, T. Featherstone, J. F. C. Olliff, J. E. S. Husband and A. Horwich
Testicular Tumour Unit and Department of Diagnostic Radiology, The Royal Marsden Hospital, Sutton SM2 5PT

Inguinal or pelvic lymph node metastases are an uncommon manifestation of testicular germ cell tumours (TGCT). They are said to occur in patients with disruption of the normal lymphatic pathways due to previous scrotal surgery or local tumour extension, or as a result of retrograde spread from large para-aortic masses. Inguinal or pelvic metastases are of importance because routine CT scanning in patients with testicular tumours does not always include these regions, and because the need for routine treatment to the pelvic and inguinal nodes has been questioned in some patients. On review of the case notes of 1191 patients with TGCT seen at the Royal Marsden Hospital between 1977 and 1989, 22 were found who had developed inguinal (11) or pelvic node (11) metastases. Six patients had a history of maldescent and orchidopexy and one patient had congenitally fused testes. Of the remaining 15 patients, eight had bulky para-aortic metastases (5 cm or more in diameter), two had histological evidence of breach of the tunical vaginalis by tumour and in five patients no predisposing cause was found. Inguinal or iliac metastases were significantly more common in patients with either previous orchidopexy or bulky para-aortic disease ($p = 0.00004$). Patients with a history of maldescent or congenital anomalies of the genitourinary system, or with bulky para-aortic disease, should routinely have the pelvis and inguinal regions included on a CT scan, and patients with a history of maldescent may be unsuitable for local treatments that do not include these areas.

Thin-slice computed tomography for assessment of tumours and responses to therapy

R. G. Sephton, D. Ball and I. Olver
Departments of Physical Sciences, Radiotherapy and Cancer Medicine, Peter MacCallum Cancer Institute, Melbourne 3000, Australia

The main use of CT in oncology is in tumour detection, and typical procedures involve scans stepping through an appreciable longitudinal distance, using relatively thick (*e.g.* 10 mm) slices. Another useful role is in assessing tumours pre- and post-therapy and, to judge from the current literature on this subject, it is common practice to use the same "thick slice" scanning procedure for this as for tumour detection. Here we show that CT can offer the best possible assessment if the tumour is covered by a set of thin (*e.g.* 2.4 mm) contiguous slices and, so long as the approximate location is already known, it is practical and cost-effective to do this. Elementary geometry and clinical examples show that even for tumours of dimensions up to 2–3 cm, thick-slice scanning may give uncertain estimates of tumour dimensions and even erroneous conclusions about post-therapy changes. In contrast, a stack of thin contiguous slices gives much better delineation not only of tumour margins but also of internal inhomogeneity, and the evaluation is less subject to positional reproducibility problems which can affect serial comparisons. Aside from the clinical examples, a simulation experiment is described which suggests that the post-therapy response of a circumscribed lung mass at a known location could be followed down to 1 mm diameter and early regrowth could be readily detected and quantified. In our experience, it is essential to use a dedicated technique for tumour assessment rather than techniques which have evolved for detection. It offers a better physical characterization (of tumour dimensions and macroscopic structure) with considerable potential for illuminating questions about tumour responses, regrowth and even physical inhomogeneity.

Paratesticular Rl abdomyosarcoma: radiological appearances of patterns of disease, presentation and relapse

J. E. Stutley, *M. Mason, J. F. C. Olliff, J. E. S. Husband and *A. Horwich
*Departments of Diagnostic Radiology and *Radiotherapy, The Royal Marsden Hospital, Sutton SM2 5PT*

We present the radiological patterns of disease presentation and relapse in 17 patients with paratesticular rhabdomyosarcoma, who presented to the Royal Marsden Hospital between 1979 and 1989 (age range 9–42 years, mean 18 years). Stages at presentation (RMH/Barts staging system) were: Stage I, 13 patients; Stage II, three patients; Stage III, one patient. All patients had baseline and follow-up CT examinations of the thorax, abdomen and pelvis, with lymphangiography in some to further investigate small volume nodal disease. Of the patients with Stage I disease, six relapsed, with five developing low-density para-aortic nodal masses; two of these patients had Stage III disease at relapse, with liver metastases, and one of these also had pulmonary metastases. The remaining patient developed pelvic nodal disease. At presentation, the three patients with Stage II disease demonstrated para-aortic metastases only. One progressed to develop posterior mediastinal disease with extradural cord compression, retroperitoneal deposits (a nodule behind the left kidney) and ascites. Another died with recurrent pelvic disease. The patient with Stage III disease at presentation had lytic bone deposits, marrow, liver and para-aortic involvement.

Ultrasound examination of regional lymph nodes: value in staging and follow-up of malignant melanoma

Th. Feyerabend, A. Mehringer, G. Treutlein, G. Schindler, R. Schmitt and M. Warmuth-Metz
Division of Diagnostic Radiology and Department of Surgery, Würzburg University Hospitals, 8700 Würzburg, West Germany

Early diagnosis and therapy of regional lymph node metastases are extremely valuable for staging and follow-up of malignant melanoma. We analysed 141 examinations of 100 patients with malignant melanoma using a 5 MHz linear array. The sonographic findings were confirmed either histologically (39 cases) or by the course of disease (88 cases). Fourteen patients were lost to follow-up. As our study shows, ultrasound, with a sensitivity of 95%, is more sensitive than palpation (sensitivity of 78%), whereas palpation has a higher specificity (96%) than ultrasonography (88%). The nearly pathognomonic sonographic appearance of melanoma metastases (round or oval, sharply demarcated, hypoechoic) is demonstrated. Examples of diagnostic pitfalls are given as well. Due to the high sensitivity, ultrasound should be used in melanoma patients pre-therapeutically, regularly in the follow-up and in case of non-diagnostic palpation, *e.g.* due to scar tissue after lymphadenectomy or irradiation.

Endocrine Studies (10.45–12.00)

Endocrine tumour localization

S. McEwan
Edmonton, Canada

Abstract not received.

Computed tomography in phaeochromocytoma

C. S. Deacon and J. E. Adams
Department of Diagnostic Radiology, University of Manchester, Manchester M13 9PT

Phaeochromocytoma is an uncommon cause of hypertension, but early detection is important as surgery may be curative and complications of the tumour may be fatal. CT scans of 48 patients with strong clinical and biochemical evidence of phaeochromocytoma and a mass on CT were reviewed. Full clinical details were available in 38 patients, 34 of whom had surgery: 32 had phaeochromocytoma, and 2 benign cortical adenoma. The majority of patients had a long history of symptoms suggestive of phaeochromocytoma before the diagnosis was considered (average duration 91 weeks). Seven presented acutely (two cerebro-vascular event, one retinal artery occlusion, two malignant hypertension, one post-operative hypertension, one haematuria); five developed hypertension during pregnancy and four were diagnosed after routine medical examinations. Five patients had associated conditions (2 MEA Type II, 2 neurofibromatosis, one von Hippel-Lindau syndrome). CT demonstrated two bilateral adrenal phaeochromocytomas, 32 unilateral adrenal tumours and 10 ectopic tumours (six abdominal, one bladder, three thoracic). Two ectopic tumours (one thoracic, one bladder) were not detected by CT because the regions were not scanned. Tumours were generally large (mean maximum diameter 4.5 cm), of mixed (20) or homogeneous (24) attenuation with contrast enhancement (35/39), particularly of the periphery, some with central cystic components. Three were malignant phaeochromocytomas (1 skeletal metastasis on CT, 1 nodal metastasis not detected on CT). Of 35 patients in whom the clinical outcome after surgery was known, 23 were cured, with resolution of hypertension. CT is a quick and sensitive method for the detection of adrenal and most abdominal phaeochromocytomas, when appropriate scanning protocols are used. Other ectopic or multiple tumours can be difficult to detect, and MIBG scanning and venous sampling are important adjuncts for tumour localization.

The elusive upper parathyroid adenoma on thallium-201/technetium-99m subtraction scintigraphy

T. Y. K. Chan, J. Serpell, A. E. Young, T. O. Nunan and O. Chan
Departments of Radiology, Surgery and Nuclear Medicine, St Thomas' Hospital, London SE1 7EH

A consecutive series of 50 patients with a total of 51 surgically resected and histologically proven parathyroid adenomas was analysed to determine the sensitivity and predictive value of ^{201}Tl/^{99}Tc^{m} scintigraphy in pre-operative localization of the tumour. Twenty-four adenomas were accurately located with respect to their precise anatomical positions: an overall sensitivity of 47%. The sensitivities of precise localization of the upper, lower and ectopic adenomas were 24%, 71% and 60%, respectively. The overall predictive value of precise localization was 71%; the predictive values of positive scans indicating upper and ectopic adenomas were both 100%, although the numbers were small. For scans suggesting lower adenomas, the predictive value was 60%. The overall sensitivity of unilateral localization was 66% (right side 70%, left 56%) with a predictive value of positive scans of 92%. Our results indicate that whilst ^{201}Tl/^{99}Tc^{m} subtraction scintigraphy could be considered a reasonably accurate means of unilateral localization of a parathyroid adenoma, it is poor at detecting the precise anatomical location of the tumour. This is especially true for an upper adenoma. Two explanations for this are proposed. The upper adenoma prolapses inferiorly when pathologically enlarged, which may lead to scintigraphic misinterpretation of a lower lesion, and because of its deeper location, it is more difficult to detect.

Correlation of the ultrasound and histology of the scintigraphically hot thyroid nodule

I. Stewart, A. Ahuja, L. McGuire, K. C. Ho and C. Metreweli
Departments of Diagnostic Radiology and Organ Imaging and Pathology, Prince of Wales Hospital, Chinese University of Hong Kong, Shatin, New Territories, Hong Kong

The ultrasound and histology of 40 patients with scintigraphic "hot" nodules was correlated to determine if "hot" nodules have diagnostic ultrasound appearances. Conventional thyroid imaging starts with scintigraphy which is sensitive but non-specific. We start with high-resolution ultrasound, followed by scintigraphy if indicated. Ultrasound examination was performed with a SDU 7000 7.5 mHz static B-scanner to produce multiple axial and sagittal images. Scintigraphy was performed using 2 mCi Tc pertechnetate. Histology was obtained either by aspiration or surgery. The results show that the ultrasonic appearances of "hot" nodules covers a wide spectrum. A significant number of scintigraphically solitary "hot" nodules are part of a multinodular pathology on ultrasound. The histology of "hot" nodules is varied. Thyroid ultrasound is very sensitive to parenchymal change and the images provide a wealth of information which currently remains difficult to correlate with function and histology. Scintigraphy is no longer a useful primary investigation.

High resolution CT of the pituitary in children with growth hormone deficiency

G. Kelly, J. E. Adams and *A. Price
*Departments of Diagnostic Radiology and *Child Health, University of Manchester, Manchester M13 9PT*

The study was undertaken to assess whether structural abnormalities of the pituitary were present in children with idiopathic growth hormone deficiency (GHD). Fifty-two patients (25 boys and 27 girls), with an age range of 14 days to 15.5 years, were studied. High-resolution CT scans were performed using contiguous 1.5 mm slices through the sellar and suprasellar regions. From these data coronal and sagittal reformations were generated. Quantitative observations were made of pituitary and sella dimensions, and the integrity of the infundibulum was assessed. Structural abnormalities of the pituitary were demonstrated in almost half the patients (partially or completely empty sella, 24; attenuation in calibre or partial absence of the infundibulum, 30). In 26 patients for whom detailed clinical and biochemical information was available, there was a strong correlation between structural abnormalities (empty sella) and (1) perinatal adverse events ($p < 0.001$) and (2) multiple pituitary hormone deficiencies ($p = 0.014$). These results suggest that adverse perinatal events may cause vascular damage and ischaemia. This leads to structural damage to the pituitary gland and infundibulum with consequent growth hormone deficiency, or pan-hypopituitarism, particularly in those with a genetic predisposition to GHD.

Retroconversion of immature teratoma of the ovary: CT appearances

E. Moskovic, T. Jobling, J. Shepherd, E. Wiltshaw and C. Parsons
Department of Radiology, The Royal Marsden Hospital, London SW3 6JJ

Immature teratoma of the ovary is a rare tumour of germ cell origin which as a group constitutes less than 3% of all ovarian cancers, occurring primarily in children and women under 30. We have studied seven patients presenting to the Royal Marsden Hospital 1983–1989 with metastatic immature ovarian teratoma. All patients underwent initial surgery followed by combination chemotherapy and second-look laparotomy. Serial CT scans were performed at 3-monthly intervals until the second laparotomy, and the results were correlated with the CT appearances. Serum levels of the tumour marker alpha feto-protein (AFP) were also monitored. Before the onset of chemotherapy, CT revealed multiple, mainly low-attenuation, inhomogeneous soft-tissue masses, mostly within the pelvis but also in the abdomen in association with bowel loops, the mesentery and retroperitoneally. Within 3–4 months of the start of chemotherapy, dramatic CT changes were evident, with increasing density of these tumour masses, whose margins became better circumscribed, and they developed internal calcification, with areas of fatty density and cystic spaces. On histological examination following second-look laparotomy, these masses were found to represent mature teratoma, analogous to the commoner mature ovarian teratoma or "dermoid cyst". This phenomenon of so-called retroconversion of immature teratomatous deposits to mature disease following chemotherapy correlates exactly with normalization of the raised serum AFP levels seen initially in 6/7 patients. Slow continued growth of some of these mature deposits was seen, causing local pressure symptoms in some cases, but overall no histological relapse occurred in any patient, and all are in sustained remission, 1 to 5 years from diagnosis. Because of its rarity, there has been scanty documentation of this tumour, particularly in the radiological literature, and this is the first report of a series, showing CT evidence of retroconversion to benign pathology.

Low-field MRI in the management of high-volume testicular teratoma

L. Wilkinson and N. C. McMillan
Department of Radiology, Western Infirmary and MRI Unit, Southern General Hospital, Glasgow G11 6NT

In patients with high-volume malignant teratoma there is frequently residual soft tissue following intensive chemotherapy. It is sometimes difficult to distinguish between remaining active disease and mature teratoma, as the appearances on CT are non-specific. We have attempted to evaluate MRI as an alternative, and to determine whether surgical excision can be avoided. Approximately 30 patients were imaged by a low-field resistive MR system in addition to the routine CT protocols. Studies were performed before, and at intervals during, treatment and the results compared with the eventual surgical findings. MRI offered additional information in only a few cases and is as yet unable to replace surgery. Since it is also unsuitable for imaging the lung fields, it cannot be recommended for routine use, but may be of value in those cases in which CT is equivocal.

Notes

Teach-in: Diagnosis of Head and Neck Disease (2.30–3.45)

CT of the head and neck

J. E. Gillespie and *A. Gholkar
*Hope Hospital, Salford and *Newcastle General Hospital, Newcastle-upon-Tyne*

CT has come to be regarded as the examination of choice following initial plain radiography in the evaluation of neoplastic and traumatic abnormalities of the extra-cranial head and neck. CT allows the direct visualization of neoplastic mass lesions as well as areas of bone erosion while in cases of trauma, associated soft tissue injury can be assessed. The anatomical complexity of this region, however, demands careful pre-examination planning in order to derive the maximum amount of information possible. Decisions regarding slice width, image planes required (direct multiplane scanning or multiplanar reformatting), the need for intravenous contrast medium and its method of administration, dynamic data acquisition and scan technique factors all need to be made prior to the examination and tailored to the clinical situation. The CT approach to neoplastic and traumatic lesions affecting the head and neck is discussed, along with the normal and abnormal anatomy of this region.

Notes

Charter Suite

Radiotherapy Dose Distribution and Tumour Control Probability (9.00–12.00)

Determinants of control probability of experimental tumours

N. J. McNally
Cancer Research Campaign, Gray Laboratory, PO Box 100, Mount Vernon Hospital, Northwood, Middlesex HA6 2JR

Experimental tumours allow one to study the general mechanisms underlying the response of human tumours to therapy, to test specific hypotheses, and to investigate new methods of treatment. In general, they do not allow one to make predictions of the response of individual human tumours to therapy. The roles of the five R's of radiology — repair, reoxygenation, repopulation, radiosensitivity and reassortment — have all been studied in experimental tumours. For instance, it has been shown that reoxygenation is an important determinant of the response to fractionation, that there can be accelerated repopulation, that repair rates may be faster than those of normal tissues, that the underlying tumour cell survival characteristics are more like those of early-responding than late-responding tissues (high α/β ratio), and that inherent cellular radiosensitivity is correlated with tumour response to radiation. There are important differences between experimental and human tumours. Experimental tumours probably have a much higher clonogenic fraction than human tumours. They tend to have relatively high hypoxic fractions and grow much faster. Nevertheless, they will continue to be the testing system for new forms of treatment since if these do not work in the model systems, they will be unlikely to be of clinical value.

Dose response data for local tumour control

D. M. Tait
Department of Radiotherapy and Oncology, The Royal Marsden Hospital, Sutton SM2 5PT

Good clinical radiation dose–response data for local tumour control are extremely difficult to generate. In practice, doses are usually adjusted because of patient and/or tumour factors, and therefore reported dose variations, and their effect on outcome, must be very carefully examined. The same bias must be considered when data from many different series are amassed in an attempt to produce evidence of a dose response. Very few clinical trials have incorporated a randomization to different radiation dose levels. However, there is information of this sort for non-oatcell carcinoma of lung, carcinoma of bladder and carcinoma of the head and neck region, and these are reviewed. Other data purporting to provide dose-response information are critically assessed. The influence of the selection of clinical endpoints on the interpretation of the available data is discussed. The clinical significance of the shape of the response curve for tumour control is discussed, together with the relevance of the corresponding normal tissue dose-response curves, in terms of optimizing patient treatments.

The radiosensitivity of human tumour cells

G. Gordon Steel
Radiotherapy Research Department, The Institute of Cancer Research, Sutton SM2 5NG

It is now well established that human tumour cells differ in radiosensitivity. The differences exist in the clinically-important low-dose region up to around 2 Gy. Irradiation at low dose rate amplifies these differences. At low dose rates the less sensitive tumour cells become much more resistant and their cell survival curves become almost straight. A large amount of data has been accumulated on the radiosensitivity of human tumour cells at a dose rate of around 2 cGy/min. This is argued to be the most clinically-relevant dose rate at which to determine radiosensitivity, both fore brachytherapy and for fractionated radiotherapy. Radiosensitivity appears to correlate with clinical response to radiotherapy. Current mathematical models of radiation cell killing allow components to be identified: a linear (*i.e.* exponential, "α-component") and a bending component ("β-component"). At low dose rate, and in the low-dose region of the acute-radiation survival curve, it is the linear component that dominates. The current position is set out, in an attempt to explain the differences in radiosensitivity among human tumour cells.

Influence of dose distribution on local tumour control probability

A. E. Nahum
Joint Department of Physics, Royal Marsden Hospital and Institute of Cancer Research, Sutton SM2 5PT

Recent advances in radiobiology have indicated that the cells in human tumours can be characterized by fairly well-defined values of the radiosensitivity parameter: α. This makes it possible to perform calculations of the number of surviving clonogenic cells, n_s, after a course of fractionated radiotherapy according to $n_s = n_o \exp(-\alpha D)$ where n_o is the initial number of clonogenic cells and D is the total dose. If one assumes that local control is achieved when no single clonogenic cell survives then the tumour control probability, TCP, will be given by $\mathrm{TCP} = \exp(-n_s)$. Using a value of 0.35 for α (corresponding to a surviving fraction after 2 Gy of 0.50) derived from radiobiological data for human bladder tumour cells, a clonogenic cell density of 10^7 per cm^3, a clinically realistic mean tumour volume of 250 cm^3, and a 64 Gy tumour dose, the TCP comes out at 0.50 which is consistent with the observed clinical outcome. However, a very steep slope for the TCP vs dose curve is predicted. By assuming an inter-patient variation in α, normally distributed with $\sigma_\alpha = 0.08$, a clinically realistic slope is obtained. Modern treatment planning systems allow one to compute the dose distribution throughout the 3-dimensional tumour volume. One can thus quantify the effect of non-uniformities in the dose distribution, *e.g.* caused by a lack of beam flatness, hot and cold spots, conformal planning etc, on the expected TCP. The results of such a study for bladder cancer treatments will be reported on. The effect of non-uniform doses in targeted therapy with ^{131}I has also been analysed, revealing that TCP depends critically on tumour size.

Notes

Quantitative Bone Studies (2.30–3.45)

Bone densitometry

I. Fogelman
Department of Nuclear Medicine, Guy's Hospital, St Thomas Street, London SE1 9RT

The introduction and development of photon absorptiometry has enabled accurate bone mass measurements to become available in routine clinical use. With this technique a highly collimated beam of photons is obtained from an isotope source and the transmitted beam intensity is monitored with a well-collimated scintillation detection scheme. The use of beams of known unique photon energies, together with energy selective detection, produces a very stable and therefore precise measurement system. Single photon absorptiometry is generally used to obtain measurements of the forearm, and with the introduction of dual photon absorptiometry it is possible to measure bone mass in both spine and femur, correcting for the variable amounts of soft tissue present. Over the past 2 years dual-energy X-ray absorptiometry has become available and seems set to become the gold standard for bone mineral measurements for the foreseeable future. This latest development in absorptiometry uses an X-ray tube rather than an isotope source to produce a higher photon flux. Thus scan times are speeded up considerably and image resolution and measurement precision are also much improved.

Quantitative bone mass measurement: techniques and correlations

J. E. Adams, R. W. Whitehouse, C. W. Hart and I. Wise
Department of Diagnostic Radiology, University of Manchester, Manchester M13 9PT

Single photon absorptiometry (SPA) was introduced about 20 years ago and provides measures of cortical and integral (cortical and trabecular) bone mineral density (BMD) in various sites of the forearm. Dual-energy photon absorptiometry (DPA) came later and provides measures of integral bone mass in the lumbar spine and femoral neck, with corrections for fat and soft tissue. More recently, dual energy X-ray absorptiometry (DEXA) has been developed, in which X rays are used in place of the gadolinium radionuclide source of DPA, with resulting improved precision and faster scanning time. Quantitative CT is also an established technique for the measurement of bone mass and uniquely permits the separate assessment of cortical and trabecular bone, and is generally applied to the lumbar vertebrae. We have studied 64 patients with a variety of metabolic bone disease who have had bone mass measurements made using SPA, QCT and DXA. Correlations have been sought between different sites (DEXA femoral neck vs. DEXA spine, $r = 0.632$; DEXA spine vs. QCT, $r = 0.76$; DEXA femoral neck vs. QCT, $r = 0.629$; DEXA spine vs. SPA, $r = 0.491$) and the results confirm that measurement of BMD at a certain skeletal site by one technique cannot usefully predict the BMD elsewhere, made by the same or a different technique in the same individual. The different methods are therefore complementary, rather than competitive, in the study of bone mass and the effects of disease on the skeleton.

Notes

Dual energy quantitative computed tomography (DEQCT) for measurement of vertebral trabecular bone composition

R. W. Whitehouse and J. E. Adams
Department of Diagnostic Radiology, University of Manchester, Manchester M13 9PT

Single energy QCT is an established method for measuring vertebral trabecular bone density, but may underestimate the mineral content due to the effect of marrow fat. DEQCT can produce fat-corrected trabecular bone mineral estimates and has greater accuracy than single energy QCT, though poorer precision. The difference between single and dual-energy QCT estimates of bone mineral density is related to marrow composition, particularly fat content, but may also be influenced by increase in soft tissue components of bone, such as unmineralized osteoid in osteomalacia. DEQCT mineral estimates using the method of Genant and Boyd (1977) have been calculated in 54 "normal" patients with no evidence of metabolic bone disease and with normal bone mineral density as measured by SEQCT. Estimation of marrow composition was made from the difference (Δ) between single and dual energy QCT. These data have been compared with those of patients with asymptomatic primary hyperparathyroidism (161), Cushing's syndrome (19) and osteomalacia (14). The data from the normal patients and those with hyperparathyroidism demonstrate an increasing difference (Δ) with age, paralleling the age-related increase in yellow marrow fat content. Patients with Cushing's syndrome show greater difference values (Δ), from normal patients of the same age, suggesting increased marrow fat. Patients with osteomalacia show a decreased difference (Δ), reflecting the presence of unmineralized osteoid. DEQCT may provide information on the quantitative composition of trabecular bone in groups of patients with diseases affecting the skeleton.

An *in vitro* study of ultrasonic attenuation in bone

J. A. Evans, M. Tavakoli and M. Himeur
Department of Medical Physics, Leeds General Infirmary, Leeds LS1 3EX

The technique of Broadband Ultrasonic Attenuation (BUA) measurement of the os calcis as a means of diagnosing osteoporosis was introduced by Langton. In this study, we have investigated the factors affecting the reproducibility and accuracy of the technique and have studied the relative contribution of the attenuation of the constituent materials and the bone architecture. The study demonstrates that reducing the frequency range of the measurements from 200–600 kHz as used by the commercial system, to 400–600 kHz, improves the reproducibility significantly. The coefficient of variation of measurements *in vitro* over a 2-day period was changed from 1.17% to 0.76% by restricting the bandwidth in this way. At 1 mHz, attenuation measurements on collagen, fat and hydroxyapatite have been performed. These show attenuation values of 0.62, 0.60 and 8.0 dB/cm/MHz respectively as compared with a value of roughly 30dB/cm/MHz for cancellous bone *in vitro*. 500 kHz data is currently being acquired but the early indications are that a roughly linear relationship with frequency exists. Thus it seems clear that bone attenuation is dominated not by the nature of its constituents but rather by the internal geometry. The clinical implications of this finding are discussed.

Notes

Index to Authors

Aberle, D. R., 43, 75
Adam, E. J., 20
Adam, A., 39
Adams, H.,2, 43, 55
Adams, J. E., 14, 87, 88, 93, 94
Adler, R. S., 8
Ahuja, A., 53, 88
Akyol, M., 14
Al-Kutoubi, A., 27, 28
Allan, P. L., 53
Al-Saadi, A., 25
Anslow, P. L., 70
Aras, T., 49
Arnold, M., 46, 79
Asbury, D. L., 32, 50, 51, 52
Ash, D. V., 35, 61
Ashley, S., 76, 77, 78
Astley, S. M., 52
Ayoub, A. W., 64

Baert, A. L., 37
Baird, R., 28
Ball, D., 86
Banerjee, B., 13
Barber, C. J., 27
Barber, P. V., 16
Barker, C. S., 70
Barrington, N. A., 9
Bateman, J. E., 62
Baudouin, C. J., 60
Bauer, M., 63
Bauknecht, T., 63
Baxter, G. M., 14, 23
Beales, J. S. M., 56
Beare, R., 64
Behan, M. 21
Bekdik, C. F., 2, 24, 49
Belli, A-M., 29, 76
Benjamin, I. S., 39
Bernard, M. S., 2, 43
Berridge, D. C., 27
Best, J. J. K., 68
Beuthner, G., 63
Bingham, J. B., 4
Birchall, I., 53
Birchall, I. W. J., 72
Blamey, R. W., 52
Blamire, A. M., 69
Blane, A., 68
Bleehen, N. M., 63
Bloomberg, T. J., 42
Boggis, C. R. M., 50, 51, 52
Bohndorf, W., 64
Boxer, D. I., 10
Bradley, M., 54
Bradley, P. J., 82
Bradley, S. A., 7
Brasch, R. C., 67
Breatnach, E., 42
Brennan, A. G., 32
Brett, I., 13
Briggs, J. D., 19
Britton, P. D., 20
Brooks, S. G., 76, 77, 78
Brown, K., 75
Brown, S. C. W., 13
Browse, N. L., 74
Brueton, R. N., 7
Bryant, D. J., 60
Buckwalter, K. A., 8
Bullock, T., 69
Burt, P. A., 16
Butler-Manuel, P. A., 7
Butt, W. P., 7, 9

Caner, B., 2, 24
Caner, H., 2
Caquot, L. M., 73
Carney, D., 21
Carr, D., 44
Carrick, K., 82
Carter, D. C., 38, 68
Carty, H., 12
Carvalho, P., 44
Case, A., 44
Cassoni, A., 80
Ceder, K., 51
Chadwick, D., 15
Chan, O., 27, 39, 74, 87
Chan, T. Y. K., 39, 87
Chapman, M., 53
Chapple, C-L., 31
Charig, M. J., 58
Chennells, P. M., 73
Cherryman, G. R., 84
Chetty, M. N., 39
Chilvers, G., 72
Choudhri, A. H., 27, 28
Clarke, J. A., 14
Clarke, L. J., 62
Clarke, R. L., 17
Cobby, M., 44
Colchester, A. C. F., 4
Cole, P. H., 16
Coleman, N. J., 74
Collins, C. D., 26, 42
Collins, M. C., 45
Cook, P. G., 72
Cooke, D. I., 11
Cooke, S. G., 15, 72
Coral, A., 8, 9
Coulden, R. A., 20
Cowen, A. R., 74
Cox, T., 4
Coxon, R., 69
Craig, J. O. M. C., 31
Cramer, E., 67
Cremin, B. J., 12
Cronin, B., 25
Cumberland, D. C., 76
Cunningham, D. A., 42

Dale, R. G., 63
Dall, B. J. G., 19
Daniell, S. J. N., 62
Davies, A. M., 6, 7
Davies, R. J., 55
Dawood, R. M., 31
de Bruyn, R., 13
de Lacey, G., 71
Deacon, C. S., 87
Deal, M., 21
Dearnaley, D. P., 58
Denekamp, J., 66
Des Rochers, C., 64
Dick, R., 40
Dicks-Mireaux, C., 85
Dincer, A., 24
Dinkel, E., 3
Dische, S., 64
Dixon, A. K., 21, 34, 61
Dobson, D. B., 70
Donald, J. J., 38
Dooley, J. S., 40

Dowling, R. H., 40
Dowsett, D. J., 26
Driver, I., 61
Duffy, P., 23
Durst, M., 63
Dyet, J. F., 75

El Masri, W., 15
El Sayed, A. A., 68
El Nahas, A. M., 68
Ellis, I. O., 52
Ellul, J. P. M., 40
Ennis, J. T., 26
Erbas, B., 49
Erbengi, G., 2, 24, 49
Evans, D. B., 61
Evans, G., 23
Evans, J. A., 94
Evans, P. M., 57
Evans, R. M., 72

Facey, P., 45
Fairhurst, H. J., 38
Farman, P., 20
Faulkner, K., 31
Featherstone, T., 85
Feng, D-H., 32, 33
Ferrell, W. G., 23
Feyerabend, Th., 64, 86
Fielding, J. A., 53
Firmin, D. N., 29
Firth, J. L., 69
Flower, M. A., 25
Fogelman, I., 93
Foo, W., 81
Fowler, J., 6
Fowler, J. L., 7
Fowler, R. C., 73
Fraser, R. D., 7
Freer, C. E. L., 61
Freson, M., 71
Friedburg, H., 3
Frier, M., 27

Gaines, P. A., 46, 79
Gale, A. G., 51, 52, 70, 71
Garber, S. J., 5, 38
Gardener, J. E., 54
Garvie, N., 56
Gattamaneni, H. R., 18
Gausserand, F., 73
Gehani, A. A., 76, 77, 78
Gelister, J. S. K., 58
Gholkar, A., 90
Giakoumakis, G. E., 62
Gibbon, W. W., 6, 9
Gibbs, P., 69
Gill, K. P., 21,
Gillams, A., 40
Gillatt, D. A., 58
Gillen, G. J., 19
Gillespie, J. E., 90
Gilligan, A. C., 18
Gingell, J. C., 58
Goddard, P. R., 28, 44
Golding, S. J., 58
Graves, M. J., 4, 48
Graves, P. E., 4, 48
Gregson, R. H. S., 27
Griffin, J. G., 3
Griffiths, G. J., 53
Guy, R. L., 7

Haddaway, M., 15
Haigh, S. F., 73
Hall, L. D., 61
Hall-Craggs, M. A., 85
Hampshaw, A., 22
Hansell, D. M., 43, 75
Harmer, C. L., 25, 80
Hart, C. W., 93
Hartley, G. H., 50, 51
Hartnell, G., 23, 24, 28, 44, 77, 78
Hasan, A. H., 38
Haskin, M. E.49
Hawnaur, J. M., 1, 2, 68
Haylor, J. L., 68
Hayrapetian, A. S., 75
Hayward, M., 45
Heatley, F. W., 7
Hemingway, A. P., 29
Hendry, W. F., 58
Heron, C. W., 12
Highman, J. H., 31
Hill, C. R., 17
Himeur, M., 94
Hindley, A. C., 16
Hine, A. L., 10, 14
Ho, K. C., 8, 38, 54, 88
Holland, P., 19
Holm, H. H., 36
Horino, M., 48
Horrocks, M., 23, 24, 28, 78
Horwich, A., 34, 58, 85, 86
Hourihan, M. D., 2
Howard, T. M., 32
Huang, H. K., 75
Hughes, P. M., 2, 38
Hughes, T. H., 14
Husband, J. E. S., 83, 84, 85, 86

Ignotus, P., 20, 55
Iizuka, T., 48
Isaacs, D., 46
Isherwood, I., 1, 2, 68
Ivanoff, J., 49

James, D. C., 37
Jaques, P. F., 29
Jaspan, T., 5
Jeans, W. D., 28, 72
Jehu, F. F., 71
Jenkins, J. P. R., 1, 2, 50, 52, 68
Jenkins, R., 42
Jobling, T., 88
Johnson, F., 70
Johnson, R. J., 34
Jones, A. M., 23
Jones, J., 45
Jones, M. C., 55
Jones, T., 25
Joseph, A. E. A., 20, 55
Junor, B. J. R., 19

Kabala, J. E., 15, 24
Kapucu, O., 24
Karani, J., 19
Keal, R., 30
Kean, D., 68
Keightley, A. M., 40
Kelly, G., 88
Kennan, N., 45
Kerslake, R. W., 5, 10
Kester, R. C., 78, 79
Khan, A. N., 6
Kilner, P. J., 29
King, D. M., 58
King, S. J., 73
King, W., 54
Kinsella, D., 10

Ladam, V., 73
Laing, A. H., 25
Landwehrmann, S., 3
Latif, A. B., 78

Lavelle, J. M., 37
Lavender, J. P., 41
Lazarus, J. H., 55
Lea Thomas, M., 74
Leach, M. O., 60
Lees, W. R., 38, 54
Leese, T., 37
Leinster, S. J., 50
Leonard, R., 56
Leung, J., 38
Leung, P. C., 8
Leung, S. F., 18, 81
Leung, Y. K., 8
Lewin, E., 54
Lewis-Jones, H. G., 50, 58
Li, S-J., 32, 33
Lim, J., 17
Lin, M., 46
Lindsell, D. R. M., 46
Lintott, D. J., 73
Lizzi, F., 66
Ljubenov, T., 65
Lloyd, D. C. F., 14
Logue, J. P., 80
London, N. J. M., 37
Longmore, D. B., 29, 41, 47
Loveday, E., 39
Lovell, P., 71
Loverock, P., 64
Lowdell, C. P., 61
Lyn, B. E., 64

MacDonald, A. F., 3
MacKechnie, S., 23
Macmillan, C. H., 82
MacMillan, R. M., 49
MacVicar, D., 73
Magee, B. J., 17, 80
Mamtora, H., 9
Manns, R. A., 6
Mansfield, P., 69
Marchal, G., 37
Marcus, C., 73
Martin, D. F., 38, 45
Martinez, D., 79
Mason, M., 85, 86
Mathur, S., 40
Matthews, I. P., 31
Mattrey, R., 21
Mauro, M. A., 29
Maxwell, A. J., 14, 45
McAllister, W., 42
McAteer, E. J., 53
McCall, I. W., 10, 15
McCarty, M., 21, 28, 42
McCready, V. R., 25, 84
McCreath, G., 14
McEwan, S., 87
McGregor, E., 14
McGuire, L., 88
McHugh, D., 80
McKinney, W. M., 23
McMillan, N. C., 89
McNally, E., 71
McNally, N. J., 91
McNeill, A., 5
McNichol, M., 10
McNicholas, M. J., 3
McRitchie, H., 68
Mehringer, A., 86
Menanteau, B., 73
Merrick, M., 56
Metreweli, C., 8, 38, 46, 53, 54, 79, 88
Millar, K., 71
Mohiaddin, R. H., 29, 41
Mohrmann, U., 63
Molyneux, A. J., 70
Moody, A., 73
Moore, N. R., 61
Morcos, S. K., 68
Morgan, A., 32
Morgan, D. A. L., 82
Morley, P., 14, 19
Morris, E., 6, 19
Morris Jones, P., 18
Morris-Jones, W., 45
Morton, E. J., 62
Moscovic, E., 43, 88
Moss, F., 42
Moule, B., 38
Mourad, K. M., 72
Muir, C., 56
Mulholland, R. C., 10
Mundinger, A., 3
Mundy, J., 25
Murphy, P., 28

Nahum, A. E., 57, 91
Naik, D. R., 22
Naldoken, S., 24
Needham, G., 3
Newstead, M., 50
Ng, K., 53
Ng, Y. Y., 85
Nicholls, R. J., 39
Nicholson, D. A., 50
Niendorf, H. P., 67
Njemanze, P. C., 23
Noble-Jamieson, G., 20
Nomicos, C. D., 62
North, A. D., 10
Notley, M., 16
Nunan, T. O., 87

Occleshaw, C. J., 9, 22
O'Connell, D., 21
O'Driscoll, B. R., 16
Olliff, J. F. C., 84, 85, 86
Olver, I., 86
Ordidge, R. J., 69
O'Reilly, P. H., 13
Ostlere, S. J. O., 11
Othman, S., 55
Ott, D., 3
Ott, R. J., 25
Ozcan, O. E., 2
Özmen, M., 24
Özmen, F., 49

Padayachee, T. S., 4, 48
Page, D. R., 60
Pardy, B. J., 72
Parker, A., 68
Parkin, A., 78, 79
Parsons, C., 56, 88
Patel, B., 45
Paz, R., 41
Pearce, M., 32
Pennell, D. J., 47
Penry, J. B., 15, 58
Perkins, A. C., 27
Persad, R. A., 58
Peterson, S., 21
Pickworth, F. E., 15
Pinkerton, C. R., 84
Pollard, S. G., 21
Porter, A. W., 31
Porter, K. M., 7
Power, W. J., 3
Pratt, B., 25
Pratt, C., 10
Pratt, T. A., 30
Prendergast, C. M., 43
Price, A., 88
Pringle, J., 84
Procter, A. E., 76
Pullicino, V. C., 10, 15

Qi, D-Y., 32, 33

Ramsay, J., 63
Redpath, T. W., 61
Reek, C., 30
Rees, J., 6
Rees, M. R., 26, 49, 76, 77, 78, 79
Rees, R. S. O., 29, 47
Regan, F., 20, 27, 28, 45
Renwick, I., 7
Rhodes, J., 45
Ribeiro, G. G., 17
Richards, C. J., 55
Richter, E., 64
Rickards, D., 5
Rish, S., 62
Rivens, I., 17
Robinson, A. C., 18
Robinson, M. H., 80
Robinson, P. J. R., 11, 79
Roebuck, E. J., 51, 52
Romaniuk, C. S., 9, 26
Rowlands, P. C., 21
Rubens, M. B., 43
Rugg, T., 64
Russell, J. G. B., 70
Rustin, G., 34

Sagar, S. M., 82
Sampson, C., 42
Sandhu, A., 7
Sandrasagra, F. A., 20, 55
Sasaki, Y., 48
Saunders. M. I., 64
Schindler, G., 86
Schlief, R., 67
Schmitt, R., 64, 86
Schulz-Wendtland, R., 63
Seedhom, B. B., 11
Sefton, G. K., 11
Sen, M., 39
Sephton, R. G., 86
Serpell, J., 87
Servomaa, A., 51
Sharma, A., 46
Shaw, A. J., 30
Sheard, K., 79
Shelton, C. G., 62
Shepherd, J., 88
Sherborne, R., 72
Sims, C., 61
Sissons, G. R. J., 46
Smith, A. C., 38
Smith, S. R., 58
Somers, J. M., 21
Spencer, J. A., 46, 70
Steel, G. G., 91
Steele, B., 7
Stehling, M. K., 69
Stenning, S., 63
Stewart, I., 8, 38, 54, 88
Stout, R., 16
Stutley, J. E., 86
Sugrue, D., 26
Sutton, M. L., 17
Swallow, J., 54
Swann, A. C., 11
Swindell, R., 17, 80
Swindell, W., 57

Tait, D. M., 91
Tapiovaara, M., 51
Tarnawski, M., 4, 48
Tateno, M., 48
Tavakoli, M., 94
Taylor, C., 23
Taylor, M. G., 4
Taylor, C. J., 52
Taylor, W., 40
Tennant, S., 22
Teo, P., 81
ter Haar, G. R., 17, 64
Theodoropoulos, S., 41
Thirsk, G., 22
Thomas, G. V., 6
Thomas, J. M., 80
Thomas, R. J., 82
Thorley, P. J., 79
Tiller, G., 73
Todd-Pokropek, A., 31
Tran, T., 20, 27, 28, 45
Treutlein, G., 86
Ts'ao, S. Y., 18, 81
Tung, K. T., 27
Turnbull, L.W., 68
Turner-Warwick, R., 5
Turul, H., 2
Twining, P., 54, 55

Underwood, S. R., 29, 47
Ünlü, M., 49
van Holsbeck, M., 8
van Tiggelen, R., 71
Vernon, J., 71
Vivian, G. C., 15

Wakely, C. J., 78
Walker, G. E., 51, 52
Ward, S. C., 75
Warmuth-Metz, M., 86
Wastie, M. L., 27
Watkinson, A. F., 76
Watt, I., 8
Webb, S., 62
Welch, T., 71
Wellings, R., 6
West, D. J., 21
Westbury, G., 80
Whitehouse, G. H., 50
Whitehouse, R. W., 93, 94
Wilde, P., 10
Wilde, R. P. H., 28
Wilkinson, L., 89
Williams, L. A., 6
Williams, J., 9
Williams, L. B., 10
Williams, M. P., 34, 83, 84
Williams, C. E., 58
Wilson, C. B., 25
Wilson, A. R. M., 51, 52
Wilson, N. M., 74
Wiltshaw, E., 80, 88
Wise, I., 93
Wisheart, J. D., 28
Wood, A. M., 51
Workman, A., 74
Worthington, B. S., 1, 5, 10, 51, 52, 69, 70, 71
Wright, D. J., 40
Wyatt, M. G., 23, 24, 78
Wylie, E., 83

Yacoub, M., 41
Yates, D., 31
Yeung, E. Y. C., 39
Yiakoumakis, E. N., 62
Young, A. E., 87
Young, I. R., 60
Yu, P., 81

Zuccollo, J., 55

BIR Bulletin

Honorary Editor, BIR Bulletin: D. Rickards, LRCP, MRCS, FFR(D)SA, FRCR
Please address all correspondence to: Honorary Editor, BIR Bulletin, The British Institute of Radiology,
36 Portland Place, London W1N 4AT

The British Institute of Radiology is not responsible for opinions expressed in the BIR Bulletin

Radiology 90
Harrogate, 11-13 June 1990

Radiology 90 — Cementing the Partnership between Science and Medicine

by Tim Hogan (BIR Publications Manager)

Radiology 90, the 48th Annual Congress of the British Institute of Radiology, was held in Harrogate on 11–13 June 1990. For the first time, the BIR meting was held concurrently with the Annual Congress of the College of Radiographers. This meant that MED X RAY, the joint technical exhibition of the two bodies, was held over three days only, and was especially well attended by both delegates and companies.

Radiology 90 was designed to provide an interface for science and medicine, to show that disease can be tackled successfully by employing an integrated approach in which workers with different specialist backgrounds and using different techniques combine their efforts. The guiding philosophy was that the radiological sciences need a multidisciplinary approach to evolve, a reflection of the very nature of the BIR itself.

The Scientific Programme Chairman was Dr Ralph McCready, who implemented a new format for the scientific sessions. Typically, a session began with an Invited Review lecture which was followed by proffered papers on a related theme. In addition, Consensus Workshops were introduced in which difficult topics were debated with the aim of providing guidelines. Teach-ins provided an opportunity for delegates to become more familiar with new and evolving techniques and to discuss their own experiences. The Work in Progress sessions enabled current research findings to be transmitted without delay. The scientific poster session was coordinated by Dr Marilyn Law and contained a record number of posters — 119 in all. In total, the Congress featured 301 presentations with sessions held in parallel in four different locations.

The Harrogate International Centre proved to be a popular choice of venue, with scientific sessions held in the Moat House Hotel.

Gathered at the Registration desk are, from left to right, Dr Marylin Law, Tony Hudson, Nelleke van Helfteren, Jackie Feenstra, Claire Brice, Terry Moran and Charlotte McLeish

CENTRAL LIBRARY

MED X RAY and all the other locations were linked by a covered walkway, giving the impression that all the events occurred under one roof. Harrogate itself was easily reached by road and via Intercity trains to York and Leeds, and the town provided pleasant surroundings with good local amenities.

Of course, the BIR Annual Congress is not only an excellent opportunity for delegates to catch up on the latest radiological developments: it is also a great social occasion with a wide variety of enjoyable events to share with partners and colleagues. As well as the evening functions, there were golf and angling competitions and a full accompanying persons programme.

In the report that follows, I hope to illustrate some of the highlights of the meeting and hint at the vast range of radiological interests addressed. As I can only skim over the surface of the meeting there will be many notable points omitted.

I would like to thank all those who have helped me write this article, especially Professor Hill, Dr McCready and many of the Session Chairmen. I have quoted freely from the speakers themselves, so must apologize if there are any inaccuracies or remarks taken out of context.

The Bulletin will be delighted to publish comments and recollections of members, so please do send in your contributions.

Monday

As in last year's meeting, BIR Past President Professor Brian Worthington contributed to many of the sessions both in his capacity as session chairman and as a presenter/coauthor of papers (8 papers in all!). Professor Worthington opened the session *Central Nervous System* with a paper on MRI disorders of the spinal column.

Professor Worthington reported that MRI is becoming the preferred method of addressing clinical problems based on disc pathology. Disc degeneration is part of normal senescence, and its pathophysiology is complex and incompletely understood. There is also a high incidence of premature disc degeneration in adolescents with disc protrusion. Animal model studies have demonstrated the evolution of changes occurring in disc space infection and have emphasized the value of MRI in early diagnosis.

Many of the papers in this session illustrated the development of MRI and CT in central nervous system studies.

For instance, paranasal sinus disease, which is an area of confusion both in ENT practice and for radiologists, can be elucidated by CT demonstration of the ethmoid sinuses. G. Needham reported that sinus occurred in 26% of patients referred for cranial CT for non-sinus-related problems, and went on to discuss the implications, with particular reference to ENT collaboration and new techniques in endoscopic surgical treatment.

MRI has been recommended in the detection of dural sinus thrombosis. A high signal in the sinuses is a reliable indicator of thrombosis; conventional X-ray angiographic techniques have been previously relied upon to demonstrate flow obstruction. T. S. Padayachee described how MR venous angiography can augment MR assessment, and concluded that combined MR imaging and angiography enable a more complete assessment — since this does not involve ionizing radiation, contrast media or vessel puncture it may be the imaging modality of choice for assessing this condition.

Concurrently, a well attended session on *Renal Studies* was proceeding. Several contributions considered paediatric renal disease. R. de Bruyn reviewed the role of prenatal ultrasound in identifying fetuses requiring investigation for congenital urological abnormalities, as well as discussing current trends in post-natal management. F. E. Pickworth reported success with ^{99}Tc^{m}-MAG3, a new Hippuran substitute for renograpy and indirect micturating cystography, in the investigation of children with renal tract disease. This is safe and sensitive, giving more information than any other single imaging modality, and may reduce the need for other investigations with higher radiation doses.

J. A. Clarke pointed out that critical analysis of current radiological practice is necessary to ensure that limited resources are used effectively. With this in mind, a study was designed to investigate the use of intravenous urography in a large teaching hospital. It was found that, with more selective and appropriate use of IVUs, not only could financial savings be made but also exposure of patients to potential reaction to IV contrast media and unnecessary ionizing radiation could be reduced.

With the present interest in systemic therapy, the session *Radioisotope Diagnosis and Therapy in Oncology* was especially interesting. The main messages that came out of the session were the very real potential of a treatment to relieve the pain of prostatic carcinoma by the use of strontium-90, and the controversy as to the best way to treat hyperthyroidism with radioactive iodine to avoid hypothyroidism.

This session ran on to a general *Radiotherapy* session. R. Stout reported that intraluminal radiotherapy is now a simple, safe and effective palliative for selected patients with inoperable lung cancer, achieving results comparable to those of conventional X-ray therapy and with less morbidity. G. R. ter Haar discussed a strategy for the use of highly focused ultrasound for the non-invasive destruction of deep seated tumours *in vivo*. The strategy for damaging tissue volumes was discussed in terms of exposure times, the proximity of adjacent lesions and the planning of the positions in which successive lesions should be placed.

The well attended session on *Cardiovascular Studies* contained some fascinating presentations. D. C. Berridge reported that monoclonal platelet-specific antibody imaging may help detect sites of recent arterial thrombosis and define those patients most likely to benefit from intra-arterial thrombolysis, so avoiding major surgery.

Thoracic aortic MRI has been shown to be an accurate method for demonstrating a wide variety of abnormalities, and this procedure has been advocated as a routine investigation following thoracic aortic surgery as there can be unexpected complications. G. Hartnell presented results that do not favour this policy — MRI is worthwhile if there are objective signs of deterioration following surgery, but otherwise routine scanning is unlikely to demonstrate important abnormalities that would affect management.

P. Murphy reported a retrospective study of the fate of asymptomatic superficial artery stenoses, and warned that the fact that such a stenosis is asymptomatic is no reason for complacency and no guarantee that a limb-threatening situation may not develop in the future.

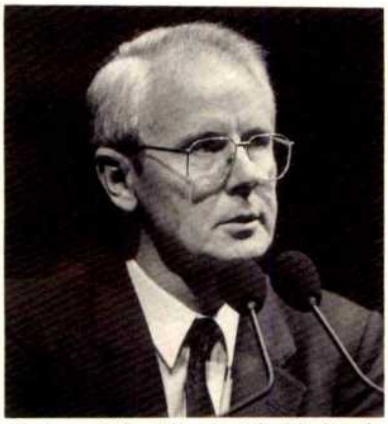
Professor Holm delivering The MacKenzie Davidson Lecture

The *MacKenzie Davidson Memorial Lecture* was delivered by H. H. Holm of Herlev Hospital, University of Denmark. His lecture was entitled "Interventional Ultrasound". Ultrasound is the most convenient, rapid and precise method to guide a puncture needle, and thus interventional ultrasound is playing an increasingly important role in the management of more and more patients. Material can be removed from or deposited into the body for both diagnostic and therapeutic reasons, and hence there are a large and increasing number of applications. Professor Holm reviewed the newest and most important applications in this field, and concluded that this is a valuable low risk tool which spares many patients much more traumatic procedures and that many new applications of the technique will be discovered.

Later in the day was the session on *Quality Assurance and Protection*, chaired by the BIR President, Professor C. R. Hill. Though sometimes regarded as a tedious chore, QA remains an inescapable necessity for every modern film-based X-ray department. R. M. Dawood discussed the role of QA in PACS — the arrival of new digital technology brings unfamiliar problems that have important practical consequences for the viability of these systems. Dr Dawood examined the problems of setting up and monitoring the performance of TV display systems.

M. Pearce reminded us that good QA cannot compensate for poor inherent performance, as illustrated by his diary of a "rogue" mobile breast screening unit. Clinical problems included poor repeatability, poor reproducibility, premature termination of exposure and refusal to expose, but provided an excellent opportunity to test all aspects of their QA programme.

I. P. Matthews reported that an observational study of radiographic practice in Wales showed a wide interdepartmental variation in patients' exposure for the same type of examination. A significant determinant in this variation was the choice of projection. Guidelines are being evaluated which, if successfully implemented, would have important implications for prevention of radiogenic cancers attributable to current use of diagnostic radiology in the UK.

Tuesday

Tuesday began with a popular session on the *Liver and Biliary System*, which provoked informed and entertaining discussion.

J. J. Donald described a prospective study of patients with ultrasound diagnosis of cholangiocarcinoma who underwent endoscopic retrograde cholangiopancreatography (ERCP). Knowledge of the distribution of the tumour is essential for successful treatment either by palliative stenting or by surgery. The ERCP findings agreed precisely with ultrasonography in 56% of cases and estimated greater tumour extent in 22%. Ultrasonography is an accurate diagnostic method which maps the biliary tree and provides information on tumour load, important in planning treatment.

Patients with symptomatic benign biliary strictures provide a therapeutic dilemma when surgery is not considered appropriate and when an endoscopic approach is not possible. A. Gillam described the treatment of 21 patients with either percutaneous insertion of an endoprosthesis or percutaneous balloon dilation.

The data do not suggest any preference for either technique.

In the Consensus Workshop *Evaluation of Skeletal Metastases*, a practising clinical oncologist, a general radiologist and a nuclear medicine specialist reviewed the clinical role of bone scintigraphy in lung, breast, prostate and bladder cancer and in the lymphomas. The panel, with much audience participation, were able to come to a consensus defining the most effective use of skeletal investigations of these conditions, and the conclusions will be published shortly.

Of particular interest in the session on *Chest Radiology* was the presentation on CT evaluation of pulmonary involvement in systemic lupus erythematosus by C. M. Prendergast. High resolution CT of the chest has an established role in the assessment and monitoring of diffuse diseases of the lung parenchyma. Dr Prendergast described a review of patients with this disease who had high resolution CT of the thorax. The pathological explanation of the appearances needs clarification since it remains uncertain whether they represent areas of lupus pneumonitis, infarction due to vasculitis, or intercurrent infection.

Several papers in the session on *Mammography* were concerned with the accuracy and objectivity of mammographic interpretation.

Even though radiologists employ systematic analysis methods, significant observer variability exists. S. M. Astley presented results showing that computer-based image analysis methods can increase diagnostic confidence, although difficulties were encountered in defining microcalcification.

Elucidating the mammographic areas radiologists visually examine in detail is a key factor in understanding the dificulties and sources of errors. A. G. Gale compared eye movement data from trainees and experts, based on overall visual search strategy, areas examined and the amount of time spent on specific areas. G.E. Walker considered aptitude and personality assessments and related the reasons for variable performance to training offered.

The mammography theme was continued later on that day with a Teach-in *Interpretation of Mammograms*. The session concentrated on the implications of normal variants and abnormalities seen on mammograms, with the following essential questions. (1) What, if anything, do you do once an abnormality has been observed? (2) Why are the patients managed as they are? (3) How well does the natural history of breast disease support current practice?

In the Charter Suite, Tuesday started off with *Advances in Oncology*. Improvements in the local control of tumours in a significant number of patients could be achieved by increasing the dose to the tumour; however, the tolerance of normal tissues to radiation damage is frequently the limiting factor. A. E. Nahum described conformal therapy, which aims to shape the high-dose volume to conform to that of the target volume, thereby reducing the volume of normal tissues irradiated. W. Swindell later pointed out that great care must be taken when positioning the patient on the treatment machine to ensure that the target volume (which is referenced to the patient) is correctly positioned relative to the treatment volume (which is referenced to the machine).

Several papers addressed carcinoma of the bladder. R. A. Persad discussed the role of MRI for staging bladder cancer. It is important to perform accurate staging since the detection of invasion into the muscle layers or into adjacent organs will affect both prognosis and the treatment available. It was shown that MRI offers an accurate method of imaging transitional cell carcinoma that has extended beyond the wall of the bladder. The main problem is the differentiation of non-invasive from muscle-invasive disease. M. J. Charig described a study undertaken to determine the role of CT in the management of carcinoma of the bladder. The implications for the planning of examinations and for the allocation of CT appointments were discussed.

The session *Oncology* took place on Tuesday afternoon. R. G. Dale reviewed the current status of radiobiological modelling, and emphasized the versatility of the linear-quadratic model. G. R. ter Haar discussed the effect of ultrasound on the cytotoxicity of some chemotherapeutic agents — ultrasound enhances the toxicity of daunomycin at 37°C but has no effect on that of chlorambucil at this temperature. C. Des Rochers gave a most interesting talk in which she warned of possible consequences of cigarette smoking by patients undergoing radiotherapy for head and neck tumours. Patients should be encouraged to stop smoking altogether prior to radiotherapy to minimize mucositis. Patients can prove very resistent to such advice, and patient counselling was discussed.

The Congress Theatre was the venue for the *Mayneord Memorial Lecture*, "Conjoint Application of Diagnostic and Therapeutic Ultrasound", given by F. L. Lizzi (of the

To mark the success of the seventh BIR/3M Mayneord Memorial Lecture, Professor Frederic Lizzi is presented with the commemorative Mayneord Lecture plaque. Handing it over is Ken Roche (2nd left), General Marketing Manager of 3M Medical Imaging Systems Group, who sponsor the annual lecture. They are joined by Mrs Audrey Mayneord and BIR President Kit Hill

Riverside Research Institute, New York), and financed by 3M UK plc. New diagnostic ultrasound techniques are permitting more precise quantification of tissue microstructure in terms of the sizes, concentrations and mechanical properties of tissue elements. The presentation reviewed the theory and practical applications of tissue characterization techniques, and included the theoretical model and clinical instrumentation developed for ophthalmic therapeutic ultrasound, and how the diagnostic and therapeutic results are combined, using three-dimensional computer graphics, to plan therapy sessions and monitor alterations induced within tumours.

The *Sylvanus Thompson Memorial Lecture* was given by Professor J. Denekamp, CRC Gray Laboratory, Mount Vernon Hospital, and was entitled "Tumour Vasculature: a Bother or a Boon to the Cancer Therapist?".

Professor Denekamp recalled that poor vascular supply to solid tumours has been recognized as a common feature, giving rise to concern about hypoxic radioresistance and poor drug delivery. Recently, the neovasculature has been cited as a possible target for tumour attack. Over a decade ago, it was proposed that cytotoxic drugs could be targetted at the proliferating endothelium because the endothelial turnover is 50–100 times higher than in normal vessels.

Since then it has become apparent that the biochemical features of immature endothelium may influence the possibility of causing localized vascular collapse or occlusion, or the activation of prodrugs. Vascular effects may be an important component in the tumour response to many forms of therapy, such as hyperthermia, photodynamic therapy, biological response modifiers and certain cytotoxic drugs. The potential avalanche effect, in which ischaemic death of thousands of cells can occur for each vessel occluded, should not be discarded lightly. With this common aim, studies of neovascular pathology, physiology and morphology, endothelial proliferation and differentiation and haemodynamic properties must be brought together.

Professor Denekamp giving the Sylvanus Thompson Memorial Lecture

Wednesday

The final day of this full and varied meeting began with *Contrast Studies* and an Invited Review entitled "Contrast-enhanced MRI: Gd-DTPA and Beyond", given by R. C. Brasch, and supported by Schering Healthcare. Contrast media, by providing functional information and clues to specificity, can enhance the diagnostic value of the MR examination. The most successful approach has been to manipulate the MR tissue intensity chemically, by instilling small amounts of paramagnetic or superparamagnetic substances that reduce tissue relaxation times. Gd-DTPA was the first such agent to be used widely in clinical practice. Side effects, such as nausea and headache, occur with only a very low frequency.

Several other papers contributed results on Gd-DTPA. Professor Worthington reported that the overall effects of intravenous Gd-DTPA on tissue signal in intracranial tumours are complex, depending on dosage, time of administration, pulse sequence and tissue type. High speed EPI permits the kinetics of tissue enhancement to be analysed for the first time. Dynamic scanning is a valuable adjunct to a morphological study of tumours. The temporal profile of enhancement may allow discrimination between different tumour types and assessment of the malignant potential of a single type.

R. Schlief gave an Invited Review on contrast agents for diagnostic ultrasound. The effects of ultrasound contrast media are based on small bubbles of air (microbubbles) which do not diffuse in the body like X-ray or MRI contrast media, but remain within the vascular system. Such contrast agents extend the capability of diagnostic ultrasound, *e.g.* in the broad spectrum of vascular imaging, transcranial Doppler, tumour delineation, tissue/tumour perfusion, urology and gynaecology.

Two oncology sessions were held on Wednesday. V. R. McCready looked at clinical applications of SPECT. Recent developments in equipment and radiopharmaceuticals have resulted in a great improvement in the images from tomographic examinations, available seconds after acquisition. However, there must be good quality control with the correct use of filters. R. G. Sephton discussed the use of thin-slice CT for assessment of tumours and responses to therapy, and proposed that CT can offer the best assessment if the tumour is covered by a set of thin contiguous slices and that if the approximate location is known it is practical and cost effective to do this.

The optimal treatment for soft tissue sarcomas is wide surgical resection; such optimal surgery will be followed by local recurrence in 40–60% of patients unless radiotherapy is also given. C. L. Harmer reported that pre-operative radiotherapy can render an initially inoperable tumour removable, although there is no apparent radiobiological advantage in routinely delivering radiation before surgery.

During irradiation of volumes which incorporate the olefactory system, some patients complain of a pungent smell. S. M. Sagar concluded that the formation of ozone is to blame, and that patients should be forewarned and reassured before treatment.

The session on *Quantitative Bone Studies* transmitted the important message that bone density measurements are now well established in routine clinical practice. Single photon absorptiometry is used to obtain measurements of the forearm, and with the introduction of dual photon absorptiometry it is possible to measure bone mass in both spine and femur. Over the past two years, dual-energy X-ray absorptiometry has become available and seems set to become the gold standard for bone mineral measurements for the foreseeable future. In future, more women may be screened at the time of the menopause to detect osteopoenia with a view to predicting those who are at greatest risk of developing osteoporosis.

Professor C. R. Hill's BIR Presidential Address considered the question "A Future for Radiological Science?". Professor Hill recounted that the past 20 years have been an exciting and productive period, but that continuation at the current level of activity cannot be taken for granted. In the first place, society seems to have undergone a cultural shift away from science, even when it seems to support health care; secondly, the scientific basis of some, although not all, branches of radiology and radiotherapy seems to be approaching a point of complete exploitation.

Professor Hill's BIR Presidential Address: "A Future for Radiological Science"

A number of branches of the subject were examined in turn, and it was concluded that, whilst advances corresponding to systematization of existing knowledge will continue it is in only certain areas, such as nuclear medicine and ultrasound, where there is potential for substantial and fundamentally based advances.

On duty at the BIR stand: (from right to left) Mary-Anne Piggott (General Secretary), Tim Hogan (Publications Manager) and Tony Hudson (Administration Manager).

I hope that my selection from Radiology 90 will provide interesting reading. This was my first Radiology meeting and I came away with many strong impressions. Not least of all, I enjoyed having the opportunity to meet BIR members at the newly instigated BIR stand.

Radiology and Oncology 91

The 49th BIR Annual Congress, Radiology and Oncology 91, and MED X Ray will be held in Brighton on 29 April–1 May 1991, and will again be concurrent with the COR meeting. The work behind the scenes by BIR Committee members and staff to ensure the success of such a large and important meeting is daunting and is well under way now. This includes production and distribution of promotional literature, assessment of proffered papers followed by publication of the Abstracts, and liaison with MED X RAY exhibitors, to name but several aspects. Dr Stephen Golding is at the helm as Scientific Programme Chairman.

Do come to Radiology and Oncology 91 to help make this an even more successful meeting. You will be very welcome.

RADIOLOGY AND ONCOLOGY 91

Brighton 29 April–1 May 1991

British Institute of Radiology 49th Annual Conference

Radiology and Oncology 91 will incorporate all aspects of modern radiology for all those concerned with diagnostic radiology and radiotherapy.

Proffered abstracts are invited for oral and poster presentation and will form a major element of the meeting. Deadline for receipt of abstracts: **20 November 1990**

Library Progress

Major developments have taken place recently in the library. The computers have now been installed. We have opted for "Lending Library" which is a fully integrated library automation software package run on compaq hardware and supplied by Fretwell Downing Ltd. "Lending Library" and the other shortlisted package, CALM from Pyramid Computers, were demonstrated by the two companies at 36 Portland Place last month for the benefit of BIR management and Mr Carl Pavey of Nucletron Trading UK, one of the BIR's sponsors. The final choice was only made after visits to already installed sites to see the software in operation in a working environment.

The library has also installed its purpose-built issue counter/inquiry desk, a revolving periodicals rack and an information display unit. The library has also been recarpeted to match the ensuite du Boulay Members' Room which is now open for use, having been furnished.

The library is open 9 a.m.–5 p.m. on Monday, Wednesday and Friday and 9 a.m.–7. p.m. every Tuesday and Thursday.

Stephen Johnson
Systems Librarian

The journal stock includes more than 100 titles. Although journals may not be taken out of the library, there is a photocopy service, also available by post or FAX. A list of current journals is available on request and is also published in the March and September issues of the Bulletin. Most books (except the historical collection) are available on loan.

Members can apply to the BIR librarian for a visitor's card which allows limited use of the RSM library for reference purposes, including photocopying and searches.

The BIR Library is open weekdays 9 a.m.–5 p.m. (7 p.m. on Tuesdays and Thursdays).

Recent additions to the library

Babcock, D. S. (Ed.), 1989. Neonatal and Pediatric Ultrasonography. (Clinics in Diagnostic Ultrasound, 24).

Baverstock, K. F. & Stather, J. W. (Eds), 1989. Low Dose Radiation: Biological Bases of Risk Assessment.

Breton, J.-L., 1987. Rayons Cathodiques et Rayons X.

Cahill, D. R., Orland, M. J. & Reading, C. C., 1990. Atlas of Human Cross-sectional Anatomy, with CT and MR Images, 2nd edn.

Carr, D. H. (Ed.), 1988. Contrast Media.

Chiu, L., Stanford, W. & Yiu-Chiu, V., 1986. Computed Tomographic Angiography of the Mediastinum.

Commission of the European Communities, 1989. Radiation Protection Training and Information for Workers. Proceedings of a Seminar held in Luxembourg 28–30 November, 1988, EUR 12177 EN.

Fitzgerald, M. et al, 1989. The Commissioning and Routine Testing of Mammographic X-ray Systems. A Protocol Produced by a Working Party of the Diagnostic Radiology Topic Group. IPSM Report 59.

Fogelman, I. & Collier, B. D., 1989. Atlas of Planar and SPECT Bone Scans.

Goldstein, S. R., 1989. Endovaginal Ultrasound.

Hagan, A. D. & DeMaria, A. N., 1989. Clinical Applications of Two-dimensional Echocardiography and Cardiac Doppler, 2nd edn.

Herlinger, H. & Maglinte, D. (Eds), 1989. Clinical Radiology of the Small Instestine.

Madkour, M. M., 1989. Brucellosis.

Neal, M. P., Tisnado, J. & Cho, S. R. (Eds), 1989. Emergency Interventional Radiology.

Sharp, P. F., Gemmell, H. G. & Smith, F. W., 1989. Practical Nuclear Medicine.

Silverman, P. M. & Zeman, R. K. (Eds), 1990. CT and MRI of the Liver and Biliary System.

Stevens, J. M., Valentine, A. R. & Kendall, B. E., 1988. Computed Cranial and Spinal Imaging: a Practical Introduction.

Sughara, T. & Saito, M. (Eds), 1988. Hyperthermic Oncology. Proceedings of the 5th International Symposium, Kyoto 1988.

Vanel, D. & McNamara, M. T. (Eds), 1989. MRI of the Body.

Weaver, D. D., 1989. Catalog of Prenatally Diagnosed Conditions.

New BIR Members

Medical

Dr S. I. Al-Agha, MB, DcH
(Ireland) Diagnostic Radiologist
Dr Sally A. Bradley, MB, ChB, FRCR
(Birmingham) Diagnostic Radiologist
Dr Mark J. Charig, DSc, MRCP, FRCR
(Oxford) Diagnostic Radiologist
Dr A. Kadir H. Hasan, MB, ChB, PhD, FRCR (Part 1)
(Glasgow) Diagnostic Radiologist
Dr Caroline L. Holland, MB, ChB, MRCP, FRCR Part 1
(Birmingham) Diagnostic Radiologist
Dr Philip Jones, BA, Bm, BCh, MRCP
(London) Radiotherapist/Oncologist
Dr Vaneeta Kapur, MB, BS
(India) Diagnostic Radiologist
Dr Apostolos Karantanas, MD, PhD
(Greece) Diagnostic Radiologist
Dr Nirmala Nagaraj, MB, BS
(London)
Dr Christopher S. Romaniuk, MB, ChB, MRCP, FRCR
(Leeds) Diagnostic Radiologist
Dr Santosh K. Sarkar, MB, BS, DCH, DMRD
(London) Diagnostic Radiologist

Dr John A. Spencer, MA, MB, MRCP, FRCR
(Oxford) Diagnostic Radiologist
Prof. Carl-Gustav Standertskjold-Nordenstam, Professor and Chairman
(Finland) Diagnostic Radiologist
Dr Elizabeth J. N. Stockdale, MB, ChB, DMRD, FRCR
(Aberdeen) Diagnostic Radiologist
Dr Hywel G. Thomas, MB, ChB, MRCP
(Oxford) Diagnostic Radiologist
Mr Richard M. Wellings, FRCS Ed, MB, ChB
(Birmingham) Diagnostic Radiologist
Dr David J. Wilcock, MA, MB, BChir, MRCP
(Nottingham) Diagnostic Radiologist
Dr Michael Williams, MA, FRCR
(Plymouth) Diagnostic Radiologist

Non-Medical

Mr Timothy P. Allen
(Wolverhampton) Engineer
Dr Diane C. Crawford, BSc, MSc, PhD
(Sutton) Physicist
Miss Pamela M. Kimber, FCR(R)
(Southampton) Radiographer
Miss Rosemary P. Klem, TDCR
(Birmingham) Radiographer
Mr J. Alistair R. McIntosh, BSc, FIPSM
(Coventry) Physicist
Mr Call R. Pavey, BSc
(Nucletron Trading Ltd), Executive
Mrs Leslie Robinson, DCR(R)
(Birmingham) Radiographer
Mr Bryan Stubbs, BSc, MSc, FIPSM
(Leeds) Physicist
Mr David Travis, HDCRT, MDCR
(Reading) Radiographer
Miss Diana Whait, TDCR(T)
(Northwood) Radiographer

Is there a seminar, conference or evening get-together you want to organize, but you don't have the time? The BIR Conference Office may be able to help you. Please call Vanessa Whitehead, Conference Manager, to discuss possibilities. Tel: **071-580 4085**

BIR Calendar

Current Progress in Magnetic Resonance: Scientific and Clinical Developments in the UK
October 15, 1990
Middlesex Hospital
Organizer: Prof. B. S. Worthington

Cracking Gallbladder and Bile Duct Problems
October 18, 1990
All day meeting
Chairmen: Drs A. Adam and R. Dick
Organizer: Dr A. Adam, London
Speakers: Drs J. Walters, C. Russell, P. R. Mueller, W. R. Lees, D. Martin, R. Dick, I. S. Benjamin and A. Adam

Prediction and Measurement of Tumour Response to Treatment
November 9, 1990
Organizer: Dr R. Camplejohn
Speakers: Drs P. R. Twentyman, J. Ramsey, S. E. Davidson, C. Mothersill, P. Price, J. C. M. Bremner, P. Anderson, J. E. D. Dyson, C. S. Parkins, G. D. Wilson, S. M. O'Reilly, and A. E. Johnson and Prof. S. Dische.

IPSM/Nuclear Medicine Radionuclide Tomography Update
November 21, 1990
All day meeting organized by IPSM

Planning for 1992 — A Review of Radiation Protection Practice in Member States of the EEC
December 5, 1990
Institution of Electrical Engineers
Organizer: Dr M. Fitzgerald

Practical Issues in Breast Cancer Screening
January 17, 1991
Scientific Societies Lecture Theatre
Joint BIR/RCR/RSM all day meeting
Organizer: Prof. G. H. Whitehouse
Speakers: Drs J. Law, N. M. Perry, G. J. Bickler, A. R. M. Wislon, C. Rubin, M. J. Michell, F. E. White, J. Austoker, A. K. Tucker and Prof. J. Chamberlain

Cerebral Blood Flow Practical Measurement and Clinical Relevance — a Multimodality Approach
February 12, 1991
All day Meeting
Organizer: Dr A. H. Smith
Abstract deadline: 5 October 1990

CT — Are the Bells and Whistles Worthwhile?
February 20, 1991
All day meeting
Organizers: Drs A. Dixon and S. Golding

Radiobiology Proffered Papers
February 22, 1991
Organizer: Dr R. Camplejohn

Radiation Oncology/IPSM
April 10, 1991
All day meeting organized by IPSM

RADIOLOGY AND ONCOLOGY 91 and MED X RAY
29 April–1 May
Metropole Hotel, Brighton

Radiation Oncology and Radiobiology: Particle Therapy
June 7, 1991

The New Legislation — Friend or Foe (After the White Paper ... and into Europe)
June 13, 1991
All day meeting orginized by the Industry Committee
Chairmen: C. A. Joslin, O. Craig and D. Rigg
Speakers include J. Roylance, I. Watt, E. Sutherland, I. Isherwood and P. Richardson

Conversazione
June 27, 1991
Painter's Hall, London
Lecture: " Half an Eye on the Sty", by Sir Stephen Furness.

Unless otherwise indicated, enquiries about the following events should be addressed to the Conference Manager, British Institute of Radiology, 36 Portland Place, London W1N 4AT (Tel. 071-580 4085).

Industry news

F50 Stress Electrode from Abingdon

Abingdon Instruments have introduced a new foam carbon fibre stress electrode for ECG monitoring under stringent conditions.

The F-50 has all the benefits of carbon fibre with a higher signal, longer operating life and lower cost. Carbon fibre electrodes do not need gel, are non-irritant and are reactivated by the patients' sweat. They can be used with carbon fibre leads for MRI and X-ray applications.

For further information and samples contact Abingdon Instruments, Hamlyn House, Buckfastleigh, Devon TQ11 ONR. Tel. 0364 42537.

Radiotherapy Simulator Enhancements from Varian

Varian has announced that its Zimatron C-Series line of radiotherapy simulators has been enhanced with new software, control system console and a newly designed hand pendant. The new Ximatron version 3.5 software provides auto functions for 20 standard anatomical setups which are customer definable to bring all Ximatron parameters into end positions with a touch of a single button. This saves much time during patient setup.

The new operator console has dedicated controls for rotational, vertical, lateral and longitudinal movements, as well as separate controls for asymmetric and symmetric wires and blades. A new microprocessor-controlled hand pendant is also available. LED displays and backlit function keys make the pendant easy to read in a dimly lit simulation or treatment room.

Varian recently celebrated the shipment of the 200th Ximatron C-Series simulator to St John's Hospital in Springfield, Missouri. The first C-Series Ximatron was installed in 1986 in St Luke's Hospital, Guildford, England. Since then the equipments has been installed in more than 30 countries.

For further information please contact Varian International AG, Medical Equipment, Kollerstrasse 38, CH-6300 Zug, Switzerland.

Gyroscan Passes 1000 Marker

On Wednesday 8th August 1990 the 1000th person was scanned by the Philips Gyroscan T5 Magnetic Resonance Scanner at the King Edward VII Hospital in Midhurst, Surrey.

The Gyroscan T5 has been a major success for Philips; in less than two years over 150 systems have been sold worldwide. The system can be installed in a comparatively small space thanks to the newly designed actively shielded 0.5 tesla magnet.

New Expanded Line of Clear-Pb Mobile X-ray Barriers from Victoreen

Although lead aprons are used for protection from secondary radiation, a full-height radiation barrier provides practically total body shielding during extended X-ray procedures. Most barriers have small lead–glass windows which limit the user's field of view and freedom of movement. Clear Pb-mobile X-ray barriers are an ideal alternative.

Each full-height radiation barrier consists of a transparent Clear-Pb lead–plastic viewing panel with smooth rolling casters for mobility and is shatter-resistant. Barriers are available in four sizes; in addition, a choice of window thickness is offered in the two larger models.

For further information contact Nuclear Associates, 100 Voice Road, Carle Place, NY11514-1593 USA.
Tel. 516 741 5414.

From left to right: Dr E. Burrows, Consultant Radiologist, Mr Robert Davies, Philips Medical Systems, Miss Agnes Shiels, the 1000th person to be imaged, Dr I. Gabe, Senior Physician, Miss Jenny Davies, Matron.

BIR Company Subscriber Scheme

The BIR company subscriber scheme is aimed at all companies with and interest in radiology and addied sciences.

For and annual subscription of £250 p.a. member companies are offered an attractive benefits package.

To find out why your company should join the leading edge companies listed below, please contact Mr Tony Hudson, Administration Manager, British Institute of Radiology, 36 Portland Place, London W1N 4AT. Tel: 071-580 4085.

Agfa-Gevaert Ltd
27 Great West Road, Brentford, Middlesex TW8 9AX. Tel. 081-560 2131.
Product Areas 1. Contact Mr G. Mountford, Director.

American Medical Ltd
PO Box 971, London SW10.
Tel. 071-352 8051. Fax: 071-376 4508.
Product areas 1, 3, 4, 5, 7, 8.
Contact Betsy Riley, Managing Director.

Amersham International PLC
Lincoln Place, Green End, Aylesbury, Bucks HP20 2TP. Tel. 0296 395222.
Product areas 4, 5, 6.
Contact Mr James McLaughlin, Sales and Marketing Manager.

Bard Ltd
Forest Houe, Brighton Road, Crawley, West Sussex RH 11 9BP.
Tel. 0293 27888, ext. 2204.
Product area 2.
Contact Anna Shores, Product Manager.

British Nuclear Fuels plc
Room 525, Hinton House, Risley, Warrington, Cheshire WA3 6AS.
Tel. 0925 835022.
Product areas 8, 11. Contact Dr R. J. Berry, Director of Health and Safety and Environmental Protection.

Bruel & Kjaer (UK) Ltd
92 Uxbridge Road, Harrow, Middlesex, HA3 6BZ.
Tel. 081-954 2366.
Product areas 3, 6.
Contatct Mr Dennis Lewis, Sales Manager.

Cardiac Services Ltd
95A Finaghy Road, South Belfast BT10 OBY. Tel. 0232-625566.
Product areas 1, 3, 4, 5, 6.
Contact Mr R. J. Brown. Managing Director.

Du Pont (UK) Ltd
Wedgwood Way, Stevenage, Hertfordshire SG1 4QN. Tel. 0438 734000.
Product areas 1, 3, 4, 5, 6, 7, 9 and 10.
Contact Mr E. G. Lovat, Product Manager, Diagnostic Imaging.

E. G. & G. Limited
Vale Road, Windsor, Berkshire SL4 5JP. Tel. 0753 855611.
Product areas 1, 6, 7, 8.
Contact Miss Susan Holgate, Sales Executive (Therapy).

Elscint (GB) Ltd
Colonial Business Park, Colonial Way, Watford, Herts WD2 4PT.
Tel. 0865 340900.
Product areas 1, 3, 4.
Contact Faith Gorman, Marketing Manager.

E-Z-EM Ltd
1230 High Road, Whetstone, London N20. Tel. 081-446 9714.
Product areas 1, 2, 8.
Contact Mr D. F. Wills, Sales and Marketing Manager.

Fuji Photo Film (UK) Ltd
125 Finchley Road, London NW3 6JH.
Tel. 071-586 9351.
Product areas 1, 3.
Contact Mr R. G. Brown, Marketing and Administration Manager.

Gammex-RMI Ltd
34 Shakespeare Street, Nottingham NG1 4FQ. Tel. 0602 483807.
Product areas 1, 3, 4, 5, 6.
Contact Miss Eileen Parr, Commercial Manager.

IGE Medical Systems Ltd
352 Buckingham Avenue, Slough, Berks SL1 4ER. Tel. 0753 874000.
Product areas 1, 2, 3, 4, 5, 6, 8, 9.
Contact Jill Mitchell, UK Sales Support.

Kodak Ltd
PO Box 66, Station Road, Hemel Hempstead, Herts HP1 1JU.
Tel. 0442 61122.
Product area 1.
Contact Mr P. E. Blackwell, Manager, Health Sciences Division.

3M UK PLC
3M House, Bracknell, PO Box 1, Berks RG12 1JU. Tel. 0344 426726.
Product area 1.
Contact Mr Alan Budge, Marketing Manager.

Mallinckrodt Diagnostica (UK) Ltd
11 North Portway Close, Round Spinney, Northampton NN3 4RQ.
Tel. 0604-46132.
Product areas 4, 5.
Contact Mr D. G. L. Wood, Business Manager.

M. A. S. Medical Ltd
Armytage Road, Brighouse, West Yorkshire HD6 1QF. Tel. 0484 721906.
Contact Martin York, Managing Director.

Merit Health Systems Ltd
1 Viking Close, Great Gutter Lane, Willerby, North Humberside HU10 6DZ. Tel. 0482 652252.
Product area 13.
Contact Mr W. Blakemore, Director.

Medical XraySupplies Ltd
Unit 12, Kingsbury Industrial Estate, Church Lane, Kingsbury, London NW9 8AU. Tel. 081-205 9500.
Product area 1.
Contact Mr R. J. Laird, Sales Director/Mr K. Wartnaby, Managing Director.

Mitsubishi Electric UK Ltd
Travellers Lane, Hatfield, Herts AL10 8XB. Tel. 07072 78756.
Product area 14.
Contact T. F. McCloud, Sales and Marketing Manager.

National Power plc
14 Newgate Street, London EC1A 7AM. Tel: 071-634 6898.
Product areas 7, 8.
Contact Mr A. J. Swanson, Assistant Company Secretary.

Nuclear Associates
100 Voice Road, Carle Place, New York 11514-1593, USA.
Tel. 516-741 7614.
Product areas 1, 3, 4, 5, 6, 8.
Contact Mr H. Glasser, General Manager.

Nucletron Trading Ltd
Nucletron House, Tarporley Business Centre, Tarporley, Cheshire, CW6 9UY. Tel: 0829 733611.
Product areas 6, 8.
Contact Mrs Marilyn A. Hart, Office Manager.

Nycomed (UK) Ltd
Nycomed House, 2111 Coventry Road, Sheldon, Birmingham B26 3EA.
Tel. 021-742 2444.
Product areas 1, 3.
Contact Mr L. Birch Hansen, Managing Director.

Oxford Magnet Technology
Wharf Road, Eynsham, Oxford.
Tel. 0865 880880.
Product area 1.
Contact Pauline Hobday, Director of Sales and Marketing.

Philips Medical Systems
Kelvin House, 63–75 Glenthorne Road, Hammersmith, London W6 OLJ. Tel. 081-741 1666.
Product areas 1, 3–8.
Contact J. M. Woolston, Sales and Marketing Manager.

Polaroid (UK) Ltd
Ashley Road, St Albans, Herts AL1 5PR. Tel. 0727 59191.
Product areas 1, 3.
Contact David Hollingworth, Marketing Manager.

Premise Engineering Ltd
Tibbs Hill Road, Abbots Langley, Watford, Herts WD5 ODR.
Tel. 09277-67433/63320.
Product area 8.
Contact Mr R. K. Beach, Director.

Radiological Protection Services Ltd
61 Lind Road, Sutton, Surrey SM1 4PP. Tel. 081-643 6374.
Product area 8.
Contact B. H. Cutting, Managing Director.

Quantel Ltd
Administration Centre, Kiln Road, Newbury, Berkshire RG13 2HA.
Tel. 0444 232323.
Product areas 2, 10.
Contact Mr Christopher Trim, Publicity Officer.

Schering Health Care Ltd
The Brow, Burgess Hill, West Sussex RH15 9NE. Tel. 04446 6011.
Product areas 1, 2, 3.
Contact Mr A. Greaves, Product Manager.

Sony (UK) Ltd
Jays Close, Viables, Basingstoke, Hants RG22 4SB. Tel. 0256 483564.
Product areas 1, 3, 4, 5, 7, 8.
Contact Richard Holt, Marketing Manager.

Toshiba Medical Systems UK
Manor Court, Manor Royal, Crawley, West Sussex RH10 2PY.
Tel. 0293 560772.
Product areas 1, 2, 3, 4, 9, 10.
Contact Mr S. M. Weeden, Manager X-ray Products.

Toshiba Medical Systems Europe BV
Schieweg 1, 2627 An Delft, The Netherlands. Tel. 015 61 0121.
Product areas 1, 2, 3, 4, 9, 10.
Contact Mr P Blonk, Office Manager, X-ray BU.

X-rite (H. Miller Graphics Ltd)
8 Moody Street, Congleton, Cheshire CW12 4AP. Tel. 0260 279988.
Product areas 1, 12.
Contact Mrs P. Dhanani, Medical Sales.

Wardray Products Ltd
Hampton Court Estate, Summer Road, Thames Ditton, Surrey KT7 OSP. Tel. 081-398 9911.
Product area 8.
Contact Mr R. B. Wardley, Managing Director.

KEY TO PRODUCT AREAS

1: Diagnostic X-ray including NMR and CT
2: Interventional radiology
3: Ultrasound
4: Nuclear medicine
5: Radiopharmaceuticals
6: Radiotherapy and oncology
7: Radiobiology
8: Radiation protection
9: PACS
10: Image processing
11: Nuclear fuel cycle services
12: Quality assurance.
13. Radiology data management computer systems
14. Video printing

Meetings and Courses

Imaging and Interventional Techniques in Uro-Radiology
October 31, 1990
Surrey
Further details: Dr E. A. North, Consultant Radiology, Department of Radiology, St. Helier Hospital, Wrythe Lane, Carshalton, Surrey, SM5 1AA.

Successful Financial Management in the NHS of the Future
November 6–7, 1990
Birmingham
Further details: Paul Groves, ICM Marketing Ltd, 50 Occam Road, Surrey Research Park, Guildford, Surrey, GU2 5YS. Tel: 0483 37107.

Radiotherapy for the 90s: a 2-day Meeting
November 8–9,1990
Manchester
Further details: B. Magee/R. D. Hunter, Radiotherapy Department, Christie Hospital and Holt Radium Institute, Wilmslow Road, Withington, Manchester M20 9BX. Tel: 061 445 8123, Ext. 293/310.

Iranian Congress of Medicine and Image
November 11–16, 1990
Mashhad, Iran
Further details: Congress Secretariat, Imam Reza Hospital , PO Box 1339, 91735, Mashhad, Iran. Tel: 051-93034; Fax: 512015 IR.

Endo-urology and Percutaneous Access Course
November 22–24, 1990
Newcastle upon Tyne
Further details: Mrs D. Lees, Teaching Centre, Freeman Hospital, Freeman Road, Newcastle upon Tyne NW7 7DN. Tel. (091) 2843111, Ext. 3051.

British Medical Ultrasound Society 22nd Annual Scientific Meeting
December 4–6, 1990
Harrogate
Further details: Miss Anne Summers, British Medical Ultrasound Society, 36 Portland Place, London W1N 3DG.

The Biological Council 6th Annual Symposium
December 13–14, 1990
London
Further details: Mrs B. Cavilla, c/o Institute of Biology, 20 Queensberry Place, London SW7 2DZ.

MRI Update
December 13–15, 1990
New York
Further details: Radiology Postgraduate Education Office, Cornell University Medical College, 1300 York Avenue, New York, NY 10021, USA. Tel: (212) 746 2522.

Diagnostic Radiology in Aruba
January 20–26, 1991
Aruba
Further details: Radiology Postgraduate Education Office, Cornell University Medical College, 1300 York Avenue, New York, NY 10021, USA. Tel: (212) 746 2522.

Computed Body Tomography 1991 — The Cutting Edge
February 7–10, 1991
Florida, USA
Further details: Program Coordinator,The Johns Hopkins Medical Institutions, Office of Continuing Education, Turner Building, 720 Rutland Avenue, Baltimore, Maryland 21205. Tel: (301) 955-2959.

Principles and Practice of Clinical MRI
February 28–March 5, 1991
Florida, USA
Further details: Program Coordinator,The Johns Hopkins Medical Institutions, Office of Continuing Education, Turner Building, 720 Rutland Avenue, Baltimore, Maryland 21205. Tel: (301) 955-2959.

Dosimetry in Diagnostic Radiology
March 19–21, 1991
Kirchberg, Luxembourg
Further details: CEC Mr K. Schnuer, Bat. Wagner C 331, L-2920, Luxembourg. Tel: (352) 4301-6388; Fax: (352) 4301-4646.

2nd European Meeting on Contrast Media Research
March 26–27, 1991
Lyon, France
Further details: P. G. Promotion, 17 rue Childebert, 69002 Lyon, France. Tel: (33) 78 42 67 70.

Radiology and Oncology 91
April 29–May 1, 1991
Brighton
Further details: The Conference Office, The British Institute of Radiology, 36 Portland Place, London W1N 4AT. Tel: 071-580 4085.

CAR '91 (Computer Assisted Radiology)
July 3–6, 1991
Berlin, Germany
Further details: Professor Heinz U. Lemke, c/o University Klinikum, Rudolf Virchow - Wedding, Altes Rontgenhaus - Raum 1005, Augustenburger Platz 1, D-1000 Berlin 65. Abstract deadline: November 15, 1990.

9th International Congress of Radiation Research
July 7–12, 1991
Toronto, Canada
Further details: 9th International Congress of Radiation Research, 1891 Preson White Drive, Reston, VA 22091, Canada. Tel: (703) 648-3780. Deadline for abstracts: January 15, 1991 and for Junior Investigators Awards: October 15, 1990. Alternatively, contact Miss B. M. de Vere, The Royal Society, 6 Carlton House Terrace, London SW1Y 5AG.

6th World Congress in Ultrasound
September 1–6, 1991
Copenhagen, Denmark
Further details: Torben Larsen, Department of Gynecology, Herlev Hospital, DK-2730 Herlev, Denmark.

European Congress of Radiology '91
September 15–20, 1991
Vienna, Austria
Further details: The Congress Secretariat ECR '91, c/o Vienna Academy of Postgraduate Medical Education and Research, Alser Straße 4, A-1090 Vienna, Austria. Tel: (1) 421383; Fax: (1) 42138323.

6th Asian Oceanian Congress of Radiology
December 14–18, 1991
New Delhi, India
Further details: M. L. Malhotra, Executive Secretary, Aggarwal Imaging Research Centre, 10-B, Kasturba Gandhi Marg, New Delhi-110 001, India.

As a service to our readers, notice of meetings or courses will be inserted free of charge. Please send full details to the Honorary Editor, BIR Bulletin.

Please send articles for the Bulletin or any comments or suggestions you may have about the Bulletin to The Honorary Editor, BIR Bulletin, 36 Portland Place, London W1N 4AT.

BIR Bulletin

Honorary Editor, BIR Bulletin: D. Rickards, LRCP, MRCS, FFR(D)SA, FRCR
Please address all correspondence to: Honorary Editor, BIR Bulletin, The British Institute of Radiology, 36 Portland Place, London W1N 4AT
The British Institute of Radiology is not responsible for opinions expressed in the BIR Bulletin

The New Code of Practice for High Energy Photon Therapy Dosimetry

Based on the NPL Absorbed Dose Calibration Service

Bill Owen
Division of Radiation Science and Acoustics
National Physical Laboratory

The code, published by the Institute of Physical Sciences in Medicine (IPSM, 1990) recommends that the type NE 2561 therapy-level ionization chamber, manufactured by NE Technology Ltd, should continue as the secondary standard chamber when calibrated by the National Physical Laboratory (NPL) in terms of absorbed dose to water. The NPL absorbed dose calibration service offers calibrations for cobalt-60 γ radiation and seven X-ray qualities between 4 and 19 MV with beam filtrations matching those of clinical beams where possible. Absorbed dose to water is given by the product of the corrected electrometer reading with the secondary standard in water and the NPL calibration factor for the incident radiation quality. The NPL beam quality is expressed in terms of quality index, *i.e.* tissue to phantom ratio of 20 to 10 cm depths in water with a constant field size of 10 x 10 cm. The NPL calibration factors are applicable to the secondary standard chamber in a thin-walled Perspex sheath at the appropriate International Commission on Radiation Units and Measurements reference depth (ICRU, 1973) in water. The factors are for chamber air conditions of 20°C, 1013.3 mbar and 50% relative humidity, and are corrected for losses due to ion recombination. The NPL primary standard is a graphite calorimeter which is used to calibrate three type NE 2561 ionization chambers as working standards in terms of absorbed dose to water. Secondary standards are then calibrated at NPL by comparison with the working standards in a water phantom. The secondary standard calibration factors have an overall uncertainty of ±1.5% at the 95% confidence level.

The Code recommends that the secondary standard is used to calibrate a field instrument by comparison in either a water or Perspex phantom using a 10 x 10 cm field at the appropriate ICRU reference depth in that both the secondary standard and the field instrument should be in their respective waterproof sheaths so that the size of the air gap between the chamber and its sheath is the same at calibration as when used in a water phantom. The calibration should be carried out using the machines and radiation qualities that will subsequently be measured by the field instrument. The quality index for the comparison beam should be measured and used to interpolate the appropriate secondary standard calibration factor from the NPL calibration data.

The Code recommends that a calibrated field instrument should be used in a full-scatter water phantom for the measurement of dose rate from a cobalt-60 unit or for the calibration of a machine dose monitor. For routine check measurements the Code recommends that the calibrated field instrument be used in a Perspex phantom for convenience.

The current UK Code of Practice for high energy photon dosimetry (Hospital Physicists' Association (HPA), 1983) is based on an NPL 2 MV air kerma calibration of a secondary standard and on energy-dependent conversion factors, Cλ, quoted in the Code in terms of machine MV. Apart from the difficulty of measuring MV, NPL measurements have shown that absorbed dose to water calibration factors are dependent on the degree of beam filtration as well as MV. The advantage of quality index is that it is a practical measurement which takes account of both MV and the relatively heavy beam filtration of clinical beams. The agreement between absorbed dose to water derived from the HPA 1983 Code with an uncertainty of up to 3.5%, and that from the new Code is within 1.5%.

References

HPA, 1983. Revised code of practice for the dosimetry of 2 to 35 MV X-ray, and of caesium-137 and cobalt-60 gamma ray beams. *Physics in Medicine and Biology, 28,* 1097–1104.

ICRU, 1973. *Measurement of Absorbed Dose in a Phantom Irradiated by a Single Beam of X or gamma Rays. ICRU Report 23* (ICRU, Washington DC, USA).

IPSM, 1990. Code of practice for high energy photon therapy dosimetry based on the NPL Absorbed Dose Calibration Service. *Physics in Medicine and Biology* (in press).

Another Gold for British Radiology

Congratulations to Professor Brian Worthington, BIR Past President, who has been awarded the 1990 Gold Medal of the Society of Magnetic Resonance in Medicine: the USA-based, major organization in the field internationally. This news is particularly good as it means that seven out of a total 17 of these awards have now come to our UK colleagues. The news is all the more remarkable in view of the disparity of provision of scanners in this country (33 installed) and in the USA (2000).

Congratulations also to Dr Ian Young on becoming President-elect of the SMRM.

C. R. Hill

Patrick Bishop

It is with regret that we announce the death of Patrick James Bishop, who worked as part-time BIR Librarian from 1971 to 1982. He was also the librarian of the Cardiothoracic Institute in Brompton.

BIR Calendar

Unless otherwise indicated, enquiries about the following events should be addressed to the Conference Manager, British Institute of Radiology, 36 Portland Place, London W1N 4AT (Tel. 071-580 4085).

Prediction and Measurement of Tumour Response to Treatment
November 9, 1990
Organizer: Dr R. Camplejohn
Speakers: Drs P. R. Twentyman, J. Ramsey, S. E. Davidson, C. Mothersill, P. Price, J. C. M. Bremner, P. Anderson, J. E. D. Dyson, C. S. Parkins, G. D. Wilson, S. M. O'Reilly, and A. E. Johnson and Prof. S. Dische.

IPSM/Nuclear Medicine Radionuclide Tomography Update
November 21, 1990
All day meeting organized by IPSM

Planning for 1992 — A Review of Radiation Protection Practice in Member States of the EEC
December 5, 1990
Institution of Electrical Engineers
Organizer: Dr M. Fitzgerald
Chairmen: Prof. C. A. Joslin, Mr D. Gifford, Prof. E. Rhys Davies and Dr R. J. Berry.
Speakers: Mr H. Eriskat, Mr M. O. Hjardemaal, Dr A. Hufton, Mr C. Maccia, Prof. J. J. Broerse, Prof. E. Vano-Carruana, Dr H. M. Kramer, Dr B. M. Moores and Dr R. J. Berry.

Practical Issues in Breast Cancer Screening
January 17, 1991
Scientific Societies Lecture Theatre
Joint BIR/RCR/RSM all day meeting
Organizer: Prof. G. H. Whitehouse
Speakers: Drs J. Law, N. M. Perry, G. J. Bickler, A. R. M. Wislon, C. Rubin, M. J. Michell, F. E. White, J. Austoker, A. K. Tucker and Prof. J. Chamberlain

Cerebral Blood Flow Practical Measurement and Clinical Relevance — a Multimodality Approach
February 12, 1991
All day Meeting
Organizer: Dr A. H. Smith

CT — Are the Bells and Whistles Worthwhile?
February 20, 1991
All day meeting
Organizers: Drs A. Dixon and S. Golding

Radiobiology Proffered Papers
February 22, 1991
Organizer: Dr R. Camplejohn

Radiation Oncology/IPSM
April 10, 1991
All day meeting organized by IPSM

RADIOLOGY AND ONCOLOGY 91 and MED X RAY
29 April–1 May
Metropole Hotel, Brighton

Radiation Oncology and Radiobiology: Particle Therapy
June 7, 1991

The New Legislation — Friend or Foe (After the White Paper ... and into Europe)
June 13, 1991
All day meeting orginized by the Industry Committee
Chairmen: Prof. C. A. Joslin, Dr O. Craig and Miss D. Rigg
Speakers include Dr J. Roylance, Dr I. Watt, Mr E. Sutherland, Prof. I. Isherwood and Mr P. Richardson

Conversazione
June 27, 1991
Painter's Hall, London
Lecture: " Half an Eye on the Sty", by Sir Stephen Furness.

Is there a seminar, conference or evening get-together you want to organize, but you don't have the time? The BIR Conference Office may be able to help you. Please call Vanessa Whitehead, Conference Manager, to discuss possibilities.

The Rolex Awards for Enterprise

The Rolex Awards provide financial assistance to people with a spirit of enterprise linked with perseverance and originality, to allow them to carry out unconventional projects in one of the following fields:

Applied sciences and invention
Exploration and discovery
The environment

Five laureates are chosen by a Selection Committee traditionally composed of prominent figures of international renown.

Numerous candidates who receive an Honorable Mention also receive a gold and steel watch, as well as the publicity which may lead to opportunities. For the 1990 Awards, 35 of the entries received an Honorable Mention.

Awards are given every three years; the next five laureats will be selected in 1993.

For more information, contact Christiane Ricou, Relations Publiques, Montres Rolex S. A., Rue François-Dussaud, 1211 Genève 24. Tel. (022) 43 22 00.

Lecture, Conference and Meeting Facilities

Available for use at 36 Portland Place, London W1

The BIR lecture Theatre, with raked seating and extensive audiovisual equipment, accomodates 100 people in air conditioned comfort.

The conference room accommodates a maximum of 34 people with modular furniture which can be arranged to suit the needs of individual users.

For further information please contact the House Manager, British Institute of Radiology, 36 Portland Place, London W1N 4AT. Tel. 071-580 4085.

Library News

The BIR Library is open weekdays 9 a.m.–5 p.m. (7 p.m. on Tuesdays and Thursdays).

The journal stock includes more than 100 titles. Although journals may not be taken out of the library, there is a photocopy service, also available by post or Fax. A list of current journals is available on request and is also published in the March and September issues of the Bulletin. Most books (except the historical collection) are available on loan.

Members can apply to the BIR librarian for a visitor's card which allows limited use of the RSM library for reference purposes, including photocopying and searches.

Recent additions to the library

IAEA, 1989. Measurement of Radionuclides in Food and Environment. A Guidebook. IAEA Technical Reports Series, 295.

Lemke, H. U. et al (Eds), 1989. Computer Assisted Radiology. Proceedings of the 3rd International Symposium CAR '89.

Paliwal, B. R. et al (Eds), 1988. Biological, Physical and Clinical Aspects of Hyperthermia.

Persson, B. R. & Ståhlberg, F., 1989. Health and Safety of Clinical NMR examinations.

Ring, E. F. J. (Ed.), 1990. Current Research in Osteoporosis and Bone Mineral Measurement. Proceedings of the 2nd Bath Conference 25–27 June, 1990.

K. C. Simpkins (Ed.), 1988. A Textbook of Radiological Diagnosis. 5th edn. Vol. 4. The Alimentary Tract: the Hollow Organs and Salivary Glands. (RCR.)

Tio, T. L., 1988. Endosonography in Gastroenterology.

White, D. R. & Cull, P., 1988. Radiation Saftey for Domestic Staff. (1) X-ray and Radiotherapy Departments, Wards and Theatres. Tape and Slides (Graves medical Audiovisual Library 85-5).

New periodical:
Documents of the NRPB.

Industry News

Matchmaker '90 Brings American Medical Equipment Firms to the UK

The first Medical Matchmaker to be held in the UK, featuring products and services from the medical and dental equipment industries, is to be held November 26–28, 1990, in the International Marketing Centre at the American Embassy, London. Over 40 American companies will take part.

Companies will be exhibiting the latest in medical and dental products such as hospital management and medical software, diagnostic testing kits, medical disposables, orthopaedic products and other surgical and medical equipment/products.

Attendance at Matchmaker '90 is by appointment only, ensuring that each participant is properly matched with its UK counterpart.

The programme has been fostering British and American business co-operation since 1984, and has served as a model for other embassies.

Companies interested in meeting American participants are encouraged to contact the International Marketing Centre at the US Embassy in London. A catalogue will soon be available detailing the participating American companies.

For further information, contact Mrs Mickey Boxer, International Marketing Centre, Embassy of the United States of America, 24/31 Grosvenor Square, London W1A 1AE. Tel: 071-409 2927. Fax: 071-491 4022.

BIR Company Subscriber Scheme

The BIR company subscriber scheme is aimed at all companies with and interest in radiology and addied sciences.

For and annual subscription of £250 p.a. member companies are offered an attractive benefits package.

To find out why your company should join the leading edge companies listed below, please contact Mr Tony Hudson, Administration Manager, British Institute of Radiology, 36 Portland Place, London W1N 4AT. Tel: 071-580 4085.

Agfa-Gevaert Ltd
27 Great West Road, Brentford, Middlesex TW8 9AX. Tel. 081-560 2131.
Product Areas 1. Contact Mr G. Mountford, Director.

American Medical Ltd
PO Box 971, London SW10.
Tel. 071-352 8051. Fax: 071-376 4508.
Product areas 1, 3, 4, 5, 7, 8.
Contact Betsy Riley, Managing Director.

Amersham International PLC
Lincoln Place, Green End, Aylesbury, Bucks HP20 2TP. Tel. 0296 395222.
Product areas 4, 5, 6.
Contact Mr James McLaughlin, Sales and Marketing Manager.

Bard Ltd
Forest Houe, Brighton Road, Crawley, West Sussex RH 11 9BP.
Tel. 0293 27888, ext. 2204.
Product area 2.
Contact Anna Shores, Product Manager.

British Nuclear Fuels plc
Room 525, Hinton House, Risley, Warrington, Cheshire WA3 6AS.
Tel. 0925 835022.
Product areas 8, 11. Contact Dr R. J. Berry, Director of Health and Safety and Environmental Protection.

Bruel & Kjaer (UK) Ltd
92 Uxbridge Road, Harrow, Middlesex, HA3 6BZ.
Tel. 081-954 2366.
Product areas 3, 6.
Contatct Mr Dennis Lewis, Sales Manager.

Cardiac Services Ltd
95A Finaghy Road, South Belfast BT10 OBY. Tel. 0232-625566.
Product areas 1, 3, 4, 5, 6.
Contact Mr R. J. Brown. Managing Director.

Du Pont (UK) Ltd
Wedgwood Way, Stevenage, Hertfordshire SG1 4QN. Tel. 0438 734000.
Product areas 1, 3, 4, 5, 6, 7, 9 and 10.
Contact Mr E. G. Lovat, Product Manager, Diagnostic Imaging.

E. G. & G. Limited
Vale Road, Windsor, Berkshire SL4 5JP. Tel. 0753 855611.
Product areas 1, 6, 7, 8.
Contact Miss Susan Holgate, Sales Executive (Therapy).

Elscint (GB) Ltd
Colonial Business Park, Colonial Way, Watford, Herts WD2 4PT.
Tel. 0865 340900.
Product areas 1, 3, 4.
Contact Faith Gorman, Marketing Manager.

E-Z-EM Ltd
1230 High Road, Whetstone, London N20. Tel. 081-446 9714.
Product areas 1, 2, 8.
Contact Richard Bayliss, Sales and Marketing Manager.

Fuji Photo Film (UK) Ltd
125 Finchley Road, London NW3 6JH.
Tel. 071-586 9351.
Product areas 1, 3.
Contact Mr R. G. Brown, Marketing and Administration Manager.

Gammex-RMI Ltd
34 Shakespeare Street, Nottingham NG1 4FQ. Tel. 0602 483807.
Product areas 1, 3, 4, 5, 6.
Contact Miss Eileen Parr, Commercial Manager.

IGE Medical Systems Ltd
352 Buckingham Avenue, Slough, Berks SL1 4ER. Tel. 0753 874000.
Product areas 1, 2, 3, 4, 5, 6, 8, 9.
Contact Jill Mitchell, UK Sales Support.

Kodak Ltd
PO Box 66, Station Road, Hemel Hempstead, Herts HP1 1JU.
Tel. 0442 61122.
Product area 1.
Contact Mr P. E. Blackwell, Manager, Health Sciences Division.

Lanmark
PO Box 317, Beaconsfield, Bucks HP9 2LR.
Tel. 0494 791615/670586.
Product areas 1, 3, 4, 5, 9, 10, 15, 16.
Contact Liz Beckmann, Director.

3M UK PLC
3M House, Bracknell, PO Box 1, Berks RG12 1JU. Tel. 0344 426726.
Product area 1.
Contact Mr Alan Budge, Marketing Manager.

Mallinckrodt Diagnostica (UK) Ltd
11 North Portway Close, Round Spinney, Northampton NN3 4RQ.
Tel. 0604-46132.
Product areas 4, 5.
Contact Mr D. G. L. Wood, Business Manager.

M. A. S. Medical Ltd
Armytage Road, Brighouse, West Yorkshire HD6 1QF. Tel. 0484 721906.
Contact Martin York, Managing Director.

Merit Health Systems Ltd
1 Viking Close, Great Gutter Lane, Willerby, North Humberside HU10 6DZ. Tel. 0482 652252.
Product area 13.
Contact Mr W. Blakemore, Director.

Medical Xray Supplies Ltd
Unit 12, Kingsbury Industrial Estate, Church Lane, Kingsbury, London NW9 8AU. Tel. 081-205 9500.
Product area 1.
Contact Mr R. J. Laird, Sales Director/Mr K. Wartnaby, Managing Director.

Mitsubishi Electric UK Ltd
Travellers Lane, Hatfield, Herts AL10 8XB. Tel. 07072 78756.
Product area 14.
Contact T. F. McCloud, Sales and Marketing Manager.

National Power plc
14 Newgate Street, London EC1A 7AM. Tel: 071-634 6898.
Product areas 7, 8.
Contact Mr A. J. Swanson, Assistant Company Secretary.

Nuclear Associates
100 Voice Road, Carle Place, New York 11514-1593, USA.
Tel. 516-741 7614.
Product areas 1, 3, 4, 5, 6, 8.
Contact Mr H. Glasser, General Manager.

Nucletron Trading Ltd
Nucletron House, Tarporley Business Centre, Tarporley, Cheshire, CW6 9UY. Tel: 0829 733611.
Product areas 6, 8.
Contact Mrs Marilyn A. Hart, Office Manager.

Nycomed (UK) Ltd
Nycomed House, 2111 Coventry Road, Sheldon, Birmingham B26 3EA.
Tel. 021-742 2444.
Product areas 1, 3.
Contact Mr L. Birch-Hansen, Managing Director.

Oxford Magnet Technology
Wharf Road, Eynsham, Oxford.
Tel. 0865 880880.
Product area 1.
Contact Pauline Hobday, Director of Sales and Marketing.

Philips Medical Systems
Kelvin House, 63–75 Glenthorne Road, Hammersmith, London W6 OLJ. Tel. 081-741 1666.
Product areas 1, 3–8.
Contact J. M. Woolston, Sales and Marketing Manager.

Polaroid (UK) Ltd
Ashley Road, St Albans, Herts AL1 5PR. Tel. 0727 59191.
Product areas 1, 3.
Contact David Hollingworth, Marketing Manager.

Premise Engineering Ltd
Tibbs Hill Road, Abbots Langley, Watford, Herts WD5 ODR.
Tel. 09277-67433/63320.
Product area 8.
Contact Mr R. K. Beach, Director.

Radiological Protection Services Ltd
61 Lind Road, Sutton, Surrey SM1 4PP. Tel. 081-643 6374.
Product area 8.
Contact B. H. Cutting, Managing Director.

Quantel Ltd
Administration Centre, Kiln Road, Newbury, Berkshire RG13 2HA.
Tel. 0444 232323.
Product areas 2, 10.
Contact Mr Christopher Trim, Publicity Officer.

Schering Health Care Ltd
The Brow, Burgess Hill, West Sussex RH15 9NE. Tel. 04446 6011.
Product areas 1, 2, 3.
Contact Mr A. Greaves, Product Manager.

Sony (UK) Ltd
Jays Close, Viables, Basingstoke, Hants RG22 4SB. Tel. 0256 483564.
Product areas 1, 3, 4, 5, 7, 8.
Contact Richard Holt, Marketing Manager.

Toshiba Medical Systems UK
Manor Court, Manor Royal, Crawley, West Sussex RH10 2PY.
Tel. 0293 560772.
Product areas 1, 2, 3, 4, 9, 10.
Contact Mr S. M. Weeden, Manager X-ray Products.

Toshiba Medical Systems Europe BV
Schieweg 1, 2627 An Delft, The Netherlands. Tel. 015 61 0121.
Product areas 1, 2, 3, 4, 9, 10.
Contact Mr P Blonk, Office Manager, X-ray BU.

X-rite (H. Miller Graphics Ltd)
8 Moody Street, Congleton, Cheshire CW12 4AP. Tel. 0260 279988.
Product areas 1, 12.
Contact Mrs P. Dhanani, Medical Sales.

Wardray Products Ltd
Hampton Court Estate, Summer Road, Thames Ditton, Surrey KT7 OSP. Tel. 081-398 9911.
Product area 8.
Contact Mr R. B. Wardley, Managing Director.

KEY TO PRODUCT/SERVICE AREAS

1: Diagnostic X-ray including NMR and CT
2: Interventional radiology
3: Ultrasound
4: Nuclear medicine
5: Radiopharmaceuticals
6: Radiotherapy and oncology
7: Radiobiology
8: Radiation protection
9: PACS
10: Image processing
11: Nuclear fuel cycle services
12: Quality assurance.
13. Radiology data management computer systems
14. Video printing
15. Equipment leasing
16. Hospital-shared services

Meetings and Courses

1st International Conference on Digital Radiology and PACS
November 11–13, 1990
Bologna, Italy
Further details: Organizing Secretariat, SO.GE.PA.CO, P.zza Costituzione 4 – 40128 Bologna, Italy. Tel: 051-6435111; Fax: 051-6435149.

Advanced Oncology: Head and Neck Cancer
November 23–24, 1990
London
Further details: The Conference Office, The Royal College of Radiologists, 38 Portland Place, London W1N 4DG. Tel: 071-323 3100.

The Second National Congress on Radiation Oncology
November 25–28, 1990
Shandong, China
Further details: Hu Yimin, Executive Secretary, Radiation Oncology Dept., Cancer Institute (Hospital), Chinese Academy of Medical Sciences, Beijing 100021, China.

The John Rylands Medical Book Fair 1990
Manchester
November 26–30, 1990
Further details: Mrs Jill Rawlinson, Haigh & Hochland Ltd, The Precinct Centre, Oxford Road, Manchester, M13 9QA. Tel: 061 273-4156. Fax: 061 273-4340.

New Interventional Techniques in the Vascualr System
November 28, 1990
London
Further details: Dr R. E. Smith, Surgical Professiorial Unit, St Bartholomew's Hospital, London, EC1A 7BE. Tel: 071-606 5943.

Continuing Care for Elderly People — What future?
November 30, 1990
London
Further details: Susan Hodge, King's Fund Centre, 126 Albert Street, London, NW1 7NF. Tel: 071-267 6111; Ext. 210.

Environmental Implications of a single European Market
December 5, 1990
London
Further details: Liz Hide, IBC Technical Services Ltd, IBC House, Canada Road Industrial Estate, Byfleet, Surrey, KT14 7JL. Tel: 071-236 4080.

Remote Technology for the Nuclear Industry
December 10–11, 1990
London
Further details: Katie Lye, IBC Technical Services Ltd, IBC House, Canada Road Industrial Estate, Byfleet, Surrey, KT14 7JL. Tel: 071-236 4080.

Radiotherapy User-club: Meeting on Dosimetry for Users of NPL Calibration Services
December 13, 1990
Middlesex
Further details: Mr C. J. Moretti, Building 62, NPL, Teddington, Middlesex TW11 0LW. Tel: 081-943 6083.

Personal Dosimetry — Present and Future
January 22, 1991
London
Further details: Dr D. N. S. Dixon, Programme Committee Secretary, The Society for Radiological Protection, 67 Oatlands Park, Linlithgow, West Lothian EH49 6AS. Tel: 031-244 2779.

The Seventh International Conference on Chemical Modifiers of Cancer Treatment
February 2–5, 1991
Florida, USA
Further details: Ms Suzanne Bohn, Projects Coordinator, American College of Radiology, 1101 Market St, 14th Floor, Philadelphia, PA 19107, USA. Tel: 215 574-3181.

The Bart's/London FRCR II Revision Course (MCQs, Film Reporting and Practice Vivas)
February 11–13, 1991
London
Further details: Mrs C. Burrage, Course Secretary, Room 26, Dunn Laboratories, St Bartholomew's Hospital, London EC1A 7BE. Tel: 071-601 7531. Fax: 071-607 7024.

Brain Chemistry and Behaviour: Advances in PET and SPECT Imaging
March 14–16, 1991
Maryland, USA
Further details: Patty Campbell, Program Coordinator, Office of Continuing Education, 720 Rutland Avenue, Baltimore, Maryland 21205, USA. Tel: (301) 955-3839.

Breast Imaging Update
March 16–18, 1991
California, USA
Further details: UCSF School of Medicine, Radiology Postgraduate Education, Box 0628, Room C-324, San Francisco, CA 94143-0628, USA. Tel: (415) 476-5731. Fax: (415) 476-9213.

Spectrum of Development Disabilities XIIss: Cerebral Palsy: Issues of Early Detection and Intervention
March 18–20, 1991
Maryland, USA
Further details: Program Coordinator, The Johns Hopkins Medical Institutions, Office of Continuing Education, Turner Building, 720 Rutland Avenue, Baltimore, Maryland 21205, USA. Tel: (301) 955-2959

The Fourth Annual International Intradiscal Therapy Society Meeting
April 3–7, 1991
Texas, USA
Further details: Ellen M. Yolich, Meeting Coordinator, IIts, PO Box 679, Grayslake, IL 60030-0679, USA. Tel: 1/800-426-4868 or 1/708-223-2684.

Eurodop '92: Major International Symposium on the Medical Applications of the Doppler Effect in Diagnostic Ultrasound
April 5–8, 1992
Brighton
Further details: Eurodop '92, Bell Howe Conferences, 1 Willoughby Street, Beeston, Nottingham NG9 2LT. Tel: 0602 436323.

As a service to our readers, notice of meetings or courses will be inserted free of charge. Please send full details to the Honorary Editor, BIR Bulletin.

Please send articles for the Bulletin or any comments or suggestions you may have about the Bulletin to The Honorary Editor, BIR Bulletin, 36 Portland Place, London W1N 4AT.